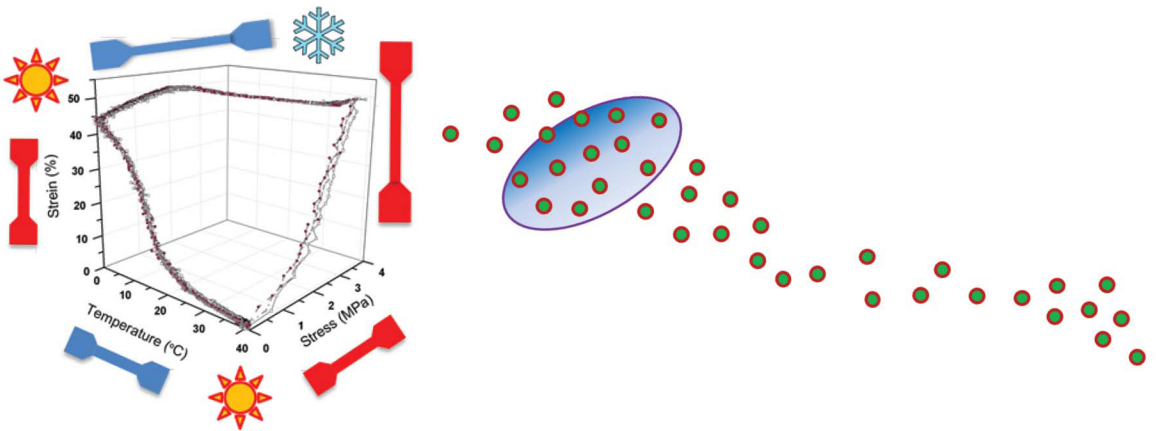


How Smart are the Polymers?



Laura Peponi, PhD,
Jean Marie Raquez, PhD
Editors

NOVA

Complimentary Contributor Copy

HOW SMART ARE THE POLYMERS?

No part of this digital document may be reproduced, stored in a retrieval system or transmitted in any form or by any means. The publisher has taken reasonable care in the preparation of this digital document, but makes no expressed or implied warranty of any kind and assumes no responsibility for any errors or omissions. No liability is assumed for incidental or consequential damages in connection with or arising out of information contained herein. This digital document is sold with the clear understanding that the publisher is not engaged in rendering legal, medical or any other professional services.

Complimentary Contributor Copy

POLYMER SCIENCE AND TECHNOLOGY

Additional books and e-books in this series can be found
on Nova's website under the Series tab.

Complimentary Contributor Copy

POLYMER SCIENCE AND TECHNOLOGY

HOW SMART ARE THE POLYMERS?

LAURA PEPONI
AND
JEAN-MARIE RAQUEZ
EDITORS



Complimentary Contributor Copy

Copyright © 2018 by Nova Science Publishers, Inc.

All rights reserved. No part of this book may be reproduced, stored in a retrieval system or transmitted in any form or by any means: electronic, electrostatic, magnetic, tape, mechanical photocopying, recording or otherwise without the written permission of the Publisher.

We have partnered with Copyright Clearance Center to make it easy for you to obtain permissions to reuse content from this publication. Simply navigate to this publication's page on Nova's website and locate the "Get Permission" button below the title description. This button is linked directly to the title's permission page on copyright.com. Alternatively, you can visit copyright.com and search by title, ISBN, or ISSN.

For further questions about using the service on copyright.com, please contact:

Copyright Clearance Center

Phone: +1-(978) 750-8400

Fax: +1-(978) 750-4470

E-mail: info@copyright.com.

NOTICE TO THE READER

The Publisher has taken reasonable care in the preparation of this book, but makes no expressed or implied warranty of any kind and assumes no responsibility for any errors or omissions. No liability is assumed for incidental or consequential damages in connection with or arising out of information contained in this book. The Publisher shall not be liable for any special, consequential, or exemplary damages resulting, in whole or in part, from the readers' use of, or reliance upon, this material. Any parts of this book based on government reports are so indicated and copyright is claimed for those parts to the extent applicable to compilations of such works.

Independent verification should be sought for any data, advice or recommendations contained in this book. In addition, no responsibility is assumed by the publisher for any injury and/or damage to persons or property arising from any methods, products, instructions, ideas or otherwise contained in this publication.

This publication is designed to provide accurate and authoritative information with regard to the subject matter covered herein. It is sold with the clear understanding that the Publisher is not engaged in rendering legal or any other professional services. If legal or any other expert assistance is required, the services of a competent person should be sought. FROM A DECLARATION OF PARTICIPANTS JOINTLY ADOPTED BY A COMMITTEE OF THE AMERICAN BAR ASSOCIATION AND A COMMITTEE OF PUBLISHERS.

Additional color graphics may be available in the e-book version of this book.

Library of Congress Cataloging-in-Publication Data

Names: Peponi, Laura, editor. | Raquez, Jean-Marie, editor.

Title: How smart are the polymers? / Laura Peponi, PhD, ICTP-CSIC, and Jean Marie Raquez, PhD, University of Mons, editors.

Description: Hauppauge, New York: Nova Science Publishers, Inc., [2018] |

Series: Polymer science and technology | Includes bibliographical references and index.

Identifiers: LCCN 2018032695 (print) | LCCN 2018034395 (ebook) | ISBN

9781536139617 (ebook) | ISBN 9781536139600 (hardcover) | ISBN 9781536139617 (ebook)

Subjects: LCSH: Polymers. | Smart materials.

Classification: LCC TA455.P58 (ebook) | LCC TA455.P58 H69 2018 (print) | DDC 620.1/92--dc23

LC record available at <https://lccn.loc.gov/2018032695>

Published by Nova Science Publishers, Inc. † New York

Complimentary Contributor Copy

CONTENTS

Preface		ix
Challenges and Perspectives in Smart Polymer Materials		xv
	<i>Jean-Marie Raquez and Laura Peponi</i>	
Chapter 1	Stimuli-Responsive Polymeric Materials with Shape Memory Ability	1
	<i>Valentina Sessini, Jean-Marie Raquez, Philippe Dubois, José M. Kenny and Laura Peponi</i>	
Chapter 2	Thermally-Activated Shape Memory Behavior of Different Nanocomposites Based on Ethylene Copolymers	35
	<i>Valentina Sessini, David Brox, Antonio Julio López, Alejandro Ureña, Jean-Marie Raquez, Philippe Dubois, José M. Kenny and Laura Peponi</i>	
Chapter 3	Shape-Memory Nanocomposites for Multi-Responsive Polymer Materials	59
	<i>Antoniya Toncheva, Florence Pilate, Philippe Dubois and Jean-Marie Raquez</i>	
Chapter 4	Intrinsically Healable Polymers	95
	<i>Robert H. Aguirresarobe, Sil Nevejans, Nicholas Ballard, June Aizpurua, Lourdes Irusta and Haritz Sardon</i>	
Chapter 5	Intrinsic Self-Healing Elastomers Based on Covalent Bonding	123
	<i>Marianella Hernández, Raquel Verdejo and Miguel Angel López-Manchado</i>	

Chapter 6	Healing Ability of Ionomeric Polymers under Low-Energy Transfer Damages <i>Antonio Julio López, Jorge Teno, Alejandro Ureña and Joaquin Rams</i>	149
Chapter 7	Photo-Responsive Polymers Based on Coumarin <i>Cástor Salgado Soneira, Laura Peponi, Marina P. Arrieta, Daniel López and Marta Fernández-García</i>	175
Chapter 8	Thermo-Responsive Polymer Dispersed Liquid Crystals Based on Block Copolymers <i>Sheyla Carrasco-Hernandez, Joseba Gomez-Hermoso de Mendoza, Junkal Gutierrez and Agnieszka Tercjak</i>	199
Chapter 9	Frontal Polymerization for Smart Hydrogels <i>Ivan Navarro Baena, Valeria Alzari and Laura Peponi</i>	223
Chapter 10	Tuning Polymer Thermosensitivity in Aqueous Media for Biomedical Applications <i>M. Eugenia Pérez-Ojeda, Enrique Martínez-Campos, Carlos Elvira and Alberto Gallardo</i>	245
Chapter 11	Smart Antimicrobial Surfaces <i>Alexandra Muñoz-Bonilla and Marta Fernández-García</i>	275
Chapter 12	Polymers for Smart Packaging Solutions <i>Marco Monti and Marta Zaccone</i>	295
Chapter 13	Smart Coatings: Development of Antioxidant Edible Films Based on Sodium Caseinate and Hydroxytyrosol <i>Marina Patricia Arrieta and Mercedes Ana Peltzer</i>	309
Chapter 14	Is Your Polymer Smart Enough? Better Make A Hybrid! <i>Daniela Anahí Sánchez-Téllez, Lucía Téllez-Jurado and Luís María Rodríguez-Lorenzo</i>	335
Chapter 15	Polymers for Additive Manufacturing <i>Thibault Ghigonetto, Carmen M. González-Henríquez, Mauricio A. Sarabia-Vallejos and Juan Rodriguez-Hernandez</i>	355
Chapter 16	From 3D to 4D-Printing: On the Road to Smart 3D-Printed Polymer Devices <i>Jérémy Odent, Antoniya Toncheva, Philippe Dubois and Jean-Marie Raquez</i>	391

Editor Contact Information

423

Index

425

PREFACE

Smart polymer materials represent an exciting range of novel materials for advanced applications such as aeronautics and biomedical devices. These materials are able to sustain any external stimuli including temperature, pH, electric and magnetic fields and response in an adaptive and proportional manner to this environmental change. Two main categories of smart materials are able to encompass these features, i.e., self-evolving materials and self-healing materials. Self-evolving materials can, for instance, reconfigure themselves on-the-fly to react upon changing environmental conditions. A variety of possible material candidates can be described as self-evolving materials including shape-memory polymers, adaptive hydrogels and actuators changing their properties in response to external stimulation. In addition to them, intrinsic self-healing polymers encompass these responsiveness features and are constructed on the basis of reversible bonding such as Diels-Alder reactions for locally healing these materials after experiencing damage.

This book intends to propose a comprehensive knowledge on smart materials that encompass self-evolving materials and self-healing materials, including their implementation of 3D-printing technology. Combining smart materials and additive manufacturing has thereby been introduced as an inspiring way to provide more complex 3D objects with elevated adaptive properties. They are myriad issues that are still challenging with the construction of these smart materials, including their additive manufacturing, but the book will offer novel opportunities to obtain multi-responsive materials in advanced technology.

Chapter 1 - Shape memory materials are able to change their shape upon application of an external stimulus such as temperature, humidity, light, electric or magnetic fields, etc. Due to their scientific and technological relevance, this book chapter reviews the main shape memory materials, briefly introducing metals, ceramics and polymers. In particular, shape memory polymers are discussed following the nature of the stimulus that allows their shape memory response, including their characterization methods.

Polymeric materials show a wide range of relevant properties such as processability, versatility and biocompatibility, among others, characteristics that are responsible for the increased interest in recent years in the shape memory field.

Chapter 2 - Shape memory materials are able to change their shape upon application of an external stimulus such as temperature, humidity, light, electric or magnetic fields, etc. This chapter wants to focus the attention on nanocomposite systems with shape memory response due to their high scientific and technological relevance. In particular, three different nanocomposites based on ethylene copolymers are presented with different thermally-activated mechanisms such as Nucrel® and Surlyn® reinforced with silica nanoparticles, blends of EVA/thermoplastic starch reinforced with natural bentonite and EVA reinforced with starch nanocrystals. All of these systems present shape memory ability, evidencing how the addition of well dispersed nanoparticles can affect the shape memory response of the neat matrix.

Chapter 3 - Shape-memory polymers (SMPs) are currently a subject of tremendous attention from both - the academic and industrial fields and are playing a major role in inspiring the design of a class of polymer materials. Their attractive properties related to multi-step shape-changing upon exposure to an appropriate stimulus, as well as high elastic deformation, low density, relatively low cost, ease of processing, chemical stability and biocompatibility make SMPs suitable for numerous real world applications. As if that's not enough, fabricating nanocomposites *via* the incorporation of nanofillers offers the possible applications as innovative materials with designed functionalities and multi-responsiveness even further. Nowadays, these polymer materials can be used as biomedical devices (implants, sutures, stents, drug delivery systems), actuator systems, sensors or deployable hinges for automotive, electronics and aerospace industries. In this chapter, a short description on SMPs chemical architecture, nanofillers incorporation and approaches for 3D printing are outlined. The content would also mention some potential application of the printed parts and final critical remarks.

Chapter 4 - The introduction of healing characteristics into synthetic polymers has represented a step forward in the development of safer, more durable and more reliable materials. Ideally, a healable material should be able to restore its performance after being damaged, even for multiple damage/healing events. In this sense, the current knowledge about material science, polymer physicochemistry and polymer synthesis has led to the development of new types of healable polymers capable of fulfilling these prerequisites: Intrinsically healable polymers. These materials contain active elements, which are covalently incorporated into the polymer structure and impart repairing characteristics to the final material. Herein, the authors summarize the most relevant parameters in the development of intrinsically healable polymers as well as the most recent synthetic approaches reported in the literature.

Chapter 5 - Self-healing materials have intensively been investigated over the past 15 years. Several approaches have been developed, resulting in materials capable of dealing

with damage events in a more or less independent way, thereby extending their service life, and thus reducing waste. Large interest has been drawn to self-healing elastomeric materials, following either extrinsic or intrinsic approaches. In this chapter the authors discuss Diels-Alder chemistry and disulfide exchange reactions as the most prominent examples currently used in the development of intrinsic self-healing elastomers based on reversible covalent bonds.

Chapter 6 - The self-healing ability of poly(ethylene-co-metacrylic acid) (EMAA) copolymer neutralized with sodium salt forming the ionomer known as Surlyn® has been investigated using various types of low-velocity damage: indentation, puncture and scratch with razor blade, and puncture with different sharp metallic pointers. These types of macroscopic damages create low-energy heat transfer to the tested material and therefore, thermal energy must be externally added to the material to trigger its healing properties. Different thermal treatments have been carried out using a range of temperatures (40, 55, 70 and 105°C) and heating times, to determine the healing abilities of the material and to optimize the healing procedure for each type of damage. The use of 70°C for 40 min is an effective healing route for the most of the damages, but only complete healing values were obtained when using 105°C.

Chapter 7 - In this chapter, photo-responsive polymers (PRP) with extraordinary consideration in the polyurethane field and in particular, coumarin-based polymers are reviewed. But it also summarizes other representatives photo-reactive compounds used in polymer science (i.e., azobenzene, spiropyran, cinnamic acid/ester, anthracene and coumarin derivatives). Firstly, this chapter offers an overview of the photo-responsive mechanism of these photo-reactive compounds. Since light is an ideal way to modify physical and chemical properties on material surfaces, smart properties such as self-healing and/or shape memory behavior can be performed with the correct useful of this source. For these reason, PRP can be used as films, hydrogels as well as supramolecular systems with interesting properties for several applications such as laser dyes, drug delivery systems and mainly as coatings. Well-dispersed nano-sized fillers are able to enhance several properties of PRF, including hydrophilic/hydrophobic, thermal and mechanical properties, as well as the release ability, etc. Thus, recent developments in PRP are summarizes here with a special emphasis on PU-coumarin based systems as well as on their nanocomposites.

Chapter 8 - This Chapter deals with an extensive description related to polymer dispersed liquid crystals based on block copolymers. In addition, a short introduction related to liquid crystals with an emphasis on nematic liquid crystals and polymer dispersed liquid crystals (PDLC) will be given. The introductory part will be followed by a comprehensive discussion related to polymer dispersed liquid crystals and their reversible properties under external stimuli such as thermal gradients or electric and magnetic fields. Finally, different examples of PDLC blends based on block copolymers such as a polymeric matrix will be presented. Furthermore, special attention will be paid

to the reversible switching of these smart materials using different characterization techniques such as differential scanning calorimetry (DSC), optical microscopy (OM), photoluminescence spectroscopy (PL), UV-visible spectroscopy (UV-vis), and others.

Chapter 9 - A short review on current work in smart hydrogels field has been presented in this chapter, focusing the attention on the different stimuli to be used for activating hydrogels. Special attention was paid on frontal polymerization as suitable synthetic route for smart hydrogels and their nanocomposites. Therefore, after a brief review on frontal polymerization to design smart hydrogels, a case study has been presented based on the use of the frontal polymerization to obtain smart hydrogels nanocomposites of poly(N-vinylcaprolactam) (PVCL) and its nanocomposites. In particular, hydrogels were reinforced with both silver and hydroxyapatite nanoparticles. Because of the unique properties of these nanoparticles, the nanocomposites presented herein can be considered as very interesting materials for biomedical and antibacterial applications.

Chapter 10 - Thermoresponsive polymers have been thoroughly investigated for biomedical uses in many areas; from theragnostics, drug and gene delivery to cell harvesting and tissue engineering. The use of biocompatible smart polymers requires precisely tuning the structure, composition (hydrophobic/hydrophilic balance), polymer length, molecular weight, lateral chains, etc. in order to achieve physical changes in aqueous media at physiological temperature. This chapter intends to describe these issues and how the alteration of the chemical structure of the repetition unit within the backbone, the polymerization degree or end-functionalization, affect the thermal, mechanical and degradation properties of the resulting (co)polymers upon the final application.

Chapter 11 - Bacterial colonization and biofilm formation on material surfaces is a serious problem in medical devices and, in general, in human healthcare. In recent years, polymeric coatings with inherent antibacterial properties have acquired relevance as a practical alternative to combat biofilm formation. Basically, there are two main types of antimicrobial surfaces, bactericidal and antifouling surfaces, in which each type presents its inherent drawbacks. Thus, many efforts have been made to develop surfaces with both characters, bactericidal and bacteria-resistant properties. Of particular interest results smart antimicrobial surfaces that can reversibly switch in response to external stimuli between bactericidal and antifouling character to release dead bacteria attached onto the surfaces. In this chapter, the authors highlight the recent developments performed on smart surfaces with switchable capacity between biocidal activity and self-cleaning properties in response to stimulus such as pH, temperature, aqueous environment, ionic strength, light and electrical field.

Chapter 12 - In the last years, smart (or intelligent) packaging has been one of the most promising technologies in the food packaging industry. In fact, the possibility of making people aware of the safety and the quality of the food they are going to eat, has a

huge potential impact in terms of both health of the consumer and reduction of food waste. In this field, many technical opportunities have been developed, based on a physical or a chemical reaction that results in a visible change of color which communicates to the consumer the change in the food quality. Being some of the most used materials in food packaging, polymers have often a main role also in the smart solutions, also thanks to their versatility and the possibility to be modified and tailored to obtain the expected features. This chapter represents a brief overview of the smart packaging solutions related to the polymer world.

Chapter 13 - The increasing production of biobased and biodegradable polymers provides to the food industry the opportunity to offer alternative solutions with lower environmental impact. Among the available biopolymers, caseinates show excellent edible film formability, the ability to form thin and flexible layers, interesting for edible coating systems. Hydroxytyrosol (HT) is a natural antioxidant occurring in olives and mostly recovered from residues of olive oil production. However, many authors suggested that it is also available in olive oil. The HT is an ortho-diphenol with a marked antioxidant activity related to the electron donating ability of hydroxyl groups in the ortho position and subsequent formation of stable intramolecular hydrogen bonds with the phenoxylic radical. This chapter begins with generalities regarding the interest of smart materials in the food packaging field, focusing the attention on antioxidant active packaging systems as well as the interest on the use of edible active coatings for these applications. Then, it is reported the development of active edible films based on sodium caseinate and HT. The most important results regarding a full characterization of the obtained active films in terms of visual, structural, thermal, mechanical and barrier properties; together with the evaluation of the antioxidant properties of the developed films are described throughout this chapter and it was possible to conclude that this system is a good alternative to avoid or retard foodstuff oxidation and though increase food shelf life.

Chapter 14 - The main advantages of inorganic–organic hybrids are the combination of frequent dissimilar properties of organic and inorganic components in one material and the opportunity to develop an almost unlimited set of new materials with a large spectrum of known and yet unknown properties, because of the many possible combinations. Usually, in composite materials, polymer networks serve as organic matrices and inorganic components (Si, Ti, Sn, Al-based compounds, etc.) serve as fillers dispersed into the polymer network. These composites can be considered within Class I hybrids. In this class, weak bonds between components can be found such as Van der Waals forces or hydrogen bonds. Moreover there is Class II hybrids where components are linked by strong chemical bonds such as ionic or ionic-covalent bonds. Two types of reactions can be used to synthesize Class II hybrids: the simultaneous polymerization and the sequential polymerization of organic and inorganic monomers. Different structures can be obtained by altering the polymerization procedure: inorganic phase nanodomains

dispersed into the organic matrix; networks with bicontinuous phase structure; networks with ordered inorganic phase; and organic-inorganic block copolymer networks with inorganic junction domains. The chemistry of inorganic-organic network hybrids is mainly developed using hybrid molecular precursors such as organically modified metal-alkoxides or oligomers of general formula $R'_n\text{Si}(\text{OR})_{4-n}$ or $(\text{OR})_{4-n}\text{Si-R}''-\text{Si}(\text{OR})_{4-n}$ with $n = 1, 2, 3$, respectively. Several stimuli responsive hybrids have been manufactured for different applications: drug delivery systems based on mesoporous silica supports (MSS) have been described responding to physical, chemical or biochemical stimuli; antibacterial hybrids based on photocatalyst reactions; smart biosensing systems based on thin metallic and inorganic nanofilms with natural peptides, glutathione or aminothiols are also being described responding to complex opto-electronic interactions; graphene-based bilayer and multilayer actuators made from graphene and conducting polymers are described responding to chemical variations; and self-healing graphene-polymer hybrids are described responding to near-infrared region (NIR) irradiation. These materials are among the highlighted examples of hybrid smart materials.

Chapter 15 - Additive manufacturing (AM), also generally known as 3D printing permits the fabrication of fully customized objects with a high level of geometrical complexity implying rapid fabrication time as well as low cost. Among the materials used for additive manufacturing include metals and ceramics in addition to polymers. Nevertheless, the synthetic versatility as well as the wide range of material properties that can be achieved using polymers have established this type of materials amongst the most widely employed. Herein, the authors describe the basic principles applied when considering printing mechanisms, as well as the advantages and disadvantages of the most relevant AM technologies. Moreover, the characteristics of the polymers employed for each technology are described including discussion of some illustrative examples of their principal applications.

Chapter 16 - The scientific and technological progress reached a point that allows for exciting 3D printing technologies. Applied to the additive manufacturing industry, said technologies offer the possibility to create polymer devices with controlled architectures such as personalized prototypes, hydrogels, biomedical and flexible electronic devices, as well as sensors and actuators with controlled properties and a specific set of desired functionalities. Alongside this advancement, a new class of polymers defined as “smart polymer materials”, are described, with a main utility built around the capacity to exhibit adaptive properties that fulfill previously impossible functions post application of environmental changes. Direct 3D printing of such stimuli-responsive materials allowed the development of a brand new 4D printing technology with an outlined time dimension. This chapter will cover a comparative review of the two most frequently explored AM technologies - fused deposition modeling and stereolithography with a specific focus on the practical use in “smart materials” 3D printing. Potential applications for the printed parts and some critical remarks are also mentioned.

CHALLENGES AND PERSPECTIVES IN SMART POLYMER MATERIALS

Jean-Marie Raquez¹ and Laura Peponi²

¹Laboratory of Polymeric and Composite Materials,
University of Mons, Mons, Belgium

²Instituto de Ciencia y Tecnología de Polímeros,
ICTP-CSIC, Madrid, Spain

Nothing than both scientific and technological progresses has pushing the emergency of smart polymer materials for advanced applications such as aeronautics. Nature is thereby inspiring scientists to design these smart polymers in such a way to biomimic the behavior of living organisms. The most inspiring feature is the ability of a material able to interact with its surrounding environment and to provide an adaptive and proportional response given any environmental change. This corresponds to a large range of properties (stiffness, etc.) that can be adapted upon the application of an external stimulus as well as upon the nature of stimuli including temperature, pH, electric and magnetic fields. The adaption of biomimetic principles for materials research generally encompasses two main categories of materials, i.e., *self-evolving materials* and *self-healing materials*. *Self-evolving materials* can, for instance, reconfigure themselves on-the-fly to react upon changing environmental conditions. A variety of possible material candidates can be described as self-evolving materials including shape-memory polymers, adaptive hydrogels and actuators changing their properties in response to external stimulation. For instance, shape memory polymers (SMPs) represent a new class of high-performance materials, having the potential to be applied as biomedical materials as well as engineering thermoplastics. Resulting from the association between the polymer morphology and a specific program, these materials have the ability to deform themselves from a temporary shape to a permanent shape upon application of an external

stimulus like a change in temperature or exposition to light. Since the 1980s, *self-healing polymers* have been widely developed to overcome any mechanical stress or degradation (damage, fracture, photo or thermal degradation...) that cause failure or microcracks, reducing the lifetime, the sustainability and the safety of the material during their utilization. *Intrinsic self-healing polymers* based on reversible bonding such as Diels-Alder reactions have shown to be an interesting alternative to heal in a repeatable and infinite manner.

In this respect, we are also facing an era where combining *Smart Materials* and *Additive Manufacturing* will alter our lives by providing complex 3D objects with unique abilities given environmental changes, among which *Self-Evolving Materials* will definitely fall down as the most important descendant. Based on a layer-by-layer fabrication process to design custom 3D objects using computer-aided models, *3D-printing technology* significantly speed up the product development using a single build station at sub-microscale. As the number of studies conducted on this technology increases, the new 4D printing has been coined as the fourth dimension of time.

The motivation of this book was thereby to propose a comprehensive knowledge on smart materials that encompass *self-evolving materials* and *self-healing materials*, including their implementation of 3D-printing technology. The authors of this book are leading in the realm of smart materials and provide up-to-date research and related methodologies all long the book. They are myriad issues that are still challenging with the construction of smart materials, including their additive manufacturing, but it also offers novel opportunities to obtain multi-responsive materials in the advanced technology.

The chapters of this book have been divided into four main sections as shape-memory polymers (Chapters 1-3), self-healing polymers (Chapters 4-7), smart materials made of liquid crystals and hydrogels (Chapters 8-13) and 3D- and 4D-printing technology (Chapters 14-15). The first chapters discuss about the multi-responsiveness of shape-memory polymers including the design of related nanocomposites. In particular, shape memory polymers and nanocomposites are one the of most important class of multi-responsive smart materials, providing excellent and new opportunities for scientific developments in the field of polymer synthesis and functionalization, molecular architecture design, processing of polymer blends and interpenetrating networks and multifunctional materials. The second section discusses about self-healing polymers that can be intrinsically healed under mild conditions. For instance, Diels-Alder chemistry and disulfide exchange reactions as the most prominent examples currently used in the development of intrinsic self-healing elastomers based on reversible covalent bonds. In the third section, the ability to respond with any environmental change has been discussed within large range of smart materials such as liquid crystals and coating, thermoresponsive polymers and hydrogels. For instance, thermoresponsive polymers have been thoroughly investigated for biomedical uses in many areas. The use of

biocompatible polymers showing a physical change in physiological aqueous media at body temperature requires precisely tuning the structure, composition (hydrophobic/hydrophilic balance), polymer length, molecular weight, lateral chains, etc., giving access from theragnostics, drug and gene delivery to cell harvesting and tissue engineering. The final section highlights the key-feature related to Additive manufacturing, also generally known as 3D printing, permitting the fabrication of fully customized objects with a high level of geometrical complexity implying quite limited time to fabrication as well as low cost. Direct 3D printing of such stimuli-responsive materials allows the development of an original 4D printing technology where the time dimension is herein outlined.

Thanks to the great efforts made by the authors and valuable writing, the book thereby attempts to outline the most recent progress and important concepts underlying smart materials as the scientists continue to pursue. We do hope that this book will construct new solidified pathways in the realm of smart materials inspiring researchers from the multidisciplinary fields of material science, chemistry and engineering.

Complimentary Contributor Copy

Chapter 1

STIMULI-RESPONSIVE POLYMERIC MATERIALS WITH SHAPE MEMORY ABILITY

Valentina Sessini^{1,3,}, Jean-Marie Raquez², Philippe Dubois²,
José M. Kenny¹ and Laura Peponi³*

¹Dipartimento di Ingegneria Civile e Ambientale,
University of Perugia, Terni, Italy

²Laboratory of Polymeric and Composite Materials,
University of Mons, Mons, Belgium

³Instituto de Ciencia y Tecnología de Polímeros,
ICTP-CSIC, Madrid, Spain

ABSTRACT

Shape memory materials are able to change their shape upon application of an external stimulus such as temperature, humidity, light, electric or magnetic fields, etc. Due to their scientific and technological relevance, this book chapter reviews the main shape memory materials, briefly introducing metals, ceramics and polymers. In particular, shape memory polymers are discussed following the nature of the stimulus that allows their shape memory response, including their characterization methods. Polymeric materials show a wide range of relevant properties such as processability, versatility and biocompatibility, among others, characteristics that are responsible for the increased interest in recent years in the shape memory field.

Keywords: stimuli-responsive, shape memory polymers, humidity, temperature

* Corresponding Author Email: valentina.sessini@gmail.com

INTRODUCTION

Nature is a vast source of inspiration for engineering functional materials. Indeed, chemists and material scientists often follow the principles of nature for the design of new synthetic materials (“bio-inspired materials”) [1]. In this context, one of the most inspiring features is the ability to change a specific property upon the application of an external trigger. The variety of the properties that can be changed upon application of an external stimulus is enormous, as well as the nature of the applied stimulus. Variation of mechanical properties is one feature, which for example can be found in sea cucumbers as reported from Bellamkonda et al. [2]. These animals are able to change their skin stiffness by several orders of magnitude in case of danger (i.e., an attack by a predator) [2]. In addition to these macroscopic changes, natural materials show a stimuli-responsiveness on the level of single molecules. For instance, proteins adopt different shapes depending on the conditions used (e.g., temperature, pH-value, salt concentration, etc.) [3]. Simplifying nature’s inspiring examples, many stimuli-responsive polymeric systems have been developed by researchers over the last decades [4-5].

Among stimuli-responsive materials, shape-memory materials (SMMs) can respond by changing their shape toward the application of a specific stimulus. SMMs are characterized by the shape memory effect (SME), which is defined as the ability to recover their original shape at the presence of the right stimulus, after being severely and quasi-plastically distorted [6]. The growing interest on SMMs production is well-highlighted by the number of publications during the last seventeen years (Figure 1).

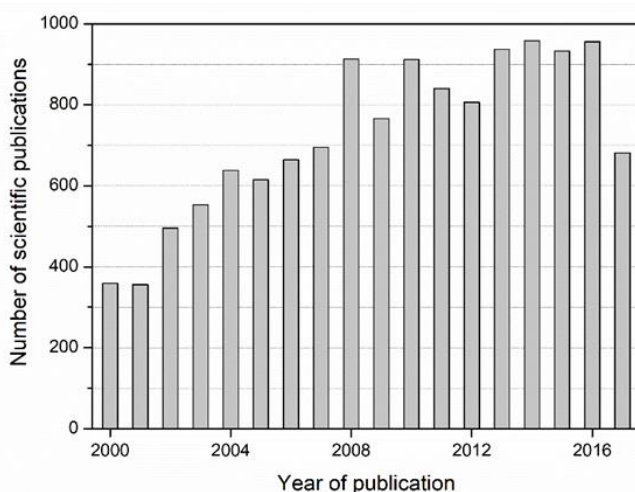


Figure 1. Number of scientific publications per year on the SMMs. Data Source: Scopus®; data research made on August, 2017.

SME has been observed in different kinds of materials like metal alloys [7-9], ceramic materials [10-12], hybrids [13-14] and gels [15-16] as well as polymeric materials [17-19]. A briefly state of the art of these materials is presented in the next pages.

METAL ALLOYS

Shape memory alloys (SMAs) or “smart alloys” was firstly discovered by Arne Ölander in 1932 [20], but the importance of SMMs was not recognized until William Buehler and Frederick Wang whom revealed the SME in a nickel-titanium (NiTi) alloy in 1962 [21], also known as Nitinol [22]. SMAs are a group of metallic alloys that can return to their original form (shape or size) when subjected to a memorization process between two transformation phases, which are temperature or magnetic field dependent [23]. In brief, SMAs can exist in two different phases with three different crystal structures, i.e., twinned martensite, detwinned martensite and austenite. The austenite structure is stable at high temperature, while the martensite structure is stable at lower temperatures. When a SMA is heated, it begins to transform from martensite into the austenite structure, i.e., to recover its original form. This transformation is possible even under high applied loads, and therefore, results in high actuation energy densities [23]. The SME in SMAs is a diffusionless solid phase transition between martensitic and austenitic crystal structures [24-25]. While at low temperatures, SMAs present the SME, at high temperatures, recovery can be achieved instantly and simultaneously upon releasing the applied load, just like rubber band. This is called “superelasticity” [26]. The SME and the superelasticity (or pseudoelasticity) on metallic materials, can be categorised into three shape memory characteristics as follows:

- One-way shape memory effect. The one-way SMAs retain a deformed state after the removal of an external force, and then they are able to recover their original shape upon heating.
- Two-way shape memory effect or reversible SME. In addition to the one-way SMAs, two-way SMAs can remember their shape at both high and low temperatures. However, two-way SMAs are commercially less applied due to the ‘training’ requirements and to the fact that they usually produce about half of the recovery strain provided by the one-way SMAs for the same material [27-28]. Furthermore, their strain tends to deteriorate quickly, especially at high temperatures [29]. Therefore, the first one provides more reliable and economical solution [23].
- Pseudoelasticity (PE) or Superelasticity (SE): The SMAs revert to their original shape after applying mechanical loading at temperatures between the temperature

where the transformation in austenite structure is complete and the highest temperature at which martensite can no longer be stress induced, without the need for any thermal activation [30].

Other forms or types of SMMs have been explored due to some obvious limitations or disadvantages of SMAs, such as high manufacturing cost, limited recoverable deformation, limited operating temperature and low bandwidth [17].

CERAMIC MATERIALS

Shape memory ceramics (SMCs) are inorganic or ceramic compounds that undergo martensitic or displacive transformations can be either stress or thermally-activated. Anyway, most of ceramics are very brittle and the transformations needed to active the SME, i.e., martensitic transformation, can cause cracking, most often because shape distortions in adjacent crystal grains are incommensurate with one to another, inducing large mismatch stresses and triggering fracture [10]. As a matter of fact, unlike SMAs such as Ni-Ti that can withstand low strains up to $\sim 8\%$ and at lower strain levels they can be reversibly transformed up to millions of cycles [31], in SMCs such as zirconia, at strains of only about $\sim 2\%$, cracking is observed after only a few transformation cycles [32]. Using ceramics, some new shape memory device can be designed for high temperature application where ordinary SMAs are not applicable. However, the technological application of the shape-memory capacity is limited by the small magnitudes of recoverable strains and the tendency of the ceramics to microcracking. It is possible to classify these materials in terms of their shape memory mechanisms [13]:

- Martensitic SMCs are the most known and widespread one. The mechanism is analogous to the metallic alloys: a transition between two crystalline phases is able to produce shape changes. For these materials, the maximum strain achieved is not more than 4%. More displacive or martensitic-like transformations and potential shape-memory materials can be found in a variety of structural ceramics such as zirconia based ceramics [11, 33] or partially stabilized zirconia [34].
- Viscoelastic SMCs are sintered ceramics that contain very little glass phase including mica ($\text{KMg}_3\text{AlSi}_3\text{O}_{10}\text{F}_2$), silicon nitride (Si_3N_4), carbon nitride (SiC), zirconia (ZrO_2) and alumina (Al_2O_3) [35]. Some mica glass-ceramics typically have a heterostructure characterized by a volume fraction in between 0.4 and 0.6 of mica, as the principal crystalline phase, dispersed in a continuous glassy phase. These materials exhibit clear shape-memory phenomenon: after high-temperature plastic deformation, cooling under load to room temperature in order to fix the temporary shape thanks to mica phase, and then reheating to recover

the original shape [36]. Because the sliding through dislocations in mica is not possible at low temperature, the deformation of the material at elevated temperatures will be retained even if the load is removed, after cooling under load to ambient temperatures. The elastic strain energy stored in the glassy phase will thus provide a driving force for recovering the original shape. If the deformed mica is reheated to a high temperature at which the stored elastic strain energy is sufficient to activate the dislocation slide, the phase mixture will reverse the original plastic deformation. In these materials, the shape-recovery percentage shows a strong dependence on the deformation temperature, deformation rate, reheating temperature and heating time [36].

- Ferroelectric SMCs are perovskite-type oxides where the crystallite domains may exist in a variety of states such as cubic, tetragonal, rhombohedral or orthorhombic, which may be either paraelectric, ferroelectric or antiferroelectric, depending on the exact composition, as well as external conditions such as temperature, stress and electric field. The phase transitions between the different structures, such as the paraelectric-ferroelectric transition and the antiferroelectric-ferroelectric transition may be accompanied by a considerable strain in the ceramics. When the electric field is removed, conventional electroceramics will return to their original state [37]. This is a typical ferroelectric behaviour. Although the shape-memory ceramics have lower strain levels than shape-memory alloys, they have some clear advantages and may be more suitable for certain applications. For instance, because an electric field can be readily changed at much higher rates than temperature, the shape-memory ceramics may be actuated at higher bandwidths, with the maximum response speed of only a microsecond.
- Ferromagnetic SMCs are transition metal oxides that undergo paramagnetic-ferromagnetic, paramagnetic-antiferromagnetic transformation, or orbital order-disorder transitions and the reversible transformations are also accompanied by recoverable lattice distortions. Because of spontaneous magnetization of these compounds is only achievable at very low temperatures, the effects of the magnetic field on the transformation and ferromagnetic shape-memory effect in these compounds are less investigated.

POLYMERIC MATERIALS

Shape memory polymers (SMPs) are polymers which are able to “memorize” a permanent shape and that can be manipulated in a way that a certain temporary shape will be “fixed” under appropriate condition [4]. Thanks to a several great features, SMPs show several advantages in comparison with SMAs [26]. In particular, some of these are

low density, high recoverable strain within a wide range of stimuli (by means of direct heating or by Joule heating, induction heating, infrared/radiation heating, laser heating, moisture or solvent or changes in pH value, light, etc.), as well as, transparency, chemical stability, easy chemical modification, well processability, high potential to be easy recyclable and reusable at low cost [38] and eventually, biocompatibility and biodegradability. Regarding the costs, not only the cost of raw material as well as the cost in fabrication and processing remain lower than for SMAs [26].

The first publication mentioning SME in polymers is due to L. B. Vernon in 1941 in a United States patent [39], who claimed a dental material made of methacrylic acid ester resin able to recover its original shape upon heating. Despite this early discovery, recognition of the importance of SMPs did not occur until the 1960s, when covalently cross-linked polyethylene was found to have shape memory capability [40]. Significant efforts began in the late 1980s and this trend continues to grow until nowadays. Dozens of other polymers have been designed and synthesized demonstrating shape memory properties for different applications.

Shape memory effect has been reported in many types of polymers like thermosets [41-42], thermoplastics [43-44], elastomers [45-46], hydrogels [47-48] and liquid crystals [49-50]. Despite their unique properties, the potential applications of SMPs are often limited due to their low thermal conductivity, inertness to electrical stimulus, slow light and electromagnetic stimuli responsiveness and low recovery time during actuation [5].

To overcome these difficulties new generation of shape memory polymeric nanocomposites (SMCs) have been designed. Generally, they are produced by the incorporation of one or more nanofillers as, nanotubes [51], nanofibers [52-53], nanocrystals [54-55], etc., within the polymer matrix. The advantages of the incorporated nanoreinforcing agents are based on their high specific surface area, high stiffness and their inherent functionalities.

The SME in SMPs is based on a totally different mechanism compared to the other SMMs. In order to show SME, SMPs have to be composed by two basic phases/domains, one is the “fixing” domain, and the other is the transition or “switching” domain. While the fixing domain always maintains its shape within the whole SME cycle, the switching domain changes its stiffness significantly at the presence of the right stimulus. This property is not intrinsic to the material. A combination of a determined polymer molecular structure, morphology, and a specific tailored processing known as a “programming” and “recovery” processes is needed in order to obtain SME [18]. First, the material is formed into its initial permanent shape by conventional processing methods, such as solvent casting, extrusion or injection molding. In the “programming” process, with the application of an external stimulus, the material is deformed and fixed in a “temporary shape.” Afterwards, upon the application of the external stimulus, the material recovers its initial permanent shape, during the “recovery” process [56].

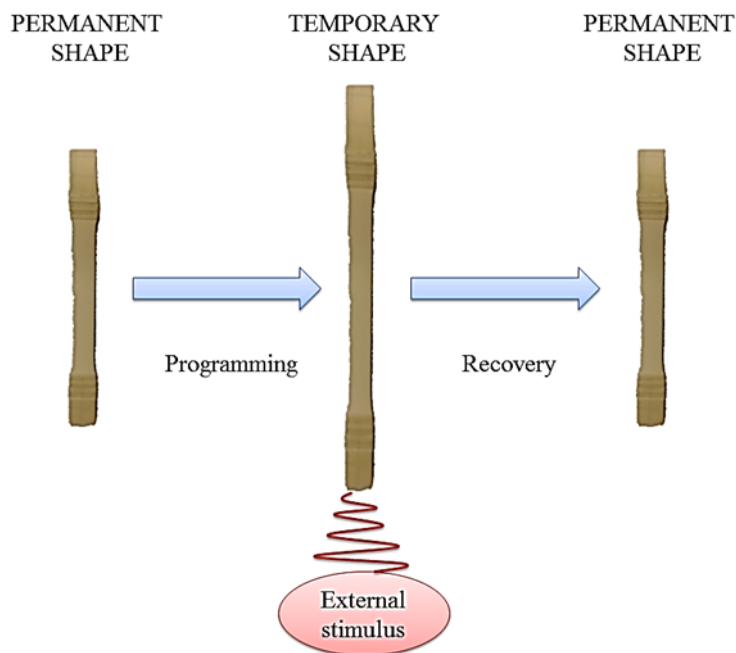


Figure 2. Schematic representation of the shape-memory effect (SME).

Programming-recovery cycles have to be repeated several times. Moreover, depending on the structure of the polymer, it is possible to fix two or more temporary shapes in each cycle [57]. SME can be utilized on surfaces (i.e., polymer coating) [58] in order to tune the surface properties by changing the shape of the polymer surface. Furthermore, bulk materials are of great interest where the polymeric material is able to change its overall shape. The properties of shape memory polymers render them attractive for a variety of application in both technical industries (i.e., aeronautics, electronics, textile and packaging) and biomedical applications (i.e., stents, scaffold, etc.).

Design of Shape Memory Polymers and Classification

As mentioned in the previous paragraph, SMPs are generally composed by structural pre-requisites: one consisting of netpoints that define a stable “network” structure or stable domain and the other one is named as switching domain, which can be influenced and change its properties by means of the external trigger and can enable fixation of the temporary shape. The first domain stabilizes the whole SMP and is responsible to retain the original shape. Indeed, the deformation of this phase is the driving force for the shape recovery. In fact, in the permanent shape, the molecular chains within the SMP are at the

lowest energy (highest entropy) state. As long as this is stable, any macroscopic deformation imposed on the permanent shape would change the conformation of the polymeric chains raising the energy state of the material. At this point, thanks to the influence of the external trigger, a depression of the molecular mobility can be induced and it serves to maintain the system in high energy state. Once it is removed out by reactivating the chain mobility, with the external trigger (i.e., by heating), the entropic energy is released, driving the molecular chains back to their lowest energy state. Therefore, the materials recover their original shape [59]. In SMPs, this stable domain (network) can be achieved by the introduction of either chemical covalent bonds or physical interactions, i.e., crystallites, glassy hard domains, hydrogen bonding, ionic clusters, chain entanglements and interpenetrating networks [18, 60-61]. The netpoints can be sufficiently stable to withstand the mechanical conditions encountered in the shape memory cycles without plastic deformation; otherwise, the permanent shape would not fully recover. The second phase fixes the temporary shape by crystallization (i.e., a melting transition will lead to the shape recovery), glass transition, a transition between different liquid crystalline phases, reversible covalent or non-covalent bonds (i.e., photodimerization of coumarine [63], Diels–Alder reactions [63], supramolecular interactions [64] and dipolar interaction [65]). Furthermore, SMPs can be designed as “multimaterial” systems such as multi-block copolymer as well as covalent polymer networks can be used as components forming “multimaterial” with shape memory properties. The preparation of binary blends from two polymers by a physical process is also an efficient method for the creation of “multimaterial” systems, in which the properties of the resulting binary polymer blends can be systematically varied.

Often one of the blend component is a polymer able to provide the flexible SMP matrix. The second blend component is used for the modification of the properties of one or both domains.

The covalent polymer network approach to create “multimaterials” is applied in interpenetrating polymer networks (IPN). Here, both polymer networks are not covalently linked to each other [60]. IPN can be obtained by two crosslinking processes occurring sequentially or both at the same time by using two different, not interfering chemical reactions forming the two different networks. Each polymer network provides permanent net-points contributing to the permanent shape [66].

In literature, SMPs have been classified in several ways, for example, through the nature of the fixed or fixity bonds, the nature of the stimulus, which allows the shape memory properties, the transition able to activate the recovery process. In the next paragraphs, SMPs will be classified depending on the nature of the stimulus, which allows the shape memory properties: temperature, solvent/water and humidity, light and other stimuli (electric and magnetic field, etc.).

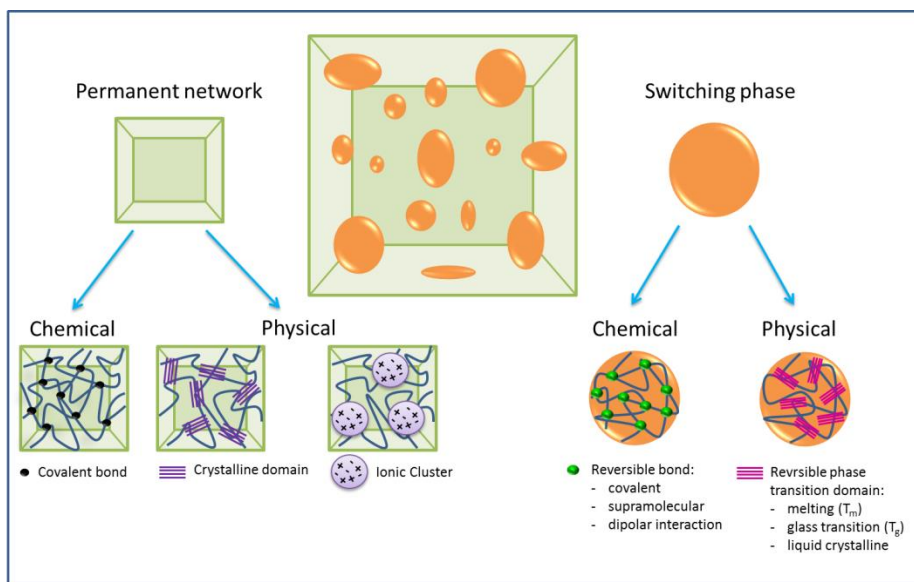


Figure 3. Schematic representation of different permanent networks and switching phases that can constitute shape memory polymers.

Temperature Responsiveness

The shape memory behavior of thermally-activated SMPs is generally triggered by heating the specimen above a specific transition temperature (T_{trans}) belonging to the switching domain. The most important transitions, which are used for thermally-activating SMPs are the melting/crystallization transition ($T_{\text{trans}} = T_m$) and the glass/rubber transition ($T_{\text{trans}} = T_g$) [4]. The T_m can be utilized in chemically crosslinked rubbers, in semicrystalline polymeric networks as well as in physically crosslinked polymers (i.e., copolymers with a low melting temperature phase, which is responsible for the switching, and a high melting temperature phase, which constitutes the permanent network) [67]. Indeed, one possibility for the shape fixation is the crystallization of the switching domain. The melting of this phase will lead to the shape recovery of the SMP. Most of these SMPs are based on polyolefins (including ethylene copolymers i.e., ethylene vinyl acetate), polyethers, or polyesters (in particular polycaprolactone, PCL).

Hereby two different mechanisms related with T_m have been developed: The first concept is based on the strain induced-crystallization. In particular, the strain induced-crystals act as thermo-responsive switching domain responsible for fixing the temporary shape. The other strategy is based on the melting of the crystalline switching domain of a two-component system such as blends [43], block copolymers [68] as well as polyurethanes [69]. Polyethers are a polymer class, which feature typically low melting temperatures, which makes them promising materials for the switching domain on SMPs. For instance, polyethylene oxide was utilized as soft block (switching domain) in

segmented multiblock copolymers with poly(ethylene terephthalate) hard block (stable domain) [70]. In segmented materials, an increase of the soft block content, resulted in higher T_{trans} due to the better crystallization of the soft block. Low melting aliphatic polyesters are probably the most often utilized soft block (in particular PCL). These soft blocks have also been applied in polyurethane systems [69]. Lower molar masses of the polyester results in lower T_{trans} , so that temperature (40°C) in the region of the human body temperature could be achieved [54]. Additionally, polymer blends containing PCL have been previously reported in the context of SMPs. The biodegradability of the soft PCL blocks opens the possibility to design SMPs for biological applications [71].

In a similar way, the T_g can be utilized in chemically crosslinked thermosets as well as physically crosslinked thermoplastics. Polymeric materials with a T_g above room temperature can be utilized. Within this context, large varieties of different materials have been investigated. In comparison to the SMPs based on T_m , in general, when T_g is used as T_{trans} , a slower shape recovery is shown due to the broad glass transitions (representing a second order phase transition). Consequently, these SMPs are not ideal for applications where a sudden shape recovery is required. On the other hand, the slow recovery makes them interesting candidates for certain biomedical applications [72]. Different studies show that it is possible to reduce the broadness of T_g . For example, epoxy resins, as a classical thermoset, were also utilized as SMPs based on T_g [73]. Rousseau et al. [74] reported that, the T_g could be tuned out by the thermoset composition between 31°C and 93°C and that a higher crosslinking density resulted in a faster shape recovery of these materials. Polyurethanes (PUs) containing a switching domain with a glass transition instead of a semicrystalline switching domain can also feature SME, as previously reported in literature. In contrast to the shape memory PUs based on T_m , these systems are transparent and are more prone to biodegradation due to the absent crystallinity of the switching domain [75]. Classical thermoplastic elastomers like PUs or EVA feature an excellent processability. However, the lack of chemical crosslinks lead to inferior properties compared with covalently crosslinked polymer. Indeed, latter materials show higher recovery stresses and higher cyclic recoverable strains [76]. Most methacrylate-based covalently crosslinked shape memory polymers are based on the T_g of the soft domain [77]. These materials are also interesting for bio-applications due to their biocompatibility and biodegradability [78].

Another biocompatible and biodegradable polymer that show shape memory effect based on its T_g is the polylactic acid (PLA), but its intrinsic brittleness limited the shape-memory effect for wide application. Zhang et al. [79] found that melt-blending PLA with biodegradable polyamide elastomer (PAE) can change the mechanical properties of PLA. With the PAE contents increasing, the elongation at break of blends increased and the brittle behavior of PLA changed as a ductile behavior. PAE domains act as stress concentrators in system with the stress release locally and lead to energy-dissipation process. They will prevent breaking of PLA matrix under high deformation, and lead to

PLA molecular orientation. When the temperature is above to the T_g of PLA, at about 60°C, the shape memory behavior can be activated [79].

Regarding high temperature SMPs for new applications, the engineering polymer polyetheretherketone (PEEK) can be modified to reveal shape memory properties as well. Indeed, it was revealed that it was practically feasible to program PEEK at room temperature and to lower the recovery temperature from its melting temperature range to around its T_g only by varying the programming temperature [80]. However, the strains that can be achieved with PEEK are rather small (30%), and the shape memory behavior is relatively poor due to creep issues. In contrast, dual and triple shape memory polymers can be prepared from sulfonated PEEK ionomers and a high temperature fatty acid salt, in particular sodium oleate (NaOl) [81]. Therefore, metal salts of sulfonated PEEK exhibited triple shape memory behavior, where two temporary networks are shown: one from the glassy state of the ionomer and the other from the NaOl crystals. While the ionic nano-domains due to the ionic or dipolar interactions between metal sulfonate groups provide the permanent network [81].

The switching phase, able to fix the temporary shape, can also be based on thermo-reversible bonds. An example of covalent thermo-reversible covalent bond is the Diels-Alder reaction and its corresponding retro-Diels-Alder reaction. Raquez et al. [63] synthesized cross-linked semicrystalline PCL-based polyesterurethane systems by thermo-reversible Diels–Alder reactions, and they showed that this system exhibits one-way and two-way shape-memory properties.

Instead of thermo-reversible covalent bonds, supramolecular interaction can be also utilized for the design of a reversible network. For this purpose, several possibilities exist: hydrogen bonds, ionic interactions or metal ligand interactions. Briefly, the design of shape memory polymers based on hydrogen bonds mostly depend on two binding motifs: the pyridine moiety [82] and the ureidopyrimidine unit [83]. The pyridine moiety can form inter- or intramolecular hydrogen bonds to the urethane group [84]. These interactions can be reversibly broken and, thus, they can interact as the temporary network. In order to increase the strength of the hydrogen interaction, the ureidopyrimidine unit can be installed within the polymeric structures. Due to the quadruple-hydrogen-bonded dimer a strong interaction could be achieved [85]. Regarding the other thermo-reversible supramolecular interactions, ionomers represent another approach. These unique materials exhibit physical and mechanical properties that are profoundly different from their non-ionic analogs. The most common strategies to obtain ionomers are the neutralization of sulfonated polymers with zinc salt [87-88] and the integration of the ionic group by carboxylic acid [86]. This behavior is attributed to the strong interactions that they are able to form because of coulombic difference in potential between ionic charges. While the morphology of ionomers is not fully understood, it is generally accepted that ionic groups coordinate with counter ions to further self-assemble into phase separated nano-domains (ionic clusters) thus forming a reversible ionic

network [86]. The inter-chain interaction formed the permanent network, whereas the dipolar interactions between the dispersed phase of crystalline salt and the ionomer itself resulted in the temporary network. In addition, metal-ligand interactions provide a thermo-reversibility that can be used for the design of shape-memory polymers [89]. Thanks to the development of reversible covalent and non-covalent chemistry, opportunities for designing switching domains or segments at the molecular level have emerged. While phase transitions are largely related to a thermal effect, molecular switches bring more options in terms of triggering mechanisms.

Moreover, it is also important to emphasize that for certain application direct heating methods are not applicable and a solution can be found using indirect trigger methods. Therefore, electrical, magnetic, optical, acoustic and chemical energies can all be converted into thermal energy and cause heating within the materials. Normally, it is necessary to incorporate functional fillers into a SMP matrix in order to achieve the energy transformation, i.e., carbon fiber, carbon nanotubes, carbon nanofibers, metal powder, etc. [59]. In the next sections, non-thermal triggers are briefly described.

Solvent/Water/Humidity Responsiveness

Only few SMPs responsive to solvent/water/humidity (also called chemo-responsive) have been reported in the literature. The programming procedure for the water-responsive SME is basically the same as that in the thermo-responsive SME. However, instead of heating to above the T_{trans} to activate the SME, the approach applied to trigger the water-responsive SME is to soften/dissolve the switching domain or, the transition temperature of the switching domain can be lowered below room temperature [19, 90]. Indeed, solvent molecules can have a plasticizing effect on polymeric materials, and they can then increase the flexibility and the macromolecule chains mobility of SMPs [91]. On the other hand, it is possible to design a special dual-component material, which has a switching component that can be softened by a particular chemical agent under its working environment. Instead of softening, in dual-component materials, shape recovery may be induced by removing (dissolving/swelling) the switching component, so that the elastic component can freely release the elastic energy stored during the programming [19].

Regarding humidity/water responsiveness, in literature are reported different strategies in order to obtain humidity/water-activated SME. One strategy is the plasticizing effect of water of the polymer matrixes. In fact, water molecules, which diffuse into the polymeric sample, disrupt the intramolecular hydrogen bonds and then mobilize the previously vitrified chains, thereby shifting the T_g to lower temperatures and allow for room temperature actuation [92]. Yang et al. [93] reported that water-absorbed in shape memory polyurethanes can be split into two parts, namely, free water and bound

water. They showed that free water absorbed into the polyurethanes has negligible effects on the T_g and the uniaxial tensile behavior, while bound water significantly reduces the T_g in an almost linear way and it has significant influence on the uniaxial tensile behavior [93]. The shape memory effect associated with the lowering of transition temperature has also been shown for polyurethanes composites reinforced with carbon nanotubes [94]. In all cases, the shape memory effect was reported to be slow, with recovery taking at least 140 min. Furthermore, in these cases, strain recovery is limited to water and it could not be triggered by only moisture due to their very low moisture absorption. Chen et al. [95] synthesized novel moisture-sensitive shape memory polyurethane based on pyridine derivative. They showed that the mechanism of moisture-sensitive SME is based on the dissociation or disruption of hydrogen bonding in the pyridine ring, induced by moisture absorption.

A different strategy for humidity/water-induced shape memory effect can be realized by incorporating a hydrophilic or water swellable component into the structure [96]. In this way, the shape recovery can be greatly accelerated [97-98]. Mei-Chin Chen et al. [99] developed a biodegradable water-activated stent, made of chitosan films cross-linked with an epoxy compound with shape-memory properties. The raw materials used in the fabrication of the developed stent are relatively hydrophilic and a subsequent immersion in water led to rapid hydration and recovery in a short period of 150 s. The hydrophilic component could be a polymeric component belonging a copolymer or a blend as well as hydrophilic filler, organic as much as inorganic [100-102]. Wu et al. [103] developed an enzymatically degradable nanocomposites with water-activated SME by using hydrophilic cellulose nanocrystals (CNCs) and hydrophobic poly(glycerol sebacate urethane). The presence of CNCs improved the mechanical properties and thanks to the water absorption/desorption, the elastic modulus of the material can be reversible changed. This is because CNCs are hydrophilic and absorb a higher amount of water, increasing the water content in the polymeric matrix. Thus, the incorporation of CNCs into the polymeric matrix, triggers the water-activated SME in the corresponding nanocomposite. Wu et al. [104] successfully synthesized composites with excellent water-activated SMEs by using clay as switching component and thermoplastic polyurethane (TPU) as the matrix.

Light and Others Stimuli

Another stimulus that can be used as trigger, in order to activate SME, is the light. Light can be used as a precise stimulus by selecting suitable wavelengths, polarization directions, and intensity, allowing non-contact remote. A wide range of polymeric materials have been found to change different properties in response to light [62, 105]. From the view point of the mechanism of light-activated SME, light-responsive SMPs

can be divided into two categories. The first approach, also the most obvious way, is to heat above the T_{trans} via photo-thermal effect. In this case, generally, light is used only for the shape recovery process but is not involved in the processing of fixing the temporary shape. In order to achieve effective heating when exposed to light, the SMPs should contain some kind of additive or filler that is not only a strong light absorber but also presents high efficiency to convert optical energy to heat through non-radiative energy decay of excited electrons. The nanofillers could be organic dyes, ligands, gold nanoparticles, gold nanorods, carbon nanotubes and graphene for example [106-111]. This kind of light-activated SME is essentially a thermally-activated mechanism because the thermal effect is still involved to activate the shape-memory behavior. Photothermal SMPs have the advantages of fast response (from a few seconds to a few minutes) and good shape memory properties, just as those thermally-activated. The second approach has a different mechanism based on the use of a reversible photochemical reaction without any other energy conversion. Actually, the most extensively studied photo-responsive polymers in the literature include light responsive moieties based on azobenzenes, spiropyrans and spirooxazines and groups undergoing [2 + 2] cycloaddition upon light irradiation such as cinnamic esters, coumarin and diarylethenes [112-123]. In the case of photo-crosslinking reaction, light takes action in both processes of temporary shape fixity and permanent shape recovery. After deforming the polymer to a temporary shape, light at a certain wavelength is applied to induce the photo-crosslinking of the SMP. Therefore, this photo-induced network structure formed with polymer chains in a deformed state is able to retain a certain degree of deformation after removal of the external trigger. For the recovery of the permanent shape, light at a different wavelength is used to de-crosslinking the polymeric network [62, 124]. Other stimuli can be used in order to activate SME such as electric and magnetic fields, pH, etc.

Electro-activated SMPs are materials that respond to an applied electric field by changing their size or shape. They have attracted rapidly expanding scientific and technological interest, due to their potential applications in sensors and actuators, robotics and artificial muscles, optical systems, drug delivery, space, ocean and energy storage applications [125]. Electro-activated SMPs are divided into two types: ionic type [125] and dielectric type [126]. In the first type the electro-responsiveness is a result of an electric field driven mobility of free ions to create a change in the local concentration of the ions within the material. The ionic type includes the conducting polymers [127], the ionic polymers [128], and polymer gels [129], as well as the so-called ionic polymer-metal composites [130]. They require low actuation voltages but suffer low deformations and response rates, while they also normally operate under wet conditions. Dielectric type materials, whose deformation is induced by electrostatic forces developed between two electrodes, comprise the dielectric elastomers [131] and the electrostrictive polymers [132]. They exhibit fast response and high deformations and they operate under dry conditions, but they require high activation electric fields [91, 113].

Magnetic-activated SMPs show magnetic-activated SME with the change in an applied magnetic field [133]. They are composites of elastomers (magnetically active elastomers) or gels (magnetically active polymeric gels) filled with small magnetic particles [134]. They are also called magnetoelastic or magnetostrictive polymeric composites. Magnetic-active elastomers are composites of high elastic polymeric elastomers filled with small nano- or micro-sized magnetic particles [135]. When a magnetic field is applied to the composite, all forces acting on the magnetic particles are transmitted to the elastomeric matrix resulting in the shape change of the sample [91]. Magnetic-active polymeric gels, also called as ferrogels, are super-paramagnetic particles filled swollen networks [136-137]. The finely distributed ferromagnetic particles are attached to the flexible network by adhesive forces, resulting in direct coupling between magnetic and mechanical properties of the magnetic-active polymeric gel [91-113].

pH-responsive polymeric systems provide the possibility to fabricate tailorable “smart” functional materials; hence they have found many potential commercial applications, such as in controlled drug delivery, personal care, industrial coatings, etc [138]. pH-responsive polymeric systems are polymers whose solubility, volume, configuration and conformation can be reversibly manipulated by changes in external pH. Indeed, a polymer is considered as pH-responsive when it features moieties that are capable of donating or accepting protons upon an environmental change in pH [139].

Ultrasound is the high-frequency waves created by mechanical oscillations of a piezoelectric material when an alternating current is applied. Ultrasounds can provoke shape changes in polymeric materials due to the unique heating mechanism based on polymer chain shearing and friction activated by ultrasonic energy [113]. Ultrasound is used in many different fields including ultrasonic devices for object detection and distance measurements, for imaging in medicine and for cleaning, mixing and accelerating chemical processes in industry [140-141].

SHAPE MEMORY EFFECT CHARACTERIZATION

During the last years, various methods for the characterization of SME have been used. In this context, a wide variety of different procedures such as the determination of the polymer’s shrinkage, the application of simple bending tests, compression tests (i.e., in case of SMP foams), three-point flexural tests, application oriented tests (e.g., for SMP textiles or medical devices), cyclic and thermo-mechanical as well as photo-mechanical or magneto-mechanical tensile tests have been reported in the literature for quantification of the shape-memory properties on the macroscopic level [142]. Furthermore, several test methods focusing on the examination of the SME on the micro- and nano-scale have been described [143-144]. Two key values for quantification of SME in polymers have been introduced describing the ability of fixing the temporary shape, called strain fixity ratio

(R_f), and the ability of recovering the original shape, called strain recovery ratio (R_r). In the next paragraph, a brief overview about the main cyclic thermo-mechanical tests for macroscopic quantification of SME is given as example.

Thermo-Mechanical Cycle Experiments

One of the most powerful test methods for quantification of the SME of SMPs are the thermo-mechanical cycle experiments [145]. These can be defined as continuous and repeatable testing protocol for studying the SME of polymers. Besides thermo-mechanical cycles allow accurate simultaneous control of physical parameters such as strain, stress and temperature, during programming and recovery, in contrast to other testing methods. Such experiments are typically performed with a conventional tensile machine equipped with a thermo-chamber enabling an accurate temperature control during mechanical deformation of the specimen (programming) and recovery [18, 54]. Alternatively, dynamic mechanical thermal analyzer (DMTA) can be applied, which allow conducting experiments in tensile and bending mode [44, 146]. It is possible to divide thermo-mechanical cycle experiments in different methods according to the geometry of the test setup as reported bellow.

Cyclic Thermo-mechanical Tensile Tests follow tailored test procedures. These test procedures consist to a programming step, where the temporary shape is fixed, and a recovery step where the permanent shape is recovered. The programming step can be performed under stress-controlled or strain-controlled conditions and the recovery step can be carried out under stress-free conditions or under constant strain. Several thermo-mechanical testing parameters influence the shape-memory properties, such as the applied strain, the strain rate, cooling and heating rates, number of operates cycles (N) as well as the applied temperatures, to stretch or deform the sample (T_d), to fix the temporary shape (T_{fix}), and to recover the original shape, the switching temperature (T_{sw}). The programming procedure can be performed based on different test protocols, such as cold drawing process ($T_d < T_{sw}$) or a heating-stretching-cooling process ($T_d = T_{sw}$). In general, the programming step is composed by three steps, (1) heating of the sample to the T_d and deforming of the specimen with a defined strain rate; (2) cooling to T_{fix} with a certain cooling rate, while the elongation is kept constant for the fixation of the temporary shape; (3) unloading the applied stress at T_{fix} resulting in the fixed temporary shape. After the temporary shape is fixed the recovery process can be initialized in step (4) consisting on heating from T_{fix} to T_{sw} with a constant heating rate, allowing the recovery of the original shape when performed under stress-free conditions.

Bending test. There are two types of tests that are based on bending the polymeric samples in order to characterize the SME. One is called “simple bending test” and the other one is the so-called “three-point flexural test.” Bending tests are preferred in brittle

materials, since the interpretation of the tensile test result is difficult due to breaking of the sample near the clamps. Additionally, large deflections can be achieved at modest strain levels. Another aspect to be mentioned is that several applications require information obtained by the bending rather than the tensile properties of the samples [142]. In a bending test the sample is bent to a certain angle at T_d and it is kept in this shape. The deformed sample is cooled to a lower temperature, T_{fix} , and the remaining stress is released. In the last step, the sample is heated up to the T_{sw} and the recovery of the permanent shape is recorded in terms of a series of deformation angles depending on T [147-148].

The three-point flexural tests is able to provide values for the elastic modulus in bending, flexural stress, flexural strain, and the flexural stress–strain response of the tested material, *i.e.*, the determination of strain recovery and stress recovery ratio [146, 149-150]. Compared to uniaxial cyclic tensile tests the main advantage of simple bending tests and three-point flexural tests are the rather simple specimen preparation and testing. The maximal deformation in three-point flexural tests is significantly lower than in tensile tests. While in tensile tests it is possible to reach values up to about 200% of deformation (depending on the instrument used), in three-point flexural tests, the maximal deformation is only about 20–30%. In tension or compression, thermal stresses arise from constrained thermal expansion or contraction, leading to difficulties in separating the various mechanisms during deformation. Upon cooling, after tensile deformation, the applied stress can increase at a fixed strain, while in the flexural deformation the thermal contraction is not as severely constrained [18, 147].

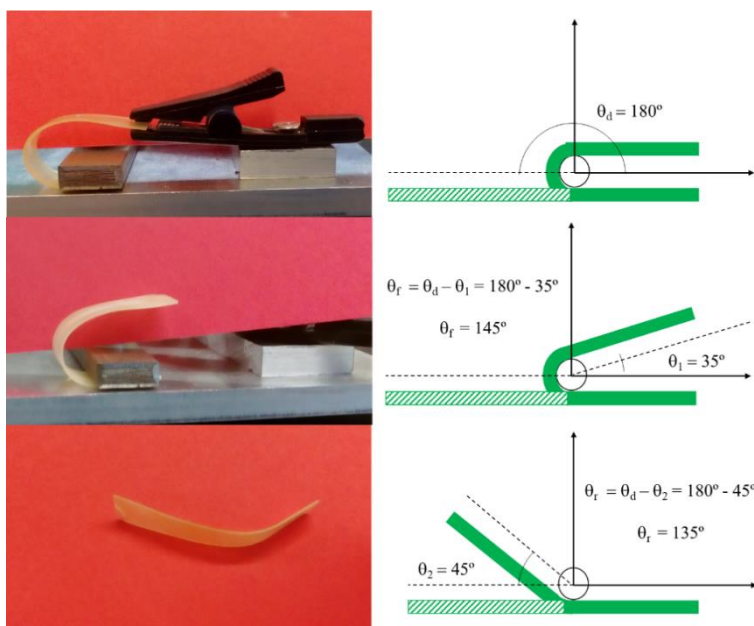


Figure 4. Schematic representation of simple bending test.

Cyclic Thermo-mechanical Compression Tests. A compressive stress reduces the length of the sample by the uniaxial application of two plates on the sample. Various sample geometries with two opposite planar surfaces can be tested in a compression test. Cyclic thermo-mechanical compression tests have been mainly applied for porous test specimens [142]. Indeed, such foams can be subjected to large compressive strains, above 90% depending on the foam morphology and density considering that many applications of foams involve compression. In a standard compression test of foams, bending of the pores occurs during the elastic regime, which can be followed by buckling, as represented by a stress plateau at increasing strains [151]. In such a cyclic thermo-mechanical test, the foam is inserted in the temperature controlled testing machine and subsequently increasing the temperature to T_d in order to perform compression of the foam at the programmed strain rate. Next, the foam is cooled maintaining the compressive stress until T_{fix} . The compressive stress is then unloaded to obtain the temporary shape of the sample. While cooling, thermal contraction occurs, leading to an additional compression of the SMP foams. Consequently, the sample would lose contact to the compression plates, if cooled under constant strain conditions below T_{trans} . By heating the foam under stress-free conditions the recovery strain is obtained, while the evolution of the recovery stress can be observed by heating under constant strain conditions [152-153]. The parameters R_f and R_r are calculated in the identical manner as for cyclic thermo-mechanical tensile tests [142].

SHAPE MEMORY POLYMERS APPLICATIONS

The interesting properties of SMPs make them good candidates for many applications, from industrial to biomedical application, self-healing materials using the SME as well as application in aerospace field [81, 124, 154]. SMPs have been applied in commercial products as early as the 1960s in the form of heat-shrinkable polyethylene tubes used as wire wraps for the purpose of electrical insulation [155-156]. Over the past three decades, reports of SMPs activated by different stimuli and exhibiting a variety of features have been increasingly published. In many applications, SMPs have some limitations compared to metallic materials, especially due to the low mechanical properties of polymers. In order to improve the mechanical properties as well as to obtain smart multifunctional materials, many researchers reported new shape memory nanocomposites filled with different types of reinforcement [157].

Many applications of SMCs in aerospace field have been reported in the literature [4]. In this area, SMPs have one decisive advantage, i.e., their lightweight. The lightweight of the applied materials is one of the most crucial issues in the design of new systems in aerospace. SMPs are of great interest for low-cost self-deployable structure [157-158], i.e., solar arrays, solar sails, sunshields, or radar and reflector antennas [124,

159-161]. Beyond this sector many other potential applications in different areas are reported in the literature, but in this chapter, we will focus more on the potential applications in the biomedical field, whereby there have been many advances in recent years [56, 162].

Shape memory polymers have tremendous applications in biology and biomedicine. For this application field, several requirements must be fulfilled and a range of problems must be overcome [163]. As a matter of fact, these requirements for biomedical applications are related to the biocompatibility and non-toxicity [164], biodegradability [165], sterilizability [166], specific mechanical properties [167], and a trigger adapted to the human body [56, 163, 168]. As explained in the previous paragraphs, thermally-activated SMPs must be heated above their characteristic T_{trans} to induce their shape change. For SMPs with T_{trans} close to body temperature, actuation can be accomplished by simply placing the SMP into the body. However, if the T_{trans} required is higher than the body temperature, addition of fillers to the SMPs has enabled several heating schemes using external energy sources to selectively heat the SMPs into the body [133]. Small et al. demonstrated photothermal actuation using IR laser light [169]. Moisture-activation of SMPs has been demonstrated by Chen et al. [95], in which the solvent depresses the glass transition temperature of the material via plasticization. Therefore, actuation can be achieved at the body temperature. This technique is feasible for deployment of SMP medical devices in body fluids. One of the most important design considerations of any material for potential biomedical applications is biocompatibility, which is the ability of the material to perform *in vivo* with an appropriate host response [56]. Preliminary biocompatibility results of polymeric materials for biomedical applications were widely reported in the literature [170]. For example, the first commercially available SMPs from Mitsubishi Heavy Industries, Ltd. (Nagoya, Japan), which are now distributed through a subsidiary (DiAPLEX, Ltd.), are polyurethane-type SMPs [171-173]. Other published biomedical academic studies on SMPs include PCL, PLA-polyurethanes, PEO based shape memory polymers that were found to be non-toxic [166, 174-175]. If these basic requirements are fulfilled, shape memory polymers can be applied in several biomedical applications such as SMP-based medical devices [175-177] (SMP-based stents, clot removal devices, aneurysm occlusion devices, etc.), SMP-based drug delivery devices [178-180] and SMP-based biomaterials for tissue engineering [181-183] (i.e., scaffold for vascular tissue, for bone tissue, etc.) [162]. The first example of fully biodegradable body thermo-responsive SMP stent were based on poly(L-lactic acid) (PLLA) and poly(glycolic acid) (PLGA) bilayers [184]. Beilvert et al. reported in a recent study that natural starch, without chemical grafting, can now be considered for manufacturing innovative biodegradable devices for less-invasive surgery.

CONCLUSION

In this chapter, a comprehensive overview of recent developments and progress in shape memory materials has been presented. In particular, shape memory polymers and nanocomposites are one of the most important class of multi-responsive smart materials providing excellent and new opportunities for scientific developments in the field of polymer synthesis and functionalization, molecular architecture design, processing of polymer blends and interpenetrating networks as well as of multifunctional materials. Indeed, within the last few years, tremendous efforts were devoted to the area of stimuli-responsive materials, driven by the need for precisely controllable material properties. Due to the high degree of control, external stimuli as triggers that induce changes of the physical properties of polymeric materials proved to be a very promising approach. The interesting properties of SMPs make them good candidates for many applications, from industrial to biomedical application, as self-healing materials with SME as well as application in aerospace field.

ACKNOWLEDGMENTS

Authors thank Spanish Ministry of Economy, Industry and Competitiveness, MINEICO, (MAT2017- 88123-P) for the economic support cofinanced with FEDER funds and the Regional Government of Madrid MULTIMAT Challenge: S2013/MIT-2862. L.P. acknowledges MINEICO for the “Ramon y Cajal” (RYC-2014-15595) contract. Authors thanks also CSIC for the I-LINK project, I-LINK1149. Jean Marie Raquez is FNRS researcher associate.

REFERENCES

- [1] Kempaiah, R.; Nie, Z., From nature to synthetic systems: shape transformation in soft materials. *Journal of Materials Chemistry B* 2014, 2 (17), 2357-2368.
- [2] Bellamkonda, R. V., Biomimetic materials: Marine inspiration. *Nat Mater* 2008, 7 (5), 347-348.
- [3] Gracias, D. H., Stimuli responsive self-folding using thin polymer films. *Current Opinion in Chemical Engineering* 2013, 2 (1), 112-119.
- [4] Hager, M. D.; Bode, S.; Weber, C.; Schubert, U. S., Shape memory polymers: Past, present and future developments. *Progress in polymer science* 2015, 49, 3-33.

- [5] Pilate, F.; Toncheva, A.; Dubois, P.; Raquez, J. M., Shape-memory polymers for multiple applications in the materials world. *European Polymer Journal* 2016, *80*, 268-294.
- [6] Huang, W.; Ding, Z.; Wang, C.; Wei, J.; Zhao, Y.; Purnawali, H., Shape memory materials. *Materials Today* 2010, *13* (7), 54-61.
- [7] Perkins, J., *Shape memory effects in alloys*. Springer Science & Business Media: 2012.
- [8] Ferguson, J.; Schultz, B.; Rohatgi, P., Zinc alloy ZA-8/shape memory alloy self-healing metal matrix composite. *Materials Science and Engineering: A* 2015, *620*, 85-88.
- [9] Shahverdi, M.; Czaderski, C.; Motavalli, M., Iron-based shape memory alloys for prestressed near-surface mounted strengthening of reinforced concrete beams. *Construction and Building Materials* 2016, *112*, 28-38.
- [10] Lai, A.; Du, Z.; Gan, C. L.; Schuh, C. A., Shape memory and superelastic ceramics at small scales. *Science* 2013, *341* (6153), 1505-1508.
- [11] Zeng, X. M.; Lai, A.; Gan, C. L.; Schuh, C. A., Crystal orientation dependence of the stress-induced martensitic transformation in zirconia-based shape memory ceramics. *Acta Materialia* 2016, *116*, 124-135.
- [12] Uchino, K., Shape memory ceramics. *Shape Memory Materials* 1998, 184-202.
- [13] Wei, Z.; Sandström, R.; Miyazaki, S., Shape-memory materials and hybrid composites for smart systems: Part I Shape-memory materials. *Journal of Materials Science* 1998, *33* (15), 3743-3762.
- [14] Fan, K.; Huang, W.; Wang, C.; Ding, Z.; Zhao, Y.; Purnawali, H.; Liew, K.; Zheng, L., Water-responsive shape memory hybrid: Design concept and demonstration. *eXPRESS Polym. Lett* 2011, *5*, 409-416.
- [15] Gong, J. P., Why are double network hydrogels so tough? *Soft Matter* 2010, *6* (12), 2583-2590.
- [16] Miyamae, K.; Nakahata, M.; Takashima, Y.; Harada, A., Self-Healing, Expansion–Contraction, and Shape-Memory Properties of a Preorganized Supramolecular Hydrogel through Host–Guest Interactions. *Angewandte Chemie International Edition* 2015, *54* (31), 8984-8987.
- [17] Peponi, L.; Navarro-Baena, I.; Kenny, J. M., Smart Polymers and their Applications. In *Smart Polymers and their Applications*, First Edition ed.; Aguilar, M. R.; Román, J. S., Eds. Woodhead Publishing: 2014, pp 204-236.
- [18] Lendlein, A.; Kelch, S., Shape-memory polymers. *Angewandte Chemie International Edition* 2002, *41* (12), 2034-2057.
- [19] Huang, W.; Zhao, Y.; Wang, C.; Ding, Z.; Purnawali, H.; Tang, C.; Zhang, J., Thermo/chemo-responsive shape memory effect in polymers: a sketch of working mechanisms, fundamentals and optimization. *Journal of Polymer Research* 2012, *19* (9), 1-34.

- [20] Ölander, A., An electrochemical investigation of solid cadmium-gold alloys. *Journal of the American Chemical Society* 1932, 54 (10), 3819-3833.
- [21] Buehler, W. J.; Gilfrich, J.; Wiley, R., Effect of low-temperature phase changes on the mechanical properties of alloys near composition TiNi. *Journal of applied physics* 1963, 34 (5), 1475-1477.
- [22] Kauffman, G. B.; Mayo, I., The story of nitinol: the serendipitous discovery of the memory metal and its applications. *The chemical educator* 1997, 2 (2), 1-21.
- [23] Jani, J. M.; Leary, M.; Subic, A.; Gibson, M. A., A review of shape memory alloy research, applications and opportunities. *Materials & Design* 2014, 56, 1078-1113.
- [24] Firstov, G.; Koval, Y.; Van Humbeeck, J.; Timoshevskii, A.; Kosorukova, T.; Verhovlyuk, P., Some Physical Principles of High Temperature Shape Memory Alloys Design. *Materials Science Foundations* 2015.
- [25] Vinokur, A. I.; Fredrickson, D. C., Toward Design Principles for Diffusionless Transformations: The Frustrated Formation of Co-Co Bonds in a Low-Temperature Polymorph of GdCoSi₂. *Inorganic chemistry* 2016.
- [26] Sun, L.; Huang, W. M.; Ding, Z.; Zhao, Y.; Wang, C. C.; Purnawali, H.; Tang, C., Stimulus-responsive shape memory materials: A review. *Materials & Design* 2012, 33, 577-640.
- [27] Huang, W.; Toh, W., Training two-way shape memory alloy by reheat treatment. *Journal of materials science letters* 2000, 19 (17), 1549-1550.
- [28] Cisse, C.; Zaki, W.; Zineb, T. B., A review of constitutive models and modeling techniques for shape memory alloys. *International Journal of Plasticity* 2016, 76, 244-284.
- [29] Ma, J.; Karaman, I.; Noebe, R. D., High temperature shape memory alloys. *International Materials Reviews* 2010, 55 (5), 257-315.
- [30] Savi, M. A.; Paiva, A.; de Araujo, C. J.; de Paula, A. S., Shape Memory Alloys. In *Dynamics of Smart Systems and Structures*, Springer: 2016, pp 155-188.
- [31] Simha, N., Twin and habit plane microstructures due to the tetragonal to monoclinic transformation of zirconia. *Journal of the Mechanics and Physics of Solids* 1997, 45 (2), 261-292.
- [32] Reyes-Morel, P. E.; Cherng, J. S.; Chen, I. W., Transformation Plasticity of CeO₂-Stabilized Tetragonal Zirconia Polycrystals: II, Pseudoelasticity and Shape Memory Effect. *Journal of the American Ceramic Society* 1988, 71 (8), 648-657.
- [33] Heuer, A. H.; Ruhle, M.; Marshall, D. B., On the thermoelastic martensitic transformation in tetragonal zirconia. *Journal of the American Ceramic Society* 1990, 73 (4), 1084-1093.
- [34] Swain, M., Shape memory behaviour in partially stabilized zirconia ceramics. *Nature* 1986, 322, 234-236.

- [35] Itoh, A.; Miwa, Y.; Iguchi, N., Shape memory phenomena of glass-ceramics and sintered ceramics. *Nippon Kinzoku Gakkaishi/Journal of the Japan Institute of Metals* 1990, 54 (1), 117-124.
- [36] Schurch, K.; Ashbee, K., A near perfect shape-memory ceramic material. *Nature* 1977, 266, 706-707.
- [37] Haertling, G. H., Ferroelectric ceramics: history and technology. *Journal of the American Ceramic Society* 1999, 82 (4), 797-818.
- [38] Inoue, K.; Yamashiro, M.; Iji, M., Recyclable shape-memory polymer: Poly (lactic acid) crosslinked by a thermoreversible Diels–Alder reaction. *Journal of Applied Polymer Science* 2009, 112 (2), 876-885.
- [39] Vernon, L. B.; Vernon, H. M., *Process of manufacturing articles of thermoplastic synthetic resins*. Google Patents: 1941.
- [40] Rainer, W. C.; Redding, E. M.; Hitov, J. J.; Sloan, A. W.; Stewart, W. D., *Polyethylene product*. Google Patents: 1964.
- [41] Yao, Y.; Wang, J.; Lu, H.; Xu, B.; Fu, Y.; Liu, Y.; Leng, J., Thermosetting epoxy resin/thermoplastic system with combined shape memory and self-healing properties. *Smart Materials and Structures* 2015, 25 (1), 015021.
- [42] Zheng, N.; Fang, G.; Cao, Z.; Zhao, Q.; Xie, T., High strain epoxy shape memory polymer. *Polymer Chemistry* 2015, 6 (16), 3046-3053.
- [43] Navarro-Baena, I.; Sessini, V.; Dominici, F.; Torre, L.; Kenny, J. M.; Peponi, L., Design of biodegradable blends based on PLA and PCL: From morphological, thermal and mechanical studies to shape memory behavior. *Polymer Degradation and Stability*.
- [44] Samuel, C.; Barrau, S.; Lefebvre, J. M.; Raquez, J. M.; Dubois, P., Designing Multiple-Shape Memory Polymers with Miscible Polymer Blends: Evidence and Origins of a Triple-Shape Memory Effect for Miscible PLLA/PMMA Blends. *Macromolecules* 2014, 47 (19), 6791-6803.
- [45] Sessini, V.; Raquez, J. M.; Lo Re, G.; Mincheva, R.; Kenny, J. M.; Dubois, P.; Peponi, L., Multiresponsive Shape Memory Blends and Nanocomposites Based on Starch. *ACS Applied Materials and Interfaces* 2016, 8 (30), 19197-19201.
- [46] Feng, X. Q.; Zhang, G. Z.; Bai, Q. M.; Jiang, H. Y.; Xu, B.; Li, H. J., High Strength Self-Healing Magnetic Elastomers With Shape Memory Effect. *Macromolecular Materials and Engineering* 2016, 301 (2), 125-132.
- [47] Bilici, C.; Can, V.; Nöchel, U.; Behl, M.; Lendlein, A.; Okay, O., Melt-Processable Shape-Memory Hydrogels with Self-Healing Ability of High Mechanical Strength. *Macromolecules* 2016.
- [48] Zhang, Y.; Li, Y.; Liu, W., Dipole–Dipole and H-Bonding Interactions Significantly Enhance the Multifaceted Mechanical Properties of Thermoresponsive Shape Memory Hydrogels. *Advanced Functional Materials* 2015, 25 (3), 471-480.

- [49] Michal, B. T.; McKenzie, B. M.; Felder, S. E.; Rowan, S. J., Metallo-, thermo-, and photoresponsive shape memory and actuating liquid crystalline elastomers. *Macromolecules* 2015, 48 (10), 3239-3246.
- [50] Ware, T. H.; McConney, M. E.; Wie, J. J.; Tondiglia, V. P.; White, T. J., Voxellated liquid crystal elastomers. *Science* 2015, 347 (6225), 982-984.
- [51] Terenzi, A.; Natali, M.; Petrucci, R.; Rallini, M.; Peponi, L.; Beaumont, M.; Eletskii, A.; Knizhnik, A.; Potapkin, B.; Kenny, J., Analysis and simulation of the electrical properties of CNTs/epoxy nanocomposites for high performance composite matrices. *Polymer Composites* 2015.
- [52] Shirole, A.; Sapkota, J.; Foster, E. J.; Weder, C., Shape Memory Composites Based on Electrospun Poly (vinyl alcohol) Fibers and a Thermoplastic Polyether Block Amide Elastomer. *ACS applied materials & interfaces* 2016, 8 (10), 6701-6708.
- [53] Tan, L.; Gan, L.; Hu, J.; Zhu, Y.; Han, J., Functional shape memory composite nanofibers with graphene oxide filler. *Composites Part A: Applied Science and Manufacturing* 2015, 76, 115-123.
- [54] Navarro-Baena, I.; Kenny, J. M.; Peponi, L., Thermally-activated shape memory behaviour of bionanocomposites reinforced with cellulose nanocrystals. *Cellulose* 2014, 21 (6), 4231-4246.
- [55] Sonseca, Á.; Camarero-Espinosa, S.; Peponi, L.; Weder, C.; Foster, E. J.; Kenny, J. M.; Giménez, E., Mechanical and shape-memory properties of poly(mannitol sebacate)/cellulose nanocrystal nanocomposites. *Journal of Polymer Science, Part A: Polymer Chemistry* 2014, 52 (21), 3123-3133.
- [56] Chan, B. Q. Y.; Low, Z. W. K.; Heng, S. J. W.; Chan, S. Y.; Owh, C.; Loh, X. J., Recent Advances in Shape Memory Soft Materials for Biomedical Applications. *ACS applied materials & interfaces* 2016, 8 (16), 10070-10087.
- [57] Meng, H.; Li, G., A review of stimuli-responsive shape memory polymer composites. *Polymer* 2013, 54 (9), 2199-2221.
- [58] Wang, L.; Deng, L.; Zhang, D.; Qian, H.; Du, C.; Li, X.; Mol, J. M.; Terryn, H. A., Shape memory composite (SMC) self-healing coatings for corrosion protection. *Progress in Organic Coatings* 2016, 97, 261-268.
- [59] Zhao, Q.; Qi, H. J.; Xie, T., Recent progress in shape memory polymer: New behavior, enabling materials, and mechanistic understanding. *Progress in polymer science* 2015, 49, 79-120.
- [60] Behl, M.; Razaq, M. Y.; Lendlein, A., Multifunctional Shape-Memory Polymers. *Advanced Materials* 2010, 22 (31), 3388-3410.
- [61] Cavicchi, K. A.; Pantoja, M.; Cakmak, M., Shape memory ionomers. *Journal of Polymer Science Part B: Polymer Physics* 2016, 54 (14), 1389-1396.
- [62] Habault, D.; Zhang, H.; Zhao, Y., Light-triggered self-healing and shape-memory polymers. *Chemical Society Reviews* 2013, 42 (17), 7244-7256.

- [63] Raquez, J. M.; Vanderstappen, S.; Meyer, F.; Verge, P.; Alexandre, M.; Thomassin, J. M.; Jérôme, C.; Dubois, P., Design of Cross-Linked Semicrystalline Poly (ϵ -caprolactone)-Based Networks with One-Way and Two-Way Shape-Memory Properties through Diels–Alder Reactions. *Chemistry–A European Journal* 2011, 17 (36), 10135-10143.
- [64] Karger-Kocsis, J., Biodegradable polyester-based shape memory polymers: Concepts of (supra) molecular architecturing. *Express polymer letters* 2014, 8 (6), 397-412.
- [65] Dolog, R.; Weiss, R., Shape memory behavior of a polyethylene-based carboxylate ionomer. *Macromolecules* 2013, 46 (19), 7845-7852.
- [66] Liu, G.; Ding, X.; Cao, Y.; Zheng, Z.; Peng, Y., Novel Shape-Memory Polymer with Two Transition Temperatures. *Macromolecular Rapid Communications* 2005, 26 (8), 649-652.
- [67] Behl, M.; Lendlein, A., Shape-memory polymers. *Materials Today* 2007, 10 (4), 20-28.
- [68] Navarro-Baena, I.; Kenny, J. M.; Peponi, L., Crystallization and thermal characterization of biodegradable tri-block copolymers and poly(ester-urethane)s based on PCL and PLLA. *Polymer Degradation and Stability* 2014, 108, 140-150.
- [69] Peponi, L.; Navarro-Baena, I.; Sonseca, A.; Gimenez, E.; Marcos-Fernandez, A.; Kenny, J. M., Synthesis and characterization of PCL–PLLA polyurethane with shape memory behavior. *Eur. Polym. J.* 2013, 49 (4), 893-903.
- [70] Luo, X.; Zhang, X.; Wang, M.; Ma, D.; Xu, M.; Li, F., Thermally stimulated shape-memory behavior of ethylene oxide-ethylene terephthalate segmented copolymer. *Journal of Applied Polymer Science* 1997, 64 (12), 2433-2440.
- [71] Navarro-Baena, I.; Arrieta, M. P.; Sonseca, A.; Torre, L.; López, D.; Giménez, E.; Kenny, J. M.; Peponi, L., Biodegradable nanocomposites based on poly(ester-urethane) and nanosized hydroxyapatite: Plasticant and reinforcement effects. *Polymer Degradation and Stability* 2015, 121, 171-179.
- [72] Ratna, D.; Karger-Kocsis, J., Recent advances in shape memory polymers and composites: a review. *Journal of Materials Science* 2008, 43 (1), 254-269.
- [73] Kumar, K. S.; Biju, R.; Nair, C. R., Progress in shape memory epoxy resins. *Reactive and Functional Polymers* 2013, 73 (2), 421-430.
- [74] Rousseau, I. A.; Xie, T., Shape memory epoxy: composition, structure, properties and shape memory performances. *Journal of Materials Chemistry* 2010, 20 (17), 3431-3441.
- [75] Jeong, H. M.; Lee, S. Y.; Kim, B. K., Shape memory polyurethane containing amorphous reversible phase. *Journal of Materials Science* 2000, 35 (7), 1579-1583.
- [76] Xie, T., Recent advances in polymer shape memory. *Polymer* 2011, 52 (22), 4985-5000.

- [77] Safranski, D. L.; Gall, K., Effect of chemical structure and crosslinking density on the thermo-mechanical properties and toughness of (meth)acrylate shape memory polymer networks. *Polymer* 2008, *49* (20), 4446-4455.
- [78] Song, L.; Hu, W.; Wang, G.; Niu, G.; Zhang, H.; Cao, H.; Wang, K.; Yang, H.; Zhu, S., Tailored (Meth) Acrylate Shape-Memory Polymer Networks for Ophthalmic Applications. *Macromolecular bioscience* 2010, *10* (10), 1194-1202.
- [79] Zhang, W.; Chen, L.; Zhang, Y., Surprising shape-memory effect of polylactide resulted from toughening by polyamide elastomer. *Polymer* 2009, *50* (5), 1311-1315.
- [80] Wu, X. L.; Huang, W. M.; Ding, Z.; Tan, H. X.; Yang, W. G.; Sun, K. Y., Characterization of the thermoresponsive shape-memory effect in poly (ether ether ketone)(PEEK). *Journal of Applied Polymer Science* 2014, *131* (3).
- [81] Shi, Y.; Yoonessi, M.; Weiss, R., High temperature shape memory polymers. *Macromolecules* 2013, *46* (10), 4160-4167.
- [82] Chen, S.; Hu, J.; Zhuo, H.; Yuen, C.; Chan, L., Study on the thermal-induced shape memory effect of pyridine containing supramolecular polyurethane. *Polymer* 2010, *51* (1), 240-248.
- [83] Li, J.; Viveros, J. A.; Wrue, M. H.; Anthamatten, M., Shape-Memory Effects in Polymer Networks Containing Reversibly Associating Side-Groups. *Advanced Materials* 2007, *19* (19), 2851-2855.
- [84] Shabbir, A.; Javakhishvili, I.; Cervený, S.; Hvilsted, S.; Skov, A. L.; Hassager, O.; Alvarez, N. J., Linear Viscoelastic and Dielectric Relaxation Response of Unentangled UPy-Based Supramolecular Networks. *Macromolecules* 2016.
- [85] Feldman, K. E.; Kade, M. J.; Meijer, E.; Hawker, C. J.; Kramer, E. J., Model transient networks from strongly hydrogen-bonded polymers. *Macromolecules* 2009, *42* (22), 9072-9081.
- [86] Lewis, C. L.; Dell, E. M., A review of shape memory polymers bearing reversible binding groups. *Journal of Polymer Science Part B: Polymer Physics* 2016.
- [87] Weiss, R.; Izzo, E.; Mandelbaum, S., New design of shape memory polymers: mixtures of an elastomeric ionomer and low molar mass fatty acids and their salts. *Macromolecules* 2008, *41* (9), 2978-2980.
- [88] Dong, J.; Weiss, R., Shape memory behavior of zinc oleate-filled elastomeric ionomers. *Macromolecules* 2011, *44* (22), 8871-8879.
- [89] Whittell, G. R.; Hager, M. D.; Schubert, U. S.; Manners, I., Functional soft materials from metallopolymers and metallosupramolecular polymers. *Nat Mater* 2011, *10* (3), 176-188.
- [90] Du, H.; Zhang, J., Shape memory polymer based on chemically cross-linked poly (vinyl alcohol) containing a small number of water molecules. *Colloid and Polymer Science* 2010, *288* (1), 15-24.

- [91] Meng, H.; Hu, J., A brief review of stimulus-active polymers responsive to thermal, light, magnetic, electric, and water/solvent stimuli. *Journal of Intelligent Material Systems and Structures* 2010, 21 (9), 859-885.
- [92] Huang, W.; Yang, B.; An, L.; Li, C.; Chan, Y., Water-driven programmable polyurethane shape memory polymer: demonstration and mechanism. *Applied Physics Letters* 2005, 86 (11), 114105.
- [93] Yang, B.; Huang, W.; Li, C.; Li, L., Effects of moisture on the thermomechanical properties of a polyurethane shape memory polymer. *Polymer* 2006, 47 (4), 1348-1356.
- [94] Yang, B.; Huang, W. M.; Li, C.; Chor, J. H., Effects of moisture on the glass transition temperature of polyurethane shape memory polymer filled with nano-carbon powder. *European Polymer Journal* 2005, 41 (5), 1123-1128.
- [95] Chen, S.; Hu, J.; Yuen, C. W.; Chan, L., Novel moisture-sensitive shape memory polyurethanes containing pyridine moieties. *Polymer* 2009, 50 (19), 4424-4428.
- [96] Willett, J. L., Humidity-Responsive Starch-Poly (methyl acrylate) Films. *Macromolecular Chemistry and Physics* 2008, 209 (7), 764-772.
- [97] Chae Jung, Y.; Hwa So, H.; Whan Cho, J., Water-Responsive Shape Memory Polyurethane Block Copolymer Modified with Polyhedral Oligomeric Silsesquioxane. *Journal of Macromolecular Science, Part B* 2006, 45 (4), 453-461.
- [98] Gu, X.; Mather, P. T., Water-triggered shape memory of multiblock thermoplastic polyurethanes (TPUs). *Rsc Advances* 2013, 3 (36), 15783-15791.
- [99] Chen, M. C.; Tsai, H. W.; Chang, Y.; Lai, W. Y.; Mi, F. L.; Liu, C. T.; Wong, H. S.; Sung, H. W., Rapidly self-expandable polymeric stents with a shape-memory property. *Biomacromolecules* 2007, 8 (9), 2774-2780.
- [100] Zhu, Y.; Hu, J.; Luo, H.; Young, R. J.; Deng, L.; Zhang, S.; Fan, Y.; Ye, G., Rapidly switchable water-sensitive shape-memory cellulose/elastomer nanocomposites. *Soft Matter* 2012, 8 (8), 2509-2517.
- [101] Wu, T.; O'Kelly, K.; Chen, B., Poly (vinyl alcohol) particle-reinforced elastomer composites with water-active shape-memory effects. *European Polymer Journal* 2014, 53, 230-237.
- [102] Mendez, J.; Annamalai, P. K.; Eichhorn, S. J.; Rusli, R.; Rowan, S. J.; Foster, E. J.; Weder, C., Bioinspired Mechanically Adaptive Polymer Nanocomposites with Water-Activated Shape-Memory Effect. *Macromolecules* 2011, 44 (17), 6827-6835.
- [103] Wu, T.; Frydrych, M.; O'Kelly, K.; Chen, B., Poly (glycerol sebacate urethane)-cellulose nanocomposites with water-active shape-memory effects. *Biomacromolecules* 2014, 15 (7), 2663-2671.
- [104] Wu, T.; O'Kelly, K.; Chen, B., Poly (methacrylic acid)-grafted clay-thermoplastic elastomer composites with water-induced shape-memory effects. *Journal of Polymer Science Part B: Polymer Physics* 2013, 51 (20), 1513-1522.

- [105] Jiang, H.; Kelch, S.; Lendlein, A., Polymers move in response to light. *Advanced Materials* 2006, 18 (11), 1471-1475.
- [106] Koerner, H.; Price, G.; Pearce, N. A.; Alexander, M.; Vaia, R. A., Remotely actuated polymer nanocomposites—stress-recovery of carbon-nanotube-filled thermoplastic elastomers. *Nature materials* 2004, 3 (2), 115-120.
- [107] Leng, J.; Wu, X.; Liu, Y., Infrared light-active shape memory polymer filled with nanocarbon particles. *Journal of Applied Polymer Science* 2009, 114 (4), 2455-2460.
- [108] Liang, J.; Xu, Y.; Huang, Y.; Zhang, L.; Wang, Y.; Ma, Y.; Li, F.; Guo, T.; Chen, Y., Infrared-Triggered Actuators from Graphene-Based Nanocomposites. *The Journal of Physical Chemistry C* 2009, 113 (22), 9921-9927.
- [109] Zhang, H.; Xia, H.; Zhao, Y., Optically triggered and spatially controllable shape-memory polymer–gold nanoparticle composite materials. *Journal of Materials Chemistry* 2012, 22 (3), 845-849.
- [110] Zhang, H.; Zhao, Y., Polymers with dual light-triggered functions of shape memory and healing using gold nanoparticles. *ACS applied materials & interfaces* 2013, 5 (24), 13069-13075.
- [111] Hribar, K. C.; Metter, R. B.; Ifkovits, J. L.; Troxler, T.; Burdick, J. A., Light-Induced Temperature Transitions in Biodegradable Polymer and Nanorod Composites. *Small* 2009, 5 (16), 1830-1834.
- [112] He, J.; Zhao, Y.; Zhao, Y., Photoinduced bending of a coumarin-containing supramolecular polymer. *Soft Matter* 2009, 5 (2), 308-310.
- [113] Manouras, T.; Vamvakaki, M., Field responsive materials: photo-, electro-, magnetic-and ultrasound-sensitive polymers. *Polymer Chemistry* 2016.
- [114] Xie, H.; Cheng, C. Y.; Du, L.; Fan, C. J.; Deng, X. Y.; Yang, K. K.; Wang, Y. Z., A Facile Strategy To Construct PDLLA-PTMEG Network with Triple-Shape Effect via Photo-Cross-Linking of Anthracene Groups. *Macromolecules* 2016, 49 (10), 3845-3855.
- [115] Lendlein, A.; Jiang, H.; Jünger, O.; Langer, R., Light-induced shape-memory polymers. *Nature* 2005, 434 (7035), 879-882.
- [116] Sodhi, J. S.; Rao, I. J., Modeling the mechanics of light activated shape memory polymers. *International Journal of Engineering Science* 2010, 48 (11), 1576-1589.
- [117] Rochette, J. M.; Ashby, V. S., Photoresponsive polyesters for tailorable shape memory biomaterials. *Macromolecules* 2013, 46 (6), 2134-2140.
- [118] Zhang, X.; Zhou, Q.; Liu, H.; Liu, H., UV light induced plasticization and light activated shape memory of spiropyran doped ethylene-vinyl acetate copolymers. *Soft Matter* 2014, 10 (21), 3748-3754.
- [119] Kumpfer, J. R.; Rowan, S. J., Thermo-, photo-, and chemo-responsive shape-memory properties from photo-cross-linked metallo-supramolecular polymers. *Journal of the American Chemical Society* 2011, 133 (32), 12866-12874.

- [120] Xie, H.; He, M. J.; Deng, X. Y.; Du, L.; Fan, C. J.; Yang, K. K.; Wang, Y. Z., Design of Poly (l-lactide)–Poly (ethylene glycol) Copolymer with Light-Induced Shape-Memory Effect Triggered by Pendant Anthracene Groups. *ACS applied materials & interfaces* 2016, 8 (14), 9431-9439.
- [121] Nagata, M.; Yamamoto, Y., Synthesis and characterization of photocrosslinked poly (ϵ -caprolactone) s showing shape-memory properties. *Journal of Polymer Science Part A: Polymer Chemistry* 2009, 47 (9), 2422-2433.
- [122] Li, J.; Lewis, C. L.; Chen, D. L.; Anthamatten, M., Dynamic Mechanical Behavior of Photo-Cross-linked Shape-Memory Elastomers. *Macromolecules* 2011, 44 (13), 5336-5343.
- [123] Wu, L.; Jin, C.; Sun, X., Synthesis, Properties, and Light-Induced Shape Memory Effect of Multiblock Polyesterurethanes Containing Biodegradable Segments and Pendant Cinnamamide Groups. *Biomacromolecules* 2011, 12 (1), 235-241.
- [124] Leng, J.; Lan, X.; Liu, Y.; Du, S., Shape-memory polymers and their composites: Stimulus methods and applications. *Progress in Materials Science* 2011, 56 (7), 1077-1135.
- [125] du Toit, L. C.; Kumar, P.; Choonara, Y. E.; Pillay, V., Electroactive Polymers and Coatings. In *Industrial Applications for Intelligent Polymers and Coatings*, Springer: 2016, pp 51-89.
- [126] Pelrine, R.; Kornbluh, R., Dielectric Elastomers as Electroactive Polymers (EAPs): Fundamentals. *Electromechanically Active Polymers* 2016, 671.
- [127] Chandrasekhar, P., *Conducting polymers, fundamentals and applications: a practical approach*. Springer Science & Business Media: 2013.
- [128] Wilson, A. D., *Developments in Ionic Polymers—2*. Springer Science & Business Media: 2012.
- [129] Bar-Cohen, Y.; Zhang, Q., Electroactive polymer actuators and sensors. *MRS bulletin* 2008, 33 (03), 173-181.
- [130] Shahinpoor, M.; Bar-Cohen, Y.; Simpson, J. O.; Smith, J., Ionic polymer-metal composites (IPMCs) as biomimetic sensors, actuators and artificial muscles - a review. *Smart Materials and Structures* 1998, 7 (6), R15.
- [131] Romasanta, L.; Lopez-Manchado, M.; Verdejo, R., Increasing the performance of dielectric elastomer actuators: A review from the materials perspective. *Progress in polymer science* 2015, 51, 188-211.
- [132] Su, J.; Tajitsu, Y., Piezoelectric and Electrostrictive Polymers as EAPs: Materials. *Electromechanically Active Polymers* 2016, 509.
- [133] Behrens, S.; Appel, I., Magnetic nanocomposites. *Current Opinion in Biotechnology* 2016, 39, 89-96.
- [134] Thévenot, J.; Oliveira, H.; Sandre, O.; Lecommandoux, S., Magnetic responsive polymer composite materials. *Chemical Society Reviews* 2013, 42 (17), 7099-7116.

- [135] Stepanov, G.; Borin, D. Y.; Kramarenko, E. Y.; Bogdanov, V.; Semerenko, D.; Storozhenko, P., Magnetoactive elastomer based on magnetically hard filler: synthesis and study of viscoelastic and damping properties. *Polymer Science Series A* 2014, 56 (5), 603-613.
- [136] Šafařík, I.; Pospíšková, K.; Horská, K.; Maděrová, Z.; Šafaříková, M., Magnetically Responsive (Nano) Biocomposites. In *Intracellular Delivery II*, Springer: 2014, pp 17-34.
- [137] Attaran, A.; Brummund, J.; Wallmersperger, T., Modeling and finite element simulation of the magneto-mechanical behavior of ferrogels. *Journal of Magnetism and Magnetic Materials* 2016.
- [138] Dai, S.; Ravi, P.; Tam, K. C., pH-Responsive polymers: synthesis, properties and applications. *Soft Matter* 2008, 4 (3), 435-449.
- [139] Hoffman, A. S., Stimuli-responsive polymers: Biomedical applications and challenges for clinical translation. *Advanced drug delivery reviews* 2013, 65 (1), 10-16.
- [140] Mura, S.; Nicolas, J.; Couvreur, P., Stimuli-responsive nanocarriers for drug delivery. *Nature materials* 2013, 12 (11), 991-1003.
- [141] Xia, H.; Zhao, Y.; Tong, R., Ultrasound-Mediated Polymeric Micelle Drug Delivery. In *Therapeutic Ultrasound*, Springer: 2016, pp 365-384.
- [142] Sauter, T.; Heuchel, M.; Kratz, K.; Lendlein, A., Quantifying the shape-memory effect of polymers by cyclic thermomechanical tests. *Polymer Reviews* 2013, 53 (1), 6-40.
- [143] Fulcher, J. T.; Lu, Y. C.; Tandon, G. P.; Foster, D. C., Thermomechanical characterization of shape memory polymers using high temperature nanoindentation. *Polymer Testing* 2010, 29 (5), 544-552.
- [144] Wornyo, E.; Gall, K.; Yang, F.; King, W., Nanoindentation of shape memory polymer networks. *Polymer* 2007, 48 (11), 3213-3225.
- [145] Heuchel, M.; Sauter, T.; Kratz, K.; Lendlein, A., Thermally induced shape-memory effects in polymers: Quantification and related modeling approaches. *Journal of Polymer Science Part B: Polymer Physics* 2013, 51 (8), 621-637.
- [146] Gall, K.; Yakacki, C. M.; Liu, Y.; Shandas, R.; Willett, N.; Anseth, K. S., Thermomechanics of the shape memory effect in polymers for biomedical applications. *Journal of Biomedical Materials Research Part A* 2005, 73 (3), 339-348.
- [147] Wagermaier, W.; Kratz, K.; Heuchel, M.; Lendlein, A., Characterization methods for shape-memory polymers. In *Shape-memory polymers*, Springer: 2009, pp 97-145.
- [148] Biju, R.; Gouri, C.; Nair, C. R., Shape memory polymers based on cyanate ester-epoxy-poly (tetramethyleneoxide) co-reacted system. *European Polymer Journal* 2012, 48 (3), 499-511.

- [149] Gall, K.; Dunn, M. L.; Liu, Y.; Finch, D.; Lake, M.; Munshi, N. A., Shape memory polymer nanocomposites. *Acta Materialia* 2002, 50 (20), 5115-5126.
- [150] Liu, Y.; Gall, K.; Dunn, M. L.; McCluskey, P., Thermomechanical recovery couplings of shape memory polymers in flexure. *Smart Materials and Structures* 2003, 12 (6), 947.
- [151] Hearon, K.; Singhal, P.; Horn, J.; Small IV, W.; Olsovsky, C.; Maitland, K. C.; Wilson, T. S.; Maitland, D. J., Porous shape-memory polymers. *Polymer Reviews* 2013, 53 (1), 41-75.
- [152] Hasan, S. M.; Nash, L. D.; Maitland, D. J., Porous shape memory polymers: Design and applications. *Journal of Polymer Science Part B: Polymer Physics* 2016.
- [153] Warwar Damouny, C.; Silverstein, M. S., Hydrogel-filled, semi-crystalline, nanoparticle-crosslinked, porous polymers from emulsion templating: Structure, properties, and shape memory. *Polymer* 2016, 82, 262-273.
- [154] Barvosa-Carter, W.; Johnson, N. L.; Browne, A. L.; Herrera, G. A.; Mc Knight, G. P.; Massey, C., Reversibly expandable energy absorbing assembly utilizing shape memory foams for impact management and methods for operating the same. Google Patents: 2007.
- [155] Kirkpatrick, W. C.; Baird, J. W. G.; Ford, T. E., *Encapsulation of electrical components and other articles*. Google Patents: 1963.
- [156] Ota, S., Current status of irradiated heat-shrinkable tubing in Japan. *Radiation Physics and Chemistry (1977)* 1981, 18 (1), 81-87.
- [157] Liu, Y.; Du, H.; Liu, L.; Leng, J., Shape memory polymers and their composites in aerospace applications: a review. *Smart Materials and Structures* 2014, 23 (2), 023001.
- [158] Sokolowski, W. M.; Tan, S. C., Advanced self-deployable structures for space applications. *Journal of Spacecraft and Rockets* 2007, 44 (4), 750-754.
- [159] Zhang, R.; Guo, X.; Liu, Y.; Leng, J., Theoretical analysis and experiments of a space deployable truss structure. *Composite Structures* 2014, 112, 226-230.
- [160] Feng, C. M.; Liu, T. S., A bionic approach to mathematical modeling the fold geometry of deployable reflector antennas on satellites. *Acta Astronautica* 2014, 103, 36-44.
- [161] Bergman, D.; Yang, B., An analytical shape memory polymer composite beam model for space applications. *International Journal of Structural Stability and Dynamics* 2016, 16 (02), 1450093.
- [162] Cutter, C. N., Opportunities for bio-based packaging technologies to improve the quality and safety of fresh and further processed muscle foods. *Meat Science* 2006, 74 (1), 131-142.

- [163] Ward Small, I.; Singhal, P.; Wilson, T. S.; Maitland, D. J., Biomedical applications of thermally activated shape memory polymers. *Journal of Materials Chemistry* 2010, 20 (17), 3356-3366.
- [164] Arrieta, M. P.; López, J.; Rayón, E.; Jiménez, A., Disintegrability under composting conditions of plasticized PLA-PHB blends. *Polymer Degradation and Stability* 2014.
- [165] Tokiwa, Y.; Suzuki, T., Hydrolysis of polyesters by lipases. *Nature* 1977, 270 (5632), 76-78.
- [166] Arrieta, M. P.; López, J.; López, D.; Kenny, J. M.; Peponi, L., Biodegradable electrospun bionanocomposite fibers based on plasticized PLA-PHB blends reinforced with cellulose nanocrystals. *Industrial Crops and Products* 2016, 93, 290-301.
- [167] Drumright, R. E.; Gruber, P. R.; Henton, D. E., Polylactic acid technology. *Advanced Materials* 2000, 12 (23), 1841-1846.
- [168] Nair, L. S.; Laurencin, C. T., Biodegradable polymers as biomaterials. *Progress in polymer science* 2007, 32 (8-9), 762-798.
- [169] Lucas, N.; Bienaime, C.; Belloy, C.; Queneudec, M.; Silvestre, F.; Nava-Saucedo, J. E., Polymer biodegradation: Mechanisms and estimation techniques—A review. *Chemosphere* 2008, 73 (4), 429-442.
- [170] Chandra, R.; Rustgi, R., Biodegradable polymers. *Progress in polymer science* 1998, 23 (7), 1273-1335.
- [171] Vroman, I.; Tighzert, L., Biodegradable polymers. *Materials* 2009, 2 (2), 307-344.
- [172] Bastioli, C., *Handbook of biodegradable polymers*. iSmithers Rapra Publishing: 2005.
- [173] Raquez, J. M.; Narayan, R.; Dubois, P., Recent Advances in Reactive Extrusion Processing of Biodegradable Polymer-Based Compositions. *Macromolecular Materials and Engineering* 2008, 293 (6), 447-470.
- [174] Ferri, J.; Garcia-Garcia, D.; Sánchez-Nacher, L.; Fenollar, O.; Balart, R., The effect of maleinized linseed oil (MLO) on mechanical performance of poly (lactic acid)-thermoplastic starch (PLA-TPS) blends. *Carbohydrate Polymers* 2016, 147, 60-68.
- [175] Sabetzadeh, M.; Bagheri, R.; Masoomi, M., Effect of nanoclay on the properties of low density polyethylene/linear low density polyethylene/thermoplastic starch blend films. *Carbohydrate Polymers* 2016, 141, 75-81.
- [176] Peres, A. M.; Pires, R. R.; Oréface, R. L., Evaluation of the effect of reprocessing on the structure and properties of low density polyethylene/thermoplastic starch blends. *Carbohydrate Polymers* 2016, 136, 210-215.
- [177] Samper-Madrigal, M. D.; Fenollar, O.; Dominici, F.; Balart, R.; Kenny, J., The effect of sepiolite on the compatibilization of polyethylene-thermoplastic starch blends for environmentally friendly films. *Journal of Materials Science* 2015, 50 (2), 863-872.

- [178] Suvorova, A. I.; Tujkova, I. S.; Trufanova, E. I. In *Viscosity, sorption of water and biodegradation of starch/copolyamide blends*, Macromolecular Symposia, Wiley Online Library: 1999; pp 331-337.
- [179] Nakamura, E.; Cordi, L.; Almeida, G.; Duran, N.; Mei, L. I., Study and development of LDPE/starch partially biodegradable compounds. *Journal of Materials Processing Technology* 2005, *162*, 236-241.
- [180] Averous, L., Biodegradable multiphase systems based on plasticized starch: a review. *Journal of Macromolecular Science, Part C: Polymer Reviews* 2004, *44* (3), 231-274.
- [181] Maiti, S.; Ray, D.; Mitra, D.; Mukhopadhyay, A., Isolation and characterisation of starch/polyvinyl alcohol degrading fungi from aerobic compost environment. *International Biodeterioration & Biodegradation* 2013, *82*, 9-12.
- [182] Jiménez, A.; Fabra, M. J.; Talens, P.; Chiralt, A., Effect of sodium caseinate on properties and ageing behaviour of corn starch based films. *Food hydrocolloids* 2012, *29* (2), 265-271.
- [183] Arrieta, M. P.; Peltzer, M. A.; del Carmen Garrigós, M.; Jiménez, A., Structure and mechanical properties of sodium and calcium caseinate edible active films with carvacrol. *Journal of Food Engineering* 2013, *114* (4), 486-494.
- [184] Espigulé, E.; Puigvert, X.; Vilaseca, F.; Mendez, J. A.; Mutjé, P.; Girones, J., Thermoplastic starch-based composites reinforced with rape fibers: Water uptake and thermomechanical properties. *BioResources* 2013, *8* (2), 2620-2630.

Chapter 2

**THERMALLY-ACTIVATED SHAPE MEMORY
BEHAVIOR OF DIFFERENT NANOCOMPOSITES
BASED ON ETHYLENE COPOLYMERS**

*Valentina Sessini¹, David Brox¹⁻², Antonio Julio López²,
Alejandro Ureña², Jean-Marie Raquez³, Philippe Dubois³,
José M. Kenny¹ and Laura Peponi^{1,*}*

¹Instituto de Ciencia y Tecnología de Polímeros, ICTP-CSIC, Spain

²Departamento de Matemática Aplicada, Ciencia e Ingeniería de Materiales
y Tecnología Electrónica. Universidad Rey Juan Carlos, Spain

³Laboratory of Polymeric and Composite Materials, University of Mons, Belgium

ABSTRACT

Shape memory materials are able to change their shape upon application of an external stimulus such as temperature, humidity, light, electric or magnetic fields, etc. This chapter wants to focus the attention on nanocomposite systems with shape memory response due to their high scientific and technological relevance. In particular, three different nanocomposites based on ethylene copolymers are presented with different thermally-activated mechanisms such as Nucrel® and Surlyn® reinforced with silica nanoparticles, blends of EVA/thermoplastic starch reinforced with natural bentonite and EVA reinforced with starch nanocrystals. All of these systems present shape memory ability, evidencing how the addition of well dispersed nanoparticles can affect the shape memory response of the neat matrix.

Keywords: ethylene copolymers, ionomeric resin, nucrel®, surlyn®, stimuli-responsive, shape memory, thermally-activated, nanocomposites

* Corresponding Author Email: lpeponi@ictp.csic.es.

INTRODUCTION

Smart materials have the ability to respond to an external stimulus. Between smart materials, there is a class of polymers known as shape memory polymers (SMPs), able to change their shape by fixing a temporary one upon the application of an external stimulus [1]. Moreover, shape memory materials have the capability to recover the original shape once the external stimulus is applied again.

Shape memory process in polymers involves the retention of the deformation entropy as internal energy and its activation due to an external stimulus, which means the relaxation of the polymer chains and therefore, the recovery of the original shape [2]. To obtain this response, a particular polymer structure is needed and viscoelastic relaxation is necessary to create an elevated mobility to the macromolecular chains.

Different are the external stimuli able to produce the shape change in polymeric materials, such as temperature [3-7], humidity [8, 9], pH [10], light [11] and electric or magnetic field [12]. However, thermal stimulus is the most common one [13-15]. In general, the shape memory mechanism in the SMPs encompasses two main stages: the programming stage and the recovery stage as schematically shown in Figure 1. In the first stage, a temporary shape (shape B) is fixed by the application of an external stimulus. In the second stage, the original shape is recovered (shape A) after applying the same stimulus as can be seen in Figure 1 [16].

Moreover, shape memory polymers are formed by two different phases: the reversible phase, also called “switching phase”, which is able to fix the temporary shape and the “permanent phase”, responsible for recovering the original shape of the polymeric material (Figure 1). Both phases can be formed by chemical or physical domains, affecting the thermal response of the polymeric materials. The external stimulus, such as temperature, can fix the temporary shape and counteracts the elastic forces, which tend to return the material to its original shape [17]. This is the reason why a reversible thermal transition to a specific temperature (T_{trans}) is needed. In particular, permanent bonds are retained at temperatures higher than T_{trans} , while reversible and permanent domains are both presented at temperatures lower than T_{trans} [18].

The above-mentioned SMPs are the most common ones and they are usually referred as “one-way shape memory polymers”, with two active phases – i.e., the switching and the permanent domains – with an external stimulus triggering the change from one shape to another, Figure 1.

In general, shape memory properties are characterized by thermo-mechanical cycle experiments [19, 20]. Figure 2 shows a 3D representation of a thermo-mechanical shape memory cycle.

The curve shows the process starting with a deformation of the sample at the switching temperature (T_{sw}). Afterwards, a quick cooling stage is done to temperature lower than T_{trans} (fixing temperature, T_{fix}) maintaining the applied load until the

temporary shape is fixed. After, the unloading of the applied stress is followed by an increase of the temperature above T_{trans} (T_{sw}) to activate the recovery of the permanent shape.

When the polymer shows two temporary shapes and only one permanent shape, it is known as “triple” shape memory polymer [21]. These polymers need one programming stage, to program both temporary shapes, and two different triggers to recover firstly the intermediate temporary shape and subsequently the original one, as schematically shown on Figure 3.

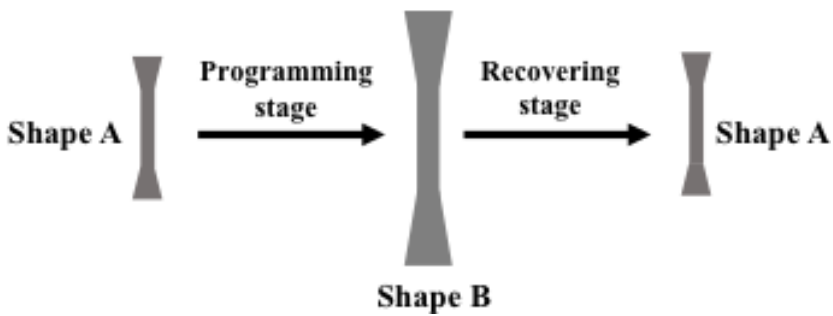


Figure 1. Scheme of the shape memory process.

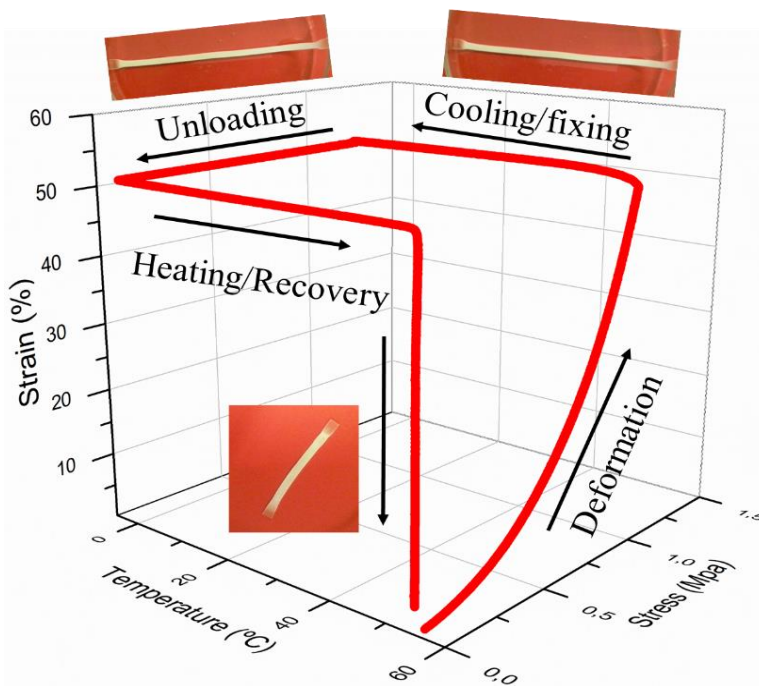


Figure 2. Scheme of 3D thermo-mechanical shape memory cycle.

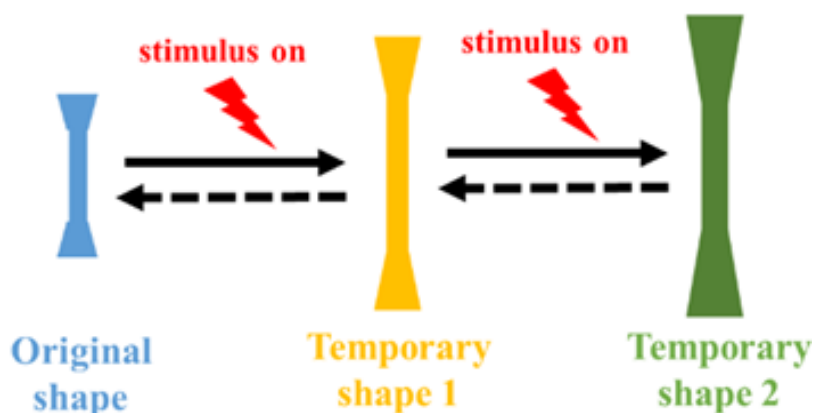


Figure 3. Scheme of triple shape memory process.

Therefore, depending on the chemical or physical structure of the switching domains, the melting temperature, T_m , or the glass transition temperature, T_g , will be considered as the T_{trans} [22].

In particular, in semicrystalline polymers, T_m is used as T_{trans} . Polymers with chemical crosslinking, i.e., covalent or thermoreversible bonds [23] or physically crosslinked by means of segregated domains [24] or a mixture of both types forming copolymers [25] are representative of SMPs constructed around T_m . In general, in the copolymers the phase with higher T_{trans} is the responsible for the preservation of the physical structure, maintaining the permanent shape. Meanwhile, the phase with the lower T_{trans} is the responsible for the fixation of the temporary shape [26] as shown in the next paragraphs of this chapter. When SMPs are based on T_g , they are able to fix a temporary shape to a temperature below their T_g and to recover the permanent one above this temperature [18].

It is important to note also that in the last years shape memory nanocomposites [27] have obtained a great interest from both academic and industrial sectors studying the incorporation of nanofillers such as carbon nanotube, layered silicates, titanium oxide, etc. into the polymer matrix [28]. The addition of nanoparticles, characterized by high surface area, and the obtention of favorable interactions between the matrix and the nanofillers, result in the improvement of numerous properties including thermal stability, flame retardancy, mechanical properties, gas barrier properties, and so on as compared with neat polymers [29].

Moreover, in recent years, nanowhiskers and nanocrystals prepared from natural polymers, such as cellulose and starch, have been applied to reinforce biodegradable or non-biodegradable polymeric matrix [13, 30-33]. In particular, starch is an abundant biopolymer, which is totally biodegradable. Starch nanocrystals (SNCs) have been used as fillers in polymeric matrices such as natural rubber [34], poly-vinyl alcohol [35] and thermoplastic starch, TPS [36]. The physical properties of the resulting nanocomposites were improved by the incorporation of SNCs [37].

Copolymers of ethylene-vinyl acetate (EVA) are a class of widely used polymers, with a variety of industrial applications such as flexible packaging, membranes, cable and wire, hose and tube, photovoltaic encapsulants, footwear and biomedical applications [38-40]. Recent developments in the field of shape memory polymers have drawn increasing attention to EVA copolymers for potential non-structural applications (microfluidic devices, soft actuators, etc.). However, most of the studies reported in literature of the shape memory behavior of EVA are about crosslinked EVA [41-43]. Nevertheless, Wu et al. reported the study of the shape recovery of a commercial EVA by studying its creep and the thermo-responsive shape memory effect presenting two potential applications [44].

However, in many cases, EVA application is limited due to its low tensile strength, thermal stability, and high flammability [28, 45]. To overcome these deficiencies, commonly either the vinyl acetate (VA) content of EVA varies or suitable nanofillers are incorporated in the EVA matrix. Indeed, varying the VA content, many properties of EVA change while the polar groups of vinyl acetate could get involved with a strong interaction with nanofillers, making its dispersion homogeneous. At this regard, several investigations have been reported in literature, including the incorporation of graphite oxide [46], sepiolite [47], montmorillonite [39, 48], carbon nanotube [49], and so on.

Commercial poly(ethylene-co-methacrylic acid) copolymer, named Nucrel® and its sodium neutralized counterpart with the tradename of Surlyn® are manufactured by Dupont™ Company. The self-healing properties of ionomeric resin under high speed impact, i.e., ballistic damage [50, 51], and even under hyper-velocity impacts (1-4 km/s) simulating space debris impacts [52] have been studied.

This ionomeric material presents ionic groups integrated by the carboxyl groups of the polymer that create strong interactions by coulombic potentials between the ionic charges, forming the ionic clusters. These clusters are able to form reversible ionic networks [53] and the inter-chain interactions designed the permanent network. Due to the presence of two different phases in these polymers, it is possible to use them for designing shape memory polymers.

In this chapter, different nanocomposites based on ethylene copolymers are presented with different mechanisms used to obtain the shape memory response.

In particular three different systems are studied based on Nucrel® and Surlyn® reinforced with silica nanoparticles, blends of EVA/thermoplastic starch reinforced with natural bentonite and EVA reinforced with SNCs.

THERMALLY-ACTIVATED SHAPE MEMORY CHARACTERIZATION

Thermally-activated shape memory behavior of our nanocomposites was studied through thermo-mechanical cycle experiments using an Instron Universal Testing

Machine equipped with a temperature chamber. For each material, the right transitions, the switching temperature and the fixing temperature, were found based on the thermal and dynamo-mechanical characterization.

Therefore, with the aim to get a quantitative estimation of the shape memory properties of the materials, the strain fixity ratio (R_f) and the strain recovery ratio (R_r) have been calculated [20]. In particular, R_r , the ability to recover the initial shape, was taken as the ratio of the recovered strain to the total strain, as given by the following equation:

$$R_r(N) = \frac{(\varepsilon_m - \varepsilon_p(N))}{\varepsilon_m - \varepsilon_p(N-1)} \times 100\% \quad (1)$$

R_f , the ability to fix the temporary shape, is the amplitude ratio of the fixed strain to the total strain, as presented by the Equation 2:

$$R_f(N) = \frac{\varepsilon_u(N)}{\varepsilon_m} \times 100\% \quad (2)$$

where, ε_m is the deformed strain, ε_u the fixed strain, ε_p the recovered strain and N is the number of cycles.

POLY(ETHYLENE-CO-METHACRYLIC ACID) RANDOM COPOLYMER AND IONOMERS

Commercial poly(ethylene-co-methacrylic acid) random copolymer (EMAA) named Nucrel® 960 (containing 15 wt% of methacrylic acid (MAA) comonomer) and its ionomer, Surlyn® 8940, with 30% of the MAA comonomer neutralized by sodium (EMAA-Na), were kindly provided by Dupont™ Company. Silicon Dioxide Nanopowder (SiO_2) with a particle average size of 7-14 nm and specific surface higher than 200 m^2/g was supplied by EMFUTUR.

Shape memory properties of a commercial poly(ethylene-co-methacrylic acid) random copolymer named Nucrel® 960 and its ionomeric resin, Surlyn® 8940, were studied. With the purpose of select the parameters for thermo-mechanical cycles, dynamic thermo-mechanical analysis was performed in order to study the main chain relaxation of the materials. $\text{Tan}\delta$ curves are reported in Figure 4 for Nucrel® as well as Surlyn®. Both materials have similar elastic properties. Nucrel® showed three main relaxations in the range of temperature between - 140 and 100°C.

In particular, around - 70°C a relaxation was observed and it was ascribed to the local molecular motion of the amorphous segment of PE while at ~ 30°C the relaxation

corresponding to the melting of the secondary crystals of PE was detected. Moreover, after $\sim 70^{\circ}\text{C}$ the relaxation corresponding to the primary crystallites of PE was observed [54, 55]. For Surlyn®, the same relaxations were detected but the relaxation below 0°C were more evident and were ascribed not only to the molecular motion of the amorphous phase of PE but also to the ion-depleted in the amorphous region, although different explanation have been proposed in literature for this relaxation over the year [56]. The relaxation corresponding to the melting of the secondary crystals of PE was shifted to higher temperature for Surlyn® ($\sim 60^{\circ}\text{C}$) as well as that one of the primary crystals, starting from $\sim 85^{\circ}\text{C}$. In this case, three types of physical crosslinks are present due to the ionic domains, primary and secondary polyethylene crystallites. Above 100°C , where all the polyethylene crystals have melted, the Surlyn® is a physically crosslinked rubber with a supramolecular network formed by ionic interactions [57].

Polyethylene crystals provide the temporary network, therefore the switching temperature for shape memory is determined by their melting temperature. In order to compare the shape memory properties of both Nucrel® and Surlyn® and their nanocomposites reinforced with 1 wt% of silica nanoparticles, a common switching temperature was taken, that is, at 60°C . Thus, the crystallites that melt below 60°C (mainly the secondary crystallites) are used as the temporary network for generating shape memory effects. In particular, for Nucrel® the permanent shape is achieved through the largest and strongest primary polyethylene crystals that create a physical network with the amorphous chains of the material. While for Surlyn®, the presence of the Na^+ ions allows to obtain a more stable permanent network due to the presence of the ionomeric aggregates in addition to the physical network formed by the PE primary crystals.

Once the T_{sw} was selected, the mechanical response of our materials was studied at that temperature (60°C). A stress-strain test (Figure 5) was carried out to determine the maximum deformation that the material could withstand at the T_{sw} .

In Figure 5, it is possible to note that Surlyn® showed different mechanical properties compared to Nucrel®. In fact, Surlyn® showed higher elastic modulus and higher maximum stress, while the elongation at break decreased for Surlyn® due to the Na^+ neutralization of methacrylic acid groups. The presence of SiO_2 improves the mechanical properties of both neat materials, Nucrel® and Surlyn®. Even if the elongation at break decreased due to the ionomer structure as well as to the presence of SiO_2 in both matrices, the maximum deformation at 60°C for the shape memory test was higher than 500% for all the materials.

Thermally-activated shape memory properties were studied using an Instron Machine equipped with a temperature chamber. Samples for the thermo-mechanical cycles were cut from compression-molded films into rectangular specimens of approximately 20 mm x 5 mm x 0.50 mm. The samples were heated at the T_{sw} of 60°C for 5 min, followed by a strain-controlled uniaxial stretching applied until a fixed percentage of deformation, i.e.,

50% and 100%. They were then quenched at 0°C (T_{fix}) under the same constant stress, which after 10 minutes was released. A free-strain recovery was then performed at the selected T_{sw} . The 2D stress-strain and 3D thermo-mechanical stress-strain-temperature cycle diagrams for neat Nucrel® and its nanocomposite counterpart are shown in Figure 6 and Figure 7 at 2 different deformation values, 50% and 100%, respectively. In order to evaluate the repeatability of the shape memory properties, four thermo-mechanical cycles were completed for each sample.

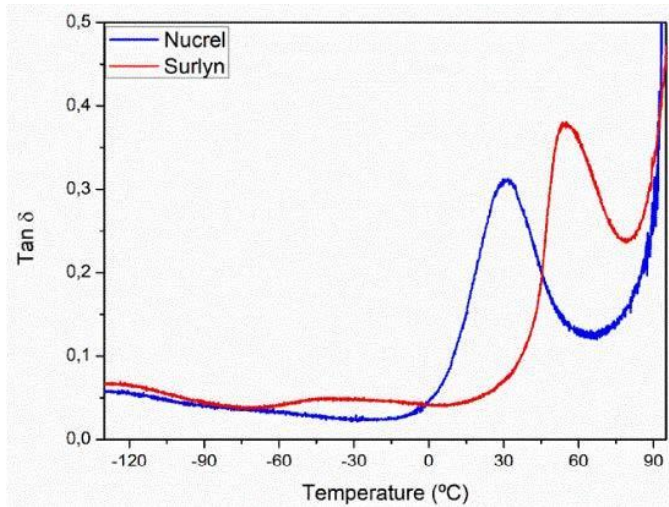


Figure 4. Damping factor ($Tan\delta$) as a function of temperature for both Nucrel® and Surlyn®.

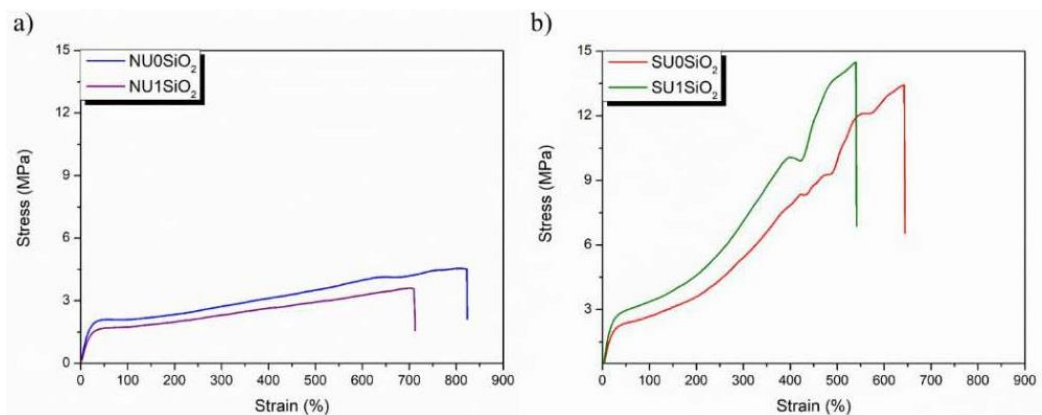


Figure 5. Stress-strain curves performed at 60°C for the neat materials and their respective nanocomposites. a) Nucrel® and b) Surlyn®.

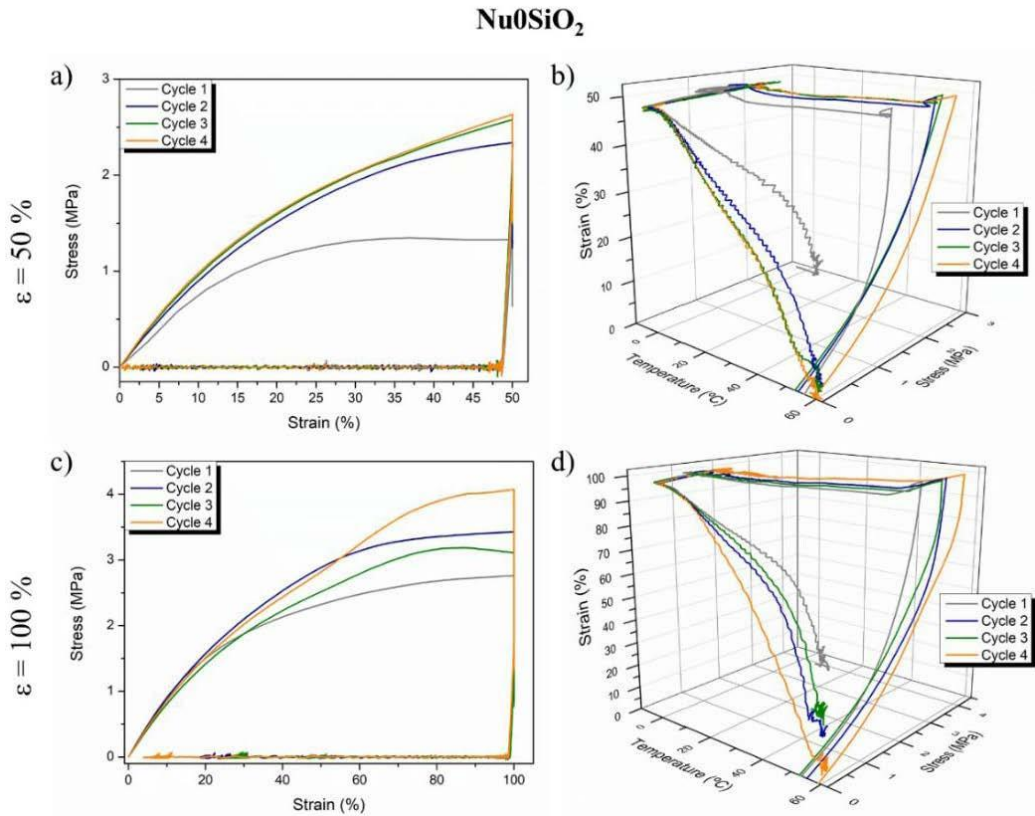


Figure 6. Thermo-mechanical cycles for neat Nucrel®. 2D stress-strain cycles and 3D stress-strain-temperature cycle diagrams at 50% (a-b) and 100% (c-d) of deformation.

All the samples show a good ability to fix the deformed shape at the selected T_{fix} while the recovery process begun before reaching the selected T_{sw} , as it was expected by observing Figure 4, where the peak related to the melting of PE secondary crystals is at around 25°C. Moreover, it is possible to notice that increasing the number of cycles, the stress needed to reach the same value of elongation (50% or 100%) is higher than the stress applied during the first cycle. This is probably due to a reorganization of the polymeric structure after the first cycle.

In Table 1, the results of thermo-mechanical cycles in terms of R_r and R_f are summarized for Nucrel® and its SiO₂ reinforced nanocomposite. Between the samples based on Nucrel®, we can conclude that higher values of R_r were observed for a deformation of 50% and in particular for the sample reinforced with 1 wt% of SiO₂. In fact, for 100% of deformation the R_r values were drastically dropped towards lower values compare with that obtained for 50% of deformation. Furthermore, R_r values improved increasing the number of cycles. This is probably due to a progressive rearrangement of the polymeric structure cycle by cycle, until reaching a constant value. Whereas the R_f values are higher for the sample reinforced with silica nanoparticle for

both applied deformations. The presence of silica nanoparticles increases the ability to fix the temporary shape, probably due to a decrease of the polymeric chain mobility. Thermo-mechanical cycles were performed also for the samples based on Surlyn® following the same procedure than Nucrel®.

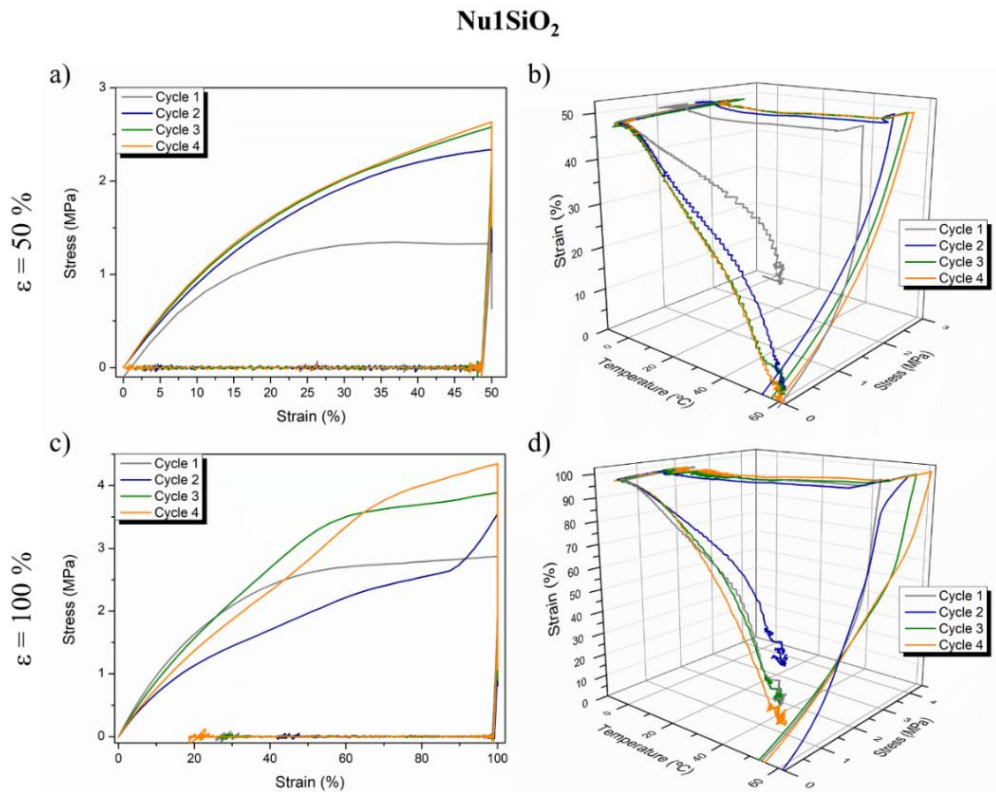


Figure 7. Thermo-mechanical cycles for Nucrel® nanocomposite reinforced with 1 wt% of SiO₂. 2D stress-strain cycles and 3D stress-strain-temperature cycle diagrams at 50% (a-b) and 100% (c-d) of deformation.

Table 1. Values of R_r and R_f obtained by thermo-mechanical cycles at 50% and 100% of deformation for Nucrel® and its SiO₂ nanocomposite

Sample	ϵ (%)	R_r (%)				R_f (%)			
		1	2	3	4	1	2	3	4
NU0SiO ₂	50	81	74	96	97	97	97	95	97
	100	55	81	73	93	99	99	99	98
NU1SiO ₂	50	59	94	96	98	99	97	95	97
	100	73	59	74	81	99	99	99	99

The 2D stress-strain and 3D thermo-mechanical stress-strain-temperature cycle diagrams for neat Surlyn® and its nanocomposite counterpart are shown in Figure 8 and Figure 9 at 2 different deformation values, 50% and 100%, respectively.

As noted for Nucrel® based materials also the samples based on Surlyn® show a good ability to fix the deformed shape at the selected T_{fix} . Compared with Nucrel®, Surlyn® based materials are more stable during the recovery, maintaining the temporary shape longer but not until the selected T_{sw} , as was expected observing Figure 4, where the peak related to the melting of PE secondary crystals is at around 60°C. Moreover, it is possible to notice that increasing the number of cycles, the stress needed to reach the same value of elongation is higher than the stress applied during the first cycle when 100% of elongation was applied. On the contrary, when 50% of elongation was applied, the value of applied stress was almost constant during the different cycles. This is probably due to the strongest physical network formed by ionic interaction in Surlyn®.

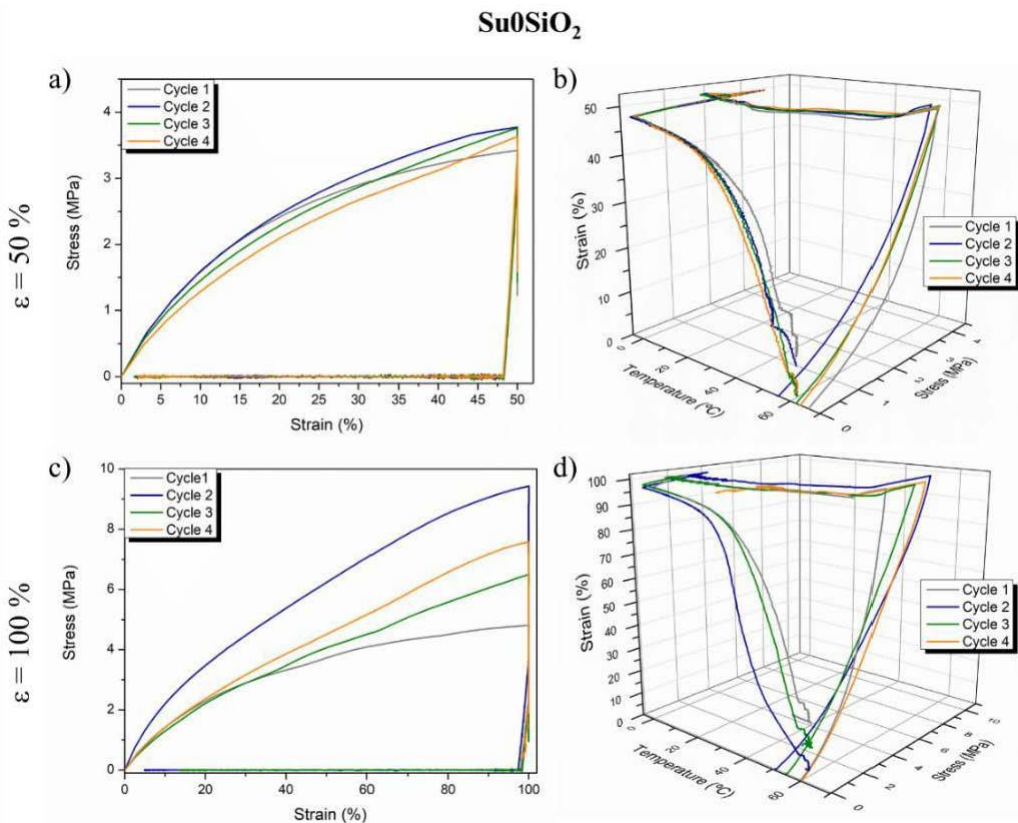


Figure 8. Thermo-mechanical cycles for neat Surlyn®. 2D stress-strain cycles and 3D stress-strain-temperature cycle diagrams at 50% (a-b) and 100% (c-d) of deformation.

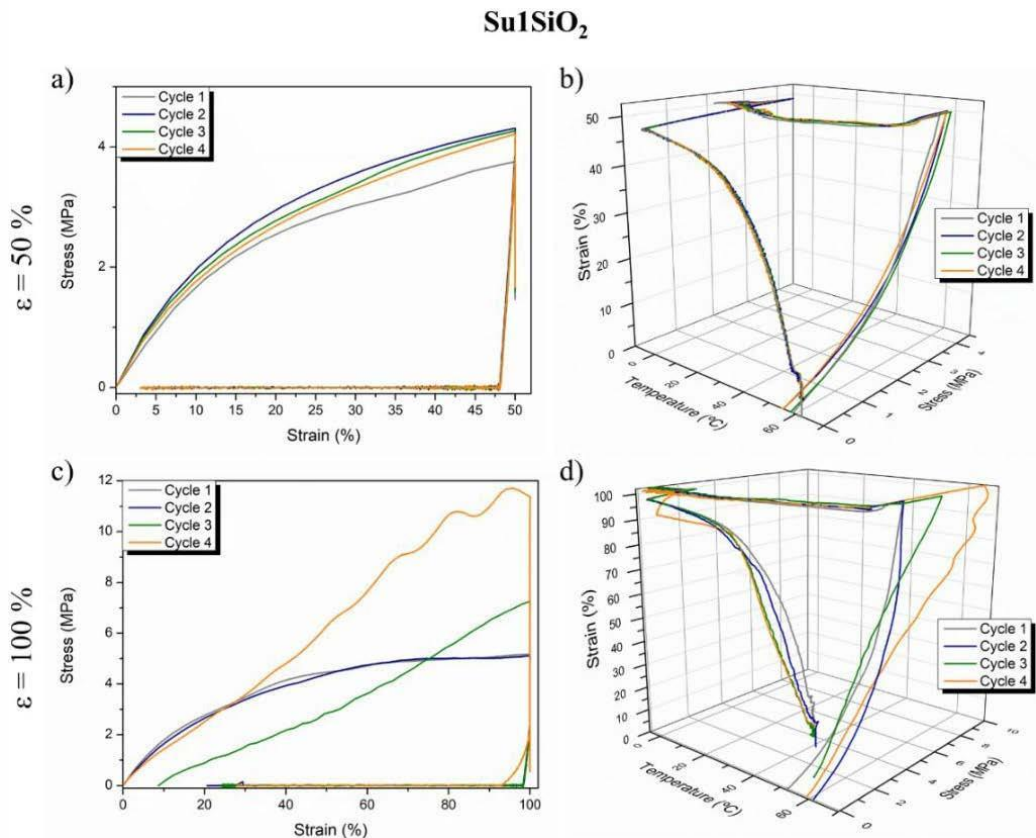


Figure 9. Thermo-mechanical cycles for Surlyn® nanocomposite reinforced with 1 wt% of SiO₂. 2D stress-strain cycles and 3D stress-strain-temperature cycle diagrams at 50% (a-b) and 100% (c-d) of deformation.

Table 2. Values of R_r and R_f obtained by thermo-mechanical cycles at 50% and 100% of deformation for Surlyn® and its respective nanocomposite

Sample	ϵ (%)	R_r (%)				R_f (%)			
		1	2	3	4	1	2	3	4
SU0SiO ₂	50	81	85	96	95	97	96	97	96
	100	76	95	86	88	98	97	98	97
SU1SiO ₂	50	86	93	93	94	96	96	98	96
	100	70	79	78	72	98	98	98	92

In Table 2, the results of thermo-mechanical cycles in terms of R_r and R_f are summarized for Surlyn® and its SiO₂ reinforced nanocomposite.

As observed for Nucrel®, higher values of R_f were observed for 50% of deformation also for the samples based on Surlyn®, in particular for the sample reinforced with 1 wt% of SiO₂. Compared with Nucrel®, the decrease of the R_r values when 100% of

deformation is applied, was less evident due to the higher mechanical properties of Surlyn® thanks to the ionomeric network. However, R_r values improved after increasing the number of cycles. Moreover, the high R_f values are the same for neat sample as well as for the sample reinforced with silica nanoparticle, higher than 95%.

POLY(ETHYLENE-CO- VINYL ACETATE) RANDOM COPOLYMER/THERMOPLASTIC STARCH BLENDS AND NANOCOMPOSITES

Native pea starch was used as received to obtain thermoplastic starch (TPS). Commercial EVA copolymer with 19 wt% VA content was purchased from Exxon Mobil Chemical Company. Glycerol (purity 97%) was used as starch plasticizer and commercial natural bentonite, Cloisite- Na^+ (CLNa^+), with a typical dimension, ranging from 2 to 13 μm , was used as nanofillers.

In our previous work [40], the thermally-activated shape memory effect of neat ethylene-vinyl acetate copolymer and its blends with thermoplastic starch has been studied by using the stretch-induced crystallization mechanism to program the temporary shape. In particular, two different blends with different TPS content, i.e., 40 and 50 wt%, have been tested and compared with neat EVA, as well as EVA/TPS blends based nanocomposites reinforced with 1 wt% of natural bentonite, (CLNa^+). Indeed was demonstrated that a new poorly organized crystalline structure (A phase), induced by stretching the sample until 250% of elongation, was used as switching phase of EVA. Therefore, the melting temperature of the crystalline phase A was considered the switching temperature of our system. The presence of the two different crystal phases in EVA was first confirmed by DSC analysis using the same programming condition used for the shape memory activation, i.e., after stretching 250% of elongation at 40°C. The DSC thermograms related to the first heating scan of non-stretched and stretched samples, blends and their nanocomposites are showed in Figure 10.

It easy to note that, as for pure EVA [40], while both non-stretched blends and nanocomposites present only B-phase crystals, a new crystalline phase with a T_m of about 50°C is presented after stretching the EVA-based samples. Thus, the desired two different crystal phases A and B were obtained in these EVA-based materials. Therefore, the new induced crystal phase A is the phase responsible for fixing the temporary shape of our system while amorphous EVA, thermoplastic starch and B crystal phase network was that responsible for memorize the original shape, as reported in our previous work [40]. When the heating is applied, the crystalline phase A melts and the system recovers its permanent shape.

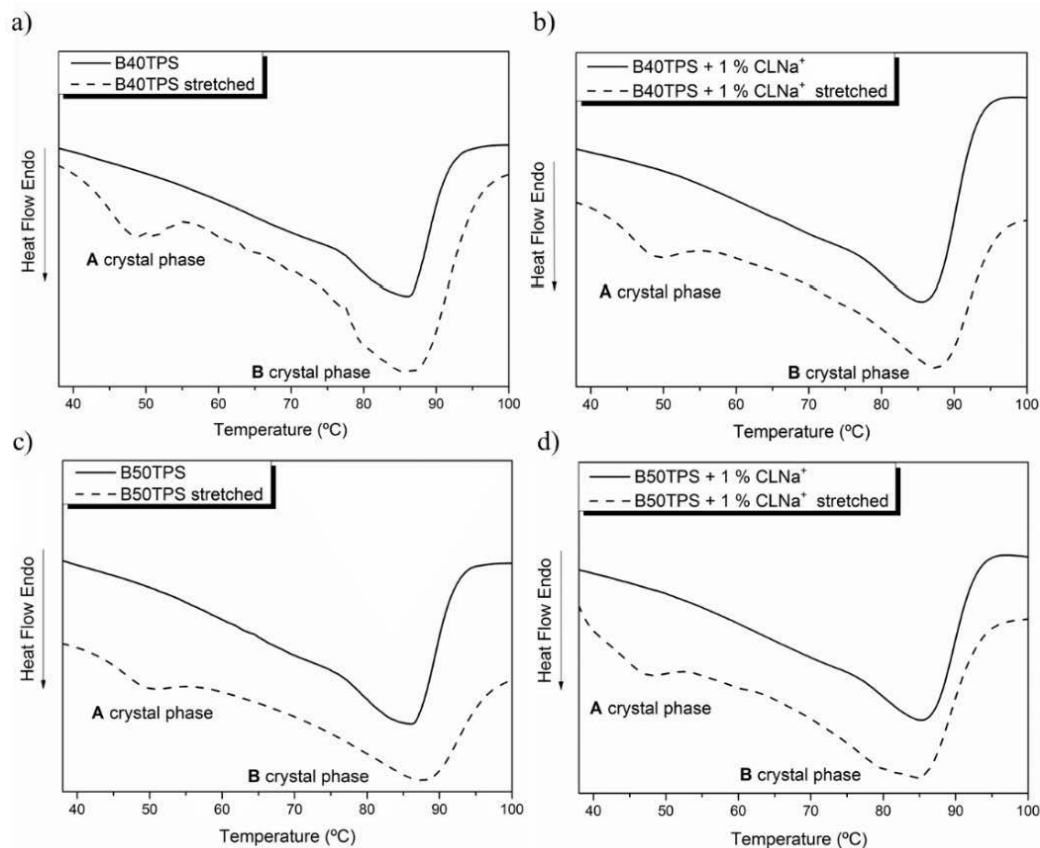


Figure 10. First cycle DSC thermograms for non-stretched and stretched blends and their nanocomposites: a) B40TPS, b) B40TPS + 1% CLNa⁺, c) B50TPS and d) B50TPS + 1% CLNa⁺.

The thermally-activated shape memory properties of neat EVA, the blends and their nanocomposites were characterized by Instron Machine. In brief, the parameter used were 40°C as stretching temperature (T_s), 250% of elongation, $T_{fix} = 10^\circ\text{C}$ and 60°C as T_{sw} . 3D thermo-mechanical stress-strain-temperature cycles and the 2D stress-strain diagram were determined for all the samples studied (Figure 11). In order to evaluate the repeatability of the shape memory properties, five different thermo-mechanical cycles were performed for each sample.

The values obtained in every cycle for both the R_r and the R_f are summarized in Table 3. The results show that the presence of TPS did not affect the induced thermo-responsive mechanism of EVA.

The values reflect that the ability to recover the initial shape is excellent, showing R_r values higher than 90%. Moreover, the very high EVA ability to fix the temporary shape during the first cycle slightly decreases during the following thermo-mechanical cycles from 99% to 85%. When the TPS is added, the R_f values are maintained quite constant during all the thermo-mechanical cycles at about 88%. Moreover, the addition of the

nanoclays did not affect the optimum results for R_f and R_r values presented by the neat blends in the heating responsiveness of these blends. Besides, also the samples containing 50% of TPS reached high values in the latest cycles demonstrating that also with the highest TPS content the shape memory properties of EVA are extraordinary.

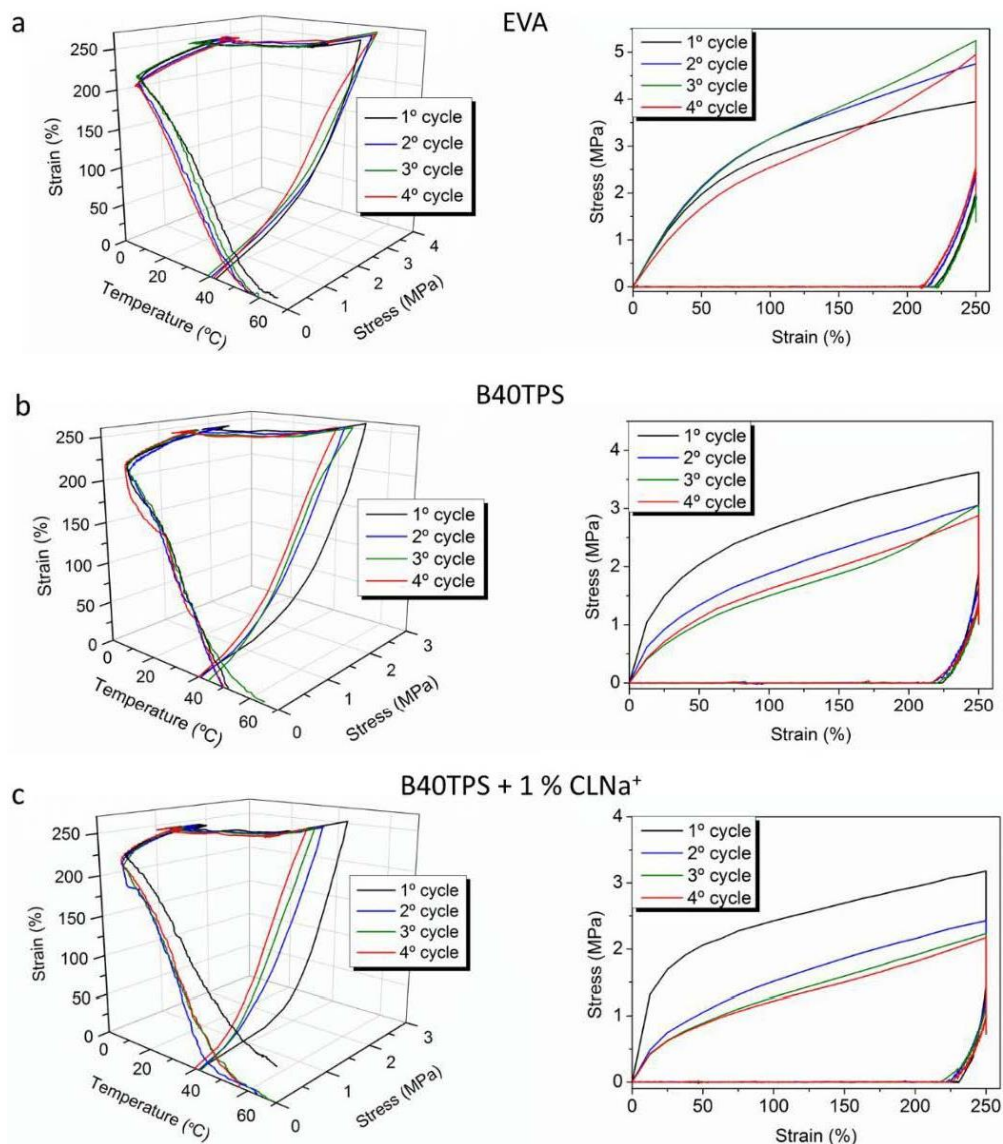


Figure 11. 3D thermo-mechanical stress-strain-temperature cycle and the 2D stress-strain diagram for (a) Neat EVA, (b) B40TPS, (c) B40TPS + 1% CLNa⁺, (d) B50TPS, (e) B50TPS + 1% CLNa⁺. Reprinted with permission from (Sessini V, Raquez J-M, Lo Re G, et al. Multiresponsive Shape Memory Blends and Nanocomposites Based on Starch. ACS applied materials & interfaces. 2016 2016/08/03;8(30):19197-19201) [40]. Copyright 2016 American Chemical Society.

Table 3. Values of R_r and R_f for the thermally-activated shape memory test for all the samples studied

Sample	R_r (%)				R_f (%)			
	1	2	3	4	1	2	3	4
EVA	94	97	97	100	99	86	89	85
B40TPS	100	100	99	100	89	87	89	87
B40TPS + 1% CLNa ⁺	98	96	97	100	91	91	88	88
B50TPS	82	99	98	100	92	89	87	90
B50TPS + 1% CLNa ⁺	81	90	100	100	93	91	89	87

Adapted with permission from (Sessini V, Raquez J-M, Lo Re G, et al. Multiresponsive Shape Memory Blends and Nanocomposites Based on Starch. ACS applied materials & interfaces. 2016 2016/08/03;8(30):19197-19201) [40]. Copyright 2016 American Chemical Society.

The analysis of the strain energy involved in the shape memory experiments was carried out for all the samples following the same procedure reported previously [58]. In fact, the strain energy of an ideal shape memory polymer was estimated taking into account that the ϵ_u overlaps with ϵ_m in the stress-strain curves, and that an ideal material is able to recover all the applied deformation. Thus, based on this hypothesis, we were able to calculate the ideal as well as the real strain energy of the samples. In Figure 12, the values of the strain energy and strain recovery ratio obtained during the different cycles are showed for all the samples.

The un-filled symbols in Figure 12 correspond to the real values and the filled ones to the ideal values. It is possible to note as the different symbols (filled and un-filled) are overlapped, thus in Table 4 the energy efficiency values are reported, as the ratio between the real and the ideal strain energies.

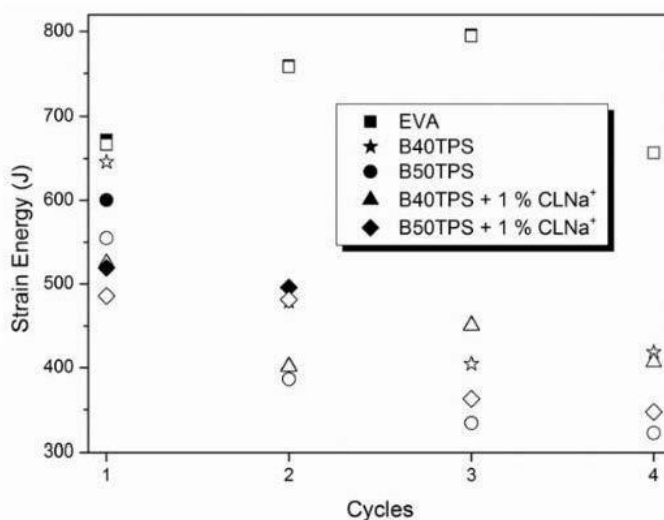


Figure 12. Strain energy for the different materials based on EVA/TPS blends.

Table 4. The values obtained for the energy efficiency for all the samples

Sample	Energy Efficiency			
	1	2	3	4
EVA	99.2	99.7	99.7	100.0
B40TPS	100.0	100.0	99.9	100.0
B40TPS + 1% CLNa ⁺	99.9	99.7	99.8	100.0
B50TPS	92.4	99.9	99.9	100.0
B50TPS + 1% CLNa ⁺	93.5	97.1	100.0	100.0

For all the samples the energy efficiency is very high after obtaining the better results for the sample B40TPS, showing values of 100% also in the first cycle. Thus, the blends and their nanocomposites present behavior almost ideal being capable to recover nearly all the deformation applied.

POLY(ETHYLENE-CO-VINYL ACETATE) RANDOM COPOLYMER/STARCH NANOCRYSTALS NANOCOMPOSITES

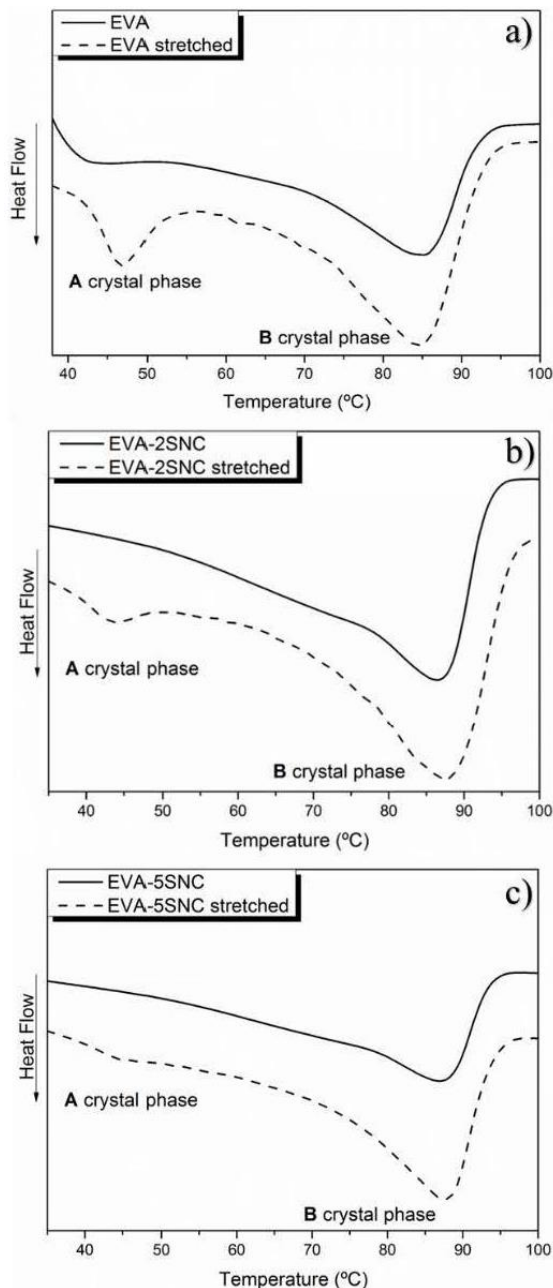
Starch nanocrystals were synthesized by acid hydrolysis applying 100 rpm of mechanical stirring at 40°C, using a silicon oil bath, for 5 days. The final suspensions were washed by successive centrifugations in distilled until reaching neutral pH. Finally, it was freeze-dried to obtain SNCs powder.

Following the same mechanism and the same procedure used for EVA-based materials previously described, thermally-activated shape memory properties were studied for EVA reinforced with 2 wt% and 5 wt% of SNCs.

In order to study the effect of starch nanocrystals on the induced-crystallization mechanism of EVA, DSC analyses were performed at the same conditions of shape memory test. The DSC thermogram related to the first heating scan of non-stretched and stretched neat EVA and its nanocomposites are reported in Figure 13. Surprisingly, increasing the amount of SNCs on EVA matrix, the stretch-induced crystallization of the A crystal phase was inhibited. The thermograms showed as the melting enthalpy of the crystalline phase A peak decreased for stretched EVA-2SNC compared to that of stretched neat EVA and much more for stretched EVA-5SNC. Indeed, for EVA-5SNC the crystal phase A was almost absent although the sample was stretched at 250% of elongation. Moreover, an increase of the melting enthalpy of crystalline phase B was observed in the nanocomposites.

This behavior and the induced-crystallization of the crystalline phase B rather than the crystalline phase A was reflected in the shape memory results. The 2D stress-strain and 3D thermo-mechanical stress-strain-temperature cycle diagram are shown in Figure 14. In order to evaluate the repeatability of the shape memory properties, different

thermo-mechanical cycles were completed for each sample. It was not possible to do more than 3 cycles because the EVA/SNC nanocomposites were broken.



Adapted with permission from (Sessini V, Raquez J-M, Lo Re G, et al. Multiresponsive Shape Memory Blends and Nanocomposites Based on Starch. ACS applied materials & interfaces. 2016 2016/08/03;8(30):19197-19201) [40]. Copyright 2016 American Chemical Society.

Figure 13. DSC thermogram of first scan of non-stretched and stretched neat EVA and its nanocomposites: a) Neat EVA, b) EVA-2SNC and c) EVA-5SNC.

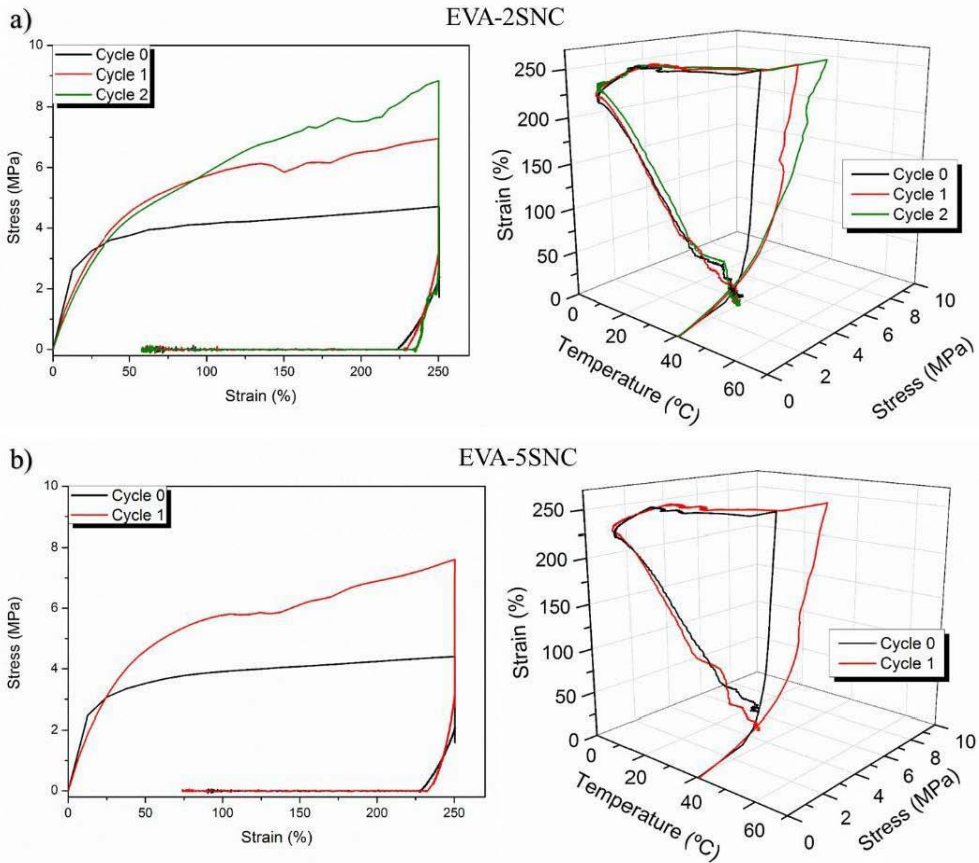


Figure 14. 2D stress-strain and 3D thermo-mechanical stress-strain-temperature cycle diagram for: a) EVA-2SNC and b) EVA-5SNC.

Observing Figure 14, it is easy to notice that after the cycle 0 (named 0 because is used to delete the thermal history of the materials and in general is not reported) the value of stress strongly increases. This is due to the progressive increase of the B crystal phase, which is able to fix more toughly the permanent network formed by amorphous EVA, SNCs and B crystal phase. The values obtained in every cycle for both the R_r and the R_f are summarized in Table 5. The results showed that the presence of SNCs affected the thermo-responsiveness of EVA based on induced-crystallization mechanism.

Table 5. Values of R_r and R_f for the thermally-activated shape memory test of the samples studied

Sample	R_r (%)			R_f (%)		
	0	1	2	0	1	2
EVA	96	94	97	90	99	96
EVA-2SNC	73	77	77	92	94	96
EVA-5SNC	64	70	-	94	95	-

The values reflected that the ability to recover the initial shape decrease when the amount of SNCs increase into the EVA matrix, showing R_r values of 20% less for EVA-2SNC and almost 30% less for EVA-5SNC compared to neat EVA. Contrarily, the high EVA ability to fix the temporary shape did not undergo any significant change though the amount of SNCs increased into the EVA matrix.

FINAL REMARKS

In brief, shape memory polymers are a special class of smart materials capable to memorize and to recover, triggered by an external stimulus, their original shape from a temporary shape programmed by mechanical deformation.

This chapter focuses the attention on polymeric nanocomposite systems with shape memory response due to their scientific and technological relevance.

In particular, three different systems were studied based on ethylene copolymers such as Nucrel® and Surlyn® reinforced with silica nanoparticles, blends of EVA/thermoplastic starch reinforced with natural bentonite and EVA reinforced with starch nanocrystals. The three different studied systems present very good shape memory ability and the addition of well dispersed nanoparticles affects positively the shape memory response of the neat matrices.

ACKNOWLEDGMENTS

Authors thank Spanish Ministry of Economy, Industry and Competitiveness, MINEICO, (MAT2017-88123-P) and the Regional Government of Madrid (MULTIMAT-CHALLENGE, S2013/MIT-2862) for the economic support. LP acknowledges MINEICO for the “Ramon y Cajal” (RYC-2014-15595) contract. Authors thanks also CSIC for the I-LINK project, I-LINK1149. JMR is a FRS-FNRS research associate.

REFERENCES

- [1] Wei, Z; Sandstroröm, R; Miyazaki, S. Shape memory materials and hybrid composites for smart systems: Part I Shape memory materials. *Journal of Materials Science*, 1998, 33(15), p. 3743-3762.
- [2] Koerner, H; et al., Polymer design for high temperature shape memory: Low crosslink density polyimides. *Polymer*, 2013, 54(1), p. 391-402.

- [3] Rousseau, IA. Challenges of shape memory polymers: A review of the progress toward overcoming SMP's limitations. *Polymer Engineering & Science*, 2008, 48(11), p. 2075-2089.
- [4] Sessini, V; et al., Humidity-Activated Shape Memory Effects on Thermoplastic Starch/EVA Blends and Their Compatibilized Nanocomposites. *Macromolecular Chemistry and Physics*, 2017, 218(24).
- [5] Navarro-Baena, I; et al., Design of biodegradable blends based on PLA and PCL: From morphological, thermal and mechanical studies to shape memory behavior. *Polymer degradation and stability*, 2016, 132, p. 97-108.
- [6] Arrieta, MP; Sessini, V; Peponi, L. Biodegradable poly(ester-urethane) incorporated with catechin with shape memory and antioxidant activity for food packaging. *European Polymer Journal*, 2017, 94, p. 111-124.
- [7] Peponi, L; et al., Thermally-activated shape memory effect on biodegradable nanocomposites based on PLA/PCL blends reinforced with hydroxyapatite. *Polymer degradation and stability*, 2018, 10.1016/j.polymdegradstab.2018.02.019.
- [8] Wang, CC; et al., Cooling-/water-responsive shape memory hybrids. *Composites science and technology*, 2012, 72(10), p. 1178-1182.
- [9] Sessini, V; et al., Humidity-activated shape memory effect on plasticized starch-based biomaterials. *Carbohydrate polymers*, 2018, 179, p. 93-99.
- [10] Lee, YM; Kim, SH; Cho, CS. Synthesis and swelling characteristics of pH and thermoresponsive interpenetrating polymer network hydrogel composed of poly (vinyl alcohol) and poly (acrylic acid). *Journal of Applied Polymer Science*, 1996, 62(2), p. 301-311.
- [11] Lendlein, A; et al., Light-induced shape memory polymers. *Nature*, 2005, 434(7035), p. 879.
- [12] Liu, Y; et al., Review of electro-active shape memory polymer composite. *Composites science and technology*, 2009, 69(13), p. 2064-2068.
- [13] Navarro-Baena, I; Kenny, JM; Peponi, L. Thermally-activated shape memory behaviour of bionanocomposites reinforced with cellulose nanocrystals. *Cellulose*, 2014, 21(6), p. 4231-4246.
- [14] Odent, J; et al., Ultra-stretchable ionic nanocomposites: From dynamic bonding to multi-responsive behavior. *Journal of Materials Chemistry A*, 2017, 5(26), p. 13357-13363.
- [15] Odent, J; et al., Shape memory Behavior of Polylactide/Silica Ionic Hybrids. *Macromolecules*, 2017, 50(7), p. 2896-2905.
- [16] Mather, PT; Luo, X; Rousseau, IA. Shape memory polymer research. *Annual Review of Materials Research*, 2009, 39, p. 445-471.
- [17] Heuchel, M; et al., Relaxation based modeling of tunable shape recovery kinetics observed under isothermal conditions for amorphous shape memory polymers. *Polymer*, 2010, 51(26), p. 6212-6218.

- [18] Karger-Kocsis, J. Biodegradable polyester-based shape memory polymers: Concepts of (supra) molecular architecturing. *Express Polymer Letters*, 2014, 8(6), p. 397-412.
- [19] Olalla, A; et al., Smart Nanocellulose Composites With Shape memory Behavior, in *Multifunctional Polymeric Nanocomposites Based on Cellulosic Reinforcements*, 2016, Elsevier. p. 277-312.
- [20] Peponi, L; Navarro-Baena, I; Kenny, J. Shape memory polymers: properties, synthesis and applications, in *Smart polymers and their applications*, 2014, Elsevier. p. 204-236.
- [21] Bellin, I; Kelch, S; Lendlein, A. Dual-shape properties of triple-shape polymer networks with crystallizable network segments and grafted side chains. *Journal of Materials Chemistry*, 2007, 17(28), p. 2885-2891.
- [22] Lendlein, A; Kelch, S. Shape-memory polymers. *Angewandte Chemie International Edition*, 2002, 41(12), p. 2034-2057.
- [23] Pandini, S; et al., One-way and two-way shape memory behaviour of semi-crystalline networks based on sol-gel cross-linked poly (ϵ -caprolactone). *Polymer*, 2013, 54(16), p. 4253-4265.
- [24] Luo, H; et al., Novel Biodegradable Shape Memory Material Based on Partial Inclusion Complex Formation between α -Cyclodextrin and Poly (ϵ -caprolactone). *Biomacromolecules*, 2008, 9(10), p. 2573-2577.
- [25] Tan, LS; Wang, DH. *Multifunctional crosslinkers for shape memory polyimides, polyamides and poly (amide-imides) and methods of making the same*, 2015, Google Patents.
- [26] Gordon, M; Taylor, JS. Ideal copolymers and the second-order transitions of synthetic rubbers. I. Non-crystalline copolymers. *Journal of Chemical Technology and Biotechnology*, 1952, 2(9), p. 493-500.
- [27] Pilate, F; et al., Shape memory polymers for multiple applications in the materials world. *European Polymer Journal*, 2016, 80, p. 268-294.
- [28] Bidsorkhi, HC; et al., Preparation and characterization of ethylene-vinyl acetate/halloysite nanotube nanocomposites. *Journal of Materials Science*, 2015, 50(8), p. 3237-3245.
- [29] Peponi, L; et al., Processing of nanostructured polymers and advanced polymeric based nanocomposites. *Materials Science and Engineering R: Reports*, 2014, 85(1), p. 1-46.
- [30] Sessini, V; et al., Processing of edible films based on nanoreinforced gelatinized starch. *Polymer degradation and stability*, 2016, 132, p. 157-168.
- [31] Sonseca, Á; et al., Mechanical and shape memory properties of poly(mannitol sebacate)/cellulose nanocrystal nanocomposites. *Journal of Polymer Science, Part A: Polymer Chemistry*, 2014, 52(21), p. 3123-3133.

- [32] Mujica-Garcia, A; et al., Poly (lactic acid) melt-spun fibers reinforced with functionalized cellulose nanocrystals. *RSC Advances*, 2016, 6(11), p. 9221-9231.
- [33] Peponi, L; et al., Smart Polymers, in *Modification of Polymer Properties*, 2016, p. 131-154.
- [34] Rajisha, K; et al., Preparation and characterization of potato starch nanocrystal reinforced natural rubber nanocomposites. *International journal of biological macromolecules*, 2014, 67, p. 147-153.
- [35] Chen, Y; et al., Comparative study on the films of poly (vinyl alcohol)/pea starch nanocrystals and poly (vinyl alcohol)/native pea starch. *Carbohydrate polymers*, 2008, 73(1), p. 8-17.
- [36] Li, X; et al., Mechanical, barrier and morphological properties of starch nanocrystals-reinforced pea starch films. *Carbohydrate polymers*, 2015, 121, p. 155-162.
- [37] Darder, M; Aranda, P; Ruiz-Hitzky, E. Bionanocomposites: a new concept of ecological, bioinspired, and functional hybrid materials. *Advanced Materials*, 2007, 19(10), p. 1309-1319.
- [38] Henderson, AM. Ethylene-vinyl acetate (EVA) copolymers: a general review. *IEEE Electrical Insulation Magazine*, 1993, 9(1), p. 30-38.
- [39] Alakrach, A; et al. Thermal properties of ethyl vinyl acetate (EVA)/montmorillonite (MMT) nanocomposites for biomedical applications. in *MATEC Web of Conferences*, 2016. EDP Sciences.
- [40] Sessini, V; et al., Multiresponsive Shape Memory Blends and Nanocomposites Based on Starch. *ACS applied materials & interfaces*, 2016, 8(30), p. 19197-19201.
- [41] Nöchel, U; et al., Triple-Shape Effect with Adjustable Switching Temperatures in Crosslinked Poly [ethylene-co-(vinyl acetate)]. *Macromolecular Chemistry and Physics*, 2014, 215(24), p. 2446-2456.
- [42] Li, F; et al., Shape memory effect of ethylene–vinyl acetate copolymers. *Journal of Applied Polymer Science*, 1999, 71(7), p. 1063-1070.
- [43] Li, J; Rodgers, WR; Xie, T. Semi-crystalline two-way shape memory elastomer. *Polymer*, 2011, 52(23), p. 5320-5325.
- [44] Wu, X; Huang, W; Tan, H. Characterization of shape recovery via creeping and shape memory effect in ether-vinyl acetate copolymer (EVA). *Journal of Polymer Research*, 2013, 20(8), p. 150.
- [45] Gao, F; Beyer, G; Yuan, Q. A mechanistic study of fire retardancy of carbon nanotube/ethylene vinyl acetate copolymers and their clay composites. *Polymer degradation and stability*, 2005, 89(3), p. 559-564.
- [46] Sengupta, R; et al., A review on the mechanical and electrical properties of graphite and modified graphite reinforced polymer composites. *Progress in polymer science*, 2011, 36(5), p. 638-670.

- [47] Bidsorkhi, HC; et al., Mechanical, thermal and flammability properties of ethylene-vinyl acetate (EVA)/sepiolite nanocomposites. *Polymer Testing*, 2014, 37, p. 117-122.
- [48] Zanetti, M; et al., Synthesis and thermal behaviour of layered silicate–EVA nanocomposites. *Polymer*, 2001, 42(10), p. 4501-4507.
- [49] Morlat-Therias, S; et al., Polymer/carbon nanotube nanocomposites: influence of carbon nanotubes on EVA photodegradation. *Polymer degradation and stability*, 2007, 92(10), p. 1873-1882.
- [50] Varley, RJ; Shen, S; van der Zwaag, S. The effect of cluster plasticisation on the self healing behaviour of ionomers. *Polymer*, 2010, 51(3), p. 679-686.
- [51] Varley, RJ; van der Zwaag, S. Towards an understanding of thermally activated self-healing of an ionomer system during ballistic penetration. *Acta Materialia*, 2008, 56(19), p. 5737-5750.
- [52] Francesconi, A; et al., Comparison of self-healing ionomer to aluminium-alloy bumpers for protecting spacecraft equipment from space debris impacts. *Advances in Space Research*, 2013, 51(5), p. 930-940.
- [53] Lewis, CL; Dell, EM. A review of shape memory polymers bearing reversible binding groups. *Journal of Polymer Science Part B: Polymer Physics*, 2016, 54(14), p. 1340-1364.
- [54] Eisenberg, A; Navratil, M. Ion clustering and viscoelastic relaxation in styrene-based ionomers. IV. X-ray and dynamic mechanical studies. *Macromolecules*, 1974, 7(1), p. 90-94.
- [55] Tachino, H; et al., Dynamic mechanical relaxations of ethylene ionomers. *Macromolecules*, 1993, 26(4), p. 752-757.
- [56] Wakabayashi, K; Register, RA. Morphological origin of the multistep relaxation behavior in semicrystalline ethylene/methacrylic acid ionomers. *Macromolecules*, 2006, 39(3), p. 1079-1086.
- [57] Zhao, Z; et al., Three-Dimensional Printed Shape Memory Objects Based on an Olefin Ionomer of Zinc-Neutralized Poly (ethylene-co-methacrylic acid). *ACS applied materials & interfaces*, 2017, 9(32), p. 27239-27249.
- [58] Peponi, L; et al., Synthesis and characterization of PCL–PLLA polyurethane with shape memory behavior. *European Polymer Journal*, 2013, 49(4), p. 893-903.

Chapter 3

SHAPE-MEMORY NANOCOMPOSITES FOR MULTI-RESPONSIVE POLYMER MATERIALS

Antoniya Toncheva^{1,2,}, Florence Pilate¹,
Philippe Dubois¹ and Jean-Marie Raquez^{1,*}*

¹Laboratory of Polymeric and Composite Materials,
Center of Innovation and Research in Materials And Polymers,
University of Mons, Mons, Belgium

²Laboratory of Bioactive Polymers, Institute of Polymers,
Bulgarian Academy of Sciences, Sofia, Bulgaria

ABSTRACT

Shape-memory polymers (SMPs) are currently a subject of tremendous attention from both - the academic and industrial fields and are playing a major role in inspiring the design of a class of polymer materials. Their attractive properties related to multi-step shape-changing upon exposure to an appropriate stimulus, as well as high elastic deformation, low density, relatively low cost, ease of processing, chemical stability and biocompatibility make SMPs suitable for numerous real world applications. As if that's not enough, fabricating nanocomposites *via* the incorporation of nanofillers offers the possible applications as innovative materials with designed functionalities and multi-responsiveness even further. Nowadays, these polymer materials can be used as biomedical devices (implants, sutures, stents, drug delivery systems), actuator systems, sensors or deployable hinges for automotive, electronics and aerospace industries. In this chapter, a short description on SMPs chemical architecture, nanofillers incorporation and approaches for 3D printing are outlined. The content would also mention some potential application of the printed parts and final critical remarks.

* Corresponding Author Email: antoniya.toncheva@umons.ac.be;
jean-marie.raquez@umons.ac.be.

Keywords: shape-memory polymer, shape-memory composite, nanofiller, smart materials, 3D-printing

INTRODUCTION

1. General Overview

1.1. Historical Prologue

The study of the technological development of humanity has been a subject of passionate discussion, leading to the definition of different stages - from most primitive to present day. This vision was proposed by a Danish archaeologist named Christian Jürgensen Thomsen (1788-1865) who suggested that no one would have used stone tools once their bronze equivalent had been produced. Respectively, nobody would have used the bronze tools while iron tools were available. Today, there is little doubt that, the use and discovery of new materials has been a major factor in the development of human civilization. Traditional structural materials like wood, glass, steel, iron, and others, are still plentifully used. Slowly yet steadily, over the years new functional materials have appeared to replace them. As one of those newcomers, synthetic materials were developed by the relatively young plastic industry, but in 1989 the manufacturing of plastics managed to finally surpass even steel production [1] giving the birth of the current “Smart Materials” age [2] (Figure 1).

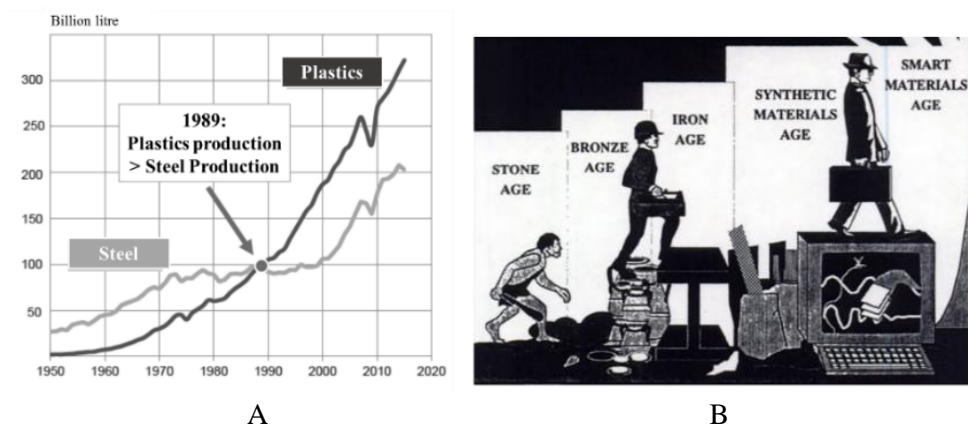


Figure 1. Volumetric comparison between steel and plastics production between 1950 and 2015 [Plastics Europe Market Research group] [1] (A) and caricature of the Human evolution relative to the materials growth [2] (B).

1.2. Shape-Memory Materials

Shape-memory materials (SMMs) are a new class of smart materials including shape-memory alloys (SMAs), polymers (SMPs), hybrids (SMHs), ceramics (SMCs) and gels (SMGs) (Figure 2). They carry a very interesting main characteristic - they can memorize a second (temporary) shape in addition of their original shape, while still being able to revert to the state of origin exposed to an appropriate stimulus.

This behavior - called a shape-memory effect (SME) was mentioned for the first time in a patent from Vernon in 1941. The invention relied upon the “elastic memory” of a synthetic resin and the listed application was molding of dental objects [4]. Later in the 1960s, cross-linked polyethylene with new shrinking properties was a subject of another patent by Rainier [5].

This work gave the possibility to produce at industrial level heat shrinkage tubing and films, later successfully commercialized without being actually recognized as SMPs. In the late 1980s, the CDF Chimie Company (France) developed the polynorbornene-based SMPs, followed by another significant scientific effort only 10 years after - the discovery of polyurethane-based SMPs by Mistubishi Heavy Industries Ltd.

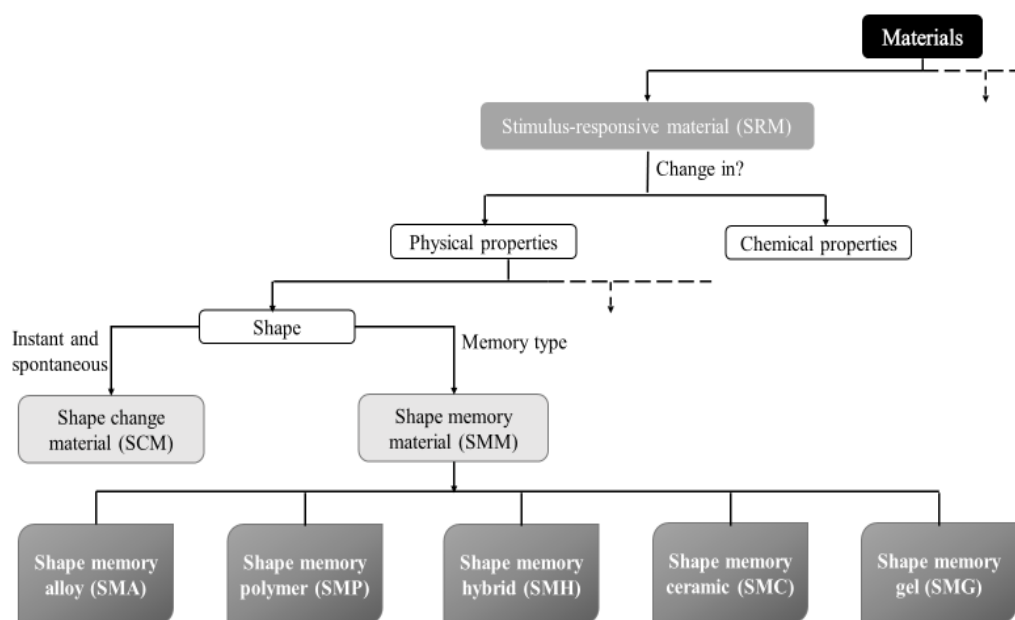


Figure 2. Classification of different SMMs [3].

1.3. Shape-Memory Polymers and Nanocomposites

In this historical context, out of the different SMM classes, SMPs have enjoyed a remarkable interest from both scientific and industrial community, and are consistently studied in the literature as evidenced by an increasing number of publications over the last twenty-five years [6-10] (Figure 3). A very likely reason for this focused interest are

the multitude of interesting qualities those materials possess - a low density, relatively low cost, high potential of recyclability and processing, transparency, high recoverable strain within a wide range of stimuli, chemical stability and modification, biocompatibility and various degradation rate of biodegradability [3]. Remarkably, SMPs can even be programmed for (multi)stimuli-responsiveness and recover their initial shape upon direct or Joule heating, heating from radiation and laser source heating, microwaves [11, 12], pressure-responsive [13], moisture, solvent or solvent vapors [14], as well as change in the pH values [15]. With all those advantages, however, come several severe limitations - a low tensile strength and stiffness, stimuli-responsive actuation restricted mostly to heat-related treatment and an absence of proper function. We could also add to the list relatively low thermal conductivity, low stiffness and high SME inertness to external stimuli (light and electro-magnetic) during actuation procedures.

One promising strategy to overcome these difficulties is the incorporation of one or more (in)organic nanofillers (nanotubes, nanofibers, nanospheres, nanorods, etc.) within the SMPs polymer matrix, thus giving origin to the shape-memory nanocomposites (SMNCs) [16, 17]. Due to their high specific surface area, high stiffness and inherent functionalities (electrical conductivities, water-responsive, etc.) the nanofillers play the role of reinforcement agents leading to an all around improvement of the physico-mechanical, thermal, mechanical and electrical properties of the materials [18]. Subsequently, it is possible to confer to the materials the desired multi-stimuli-responsiveness and functionalities enlarging the field of their potential application as smart textiles [19], medical [20] and flexible electronic devices [21], sensor and actuators [22], high performance water-vapor permeability membranes [23], self-deployable structures [24, 25], filaments for 3D printing [26] and many others. As of late, SMNCs have gained already attention in the production of innovative polymer materials as confirmed by the number of published scientific articles (Figure 3).

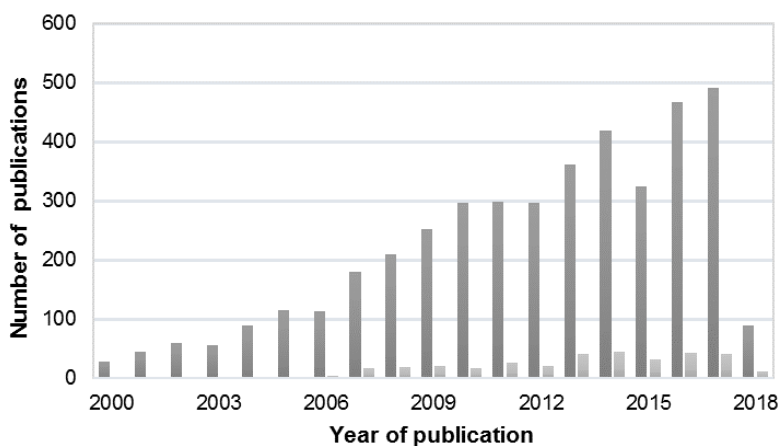


Figure 3. Number of scientific publications per year on the SMPs (darkest bars) and SMNCs (brighter bars). The data research was made on Scopus®, Elsevier B.V. on February 2018.

In the frame of this chapter, a brief review of the SMPs chemical architecture and recent trends in the field is presented with particular focus on SMNCs their structure, shape-memory effects and working mechanism.

2. SMPs for Multi-Responsive Materials

2.1. Definitions and Generalities

Accepted by the scientific community, SMPs are described as polymers capable to memorize a permanent shape, to acquire a temporary one upon deformation during the programming step and to revert back to their original shape when an appropriate stimulus is applied during the recovery step (Figure 4). The capacity of the polymer for recovery from a fixed shape to the initial one is defined as the SME [27]. This effect can be reversible upon subsequent programming process and quantified by the fixity ratio (R_f) or the capacity of the polymer to fix the temporary shape and the recovery ratio (R_r) related to its possibility to reach the original shape [28].

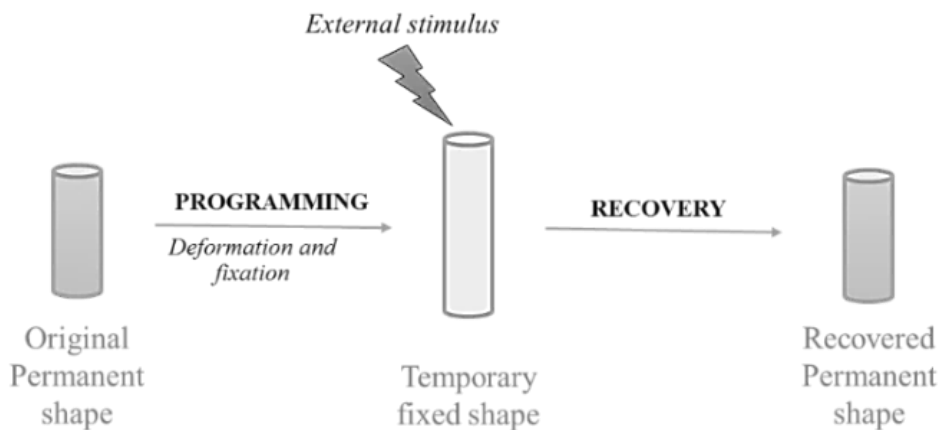


Figure 4. Schematic illustration of SME.

The SME is not an intrinsic property of the polymers but rather results from the combination between a particular polymer morphology (switching and permanent domains) and a stimulus program. To elaborate, a key element is the predefined arrangement between the polymer structure/morphology and the applied programming process [29]. In general, the SMP chemical architecture results in the coexistence of a permanent and a switching domain: the former is made of chemical or physical cross-links [interpenetrated network (IPN) [30-32] or interlocked cyclodextrin supramolecular complex [33-35]] and the latter of stimuli sensitive fragments (crystallization/melting transition, vitrification/glass transition or liquid crystal anisotropic/isotropic transition in

the case of heating-responsive SMPs) [36] (Figure 3). The fixation of the temporary shape and the shape recovery to the initial one results in so-called controlled reversible triggered switches (reversible molecule cross-linking and a supramolecular association/dissociation). In all types of actuations, the entropic elasticity of the polymer network is a driving force for the shape recovery process [37].

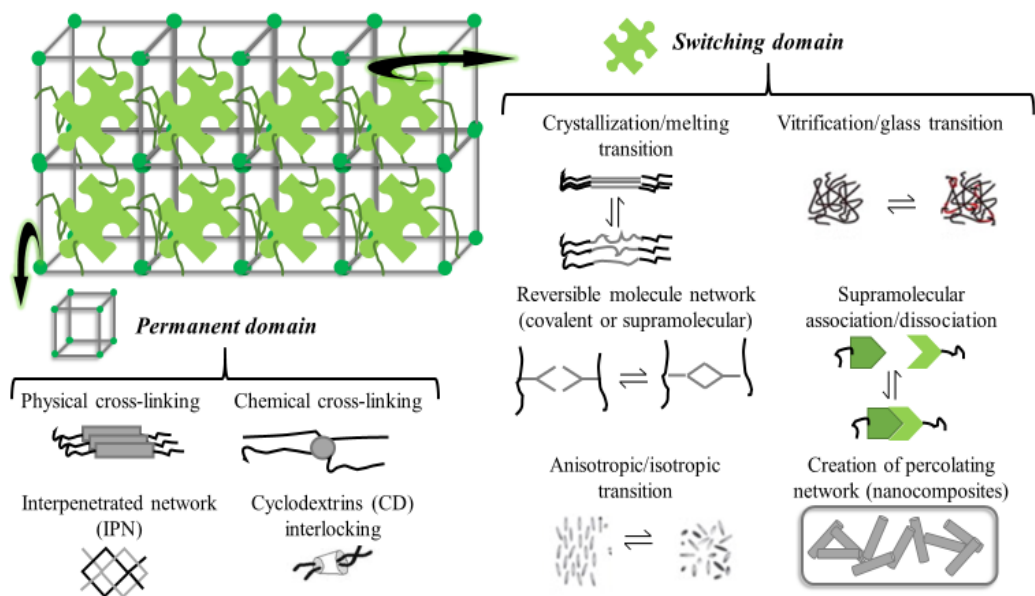


Figure 5. General presentation of SMP chemical architecture and permanent and switching domain building blocks concept.

Most of the SMPs systems are characterized with “one-way” (1W-SME) heating-triggered response in relation to their thermal transitions [glass transition temperature (T_g) and melting temperature (T_m)]. “Two- (2W-SME) and multi-way” polymers are the subject of several studies for their ability to change reversibly their shape with multi-stimuli responsiveness, thus offering an even greater to design polymer actuators [38]. This could be of interest for artificial muscles fabrication as well as devices with multiple degree of freedom for endoscopic surgery application and obtained from: cross-linked semi-crystalline polymers [39-42], nematic liquid-crystalline elastomers [43, 44], and glass-forming polydomain nematic networks [45]. Usually, the actuation phenomenon occurs during the heating and cooling step by reversible chain conformations in presence or absence of external stress. Polymer devices with actuator behavior were described by Chung et al. for poly(cyclooctene) (PCO) films covalently cross-linked by dicumyl peroxide [42].

2.2. Polymeric Actuators

Previously, it was reported that the “2W-SME” of the semi-crystalline thermosets can be easily controlled by adjusting the degree of the polymer matrix cross-linking [46]. Using a working temperature close to the material T_m it was possible to increase the strain during the cooling step revealing the reversible shape effect. In addition, when the sample was heated upon constant stress, a tensile contraction of the PCO appeared responsible for the shape recovery similar to the one observed before crystallization. More complex systems based on crystallization induced elongation and melting induced contraction phenomena were described for multiphase polymer networks [star-precursors of poly(pentadecalactone) (PPDL) and PCL] [47] (Figure 6). Potentially interesting, thermo-reversible cross-linked PCL-based PU networks with pronounced “2W-SME” were reported by Raquez et al. in 2011 using reactive extrusion as technology of choice [48]. The main advantage of the used Diels-Alder cycloaddition reactions (between furan and maleimide moieties), was the easy control of the microstructure and the cross-linking density by partially replacing PCL-diol with PCL-tetraol. This SME can be also obtained without applying a constant stress as in the case of a multiphase copoly(ester-urethane) network made of, at least, two semi-crystalline polyester segments (PCL and PPDL) [49]. Another strategy is to form an internal skeleton based on crystallites huddled in nano-clusters playing the role of physical network and adjusting the degree of actuation of the domains [50]. For this purpose, cross-linked poly[ethylene-*co*-(vinyl acetate)] (cPEVA), with a broad T_m (in the range from 25°C to 90°C), allowed the formation of two types of polyethylene (PE) crystallites. By taking advantage of the presence of two T_m it was possible to actuate step by step the device: lower T_m defined as the actuation domain (from $T_{m,onset}$ to intermediate T_m) and the other thermal transition was activated by the upper range (from the intermediate T_m to $T_{m,offset}$). As a result, the main network was created after applying a certain stress directly after the cooling step ($T_{m,onset}$, 25°C). Another strategy is the design of IPN combining the crystalline component of PCL (switching domain) and the elastomer poly(tetramethylene ether)glycol (PTMEG) acting as a spring [51]. In this case Pre-IPN was first obtained by previously dissolving macromonomers and cross-linkers in dimethylformamide, leading to the production of photo-crosslinked acrylate-PCL. Stretching the resulted gel-like structure and the subsequent curing/cooling step of the PTMEG at 80°C allowed the formation of the elastomeric network.

The reheating of the sample allowed the PCL to melt by “opening of the switch.” Then the PTMEG underwent a compression movement and the polyester segment can crystallize upon cooling following the “spring direction.” With this example, the authors demonstrated the possibility to build tension-free 2W-SMP systems for artificial muscles or tendon application (Figure 7).

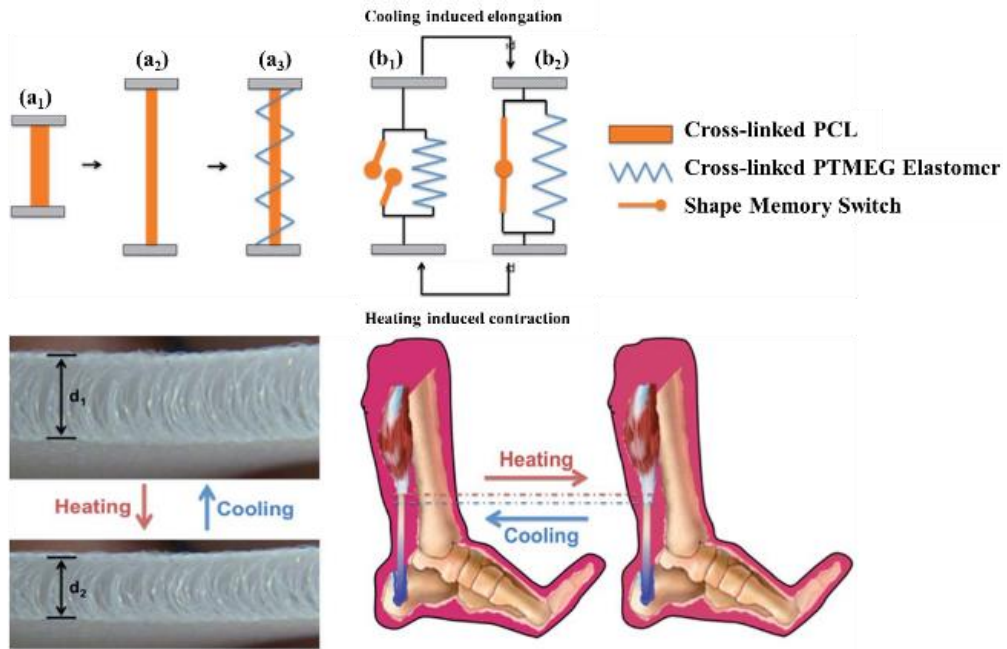


Figure 7. “2W-SME switch spring” actuated system for artificial muscles or tendon application; a₁ - cross-linked PCL, a₂ - stretched fixed PCL, a₃ - cross-linked PTMEG, b₁ - compressed shape, b₂ - elongated shape [51].

3. Multi-Responsive SMNCs

In the previous section, one of the more common and convenient way to actuate the SMP materials was described - direct sample heating or increasing the environmental temperature. However, this is not really suitable for all applications. An elegant strategy to increase the sample temperature is to incorporate functional nanofillers into the SMP matrix. In this way it will be possible to convert various energy (electrical, magnetic, optical, acoustic or chemical) to heat and to act on the thermal transitions of polymer devices. In the following section, the possibility to produce temperature- or magnetic field-memory, as well as water-sensitive SMPs is outlined and some of the potential applications are pointed out.

3.1. SMNCs Containing Carbon-Based Nanofillers

Up to date, one of the most studied SMPs materials are the electrically conductive polymeric nanocomposites. They can be easily obtained by the incorporation of nanofillers capable to convert the electrical current into heat through Joule effect such as: single-walled carbon nanotubes (SWCNTs), multi-wall carbon nanotubes (MWCNTs), carbon nanofibers (CNFs), carbon nanopaper, aligned conductive carbon-based nanofillers, carbon black (CB) and graphene.

Carbon nanotubes is the most promising reinforcement materials, capable of carrying a current density as high as 1×10^9 amp/cm² [52] while showing good flexibility compared to conventional fibers [53]. The good overall performance of electrically conductive SMNCs is directly related to the dispersion of the nanofillers in the polymer matrix, the interaction with the polymer chains and the establishing of the percolation network. In return, this affects the materials' final mechanical and thermal properties and restricts their potential applications. In order to overcome said difficulties, several strategies have been developed: (i) direct blending of the (MW)CNTs with the polymer, (ii) (MW)CNTs surface-modification (improvement of the interfacial interactions with the polymer macromolecules), (iii) cross-linking the (MW)CNTs with the polymer matrix, (iv) alignment of the (MW)CNTs in the polymer material or (v) conversion of the (MW)CNTs into nanopaper or film and its incorporation within the polymer system [54].

In most cases, the direct (MW)CNTs blending approach with the polymer matrix cannot avoid entirely the formation of nanofiller aggregates (lack of functional sites on the conductive nanofillers surface capable to interact with the polymer matrix). A good workaround is to prepare films and yarns, as paper-like (MW)CNTs films (nanopapers). Those are self-supporting networks of entangled CNTs hold together by Van der Waals interactions at the tube-tube junctions. Lu et al. described such three-dimensional self-assembled MWCNTs nanopaper developed using hydrophilic polycarbonate membrane synthesized by controlled pressure vacuum deposition [55]. The obtained highly conductive continuous and compact network was combined with styrene-based SMP, thus facilitating the electrically heating of the nanocomposite. It was of interest to remark that the electrical stimulation (35 V) allowed to drive up a 5 g mass object from 0 to 30 mm in height (Figure 8A) and the material acted as a sensor that responded to the changes in degree of humidity (the electrical resistivity of materials increased with the water content in the sample after immersion). Macromolecular self-assembled MWCNTs structures offer an opportunity to produce percolating conductive network for sensors, controllable devices and deployable structures application [56]. However, an even better dispersion of the nanofillers can be achieved by their surface chemical modifications as reported by Raja et al. [57]. In the PU-based nanocomposites the morphological characterization of the materials revealed good dispersion level for the due to the improved interfacial interaction between the polymer macromolecules and the MWCNTs. Moreover, the PU/PVDF films got improved tensile strength and dynamic storage modulus, as well as good electrical and thermal conductivity. The shape-memory behavior of "U" shaped structures showed R_f of 95% upon constant voltage (40 V).

Another set of SMNCs with good performance indicators were obtained using triethanolamine-functionalized MWCNTs (TEA-f-MWCNTs, MWCNTs up to 2 wt%) by using hyperbranched polyurethanes (HPU) as polymer matrix [58]. Taking advantage of the strong interfacial interaction of TEA-f-MWCNTs with the PU chains (hydrogen bonding and polar-polar interactions), it was possible to reach significant thermal stability

accompanied with increased degree of crystallinity, enhanced tensile strength (28.5 MPa) and scratch resistance (7 kg). Combining two or more electrically sensitive nanofillers, such as carboxylic acid-functionalized CNTs grafted onto the CNFs and then self-assembled, was an elegant way to generate Joule heating shape recovery [59].

Recently, the effect of epoxy-*graft*-polyoxyethylene octyl phenyl ether (EP-g-TX100) on the processing and t-SME of the novel CNT/water-borne epoxy (WEP) nanocomposites was investigated [60]. The introduction of EP-g-TX100 in homogenous way in the CNT-epoxy system renders possible the design of the SMP materials with good mechanical properties and two- and triple-shape-memory properties (Figure 8B). Surface (MW)CNTs decoration with metals (Cu, Fe, Ag and Pt) was yet another promising and simple method to nanoreinforce and electrically actuate the SMNCs (Cu-CNT were incorporated in polylactic acid (PLA)/epoxidized soybean oil [61], Fe-MWCNTs and Ag-MWCNTs in PUs [62], combining them with boron nitride [63] or coating of the electrical nanofillers with conductive polymer (polypyrrole-coated MWCNTs) [64].

An effective way to enlarge the practical applications of nanotubes is to assemble them into highly aligned structures for electroactive polymer (EAP) actuator systems [65]. One of the most important classes of EAPs are the electrothermal actuators (ETAs), due to having low driving voltage and being electrolyte-free. Large-area CNT buckypaper (BP, layers of aligned CNT array) as flexible electrode for CNTs loaded double-layer ETA (BP and polydimethylsiloxane layers) has already been studied [66]. It was established that directional control ETAs bending is possible: bending to the BP sides along the length direction of the U-shaped electrodes, and larger deformation of the horizontally cut actuator (CNTs alignment perpendicular to the U-shaped BP band; Figure 9A). This concept gave the idea for potential bionic actuation similar in behavior acting to a human-hand with long service life (Figure 9B).



Figure 8. Electrically actuated SMNCs containing (MW)CNTs [55, 60].

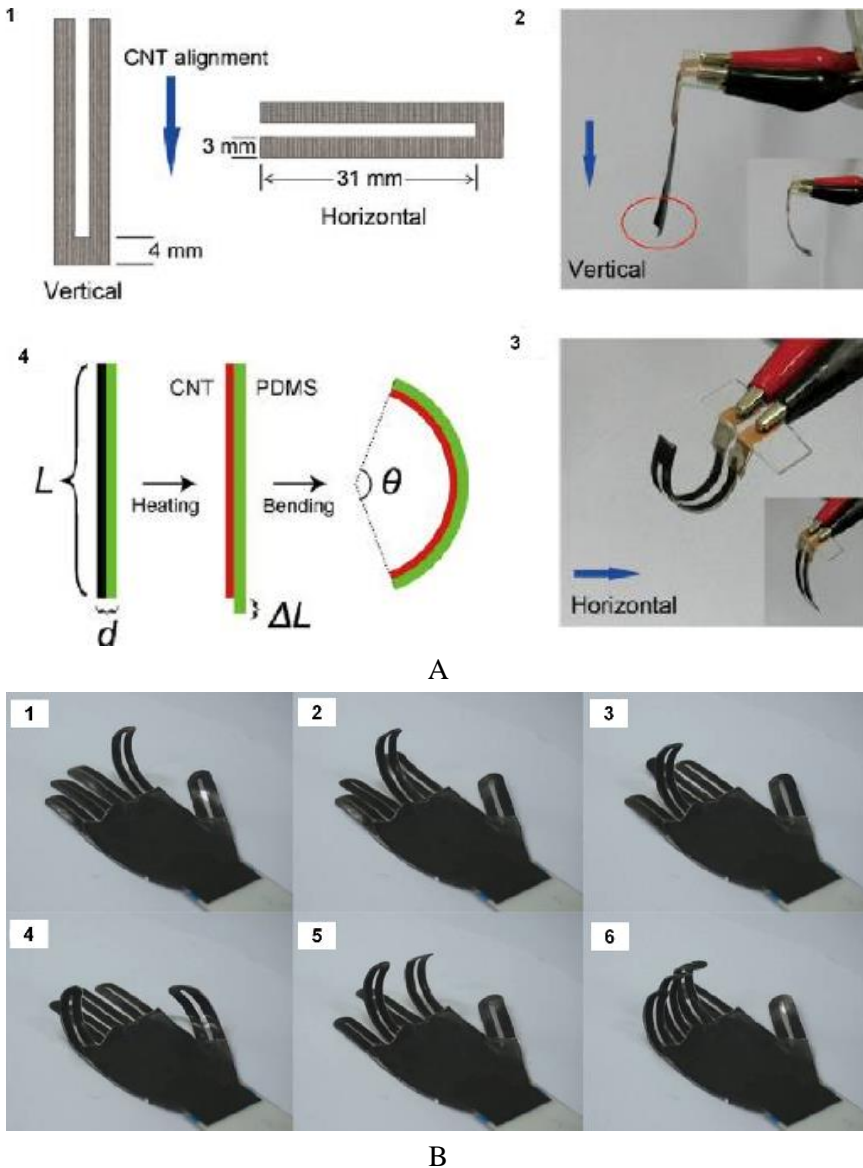


Figure 9. SMNCs bilayer structure containing A nanopaper and actuated under electrical current and B [66].

CNFs are also remarkable with their excellent thermal and electrical conductivity, but better interfacial bonding can be obtained after their surface oxidation [67]. Good dispersion of these nanofillers can be achieved by high-power sonication or by *in situ* polymerization and lamination onto styrene-based SMPs [22, 68]. Incorporating them in continuous way resulted in epoxy-based SMNCs with high-speed electrical actuation [69]. Here, of importance was the fiber morphology, as well as the nanoscale dimensioning providing the percolating conductive network.

The reinforcement of the polymer matrix and the maintenance of stable physical cross-linking polymer structure was achieved by using CB as nanofiller [70]. Often, loaded with another conductive nanofiller it is homogeneously dispersed and serves as interconnections between carbon fibres [71] or in direct interaction with MWCNT nanopaper and nickel nanostrand [72]. The resulting SMP materials showed great improvement in electrical and thermal conductivity.

The last discussed nanofiller in this section is graphene with chemical properties similar than these of the nanotubes and structure similar with layered nanoclay. It was incorporated by direct mixing with the polymer matrix for PVA water-induced SMP [73], preparation of polymer blends with embedded functionalized graphene (self-healing materials) [74] or PCL-click coupling with graphene sheet (enhanced mechanical and recovery properties) [75]. The synergistic effect of these nanofillers enhanced the bonding between carbon fiber and SMP matrix *via* Van der Waals and covalent cross-links.

3.2. SMNCs with Incorporated Noble Metals

Due to their large specific surface area and strong surface plasmonic resonance (SPR) properties, nanosized noble metals structures such as silver (Ag) and gold (Au) nanoparticles (NPs), nanorods (NRs), nanowiskers (NWs) and nanowires (NWrs) are of great interest for the production of a new generation multi-responsive SMNCs. These structures offer the advantage of absorbing specific wavelength in the range from deep UV to near IR light and to convert remotely the light energy to heat energy (photo-thermal effect) in a non-invasive way. Inspired by these particular properties, a new trend started in the design of SMP materials with a focus on proper wavelength activation and local shape actuation.

3.2.1. SMNCs with Incorporated Gold Nanofillers

During the last decade, Au NPs demonstrated their great potential as not only systems for optically controllable SME but also as agents conferring self-healing properties (SHP) to the polymer materials [76]. Based on their high efficiency, the authors showed that the incorporation of small amount of poly(ethylene glycol)methyl ether functionalized Au NPs (0.003 wt%) to a cross-linked poly(ethylene oxide) (PEO) films was sufficient to grant photo-thermally induced healable and SME properties to the films. Digital images of the self-healing and the light-induced shape recovery process are presented in Figure 10A. Light-sensitive nanocomposites based on poly(β -amino esters) containing Au NRs have been recently developed and presented SME upon local irradiation with IR light and subsequent heating above the polymer T_g and remained cytocompatibility with cells while having mild inflammatory response [77] [78]. Based on published data, it is likely that the near-IR light-sensitive SMP materials can find

biomedical application since the applied irradiation is capable of penetrating body tissue without damaging it.

Au NRs can also be used with great success in the design of light-guided smart windows, light-tracking solar panels, actuators and others. Zheng et al. produce light-responsive SMP micropillar arrays containing PEGylated Au NRs (up to 0.2 mol%) by applying poly(dimethylsiloxane) molding procedure [79]. By simply modifying and playing with the surface topology (bent-temporary shape or unbent micropillar arrays-permanent shape), it is possible to govern the film optical properties: from opaque (bent pillars) to transparent (straight pillars) upon local laser irradiation (5 sec, wavelength of 532 nm; power of 0.3 W, respectively). Material unidirectional wetting was achieved by covering SMP pillars with thin film of Au or Au-palladium [80]. Using small amount of Au NPs (0.5 wt%) enables also the controlled SPR absorption by cross-linked PEO matrix. Multi-step shape recovery was done by the formation of a temperature gradient in the temporary shape inducing anisotropic polymer chain relaxation and strain energy release [81], Figure 10B. By taking advantage of the anisotropic structure of the NRs it was possible to play on the light polarization angle for effective photo-thermal shape control as in the case of PVA/Au NRs (nanofillers of 0.02 wt%) films [82].

3.2.2. SMNCs with Incorporated Silver Nanofillers

As a metal-ligand coordination system, silver can be successfully used for the production of physical cross-linking SMPs structures. In this direction Wang et al. described SMNCs containing Ag ions (3 wt%)-coordination polymer network (isonicotinate-functionalized polyester (PIE) and the pyrazinamide groups) [83]. The degree of cross-linking, rigidity and shape recovery were modulated by simply controlling the amount of the absorbed ions. Moreover, SMP were considered as suitable for smart wound dressings or implants with antibacterial properties against *Escherichia coli* and cytocompatibility with osteoblast cells (Figure 11A).

With their high thermal and electrical conductivity Ag NWs offer a possibility to produce metallic nanotubes, stretchable and transparent conducting electrodes and semiconductors, organic light-emitting diodes, organic solar cells, touch screens, electrochemical devices, etc. [84]. A major issue in this system is the achievement of homogeneous nanofiller dispersion for conductive percolating network formation. A novel approach in the design of SMNCs are multilayer structures such as bilayer from Ag NWs and SMPUs [85, 86]. Of great interest was the fact that the bilayer was flexible and highly conductive (DC voltage of 1.5 V) sufficient to turn on the LED upon strain stretching (elongation less than 12% and resistance of 200 Ω /sq), while the fast electro-responsive shape recovery is based on the Joule effect heating. In this context, deformable electronic devices are of interest for wearable displays, solar panels and

non-invasive biomedical devices fabrication subjects of large deformation to cope with body movements. Recently, Ag NWrs were used for highly flexible and transparent SMP bilayer electrodes (diameter of 60 nm and length of 6 μm) made of cross-linked polyacrylate-based light-emitting diodes [87]. The programming of the materials was a result of the shape-memory properties of the cross-linked network upon either compressive strain (bent up to 16% without significant resistance changes) or upon tensile strain (accompanied by a slight resistance increase). In comparison to the classical used indium-doped tin oxide (ITO) anode, the Ag NWrs/polyacrylate electrodes demonstrated slightly higher efficacy of 14 cd/A.

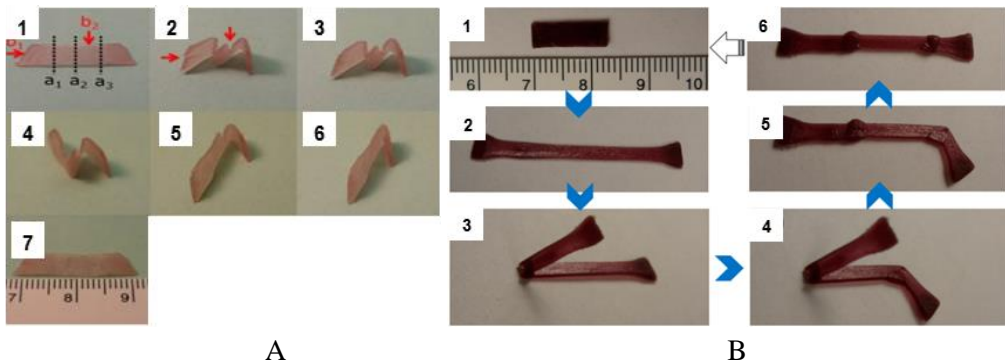
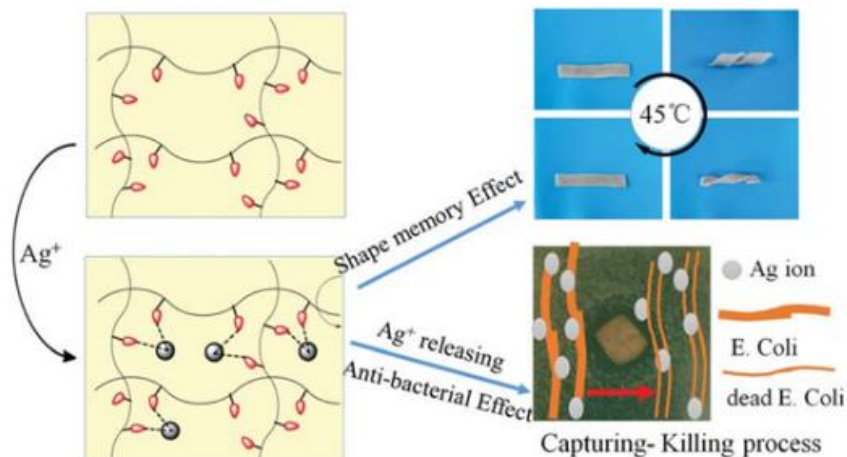


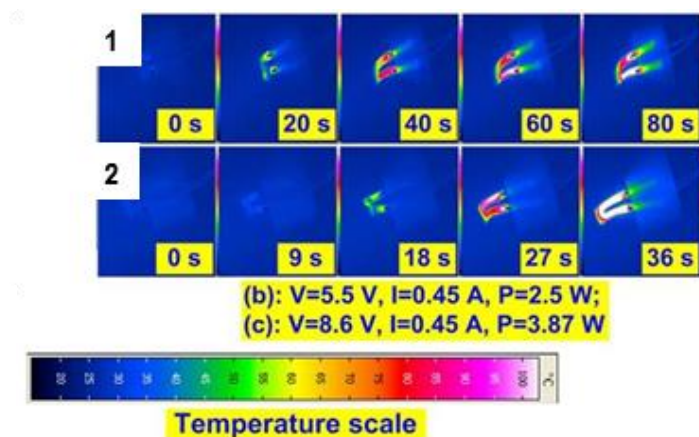
Figure 10. SMNCs materials containing Au nanofillers.

SMNCs embedded with Ag can be of interest for the flexible solar modules (polymer solar cells or semi-transparent solar cells in windows) concept [88]. The nanofiller morphology was a key element for the devices performances (Ag NWrs length) [89]. In their study, Yu et al. showed that (length of 4-10 μm) led to the production of devices with high filling factor (FF or nanowires high surface coverage) but was accompanied with low photo-current (loss of transmittance). In contrast, long Ag NWrs (length above 20 μm) were responsible for high photo-current but lower FF.

Several studies have dealt with the concept of combining multiple nanofillers in one multilayer SMNC for final synergetic effect [90, 91]. Indeed, epoxy-based thermoset SMP resin possessed enhanced electro-thermal properties and electro-activated shape recovery performance, where Ag NPs were decorated graphene oxide (GO) assembly grafted onto carbon fibers. The guiding force for the material shape recovery, resulted in Joule-heating induced process: the self-assembled GO grafted onto the carbon fibers acted as a Joule-heat-carrying layer and the Ag-NPs-decorated GO decreased the thermal dissimilarity and facilitate heat-transfer from the carbon fiber to the polymer matrix. As presented in Figure 11B(2), the SME was faster for nanofiller containing films (36 sec, DC of 8.6 V with temperature range above the polymer T_g).



A



B

Figure 11. SMNCs materials containing Ag nanofillers.

3.3. SMNCs with Incorporated Metal Oxide Nanofillers

Magnetically addressable SMPs are another interesting system, where magnetic NPs play the role of inductive heaters offering the possibility to remotely trigger the shape [92]. This kind of stimuli is of particular importance for the design of biomedical devices where it becomes possible to achieve a noncontact harmless activation of the polymer parts without heating the surround tissue [93]. Good candidates in this section are the iron oxides (Fe_3O_4) NPs, characterized with good biocompatibility and high magnetism. A whole set of possible applications opens up - the fabrication of drug targeting systems, magnetic resonance imaging for clinical diagnosis, recording materials catalysts, magnetically controlled smart implants, etc.

To overcome the general problem of NPs homogeneous dispersion in the material, their surface can be somewhat (non)covalently modified in order to enhance their miscibility within the material and create nanoscale net-points in the polymer matrix. Fe₃O₄ NPs produced from co-precipitation (divalent and trivalent iron salts) using PEG-10000 as dispersing surfactant were uniformly loaded in the biocompatible poly(D,L-lactide) (PDLLA/Fe₃O₄ weight ratios of 1:1, 2:1, 3:1). The key element in this step was the hydrogen bonding between Fe-OH group of Fe₃O₄ and C=O of the polyester resulting in enhanced tensile properties and SME activated upon alternating magnetic field (frequency of 20 kHz and strength of 6.8 kA/m) [94]. Fe₃O₄ NPs (up to 20 wt%) can be synthesized by co-precipitation method by modifying their surface with oleic acid. A clear improvement of the PLLA mechanical properties in terms of elastic modulus, tensile strength and elongation at break was noticed. The authors demonstrated that the shape recovery ratio in PLLA/Fe₃O₄ (nanofiller content 10 wt%) and the recovery speed in an alternating magnetic field were lower than the one in water at 70°C (Figure 13A) [95]. In the literature, PCL as biocompatible polymer was used for the production of cross-linked thermo- and magnetic-sensitive materials [96, 97]. The addition of Fe₃O₄ was done with the aim to accelerate the materials degree of degradation taking advantage from the hydrophilic nature of the NPs promoting the hydrolysis of the polymer ester bonds. Consequently, SMP permanent domain was altered affecting directly the SME performance. The perspective of implants fabrication with desired life time and shape-memory properties was then demonstrated.

In this aspect, non-toxic, biocompatible and highly hydrophilic polymers such as poly(ethylene glycol) (PEG) or poly(vinyl alcohol) (PVA) can be used as second switching segment to create thermo- and water-triggered SMPs appropriate for biomedical applications. What is more, it was possible to confer magnetically-responsive properties to these systems by adding Fe₃O₄ PEG-modified NPs (5 and 10 wt%) within the polymer matrix with excellent R_f and R_r ratio suitable for biomedical applications where the direct heating of the material is avoided (electrical current between 400 and 450 A, frequency of 166 kHz; Figure 12).

The idea of NPs chemical modification was explored also by Bai et al. by developing a one-pot synthesis of norbornene-capped super-paramagnetic iron oxide NPs. Successfully, the nanofillers were then integrated (up to 20 wt%) into polynorbornene by ring-opening metathesis polymerization of norbornene [98]. As described by the authors, the aim of the NPs functionalization acted as cross-links and magnetic-induction heaters in the macromolecular network architecture. The nanocomposites had a super-paramagnetic response, with saturation magnetization of around 2 and 5 emu/g for the nanocomposites with 10 and 20 wt% Fe₃O₄, respectively.

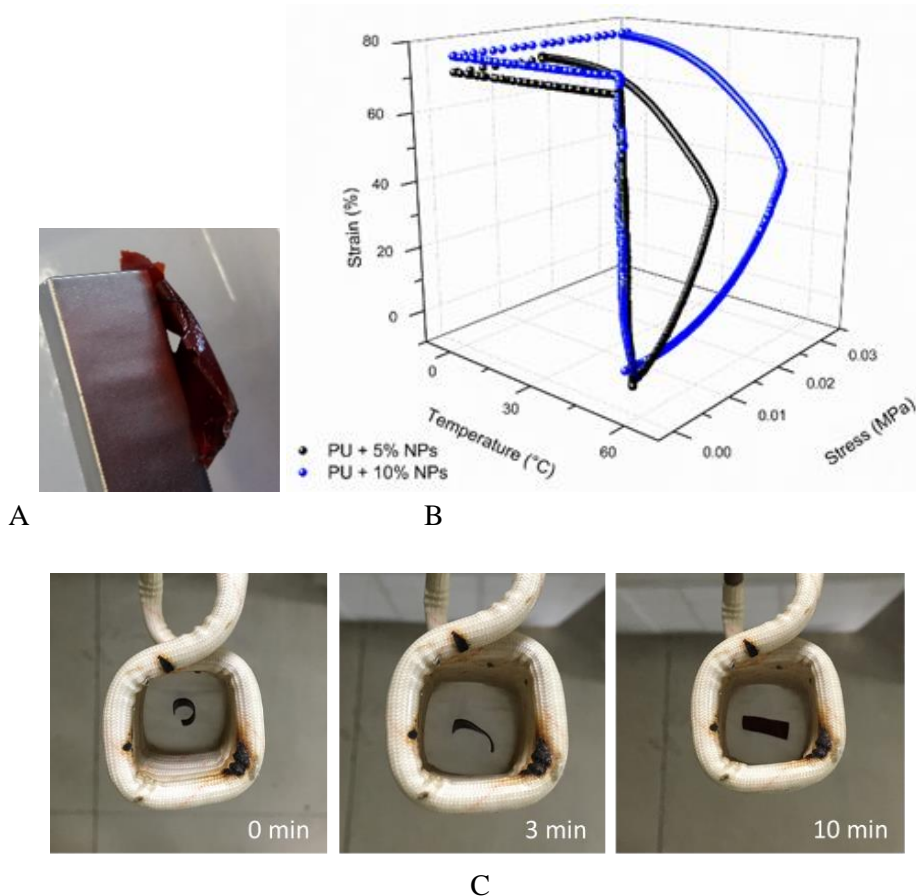


Figure 12. PCL/UPy-based PU materials containing Fe_3O_4 -PEG modified NPs with magnetic (A), shape-memory (B) properties activated upon magnetic field (C).

As an effective cross-linking agent Fe_3O_4 NPs was also used for the preparation of the polyPMMA-PEG SMP this time prevented their displacement and reaggregation in the matrix [99]. This setup granted enhanced mechanical properties to the materials accompanied with uniform heat-generation and heat-transfer upon exposure to an alternating magnetic field, when compared to the dispersed NPs. Another approach for better NPs dispersion is to directly graft oligomers on the NPs surface. Good example is the study of Schmidt et al. where oligo(ϵ -caprolactone)-grafted Fe_3O_4 superparamagnetic NPs were incorporated into thermosets of oligo(ϵ -caprolactone)dimethacrylate/butyl acrylate: the material recovered its original straight shape in 20 sec (magnetic field frequency of 300 kHz and power of 5.0 kW) [100].

The idea to combine two or more nanofillers in the material was explored also in the case of magnetically triggered devices. In 2014 Li et co-workers obtained SMNCs using biodegradable and biocompatible chemically cross-linked PCL with allyl alcohol as polymer matrix and Fe_3O_4 in order to decorate conductive MWCNTs (Fe_3O_4 @M) as a magnetism and electricity responsive source [101]. Covering the outside of the MWCNTs

with magnetic layer enhanced the magnetic properties while the non-coated MWCNTs were responsible for the electric properties of the multi-stimuli responsive material [hot water, magnetic field (frequency of 20 kHz and strength of 6.8 kA/m) and electric field (60 V); Figure 13A]. In addition, the use of semi-crystalline polyester allowed the 2W-reversible shape-memory capabilities when temperature above and below the T_m are applied.

One more group of interesting NPs are the TiO_2 for their semiconductor and photocatalytic properties, as well as photo-stability in solution, redox selectivity and strong oxidizing power. Up to date, only a few studies focus on the incorporation of TiO_2 NPs for SMNCs fabrication. In the study of Iijima et al. surface-modification of the nanofillers with anionic surfactant is proposed (anionic head group and organic chains are branched into a hydrophobic alkyl and a hydrophilic PEG chain ended by a polymerizable vinyl group) [102]. TiO_2 NPs with the conferred surfactant complex properties gave then stable suspensions in various organic solvents (alcohols, nitriles, ketones and acetates) and polymers [epoxy resin and poly-(methylmethacrylate) resin]. Afterwards, the obtained TiO_2 /epoxy nanocomposites were activated via direct heating. Surface-modification of the metal oxide NPs were also done by ring-opening polymerization of ϵ -caprolactone (g - TiO_2) in order to ensure a good dispersion in the polyester matrix of poly(L-lactide-*co*- ϵ -caprolactone) (PLCL). Further physical cross-linking, between the polymer chains of g - TiO_2 and PLCL (TiO_2 of 5 wt%), gave enhanced mechanical properties [103].

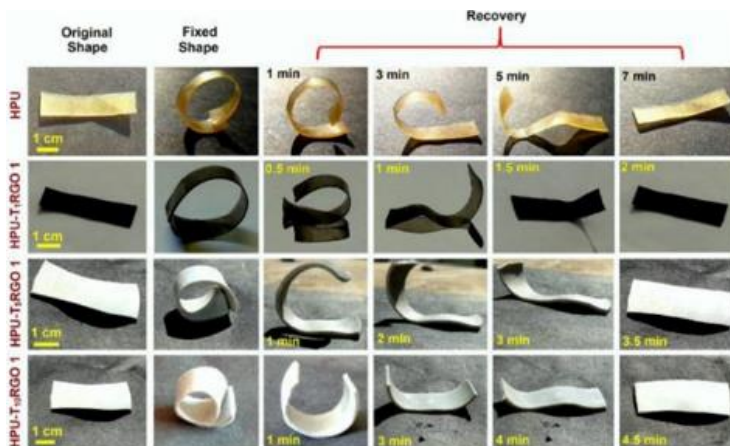
Great challenge in the SMNCs chemical architecture is the production of multi-functional materials with shape-memory, SHP and self-cleaning properties (SCP) upon sunlight exposure. Recently it was reported that the combination of TiO_2 NPs and reduced graphene oxide (RGO; up to 1 wt%) can tune easily the materials properties [104]. The high light absorbing capacity of RGO and its energy transfer allowed the heating of the HPU system (close to its T_m) under sunlight exposure and rapid shape recovery (R_r of 91-95%) was recorded (Figure 13B). Here, the nanoreinforced phenomena significantly improved tensile strength, tensile modulus, toughness and elongation at break of the nanocomposites. Of importance in this case was the good dispersion of the nanofiller, its miscibility and interfacial interactions with the polymer chains (presence of hydroxyl groups and polar Ti-O groups).

In the field of metal oxide particles, zinc oxide (ZnO) are attracting also attention for their physical and chemical properties, such as high chemical and photo-stability, good electrochemical coupling coefficient and broad range of radiation absorption. This filler is frequently used for sensor, energy generator and photocatalyst in hydrogen production based on its piezo- and pyroelectric properties. In the literature few articles discuss the ZnO SMNCs dealing with imidazole-zinc ion coordinated shape-memory hydrogel [105], triple-shape-memory poly (acrylonitrile 2-methacryloyloxyethyl phosphorylcholine) based on the dipole-dipole-zinc ion coordination [106] or epoxy-based SMP containing

metallo-supramolecular unit formed by coordinating 2,6-bis(*N*-methyl-benzimidazolyl)-pyridine ligands to zinc di[bis(trifluoromethylsulfonyl)-imide] [107], ZnO NRs in PU matrix [108, 109].



A



B

Figure 13. SMNCs materials containing Fe_3O_4 and TiO_2 NPs as nanofillers. Cross-linked PCL SMPs containing Fe_3O_4 decorated with conductive MWCNTs actuated under thermal, magnetic and electrical stimulus (A) [101] and HPU SMNCs materials loaded with TiO_2 NPs with self-healing and shape recovery properties (B) [104].

3.4. SMNCs Containing Cellulose Nanocrystals

Interesting biocompatible nanoreinforcing nanofillers are the cellulose nanocrystals (CNCs, known also as cellulose nanowiskers). This is mainly due to their anisotropic structure (high aspect ratio), renewable resources and stiffness [110]. They are also characterized with relatively low cost, low density, wide bioavailability, renewability and unique physico-chemical properties [111] [112]. The presence of hydroxyl groups in the chemical structure offers a possibility to form supramolecular interactions based on

hydrogen bonding (e.g., SMP higher-modulus as a result of the interconnected CNCs in the polymer matrix) responsible for the water-induced SME. The potential application of such SMNC is reserved for the biomedical field as self-tightening sutures and self-retractable and removable vascular stents fabrication. However, the preparation of nanocomposites by direct incorporation of CNCs into the polymeric matrix remains difficult due to the poor affinity between the hydrophilic nanofiller and the polymer chains. Often the result ends up being an insignificant increase or in some cases a failure to improve the materials physico-mechanical properties.

Interesting approach for the production of thermo-responsive and water-responsive SMNCs by using CNCs as a cross-linking agent is described by Liu et al. [113]. The nanocrystals were chemically bonded *via* their hydroxyl groups to low molecular 4,4-diphenylmethane diisocyanate end-functionalized PCL and PEG. The biocompatible nanocomposite from PEG[60]-PCL[40]-CNC[10] demonstrated excellent thermo- and water-induced SME (R_r of 85%) as presented in Figure 14A. Here, the shape recovery properties depended on the polymer degree of crystallinity and the materials degree of cross-linking.

It is of importance to notice that the CNCs gave the unique possibility to produce water-sensitive SME mechanism which is totally athermal in comparison to traditional systems where water (or other solvent) is used as plasticizers in the idea to lower the polymer T_g . Water-activated mechanically adaptive PU SMNCs with incorporated CNCs have been described in the literature with enhanced mechanical properties (nanofiller content above the percolation limit) [115]. In this flow of ideas, in 2012 Zhu et al. reported an effective strategy to design elastomeric thermoplastic PU/CNCs-based materials with rapid SME response as a result of the successful combination between the nanofiller percolation network (chemo-mechanical adaptability) and the entropic elasticity of the elastomer [116]. The obtained materials were suitable for design of breathable clothing and medical devices triggered by human body liquids. PU-based materials with enhanced tensile strength and the Young's modulus (up to 1040% and 4400%, respectively), were produced from biodegradable poly(glycerol sebacate urethane) (PGSU) were also reported in the literature. This time the nanocrystals were grafted along the polymer macromolecule: CNCs got competed with the -OH groups from PGS prepolymer and reacted with the isocyanate groups of hexamethylene diisocyanate [117]. Blending poly(ethylene glycol)-poly(ϵ -caprolactone)-based polyurethane (PECU) with functionalized CNCs (pyridine moieties CNC-C₆H₄NO₂) can lead to the production of pH-responsive films [114]. The switching units of the materials had attractive interactions from the hydrogen bonding between pyridine groups and hydroxyl moieties: at low pH value the interactions were reduced or disappeared as a result of the pyridine groups protonation (Figure 14B). The final results showed a possibility to produce new smart polymer material (biomaterials, smart actuators, and sensors). CNCs were also incorporated as a hard segment in thermoplastic PU

bionanocomposites [118]. Resulting in thermodynamic incompatibility, between both PU soft/hard segments, microphase separation was obtained and two main T_m transitions were designed. The incorporation of the CNCs led to an increase in the hard phase-degree of crystallinity and improvement of the storage modulus and the shape recovery performances. In other reported data, only 5 wt% CNCs were sufficient to six-fold increase in Young's modulus and five-fold improvement in toughness of poly(mannitol sebacate) making them suitable for biomedical applications as soft tissue engineering scaffolds [119]. In addition, the ureido-pyrimidinone [UPy(OH)₂] have the ability to highly dimerize and therefore elaborate a dynamic supramolecular network based on hydrogen bonding in PCL-based PU matrix materials. Introducing CNCs into the PU matrix will allow us the complementary hydrogen bonds with UPy in order to elaborate efficient SMNP-based materials.

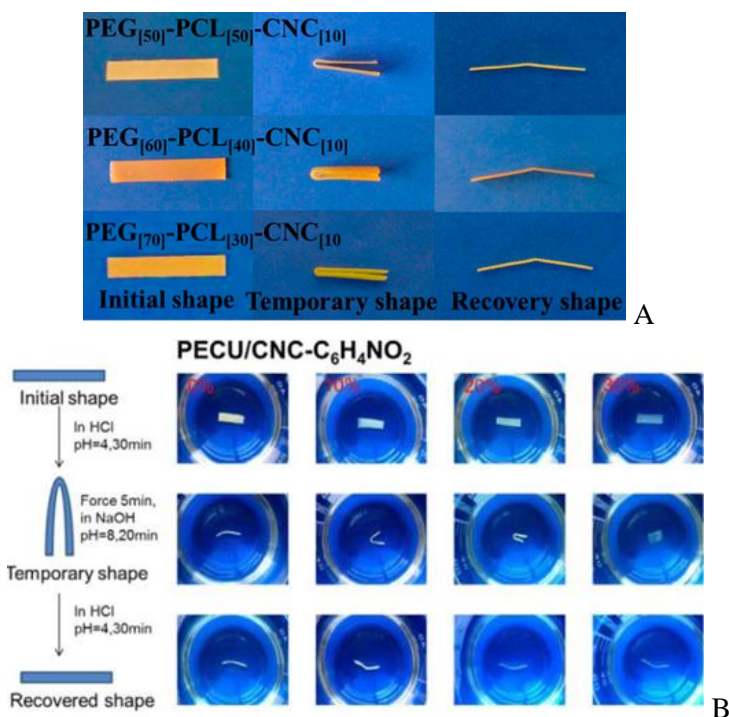


Figure 14. SMNCs materials containing CNCs: (A) Thermo-responsive shape recovery behavior of the PEG-PCL-CNC nanocomposites when heated in oven at 60°C and (B) digital photos of the shape memory process of PECU/CNC-C₆H₄NO₂ film with different CNC-C₆H₄NO₂ loading immersed in HCl (pH 4) and NaOH (pH 8) solution at room temperature [113] and [114].

In this chapter the authors presented the nanofillers most often used to trigger the polymer materials SME. In the literature SMPs can be reinforced by the incorporation of microfibers, fabrics and Kevlar mats, carbon or glass fibers. Their high elastic modulus, strength and characteristic structural morphology are remarkable and lead to enhanced mechanical load while maintaining the transvers direction [120]. The potential

application of such SMNCs can be suitable for spacecraft self-deployable and vibration control structures [121-123]. Exfoliated nanoclays as part of the hard phase have also positive impact on the materials mechanical properties [124-126]. This is also the case of SiC and SiO₂ and of cross-linking agent with PCL [127] or coupling with SMPU chains [128].

3.5. SMP as Smart 3D Printed Materials

During the last decade the scientific and technological progress has inspired the emergency of exciting 3D printing prototype technologies. As part of the additive manufacturing, stereolithography (SLA) and fused deposition modeling (FDM) techniques, have offered the possibility to expand the polymer materials application at industrial level. Combining the variety of chemical approaches to incorporate functional nanofillers within the polymer matrix and the SMPs “1W-, 2W-” and multi-shape properties, a new trend in the world of material design. SMP quickly found a key place for design of complex deployable structures. Of particular interest is the 4D printing technology where the fourth dimension was added in order to describe the material's transformation (change shape, functionality or properties over time once triggered by an external stimulus) over time [129, 130]. SLA was successfully used as method to use SMP as start material for highly elastic, transparent and electroconductive hydrogels for soft robotics application. [131], composite hydrogels with magnetic responsiveness [132], materials for biocompatible 3D scaffolds as tissue engineering for mesenchymal stem cells culturing [133] or medical devices such as vascular or tracheal stents [134] or methacrylated polycaprolactone precursor, respectively [135]. Materials with tunable SME can be also designed by another method - FDM. Filaments appropriate for 3D printing application from non-commercially available polymers with good processability are now a fact. Rapid prototyping, specific topological structuration and nanodomains formation with long relaxation times of the supramolecular crosslinks [136], as well as devices for object catching and transportation [26] or biomimetic solar tracking sensors or smart solar cell systems [137] can be obtained. The SMP 3D printing approach at structural and material design level is discussed in detail in Chapter 15 of the present book and the readers are kindly invited to consult its contents.

FUTURE DIRECTIONS AND CHALLENGES

SMPs open the door to the production and design of new generation of polymer materials with multi-responsiveness. The possibility to introduce functional nanofillers in the structures offer the unique advantage to enlarge the polymer's application in the yet unexplored field of the practical daily use. Based on current insights, several future directions and related challenges may be considered:

1. The incorporation of different nanostructured fillers in the SMP-matrix allows the enhancement of the materials mechanical properties (unfortunately, staying close to the relatively poor properties of origin). Additional efforts are needed to optimize the nanofillers dispersion and the materials characteristics (structural fatigue, relaxation, creep and duration);
2. Fabrication of biocompatible and biodegradable SMPs medical devices is of great interest for human health. Even if a great range of devices can be produced (scaffolds for tissue engineering, implants for minimally invasive surgery procedures, self-tightening sutures, self-retractable and removable stents, drug delivery systems), the main challenges remain the materials rate of degradation (enzymatic or hydrolytic) their degree of toxicity, mechanical solicitation etc.;
3. Smart materials and structures obtained by three-dimensional manufacturing (3D printing) allow the production of SMNCs as actuators for soft robotics, self-evolving structures, anti-counterfeiting system, active origami and controlled sequential folding. Today, some technological and design limitations are still unsolved, mainly relating to the limited choice of polymers to use, multi-material components fabrication, presence of microstructural defects and materials real time adapting. In this aspect promising efforts are done applying SLA and FDM;
4. Inspired by nature, scientists have designed diverse self-cleaning, self-healing and self-adapting SMPs materials suitable for the elaboration of load-bearing aircraft components, self-cleaning and light-guided windows, flexible solar modules (polymer solar cells), smart textiles, bionic robot etc. However none of those polymer systems is commercially available at present and development of new polymers and polymer blends is still needed;
5. At industrial level, SMP materials can find potential application in automobile engineering (seat and adaptive lens assemblies, reconfigurable storage bins, airflow control devices etc.), polymer solar cells, food packaging for thermal and light sensitive products, deployable structures (reflectors, ground based deployable mirrors), smart textile (life jacket, floating wheels) and others. Yet, the direct transfer from the laboratory to industrial scale remain difficult related to the final SME complexity nature (programming step and the triggering process parameters) in addition to the required quick and versatile manufacturing process, while focusing on use of low-cost additives and ensured profit gain etc.

ACKNOWLEDGMENTS

This research has been funded by the European Commission and Région Wallonne FEDER program in the frame of 'Pôle d'Excellence Materia Nova' and OPTI2MAT program of excellence, by the Interuniversity Attraction Poles program initiated by the

Belgian Federal Science Policy Office (PAI 6/27 and P7/05) and by FNRS-FRFC. Financial support from the BEWARE (BElgium WALLonia REsearch, project convention no. 410161) Fellowships Academia programme co-funded by the COFUND programme of the European Union (FP7-Marie Curie Actions) is gratefully acknowledged. Jean Marie Raquez is a FNRS researcher associate.

REFERENCES

- [1] <http://www.plasticseurope.org/>. 2016.
- [2] Gandhi, M.V. and Thompson, B.D. (1992). *Smart Materials and Structures*. Springer Netherlands Publisher.
- [3] Sun, L., Huang, W., Ding, Z., Zhao, Y., Wang, C., Purnawali, H. and Tnag, C. (2012). Stimulus-responsive shape memory materials: a review. *Materials & Design*. 33: 577-640.
- [4] Vernon, L.B. and Vernon, H.M. (1941). *Process of manufacturing articles of thermoplastic synthetic resins*. Google Patents.
- [5] Rainer, W., Redding, E., Hitov, J., Sloan, A. and Stewart, W. (1964) *Polyethylene product and process*. US Pat. 3144398.
- [6] Huang, W.M., Ding, Z., Wang C.C., Wei, J., Zhao, Y. and Purnawali, H. (2010). Shape memory materials, *Materials Today*, 13: 54-61.
- [7] Gunes, I.S. and Jana, S.C. (2008). Shape memory polymers and their nanocomposites: A review of science and technology of new multifunctional materials. *Journal of Nanoscience and Nanotechnology*. 8: 1616-37.
- [8] Hornbogen, E. (2006). Comparison of shape memory metals and polymers. *Advanced engineering materials*, 8:101-106.
- [9] El Feninat, F., Laroche, G., Fiset, M. and Mantovani, D. (2002). Shape memory materials for biomedical applications. *Advanced Engineering Materials*, 4: 91-104.
- [10] Wei, Z.G., Sandstroröm, R. and Miyazaki, S. (1998). Shape-memory materials and hybrid composites for smart systems: Part I Shape-memory materials. *Journal of Materials Sciences*, 33: 3743-3762.
- [11] Zhang, F., Zhou, T., Liu, Y. and Leng, J. (2015). Microwave synthesis and actuation of shape memory polycaprolactone foams with high speed. *Scientific reports*, 5 (11152): 1-12.
- [12] Du, H., Song, Z., Wang, J., Liang, Z., Shen, Y. and You F. (2015) Microwave-induced shape-memory effect of silicon carbide/poly(vinyl alcohol) composite. *Sensors and Actuators A: Physical*, 228: 1-8.
- [13] Fang, Y., Ni, Y., Leo, S.Y., Taylor, C., Basile, V. and Jiang, P. (2015) Reconfigurable photonic crystals enabled by pressure-responsive shape-memory polymers. *Nature Communications*, 6(7416): 1-8

- [14] Fang, Y., Ni, Y., Choi, B., Leo, S.Y., Gao, J., Ge B, Taylor, C., Basile, V. and Jiang, P. (2015) Chromogenic photonic crystals enabled by novel vapor-responsive shape-memory polymers. *Advanced Materials*, 27: 3696-3704.
- [15] Guo, W., Lu, C.H., Orbach, R., Wang, F., Qi, X.J., Cecconello, A., Seliktar, D. and Willner, I. (2015). pH-stimulated DNA hydrogels exhibiting shape-memory properties. *Advanced Materials*, 27: 73-78.
- [16] Zhao, Q., Qi, H.J. and Xie, T. (2015). Recent progress in shape memory polymer: New behavior, enabling materials, and mechanistic understanding. *Progress in Polymer Science*, 49-50:79-120.
- [17] Leng, J., Lan, X., Liu, Y. and Du, S. (2011). Shape-memory polymers and their composites: Stimulus methods and applications. *Progress in Materials Science*.56: 1077-1135.
- [18] Lu, H., Lei, M., Yao, Yi., Yu, K. and Fu, Y. (2014) Shape memory polymer nanocomposites: nano-reinforcement and multifunctionalization. *Nanoscience and Nanotechnology Letters*, 6: 772-786.
- [19] Gök, M.O., Bilir, M.Z. and Gürcüm, B.H. (2015) Shape-memory applications in textile design. *Procedia - Social and Behavioral Sciences*, 195: 2160-2169.
- [20] Sokolowski, W., Metcalfe, A., Hayashi, S., Yahia, L. and Raymond (2007). Medical applications of shape memory polymers. *Biomedical Materials*, 2: S23-S27
- [21] Ware, T., Simon, D., Hearon, K., Liu, C., Shah, S., Reeder, J., Khodaparast, N., Kilgard, M. P., Maitland, D. J., Rennaker II, R. L. and Voit, W. E. (2012). Three-dimensional flexible electronics enabled by shape memory polymer substrates for responsive neural interfaces. *Macromolecular Materials and Engineering*, 2012(297):1193-1202.
- [22] Haibao, L., Kai, Y., Yanju, L. and Jinsong, L. (2010). Sensing and actuating capabilities of a shape memory polymer composite integrated with hybrid filler. *Smart Materials and Structures*, 19: 1-7.
- [23] Mondal, S., Hu, J. L. and Yong, Z. (2006). Free volume and water vapor permeability of dense segmented polyurethane membrane. *Journal of Membrane Science*, 280: 427-432.
- [24] Santo, L., Quadrini, F., Accettura, A. and Villadei, W. (2014). Shape memory composites for self-deployable structures in aerospace applications. *Procedia Engineering*, 88: 42-7.
- [25] Mao, Y., Yu, K., Isakov, M. S., Wu, J., Dunn, M. L., Qi, J. (2015). Sequential self-folding structures by 3D printed digital shape memory polymers. *Scientific reports*, 5(13616): 1-12.
- [26] Yang, Y., Chen, Y., Wei, Y. and Li, Y. (2016). 3D printing of shape memory polymer for functional part fabrication. *The International Journal of Advanced Manufacturing Technology*, 84: 2079-2095.

- [27] Huang, W. M., Zhao, Y., Wang, C. C., Ding, Z., Purnawali, H., Tang, J. and Zhang, L. (2012). Thermo/chemo-responsive shape memory effect in polymers: a sketch of working mechanisms, fundamentals and optimization. *Journal of Polymer Research*, 19(9952):1-34.
- [28] Behl, M. and Lendlein, A. (2007). Shape-memory polymers. *Materials Today*, 10: 20-28.
- [29] Lendlein, A. and Kelch, S. (2002). Shape-memory polymers. *Angewandte Chemie International Edition*, 41: 2034-2057.
- [30] Liu, G., Guan, C., Xia, H., Guo, F., Ding, X. and Peng, Y. (2006) Novel shape-memory polymer based on hydrogen bonding. *Macromolecular Rapid Communications*, 27: 1100-1104.
- [31] Bellin, I., Kelch, S. and Lendlein, A. (2007). Dual-shape properties of triple-shape polymer networks with crystallizable network segments and grafted side chains. *Journal of Materials Chemistry*, 17: 2885-2891.
- [32] Zhang, S., Feng, Y., Zhang, L., Sun, J., Xu, X. and Xu, Y. (2007) Novel interpenetrating networks with shape-memory properties. *Journal of Polymer Science Part A: Polymer Chemistry*, 45: 768-75.
- [33] Luo, H., Liu, Y., Yu, Z., Zhang, S. and Li, B. (2008) Novel biodegradable shape memory material based on partial inclusion complex formation between α -cyclodextrin and poly(ϵ -caprolactone). *Biomacromolecules*, 9: 2573-2577.
- [34] Luo, H., Fan, M., Yu, Z., Meng, X., Li, B. and Zhang, S. (2009) Preparation and properties of degradable shape memory material based on partial α -cyclodextrin-poly(ϵ -caprolactone) inclusion complex. *Macromolecular Chemistry and Physics*, 210: 669-676.
- [35] Zhang, S., Yu, Z., Govender, T., Luo, H. and Li, B. (2008). A novel supramolecular shape memory material based on partial α -CD-PEG inclusion complex. *Polymer*, 49: 3205-3210.
- [36] Rousseau, I. A. (2008). Challenges of shape memory polymers: A review of the progress toward overcoming SMP's limitations. *Polymer Engineering and Science*, 48: 2075-2089.
- [37] Hu, J., Zhu, Y., Huang, H. and Lu, J. (2012). Recent advances in shape-memory polymers: Structure, mechanism, functionality, modeling and applications. *Progress in Polymer Science*, 37:1720-1763.
- [38] Ionov L. (2015). Polymeric Actuators. *Langmuir*, 31: 5015-5024.
- [39] Pandini, S., Dioni, D., Paderni, K., Messori, M., Toselli, M., Bontempi E. and Riccò, T. (2016). The two-way shape memory behaviour of crosslinked poly(ϵ -caprolactone) systems with largely varied network density. *Journal of Intelligent Material Systems and Structures*, 27: 1388-1403.

- [40] Pandini, S., Passera, S., Messori, M., Paderni, K., Toselli, M., Gianoncelli, A., Bontempi, E. and Riccò, T. (2012). Two-way reversible shape memory behaviour of crosslinked poly(ϵ -caprolactone). *Polymer*, 53: 1915-1924.
- [41] Ishida, K. and Yoshie, N. (2008). Two-way conversion between hard and soft properties of semicrystalline cross-linked polymer. *Macromolecules*, 41: 4753-4757.
- [42] Chung, T., Romo-Uribe, A. and Mather, P. T. (2008). Two-way reversible shape memory in a semicrystalline network. *Macromolecules*, 41: 184-192.
- [43] Küpfer, J. and Finkelmann, H. (1991). Nematic liquid single crystal elastomers. *Rapid Communications*, 12: 717-726.
- [44] Thomsen, D. L., Keller, P., Naciri, J., Pink, R., Jeon, H., Shenoy, D and Ratna B. R. (2001). Liquid crystal elastomers with mechanical properties of a muscle. *Macromolecules*, 34: 5868-5875.
- [45] Qin, H., Mather and P. T. (2009). Combined one-way and two-way shape memory in a glass-forming nematic network. *Macromolecules*, 42: 273-280.
- [46] Liu, C., Chun, S. B., Mather, P.T., Zheng, L., Haley, E. H. and Coughlin, E. B. Chemically cross-linked polycyclooctene: Synthesis, characterization, and shape memory behavior. *Macromolecules* 35: 9868-9874.
- [47] Zotzmann, J., Behl, M., Hofmann, D. and Lendlein A. (2010). Reversible triple-shape effect of polymer networks containing polypentadecalactone-and poly (ϵ -caprolactone)-segments. *Advanced Materials*, 22: 3424-3429.
- [48] Raquez, J. M., Vanderstappen, S., Meyer, F., Verge, P., Alexandre, M., Thomassin, J. M., Jérôme, C. and Dubois, P. (2011) Design of cross-linked semicrystalline poly(ϵ -caprolactone)-based networks with one-way and two-way shape-memory properties through Diels–Alder Reactions. *Chemistry - A European Journal*, 17: 10135-10143.
- [49] Behl, M., Kratz, K., Zotzmann, J., Nöchel, U. and Lendlein, A. (2013). Reversible bidirectional shape-memory polymers. *Advanced Materials*, 25: 4466-4469.
- [50] Behl, M., Kratz, K., Noechel, U., Sauter, T. and Lendlein A. (2013). Temperature-memory polymer actuators. *Proceedings of the National Academy of Sciences*, 110: 12555-12559.
- [51] Wu, Y., Hu, J., Han, J., Zhu, Y., Huang, H., Li, J. and Tang, B. (2014). Two-way shape memory polymer with “switch-spring” composition by interpenetrating polymer network. *Journal of Materials Chemistry A.*, 2: 18816-18822.
- [52] Yao, Z., Kane, C. L. and Dekker, C. (2000). High-field electrical transport in single-wall carbon nanotubes. *Physical Review Letters*, 84: 2941-2944.
- [53] Iijima, S., Brabec, C., Maiti, A. and Bernholc, J. (1996). Structural flexibility of carbon nanotubes. *The Journal of Chemical Physics*, 104: 2089-2092.

- [54] Lu, H., Yao, Y. and Lin, L. (2013). Carbon-based reinforcement in shape-memory polymer composite for electrical actuation. *Pigment & Resin Technology*, 43: 26-34.
- [55] Lu, H., Liu, Y., Gou, J., Leng, J. and Du S. (2011). Surface coating of multi-walled carbon nanotube nanopaper on shape-memory polymer for multifunctionalization. *Composites Science and Technology*, 71: 1427-1434.
- [56] Lu, H. and Gou J. (2012). Fabrication and electroactive responsive behavior of shape-memory nanocomposite incorporated with self-assembled multiwalled carbon nanotube nanopaper. *Polymers for Advanced Technologies*, 23: 1529-1535.
- [57] Raja, M., Ryu, S. H. and Shanmugaraj, A. M. (2014). Influence of surface modified multiwalled carbon nanotubes on the mechanical and electroactive shape memory properties of polyurethane (PU)/poly(vinylidene difluoride) (PVDF) composites. *Colloids and Surfaces A: Physicochemical and Engineering Aspects*, 450: 59-66.
- [58] Kalita, H. and Karak, N. (2014). Hyperbranched polyurethane/triethanolamine functionalized multi-walled carbon nanotube nanocomposites as remote induced smart materials. *Polymer International*, 63: 1295-1302.
- [59] Lu, H. and Min Huang, W. (2013). Synergistic effect of self-assembled carboxylic acid-functionalized carbon nanotubes and carbon fiber for improved electro-activated polymeric shape-memory nanocomposite. *Applied Physics Letters*, 102: 231910-2319104.
- [60] Dong, Y., Xia, H., Zhu, Y., Ni, Q. Q. and Fu, Y. (2015). Effect of epoxy-graft-polyoxyethylene octyl phenyl ether on preparation, mechanical properties and triple-shape memory effect of carbon nanotube/water-borne epoxy nanocomposites. *Composites Science and Technology*, 120: 17-25.
- [61] Alam, J., Khan, A., Alam, M. and Mohan, R. (2015). Electroactive Shape Memory Property of a Cu-decorated CNT Dispersed PLA/ESO Nanocomposite. *Materials*, 8: 6391-6400.
- [62] Raja, M., Shanmugaraj, A. M., Ryu, S. H. and Subha, J. (2011). Influence of metal nanoparticle decorated CNTs on polyurethane based electro active shape memory nanocomposite actuators. *Materials Chemistry and Physics*, 129: 925-931.
- [63] Lu, H., Yao, Y., Huang, W. M., Leng, J. and Hui, D. (2014). Significantly improving infrared light-induced shape recovery behavior of shape memory polymeric nanocomposite via a synergistic effect of carbon nanotube and boron nitride. *Composites Part B: Engineering*, 62: 256-261.
- [64] Sahoo, N. G., Jung, Y. C., Yoo, H.J. and Cho, J.W. (2007). Influence of carbon nanotubes and polypyrrole on the thermal, mechanical and electroactive shape-memory properties of polyurethane nanocomposites. *Composites Science and Technology*, 67: 1920-1929.

- [65] Falvo, M. R., Clary, G. J., Taylor, R. M., Chi, V., Brooks, F.P., Washburn, S. and Superfine, R. (1997). Bending and buckling of carbon nanotubes under large strain. *Nature*, 389: 582-584.
- [66] Li, Q., Liu, C., Lin, Y. H., Liu, L., Jiang, K. and Fan, S. (2015). Large-strain, multiform movements from designable electrothermal actuators based on large highly anisotropic carbon nanotube sheets. *ACS Nano*, 9: 409-418.
- [67] Gunes, I. S., Jimenez, G. A. and Jana, S. C. (2009). Carbonaceous fillers for shape memory actuation of polyurethane composites by resistive heating. *Carbon*, 47: 981-997.
- [68] Haibao, L., Yanju, L., Jihua, G., Jinsong, L. and Shanyi, D. (2010). Electrical properties and shape-memory behavior of self-assembled carbon nanofiber nanopaper incorporated with shape-memory polymer. *Smart Materials and Structures*, 19: 075021-075028.
- [69] Luo, X. and Mather, P. T. (2010). Conductive shape memory nanocomposites for high speed electrical actuation. *Soft Matter*, 6: 2146-2149.
- [70] Li, F., Qi, L., Yang, J., Xu, M., Luo, X. and Ma, D. (2000). Polyurethane/conducting carbon black composites: Structure, electric conductivity, strain recovery behavior, and their relationships. *Journal of Applied Polymer Science*, 75: 68-77.
- [71] Leng, J., Lv, H., Liu, Y. and Du, S. (2007). Electroactivate shape-memory polymer filled with nanocarbon particles and short carbon fibers. *Applied Physics Letters*, 91: 144105-144108.
- [72] Lu, H., Gou, J., Leng, J. and Du, S. (2011). Magnetically aligned carbon nanotube in nanopaper enabled shape-memory nanocomposite for high speed electrical actuation. *Applied Physics Letters*, 98: 174105-174108.
- [73] Qi, X., Yao, X., Deng, S., Zhou, T. and Fu, Q. (2014). Water-induced shape memory effect of graphene oxide reinforced polyvinyl alcohol nanocomposites. *Journal of Materials Chemistry A*, 2: 2240-2249.
- [74] Xiao, X., Xie, T. and Cheng, Y.T. (2010). Self-healable graphene polymer composites. *Journal of Materials Chemistry*, 20: 3508-3514.
- [75] Yadav, S. K., Yoo, H. J. and Cho, J. W. (2013). Click coupled graphene for fabrication of high-performance polymer nanocomposites. *Journal of Polymer Science Part B: Polymer Physics*, 51: 39-47.
- [76] Zhang, H. and Zhao, Y. (2013). Polymers with Dual Light-Triggered Functions of Shape Memory and Healing Using Gold Nanoparticles. *ACS Appl Mater Interfaces*, 5: 13069-13075.
- [77] Hribar, K. C., Metter, R. B. and Burdick, J. A. (2009). Novel nano-composite biomaterials that respond to light. *Departmental Papers*, 2009: 2409- 2411.

- [78] Hribar, K. C., Lee, M. H., Lee, D. and Burdick, J. A. (2011). Enhanced release of small molecules from near-Infrared light responsive polymer-nanorod composites. *ACS Nano*, 5: 2948-2956.
- [79] Zheng, Y., Li, J., Lee, E. and Yang, S. (2015). Light-induced shape recovery of deformed shape memory polymer micropillar arrays with gold nanorods. *RSC Advances*, 5: 30495-30499.
- [80] Chen, C. M., Chiang, C. L. and Yang, S. (2015). Programming tilting angles in shape memory polymer janus pillar arrays with unidirectional wetting against the tilting direction. *Langmuir*, 31: 9523-9526.
- [81] Zhang, H., Xia, H. and Zhao, Y. (2014). Light-controlled complex deformation and motion of shape-memory polymers using a temperature gradient. *ACS Macro Letters*, 3: 940-943.
- [82] Zhang, H., Zhang, J., Tong, X., Ma, D. and Zhao, Y. (2013). Light Polarization-controlled shape-memory polymer/gold nanorod composite. *Macromolecular Rapid Communications*, 34: 1575-1579.
- [83] Wang, L., Wang, W., Di, S., Yang, X., Chen, H., Gong, T. and Zhou, S. (2014). Silver-coordination polymer network combining antibacterial action and shape memory capabilities. *RSC Advances*, 4: 32276-32282.
- [84] Dinh, D. A., Hui, K. N., Hui, K., Kumar, P. and Singh, J. (2013). Silver nanowires: a promising transparent conducting electrode material for optoelectronic and electronic applications *Reviews in Advanced Sciences and Engineering*, 2: 1-22.
- [85] Luo, H., Li, Z., Yi, G., Wang, Y., Zu, X., Wang, H., H. Huang and Z. Liang (2015). Temperature sensing of conductive shape memory polymer composites. *Materials Letters*, 140: 71-74.
- [86] Luo, H., Li, Z., Yi, G., Zu, X., Wang, H., Wang, Y., Huang, H., Hu, J., Liang, Z. and Zhong, B. (2014) Electro-responsive silver nanowire-shape memory polymer composites. *Materials Letters*, 134: 172-175.
- [87] Yu, Z., Zhang, Q., Li, L., Chen, Q., Niu, X., Liu, J. and Pei, Q. (2011). Highly flexible silver nanowire electrodes for shape-memory polymer light-emitting diodes. *Advanced Materials*, 23: 664-668.
- [88] Li, G., Zhu, R. and Yang, Y. (2012). Polymer solar cells. *Nature Photonics*, 6: 153-161.
- [89] Yu, Z., Li, L., Zhang, Q., Hu, W. and Pei, Q. (2011). Silver nanowire-polymer composite electrodes for efficient polymer solar cells. *Advanced Materials*, 23: 4453-4457.
- [90] Haibao, L., Fei, L., Jihua, G., Jinsong, L. and Shanyi, D. (2014). Synergistic effect of Ag nanoparticle-decorated graphene oxide and carbon fiber on electrical actuation of polymeric shape memory nanocomposites. *Smart Materials and Structures*, 23: 085034-085041.

- [91] Lu, H., Zhu, S., Yang, Y., Huang, W. M., Leng, J. and Du, S. (2015). Surface grafting of carbon fibers with artificial silver-nanoparticle-decorated graphene oxide for high-speed electrical actuation of shape-memory polymers. *Journal of Applied Polymer Science*, 132: 41673-41680.
- [92] Mohr, R., Kratz, K., Weigel, T., Lucka-Gabor, M., Moneke, M. and Lendlein, A. (2006). Initiation of shape-memory effect by inductive heating of magnetic nanoparticles in thermoplastic polymers. *Proceedings of the National Academy of Sciences of the United States of America*, 103(10): 3540-3545.
- [93] Langer, R. and Tirrell, D. A. (2004). Designing materials for biology and medicine, *Nature*, 428: 487-492.
- [94] Zheng, X., Zhou, S., Xiao, Y., Yu, X., Li, X. and Wu, P. (2009). Shape memory effect of poly(D,L-lactide)/Fe₃O₄ nanocomposites by inductive heating of magnetite particles. *Colloids and Surfaces B: Biointerfaces*, 71: 67-72.
- [95] Zhang, X., Lu, X., Wang, Z., Wang, J. and Sun, Z. (2013). Biodegradable shape memory nanocomposites with thermal and magnetic field responsiveness. *Journal of Biomaterials Science, Polymer Edition*, 24: 1057-1070.
- [96] Yu, X., Zhou, S., Zheng, X., Xiao, Y. and Guo, T. (2009). Influence of *in vitro* degradation of a biodegradable nanocomposite on its shape memory effect. *The Journal of Physical Chemistry C*, 113: 17630-17635.
- [97] Yu, X. J., Zhou, S. B., Zheng, X. T., Guo, T., Xiao, Y. and Song, B. T. (2009). A biodegradable shape-memory nanocomposite with excellent magnetism sensitivity. *Nanotechnology*, 20: 235702-235711.
- [98] Bai, S., Zou, H., Dietsch H., Simon, Y. C. and Weder, C. (2014). Functional iron oxide nanoparticles as reversible crosslinks for magnetically addressable shape-memory polymers. *Macromolecular Chemistry and Physics*, 215: 398-404.
- [99] Shuang, X., Xingjian, L., Yaru, W., Yi, P., Zhaohui, Z., Xiaobin, D. and Yuxing, P. (2014). A remote-activated shape memory polymer network employing vinyl-capped Fe₃O₄ nanoparticles as netpoints for durable performance. *Smart Materials and Structures*, 23: 085005-085012.
- [100] Schmidt, A. M. (2006). Electromagnetic activation of shape memory polymer networks containing magnetic nanoparticles. *Macromolecular Rapid Communications*, 27: 1168-1172.
- [101] Li, W., Liu, Y. and Leng, J. (2014). Shape memory polymer nanocomposite with multi-stimuli response and two-way reversible shape memory behavior. *RSC Advances*, 4: 61847-61854.
- [102] Iijima, M., Kobayakawa, M., Yamazaki, M., Ohta, Y. and Kamiya, H. (2009). Anionic surfactant with hydrophobic and hydrophilic chains for nanoparticle dispersion and shape memory polymer nanocomposites. *Journal of the American Chemical Society*, 131: 16342-16343.

- [103] Lu, X. L., LÜ, X. Q., Wang, J. Y., Sun, Z. J., Tong, Y. X. (2013), Preparation and shape memory properties of TiO₂/PLCL biodegradable polymer nanocomposites. *Transactions of Nonferrous Metals Society of China*, 23: 120-127.
- [104] Thakur, S. and Karak, N. (2015). Tuning of sunlight-induced self-cleaning and self-healing attributes of an elastomeric nanocomposite by judicious compositional variation of the TiO₂-reduced graphene oxide nanohybrid. *Journal of Materials Chemistry A*, 3: 12334-12342.
- [105] Nan, W., Wang, W., Gao, H. and Liu, W. (2013). Fabrication of a shape memory hydrogel based on imidazole–zinc ion coordination for potential cell-encapsulating tubular scaffold application. *Soft Matter*, 9: 132-137.
- [106] Han, Y., Bai, T., Liu, Y., Zhai, X. and Liu, W. (2012). Zinc ion uniquely induced triple shape memory effect of dipole–dipole reinforced ultra-high strength hydrogels. *Macromolecular Rapid Communications*, 33: 225-231.
- [107] Wu, Y., Hu, J., Zhang, C., Han, J., Wang, Y. and Kumar, B. (2015). A facile approach to fabricate a UV/heat dual-responsive triple shape memory polymer. *Journal of Materials Chemistry A*, 3: 97-100.
- [108] Kumpfer, J. R. and Rowan, S. J. (2011). Thermo-, photo-, and chemo-responsive shape-memory properties from photo-cross-linked metallo-supramolecular polymers. *Journal of the American Chemical Society*, 133: 12866-12874.
- [109] Koerner, H., Kelley, J., George, J., Drummy, L., Mirau, P., Bell, N. S., Hsu, J. W. P. and Vaia, R. A. (2009). ZnO nanorod–thermoplastic polyurethane nanocomposites: *Morphology and Shape Memory Performance*. *Macromolecules*, 42: 8933-8942.
- [110] Habibi, Y., Lucia, L. A. and Rojas, O. J. (2010), Cellulose nanocrystals: chemistry, self-assembly, and applications. *Chemical Reviews*, 110: 3479-3500.
- [111] Šturcová, A., Davies, G. R., Eichhorn, S. J. (2005). Elastic modulus and stress-transfer properties of tunicate cellulose whiskers. *Biomacromolecules*, 6: 1055-1061.
- [112] Mendez, J., Annamalai, P. K., Eichhorn, S. J., Rusli, R., Rowan, S. J., Foster, E. J. and Weder C. (2011). Bioinspired Mechanically Adaptive Polymer Nanocomposites with Water-Activated Shape-Memory Effect. *Macromolecules*, 44: 6827-6835.
- [113] Liu, Y., Li, Y., Yang, G., Zheng, X. and Zhou, S. (2015). Multi-stimulus-responsive shape-memory polymer nanocomposite network cross-linked by cellulose nanocrystals. *ACS Applied Materials and Interfaces*, 7: 4118-4126.
- [114] Li, Y., Chen, H., Liu, D., Wang, W., Liu, Y. and Zhou, S. (2015). pH-responsive shape memory poly(ethylene glycol)–poly(ϵ -caprolactone)-based polyurethane/cellulose nanocrystals nanocomposite. *ACS Applied Materials and Interfaces*, 7: 12988-12999.

- [115] Mendez, J., Annamalai, P. K., Eichhorn, S. J., Rusli, R., Rowan, S. J., Foster, E. J. and Weder, C. (2011). Bioinspired mechanically adaptive polymer nanocomposites with water-activated shape-memory effect. *Macromolecules*, 44: 6827-6835.
- [116] Zhu, Y., Hu, J., Luo, H., Young, R. J., Deng, L., Zhang, S., Fan, Y. and Ye, G. (2012). Rapidly switchable water-sensitive shape-memory cellulose/elastomer nano-composites. *Soft Matter*. 8: 2509-2517.
- [117] Wu, T., Frydrych, M., O'Kelly, K. and Chen, B. (2014). Poly(glycerol sebacate urethane)-cellulose nanocomposites with water-active shape-memory effects. *Biomacromolecules*, 15: 2663-2671.
- [118] Saralegi, A., Gonzalez, M. L., Valea, A., Eceiza, A., Corcuera, M. A. (2014). The role of cellulose nanocrystals in the improvement of the shape-memory properties of castor oil-based segmented thermoplastic polyurethanes. *Composites Science and Technology*, 92: 27-33.
- [119] Sonseca, Á., Camarero-Espinosa, S., Peponi, L., Weder, C., Foster, E. J., Kenny, J. M. and Giménez, E. (2014). Mechanical and shape-memory properties of poly(mannitol sebacate)/cellulose nanocrystal nanocomposites. *Journal of Polymer Science Part A: Polymer Chemistry*, 52: 3123-3133.
- [120] Zhang, C. S. and Ni, Q. Q. (2007). Bending behavior of shape memory polymer based laminates. *Composite Structures*, 78: 153-161.
- [121] Douglas, C., Mark, L., Mark, S., Emmett, N. and Randal, S. Elastic memory composite material: An enabling technology for future furlable space structures. *46th AIAA/ASME/ASCE/AHS/ASC Structures, Structural Dynamics and Materials Conference: American Institute of Aeronautics and Astronautics*.
- [122] Sen, R., Zhao, B., Perea, D., Itkis, M. E., Hu, H., Love, J., Bekyarova, E. and Haddon, R. C. (2004). Preparation of single-walled carbon nanotube reinforced polystyrene and polyurethane nanofibers and membranes by electrospinning. *Nano Letters*, 4: 459-464.
- [123] Lan, X., Liu, Y., Lv, H., Wang, X., Leng, J. and Du, S. (2009). Fiber reinforced shape-memory polymer composite and its application in a deployable hinge. *Smart Materials and Structures*, 18: 024002-024008.
- [124] Kim, M. S., Jun, J. K. and Jeong, H. M. Shape memory and physical properties of poly(ethyl methacrylate)/Na-MMT nanocomposites prepared by macroazoinitiator intercalated in Na-MMT. *Composites Science and Technology*, 68: 1919-1926.
- [125] Cao, F. and Jana S. C. Nanoclay-tethered shape memory polyurethane nanocomposites. *Polymer*, 48: 3790-800.
- [126] Xu, B., Huang, W. M., Pei, Y. T., Chen, Z. G., Kraft, A., Reuben, R., De Hosson J. T. M. and Fu, Y. Q. (2009). Mechanical properties of attapulgite clay reinforced polyurethane shape-memory nanocomposites. *European Polymer Journal*, 45: 1904-1911.

- [127] Zhang, Y., Wang, Q., Wang, C. and Wang, T. High-strain shape memory polymer networks crosslinked by SiO₂. *Journal of Materials Chemistry*, 21: 9073-9078.
- [128] Park, J. S., Chung, Y. C., Lee, S. D., Cho, J. W., Chun, B. C. (2009). Shape memory effects of polyurethane block copolymers cross-linked by celite. *Fibers and Polymers*, 9: 661-666.
- [129] Tibbits, S. (2014). 4D printing: multi-material shape change. *Architectural Design*, 84: 116-121.
- [130] Campbell, T. A., Tibbits, S. and Garrett, B. (2014). The programmable world. *Scientific American*, 311(5): 60-65.
- [131] Odent, J., Wallin, T. J., Pan, W., Kruemplestaedter, K., Shepherd, R. F. and Giannelis, E. P. (2017). Highly elastic, transparent, and conductive 3D-printed ionic composite hydrogels. *Advanced Functional Materials*, 27: 1701807-1701817.
- [132] Hassan, R. U., Jo, S. and Seok, J. (2018). Fabrication of a functionally graded and magnetically responsive shape memory polymer using a 3D printing technique and its characterization. *Journal of Applied Polymer Science*, 135: 45997-56004.
- [133] Miao, S., Zhu, W., Castro, N. J., Nowicki, M., Zhou, X., Cui, H., Fisher J. P. and Zhang L. G. (2016). 4D printing smart biomedical scaffolds with novel soybean oil epoxidized acrylate. *Scientific reports*, 6: 27226-27236.
- [134] Zarek, M., Layani, M., Cooperstein, I., Sachyani, E., Cohn, D., Magdassi, S. (2016). 3D printing of shape memory polymers for flexible electronic devices. *Advanced Materials*, 28: 4449-4454.
- [135] Zarek, M., Mansour, N., Shapira, S. and Cohn, D. (2017). 4D printing of shape memory-based personalized endoluminal medical devices. *Macromolecular Rapid Communications*, 38: 1600628-1600634.
- [136] Senatov, F. S., Niaza, K. V., Zadorozhnyy, M. Y., Maksimkin, A. V., Kaloshkin, S. D. and Estrin, Y. Z. (2016). Mechanical properties and shape memory effect of 3D-printed PLA-based porous scaffolds. *Journal of the Mechanical Behavior of Biomedical Materials*, 57: 139-148.
- [137] Yang, H., Leow, W. R., Wang, T., Wang, J., Yu, J., He, K., D. Qi, Wan, C. and Chen, X. (2017). 3D printed photoresponsive devices based on shape memory composites. *Advanced Materials*, 29: 1701627-1701634.

Complimentary Contributor Copy

Chapter 4

INTRINSICALLY HEALABLE POLYMERS

Robert H. Aguirresarobe^{1,}, Sil Nevejans^{1,2}, Nicholas Ballard¹,
June Aizpurua¹, Lourdes Irusta¹ and Haritz Sardon^{1,†}*

¹POLYMAT, University of the Basque Country UPV/EHU,

Joxe Mari Korta Center, Donostia-San Sebastián, Spain

²BASF SE, Dispersion & Colloidal Materials, Ludwigshafen, Germany

ABSTRACT

The introduction of healing characteristics into synthetic polymers has represented a step forward in the development of safer, more durable and more reliable materials. Ideally, a healable material should be able to restore its performance after being damaged, even for multiple damage/healing events. In this sense, the current knowledge about material science, polymer physicochemistry and polymer synthesis has led to the development of new types of healable polymers capable of fulfilling these prerequisites: Intrinsicly healable polymers. These materials contain active elements, which are covalently incorporated into the polymer structure and impart repairing characteristics to the final material. Herein, we summarize the most relevant parameters in the development of intrinsically healable polymers as well as the most recent synthetic approaches reported in the literature.

Keywords: intrinsic healing, stimuli-responsive, dynamic chemistry

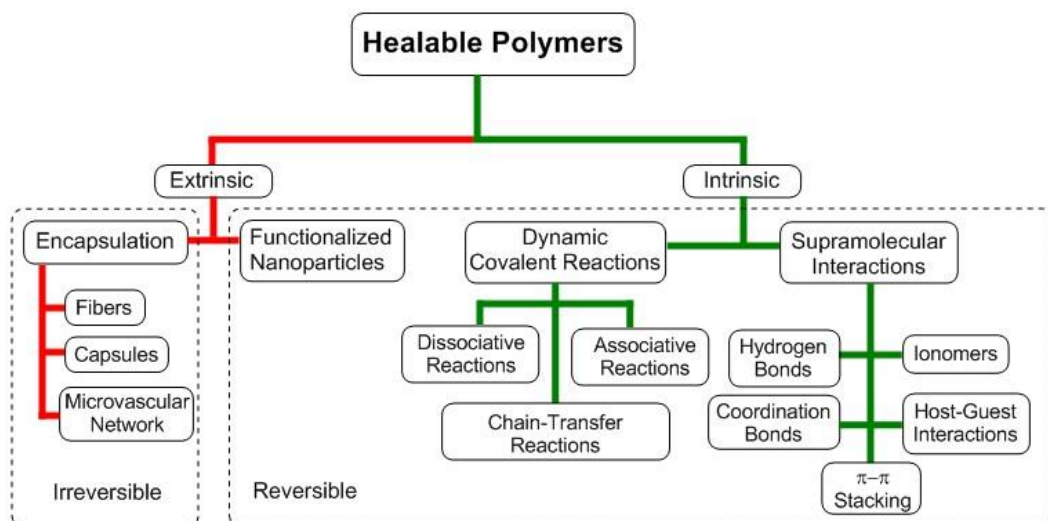
* Corresponding Author Email: roberto.hernandez@ehu.es

† Corresponding Author Email: haritz.sardon@ehu.es

1. INTRODUCTION

Self-repairing or self-healing can be defined as the ability of certain materials to *autonomically* repair (heal or recover) damage without loss of their physical properties [1]. The best known examples of these types of materials can be found in nature, considering that one of the most intriguing characteristics of natural tissues, displaying the ability to self-repair damaged structures. In biological systems, the phenomenon of self-repair is triggered by unique chemical signals released only at the specific site where damage has occurred. As a consequence of these signals, a series of chemical and physical processes lead to the transport, deposition and assembly of healing agents [2–4]. Inspired by this ability of living organisms and natural materials, researchers are trying to incorporate this concept in order to develop man-made materials capable of restoring their structural integrity in case of deterioration or failure. Research has centered in the development of healable materials such as metals, ceramics and/or polymers. Among these, polymers seem to be one of the most suitable candidates, owing to their intrinsic physical properties and the ease by which they can be functionalized [1, 5, 6]. However, mimicking the mechanisms occurring in nature is an extremely challenging issue and most of the developed healable materials need an external stimulus to trigger and produce the reparation.

Generally, healable polymers incorporate active moieties, which can act as sensing and/or reactive components. Ideally, these components would be able to sense as well as repair macroscopically invisible damages, such as pinholes or microcracks, over the lifetime of material with little to no external intervention.



Scheme 1. General classification of self-repairing polymers.

Obviously, when developing healable materials, the potential damage of the material that can suffer during its service life have to be taken into consideration. Factors such as excessive loads, fatigue or environmental conditions which affect the material in the application can alter the material performance [7–9]. As there is a wide variety of harmful conditions which are application specific, the material for a given application must be designed with careful regard to polymer synthesis, polymer physicochemistry, fracture dynamics and material science.

From a synthetic point of view, multiple strategies and approaches have been introduced to deal with the different healing requirements of particular applications. This has resulted in the development of a variety of healable polymers with very diverse characteristics in terms of physical properties, healing mechanisms and their activation. The existing healing strategies can be classified according to their intrinsic or extrinsic nature as shown in Scheme 1. Extrinsically healable materials have active fillers, so called healing agents, embedded in the polymer. Recently, the modification of nanoparticles with reversible chemistries has been described [10, 11], but most of the literature reported on these extrinsic strategies, employs the addition of liquid healing agents, such as monomers and catalysts, within brittle vessels or hollow fibers into the polymeric matrix [1, 9, 12, 13]. These healing agents are released into the matrix upon rupture; as such they act as fillers which are in charge of repairing the damaged area. Unfortunately, this process is only effective when healing agents are available on the crack's surface, moreover, the process is considered to be irreversible. Therefore, researchers have focused on the development of intrinsic healable polymers, which are polymeric materials capable of undergoing repeated healing and hence more interesting towards long term applications. In this book chapter, we will focus on intrinsically healable polymers, of which the most relevant synthetic alternatives that have produced significant repair of the polymeric material will be discussed.

2. INTRINSICALLY HEALABLE POLYMERS

Intrinsically healable materials incorporate active moieties which are directly built into the polymer chain and the repair of the material is achieved through the inherent reversibility of the interconnection of these moieties in the polymer matrix. This concept requires the presence of “weak links” in the polymer network capable of breaking in response to stress or the appearance of defects, and able to recombine afterwards. Chemical reactions involved in the healing process permit an increase of the chain mobility after the damage and/or to immobilize and restore the structural integrity of the polymer network. By selecting the appropriate chemistry, these “weak links” can recombine to reform the polymer structure so that intrinsic healing is achieved [1, 14, 15].

Ideal healable materials should work autonomously without external intervention, that is, the damage generation itself should be responsible for the activation of the healing mechanism. Accordingly, this type of materials are called self-healing materials. However, most of the current healing alternatives do not work autonomically, but operate upon external stimulation. In these cases, the healing process starts and progresses as a consequence of physicochemical reactions promoted in the active dynamic structure by the application of a certain stimulus. Therefore, the nature of the introduced dynamic structure determines the type of stimuli needed to trigger the process.

Different kinds of stimuli have been used in the field of healable materials such as heat, light, redox-reaction, mechanical stimulation or pH with the heat being the most commonly employed one [16–20]. The application of heat can promote multiple types of reactions providing energy to overcome the energy barrier for bond cleavage, and can be utilized to crosslink the polymer network as well as to break it. Indeed, heat has the capacity to influence multiple reactions; therefore the temperature must be selected accurately to avoid thermal degradation of the material.

Apart from heat, the application of light has been also widely explored to induce healing in stimuli responsive healable materials. The main advantage in comparison to heat is that the damaged area can be selectively activated by application of light, which enables to heal polymers under load [20, 21]. However, the inherent characteristics of the interaction restrict this stimulation to transparent polymers and/or polymeric surfaces. Apart from heat and light stimulation, in some circumstances other stimuli such as redox-reaction, pH or electric current are more appropriate to selectively trigger healing mechanisms in specific applications, such as hydrogels or medical applications [16, 19].

Although the field of healable materials has only been developing since the 1990s, its literature is already extensive and various concepts and chemical reactions have been applied for this purpose. In the following sections, the most established strategies to develop healable polymers are represented. As depicted in Scheme 1, the different chemistries are classified depending on the molecular principle that is used to affect the polymer matrix, dividing them into systems based on dynamic covalent reactions and those based on supramolecular interactions. Additionally, information about the required stimulation to activate the healing process in each case is included.

2.1. Dynamic Covalent Reactions

Dynamic covalent moieties are covalently linked structures or functional groups that can easily be broken or reformed as a consequence of damage or exposure to a small energy source. The main characteristic of this process is its reversibility which leads to the exchange of the dynamic moiety along the polymer network. The dynamic equilibrium established among the different moieties permits the rebuilding of the damaged polymer network by means of newly formed covalent bonds, generating the healed material.

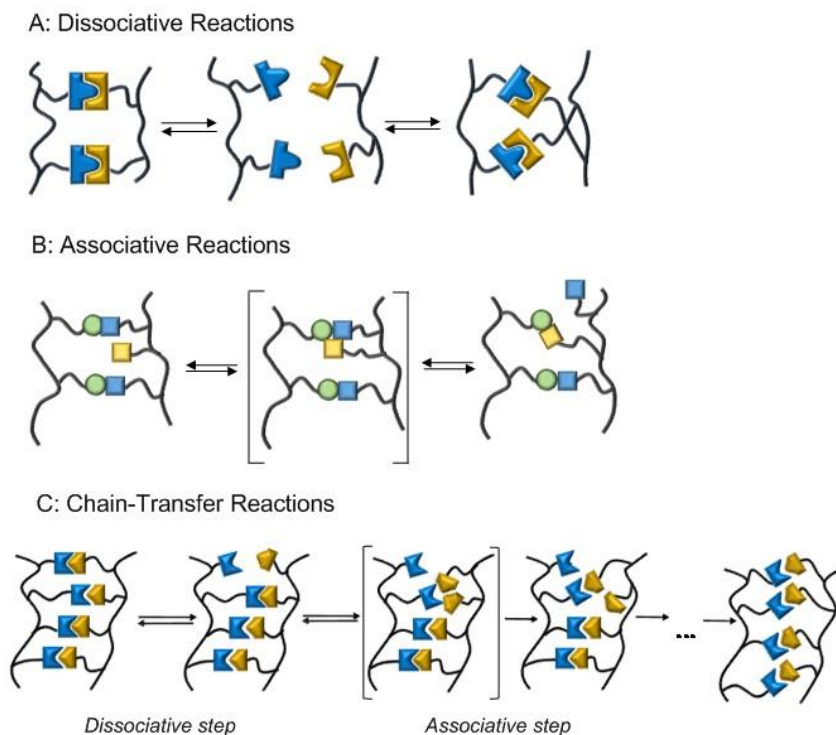


Figure 1. Schematic representations of dissociative, associative and chain-transfer mechanism for dynamic covalent reactions (Inspired by [26]).

Interest in this field has grown due to its versatility and easy implementation in different polymeric networks. In addition, the incorporation of dynamic covalent bonds permits to incorporate new features to thermosets apart from healing, such as reprocessability, solubility and/or recycling ability [22–26].

According to the dynamic mechanism involved in the process three main groups of dynamic covalent reactions have been applied in the field of healable polymers: Dissociative, associative and chain-transfer reactions.

Although the different alternatives give rise to the exchange of functional groups, the main difference relies on the reaction mechanism to produce the exchange. During a dissociative reaction (Figure 1 A), the active motif is cleaved into two components, which are able to recombine afterwards with surrounding groups. In contrast, the exchange in associative reactions (Figure 1 B) occurs because a free functional group present in the polymer chain reacts with the active motif in its vicinity. As a consequence of this reaction a new active motif is formed in the polymer structure. However, the original active structure only breaks when the new bond is formed with a free functional group (Figure 1 B). These contrasting behaviors influence the physical properties of the materials during the healing process. The cross-linking degree of the material changes when dissociative reactions take place, while it remains constant when associative processes are occurring in the material [26].

The third alternative, the chain-transfer reactions, can be considered a mixture of the previously mentioned mechanisms and resembles the degenerative chain-transfer reactions occurring in radical polymerizations. According to this mechanism (Figure 1C), the dynamic bond is activated in a first step, usually upon external stimulation, to produce two active species. These active species are able to react with the dynamic bonds in the vicinity, producing analogous dynamic bonds in the polymer backbone and new active species. As a consequence of this reaction, which occurs *via* an associative mechanism, the side groups of the polymer containing these dynamic bonds are exchanging. The process finishes when the active species lose their activity, whether by the recombination of active species or by side reactions. This third alternative usually involves radical reactions, although neutral or ionic species can also be involved this mechanism.

Dissociative Reactions

As already mentioned above, the underlying concept in this kind of materials is the formation of cross-linked polymer structures by incorporating functional moieties that are able to undergo reversible reactions, by breaking and forming covalent bonds in between two segments of the active moiety. The reversible reaction is governed by a dynamic equilibrium which can be altered by changing the experimental conditions. As a consequence, the majority of these reactions needs an external stimulus, such as heat or light, to shift the dynamic equilibrium and to activate the process.

Dissociative reactions can be divided into two categories depending on the groups resulting from the bond cleavage. The rupture of some dynamic functional groups gives rise to neutral species, while other dissociative exchanges go through radical intermediates.

Following this classification, Table 1 summarizes the most relevant dissociative reactions, involving neutral and radical components, as well as their stimuli used to trigger and maintain the healing mechanism.

Among the different dissociative reactions, the Diels-Alder reaction is one of those reversible systems that is often applied to obtain healable polymers and has been utilized to reversibly cross-link materials of very diverse physical properties [28–33, 51]. The main limitation of this reaction is that an external stimulus (heat) is necessary to activate the healing process. The reaction occurs between a diene and a dienophile, with the reaction between furans and maleimides as the most known and widely used reversible Diels-Alder reaction to obtain healable materials. However, a variety of commercially available monomers capable to undergo Diels-Alder reactions offers the possibility to tailor the reaction parameters (reaction kinetics, reaction temperature and product formation) by modifying the chemical structure of both the diene and the dienophile. Thus, different alternatives, based on cyclopentadiene, anthracene and dithioesters have also been reported [52–54].

Dissociative reversible reactions can also be used to develop optically healable polymers. The most common strategy is based on the introduction of chromophores that react *via* cycloaddition reactions upon UV light exposure. Well-established photoinduced reactions are the [2+2] cycloaddition of cinnamic acid derivatives such as coumarins, as well as the [4+4] cycloaddition reaction of anthracene [34–38, 55]. Both types of chromophores have been applied in healable coatings and elastomers, where the cycloaddition reaction allows the system to reversibly cross-link and break the material on demand.

Apart from heat- and light-stimulated materials, systems which respond to pH to obtain healing properties have also been described. Typically, these systems employ the reversible reaction between aldehydes groups and amines in which the equilibrium can be switched by changing the pH of the medium. For healable materials, the reaction of aldehydes with allylic and aromatic amines, acylhydrazine or oxime moieties have been utilized to introduce the corresponding dynamic imine, acylhydrazone and oxime-carbamate units into the polymer chain [39–42].

Hydrolysis/condensation reactions are also useful for developing healable materials, mainly hydrogels. The incorporation of boronic esters, for instance, allows reversible cross-linking and breaking of polymer networks by hydrolysis or condensation processes [43, 44].

Another alternative that has demonstrated to produce significant repairs is the incorporation of substituted ureas into the polymer backbone [45]. The dynamic nature of the substituted urea bonds permits to break the existing urea bonds into isocyanate and amines, which can later recombine. This chemistry is reminiscent of the widely used “blocked isocyanates” which are commonly applied to mask the isocyanate moiety in coating applications. However, the dissociative reactions do not produce the total disconnection of the polymer network and the concept resembles more the one proposed for associative reactions.

The essential characteristic of radical mediated dissociative reactions is the stability of the formed radicals, which avoids side reactions and produces the same dynamic bonds upon recombination. Alkoxyamine chemistry is a good example of the use of this kind of reaction to incorporate healing characteristics into polymer networks, since it forms stable radicals when breaking the C-O bond which are subsequently able to recombine along the network, typically using heat or light as activating stimulus [46–49]. Following the same concept, the dibenzofuranone structure also provides radical stabilization and its incorporation has similarly demonstrated healing in polymer materials upon activation by heat [50].

Table 1. Summary of the most relevant dissociative dynamic reactions undergoing neutral species

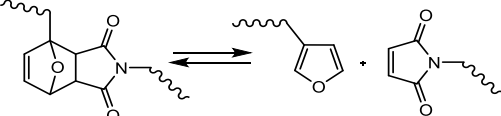
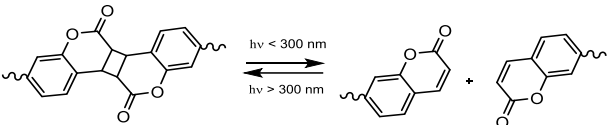
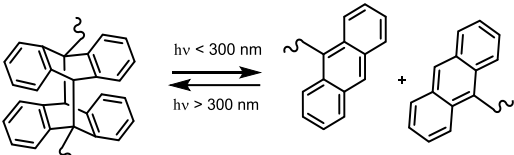
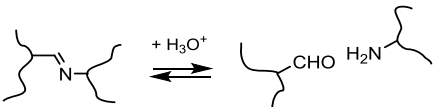
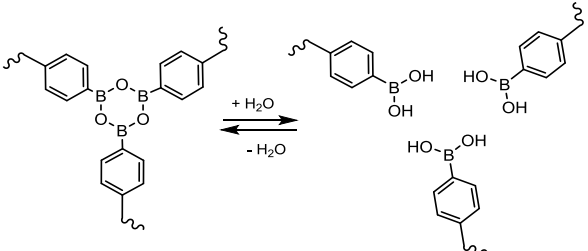
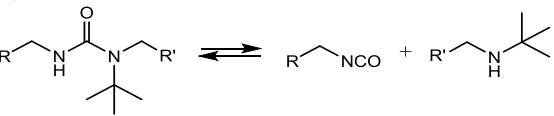
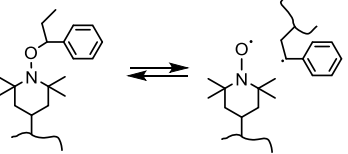
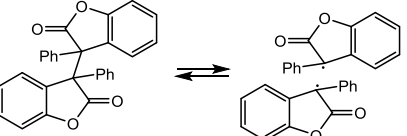
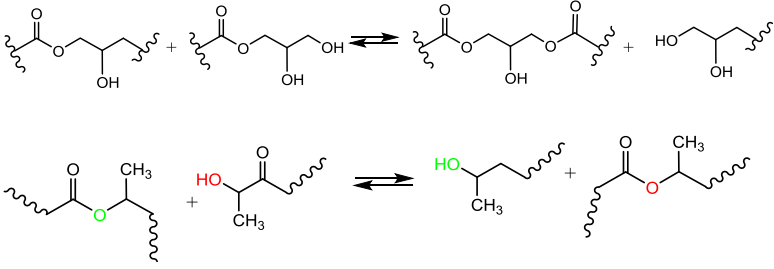
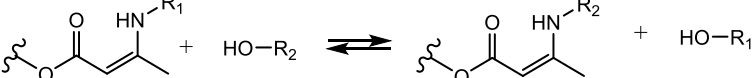
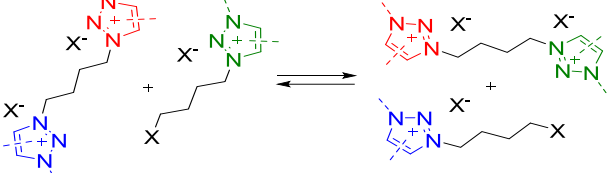
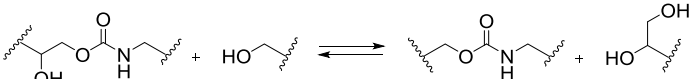
Reaction	Stimuli	Ref
<p>Diels-Alder Reaction</p> 	Heat	[27–33]
<p>Cinnamic acid derivatives</p> 	UV Light	[34–36]
<p>Anthracene derivatives</p> 	UV Light	[37, 38]
<p>Imine derivatives</p> 	pH	[39–42]
<p>Boronic acid derivatives</p> 	Water	[43, 44]
<p>Dynamic substituted ureas</p> 	Heat/SH	[45]
<p>Alkoxyamine based systems</p> 	Heat/ Light	[46-49]
<p>Diarylbibenzofuranone derivatives</p> 	Heat	[50]

Table 2. Significant reactions employed in associative healable materials

Reaction	Ref
<p>Transesterification</p> 	[23] [57]
<p>Transimination</p> $\text{Ar}-\text{C}=\text{N}-\text{R}_1 + \text{H}_2\text{N}-\text{R}_2 \rightleftharpoons \text{Ar}-\text{C}=\text{N}-\text{R}_2 + \text{H}_2\text{N}-\text{R}_1$	[58]
<p>Vinylogous urethanes</p> 	[59, 60]
<p>Transalkylation of C-N bonds</p> 	[61]
<p>Transcarbamylation of polyhydroxyurethanes</p> 	[62]

Associative Reactions

Associative reactions take advantage of interchange reactions of certain functional groups with other unreacted and free functional groups within the polymer matrix, for example by means of transesterification or metathesis reactions. According to this mechanism, the interchange of the functional groups occurs *via* an associative intermediate, that is, the functional group only breaks when a new group is formed. Thus, in contrast to dissociative processes, in associative reactions the cross-linking degree of the material remains constant along the process. This strategy has also been employed in the development of a new generation of materials so called *vitrimers*. These materials behave as crosslinked materials at low temperatures but present a glass-like fluidity at

high temperatures due to the interchange of functional groups along the polymer network [23, 26].

Although healing results for associative reactions are less frequently reported, this concept can potentially also be implemented to obtain healable materials. As occurred in the case of the reprocessing of these vitrimers, the interchange of the functional groups permits to generate covalent links between both faces of a rupture, by applying the appropriate temperature and/or pressure conditions [22, 26, 56].

The pioneering work in the field was the transesterification process in polyesters containing unreacted hydroxyl groups proposed by Leibler and coworkers, which can be seen, for example, the upper reaction in Table 2 [23]. Thus, the free hydroxyl groups are able to react with the ester groups in the main chain, producing an exchange. Taking advantage of transesterification reactions, Hillmyer et al. already produced polylactide vitrimers with healing characteristics [57].

Other alternatives to develop this kind of materials are based on transimination [58]. This reaction is thermally activated, in contrast to the dissociative reactions of imines which were produced by changes in the pH of the medium. More recently, the capability of vinylogous urethanes to produce and tailor dynamic structures has attracted attention due to its ability to be reprocessed and recycled at high temperatures [59, 60].

Similarly, the incorporation of dynamic moieties based on transalkylation reactions of C-N bonds proposed by Drockenmuler et al. has demonstrated the possibility to produce reprocessable crosslinked polymer networks [61]. These characteristics have also been reported by Hillmyer et al. for polyhydroxyurethanes [62]. These polymer networks, containing both urethane and hydroxyl groups, are able to undergo dynamic transcarbamoylation reactions at high temperatures.

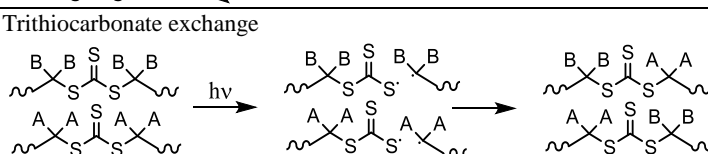
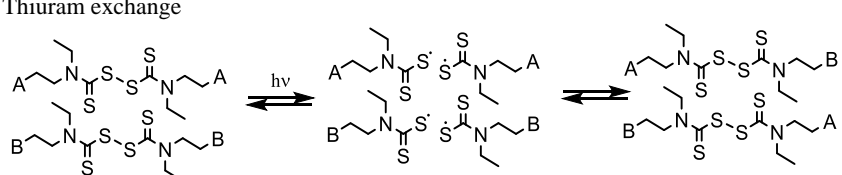
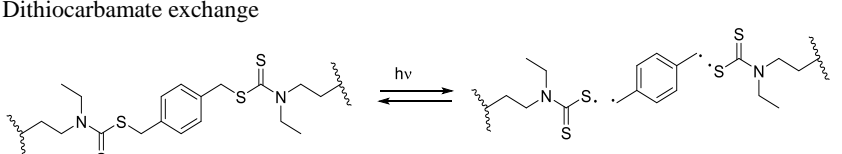
Chain-Transfer Reactions

As mentioned above, the chain-transfer reactions present features both from dissociative and associative mechanisms. Generally, this strategy involves radical mediated reactions but neutral and ionic reactions have also been used. Sulfur (and selenium) chemistry is employed in most of the examples based on chain-transfer reactions (Table 3). The simplest sulfur chemistry used in healable polymers is the dynamic exchange of disulfides through radical-mediated reactions [63, 64]. This exchange has been applied both for aliphatic and aromatic disulfides [65–68]. However, interesting to notice here it is that the exchange of aromatic disulfides can occur at room temperature without any catalyst, in contrast to aliphatic ones which need external stimulation either by heat or light to exchange satisfactorily. Thus, the incorporation of aromatic disulfides has been incorporated in very diverse polymer matrixes such polyurethanes and epoxies to provide healing characteristics at room temperature [68–71]. Even so, research is moving to selenium derivatives, enhancing the healing characteristics of sulfur counterparts, not only in terms of healing efficiency but also in

healing rates [72, 73]. Aromatic diselenides are able to exchange even more rapidly at room temperature than aromatic disulfides, which permits to develop materials with a stronger healing potential at room conditions than disulfide-based polymers.

Other alternatives based on sulfur chemistry take advantage of the redox properties of disulfide linkages to produce active species. In this case, under redox stimulation, disulfide bonds can produce thiol groups or interact with metal ions, which are responsible for the exchange of the functional groups and the recovery of the material [74, 75].

Table 3. Reactions capable to undergo chain-transfer reactions in healable polymers

Reaction	Stimuli	Ref
<p>Disulfide radical exchange</p> $\begin{array}{c} \text{R-S-S-R} \\ \text{R-S-S-R} \end{array} \rightleftharpoons \left[\begin{array}{c} \text{R-S} \cdot \cdot \text{S-R} \\ \cdot \text{S-R} \end{array} \right] \rightleftharpoons \begin{array}{c} \text{R-S} \quad \text{S-R} \\ \quad \\ \text{R-S} \quad \text{S-R} \end{array}$ <p>R= A kyl chain, Aromatic Ring</p>	Heat /Nothing	[65–68]
<p>Diselenide radical exchange</p> $\begin{array}{c} \text{R-Se-Se-R} \\ \text{R-Se-Se-R} \end{array} \rightleftharpoons \left[\begin{array}{c} \text{R-Se} \cdot \cdot \text{Se-R} \\ \cdot \text{Se-R} \end{array} \right] \rightleftharpoons \begin{array}{c} \text{R-Se} \quad \text{Se-R} \\ \quad \\ \text{R-Se} \quad \text{Se-R} \end{array}$ <p>R= A kyl chain, Aromatic Ring</p>	Heat / Nothing	[72, 73]
<p>Disulfide redox reaction</p> <p style="text-align: center;">Redox</p> $\text{~S-S~} \rightleftharpoons \text{~SH} \quad \text{HS~}$	Redox	[74, 75]
<p>Trithiocarbonate exchange</p> 	UV Light	[76]
<p>Thiuram exchange</p> 	Vis Light	[77]
<p>Dithiocarbamate exchange</p> 	UV Light	[78]

Another group of chemistries is inspired by reversible addition-fragmentation chain-transfer (RAFT) polymerization initiators. Their capacity to produce pseudo-stable radicals can be applied in the development of healable polymers by incorporating such moieties into cross-linked polymer networks. The interest has been focusing on light triggered reactions and concerns mainly thiocarbonates and thiocarbamates. Amamoto and coworkers were pioneers in the introduction of trithiocarbonate units in polymer networks to produce optically healable polymers by means of radical-mediated dissociative reactions upon UV light stimulation [76]. Afterwards, they synthesized polyurethanes containing thiuram moieties which were able to successfully recover from damage by irradiating the sample with visible light [77]. Similarly, Kloxin et al. reported UV light stimulated healable materials based on dithiocarbamate units [78].

2.2. Supramolecular Interactions

The implementation of supramolecular chemistry in the development of healable materials has known a remarkable growth in recent years. In contrast to dynamic covalent reactions, this concept is based on non-covalent interactions among polymer chains and, thanks to the reversible nature and high directionality of these interactions, these materials have presented self-assembly and self-healing characteristics in multiple polymer families, most of which act without the necessity of external intervention or stimulation [79–81]. As summarized in Table 4, different polymer systems will be described according to the supramolecular interaction responsible for the repair of undergone damage to the material.

Hydrogen Bonding

Despite not being one of the strongest non-covalent interactions, hydrogen bonds between neutral organic molecules appear frequently in self-assembled and self-healing moieties in nature. Correspondingly, they have been studied to incorporate healing abilities into different polymer matrixes [98]. In order to increase the strength of the introduced hydrogen bonds, specific species containing multiple H-bond donor and acceptors have been designed and used as active moieties for self-healing.

Several studies carried out by Meijer and coworkers [82, 99] have shown that the multiple H-bonding interaction of ureidopyrimidone (Upy) units provides self-healing and self-assembly properties to low T_g polymer thermoplastics and elastomers. Using the same concept, different donor/acceptor couples based on nucleobase derivatives have been introduced as healing motifs in polymeric elastomers and gels [80, 83, 84, 100–102].

Table 4. Supramolecular chemistries used in healable polymers

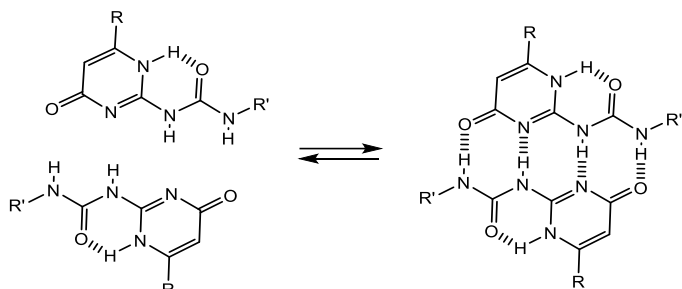
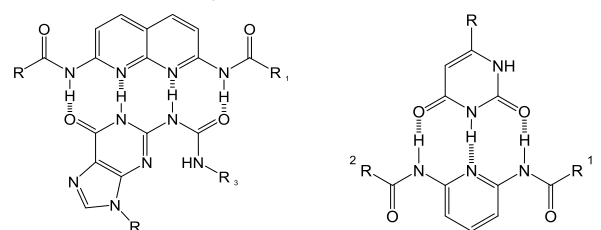
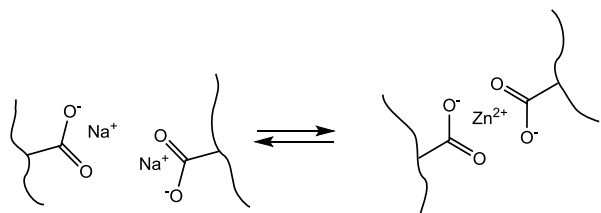
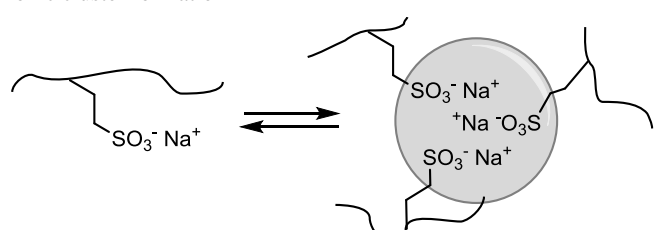
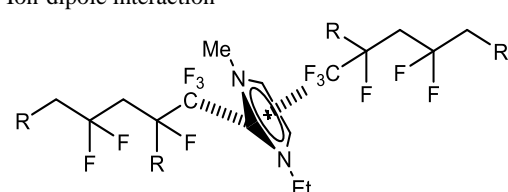
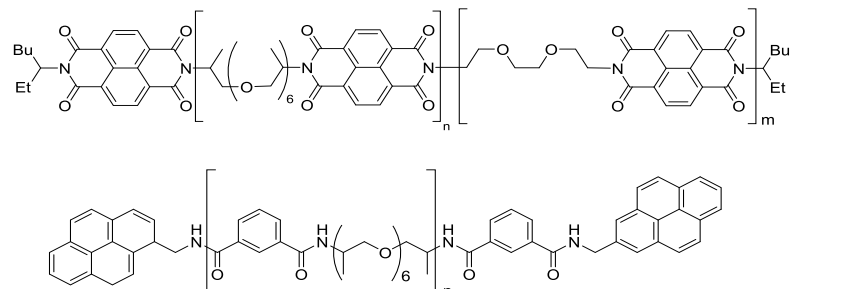
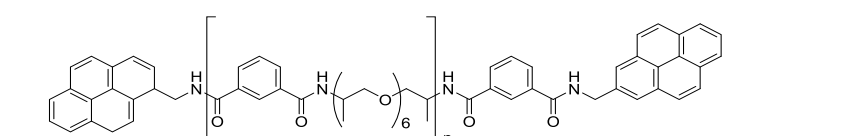
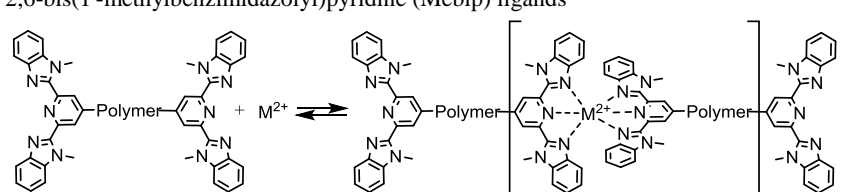
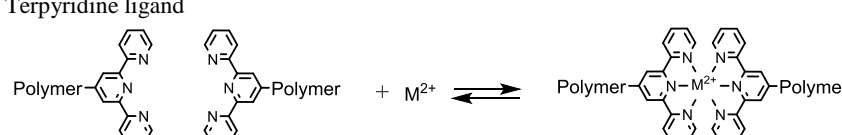
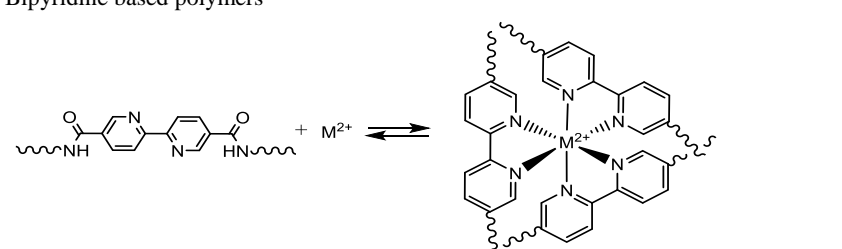
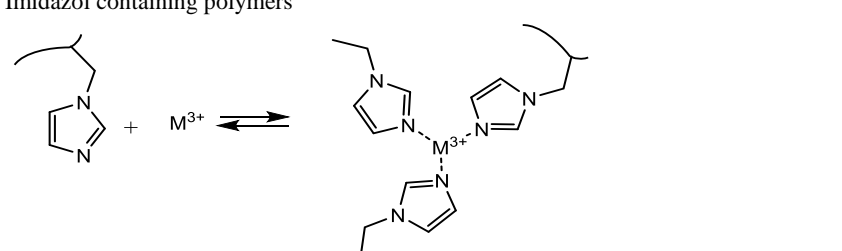
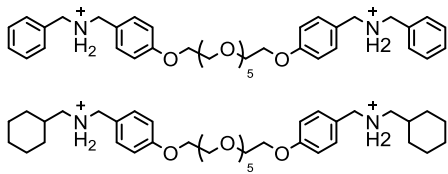
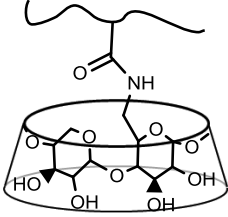
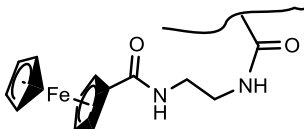
Type	Reaction	Ref
Hydrogen bonding	<p>Ureidopyrimidinone based polymers</p> 	[82]
	<p>Nuclobase derivative systems</p> 	[83] [84]
Ionomers	<p>Ionic interaction</p> 	[85]
	<p>Ionic cluster formation</p> 	[86]
	<p>Ion-dipole interaction</p> 	[87]

Table 4. (Continued)

Type	Reaction	Ref
π-π stacking	Pyrene-naphthalene diimide based polymers 	[88]
		[89]
Coordination Bonds	2,6-bis(1'-methylbenzimidazolyl)pyridine (Mebip) ligands 	[90]
	Terpyridine ligand 	[91]
	Bipyridine based polymers 	[92]
	Imidazol containing polymers 	[93]

Type	Reaction		Ref
Host-guest interactions	Host gel	Guest gel	[94]
	Crown ether		
	α and β cyclodextrines	Alkyl chains	[95]
		Ferrocene	
			[96, 97]

Ionomers

The incorporation of ionic moieties in polymer structures is widely used in polymer chemistry for imparting multiple features, such as water dispersibility and biological activity [103]. In addition to these characteristics, materials containing electric charges in their structures have demonstrated significant self-healing abilities, as the electrostatic interactions between different polymer chains act as a driving force for the repairing process [1, 104].

The pioneering work of Oyetunji et al. demonstrated the potential of this concept to produce healable materials. Partially or fully neutralized poly(ethylene-co-methacrylic acid) samples exhibited remarkable healing abilities not only in small cracks, but also in several millimeter holes when the material was able to restore its integrity after ballistic damage [85]. Since that work, various alternatives have been presented which take advantage of Coulomb interactions, using both the ionic cluster formation and the ion-dipole interaction among ionic liquids and polymer chains [86, 87].

π - π Stacking

Similar to hydrogen bonding based systems, monomers with specific π - π stacking interactions have been used to develop healable polymers. In this case, the healing occurs as a consequence of a self-assembly process of multiple polymer chains with different aromatic moieties [88, 89]. Even so, the application of this supramolecular interaction is

not very common and few examples are reported in literature due to the high insolubility of the polymer and the difficulty in finding systems capable of self-assembly by means of π - π stacking interactions.

Coordination Bonds

Metal-ligand interactions are another well-known type of supramolecular interactions that can be used to design supramolecular self-healing polymers, incorporating ligand substitutes into the polymer chain [105]. In this case, the formation of cracks involves the rupture of the coordination bonds, which can be reformed to restore the initial structure [90, 106–108]. The peculiarity of these materials is that metal ions are introduced and distributed within the polymer matrix in order to initiate the exchange process and generate the repair of the material.

Among the most relevant results comprising this category, Weder and coworkers described the use of 2,6-bis(1'-methylbenzimidazolyl)pyridine (MeBip) macromonomers to produce light-responsive healable materials [90]. These moieties were able to produce self-assembly and self-healing upon UV light stimulation and the strength of the interaction was tailored by changing the metals used in the complexation. Other alternatives take advantage of different ligands, such as terpyridine, bipyridine and imidazole motifs, incorporated as chain ends and chain extenders to produce supramolecular healable materials [91–93].

Host-Guest Interactions

The application of host-guest interactions is the most recent approach for intrinsically healable materials. The main advantage is the high selectivity of the interaction, which prevents the passivation of the healing process [109]. However, this development is at an early stage and the healing process is mainly focused in gels of low moduli. In these cases, the healing mechanism is based on the reversible interaction between macrocycles, such as cyclodextrines or crown ethers, and specific guest groups, such as ferrocene or alkyl chains [94–97, 110].

OUTLOOK AND PERSPECTIVES

Intrinsically healable polymers have led to a breakthrough in the development of synthetic materials capable of undergoing autonomous repair. In order to incorporate the dynamic chemical bonds that lead to self-healing, a wide range of synthetic approaches have already been reported. Nevertheless, the capacity to synthesize materials which match the combination of strength and healing ability of natural tissues remains a challenge. Thus, there are still significant steps to be made in order to produce polymers which display highly efficient and rapid autonomous healing. To date, most synthetic

self-healing materials depend upon external sources of energy to activate the dynamic bonds and start the healing process, which is often infeasible depending on the application. Furthermore, whether such dynamic bonds, which by their very nature are typically weaker than is common in synthetic polymers, are stable over significant periods of time is questionable.

Currently, the synthetic strategies described permit the restoration of the structural integrity of materials once both sides of the fractured surface are in contact. In this respect many materials have shown the ability to “self-heal” and to repair minor surface damage. However, healable materials should be able to repair different types of damages, such as scratches and cuts, where the fracture surfaces are not in intimate contact. This requires knowledge not just of the chemical factors that allow for reorganization of the polymer network but of the physical factors that determine the ability of a material to recover shape. With this in mind, in order to fulfill the main goal of obtaining a truly self-healing material, it is necessary to have a deeper understanding of the key factors involved in the healing processes, while designing new chemistries able to produce autonomous repairs, possibly combining self-healing and shape memory characteristics.

ACKNOWLEDGMENTS

The authors are grateful for the grant “ayudas para la especialización de personal investigador del vicerrectorado de investigación de la UPV/EHU” and “Grupo Consolidado IT618-13, IT586-13 and IT999-16. The European Union’s Horizon 2020 research and innovation programme is accredited for the financial support through Project TRACKWAY-ITN 642514 under the Marie Skłodowska-Curie grant agreement.

REFERENCES

- [1] Ghosh, S.K. 2009. *Self-Healing Materials: Fundamentals, Design Strategies and Applications*. Weinheim, Germany: Wiley-VCH Verlag GmbH & Co. KGaA. doi:10.1002/9783527625376.
- [2] Mutsaers, S.E., J.E. Bishop, G. McGrouther, and G.J. Laurent. 1997. “Mechanisms of Tissue Repair: From Wound Healing to Fibrosis.” *International Journal of Biochemistry and Cell Biology* 29 (1): 5–17. doi:10.1016/S1357-2725(96)00115-X.
- [3] Youngblood, J.P., and N.R. Sottos. 2008. “Bioinspired Materials for Self-Cleaning and Self-Healing.” *MRS Bulletin* 33 (August): 732–41. doi:10.1557/mrs2008.158.
- [4] Urban, M.W. 2011. *Handbook of Stimuli-Responsive Materials*. Weinheim, Germany: Wiley-VCH Verlag GmbH & Co. KGaA. doi:10.1002/9783527633739.

- [5] van der Zwaag, S, N.H. van Dijk, H.M. Jonkers, S.D. Mookhoek, and W.G. Sloof. 2009. "Self-Healing Behaviour in Man-Made Engineering Materials: Bioinspired but Taking into Account Their Intrinsic Character." *Philosophical Transactions. Series A, Mathematical, Physical, and Engineering Sciences* 367: 1689–1704. doi:10.1098/rsta.2009.0020.
- [6] Syrett, J.A., C.R. Becer, and D.M. Haddleton. 2010. "Self-healing and self-mendable polymers." *Polymer Chemistry I* (7): 978–87. doi: 10.1039/c0py00104j
- [7] Allen, N.S., and M. Edge. 1992. *Fundamentals of Polymer Degradation and Stabilisation*. Essex, England: Elsevier Science Publisher LTD.
- [8] Baker, A.A., R. Jones, and R.J. Callinan. 1985. "Damage Tolerance of Graphite/epoxy Composites." *Composite Structures* 4: 15–44. doi:10.1016/0263-8223(85)90018-2.
- [9] Blaiszik, B.J., S.L.B. Kramer, S.C. Olugebefola, J.S. Moore, N.R. Sottos, and S.R. White. 2010. "Self-Healing Polymers and Composites." *Annual Review of Materials Research* 40 (1): 179–211. doi:10.1146/annurev-matsci-070909-104532.
- [10] Biyani, M., J.E. Foster, and C. Weder. 2013. "Light-Healable Supramolecular Nanocomposites Based on Modified Cellulose Nanocrystals." *ACS Macro Letters* 2:236–240. doi:10.1021/mz400059w.
- [11] Schäfer, S., and G. KICKELBICK. 2015. "Self-healing polymer nanocomposites based on Diels-Alder-reactions with silica nanoparticles: The role of the polymer matrix." *Polymer* 69:357–368. doi: 10.1016/j.polymer.2015.03.017.
- [12] White, S.R., N.R. Sottos, P.H. Geubelle, J.S. Moore, M.R. Kessler, S.R. Sriram, E.N. Brown, and S. Viswanathan. 2001. "Automatic Healing of Polymer Composites." *Nature* 409:794–797.
- [13] Billiet, S., X.K.D. Hillewaere, R.F. Teixeira, F.E. Du Prez. 2013. "Chemistry of crosslinking processes for self-healing polymers." *Macromolecular Rapid Communications* 34 (4):290–309. doi: 10.1002/marc.201200689.
- [14] Garcia, S.J. 2014. "Effect of polymer architecture on the intrinsic self-healing character of polymers". *European Polymer Journal* 53 (1): 118-125. doi: 10.1016/j.eurpolymj.2014.01.026.
- [15] Yang, Y., and M.E. Urban. 2013. "Self-healing polymeric materials". *Chemical Society Reviews* 42 (17):7446–7467. doi: 10.1039/c3cs60109a.
- [16] Williams, K.A., A.J. Boydston, and C.W. Bielawski. 2007. "Towards Electrically Conductive, Self-Healing Materials." *Journal of the Royal Society* 4 (13): 359–62. doi:10.1098/rsif.2006.0202.
- [17] Caruso, M.M., D.A. Davis, Q. Shen, S.A. Odom, N.R. Sottos, S.R. White, and J.S. Moore. 2009. "Mechanically-Induced Chemical Changes in Polymeric Materials." *Chemical Reviews* 109: 5755–98. doi:10.1021/cr9001353.

- [18] Murphy, E.B., and F. Wudl. 2010. "The world of smart healable materials" *Progress in Polymer Science* 35 (1-2): 223–251. doi: 10.1016/j.progpolymsci.2009.10.006.
- [19] Zhang, Z., Y. Hu, Z. Liu, and T. Guo. 2012. "Synthesis and Evaluation of a Moisture-Promoted Healing Copolymer." *Polymer* 53 (14): 2979–90. doi:10.1016/j.polymer.2012.04.048.
- [20] Fiore, G.L, S.J. Rowan, and C. Weder. 2013. "Optically Healable Polymers." *Chemical Society Reviews* 42 (17): 7278–88. doi:10.1039/c3cs35471g.
- [21] Habault, D., H. Zhang, Y. Zhao. 2013. "Light-triggered self-healing and shape-memory polymers." *Chemical Society Reviews* 42 (17):7244–56. doi: 10.1039/c3cs35489j.
- [22] Cordier, P., F. Tournilhac, C. Soulié-Ziakovic, and L. Leibler. 2008. "Self-Healing and Thermoreversible Rubber from Supramolecular Assembly." *Nature* 451 (7181): 977–80. doi:10.1038/nature06669.
- [23] Montarnal, D., M. Capelot, F. Tournilhac, and L. Leibler. 2011. "Silica-Like Malleable Materials from Permanent Organic Networks." *Science* 334 (6058): 965–68.
- [24] Defize, T., R. Riva, J-M. Thomassin, C. Jérôme, and M. Alexandre. 2011. "Thermo-Reversible Reactions for the Preparation of Smart Materials: Recyclable Covalently-Crosslinked Shape Memory Polymers." *Macromolecular Symposia* 309–310 (1): 154–61. doi:10.1002/masy.201100036.
- [25] Imbernon, L., E.K. Oikonomou, S. Norvez, and L. Leibler. 2015. "Chemically Crosslinked yet Reprocessable Epoxidized Natural Rubber via Thermo-Activated Disulfide Rearrangements." *Polymer Chemistry* 6 (23): 4271–78. doi:10.1039/C5PY00459D.
- [26] Denissen, W., J.M. Winne, and F.E. Du Prez. 2016. "Vitrimers: Permanent Organic Networks with Glass-like Fluidity." *Chemical Science* 7 (1): 30–38. doi:10.1039/C5SC02223A.
- [27] Jin, Q., X. Liu, G. Liu, and J. Ji. 2010. "Fabrication of core or shell reversibly photo cross-linked micelles and nanogels from double responsive water-soluble block copolymers." *Polymer* 51 (6):1311–1319. doi: 10.1016/j.polymer.2010.01.026.
- [28] Du, P., X. Liu, Z. Zheng, X. Wang, T. Joncheray, and Y. Zhang. 2013. "Synthesis and Characterization of Linear Self-Healing Polyurethane Based on Thermally Reversible Diels–Alder Reaction." *RSC Advances* 3 (35): 15475–82. doi:10.1039/c3ra42278j.
- [29] Heo, Y., and H.A. Sodano. 2014. "Self-Healing Polyurethanes with Shape Recovery." *Advanced Functional Materials* 24 (33): 5261–68. doi:10.1002/adfm.201400299.

- [30] Oehlenschlaeger, K.K., J.O. Mueller, J. Brandt, S. Hilf, A. Lederer, M. Wilhelm, R. Graf, M.L. Coote, F.G. Schmidt, and C. Barner-Kowollik. 2014. "Adaptable hetero Diels-Alder networks for fast self-healing under mild conditions." *Advanced Materials* 26 (21):3561–3566. doi: 10.1002/adma.201306258.
- [31] Turkenburg, D.H., and H.R. Fischer. 2015. "Diels-Alder Based, Thermo-Reversible Cross-Linked Epoxies for Use in Self-Healing Composites." *Polymer* 79: 187–94. doi:10.1016/j.polymer.2015.10.031.
- [32] Coope, T.S., D.H. Turkenburg, H.R. Fischer, R. Luterbacher, H. Van Bracht, and I.P. Bond. 2016. "Novel Diels-Alder Based Self-Healing Epoxies for Aerospace Composites." *Smart Materials and Structures* 25 (8): 084010–19. doi:10.1088/0964-1726/25/8/084010.
- [33] Irusta, L, M.J. Fernandez-Berridi, J. Aizpurua. 2017. "Polyurethanes based on isophorone diisocyanate trimer and polypropylene glycol crosslinked by thermal reversible diels alder reactions." *Journal of Applied Polymer Science* 134 (9):44543–44552. doi: 10.1002/app.44543.
- [34] Ling, J., M.Z. Rong, and M.Q. Zhang. 2011. "Coumarin Imparts Repeated Photochemical Remendability to Polyurethane." *Journal of Materials Chemistry* 21 (45): 18373–80. doi:10.1039/c1jm13467a.
- [35] Ling, J., M.Z. Rong, and M.Q. Zhang. 2012. "Photo-Stimulated Self-Healing Polyurethane Containing Dihydroxyl Coumarin Derivatives." *Polymer* 53 (13): 2691–98. doi:10.1016/j.polymer.2012.04.016.
- [36] Aguirresarobe, R.H., L. Martin, N. Aramburu, L. Irusta, and M.J. Fernandez-Berridi. 2016. "Coumarin Based Light Responsive Healable Waterborne Polyurethanes." *Progress in Organic Coatings* 99: 314–21. doi:10.1016/j.porgcoat.2016.06.011.
- [37] Froimowicz, P., H. Frey, and K. Landfester. 2011. "Towards the Generation of Self-Healing Materials by Means of a Reversible Photo-Induced Approach." *Macromolecular Rapid Communications* 32 (5): 468–73. doi:10. 1002/marc.201000643.
- [38] Fang, Y., X. Du, Z. Du, H. Wang, and X. Cheng. 2017. "Light- and Heat-Triggered Polyurethane Based on Dihydroxyl Anthracene Derivatives for Self-Healing Applications." *Journal of Materials Chemistry A* 5 (17): 8010–17. doi:10. 1039/C7TA00871F.
- [39] Deng, G., C. Tang, F. Li, H. Jiang, and Y. Chen. 2010. "Covalent Cross-Linked Polymer Gels with Reversible Sol-Gel Transition and Self-Healing Properties." *Macromolecules* 43 (3): 1191–94. doi:10.1021/ma9022197.
- [40] Roy, N., E. Buhler, and J.M. Lehn. 2014. "Double Dynamic Self-Healing Polymers: Supramolecular and Covalent Dynamic Polymers Based on the Bis-Iminocarbohydrazide Motif." *Polymer International* 63 (8): 1400–1405. doi:10.1002/pi.4646.

- [41] Chao, A., I. Negulescu, and D. Zhang. 2016. "Dynamic Covalent Polymer Networks Based on Degenerative Imine Bond Exchange: Tuning the Malleability and Self-Healing Properties by Solvent." *Macromolecules* 49 (17): 6277–84. doi:10.1021/acs.macromol.6b01443.
- [42] Liu, W-X., C. Zhang, H. Zhang, N. Zhao, Z-X. Yu, and J Xu. 2017. "Oxime-Based and Catalyst-Free Dynamic Covalent Polyurethanes." *Journal of the American Chemical Society* 139 (25): 8678–84. jacs.7b03967. doi:10.1021/jacs.7b03967.
- [43] Cash, J.J., T. Kubo, A.P. Bapat, and B.S. Sumerlin. 2015. "Room-Temperature Self-Healing Polymers Based on Dynamic-Covalent Boronic Esters." *Macromolecules* 48 (7): 2098–2106. doi:10.1021/acs.macromol.5b00210.
- [44] Lai, J.C., J.F. Mei, X.Y. Jia, C.H. Li, X.Z. You, and Z. Bao. 2016. "A Stiff and Healable Polymer Based on Dynamic-Covalent Boroxine Bonds." *Advanced Materials* 28 (37): 8277–82. doi:10.1002/adma.201602332.
- [45] Ying, H., Y. Zhang, and J. Cheng. 2014. Dynamic urea bonds for the design of reversible and self-healing polymers. *Nature Communications* 5:1-9. doi: 10.1038/ncomms4218.
- [46] Yuan, C., M.Z. Rong, and M.Q. Zhang. 2014. "Self-Healing Polyurethane Elastomer with Thermally Reversible Alkoxyamines as Crosslinkages." *Polymer* 55 (7): 1782–91. doi:10.1016/j.polymer.2014.02.033.
- [47] Telitel, S., Y. Amamoto, J. Poly, F. Morlet-Savary, O. Soppera, J. Lalevée, and K. Matyjaszewski. 2014. "Introduction of Self-Healing Properties into Covalent Polymer Networks via the Photodissociation of Alkoxyamine Junctions." *Polymer Chemistry* 5 (3): 921. doi:10.1039/c3py01162c.
- [48] Yuan, C., M.Q. Zhang, and M.Z. Rong. 2014. "Application of Alkoxyamine in Self-Healing of Epoxy." *Journal of Materials Chemistry A* 2 (18): 6558. doi:10.1039/c4ta00130c.
- [49] Takahashi, A., R. Goseki, and H. Otsuka. 2017. "Thermally Adjustable Dynamic Disulfide Linkages Mediated by Highly Air-Stable 2,2,6,6-Tetramethylpiperidine-1-Sulfanyl (TEMPS) Radicals." *Angewandte Chemie - International Edition* 56 (8): 2016–21. doi:10.1002/anie.201611049.
- [50] Imato, K., A. Takahara, and H. Otsuka. 2015. "Self-Healing of a Cross-Linked Polymer with Dynamic Covalent Linkages at Mild Temperature and Evaluation at Macroscopic and Molecular Levels." *Macromolecules* 48 (16): 5632–39. doi:10.1021/acs.macromol.5b00809.
- [51] Liu, Y-L., and T-W. Chuo. 2013. "Self-healing polymers based on thermally reversible Diels–Alder chemistry." *Polymer Chemistry* 4 (7):2194-205. doi: 10.1039/c2py20957h.
- [52] Gacal, B., H. Durmaz, M.A. Tasdelen, G. Hizal, U. Tunca, and Y. Yagci. 2006. "Anthracene - Maleimide-Based Diels - Alder 'Click Chemistry' as a Novel Route

- to Graft Copolymers.” *Macromolecules* 39 (16): 5330–36. doi:10.1021/ma060690c.
- [53] Murphy, E.B., E. Bolanos, C. Schaffner-Hamann, F. Wudl, S.R. Nutt, and M.L. Auad. 2008. “Synthesis and Characterization of a Single-Component Thermally Remendable Polymer Network : Staudinger and Stille Revisited.” *Macromolecules* 41 (14): 5203–9. doi:10.1021/ma800432g.
- [54] Inglis, A.J., S. Sinnwell, M.H. Stenzel, and C. Barner-Kowollik. 2009. “Ultrafast Click Conjugation of Macromolecular Building Blocks at Ambient Temperature.” *Angewandte Chemie (International Edition in English)* 48 (13): 2411–14. doi:10.1002/anie.200805993.
- [55] Bassani, D.M. 2004. “The Dimerization of Cinnamic Acid Derivatives.” In *CRC Handbook of Organic Photochemistry and Photobiology* (2nd Edition), edited by Francesco Horspool, William; Lenci, 20/1-20/20. CRC Press LLC Boca Raton, Fla.
- [56] Röttger, M., T. Domenech, R. van der Weegen, A. Breuillac, R. Nicolaÿ, and L. Leibler. 2017. “High-performance vitrimers from commodity thermoplastics through dioxaborolane metathesis”. *Science* 356 (6333):62–65. doi: 10.1126/science.aah5281.
- [57] Brutman, J.P., P.A. Delgado, and M.A. Hillmyer. 2014. “Polylactide Vitrimers.” *ACS Macro Letters* 3 (7): 607–10. doi:10.1021/mz500269w.
- [58] Taynton, P., K. Yu, R.K. Shoemaker, Y. Jin, H.J. Qi, and W. Zhang. 2014. “Heat- or Water-Driven Malleability in a Highly Recyclable Covalent Network Polymer.” *Advanced Materials* 26 (23): 3938–42. doi:10.1002/adma.201400317.
- [59] Denissen, W., G. Rivero, R. Nicolaÿ, L. Leibler, J.M. Winne, and F.E. Du Prez. 2015. “Vinylogous Urethane Vitrimers.” *Advanced Functional Materials* 25 (16): 2451–57. doi:10.1002/adfm.201404553.
- [60] Denissen, W., M. Droesbeke, R. Nicolaÿ, L. Leibler, J.M. Winne, and F.E. Du Prez. 2017. “Chemical Control of the Viscoelastic Properties of Vinylogous Urethane Vitrimers.” *Nature Communications* 8: 14857. doi:10.1038/ncomms14857.
- [61] Obadia, M.M., B.P. Mudraboyina, A. Serghei, D. Montarnal, and E. Drockenmuller. 2015. “Reprocessing and Recycling of Highly Cross-Linked Ion-Conducting Networks through Transalkylation Exchanges of C-N Bonds.” *Journal of the American Chemical Society* 137 (18): 6078–6083. doi: 10.1021/jacs.5b02653.
- [62] Fortman, D.J., J.P. Brutman, C.J. Cramer, and M.A. Hillmyer. 2015. “Mechanically Activated, Catalyst-Free Polyhydroxyurethane Vitrimers.” *Journal of the American Chemical Society* 137 (44): 14019–14022. doi: 10.1021/jacs.5b08084.

- [63] Nevejans, S., N. Ballard, J.I. Miranda, B. Reck, and J.M. Asua. 2016. “The underlying mechanisms for self-healing of poly(disulfide)s”. *Physical Chemistry Chemical Physics* 18:27577–27583. doi: 10.1039/C6CP04028D.
- [64] Matxain, J.M., J.M. Asua, and F. Ruiperez. 2016. “Design of new disulfide-based organic compounds for the improvement of self-healing materials.” *Physical Chemistry Chemical Physics* 18:1758–1770. doi: 10.1039/C5CP06660C.
- [65] Lei, Z.Q., H.P. Xiang, Y.J. Yuan, M.Z. Rong, and M.Q. Zhang. 2014. “Room-Temperature Self-Healable and Remoldable Cross-Linked Polymer Based on the Dynamic Exchange of Disulfide Bonds.” *Chemistry of Materials* 26 (6): 2038–46. doi:10.1021/cm4040616.
- [66] Rekondo, A., R. Martin, A. Ruiz de Luzuriaga, G. Cabañero, H.J. Grande, and I. Odriozola. 2014. “Catalyst-Free Room-Temperature Self-Healing Elastomers Based on Aromatic Disulfide Metathesis.” *Materials Horizons* 1 (2): 237–40. doi:10.1039/C3MH00061C.
- [67] Xu, W.M., M.Z. Rong, and M.Q. Zhang. 2016. “Sunlight Driven Self-Healing, Reshaping and Recycling of Robust, Transparent and Yellowing-Resistant Polymer.” *Journal of Materials Chemistry A* 4: 10683-90. doi:10.1039/C6TA02662A.
- [68] Aguirresarobe, R.H., L. Martin, M.J. Fernandez-Berridi, and L. Irusta. 2017. “Autonomic Healable Waterborne Organic-Inorganic Polyurethane Hybrids Based on Aromatic Disulfide Moieties.” *Express Polymer Letters* 11 (4): 266–77. doi:10.3144/expresspolymlett.2017.27.
- [69] Azcune, I., and I. Odriozola. 2016. “Aromatic disulfide crosslinks in polymer systems: Self-healing, reprocessability, recyclability and more.” *European Polymer Journal* 84:147–160. doi: 10.1016/j.eurpolymj.2016.09.023.
- [70] Ruiz de Luzuriaga, A., R. Martin, N. Markaide, A. Rekondo, G. Cabañero, J. Rodríguez, and I. Odriozola. 2016. “Epoxy resin with exchangeable disulfide crosslinks to obtain reprocessable, repairable and recyclable fiber-reinforced thermoset composites.” *Materials Horizons* 3 (3):241–247. doi: 10.1039/c6mh00029k.
- [71] Ruiz de Luzuriaga, A., J.M. Matxain, F. Ruipérez, R. Martin, J.M. Asua, G. Cabañero, and I. Odriozola. 2016. “Transient mechanochromism in epoxy vitrimer composites containing aromatic disulfide crosslinks.” *Journal of Material Chemistry C* 4 (26):6220–6223. doi: 10.1039/C6TC02383E.
- [72] Ji, S., W. Cao, Y. Yu, and H. Xu. 2015. “Visible-Light-Induced Self-Healing Diselenide-Containing Polyurethane Elastomer.” *Advanced Materials* 27 (47): 7740–45. doi:10.1002/adma.201503661.
- [73] An, X., R.H. Aguirresarobe, L. Irusta, F. Ruipérez, J.M. Matxain, X. Pan, N. Aramburu, D. Mecerreyes, H. Sardon, and J. Zhu. 2017. “Aromatic Diselenide

- Crosslinkers to Enhance the Reprocessability and Self-Healing of Polyurethane.” *Polymer Chemistry* 8: 3641–46. doi:10.1039/c7py00448f.
- [74] Deng, G., F. Li, H. Yu, F. Liu, C. Liu, W. Sun, H. Jiang, and Y. Chen. 2012. “Dynamic Hydrogels with an Environmental Adaptive Self-Healing Ability and Dual Responsive Sol–Gel Transitions.” *ACS Macro Letters* 1 (2): 275–79. doi:10.1021/mz200195n.
- [75] Casuso, P., I. Odriozola, A. Pérez-San Vicente, I. Loinaz, G. Cabañero, H.J. Grande, and D. Dupín. 2015. Injectable and Self-Healing Dynamic Hydrogels Based on Metal(I)-Thiolate/Disulfide Exchange as Biomaterials with Tunable Mechanical Properties. *Biomacromolecules* 16 (11): 3552–61 doi: 10.1021/acs.biomac.5b00980.
- [76] Amamoto, Y., J. Kamada, H. Otsuka, A. Takahara, and K. Matyjaszewski. 2011. “Repeatable Photoinduced Self-Healing of Covalently Cross-Linked Polymers through Reshuffling of Trithiocarbonate Units.” *Angewandte Chemie (International Ed. in English)* 50 (7): 1660–63. doi:10.1002/anie.201003888.
- [77] Amamoto, Y., H. Otsuka, A. Takahara, and K. Matyjaszewski. 2012. “Self-Healing of Covalently Cross-Linked Polymers by Reshuffling Thiuram Disulfide Moieties in Air under Visible Light.” *Advanced Materials* 24 (29): 3975–80. doi:10.1002/adma.201201928.
- [78] Gordon, M.B., J.M. French, N.J. Wagner, and C.J. Kloxin. 2015. “Dynamic Bonds in Covalently Crosslinked Polymer Networks for Photoactivated Strengthening and Healing.” *Advanced Materials* 27 (48): 8007–10. doi:10.1002/adma.201503870.
- [79] Brunsveld, L, B.J. Folmer, E.W. Meijer, and R.P. Sijbesma. 2001. “Supramolecular Polymers.” *Chemical Reviews* 101 (12): 4071–98. doi:10.1021/cr990125q.
- [80] Herbst, F., D. Döhler, P. Michael, W.H. Binder. 2013. “Self-healing polymers via supramolecular forces.” *Macromolecular Rapid Communications* 34 (3):203–220. doi: 10.1002/marc.201200675.
- [81] de Espinosa, L. Montero, G.L. Fiore, C. Weder, J.E. Foster, and Y.C. Simon. 2015. “Healable Supramolecular Polymer Solids.” *Progress in Polymer Science* 49–50: 60–78. doi:10.1016/j.progpolymsci.2015.04.003.
- [82] Sijbesma, R.P., F.H. Beijer, L. Brunsveld, B.J. Folmer, J.H. Hirschberg, R.F. Lange, J.K. Lowe, and E.W. Meijer. 1997. “Reversible Polymers Formed from Self-Complementary Monomers Using Quadruple Hydrogen Bonding.” *Science (New York, N.Y.)* 278 (5343): 1601–4. doi:10.1126/science.278.5343.1601.
- [83] Park, T., E.M. Todd, S. Nakashima, and S.C. Zimmerman. 2005. “A Quadruply Hydrogen Bonded Heterocomplex Displaying High-Fidelity Recognition.” *Journal of the American Chemical Society* 127 (51): 18133–42. doi:10.1021/ja0545517.
- [84] Fouquey, C., J-M. Lehn, and A-M. Levelut. 1990. “Molecular Recognition Directed Self-Assembly of Supramolecular Liquid Crystalline Polymers from

- Complementary Chiral Components.” *Advanced Materials* 2 (5): 254–57. doi:10.1002/adma.19900020506.
- [85] Kalista, S.J., T.C. Ward, and Z. Oyetunji. 2007. “Self-Healing of Poly(Ethylene-Co-Methacrylic Acid) Copolymers Following Projectile Puncture.” *Mechanics of Advanced Materials and Structures* 14 (5): 391–97. doi:10.1080/15376490701298819.
- [86] Xiao, Y., H. Huang, and X. Peng. 2017. “Synthesis of Self-Healing Waterborne Polyurethanes Containing Sulphonate Groups.” *RSC Advances* 7 (33): 20093–100. doi:10.1039/C6RA28416G.
- [87] Cao, Y., T.G. Morrissey, E. Acome, S.I. Allec, B.M. Wong, C. Keplinger, and C. Wang. 2017. “A Transparent, Self-Healing, Highly Stretchable Ionic Conductor.” *Advanced Materials* 29 (10): 1605099. doi:10.1002/adma.201605099.
- [88] Burattini, S., H.M. Colquhoun, J.D. Fox, D. Friedmann, B.W. Greenland, P.J. F. Harris, W. Hayes, M.E. Mackay, and S.J. Rowan. 2009. “A Self-Repairing, Supramolecular Polymer System: Healability as a Consequence of Donor–acceptor Π – π Stacking Interactions.” *Chemical Communications*, 0: 6717–19. doi:10.1039/b910648k.
- [89] Burattini, S., B.W. Greenland, D. Hermida Merino, W. Weng, J. Seppala, H.M. Colquhoun, W. Hayes, M.E. Mackay, I.W. Hamley, and S.J. Rowan. 2010. “A Healable Supramolecular Polymer Blend Based on Aromatic Pi-Pi Stacking and Hydrogen-Bonding Interactions.” *Journal of the American Chemical Society* 132 (34): 12051–58. doi:10.1021/ja104446r.
- [90] Burnworth, M., L. Tang, J.R. Kumpfer, A.J. Duncan, F.L.O Beyer, G.L. Fiore, S.J. Rowan, and C. Weder. 2011. “Optically Healable Supramolecular Polymers.” *Nature* 472 (7343): 334–37. doi:10.1038/nature09963.
- [91] Bode, S., R.K. Bose, S. Matthes, M. Ehrhardt, A. Seifert, F.H. Schacher, R.M. Paulus, S. Stumpf, B. Sandmann, J. Vitz, A. Winter, S. Hoepfener, S.J. Garcia, S. Spange, S. van der Zwaag, M.D. Hager and U.S. Schubert. 2013. “Self-Healing Metallopolymers Based on Cadmium Bis(terpyridine) Complex Containing Polymer Networks.” *Polymer Chemistry* 4 (18): 4966. doi:10.1039/c3py00288h.
- [92] Rao, Y.L., A. Chortos, R. Pfattner, F. Lissel, Y.C. Chiu, V. Feig, J. Xu, T. Kurosawa, X. Gu, C. Wang, M. He, J.W. Chung, and Z. Bao. 2016. “Stretchable Self-Healing Polymeric Dielectrics Cross-Linked through Metal-Ligand Coordination.” *Journal of the American Chemical Society* 138 (18): 6020–27. doi:10.1021/jacs.6b02428.
- [93] Tran, N.B., J.R. Moon, Y.S. Jeon, J. Kim, and J.H. Kim. 2017. “Adhesive and Self-Healing Soft Gel Based on Metal-Coordinated Imidazole-Containing Polyaspartamide.” *Colloid and Polymer Science* 295 (4): 655–64. doi:10.1007/s00396-017-4051-7.

- [94] Liu, D., D. Wang, M. Wang, Y. Zheng, K. Koynov, G.K. Auernhammer, H.J. Butt, and T. Ikeda. 2013. "Supramolecular Organogel Based on Crown Ether and Secondary Ammoniumion Functionalized Glycidyl Triazole Polymers." *Macromolecules* 46: 4617–25. doi:10.1021/ma400407a.
- [95] Kakuta, T., Y. Takashima, M. Nakahata, M. Otsubo, H. Yamaguchi, and A. Harada. 2013. "Preorganized Hydrogel: Self-Healing Properties of Supramolecular Hydrogels Formed by Polymerization of Host-Guest-Monomers That Contain Cyclodextrins and Hydrophobic Guest Groups." *Advanced Materials* 25 (20): 2849–53. doi:10.1002/adma.201205321.
- [96] Wang, Y-F., D-L. Zhang, T. Zhou, H-S. Zhang, W-Z. Zhang, L. Luo, A-M. Zhang, B-J. Li, and S. Zhang. 2014. "A Reversible Functional Supramolecular Material Formed by Host-guest Inclusion." *Polymer Chemistry* 5: 2922. doi:10.1039/c3py01509b.
- [97] Nakahata, M., Y. Takashima, H. Yamaguchi, and A. Harada. 2011. "Redox-Responsive Self-Healing Materials Formed from Host-guest Polymers." *Nature Communications* 2. Nature Publishing Group: 511. doi:10.1038/ncomms1521.
- [98] van Gemert, G.M.L., J.W. Peeters, S.H.M. Söntjens, H.M. Janssen, and A.W. Bosman. 2012. "Self-Healing Supramolecular Polymers In Action." *Macromolecular Chemistry and Physics* 213 (2): 234–42. doi:10.1002/macp.201100559.
- [99] Folmer, B.J.B., R.P. Sijbesma, R.M. Versteegen, J.A J. van der Rijt, and E.W. Meijer. 2000. "Supramolecular Polymer Materials: Chain Extension of Telechelic Polymers Using a Reactive Hydrogen-Bonding Synthon." *Advanced Materials* 12 (12): 874–78. doi:10.1002/1521-4095(200006)12:12<874::AID-ADMA874>3.0.CO;2-C.
- [100] Chen, S., N. Mahmood, M. Beiner, and W.H. Binder. 2015. "Self-Healing Materials from V- and H-Shaped Supramolecular Architectures." *Angewandte Chemie* (International Ed. in English) 54 (35): 10188-10192. doi: 10.1002/anie.201504136.
- [101] Zhang, G., T. Ngai, Y. Deng, and C. Wang. 2016. "An Injectable Hydrogel with Excellent Self-Healing Property Based on Quadruple Hydrogen Bonding." *Macromolecular Chemistry and Physics* 217 (19):2172–2181. doi: 10.1002/macp.201600319.
- [102] Zhang, G., Y. Chen, Y. Deng, T. Ngai, and C. Wang. 2017. "Dynamic Supramolecular Hydrogels: Regulating Hydrogel Properties through Self-Complementary Quadruple Hydrogen Bonds and Thermo-Switch." *ACS Macro Letters* 6 (7):641–646. doi: 10.1021/acsmacrolett.7b00275.
- [103] Jaudouin, O., J-J. Robin, J-M. Lopez-Cuesta, D. Perrin and C. Imbert. 2012. "Ionomer-based polyurethanes: a comparative study of properties and applications". *Polymer International* 61(4): 495–510. doi: 10.1002/pi.4156.

- [104] Wu, D.Y., S. Meure, and D. Solomon. 2008. "Self-healing polymeric materials: A review of recent developments". *Progress in Polymer Science* 33(5):479–522. doi: 10.1016/j.progpolymsci.2008.02.001.
- [105] Coulibaly, S, A. Roulin, S. Balog, M.V. Biyani, J.E. Foster, S.J. Rowan, G.L. Fiore, and C. Weder. 2014. "Reinforcement of Optically Healable Supramolecular Polymers with Cellulose Nanocrystals." *Macromolecules* 47 (1): 152–60. doi:10.1021/ma402143c.
- [106] Lee, B.P., J.L. Dalsin, and P.B. Messersmith. 2002. "Synthesis and Gelation of DOPA-Modified Poly(ethylene Glycol) Hydrogels." *Biomacromolecules* 3: 1038–47. doi:10.1021/bm025546n.
- [107] Schmatloch, S., M. Fernández González, and U.S. Schubert. 2002. "Metallo-Supramolecular Diethylene Glycol: Water-Soluble Reversible Polymers." *Macromolecular Rapid Communications* 23: 957–61. doi:10.1002/1521-3927(200211)23:16<957::AID-MARC957>3.0.CO;2-W.
- [108] Hong, G., H. Zhang, Y. Lin, Y. Chen, Y. Xu, W. Weng, and H. Xia. 2013. "Mechanoresponsive healable metallosupramolecular polymers." *Macromolecules* 46 (21):8649–8656. doi: 10.1021/ma4017532.
- [109] Yang, X., H. Yu, L. Wang, R. Tong, M. Akram, Y. Chen, and X. Zhai. 2015. "Self-Healing Polymer Materials Constructed by Macrocycle-Based Host–guest Interactions." *Soft Matter* 11: 1242–52. doi:10.1039/C4SM02372B.
- [110] Nakahata, M., Y. Takashima, and A. Harada. 2016. "Highly Flexible, Tough, and Self-Healing Supramolecular Polymeric Materials Using Host-Guest Interaction." *Macromolecular Rapid Communications* 37 (1):86–92. doi:10.1002/marc.201500473.

Chapter 5

INTRINSIC SELF-HEALING ELASTOMERS BASED ON COVALENT BONDING

*Marianella Hernández**, *Raquel Verdejo*
and Miguel Angel López-Manchado

Institute of Polymer Science and Technology (ICTP-CSIC), Madrid, Spain

ABSTRACT

Self-healing materials have intensively been investigated over the past 15 years. Several approaches have been developed, resulting in materials capable of dealing with damage events in a more or less independent way, thereby extending their service life, and thus reducing waste. Large interest has been drawn to self-healing elastomeric materials, following either extrinsic or intrinsic approaches. In this chapter we discuss Diels-Alder chemistry and disulfide exchange reactions as the most prominent examples currently used in the development of intrinsic self-healing elastomers based on reversible covalent bonds.

Keywords: self-healing, elastomer, covalent bonding, Diels-Alder chemistry, disulfide exchange reaction

1. INTRODUCTION

Self-healing materials represent the forefront of recent developments in materials chemistry and engineering. Due to their built-in ability to repair physical damage, they can effectively prevent catastrophic failure and extend the material life-time. There are

* Corresponding Author Email: marherna@ictp.csic.es.

basically two well-established ways to develop self-healing polymers [Blaiszik 2010, Murphy 2010, Van Der Zwaag 2008, Wu 2008]. The first one, the so-called extrinsic concept, is based on the integration of discrete containers (capsules, fibers, or vascular networks) loaded with active components into the matrix material. When damage occurs, the containers break and release the healing agent within, which further reacts in the presence of other components embedded as other extrinsic phases in the matrix, repairing the damage. The system has a great potential for healing internally developed microcracks, but fails to repair a macroscopic cut in the material. Furthermore, the irreversible nature of the healing mechanism is a limitation. The second approach relates to the development of the so-called intrinsically self-healing materials, that is, materials containing dynamic bonds that can restore their chemical or physical connections after damage, under the influence of a non-disruptive external stimulus. A number of dynamic bonds have been demonstrated to permit healing: Diels-Alder (DA) and retro-Diels-Alder (retro-DA) based bonds; hydrogen bonding in supramolecular networks, coordination complexes, disulfides based chemistries, ionic clusters in ionomers, among others. All of these are simpler than the aforementioned extrinsic self-healing systems and due to the reversible character of the chemical/physical bonds involved in the healing (and breaking) process, they can theoretically lead to an infinite amount of healing cycles as no external healing agents are required. However, in these materials there is typically an inevitable trade-off between repairability and mechanical properties, with a high degree of self-healing being achieved mainly with materials having low mechanical strength and stiffness. Besides, the restoration of large damage areas remains a challenge because the contact between the failed surfaces is often lost.

1.1. Dynamic Covalent Bonding

The dynamic bond can be defined as any class of bond that can selectively undergo reversible breaking and reformation, usually under equilibrium conditions. The term “dynamic bond” usually encompasses two broad categories, supramolecular interactions and dynamic covalent bonds. A comparison naturally rises between both. The thermodynamic equilibration process of dynamic covalent networks is often much slower than typical supramolecular self-assemblies. However, such slow kinetics requires a less demanding stimulus and allows for a much more stable thermodynamic equilibrium compared to the relatively fragile assembly provided by non-covalent interactions. The pros and cons of these two types of systems (dynamic covalent vs. supramolecular bond) make them promising, even complementary, candidates for self-healing applications [Wojtecki 2011]. The reversibility of the dynamic bond allows repair to take place at the molecular level to fully restore the original material properties and enables the process to be repeated many times.

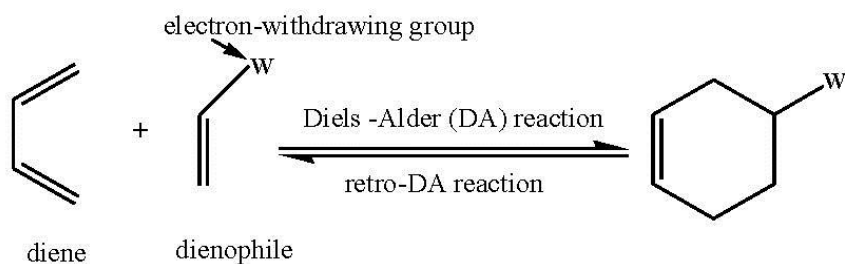


Figure 1. Schematic representation of thermally reversible Diels-Alder (DA) reaction.

One of the most studied dynamic covalent bonds is obtained from the thermoreversible Diels-Alder (DA) reaction. The [4 + 2] cycloaddition reaction between an electron-rich diene and an electron poor dienophile produces a cyclohexene adduct that could be reverted back via retro-DA reaction at elevated temperatures (see Figure 1). The reversibility feature of this reaction may endow the crosslinked polymer containing DA bonds with remoldability and healing ability.

The first self-healing polymer based on the thermoreversible DA reaction was reported by the group of Wudl [Chen 2002]. Their pioneer work proposed a crosslinked thermoset formed by DA cycloaddition of multi-furan and multi-maleimide monomers. The resulting covalent crosslinked network displayed reversibility upon heating to 150°C for 15min, leading to a cleavage of about 25% of the DA adduct. Upon cooling to 80°C and subsequent curing at this temperature, the broken bonds were allowed to fully reconnect. Self-healing experiments were performed by cutting the sample into two pieces. After damage, the two cut surfaces were brought closely into contact, healed at 150°C to allow the retro-DA reaction and, finally, cooled to room temperature. The restoration of mechanical integrity across the healed fracture surface was studied by scanning electron microscopy (SEM), which indicated almost complete recovery. The average healing efficiency was found to be about 50% of the original fracture energy. A year later [Chen 2003], the same authors improved their work by the utilization of low-melting point monomers, which feature a higher mobility in the resulting crosslinked network, thereby increasing the healing efficiency to about 80%. Though it was not the first time DA chemistry was applied to achieve reversible crosslinking, the impressive healing performance had made Wudl's work a milestone, which since then has inspired surging interest in self-healing polymers [Liu 2013, Murphy 2010, Zou 2017].

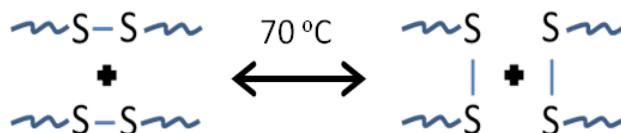


Figure 2. Disulfide exchange reaction.

DA moieties allow the implementation of self-healing capabilities to existing polymeric networks without significantly compromising the original properties. However, the main drawback of these reactions is that the healing process usually takes place at high temperatures. Weaker covalent bonds, such as disulfide (S-S) groups can therefore be beneficial to introduce a healing functionality at lower temperatures, meanwhile keeping a reasonable level of bond strength. Klumperman et al. [Canadell 2011] came up with a new self-healing concept based on the use of disulfide links incorporated in a rubber network, which was able to fully restore its mechanical properties. The exchange reaction of disulfides at moderate temperatures led to the renewal of crosslinks across damaged surfaces, as will be discussed later (see Figure 2). Disulfide bonds have been quite favored in designing self-healing and recyclable networks as their reversibility can be triggered by a variety of stimuli such as heat, light, shear forces, redox reactions, among others [Gyarmati 2013]. The healing process in such systems is mainly based on S-S bond re-shuffling. However, nucleophilic reagents such as thiol groups can also facilitate scission of S-S bonds via thiol-disulfide exchange reactions [Abdolah Zadeh 2014].

2. SELF-HEALING ELASTOMERS

In the field of elastomers, Leibler et al.'s pioneering work provided decisive motivation for the development of new rubber materials with self-healing behavior [Cordier 2008]. The authors described a supramolecular rubber based on simple low molecular weight compounds such as fatty diacids and triacids. These compounds associate with one another to form both long chains and crosslinks mainly by hydrogen bonding, exhibiting pronounced self-healing behavior. Despite the promising results, this non-covalent network is relatively fragile and the final properties of are far from those needed in real life applications. Inspired by this research, several other authors have continued working with self-healing rubbers based on supramolecular assemblies, either by hydrogen bonding and/or ionic interactions. Examples of the developments achieved in this area of research during the last two decades are listed in Table 2.1.

Many efforts have also been devoted to implement self-healing functionalities in natural or synthetic rubbers properly crosslinked by covalent bonding. Elastomers derive their excellent mechanical properties from the creation of a stable covalently bonded three-dimensional molecular network. In principle, this irreversible covalent crosslinked network does not allow for either self-healing or reprocessing. Healing requires chain mobility and, therefore, seems to be in direct contradiction with the fixation needed to form a permanent network. Therefore, the challenge of obtaining a crosslinked network with weaker covalent bonds that can infer healing capabilities to the rubber as well as

good mechanical properties still remains. Table 2.1 shows the latest results on this research line. In the next sections we will give a more detailed insight into self-healing elastomers based on DA chemistry and sulfur chemistry.

Table 2.1. Examples of self-healing elastomers and rubbery materials

Elastomer	Healing mechanism	Reference
Butadiene Rubber (BR)	Diels-Alder	[Bai 2015a, Trovatti 2015]
	Reversible disulfide crosslinks	[Xiang 2015]
	Hydrogen bonding	[Gold 2016, Wang 2015]
Natural Rubber (NR)/ Polyisoprene (IR)	Reversible disulfide crosslinks	[Hernández 2016a, Hernández 2016b]
	Hydrogen bonding	[Chino 2001, Liu 2016]
	Ionic functional groups	[Xu 2016a]
Epoxidized Natural Rubber (ENR)	Reversible disulfide crosslinks	[Imbernon 2015]
	Molecular interdiffusion/polar interaction	[Rahman 2011, Rahman 2012, Rahman 2013]
Bromobutyl Rubber (BIIR)	Ionic imidazole/bromide	[Das 2015, Le 2016, Le 2017]
Chloroprene Rubber (CR)	Reversible disulfide crosslinks	[Xiang 2016]
Nitrile Rubber (NBR)	Ionic functional groups	[Nellesen 2011, Schussele 2012]
Styrene-Butadiene Rubber (SBR)	Ionic functional groups	[Xu 2016b]
	Diels-Alder	[Kuang 2016]
Thermoplastic Elastomer (TPE)	Hydrogen bonding, brushes, two-phase separation	[Chen 2012]
	Diels-Alder	[Bai 2015b]
Supramolecular Rubber	Hydrogen bonding, vitrimers	[Cordier 2008]
Poly(dimethyl siloxane) (PDMS)	Diels-Alder	[Zhao 2016]
	Encapsulation (extrinsic)	[Cho 2012, Keller 2007, 2008, Mangun 2010]
	Thiol-silver interactions	[Martin 2012]
	Disulfide metathesis, sunlight	[Xiang 2017]
Polyurethane (PU)	Reversible alkoxyamine moieties	[Yuan 2014]
	Hydrogen bonding	[Kim 2015]
	Diels-Alder	[Fu 2016]
	Disulfide metathesis	[Aguirresarobe 2017, Amamoto 2012, Xu 2016c]
	Heat transfer	[Huang 2013, Kim 2013]
	Chain-end interaction	[Yamaguchi 2007, Yamaguchi 2012]
Poly(urea-urethane)	Disulfide metathesis, H-bonds	[Martin 2014, Martin 2016, Rekondo 2014]
Acrylic Elastomer (VHB 4910)	Hydrogen bonding, chain entanglement	[Fan 2015]
Ethylene-Propylene-Diene Monomer (EPDM)	Diels-Alder	[Polgar 2015]
Organic-inorganic sol-gel hybrid	Disulfide exchange in dual network	[Abdolah Zadeh 2014, Abdolah Zadeh 2016]
Poly(butyl acrylate-co-acrylic acid)	Metal ion-ionomer interaction	[Bose 2015a, b, Hohlbein 2015]

2.1. Diels-Alder Chemistry

The development of new mild and efficient crosslinking reactions for rubbers is of ongoing interest as the current curing approaches are not optimal for self-healing applications. Diels-Alder (DA) reactions can be considered as an alternative mechanism for crosslinking rubbers. Such a material should behave like permanently crosslinked rubbers under service conditions, while the reversibility of the crosslinks would allow healing under damage conditions. Such a concept can be applied to a broad range of rubbers. They represent a popular choice, especially because DA reactions allow for relatively fast kinetics and mild reaction conditions. One of the most iconic examples of the DA reaction is that between a furan and a maleimide [Gheneim 2002, Liu 2013, Zou 2017]. Its low coupling and high decoupling temperatures make it an excellent candidate for reversible polymer crosslinking. Polgar et al. [Polgar 2015] demonstrated this principle in a commercial ethylene-propylene rubber grafted with maleic anhydride (EPM-g-MA) in a simple two-step approach. The maleated rubber was first modified with furfurylamine to graft furan groups onto the rubber backbone. These pending furans were further crosslinked with a bismaleimide, welding a thermoreversible bridge between two furan moieties. The reversibility of the crosslinks was proven by infrared spectroscopy, solubility tests and DMTA measurements. This behavior was also demonstrated by a simple and practical healing test, by cutting the crosslinked rubber into small pieces and remolding these into a new sample with similar properties.

Trovatti et al. [Trovatti 2015] and Bai et al. [Bai 2015a] also implemented the furan/maleimide combination in polybutadiene rubber (BR) in search of recyclable tires; they added a furan heterocycle as pending group in BR (by means of a thiol-ene reaction of furfuryl thiol) and added maleimide as dienophile to crosslink the system. According to Trovatti, the forward reaction is dominant around 60°C which allows for a maximum use temperature of 60°C. The reverse reaction is dominant above 100°C, implying that there is increased mobility and theoretically the forward reaction should occur again when cooled below 60°C. Considering that the forward Diels-Alder reaction occurs at 60°C, this may lead to self-healing without any intervention in some applications. Trovatti also studied the viability of applying this approach to natural rubber (NR) [Trovatti 2017]. As expected, the process was more complex than the corresponding BR process because the chemical structure of NR, exclusively composed of long chains with double bonds, is less reactive than the pending vinyl units in BR. NR was chemically modified with furan moieties, which in the presence of bismaleimides led to the elastomer crosslinking. The modification yielded about 2% of insertion of furan motifs per poly(isoprene) unit. The reversibility of the DA reaction was successfully proven by ¹H NMR measurements. Although this research was a proof-of-concept, the possibility of crosslinking NR in a reversible fashion opens the way to a straightforward mode of recycling and/or healing elastomeric articles, such as tires. Considering that the

maximum temperature reached by an on-use tire is about 80°C under the most straining circumstances and, moreover, that the retro-DA process is rather slow, the tires would withstand these conditions without losing their performance for long time.

A similar healing reaction, but in poly(styrene-block-butadiene-block-styrene) (SBS) rubber was described by Bai et al. [Bai 2015b]. They grafted furfuryl groups to the SBS rubber which was crosslinked by introducing bismaleimide into the toluene solution. After stirring, the solution was casted and dried at 80°C for 12h. The resulting film was then cut and remolded under 10kPa of pressure at 160°C for 5min, presumably breaking the DA crosslinks. The remolded film was then cooled for 2 days, after which tensile tests showed only a slight decrease in modulus and tensile strength, indicating the reformation of the DA crosslinks.

DA chemistry should also provide an opportunity to crosslink butyl rubber (IIR). However, the application of DA chemistry to IIR has encountered some limitations due to the incomplete reactions and mixtures of products obtained during the preparation of the diene, as well as unoptimized reaction conditions for polymer grafting [Mclean 2007]. Moustafa et al. [Abd Rabo Moustafa 2013] tried to overcome these limitations by grafting poly(ethylene oxide) (PEO) or polystyrene (PS) while at the same time introducing carboxylic acid moieties along the polymer backbone. They demonstrated how the preparation of butyl rubber graft copolymers using DA chemistry could be used to tune their tensile properties as well as their thermal reversibility. This versatility opens prospects for new self-healing approaches in rubbers.

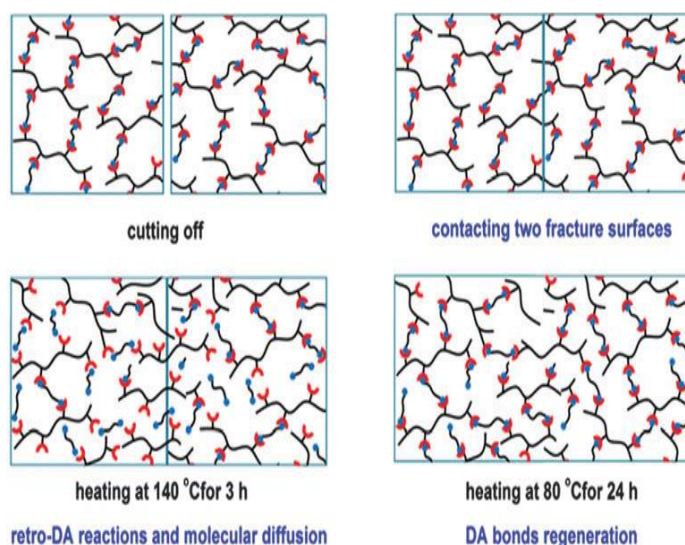


Figure reprinted and adapted with permission from [Zhao 2016]. Copyright 2015, Royal Society of Chemistry.

Figure 3. Schematic illustration of the self-healing process in polysiloxane crosslinked by DA bonds.

Self-healing poly(dimethyl siloxane) (PDMS) elastomers based on DA reactions are another rubber family facing difficulties, possibly because of limitations in finding the appropriate precursors for their synthesis. To prepare an excellent self-healing PDMS, the compatibility of the two main precursors, the reactivity of DA bond moieties (maleimide or furan) in the precursor, as well as the crosslinking network parameters such as chain mobility and crosslinking degree must be considered. Zhao et al. [Zhao 2016] reported a facile route to prepare a thermally healable polysiloxane elastomer by directly crosslinking PDMS bearing maleimide pendants (PM) with a furan-end functionalized siloxane (FS) via the DA reaction. The self-healing properties were quantitatively evaluated by tensile tests obtaining a healing efficiency of 95% after 24h at 80°C. They proposed a healing mechanism composed of 3 steps: i) adjoining two fracture surfaces, ii) retro-DA reactions and molecular diffusion, and iii) DA bond regeneration (see Figure 3). Based on this mechanism, the authors concluded that the molecular weight of the precursors plays an important role. When the molecular weight of the precursor bearing maleimide pendants is too high, the mobility of molecular chains reduces the molecular diffusion and DA bond re-formation at the fracture interface, which will decrease the self-healing efficiency. However, if the molecular weight of the precursor is too low or the DA bond content is too high, the obtained crosslinked rubber will be very brittle and not useful. In conclusion, choosing an appropriate precursor with appropriate molecular weight and maleimide content is the key to obtain a self-healing PDMS elastomer with good mechanical properties.

2.2. Disulfide Exchange Reactions

Sulfur chemistry has historically played an essential role in rubber science and engineering, since sulfur vulcanization has been the traditional method for curing polydiene rubbers. Sulfur reacts with rubber chains creating sulfur crosslinks of different lengths (i.e., mono-, di- and poly-sulfides), pendant side groups, and cyclic sulfides [Alliger 1964, Hofmann 1967]. Naturally, the study concerning disulfide bonds is of great value for the design of self-healing rubbers because they can undergo different reversible reactions (metathesis reactions) such as disulfide exchange and thiol-disulfide exchange, to obtain self healing properties [Hager 2016]. The disulfide interchange also offers a significant advantage because sulfur-sulfur (S-S) bonds can be incorporated into low T_g networks (e.g., rubbers), thus facilitating mild temperature (close to room temperature) reversibility.

Klumperman et al. [Canadell 2011] used disulfide chemistry to introduce a self-healing ability in a covalently crosslinked rubbery material. An epoxy resin containing disulfide groups in its structure was crosslinked with a tetrafunctional thiol. When a sample of this network was damaged and the fracture surfaces were immediately put into

close contact and heated at 60°C, the mechanical properties were fully restored in just 1h. As expected, longer healing times led to better healing, but even when the contact time between the two broken parts was as short as 15min, healing was observed. The results indicated that the healed samples had elastic properties similar to the original material, even after multiple healing cycles. They first ascribed the healing mechanism to disulfide exchange reactions; however, in a later article they concluded that thiol-disulfide exchange reactions were more likely responsible for the healing process [Pepels 2013].

In the same line of research, Lafont et al. [Lafont 2012] demonstrated that thermoset rubbery materials (epoxy based) containing disulfide bonds showed cohesive and multiple adhesive healing ability once cured. Inspired by this work, Abdolah Zadeh et al. [Abdolah Zadeh 2014, Abdolah Zadeh 2016] synthesized and evaluated the first generation of intrinsically healable sol-gel based polymers with reversible tetra-sulfides. They found that the macroscopic flow properties of the developed polymers were strongly affected by the content of reversible groups, the density of permanent crosslinks and the healing temperature, achieving the highest healing efficiency at 70°C.

A review by Gyarmati et al. reported that the S-S bonds in a hydrogel are able to self-heal in basic environments [Gyarmati 2013]. Here, the disulfide crosslinks were cleaved by a reducing agent (dithiothreitol), forming S-H end groups in place of the crosslink positions. Reformation of the bonds occurred through an oxidation reaction with hydrogen peroxide. This behavior was demonstrated in an alkaline medium at a pH of 9. They reported restoration of over 50% for both strength and elongation compared to the virgin material, after 24h of healing, without intervention. They also reported that these properties remain after several healing cycles, indicating that the redox-reaction that makes this self-healing behavior possible is reversible. This behavior should be possible for any polymer network, where thiol-disulfide exchange reactions are used to synthesize the material [Gyarmati 2013].

Another approach was reported by An et al. [An 2015]. They use a thiol-ene click-type radical addition of methacrylate copolymers having pendant vinyl groups with a polythiol, creating dynamic disulfide crosslinkages to yield dual sulfide-disulfide crosslinked materials. This reaction is triggered upon UV illumination and causes the formation of sulfide crosslinks, by using S-H groups of polythiol, which react with vinyl groups. They found that a material with an excess of S-H groups can be treated with iodine as an oxidizing agent, leading to disulfide linkages. These disulfide linkages were found to exhibit self-healing behavior at room temperature. The healing time appeared to be related to the size of the cuts introduced, but no external stimuli were present during healing. They also concluded that a sufficient concentration of disulfide crosslinks was required to exhibit self-healing properties. They also found that adding 6% iodine yielded full conversion of free S-H groups to disulfide linkages, which resulted in repair of cuts, as well as recovery of the storage modulus after 100% strain. However, when only 3%

iodine was used, no healing behavior was observed, hence indicating the importance of the disulfide crosslink concentration. It must be noted that healing was enabled through disulfide crosslinks, but the cuts healed were all under 0.1mm in depth.

An inconvenience arises in case of application of this technology to natural and synthetic rubbers. Since vulcanization normally occurs under high-temperature, the thermal sensitivity of the additives necessary for the sulfur self-healing must be taken into account. This prohibits the use of thiols in this application, as thiols are prone to oxidation [Xiang 2015]. Above 70°C, the accelerated oxidation hinders the exchange reaction with disulfides [Lei 2014].

To overcome this limitation, Xiang et al. introduced CuCl_2 as a new catalyst for the metathesis of sulfur bonds [Xiang 2015]. They experimented with this catalyst and found that metathesis of disulfides is possible in vulcanized BR, with an estimated content of 62% and 31% disulfide and polysulfides crosslinks, respectively. They reported self-healing behavior of its compound from temperatures above 110°C. The reaction as expected by theory is shown in Figure 4. Xiang et al. quantified the healing by comparing the tensile strength of the healed and the virgin material and found that after one healing cycle of 12h at 110°C, 75% of the tensile strength was recovered. In test specimens with the catalyst disabled, only 12% recovery of tensile strength was observed, which was attributed to molecular diffusion. By repeating the healing process, the remaining tensile strength dropped to approximately 40% after the third cycle. Xiang et al. also concluded that healing efficiency should be higher, if the non-contact zones after fracture are eliminated. They estimate that these non-contact zones in their experiments make up for 6-10% of the total fracture area. Finally, they found that the tetrasulfide greatly improves the mobility of the catalyst, which ensures a better distribution in the rubber. However, it was observed that CuCl_2 was not homogeneously distributed, which impairs the healing as less sulfide crosslinks will be able to recombine.

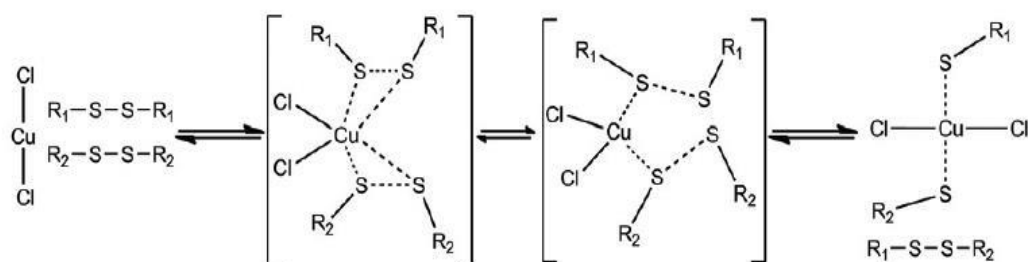


Figure reprinted and adapted with permission from [Xiang 2015]. Copyright 2015, Royal Society of Chemistry.

Figure 4. Reaction process of sulfide crosslink metathesis catalyzed by CuCl_2 .

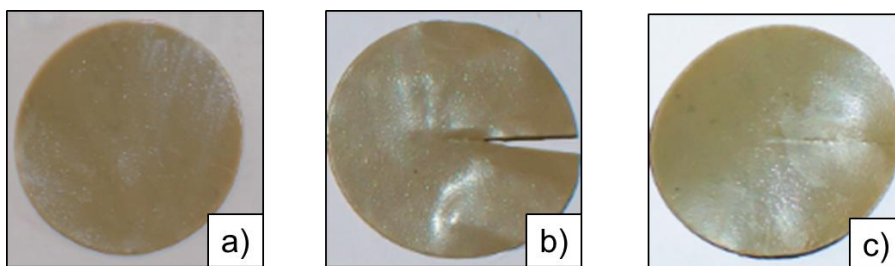


Figure 5. Photographs of: a) pristine; b) cut and c) healed NR samples.

It must be noted that further research would have to be conducted to see whether adding these catalysts after vulcanization is an option. The research by Xiang does not mention any healing at elevated temperatures without the use of the CuCl_2 catalyst. Disulfide and polysulfide bonds are known to degrade at temperatures above 60°C already over time (they are considered stable up to 50°C). So in this case, CuCl_2 would only act as a catalyst, but healing at elevated temperatures should be possible nonetheless.

Later on, Xiang et al. considered to extend the above concept to chloroprene rubber (CR), another widely used elastomer commonly vulcanized with sulfur [Xiang 2016]. It turned out that CuCl_2 could not directly be applied to CR because of its reduced catalytic effect in polar rubbers. Therefore, they considered as possible catalyst candidate copper methacrylate (MA-Cu). In presence of this catalyst the inherent sulfur crosslinks of vulcanized CR were allowed to be dynamically rearranged and reshuffled at 120°C , imparting the rubber with the functionality of repeated self-healing, reshaping and recycling.

Without the need of additional catalysts and playing with the amount of sulfur and curing degree (50% and 90%), Hernández et al. [Hernández 2016a, Hernández 2016b] reported sulfur-cured natural rubber (NR) compounds with self-healing capability without modifying conventionally used rubber formulations. Tensile tests on pristine and healed samples were performed. Macroscopic damage was introduced to rectangular samples by manually making a straight cut along the width using a fresh scalpel blade. Within 5min after cutting, the rectangular damaged samples were carefully positioned inside a home-built healing cell such that the cut surfaces were in seemingly optimal initial contact. Based on earlier work [Abdolah Zadeh 2014, Canadell 2011, Hernández 2016b, Pepels 2013], the cut samples were healed at 70°C and 1bar for 7h. Healing, here understood as the disappearance of the cut and restoration of the mechanical integrity (see Figure 5), was only observed for compounds with low sulfur content (0.7phr), resulting in a maximum recovery of tensile stress of $\sim 80\%$ [Hernández 2016a].

Interfacial damage on samples to be evaluated by Single Edge Notched Tensile (SENT) test was also created for quantification of the healing efficiency. A testing protocol based on fracture mechanics was used. It was recently demonstrated that such an

approach provides more realistic measure of the interfacial healing achieved compared to tensile experiments [Grande 2015]. The 50%-cured NR compound showed a recovery of the fracture energy of 63% (see Figure 6).

Hernández et al. [Hernández 2016b] also studied a uniform molecular network damage (due to multiple straining cycles of the entire sample) imposed to 50% and 90% sulfur-cured NR compounds. Healing of the cyclic strained samples not showing macroscale damage was done by pressure-less relaxation for 3h at 70°C. For both rubbers the instantaneous elastic modulus appeared to be completely recovered in the first cycle. However, the global tensile behavior differed after the thermal healing treatment. For the 50%-cured NR, the potentially higher availability of reversible bonds led to full recovery of the original properties thanks to the overall mobility. While for the 90%-cured rubber, the rupture of permanent bonds was irreversible, causing permanent damage and thus very low healing values (see Figure 6). Healing was quantified according to the difference in instantaneous tensile modulus between the 1st and 10th loading cycle. Such an approach was selected in order to only consider the effect of reversible bonds on the recovery of mechanical properties since the residual permanent bonds (related to the instantaneous modulus of the 10th cycle) do not contribute to the network healing.

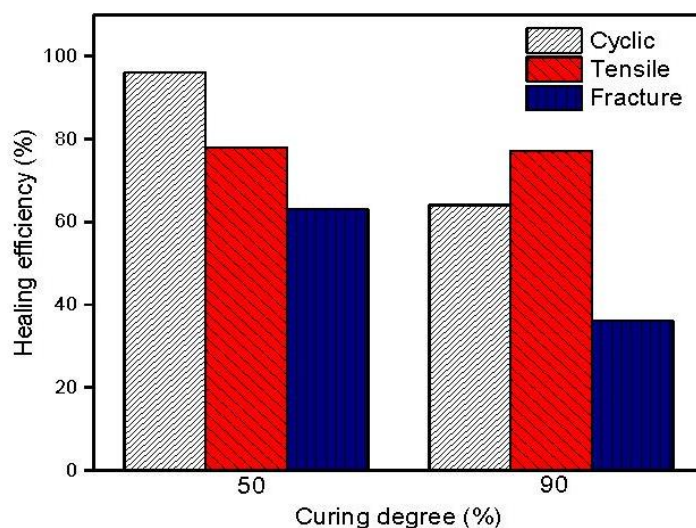
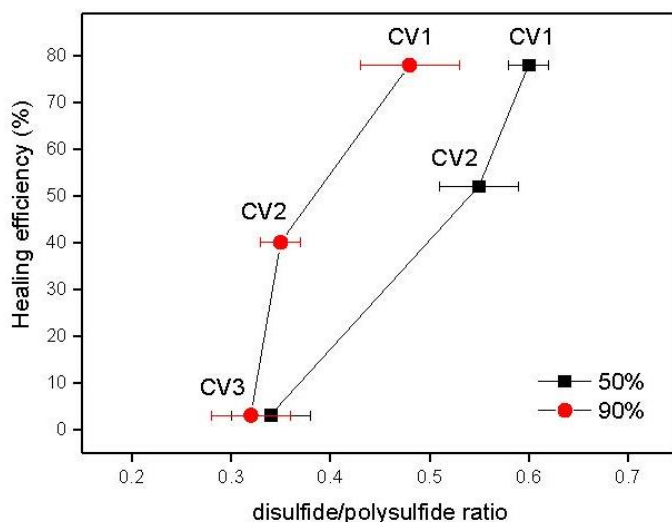


Figure 6. Healing efficiency calculated from cyclic, tensile and fracture as a function of curing degree for low sulfur content NR compounds.

The dynamic character of the di- and poly-sulfide bonds naturally present in covalently crosslinked NR was also studied and found to be responsible for the healing ability and the full recovery of mechanical properties (tensile) at moderate temperatures, provided the material was employed in a non-fully cured starting state. Hernández et al. also demonstrated that the underlying disulfide metathesis healing mechanism is based on temperature-driven sulfur radical reactions. In addition, this study revealed that the ratio

between di- and poly-sulfide bridges is an important mechanistic parameter, although other limiting factors on healing seem to be sulfur content, crosslinking density, post-curing storage time and contact time between damaged surfaces before healing treatment (see Figure 7).



Reprinted with permission from [Hernández 2016a]. Copyright 2016, American Chemical Society.

Figure 7. Mechanical healing efficiency as function of disulfide/polysulfide ratio for different NR compounds at different curing times. Sulfur content: CV1 < CV2 < CV3).

Moving a step further, Hernández et al. [Hernández 2016b] explored the potential of broadband dielectric spectroscopy (BDS) as a new tool to assess macroscale and network polymer healing processes, thanks to its unique ability to describe mobility as a function of polymer architecture. For the proof of concept, the authors studied the partially cured NR compounds referred above. The dynamic relaxations analysis gave evidence on the formation of a heterogeneous network structure at the healed interface or in the bulk, after the partial recovery of the macroscale damaged interface and/or strained polymer network, demonstrating that the polymer architecture in the healed material differs from that in the original one. A good correlation was found between crosslinking density, T_g and healing efficiency, when monitoring the healing process at a scale close to the relevant molecular processes. These results highlight the potential use of dielectric spectroscopy as a powerful technique for the development and understanding of intrinsic healing polymers. However, further tests are necessary to confirm the broader applicability of this technique.

Using alternative crosslinking systems, a study by Imbernon et al. showed disulfide healing in an epoxidized natural rubber (ENR) system crosslinked by dithiodibutyric acid (DTDB) [Imbernon 2015]. The crosslinking relies on these di-acids carboxylic groups to react with the epoxides within ENR, whereas healing is enabled through DTDB's

disulfide bonds. The healing was performed by grinding the crosslinked rubber, after which it was remoulded. After the remoulding, the maximum stress decreased significantly though (approx. 45% drop), whereas the maximum strain maintained about 85% of the maximum strain before remoulding.

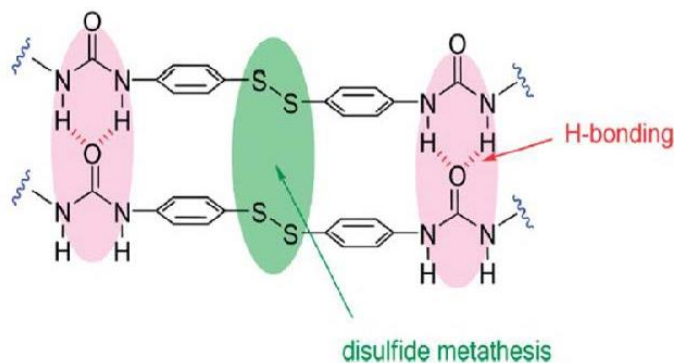


Figure reprinted and adopted with permission from [Rekondo 2014]. Copyright 2013, Royal Society of Chemistry.

Figure 8. Proposed interactions involved in the self-healing process of a poly(urea-urethane) (PUU) elastomer.

Polyurethanes (PU) are another representative rubber family of recent developments in the field of self-healing. Amamoto [Amamoto 2012] reports macroscopic self-healing on covalently crosslinked PU systems based on reshuffling of thiuram disulfide units, solely under the stimulation of visible light at room temperature and without any solvent. Aromatic disulfide structures have also been explored to ensure exchange reactions to take place at room temperature and without the need of any stimulus. The pioneering work of Rekondo et al. [Martin 2014, Rekondo 2014] is a clear example of this approach. They synthesized a poly(urea-urethane) (PUU) elastomeric system having aromatic disulfide bridges as crosslinks. The self-healing mechanism of this system was attributed to two structural features present in this crosslinking unit: i) the aromatic disulfide which is in constant exchange at room temperature, and ii) two urea groups, capable of forming a quadruple H-bond (see Figure 8). This unique combination endowed the elastomer with a healing efficiency of 80% after 2h of contact between the two broken parts of the sample, without the need for any external intervention or catalyst.

Playing with aromatic disulfides, Aguirresarobe et al. [Aguirresarobe 2017] also incorporated them as chain extenders in waterborne organic-inorganic polyurethane hybrids. The metathesis reaction of disulfide bridges provided repetitive healing abilities, as determined by tensile measurements, with a maximum value of 80% for the first healing event.

In all these examples, the disulfide exchange reaction has been regarded as the main contributor to the restoration of mechanical strength. More recently, the shape memory concept [Ahmed 2015, Kirkby 2008, Luo 2013, Nji 2010, Rodriguez 2011] has been combined with self-healing mechanisms and is attracting great research efforts. Shape-memory polymers are a class of stimuli-responsive polymers that have the capacity to reversibly change from a temporary fixed shape to a permanent pre-programmed shape on application of a stimulus [Lendlein 2002]. Xu and Chen [Xu 2016c] report for the first time a self-healing PU system based on the combination of disulfide bonds and shape memory effect. It is known that PU is a kind of polymer that has typical hard/soft segmental dual-component structure. If the soft segment is able to significantly alter its stiffness by the glass transition (T_g) or melting (T_m), while the hard segment is elastic in this range of temperature, then the PU can exhibit heating-responsive shape memory effect. Synthesized PU films were scratched with a razor blade to an approximately 50% of the thickness of the sample and then heated to 80°C. With the assistance of shape memory effect, the scratches on the material almost disappeared in just 5min. Healing was also quantified by tensile tests after a heating process of 4h, achieving 92% of recovery on tensile strength. Xu and Chen concluded that disulfide exchange reactions reestablish the chemical bonding across the crack surface during the healing process and thus lead to the almost full recovery of mechanical properties. Meanwhile, shape memory effect acts as an auxiliary recovery force. It contributes to the macroscopic scale scratch surface approaching and enables disulfide exchange reactions to be initiated rapidly, but it barely contributes to the recovery of the mechanical properties.

Finally, silicone rubber (PDMS) has attracted vast interest among the self-healing field. After the ground-breaking results by White and Sotito [Keller 2007] with microcapsules containing a healing agent embedded in a PDMS matrix, many research groups have reported diverse results by applying different healing approaches. Recently, Xiang et al. [Xiang 2017] proposed a facile route to prepare reversibly cured silicone elastomer from α,ω -dihydroxyl polydimethylsiloxane through condensation reaction with disulfide bond-containing silane coupling agent as crosslinker. A key innovative part of this investigation was that both PDMS and silane curing agent are not tailor-made in laboratory, but market available, which is conducive to the industrialization of the outcomes. Moreover, a second innovative aspect of this research was the use of sunlight for triggering disulfide bonds metathesis. They employed two light sources: sun and a xenon lamp, varying the power intensity. Xiang found that the UV component in the sunlight is the key stimulus for the exchange reaction, originating radicals from disulfide scission due to UV radiation. The healing efficiency, calculated from the restoration of mechanical strength, reached its maximum when using a light intensity of 100mW/cm² after 48h.

2.3. Self-Healing Rubber Composites

All the previous examples of rubbers based on reversible crosslinks by DA or disulfide exchange reactions can be considered successful since all of them display high healing efficiencies. However, in general terms, they suffer from poor mechanical properties. The addition of reinforcing fillers absolutely enhances their mechanical performance, but usually, this is accompanied by the disadvantage that the reinforcing agent retards the reconstruction of the network and thus its self-healing ability. A trade-off between repairability and mechanical properties is thereby often seen in self-healing rubbers. The inclusion of nanofillers in small amounts appears as a good alternative to defeat this trade-off by improving the mechanical/structural performance and generating heat within the matrix so the healing process after damage can be accelerated.

Nanofillers of different nature have been added to self-healing polyurethanes. Li et al. [Li 2014] prepared a covalently bonded graphene oxide/polyurethane (GO/PU) composite with significant reinforcement and thermally healable properties. In this work, the PU prepolymer was prepared *in situ* on the surface of GO to obtain GO/PU composites with furfuryl alcohol as the end group. The as-prepared GO/PU was then covalently crosslinked by bifunctional maleimide via the DA reaction. The results showed that with the incorporation of 0.1wt% of GO, the tensile strength of the composites increased by more than 360% with a healing efficiency of 71%.

The use of attapulgite (AT) as nanofiller in PU systems has also caught attention. A series of PU/AT nanocomposites were prepared by solution blending by Xu and Chen [Xu 2017]. AT is a natural hydrated magnesium-aluminum silicate clay with abundant hydroxyl groups covering its surface. These groups may form hydrogen bonds with various kinds of proton acceptor groups, which generally result in significant enhancement of mechanical properties. Therefore, AT can be seen as a promising low cost replacement for carbon nanotubes (CNTs) and graphene, which are far more costly. Xu and Chen added 1 to 5% of AT to the self-healing PU based on disulfide bonds and shape memory effect detailed in the previous section. Tensile strength increased continuously until AT content was 3%. After a healing process of 4h at 80°C, all samples regained different levels of their original tensile strength. With 1% of AT, 41% of tensile strength was recovered, which was the highest among samples; further increase on AT content would weaken the healing effect gradually, until almost no healing was observed when AT content was 5%. In conclusion, by modifying the amount of AT, both self-healing and mechanical properties can be tailored.

Another example of enhancement of mechanical properties without detriment of healing capability was reported by Kuang et al. [Kuang 2016], adding MWCNTs to SBR on the basis of DA bonding. Furfuryl modified SBR and furfuryl functionalized MWCNTs were reacted with bismaleimide to form a covalently bonded and reversibly

cross-linked SBR/MWCNTs composite. The nanofiller played dual roles of reinforcing and healing agent.

Using the DA strategy, Trovatti explored the possibility of binding furan-modified NR to nanocellulose customized with a maleimide function [Trovatti 2017]. Although they did not measure healing as such, they obtained an increase in modulus by a factor of 100, with respect to the non-modified nanofiller, when the maleimide-modified nanocellulose was mixed with the furan-modified NR. The chemical coupling of the modified nanocellulose with the modified NR gave therefore rise to a composite in which the reinforcing nanofiller was covalently linked to the elastomeric matrix thanks to the DA coupling.

The majority of studies covering the intrinsic healing of polymer composites report on the healing of structural properties and on the use of reinforcing agents (e.g., nanofillers) for improving the mechanical performance. However, nanofillers can also be used for restoring other functionalities, i.e., non-mechanical properties such as thermal conduction, electrical conduction and magnetic shielding, among others. Hernández et al. [Hernández 2017] aimed at restoring more than one functionality after healing a macroscopic damage in NR/graphene composites. They evaluated the restoration of electrical and thermal conductivity in a mechanically damaged sample. Different healing trends as function of the graphene content (0-2phr) were found for each of the functionalities: (i) thermal conductivity was fully restored independently of the graphene filler loading; (ii) electrical conductivity was only restored to a high degree above the percolation threshold; and (iii) tensile strength restoration increased more or less linearly with graphene content but was never complete (see Figure 9). A dedicated molecular dynamics analysis by dielectric spectroscopy of the pristine and healed samples highlighted the role of graphene-rubber interactions at the healed interphase on the overall restoration of the different functionalities. Based on the results, they suggested that the dependence of the various healing efficiencies with graphene content is due to a combination of the graphene induced lower cross-linking density, as well as the presence of strong polymer-graphene interactions at the healed interphase. Important to mention that even though the healing efficiency achieved in this study for all functionalities is significantly high, the mechanical performance of the rubber compounds was not as satisfactory as expected.

Fu et al. [Fu 2016] worked with CNTs instead. They developed a new kind of thermally reversible self-healing PU that simultaneously had good processing properties, high thermal stability and improved electrostatic dissipation capacity. They synthesized a linear polymer with multi-furan rings and a hyperbranched multi-maleimide, so the DA reaction would take place and be responsible for the self-healing capability. With small loadings of CNTs (1-2wt%), they achieved a healing efficiency as high as 93% when the sample was maintained at 130°C for 5min. The samples also showed excellent

electrostatic dissipative properties and outstanding thermal stability with a decomposition temperature 20-40°C higher than those reported for self-healing PU.

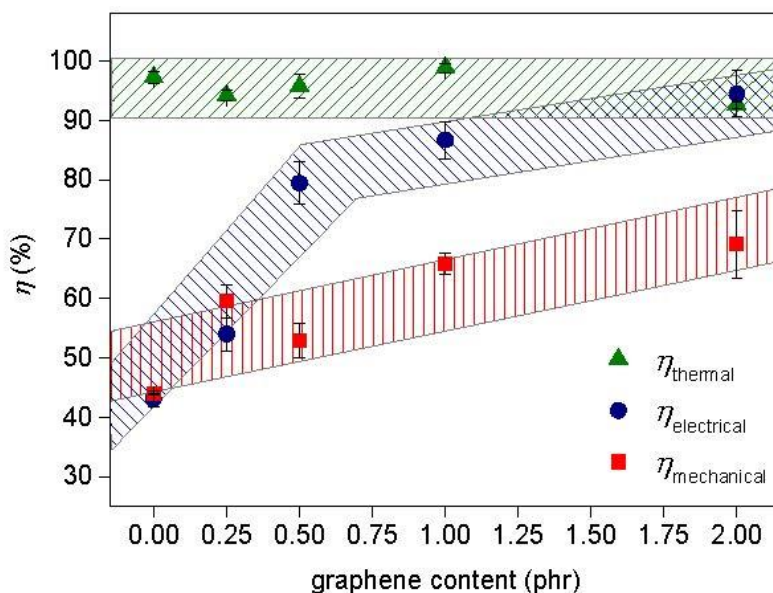


Figure reprinted with permission from [Hernández 2017]. Copyright 2017, IOP Publishing.

Figure 9. Overall healing of multi-functionalities of NR/graphene nanocomposites heated at $T = 70^{\circ}\text{C}$, as function of graphene content.

3. OUTLOOK

This chapter aimed to give an overview of the reversible covalent bonding chemistries used for crosslinking and conferring healing properties to rubbers. Special emphasis has been drawn to two reversible chemistries: Diels-Alder and disulfide exchange reactions.

The furan/maleimide combination is the leading example of Diels-Alder chemistry. In this reaction, a reversible linker moiety is cleaved, resulting in two reactive groups that subsequently react. The wide accessibility to this Diels-Alder combination offers efficient reversibility and hence healing. However, the extended reaction time and required elevated temperatures (80-130°C) compromise the application potentiality. A further opportunity to obtain self-healing based on reversible covalent bonds is the introduction of dynamic disulfide groups into the rubber. Disulfides (and higher homologs) are present in all sulfur-vulcanized rubbers, consequently the use of this approach seems more than reasonable despite certain limitations; mechanical performance is still low if we want to scale-up this concept to real life applications. Thus, depending on the application the selection of one or other chemistry might be preferable. In any case, the crucial points

will be the required healing temperature and the external trigger. Ideally, the damage itself would be the trigger.

In conclusion, we have highlighted a growing trend in self-healing elastomers that exploits the use of dynamic covalent bonds. The interest in architecture design of new dynamic rubber networks is also rising. The various examples herein discussed only constitute a small showcase of the tremendous possibilities offered by dynamic bonds for the development of self-healing rubbers and elastomers, covering a wide range of properties and applications. They represent a good prospect in aerospace, electronics and other relevant fields. It can be expected that in the future a greater range of dynamic bonds will be used to produce intrinsic self-healing polymers or maybe even of greater interest will be the possibilities of combining different dynamic bonds into the same material to allow access to a new range of properties. However, we are still a long way from commercial applications. So, research must continue as to achieve higher mechanical properties at working conditions and milder healing conditions.

ACKNOWLEDGMENTS

Dr. Marianella Hernández acknowledges the Ministry of Economics of Spain for a research contract (MAT2015-73392-JIN).

REFERENCES

- Abd Rabo Moustafa, M. & Gillies, E. (2013). "Rubber functionalization by diels–alder chemistry: From cross-linking to multifunctional graft copolymer synthesis." *Macromolecules*, no. 46, (15), 6024–6030. doi: 10.1021/ma401087v.
- Abdolah Zadeh, M., Esteves, C., van der Zwaag, S. & Garcia, S. J. (2014). "Healable dual organic-inorganic crosslinked sol-gel based polymers: Crosslinking density and tetrasulfide content effect." *Journal of Polymer Science Part A: Polymer Chemistry*, no. 52, (14), 1953–1961. doi: 10.1002/pola.27200.
- Abdolah Zadeh, M., Grande, A. M., van der Zwaag, S. & Garcia, S. J. (2016). "Effect of curing on the mechanical and healing behaviour of a hybrid dual network: A time resolved evaluation." *RSC Advances*, no. 6, (94), 91806–91814. doi: 10.1039/C6RA17799A.
- Aguirresarobe, R. H., Martin, L., Fernandez-Berridi, M. J. & Irusta, L. (2017). "Autonomic healable waterborne organic-inorganic polyurethane hybrids based on aromatic disulfide moieties." *Express Polymer Letters*, no. 11, (4), 266–277. doi: 10.3144/expresspolymlett.2017.27.

- Ahmed, N., Kausar, A. & Muhammad, B. (2015). “Advances in shape memory polyurethanes and composites: A review.” *Polymer-Plastics Technology and Engineering*, no. 54, (13), 1410-1423. doi: 10.1080/03602559.2015.1021490.
- Alliger, G. & Sjothun, I. J. eds. (1964). *Vulcanization of elastomers*. New York: Reinhold Publishing Corp.
- Amamoto, Y., Otsuka, H., Takahara, A. & Matyjaszewski, K. (2012). “Self-healing of covalently cross-linked polymers by reshuffling thiuram disulfide moieties in air under visible light.” *Advanced Materials*, no. 24, (29), 3975-3980. doi: 10.1002/adma.201201928.
- An, S. Y., Noh, S. M., Nam, J. H. & Oh, J. K. (2015). “Dual sulfide-disulfide crosslinked networks with rapid and room temperature self-healability.” *Macromolecular Rapid Communications*, no. 36, (13), 1255-1260. doi: 10.1002/marc.201500123.
- Bai, J., Li, H., Shi, Z. X. & Yin, J. (2015a). “An eco-friendly scheme for the cross-linked polybutadiene elastomer via thiol-ene and diels-alder click chemistry.” *Macromolecules*, no. 48, (11), 3539-3546. doi: 10.1021/acs.macromol.5b00389.
- Bai, J., Li, H., Shi, Z. X., Tian, M. & Yin, J. (2015b). “Dynamic crosslinked poly(styrene-block-butadiene-block-styrene) via diels-alder chemistry: An ideal method to improve solvent resistance and mechanical properties without losing its thermal plastic behavior.” *RSC Advances*, no. 5, (56), 45376-45383. doi: 10.1039/c5ra08719h.
- Blaiszik, B. J., Kramer, S. L. B., Olugebefola, S. C., Moore, J. S., Sottos, N. R. & White, S. R. (2010). “Self-healing polymers and composites.” In *Annual review of materials research*, vol 40, edited by D. R. Clarke, M. Ruhle and F. Zok, 179-211. Palo Alto: Annual Reviews.
- Bose, R. K., Hohlbein, N., Garcia, S. J., Schmidt, A. M. & van der Zwaag, S. (2015a). “Relationship between the network dynamics, supramolecular relaxation time and healing kinetics of cobalt poly(butyl acrylate) ionomers.” *Polymer*, no. 69, 228-232. doi: 10.1016/j.polymer.2015.03.049.
- Bose, R. K., Hohlbein, N., Garcia, S. J., Schmidt, A. M. & van der Zwaag, S. (2015b). “Connecting supramolecular bond lifetime and network mobility for scratch healing in poly(butyl acrylate) ionomers containing sodium, zinc and cobalt.” *Physical Chemistry Chemical Physics*, no. 17, (3), 1697-1704. doi: 10.1039/c4cp04015e.
- Canadell, J., Goossens, H. & Klumperman, B. (2011). “Self-healing materials based on disulfide links.” *Macromolecules*, no. 44, (8), 2536-2541. doi: 10.1021/ma2001492.
- Chen, X., Dam, M. A., Ono, K., Mal, A. K., Shen, H., Nutt, S. R., Sheran, K. & Wudl, F. (2002). “A thermally re-mendable cross-linked polymeric material.” *Science*, no. 295, (5560), 1698-1702. doi: 10.1126/science.1065879.
- Chen, X., Wudl, F., Mal, A. K., Shen, H. & Nutt, S. R. (2003). “New thermally remendable highly cross-linked polymeric materials.” *Macromolecules*, no. 36, (6), 1802-1807. doi: 10.1021/ma0210675.

- Chen, Y. L., Kushner, A. M., Williams, G. A. & Guan, Z. B. (2012). "Multiphase design of autonomic self-healing thermoplastic elastomers." *Nature Chemistry*, no. 4, (6), 467-472. doi: 10.1038/nchem.1314.
- Chino, K. & Ashiura, M. (2001). "Thermoreversible cross-linking rubber using supramolecular hydrogen-bonding networks." *Macromolecules*, no. 34, (26), 9201-9204. doi: 10.1021/ma011253v.
- Cho, S. H., White, S. R. & Braun, P. V. (2012). "Room-temperature polydimethylsiloxane-based self-healing polymers." *Chemistry of Materials*, no. 24, (21), 4209-4214. doi: 10.1021/cm302501b.
- Cordier, P., Tournilhac, F., Soulie-Ziakovic, C. & Leibler, L. (2008). "Self-healing and thermoreversible rubber from supramolecular assembly." *Nature*, no. 451, (7181), 977-980. doi: 10.1038/nature06669.
- Das, A., Sallat, A., Bohme, F., Suckow, M., Basu, D., Wiessner, S., Stockelhuber, K. W., Voit, B. & Heinrich, G. (2015). "Ionic modification turns commercial rubber into a self-healing material." *ACS Applied Materials & Interfaces*, no. 7, (37), 20623-20630. doi: 10.1021/acsami.5b05041.
- Fan, F. & Szpunar, J. (2015). "The self-healing mechanism of an industrial acrylic elastomer." *Journal of Applied Polymer Science*, no. 132, (25). doi: 10.1002/app.42135.
- Fu, G. H., Yuan, L., Liang, G. Z. & Gu, A. J. (2016). "Heat-resistant polyurethane films with great electrostatic dissipation capacity and very high thermally reversible self-healing efficiency based on multi-furan and liquid multi-maleimide polymers." *Journal of Materials Chemistry A*, no. 4, (11), 4232-4241. doi: 10.1039/c6ta00953k.
- Gheneim, R., Perez-Berumen, C. & Gandini, A. (2002). "Diels-alder reactions with novel polymeric dienes and dienophiles: Synthesis of reversibly cross-linked elastomers." *Macromolecules*, no. 35, (19), 7246-7253. doi: 10.1021/ma020343c.
- Gold, B. J., Hovelmann, C. H., Weiss, C., Radulescu, A., Allgaier, J., Pyckhout-Hintzen, W., Wischniewski, A. & Richter, D. (2016). "Sacrificial bonds enhance toughness of dual polybutadiene networks." *Polymer*, no. 87, 123-128. doi: 10.1016/j.polymer.2016.01.077.
- Grande, A. M., Garcia, S. J. & van der Zwaag, S. (2015). "On the interfacial healing of a supramolecular elastomer." *Polymer*, no. 56, 435-442. doi: 10.1016/j.polymer.2014.11.052.
- Gyarmati, B., Nemethy, A. & Szilagyi, A. (2013). "Reversible disulphide formation in polymer networks: A versatile functional group from synthesis to applications." *European Polymer Journal*, no. 49, (6), 1268-1286. doi: 10.1016/j.eurpolymj.2013.03.001.
- Hager, M. D., van der Zwaag, S. & Schubert, U. S. (2016). *Self-healing materials*: Springer International Publishing.

- Hernández, M., Grande, A. M., Dierkes, W., Bijleveld, J., van der Zwaag, S. & García S. J. (2016a). "Turning vulcanized natural rubber into a self-healing polymer: Effect of the disulfide/polysulfide ratio." *ACS Sustainable Chemistry & Engineering*, no. 4, (10), 5776-5784. doi: 10.1021/acssuschemeng.6b01760.
- Hernández, M., Grande, A. M., van der Zwaag, S. & Garcia, S. J. (2016b). "Monitoring network and interfacial healing processes by broadband dielectric spectroscopy: A case study on natural rubber." *ACS Applied Materials & Interfaces*, no. 8 (16), 10647-56. doi: 10.1021/acsami.6b02259.
- Hernández, M., Bernal, M. M., Grande, A. M., Zhong, N., van der Zwaag, S. & García, S. J. (2017). "Effect of graphene content on the restoration of mechanical, electrical and thermal functionalities of a self-healing natural rubber." *Smart Materials and Structures*, no. 26, (8), 085010. doi: 10.1088/1361-665X/aa71f5.
- Hofmann, W. (1967). *Vulcanization and vulcanizing agents*: Marclaren and Sons Limited.
- Hohlbein, N., Shaaban, A., Bras, A. R., Pyckhout-Hintzen, W. & Schmidt, A. M. (2015). "Self-healing dynamic bond-based rubbers: Understanding the mechanisms in ionomeric elastomer model systems." *Physical Chemistry Chemical Physics*, no. 17, (32), 21005-21017. doi: 10.1039/C5CP00620A.
- Huang, L., Yi, N., Wu, Y., Zhang, Y., Zhang, Q., Huang, Y., Ma, Y. & Chen, Y. (2013). "Multichannel and repeatable self-healing of mechanical enhanced graphene-thermoplastic polyurethane composites." *Advanced Materials*, no. 25, (15), 2224-2228. doi: 10.1002/adma.201204768.
- Imbernon, L., Oikonomou, E. K., Norvez, S. & Leibler, L. (2015). "Chemically crosslinked yet reprocessable epoxidized natural rubber via thermo-activated disulfide rearrangements." *Polymer Chemistry*, no. 6, (23), 4271-4278. doi: 10.1039/c5py00459d.
- Keller, M. W., White, S. R. & Sottos, N. R. (2007). "A self-healing poly(dimethyl siloxane) elastomer." *Advanced Functional Materials*, no. 17, (14), 2399-2404. doi: 10.1002/adfm.200700086.
- Keller, M. W., White, S. R. & Sottos, N. R. (2008). "Torsion fatigue response of self-healing poly(dimethylsiloxane) elastomers." *Polymer*, no. 49, (13-14), 3136-3145. doi: 10.1016/j.polymer.2008.04.041.
- Kim, J. T., Kim, B. K., Kim, E. Y., Kwon, S. H. & Jeong, H. M. (2013). "Synthesis and properties of near ir induced self-healable polyurethane/graphene nanocomposites." *European Polymer Journal*, no. 49, (12), 3889-3896. doi: 10.1016/j.eurpolymj.2013.10.009.
- Kim, Y. J., Huh, P. H. & Kim, B. K. (2015). "Synthesis of self-healing polyurethane urea-based supramolecular materials." *Journal of Polymer Science Part B-Polymer Physics*, no. 53, (7), 468-474. doi: 10.1002/polb.23653.

- Kirkby, E. L., Rule, J. D., Michaud, V. L., Sottos, N. R., White, S. R. & Manson, J. A. E. (2008). "Embedded shape-memory alloy wires for improved performance of self-healing polymers." *Advanced Functional Materials*, no. 18, (15), 2253-2260. doi: 10.1002/adfm.200701208.
- Kuang, X., Liu, G. M., Dong, X. & Wang, D. J. (2016). "Enhancement of mechanical and self-healing performance in multiwall carbon nanotube/rubber composites via diels-alder bonding." *Macromolecular Materials and Engineering*, no. 301, (5), 535-541. doi: 10.1002/mame.201500425.
- Lafont, U., van Zeijl, H. & van der Zwaag, S. (2012). "Influence of cross-linkers on the cohesive and adhesive self-healing ability of polysulfide-based thermosets." *ACS Applied Materials & Interfaces*, no. 4, (11), 6280-6288. doi: 10.1021/am301879z.
- Le, H. H., Böhme, F., Sallat, A., Wießner, S., auf der Landwehr, M., Reuter, U., Stöckelhuber, K. W., Heinrich, G., Radusch, H. J. & Das, A. (2016). "Triggering the self-healing properties of modified bromobutyl rubber by intrinsically electrical heating." *Macromolecular Materials and Engineering*, 10.1002/mame. 201600385: 1600385-n/a. doi: 10.1002/mame.201600385.
- Le, H. H., Hait, S., Das, A., Wiessner, S., Stockelhuber, K. W., Bohme, F., Reuter, U., Naskar, K., Heinrich, G. & Radusch, H. J. (2017). "Self-healing properties of carbon nanotube filled natural rubber/bromobutyl rubber blends." *Express Polymer Letters*, no. 11, (3), 230-242. doi: 10.3144/expresspolymlett.2017.24.
- Lei, Z. Q., Xiang, H. P., Yuan, Y. J., Rong, M. Z. & Zhang, M. Q. (2014). "Room-temperature self-healable and remoldable cross-linked polymer based on the dynamic exchange of disulfide bonds." *Chemistry of Materials*, no. 26, (6), 2038-2046. doi: 10.1021/cm4040616.
- Lendlein, A. & Kelch, S. (2002). "Shape-memory polymers." *Angewandte Chemie-International Edition*, no. 41, (12), 2034-2057. doi: 10.1002/1521-3773(20020617)41:12<2034::aid-anie2034>3.0.co;2-m.
- Li, J. H., Zhang, G. P., Deng, L. B., Zhao, S. F., Gao, Y. J., Jiang, K., Sun, R. & Wong, C. P. (2014). "In situ polymerization of mechanically reinforced, thermally healable graphene oxide/polyurethane composites based on diels-alder chemistry." *Journal of Materials Chemistry A*, no. 2, (48), 20642-20649. doi: 10.1039/c4ta04941a.
- Liu, J., Wang, S., Tang, Z. H., Huang, J., Guo, B. C. & Huang, G. S. (2016). "Bioinspired engineering of two different types of sacrificial bonds into chemically cross-linked cis-1,4-polyisoprene toward a high-performance elastomer." *Macromolecules*, no. 49, (22), 8593-8604. doi: 10.1021/acs.macromol.6b01576.
- Liu, Y. L. & Chuo, T. W. (2013). "Self-healing polymers based on thermally reversible diels-alder chemistry." *Polymer Chemistry*, no. 4, (7), 2194-2205. doi: 10.1039/c2py20957h.
- Luo, X. F. & Mather, P. T. (2013). "Shape memory assisted self-healing coating." *ACS Macro Letters*, no. 2, (2), 152-156. doi: 10.1021/mz400017x.

- Mangun, C. L., Mader, A. C., Sottos, N. R. & White, S. R. (2010). "Self-healing of a high temperature cured epoxy using poly(dimethylsiloxane) chemistry." *Polymer*, no. 51, (18), 4063-4068. doi: 10.1016/j.polymer.2010.06.050.
- Martin, R., Rekondo, A., Echeberria, J., Cabanero, G., Grande, H. J. & Odriozola, I. (2012). "Room temperature self-healing power of silicone elastomers having silver nanoparticles as crosslinkers." *Chemical Communications*, no. 48, (66), 8255-8257. doi: 10.1039/c2cc32030d.
- Martin, R., Rekondo, A., de Luzuriaga, A. R., Cabanero, G., Grande, H. J. & Odriozola, I. (2014). "The processability of a poly(urea-urethane) elastomer reversibly crosslinked with aromatic disulfide bridges." *Journal of Materials Chemistry A*, no. 2, (16), 5710-5715. doi: 10.1039/c3ta14927g.
- Martin, R., Rekondo, A., de Luzuriaga, A. R., Casuso, P., Dupin, D., Cabanero, G., Grande, H. J. & Odriozola, I. (2016). "Dynamic sulfur chemistry as a key tool in the design of self-healing polymers." *Smart Materials and Structures*, no. 25, (8). doi: 10.1088/0964-1726/25/8/084017.
- McLean, J. K., Guillen-Castellanos, S. A., Parent, J. S., Whitney, R. A. & Resendes, R. (2007). "Synthesis of graft copolymer derivatives of brominated poly(isobutylene-co-isoprene)." *European Polymer Journal*, no. 43, (11), 4619-4627. doi: 10.1016/j.eurpolymj.2007.08.009.
- Murphy, E. B. & Wudl, F. (2010). "The world of smart healable materials." *Progress in Polymer Science*, no. 35, (1-2), 223-251. doi: 10.1016/j.progpolymsci.2009.10.006.
- Nellesen, A., von Tapavicza, M., Bertling, J., Schimdt, A. M., Bauer, G. & Speck, T. (2011). "Pflanzliche selbstheilung als vorbild für selbstreparierende elastomerwerkstoffe." *GAK - Gummi, Fasern, Kunststoffe*, no. 64, (8), 472-475.
- Nji, J. & Li, G. Q. (2010). "A biomimic shape memory polymer based self-healing particulate composite." *Polymer*, no. 51, (25), 6021-6029. doi: 10.1016/j.polymer.2010.10.021.
- Pepels, M., Filot, I., Klumperman, B. & Goossens, H. (2013). "Self-healing systems based on disulfide-thiol exchange reactions." *Polymer Chemistry*, no. 4, (18), 4955-4965. doi: 10.1039/c3py00087g.
- Polgar, L. M., van Duijn, M., Broekhuis, A. A. & Picchioni, F. (2015). "Use of diels-alder chemistry for thermoreversible cross-linking of rubbers: The next step toward recycling of rubber products?" *Macromolecules*, no. 48, (19), 7096-7105. doi: 10.1021/acs.macromol.5b01422.
- Rahman, M. A., Penco, M., Peroni, I., Ramorino, G., Grande, A. M. & Di Landro, L. (2011). "Self-repairing systems based on ionomers and epoxidized natural rubber blends." *ACS Applied Materials & Interfaces*, no. 3, (12), 4865-4874. doi: 10.1021/am201417h.
- Rahman, M. A., Penco, M., Peroni, I., Ramorino, G., Janszen, G. & Di Landro, L. (2012). "Autonomous healing materials based on epoxidized natural rubber and ethylene

- methacrylic acid ionomers.” *Smart Materials and Structures*, no. 21, (3), 1-7. doi: 10.1088/0964-1726/21/3/035014.
- Rahman, M. A., Sartore, L., Bignotti, F. & Di Landro, L. (2013). “Autonomic self-healing in epoxidized natural rubber.” *ACS Applied Materials & Interfaces*, no. 5, (4), 1494-1502. doi: 10.1021/am303015e.
- Rekondo, A., Martin, R., Ruiz de Luzuriaga, A., Cabanero, G., Grande, H. J. & Odriozola, I. (2014). “Catalyst-free room-temperature self-healing elastomers based on aromatic disulfide metathesis.” *Materials Horizons*, no. 1, (2), 237-240. doi: 10.1039/c3mh00061c.
- Rodriguez, E. D., Luo, X. F. & Mather, P. T. (2011). “Linear/network poly(epsilon-caprolactone) blends exhibiting shape memory assisted self-healing (smash).” *ACS Applied Materials & Interfaces*, no. 3, (2), 152-161. doi: 10.1021/am101012c.
- Schussele, A. C., Nubling, F., Thomann, Y., Carstensen, O., Bauer, G., Speck, T. & Mulhaupt, R. (2012). “Self-healing rubbers based on nbr blends with hyperbranched polyethylenimines.” *Macromolecular Materials and Engineering*, no. 297, (5), 411-419. doi: 10.1002/mame.201100162.
- Trovatti, E., Lacerda, T. M., Carvalho, A. J. F. & Gandini, A. (2015). “Recycling tires? Reversible crosslinking of poly(butadiene).” *Advanced Materials*, no. 27, (13), 2242-2245. doi: 10.1002/adma.201405801.
- Trovatti, E., Cunha, A. G., Carvalho, A. J. F. & Gandini, A. (2017). “Furan-modified natural rubber: A substrate for its reversible crosslinking and for clicking it onto nanocellulose.” *International Journal of Biological Macromolecules*, no. 95, 762-768. doi: 10.1016/j.ijbiomac.2016.11.102.
- van der Zwaag, S. (2008). “Self-healing materials.” *Plastics Engineering*, no. 64, (4), 36-41.
- Wang, D., Guo, J., Zhang, H., Cheng, B. C., Shen, H., Zhao, N. & Xu, J. (2015). “Intelligent rubber with tailored properties for self-healing and shape memory.” *Journal of Materials Chemistry A*, no. 3, (24), 12864-12872. doi: 10.1039/c5ta01915j.
- Wojtecki, R. J., Meador, M. A. & Rowan, S. J. (2011). “Using the dynamic bond to access macroscopically responsive structurally dynamic polymers.” *Nature Materials*, no. 10, (1), 14-27.
- Wu, D. Y., Meure, S. & Solomon, D. (2008). “Self-healing polymeric materials: A review of recent developments.” *Progress in Polymer Science*, no. 33, (5), 479-522. doi: 10.1016/j.progpolymsci.2008.02.001.
- Xiang, H. P., Qian, H. J., Lu, Z. Y., Rong, M. Z. & Zhang, M. Q. (2015). “Crack healing and reclaiming of vulcanized rubber by triggering the rearrangement of inherent sulfur crosslinked networks.” *Green Chemistry*, no. 17, (8), 4315-4325. doi: 10.1039/c5gc00754b.

- Xiang, H. P., Rong, M. Z. & Zhang, M. Q. (2016). "Self-healing, reshaping, and recycling of vulcanized chloroprene rubber: A case study of multitask cyclic utilization of cross-linked polymer." *ACS Sustainable Chemistry & Engineering*, no. 4 (5), 2715-2724. doi: 10.1021/acssuschemeng.6b00224.
- Xiang, H. P., Rong, M. Z. & Zhang, M. Q. (2017). "A facile method for imparting sunlight driven catalyst-free self-healability and recyclability to commercial silicone elastomer." *Polymer*, no. 108, 339-347. doi: 10.1016/j.polymer.2016.12.006.
- Xu, C., Cao, L., Lin, B., Liang, X. & Chen, Y. (2016a). "Design of self-healing supramolecular rubbers by introducing ionic cross-links into natural rubber via a controlled vulcanization." *ACS Applied Materials & Interfaces*, no. 8, (27), 17728-17737. doi: 10.1021/acsaami.6b05941.
- Xu, C., Huang, X., Li, C., Chen, Y., Lin, B. & Liang, X. (2016b). "Design of "zn²⁺ salt-bondings" cross-linked carboxylated styrene butadiene rubber with reprocessing and recycling ability via rearrangements of ionic cross-linkings." *ACS Sustainable Chemistry & Engineering*, no. 4, (12), 6981-6990. doi: 10.1021/acssuschemeng.6b01897.
- Xu, Y. & Chen, D. (2017). "Self-healing polyurethane/attapulgitite nanocomposites based on disulfide bonds and shape memory effect." *Materials Chemistry and Physics*, no. 195, 40-48. doi: 10.1016/j.matchemphys.2017.04.007.
- Xu, Y. R. & Chen, D. J. (2016c). "A novel self-healing polyurethane based on disulfide bonds." *Macromolecular Chemistry and Physics*, no. 217, (10), 1191-1196. doi: 10.1002/macp.201600011.
- Yamaguchi, M., Ono, S. & Terano, M. (2007). "Self-repairing property of polymer network with dangling chains." *Materials Letters*, no. 61, (6), 1396-1399. doi: 10.1016/j.matlet.2006.07.039.
- Yamaguchi, M., Maeda, R., Kobayashi, R., Wada, T., Ono, S. & Nobukawa, S. (2012). "Autonomic healing and welding by interdiffusion of dangling chains in a weak gel." *Polymer International*, no. 61, (1), 9-16. doi: 10.1002/pi.3160.
- Yuan, C. E., Rong, M. Z. & Zhang, M. Q. (2014). "Self-healing polyurethane elastomer with thermally reversible alkoxyamines as crosslinkages." *Polymer*, no. 55, (7), 1782-1791. doi: 10.1016/j.polymer.2014.02.033.
- Zhao, J., Xu, R., Luo, G. X., Wu, J. & Xia, H. S. (2016). "A self-healing, re-moldable and biocompatible crosslinked polysiloxane elastomer." *Journal of Materials Chemistry B*, no. 4, (5), 982-989. doi: 10.1039/c5tb02036k.
- Zou, W., Dong, J., Luo, Y. F., Zhao, Q. & Xie, T. (2017). "Dynamic covalent polymer networks: From old chemistry to modern day innovations." *Advanced Materials*, no. 29, (14), 1606100-n/a. doi: 10.1002/adma.201606100.

Chapter 6

HEALING ABILITY OF IONOMERIC POLYMERS UNDER LOW-ENERGY TRANSFER DAMAGES

*Antonio Julio López**, *Jorge Teno*, *Alejandro Ureña*
and Joaquin Rams

Departamento de Matemática Aplicada,
Ciencia e Ingeniería de Materiales y Tecnología Electrónica,
ESCET, Universidad Rey Juan Carlos, Madrid, Spain

ABSTRACT

The self-healing ability of poly(ethylene-co-metacrylic acid) (EMAA) copolymer neutralized with sodium salt forming the ionomer known as Surlyn® has been investigated using various types of low-velocity damage: indentation, puncture and scratch with razor blade, and puncture with different sharp metallic pointers. These types of macroscopic damages create low-energy heat transfer to the tested material and therefore, thermal energy must be externally added to the material to trigger its healing properties. Different thermal treatments have been carried out using a range of temperatures (40, 55, 70 and 105°C) and heating times, to determine the healing abilities of the material and to optimize the healing procedure for each type of damage. The use of 70°C for 40 min is an effective healing route for the most of the damages, but only complete healing values were obtained when using 105°C.

Keywords: ionomer healing, scratch tests, puncture tests, thermally activated process, low-energy transfer damage

* Corresponding Author Email: antoniojulio.lopez@urjc.es.

1. INTRODUCTION

Plastic films and plates used in packaging and storage containers are subjected to different damages during the filling process and life of service; such as impact, tearing or punctures; and the product packed may become tainted or lost by leakage. Therefore, self-healing polymers are being developed and studied to extend the life of service of these packaging materials and to expand their possible applications.

Poly(ethylene-co-methacrylic acid) (EMAA) copolymer neutralized with sodium salt forming the ionomer known as Surlyn® has been extensively studied in literature due to its self-healing properties under ballistic damage [1, 2] and even under hyper-velocity impacts (1-4 km/s) simulating space debris impacts [3].

Under this high velocity deformation damages, the material suffers a first elastic recovery after the bullet penetration (elastic rebound or shape memory) and due to the friction between the bullet and the material there is a transmission of energy revealed as an increase of temperature, i.e., about 105°C are created in the tested polymer in the surrounding zone of the impact zone as reported by Fall [4]. Due to this heating process, the polymeric material suffers a viscous response creating a flow of polymer across the impact fracture sites. When this flow is high enough it involves enough number of chain entanglements, which can heal the damage as reported by some authors [1-3].

Most studies about self-healing ability of this ionomer have been focused on its ability to recover after high-heat transfer energy damages. Meanwhile, the healing ability under low-heat transfer energy damages has received much less attention although this kind of damages is probably the key ones in packaging applications. Some studies have reported the healing ability of ionomers after cone damages created by a hardness indenter [5] and some authors studied the response after nanoscratch damages created by nanoindentation using a sphere-conical diamond indenter tip [6]. In all the cases, after the low-energy heat transfer damage; the material needed some external heating to promote healing mechanisms.

It is well known in literature [7] that three factors are responsible for self-healing ability of Surlyn® material: (i) order-disorder transitions of multiplets [8] activated at about 50°C; (ii) ion hopping; and (iii) reversible hydrogen bonding.

Multiplets in ionomeric polymers are aggregates formed by several ion pairs [9, 10] which form regions with restricted molecular mobility or “physical cross-linking” sites.

However, there are other similar polymers, such as Nucrel® copolymer, with the same chemical composition that Surlyn® but with the absence of ions in its composition, which do not show these three self-healing mechanism, being reversible hydrogen bonding the only self-healing factor.

In this research, the ability of the commercial ionomer Surlyn® 8940 to heal have been evaluated after applying different types of macroscopic low energy-transfer damages: (i) indentations, (ii) scratch and pressing with razor blade and (iii) puncture

tests with metallic pointers. Different thermal stimulation treatments have been used changing: (i) temperature, (ii) heating time and (iii) continuous or discontinuous heating. Damages caused in the material and the residual damages after the healing process have been characterized using an optical 3D profiler and scanning electron microscopy (SEM). The optimal healing thermal treatment has been established for each type of damage and the effectiveness of the healing mechanisms that intervene in the difference heating treatments has been established. Moreover, mechanical properties before and after the healing treatments were evaluated to determine their possible influence in the mechanical behavior of the polymer. Additionally, Nucrel® thermoplastic polymer has been damaged as a comparative material, in order to evaluate the influence of the multiplets formed by the ionomeric parts of the polymer chains in the healing behavior of Surlyn®.

2. EXPERIMENTAL PROCEDURE

2.1. Materials

The self-healing polymer used in this work was commercially available from DuPont™ (Spain) with the name and code Surlyn® 8940. It has a melting temperature of 93°C and is a partially neutralized poly(ethylene-co-methacrylic acid) random ionomer co-polymer (EMAA). It contains a 5.4 mol.% proportion of methacrylic acid groups and of these, a 30% have been neutralized with sodium hydroxide forming the ionic chemical groups called multiplets, which are characteristics of this type of ionomers.

The polymer was received as pellets and dried in a vacuum oven at 75°C for 2 days. Coupons of approximately 2 mm and 4 mm thick were prepared using a platen press set to 160°C and applying a pressure of 5 bar (Collin P300M press) for several minutes. After that, a cooling ramp of 15°C/min was applied.

From these plates, mechanical tested specimens were prepared using metallic dies with different sizes and geometries. Plates of EMMA copolymer without metallic salt neutralization, commercially available in the form of pellets with the name of Nucrel® from Dupont™, were prepared from pellets, using the same procedure as in the case of Surlyn®.

2.2. Damages and Healing Treatment Strategies

2.2.1. Indentation Damages

Mechanical indentations using different indenter geometries were developed in both polymers. Conical indentations were performed in the surface of the ionomer using a total load of 10 kg applied during 10 s.

Shore D tests following the ASTM D2240-05 standard [11] were also conducted allowing to obtain the hardness of the specimen and to create a very sharp damage on the ionomer surface. 5 kg load was applied for 1 s with a carbon steel needle as indenter.

2.2.2. Razor Blade Damages

Sharp razor blades were used to conduct two different types of damages in the polymers: (i) pressing the surface with the blade using a manual-pressing machine (Figure 1a) with a controlled pressure of 2 Tons and (ii) manual scratches. Pattern damages of both types of macroscopic damages are shown in Figure 1b.

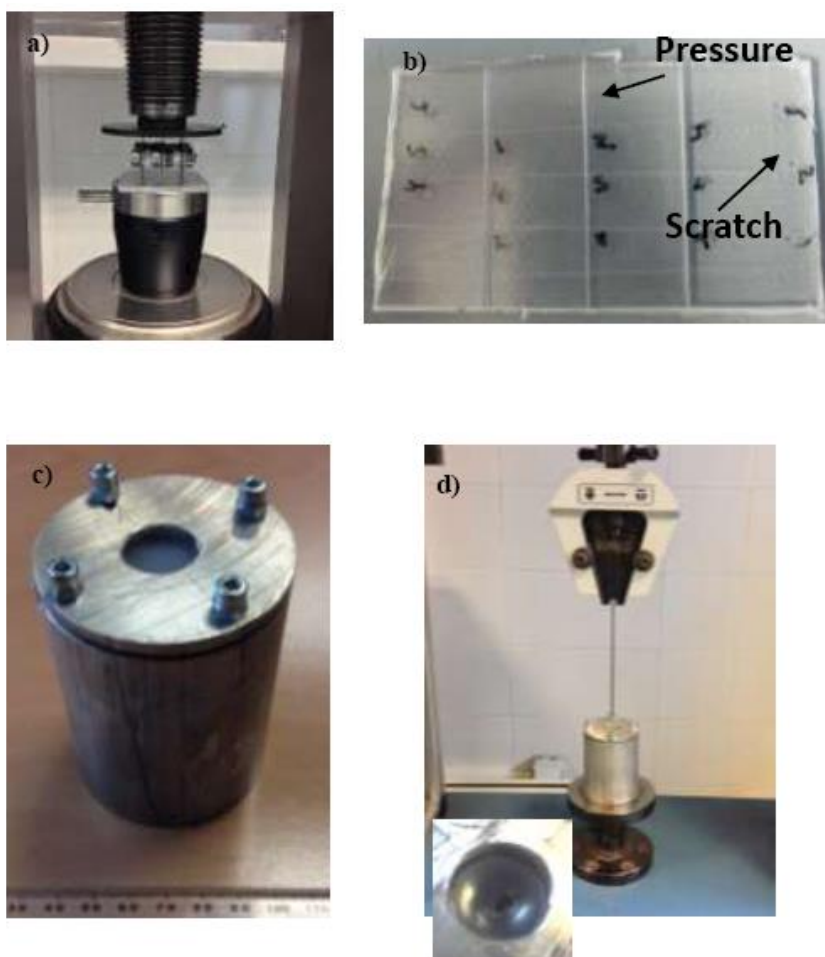


Figure 1. (a) Pressing configuration of the polymers plates using controlled load and razor blades; (b) Pattern of pressing (vertical direction) and scratch (horizontal direction) damages made with razor blade on a plate of Surlyn® (c) Magnesium sample holder (bar scale in mm) used to cause damage by penetration of a nail at a controlled speed (d) configuration used with a universal testing machine working in compression mode and damage on the material after puncture test (insert).

2.2.3. Puncture Damages

The puncture tests were conducted using a universal testing machine (Ibertest-Elib-20/W). Two different sharp metallic styluses with different diameters, 2 mm and 9 mm, were used to create penetrating damages at low deformation speed. 2 mm plates of both Surlyn® ionomer and EMMA thermoplastic polymer Nucrel® were tested. The stylus was in the superior clamp of the testing machine, which was moved in compression mode. The samples were fixed in a special magnesium sample holder fabricated for this purpose (Figure 1c). The upper magnesium plate fixed the sample at a constant torque of 0.1 (N·m) with the use of the screws, avoiding the displacement of the sample plate during the puncture test.

The upper and the lower magnesium plates of the sample holder were drilled to have a central hole to allow the penetration of the stylus.

The sampler holder was in the lower part of the testing machine (Figure 1d). A vertical displacement of the stylus of 12 mm and a controlled perforation speed of 400 mm/min were used in the puncture tests.

2.3. Healing Treatments of the Polymers

To evaluate the healing properties of the polymers, different heating temperatures were used, i.e., 40°C, 55°C, 70°C and 105°C. Furthermore, two different heating procedures were used:

- 1) *Discontinuous process*: the same coupon of damaged polymer was heated up and observed every 10 minutes from 10 to 60 minutes of treatment. After each heating time, the coupon was cooled down to room temperature and the healing ability was measured.
- 2) *Continuous process*: only one heating step was used. Different coupons of damaged polymer were used to study the different recovery times: 20, 40, and 60 minutes.

Temperature of 40°C was selected trying to elucidate the influence of the transitions in the healing abilities of the material.

Temperatures of 55 and 70°C were selected because they are above the multiple transition temperatures (35-55°C) of the ionomer material but below its melting temperature (93-97°C). Finally, temperature of 105°C was selected as an attempt to simulate the temperatures produced during ballistic tests. This temperature is above melting temperature for both, Surlyn® and Nucrel®, but we considered it would be interesting in terms of testing the material above its thermal limits. This has been also suggested by other researchers elsewhere [12].

Mechanical indentations using different indenter geometries were developed in both polymers. Conical indentations were performed in the surface of the ionomer using a total load of 10 kg applied during 10 s.

Shore D tests following the ASTM D2240-05 standard [11] were also conducted allowing to obtain the hardness.

2.4. Characterization of the Healing Process

2.4.1. Indentation and Razor Blade Damages

Indentation and razor blade damages in the polymers were characterized by using 3D Optical Profiler (Zeta-20; from Zeta Instruments). This equipment allows the acquisition of 3D micrographs of the surface of the sample at different magnifications, due to the motorized movement of the objective. Therefore, 3D micrographs of the damages were obtained.

Cross-section profiles of the damages were obtained with the Zeta 3D software. In this case, the healing ability of each material was determined by means of the percentage of recovery in depth (ϕ), using the following equation:

$$\phi (\%) = \frac{h_f - h_o}{h_o} \times 100 \quad (1)$$

where h_o is the maximum depth caused by the damage event and h_f is the residual maximum depth after the healing treatment applied, as determined by cross-profiles of the 3D micrographs through the damage.

Besides, in some healing events, the materials did not only heal the damage decreasing its depth, but also laterally closing the volume of the damage, as previously observed by Vega et al. [6]. In these cases, Mountains software (Digital Surf Company) was also used to calculate from 3D micrographs the healing of the material in terms of volumetric percentage (V%), as defined in equation 2:

$$V (\%) = \frac{V_f - V_o}{V_o} \times 100 \quad (2)$$

where V_o is the volume caused by the damage event and V_f is the volume of the damage after the application of the healing treatment.

Both, ϕ and V percentages are parameters of the viscoplastic healing ability of the material.

2.4.2. Puncture Damage

In the case of the puncture tests, the area of the hole and the length of the created lips were measured using an Optical Microscopy and Image Proplus® software just after the damage conception and after the healing treatments.

Recovery percentages (%) were established for each case.

2.5. Mechanical Tests

Mechanical characterization has been performed to characterize the possible deterioration of the mechanical properties of the ionomeric polymer due to the heating treatments used for healing.

ISO 527-standard 2 [13] has been used to conduct tensile tests in a universal testing machine (MTS-Alliance RT5). Five samples of each specimen were tested to obtain average representative values. Testing specimens with 150 x 10 x 4 mm dimensions were used. Elastic limit, tensile strength and their associated deformations were determined from the test.

Impact tests were also conducted under ISO 179-1 standard [14] in an impact tester machine (Instron/Ceast) with a pendulum energy of 7.5 J using ionomer specimens with dimensions of 80 x 10 x 4.2 mm. Notched specimens were used with a notch geometry of 45°, with a radius of 0.2 - 0.26 mm and a ligament length in the specimen in the range of 7.8 - 8.20 mm.

Average impact resistance of the polymer specimens, in terms of the different thermal treatments applied, was determined testing 5 samples for each studied condition.

3. RESULTS AND DISCUSSION

3.1. Healing of Damages Caused by Conical Indenter

Conical indenter geometry was used to create deformation damages with low energy-transfer. Depth of the damage caused by the indenter and depth of the damage after the different healing processes were characterized using a 3D optical profiler.

Figure 2 collects the 3D profile micrographs of the residual imprint after a cone indentation (Figure 2a) and the healing evolution of the damage after a general healing treatment conducted at 55°C for 30 min (Figure 2b) and 60 min (Figure 2c). It is obvious that a healing phenomenon has taken place in the material, in terms of the recovery of the depth of the residual print. This is supported by the cross-section profile obtained from the 3D micrographs after 60 minutes of heating (Figure 2d).

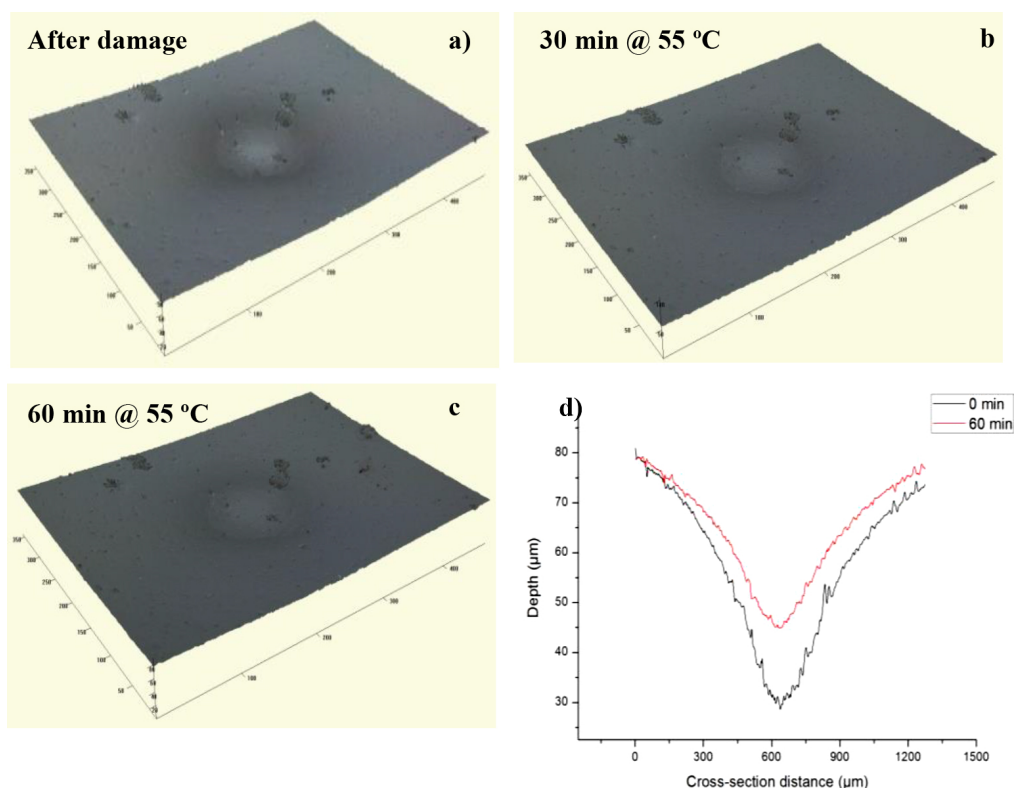


Figure 2. 3D profiler characterization of cone indentation and its evolution (a) before and after discontinuous healing treatment using general heating process in oven at 55°C during: (b) 30 min and (c) 60 min. (d) Cross-section profile of the residual imprint after damage and after 60 minutes at 55°C.

Three different residual imprints were characterized in terms of depth measurement for each tested specimen. Cross-sections data of the 3D micrographs were used to calculate the average depth recovery of each print.

For this damage produced with a conical indenter with 120° angle usually used in Rockwell C hardness test, the damage in the surface of the polymer is very wide. Therefore, the most accurate and demanding measurement of the healing process of the material resulted to be the determination of the damage's depth, rather than its volume.

In Figure 3a, the results show the average depth recovery percentage for every 10 minutes of recovery thermal treatment. The tested temperatures were 40°C, 55°C and 70°C and a discontinuous heating treatment was used. Based on this figure, 5% of depth recovery was obtained after 60 minutes of heating using a temperature of 40°C. This temperature is lower than that at which the order-disorder transition takes place, i.e., about 50°C, and it did not create an effective healing process based on the polymeric chains movement.

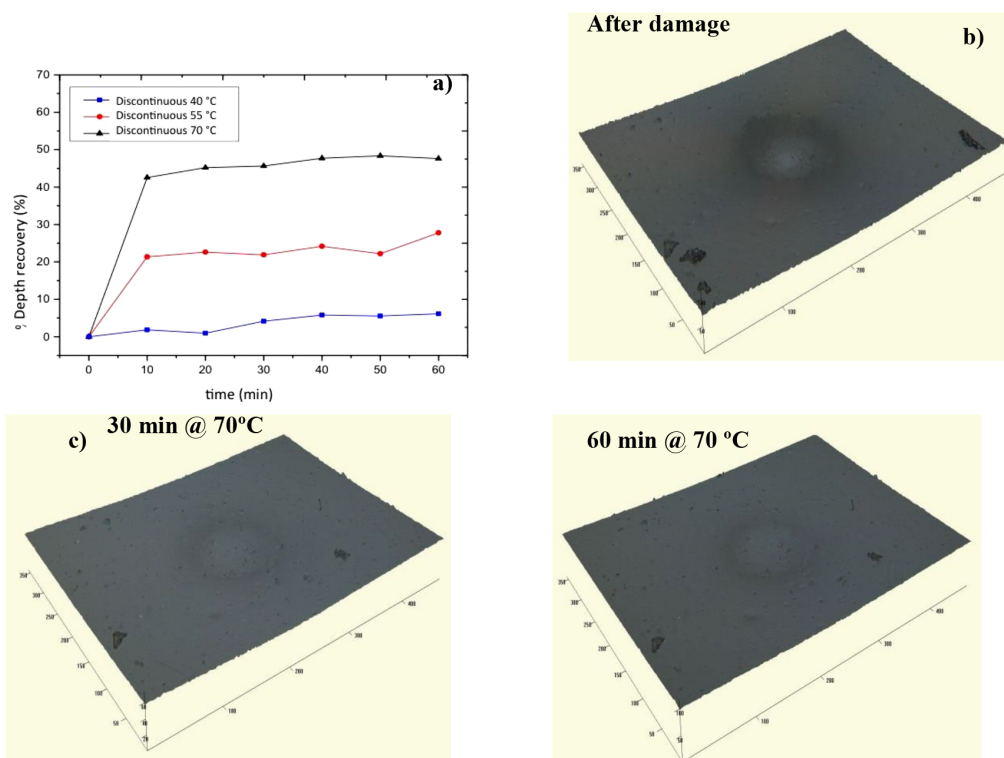


Figure 3. (a) Evolution of depth recovery after applying different temperature in the discontinuous healing process; 3D profilometer characterization of a cone indentation and its evolution in discontinuous treatment during before (b) and after healing treatment using general heating process in oven at 70°C for 30 min (c) and for 60 min (d).

Increasing the applied temperature increases the depth recovery at each individual measured time from 10 to 60 minutes (Figure 3d), allowing a final depth recovery of 28% and 48% when using heating temperatures of 55°C and 70°C, respectively. These results are also a clear indication of a thermal activation taking place in the ionomer above the order-disorder temperature and that it is essential for the movement of the polymer chains and therefore, for the healing process of Surlyn® ionomer.

In terms of heating time, in the first 10 minutes of the process is when the most of the recovery took place, a 76.4% and 70% of the total depth recovered when heating at 55°C and 70°C, respectively, regards to that obtained after 60 min of heating. After the first 10 minutes, the increase of the heating time introduces slight differences in the healing event (Figure 3a). The progressive fading of the imprint also revealed this fact. Figure 3b shows the imprint without healing process. After 30 min of heating at 70°C (Figure 3c) the 3D profile is smoother than the initial one (Figure 3b), revealing that a healing event has occurred. The 3D profile shown in Figure 3d after 60 min of heating shows little difference from the one obtained after 30 min. This confirms the fact that the healing process occurs, preferably, during the first minutes of the heating process when the discontinuous heating process was used.

The effect of the type of heating process, continuous or discontinuous, in the total healing of the polymer was also evaluated (Figure 4). When using 55°C and 70°C the continuous heating process produces higher healing of the damage than the discontinuous treatments (Figures 4a and 4b) at any single measured time (20, 40 and 60 minutes). These results reveal that the kinetic aspects of the healing process might be a key issue of the healing process. When a partial healing is achieved at an intermediate heating time in the discontinuous process, extending the heating time in a second batch is not so effective as continuous heating, because the driven force for the molecular movement, i.e., the difference in the internal energy between both ordered and disordered states, is not as higher as in the case of continuous process.

Reversible hydrogen bonding and order-disorder transition are the healing mechanisms that take place at temperatures under the melting point of the ionomer.

In addition, the higher the time and the temperature applied, the higher the promotion of the molecular movements of the polymer and therefore, the healing of the damage.

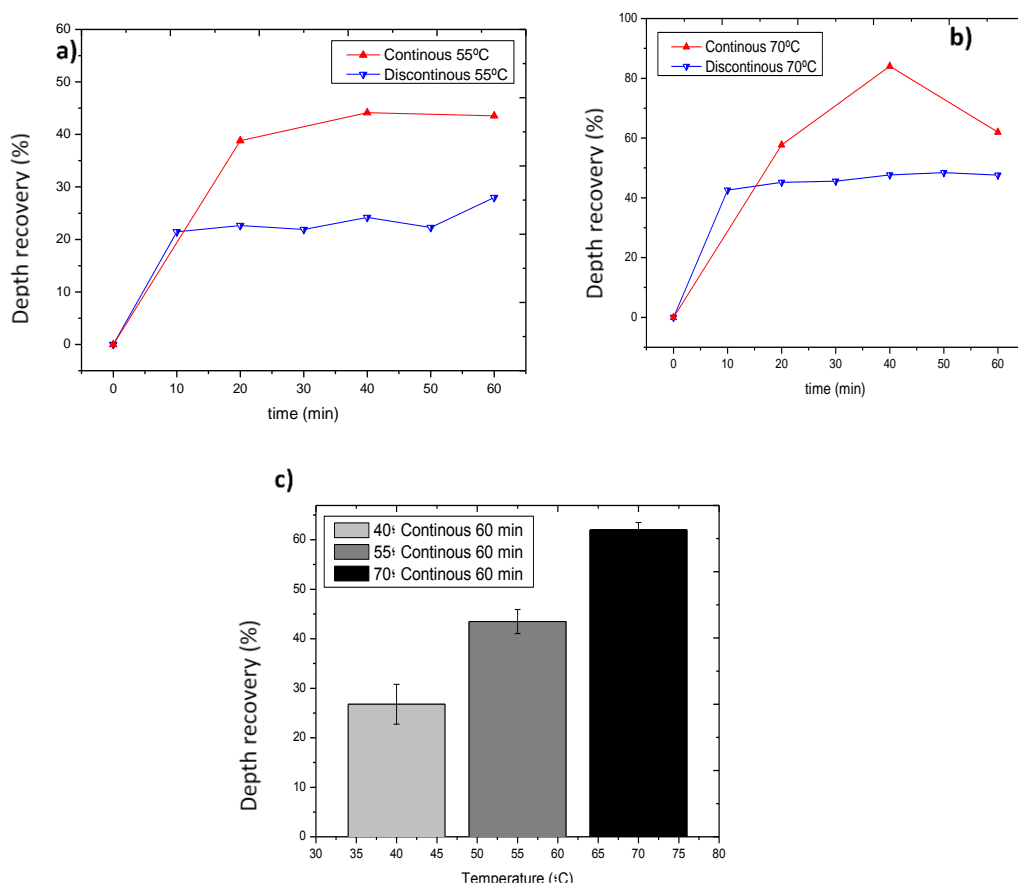


Figure 4. Surlyn® healing ability to cone indentations with discontinuous and continuous heating treatments at different times using: (a) 55°C and (b) 70°C (c) Comparative of healing ability to heal damage using 60 min continuous treatment at different temperatures.

However, the time of the heating process has a limit. Depth recovery as high as 80% was obtained after 40 minutes using 70°C (Figure 4b), but when extending the time up to 60 minutes a decrease in the depth recovery was obtained, probably because of the viscous response of the polymer at the bottom part of the damage and a permanent drawing effect arose, resulting in a decrease in the depth recovery.

In terms of time effectiveness for continuous treatments, heating times of 40 minutes resulted as the ideal one when using 55°C and 70°C, obtaining the higher recovery values.

When the thermal treatment is applied to the end, the healing of the sample is higher when using higher temperatures (Figure 4c). This can be clearly seen in Figure 5, where 3D optical micrographs are presented before and after the continuous heating treatment at different temperature for a fixed heating time (60 min).

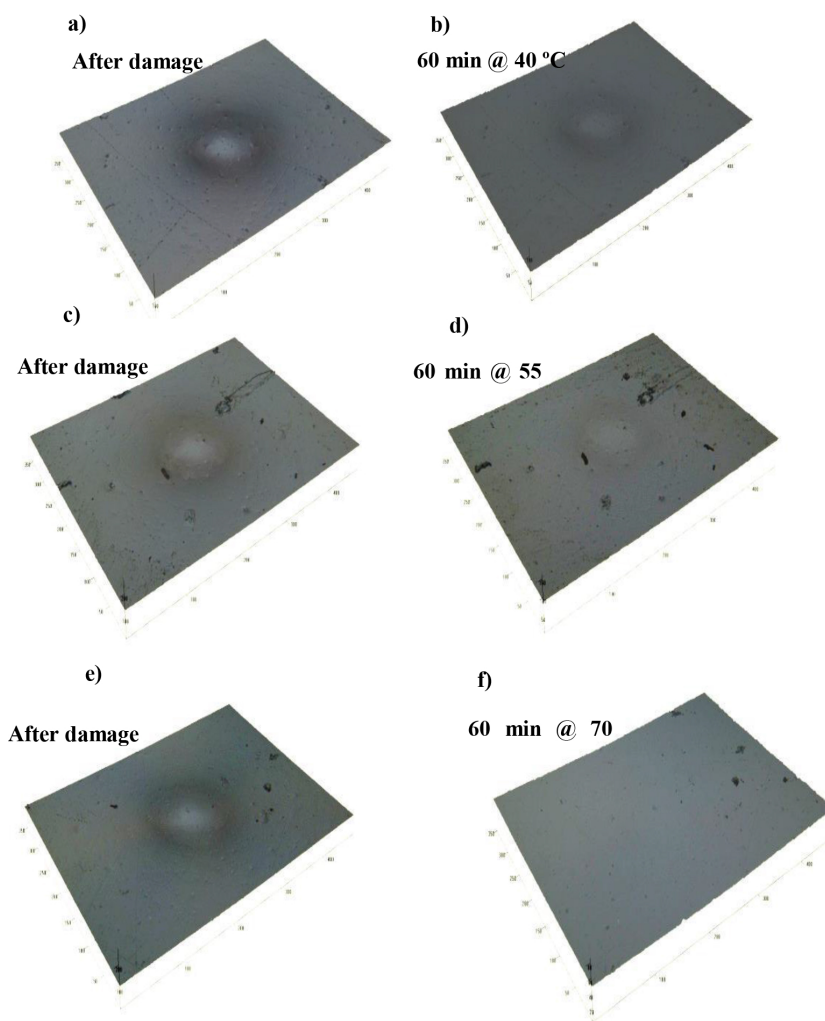


Figure 5. 3D profilometer characterization of cone indentation in Surlyn® and its evolution with continuous heating treatments up to 60 minutes: (a) before and (b) after heating at 40°C; (c) before and (d) after heating at 55°C; (e) before and (f) after heating at 70°C.

After healing at 40°C, the residual imprint was still present without a clear modification of the depth (Figure 5b), indicating that this temperature is not high enough to produce any of the healing mechanism of the ionomer.

When using 55°C for 60 min there is a recovery of the damage (Figure 5d) but the imprint can be still observed at the surface. However, 70°C produces a great recovery of the residual print (Figure 5f), even though there is still some curvature in the polymer surface detected by the cross-line profile and a 62% of depth recovery was calculated in this case (Figure 4c). Therefore, it might be stated that the time of heating is also a key point when using the continuous heating process.

To evaluate the influence of the ionic multiplets in the healing process at 70°C, Nucrel® copolymer was tested under cone damage. This material has also the ability to heal the conical damage created with the conical indenter, recovering up to 70% of the depth after continuous heating during 60 min at 70°C. Therefore, for this type of damage, reversible hydrogen bonding seems to be the main healing mechanism, although multiplet zones are needed when higher recoveries want to be obtained with this heating treatment.

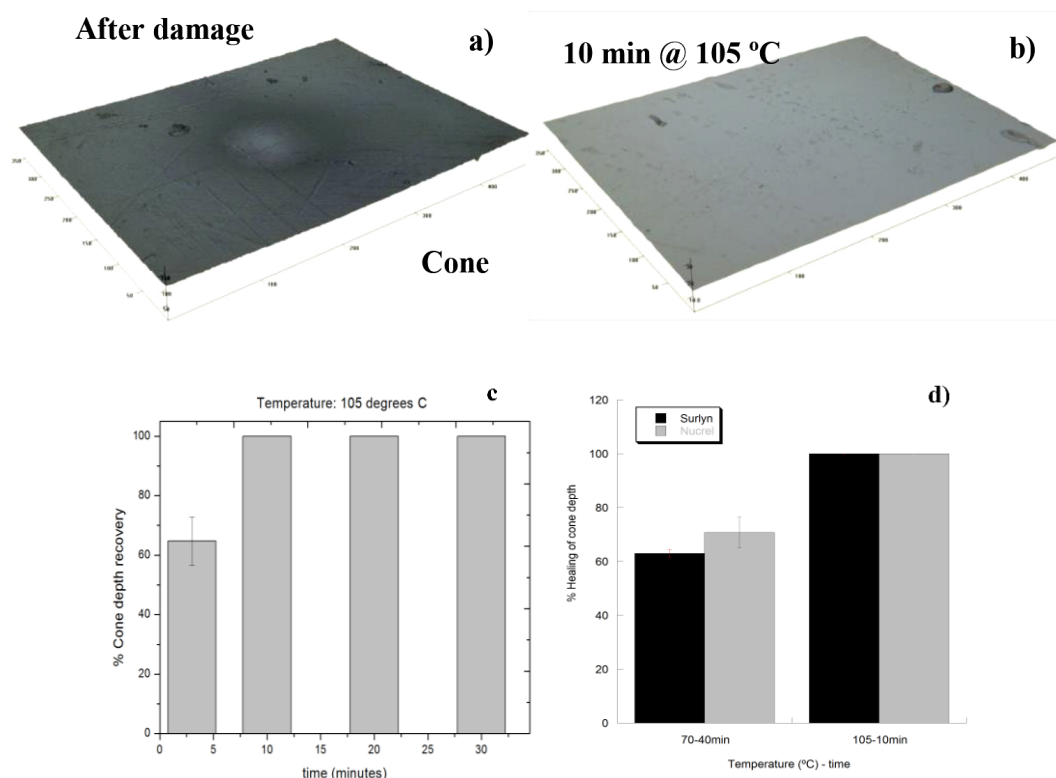


Figure 6. Conical indentation in Surlyn® characterized using 3D optical profiler. Evolution with time in continuous heating treatment at 105°C: (a) residual imprint before heating and (b) the same tested zone after 10 min heating. (c) Average and standard deviation values of % cone depth recoveries versus time of heating at 105°C. (d) Average healing for Surlyn® and Nucrel® polymers after cone damage using different healing thermal treatments.

To obtain a complete recovery of the conical damages, 105°C was used with different continuous treatment times: 3, 10, 20, 30 and 60 minutes. This is the temperature that some authors have established as the friction temperature that a ballistic impact creates in the polymer [12]. It is important to highlight that this temperature is higher than the softening temperature of the ionomer. Therefore, the ion hopping mechanism could be involved under this healing treatment condition.

Just after 3 minutes of treatment at 105°C, the same recovery as after 60 minutes at 70°C was obtained (Figure 6c). This is a clear indication that an activation of the healing phenomenon takes places at this temperature. After only 10 minutes, a total recovery of the residual cone depths was obtained, as it is shown in the 3D micrographs (Figs. 6a and 6b). Probably, viscous flow was activated due to high temperature and the ion hopping mechanism accelerates the healing process of the polymer.

Nucrel® material was also tested at 105°C after conical damages. A total recovery of the damage was obtained (Figure 6d), as in the case of Surlyn®. Therefore, for this type of damage and the use of a high temperature healing process, the recovery process of the polymer is not due to the ionic multipliers or to ion hopping, but more probably due to the viscous flow and hydrogen bonding healing mechanism.

3.2. Healing of Damages Caused by Needle-Like Indenter (Shore Hardness Tests)

Shore test creates a more destructive damage in the material due to the needle-like geometry of the indenter and the lower time (1 s) used to apply the load (5 kg), which causes a high deformation speed in the surface of the sample.

Figure 7 shows the evolution of this type of damage under different healing treatments. The healing process of the ionomer is completely different respective to that under conical damage. Under shore damage, the material does not recover the damage in depth: Instead, the material can close the volume damage healing from the lateral zones of the damaged zone. For this reason, the measurement of the damage depth is not adequate to calculate the healing ability of the material, and in this case the recovery percentage in volume will be used.

Low temperature (40°C) treatment does not create any healing event in the material even after 60 minutes, regardless of the use of discontinuous or continuous heating treatment.

The use of 55°C just creates a maximum recovery of 15.3% and 20.2% after 60 min using discontinuous and continuous treatments, respectively.

Increasing the healing temperature up to 70°C increases the healing (44.7%) after 20 min, but just after 40 min (48.4%) there is no a great variation of damage recovery when using continuous heating treatment.

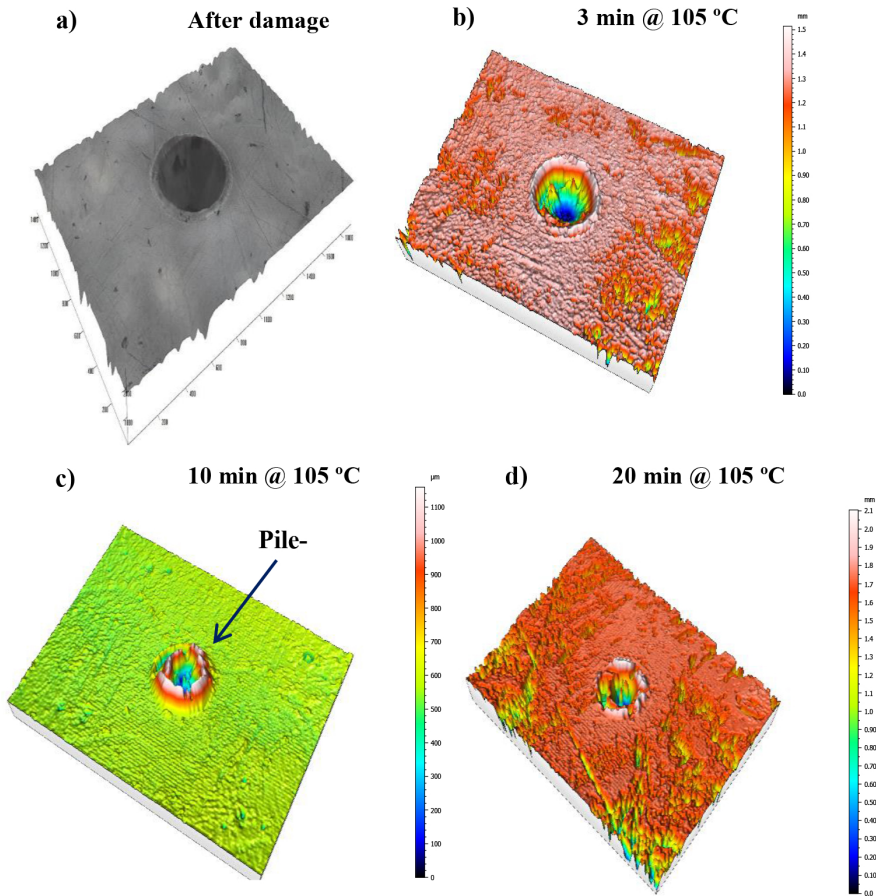


Figure 7. Characterization of shore indentation in Surlyn® using 3D profile micrographs. Evolution with time in continuous heating treatments at 105°C (a) residual imprint before heating treatment (using Zeta software); and after different heating times and using Mountain Software (b) 3 min. (c) 10 min and (d) 20 min. In figure 7c, the text in the figure must say Pile-up.

Finally, the increase of the applied temperature up to 105°C is, again, the best route to promote the healing process (Figure 7). Just after 3 minutes a $54.9\% \pm 13.8$ recovery of the damage volume was obtained, (Figure 7b). After 10 minutes, the heal reaches $85.6\% \pm 6.8\%$, creating even an extensive pile-up process in the lateral lateral zone of the deformed material (Figure 7c). This heating process was the ideal one to recover the damage.

Extending the heating process for 20 min, slightly reduces the recovery of the damaged zone. The volume recovery was $79.12 \pm 4.9\%$ and $75.74 \pm 9.0\%$, after 20 and 30 min, respectively. The viscous flow of the polymer at this relatively high temperature and the ion hopping mechanism may create also a relaxation process after 10 minutes of treatment that causes the relaxation of the pile-up zones and therefore the slight increase of the residual damage volume.

When Nucrel® polymer is damaged by a Shore needle indenter, there is no heal of the damage at any of the temperatures and times previously tested with Surlyn®. This is a clear evidence of the need for multiplsets in the polymer chains to heal the Shore damage.

Characterization of the damage created with the Shore needle indenter was also conducted using a scanning electron microscope (Figure 8) trying to find some similarities in the deformation processes to that observed by some researchers after bullet puncture tests [1]. Two basic deformation mechanisms have been observed in the material. In the outer zone surrounding the crater, striation marks were observed (arrow marked in Figure 8a) radiating from the center of the damage. The use of higher magnifications in this zone (Figure 8b) reveals a rough surface with small nodules. This suggests a ductile elastic deformation of the polymer network, responsible for the viscoelastic recovery of the material and the elastic rebound or shape memory effect. Meanwhile, when observing the borders of the crater at high magnifications polymer fibrillation is observed (Figure 8c), as in the case of ballistic puncture. These fibers were created by the severe deformation induced by the indenter and formed after the viscous flow of the polymer took place.

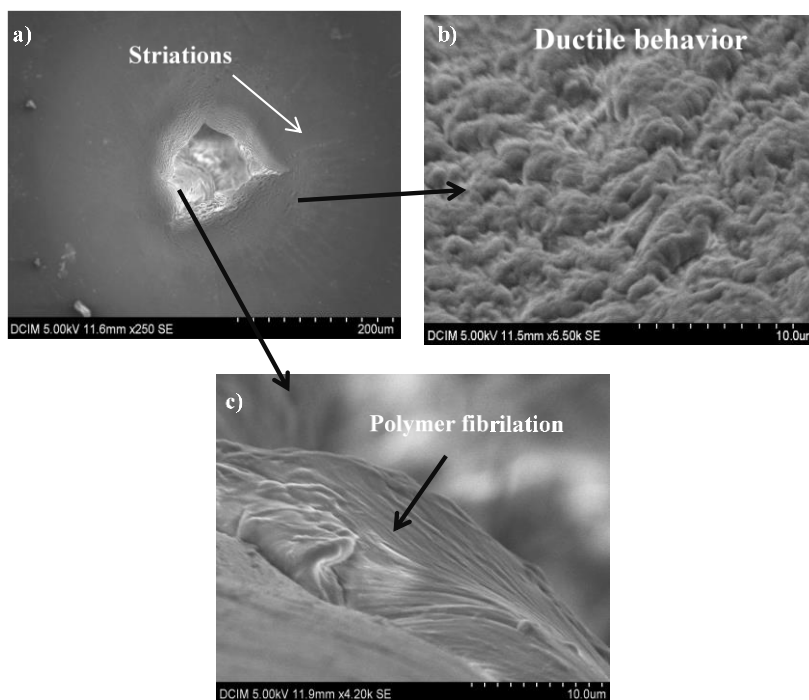


Figure 8. SEM micrographs of the damage in Surlyn® due to Shore indentation: (a) low magnification micrograph showing striations in the outer region; (b) micrograph using high magnifications of the zone near crater showing ductile behavior; (c) micrograph using high magnifications of the crater zone showing polymer fibrils.

This deformation mechanism of the ionomer was also observed under ballistic tests [1]. This might explain the fact that no complete recovery has been achieved after Shore damage, independently of the healing procedure applied. The Shore indentation damage is so aggressive as a ballistic test can be, but the elastic rebound produced in the material after a Shore indentation test is not as high as can be after a ballistic test, although some striations were also seen in the material.

This elastic rebound creates an approach between the parts of the material previously separated by the damage. The closer these parts are the higher the subsequent closure of the damage activated by temperature can be.

3.3. Healing of Damages Caused by Razor Blade

Scratch and pressing macroscopic damages created by razor blade were also performed in the surface of the ionomer. Temperatures of 55°C, 70°C and 105°C were used combined with different heating times. Optimum times and temperatures were investigated for each case. Only continuous treatment was carried out due to the higher healing values were obtained previously for cone and shore damages. Volume of the grooves created with the razor blade, before and after the healing process, was measured from micrographs obtained with optical 3D profiler and using Mountain software to analyze the data.

Figure 9a show the most-efficient thermal treatments applied after normal pressing damages to the surface with a razor blade using a manual-pressing machine with a pressure of 2 Tons and 9b shows the results after scratching the surface with a razor blade.

The use of 55°C and 70°C as healing treatment deals with an optimum heating time of 40 minutes to produce the highest average volume recovery values in terms of damage volume, 48.77% and 59.3%, respectively. Bar graph in Figure 9a also shows that the higher the temperature used in the treatment the higher the healing obtained. This fact corroborates the previous observations. Furthermore, it is obvious that this macroscopic damage caused by a razor blade needs more than order-disorder transitions to obtain high healing values.

Therefore, treatments using 105°C were also investigated. Volume recovery reached up to 79.6% when applying this temperature for 10 minutes; increasing up to 95.4% when increasing the application time to 20 min. 3D micrographs are very illustrative of the healing mechanism of the material. Surlyn®, when having enough energy to activate not only electrostatic forces inside multiplets (Figure 9d) but also ion hopping and viscous flow, the closure of the volume of the razor puncture damage from the more inner zone is almost complete, when enough time is applied (Figure 9f).

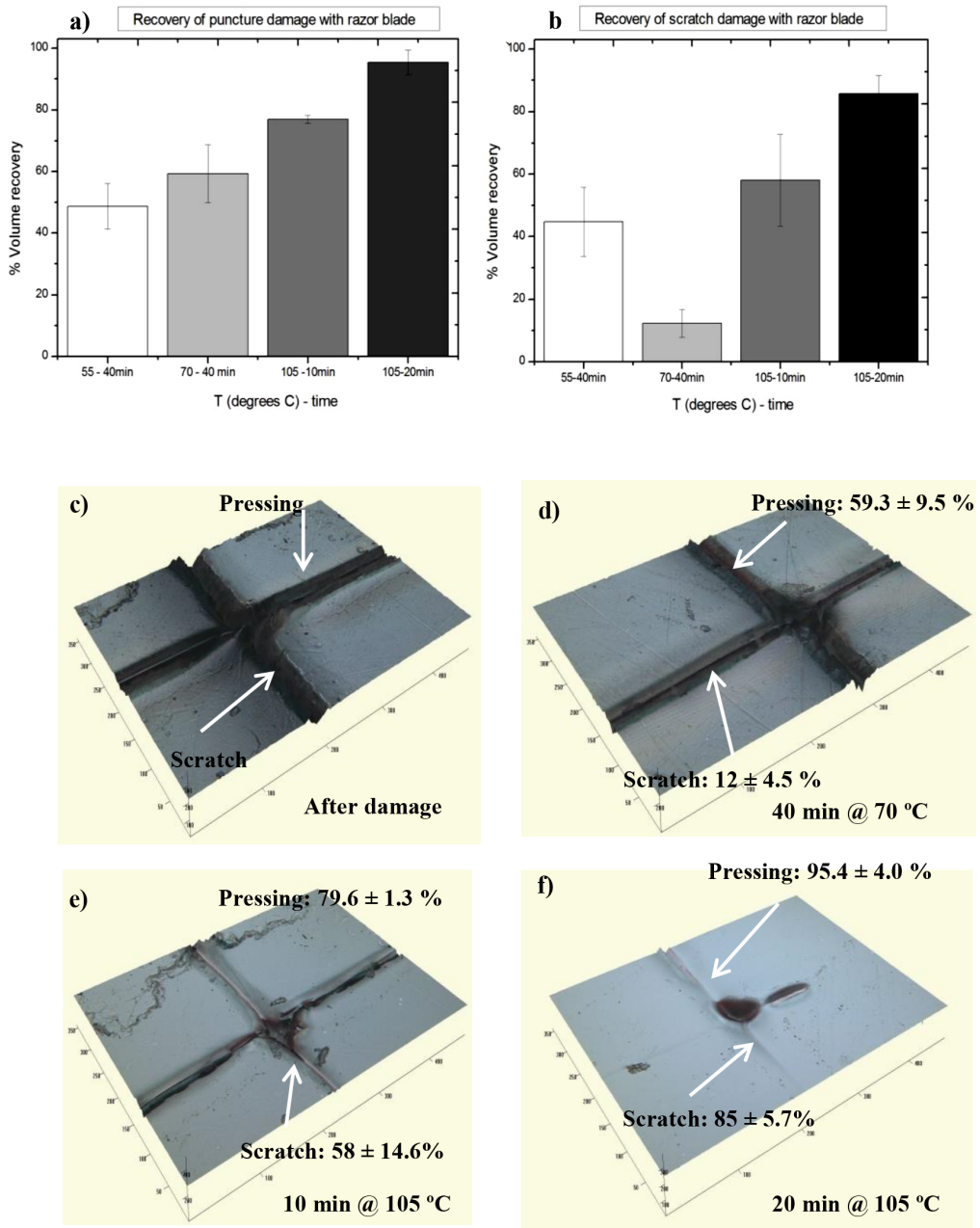


Figure 9. Average and standard deviations of volume recovery (%) of the damages created on the surface of Surlyn® by a (a) razor blade pressing (puncture) and (b) razor blade scratching after continuous thermal treatment at different temperatures and times of application: c) just after damage. Healing treatments at (d) 70°C for 40 min; (e) 105°C for 10 min and (f) 105°C for 20 min.

Scratch damage caused by razor blade is a more surface devastating event than perpendicular pressing one. In Figures 9a and 9b every single thermal treatment studied reveals that the volume percentage of the damage recovered is lower in the case of scratching than in the case of sinking the razor blade inside the material using

perpendicular pressure to the surface. A low 42% of volume recovery was obtained after 40 min at 55°C. Even after 20 min at 105°C volume recovery was only 85% in the scratch damage, mainly due to the unrecovered zone of the material groove near the confluence zone with the razor pressing (arrow marked in Figure 9f).

The use of 70°C for 40 min decreases the healing properties of the scratched sample. This can only be related to a viscous flow of the material trying to relax the deformation zones created during the scratch. Vega et al. [6] used a heating procedure at 70°C for 30 minutes and the recovery obtained was 65% in volume. The main difference with our present work is that Vega et al. focused on nanoscratch damages made using a nanoindenter and in our case the scratches are made with a razor blade in the macroscopic scale.

Meanwhile, the reference polymer, i.e., non-neutralized EMMA Nucrel® polymer, did not show any ability to heal the scratches for any of the thermal treatments applied. In all the studied cases the volume recovery was lower than 5%. This fact clearly reveals the importance of the ionomeric zones in the polymer chains of Surlyn®, that are the responsible agents, together with ion hopping at high temperatures, of healing scratches by means of heating. In absence of these carboxylic neutralized zones, the polymer is not able to activate the healing mechanism.

In the case of the pressing damages, Nucrel® showed some healing after 10 min at 105°C, 37,6% of recovery in volume, but there was no healing at lower temperatures. With pressing damages, only at higher temperatures the weak attraction that takes place between carboxylic groups is promoted in the material and it may produce some healing in the polymer [7], as it was previously described in our study in the case of the conical indentations.

3.4. Healing of Damages Caused by Puncture Tests

Figure 10 collects plain and lateral views of Surlyn® material after damages caused with 2 mm and 9 mm stylus diameters, using a stylus speed of 400 mm/min. Micrographs after different heating treatments are also shown.

The analysis of the results reveals that, as in previous exposed results, the higher the temperature applied, the higher the healing percentage obtained, not only in the case of the area of the hole but also in the case of the lips length formed due to the material perforation (Figure 10).

In the case of the lower diameter stylus, i.e., 2 mm, the hole was completely closed and deformation in depth was recovered in about 60% after 40 min at 70°C of healing treatment (Figure 10c). Hence, there is no need to promote viscous flow at 105°C to completely close the damage.

When using the 9 mm stylus diameter, due to the great hole damage formed with the perforation tool in terms of area (Figure 10e) a complete healing of the hole was not obtained, although a hole area recovery of 98.8% and a healing of 91.8% in terms of lip length was obtained after 10 minutes at 105°C of healing treatment. There was not enough molecular movement and viscous flow after 10 min to create the complete recovery of the damage and more time would be needed.

In the case of Nucrel® polymer tested with the 9 mm stylus and afterwards heated using 105°C-10 min (not shown), the recuperative abilities slightly decrease, 95.3% in the case of the hole area and a recovery of 88.9% was obtained for lip length. It seems that the hydrogen bonding recombination and mainly the viscous flow that takes place in the copolymer above the melting temperature are effective healing mechanisms for this puncture damage, even using the biggest pointer. At temperatures below melting, the recovery of this polymer is negligible.

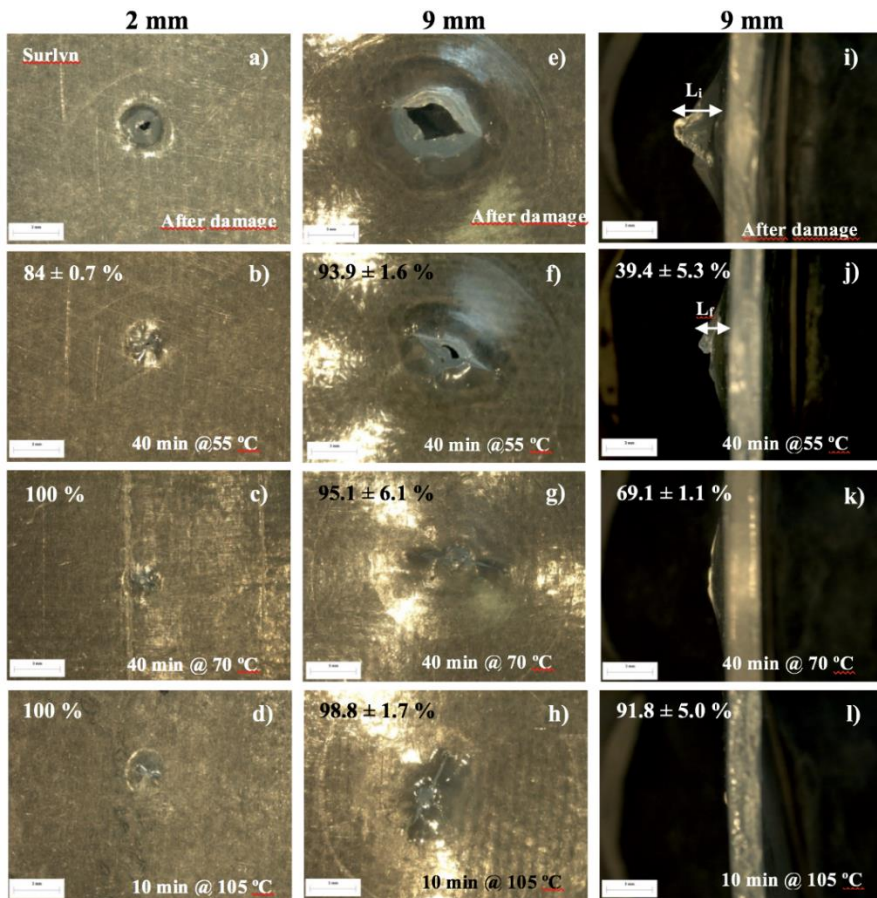


Figure 10. Optical micrographs in plain view of puncture tests at 400 mm/min speed in Surlyn® using 2 mm (a-d) and 9 mm (e-h) diameter styluses after damage and after different heating treatments. Area recovery percentage indicated on the micrographs; optical micrographs in profile view of the damage with indication of the percentage of lips length recovery (i-h) before and after the heating treatments.

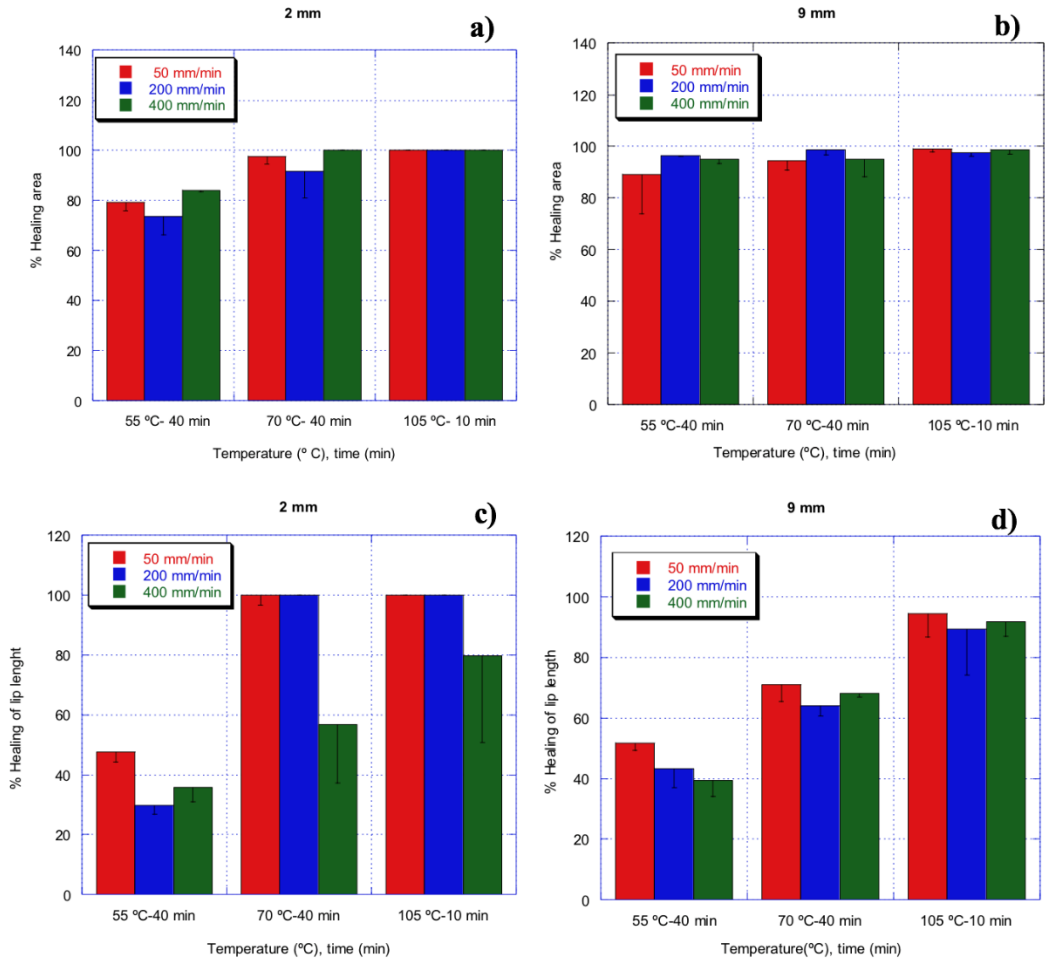


Figure 11. Average and standard deviation values of Surlyn® damage recovery: % of healed area (a, b) and % of lip length (c, d). The damage was created by puncture tests conducted at different speeds (50, 200 and 400 mm/min) and using 2 mm (a and c) and 9 mm (b and d) metallic pointer diameters.

To analyze the possible influence of the stylus speed during the perforation test on the healing ability of the ionomer plates, puncture tests at 50, 200 and 400 mm/min were also conducted and the average and standard deviation values obtained after 3 tests are collected in Figure 11.

There is no much influence of the test velocity in terms of the ability of the material to close the hole (Figures 11a and 11b). These results suggest that the friction value between the stylus and the material, which probably increases when increasing the test speed, is not high enough to increase the temperature of the punctured polymer in a significant way as to create an effective self-healing mechanism and therefore,

a subsequent heating stage is required in all the cases. Otherwise, the healing obtained after applying low temperature heating (55°C) would be clearly lower for samples tested at 200 and 400 mm/min respect to that at 50 mm/min, due to the initial closure of the damage by means of heating produce by friction (Figure 11), but this is not the case.

Furthermore, when enough time and temperature were applied during the healing treatment, at least 70°C during 40 min or 105°C in 10 min, Surlyn® has the ability to heal the damage completely without influence of the puncture speed (Figures 10a and 10b and Figures 11a and 11b).

In terms of in-depth deformation, i.e., lip's length analyzed in the profile micrographs, the most influential parameter is the healing treatment and the second one is the diameter of the stylus. The larger the stylus diameter used the lower the recovery of damage (Figures 11c and 11d). Besides, when using 2 mm stylus diameter there is a great influence of the speed, obtaining the lower healing ability when using the higher speed (Figure 11c), while the material can heal the damage completely at 70°C-40 min if it was created using 50 or 200 mm/min.

In the case of using the biggest stylus, the influence of the speed is significant when low temperature (55°C) was used and almost negligible when using 70°C or 105°C (Figure 10d). Surlyn® needs 105°C-10 min to almost heal this type of damage.

In any case, there is always a slight remnant in-depth deformation after puncture, which cannot be recovered unless 105°C is applied for 10 min.

3.5. Summary of Surlyn® Healing Ability

Table 1 shows the healing ability of Surlyn® in terms of the different damages and the different heating strategies. 40 min at 70°C is the most standard heating treatment to obtain the highest possible healing of the tested damages when using temperatures well below the melting temperature of the ionomer, except for scratch damage that only requires 40 min at 55°C. Even puncture damages are almost healed by the activation of the order-disorder transitions and hydrogen bonding healing mechanisms. To obtain higher recoveries in the material, temperatures above the melting point are required for all the tested damages. To obtain a complete or near complete healing of the material, both viscous flow and ion hopping healing mechanisms are required. Scratch and Shore damages are the most harmful damages, with healing recoveries of 85% even after activating all the healing mechanisms using 105°C for 10 or 20 minutes.

Table 1. Average and standard deviation values of the recovery obtained with the best healing treatment (with indication of the healing mechanisms taking place) applied to Surlyn® for the different tested damages

Damage	Under melting point (Order-disorder transition; hydrogen bonding)		Above melting point (Ion hopping, viscous flow)	
	Best treatment	Healing (%)	Best treatment	Healing (%)
Conical indentation	70°C-40 min	80 ± 3%	105°C-10 min	100%
Shore indentation	70°C-40 min	48.4 ± 3.4%	105°C-10 min	85.6 ± 6.8%
Razor blade <i>Pressing</i>	70°C-40 min	59.3 ± 9.5%	105°C-20 min	95.4 ± 4%
<i>Scratching</i>	55°C-40 min	42 ± 5%	105°C-20 min	85 ± 5.7%
Puncture <i>9 mm, 400 mm/min</i>	70°C-40 min	96 ± 4%	105°C-10 min	99 ± 1%

3.6. Mechanical Characterization After Healing Treatments

Mechanical characterization of the ionomer was done in order to determine the influence of the heating treatment applied to heal the damages in the mechanical properties of the material.

Shore average hardness values obtained for Surlyn® and Nucrel® specimens, both materials in the after-processing state, were 65 ± 1.2 and 54 ± 1.1 , respectively. These values were not altered by the application of any of the heating treatments applied for healing the damages.

Figure 12 presents the average mechanical values for Surlyn® in the after-processing state and after applying the different healing treatments. Tensile strength slightly decreases respect to that of the after-processing state with the application of any of the heating processes, from values around 18 MPa to values around 17 MPa (Figure 12a). Additionally, Yield strength is maintained around 21 MPa and even slightly increases to 23 MPa when increasing the heating temperature. A slight decrease in the average elongation values was obtained when increasing the temperature of the healing treatment, i.e., 14.7% for 70°C and 17.6% for 105°C regarding the initial after-processing average value of 340%.

The ionomer maintains its impact properties, as revealed by the Charpy impact tests (Figure 12b), with values around 140 (kJ/m²) regardless the heating treatment used for healing.

The cooling of the material at room temperature, i.e., out of the oven, after finishing the heating time could be allowing the maintenance of the mechanical properties of the ionomer.

Based on the above, it might be determined that the optimum healing conditions do not substantially change the mechanical properties of Surlyn® ionomer and therefore the material maintains its mechanical integrity.

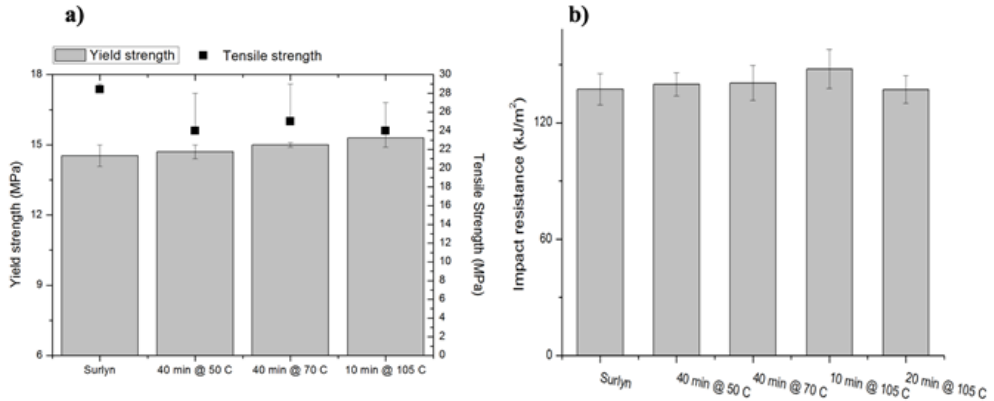


Figure 12. Average and standard deviation values for Surlyn® before and after heating process of (a) yield and tensile strength obtained in tensile tests; (b) impact resistances obtained in Charpy tests.

CONCLUSION

In this research, the ability of the commercial ionomer Surlyn® 8940 to heal has been evaluated applying different types of macroscopic low energy-transfer damages and using Nucrel® thermoplastic polymer as a reference material.

The main conclusions of this work are:

- 1) Independently of the damage type, the healing event increases when increasing the healing temperature used.
- 2) Continuous heating treatments for damage healing are more efficient than discontinuous
- 3) Damages created using a conical indenter: Surlyn® ionomer presented higher healing properties than Nucrel® copolymer when using 70°C during 40 minutes. When temperature is increased to 105°C for 10 minutes, both materials completely heal the damage.
- 4) Damages created using a needle-like indenter (Shore tests): Nucrel® polymer did not show any healing response under this damage. Therefore, reversible hydrogen bonding is not a healing mechanism involved in the healing process of this type of damage. Meanwhile, Surlyn® healed 48.4% of the volumetric

damage after 40 minutes at 70°C. This is considered the optimum healing treatment route.

- 5) Pressing with razor blade: ionomer is prone to heal this damage, with a damaged volume recovery of 60% after 40 min to 70°C. This value increases to 80% when using 105°C during 10 min and almost complete heal of the damage (95.4%) was obtained when using 105°C for 20 minutes. Nucrel® showed an absence of ability to heal under this type of damage, with only a 37% of damaged volume recovered after 10 minutes at 105°C.
- 6) Razor blade damages: Heating treatments with temperatures below melting point are not adequate to heal this macroscopic damage. The ionomer needs more than order-disorder transitions to obtain higher healing values. Therefore, heating at 105°C is needed to promote the ion hopping and viscous flow mechanism.

Scratch damage is more severe than pressing with razor blade. Sulyn® healing ability is lower than in the case of pressing damages, independently of the healing procedure used. The highest recoveries were obtained when using 105°C. Besides, Nucrel® did not show any volume recovery of the scratches after any heating processes applied.

- 7) Puncture tests with metal stylus: the speed test is not a critical parameter of the healing event. Surlyn® has a great ability to completely close the damage when using 70°C-40 min. Furthermore, Nucrel® could heal the damage almost completely, but the thermal activation required was higher (105°C-10min).
- 8) Surlyn® healing properties are based mainly on order-disorder transitions and hydrogen bonding healing mechanisms. When activating these two mechanism, using heating treatments below the melting point of the ionomer, a considerable heal is obtain in the material, with values between 42% and 96% depending on the type of damage.

To obtain higher healing values in the material, temperatures above the melting point are required to activate viscous flow and ion hopping healing mechanisms. Scratch and Shore are the most harmful damages with healing percentage above 85% even after activating all the healing mechanism using 105°C for 10 or 20 minutes, respectively.

- 9) Mechanical properties were not depleted by the healing treatments applied. Yield strength, tensile strength and impact resistance were maintained. A slight decrease in elongation capabilities was detected as increasing the temperature of the treatment.

ACKNOWLEDGMENTS

Authors wish to thank to Repsol and Universidad Rey Juan Carlos (LATEP project) and to Comunidad de Madrid (MULTIMAT-CHALLENGE S2013/MIT-2862) for funding and to DuPont™ Company for material supply.

REFERENCES

- [1] Russell J. Varley, Sybrand van der Zwaag, Towards an understanding of thermally activated self-healing of an ionomer system during ballistic penetration. *Acta Materialia* 2008;56(19):5737.
- [2] Russell John Varley, Shirley Shen, Sybrand van der Zwaag, The effect of cluster plasticization on the self-healing behaviour of ionomers. *Polymer* 2010;51(3):679.
- [3] Francesconi A., Giacomuzzo C., Grande A. M., Mudric T., Zaccariotto M., Etemadi E., Di Landro L., Galvanetto U., Comparison of self-healing ionomer to aluminium-alloy bumpers for protecting spacecraft equipment from space debris impacts. *Advances in Space Research* 2013;51(5):930.
- [4] Fall R. *Puncture Reversal of Ethylene Ionomers – Mechanistic Studies*. Masters of Science in Chemistry. Blacksburg, Virginia, 2001.
- [5] Amy Huber, Jeffrey Hinkley. *Impression Testing of Self-Healing Polymers*. National Technical Information Service (NTIS). 2005.
- [6] J. M. Vega, A. M. Grande, S. van der Zwaag, S.J. Garcia. On the role of free carboxylic groups and cluster conformation on the surface scratch healing behaviour of ionomers. *European Polymer Journal* 2014, 57: 121.
- [7] Varley R. “Ionomers as Self-healing Polymers” in *Self-healing Materials: an Alternative Approach to 20 Centuries of Materials Science*. Springer. 2007.
- [8] Eisenberg A., Rinaudo M. Polyelectrolytes and Ionomers. *Polymer Bulletin* 1990, 24(6): 671.
- [9] Eisenberg A., B. Hird, R. B. Moore. A new multiplet-cluster model for the morphology of random ionomers. *Macromolecules* 1990, 23:4098.
- [10] Moore R. B., Bittencourt D., Gauthier M., Williams C. E., Eisenberg A. Small Angle X-Ray Scattering investigations of ionomers with variable-length side chains. *Macromolecules* 1991;24:1376.
- [11] ASTM D2240-05 *Standard Test Method for Rubber Property-Durometer Hardness*. 2010.
- [12] Russell John Varley, Sybrand van der Zwaag. Development of a quasi-static test method to investigate the origin of self-healing in ionomers under ballistic conditions. *Polymer Testing* 2008; 27(1):11.

- [13] ISO 527-2. *Plastics - Determination of tensile properties-Part 2: Test conditions for moulding and extrusion plastics*. 2012.
- [14] ISO 179-1:2010. *Plastics-Determination of Charpy impact properties - Part 1: Non-instrumented impact test*. 2010.

Chapter 7

PHOTO-RESPONSIVE POLYMERS BASED ON COUMARIN

*Cástor Salgado Soneira**, *Laura Peponi*, *Marina P. Arrieta*,
Daniel López and Marta Fernández-García

Group of Macromolecular Engineering, Institute of Polymer Science
and Technology (ICTP), Spanish National Research Council (CSIC), Madrid, Spain

ABSTRACT

In this chapter, photo-responsive polymers (PRP) with extraordinary consideration in the polyurethane field and in particular, coumarin-based polymers are reviewed. But it also summarizes other representatives photo-reactive compounds used in polymer science (i.e., azobenzene, spiropyran, cinnamic acid/ester, anthracene and coumarin derivatives). Firstly, this chapter offers an overview of the photo-responsive mechanism of these photo-reactive compounds. Since light is an ideal way to modify physical and chemical properties on material surfaces, smart properties such as self-healing and/or shape memory behavior can be performed with the correct useful of this source. For these reason, PRP can be used as films, hydrogels as well as supramolecular systems with interesting properties for several applications such as laser dyes, drug delivery systems and mainly as coatings. Well-dispersed nano-sized fillers are able to enhance several properties of PRF, including hydrophilic/hydrophobic, thermal and mechanical properties, as well as the release ability, etc. Thus, recent developments in PRP are summarizes here with a special emphasis on PU-coumarin based systems as well as on their nanocomposites.

Keywords: photo-responsive, smart, light-triggered, polymer, crosslinking, dimerization, coumarin, polyurethane

* Corresponding Author Email: castorsalgado@ictp.csic.es.

1. INTRODUCTION

In the last years, light-responsive polymers attract largely interest of scientists because of their capability of combining different stimuli to obtain functional materials. In this sense, light is a clean and highly efficient stimulation source because it can be remotely and accurately controlled, quickly switched and easily focused into specific areas. Certainly, photo-reaction processes do not need any additional substances. Moreover, the wavelength and intensity of light can be modified during the reaction process to switch the properties of polymers.

When we speak about photo-responsive polymers (PRP) we refer to different classes of polymeric systems based on polyurethane, block copolymer micelles, hydrogels or supramolecular systems, among others.

In recent years, several studies based on photo-responsive polymers with different applications have been reported. For example, the formation of polymeric micelles has gained in versatility with the merge of photo-responsive systems [1]. On this topic, Zhao et al. discuss about different approaches to design rational light-responsive block copolymer micelles, by using various photochromic moieties and photochemical reactions as well as the underlying mechanisms leading to photo-induce disruption of these micelles [2]. In Figure 1, examples of light-responsive block copolymer micelles mechanisms are shown.

Several reviews of PRP have been published in recent years. Nicoletta et al. have investigated about light-driven polymer membranes, their mechanisms and their applications, with special attention on photo-responsive liquid-crystal devices [3]. On this topic, photo-responsive of different bio-materials and also surface modification with light stimulation was described by Ercole et al. [4].

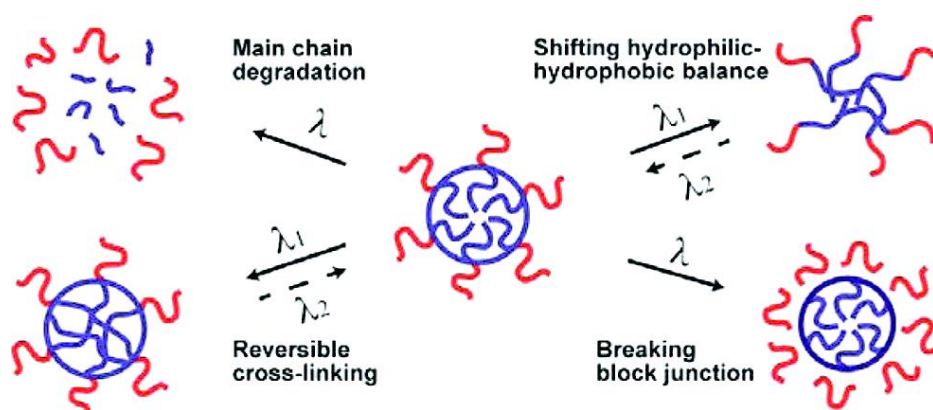


Figure 1. Different aggregations of light-responsive block copolymer micelles. Reprinted (adapted) with permission from [2]. Copyright (2012) American Chemical Society.

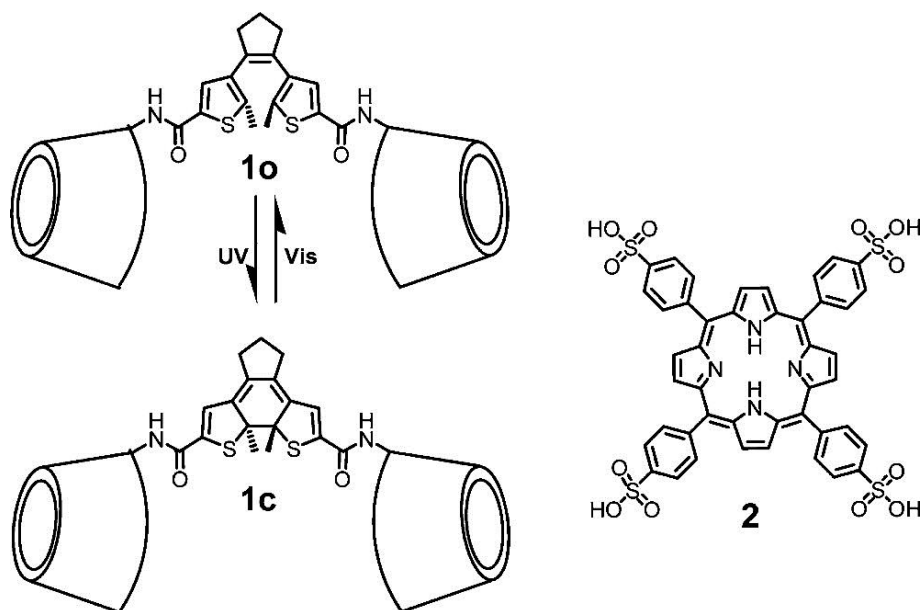


Figure 2. Photo-switchable CD dimer 1 and porphyrin guest molecule 2. Reprinted (adapted) with permission from [8]. Copyright (2015) American Chemical Society.

Moreover, photo-initiated crosslinking radical polymerization [5], thiol-based reactions or molecular crystals based on diarylethene chromophores [6] are examples of the important use of light in different physico-chemical processes. Browne et al. focused their review on the molecular switching of smart surfaces [7]. In addition, supramolecular chemistry has been updated with light-stimulated materials. Qu et al. reviewed host-guest functional systems with photo-responsive properties, such as cyclodextrin (CD) dimers as alterable receptor systems [8] (see Figure 2).

In 2009, Zhao et al. [9] developed an azobenzene-branched copolymer (Figure 3), where the *trans*-form of azobenzene bonds with a β -cyclodextrin (β -CD) derivative drives to the formation of a hydrogel. In particular, the *trans*-azobenzene form is encapsulated by β -CD after the irradiation process, the *cis*-azobenzene drive out the β -CD and recovers the sol phase. This is an example of light-responsive sol-gel controlled by UV-light through a reversible transition. This system can be used in bioengineering as drug delivery device.

In this chapter, special attention will be paid on polyurethanes (PUs) with photo-responsive properties. In particular, PUs are generally formed by reaction between polyol and isocyanate and their microstructures are characterized by the presence of soft and hard segments. Chattopadhyay et al. [10] have extensively studied the thermal stability of PUs, as well as their applications as coatings [11]. Moreover, it is expected that advances in nanotechnology, polymer science and the development of novel bioinspired surfaces have a significant impact on the growth of a new generation of environmentally friendly PU based coatings [12].

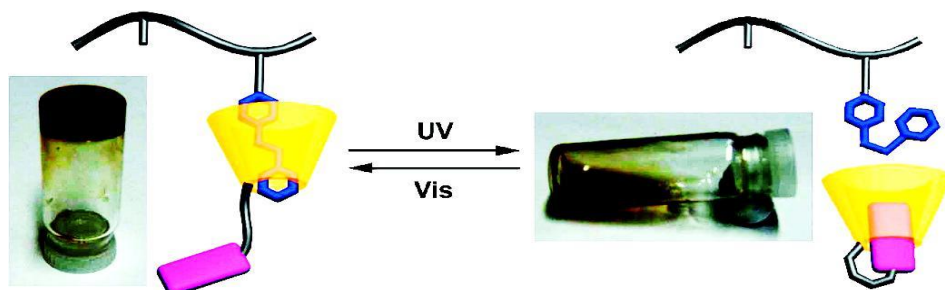


Figure 3. Photo-responsiveness azo-benzene based hydrogels with sol-gel phase transition. The trans-azobenzene form is encapsulated by the β -CD and after irradiation, the cis-azobenzene drive out the β -CD to recover the sol phase. Reprinted (adapted) with permission from [9]. Copyright (2009) American Chemical Society.

Therefore, in this chapter a brief introduction on PUs as well as on photo-switching compounds is reported. Then, the attention will be focused on coumarin-based polymers with special attention on coumarin-based polyurethanes as well as on coumarin-based nano-reinforced polymers. The chapter will conclude with some applications of PRP.

1.1. Polyurethanes

PUs are polymeric materials with a wide applicability and versatility, which are strongly related with the election of their monomers: macrodiols, diisocyanates and chain extenders (CE).

Isocyanates are very reactive systems and can react with several products such as alcohols, amines, water or acids. The basic reactions of isocyanate with different reagents are shown in Figure 4 [13].

The diisocyanate derivatives used to synthesize PUs can be aromatic or aliphatic. The most used diisocyanates are toluene diisocyanate (TDI), methylene diphenyl diisocyanate (MDI) and hexamethylene diisocyanate (HDI).

The polyol component of the PUs can be a functional polyether such as polyethylene glycol (PEG), polypropylene glycol (PPG), or polytetramethylene glycol (PTMG). Polyesters like poly(ϵ -caprolactone) diol (PCL), polylactic acid (PLA) or polycarbonate (PC) are also used. In general, the use of high molecular weight polyols as the main reactants produces polymer chains with less urethane groups and more flexible alkyl chains. Therefore, long-chain polyols with low functionality (1.8–3.0) give soft and more elastomeric PUs, while short-chain polyols with high functionality (greater than 3) give more rigid and crosslinked products [11].

Thermoplastic PUs are characterized by a linear block copolymer structure formed by hard segments (HS) and soft segments (SS). In these systems, due to the intrinsic incompatibility or thermodynamic immiscibility between HS and SS, phase separation

may be observed in the final material. Usually, the isocyanate and the chain extender form the HS, while the polyol contributes to the SS segregation.

Most of biodegradable PUs are based on PCL, PLA, PEG and polyglycolic acid (PGA) polyols. Specifically, PCL-based PUs present low crystallinity and preserve good physical properties. In 2005, Ping et al. developed segmented PCL-based PUs with shape memory behavior [14]. In 2013, Peponi et al. synthesized PUs based on triblock PLA-PCL-PLA copolymer structure with good mechanical properties and excellent shape memory behavior [15].

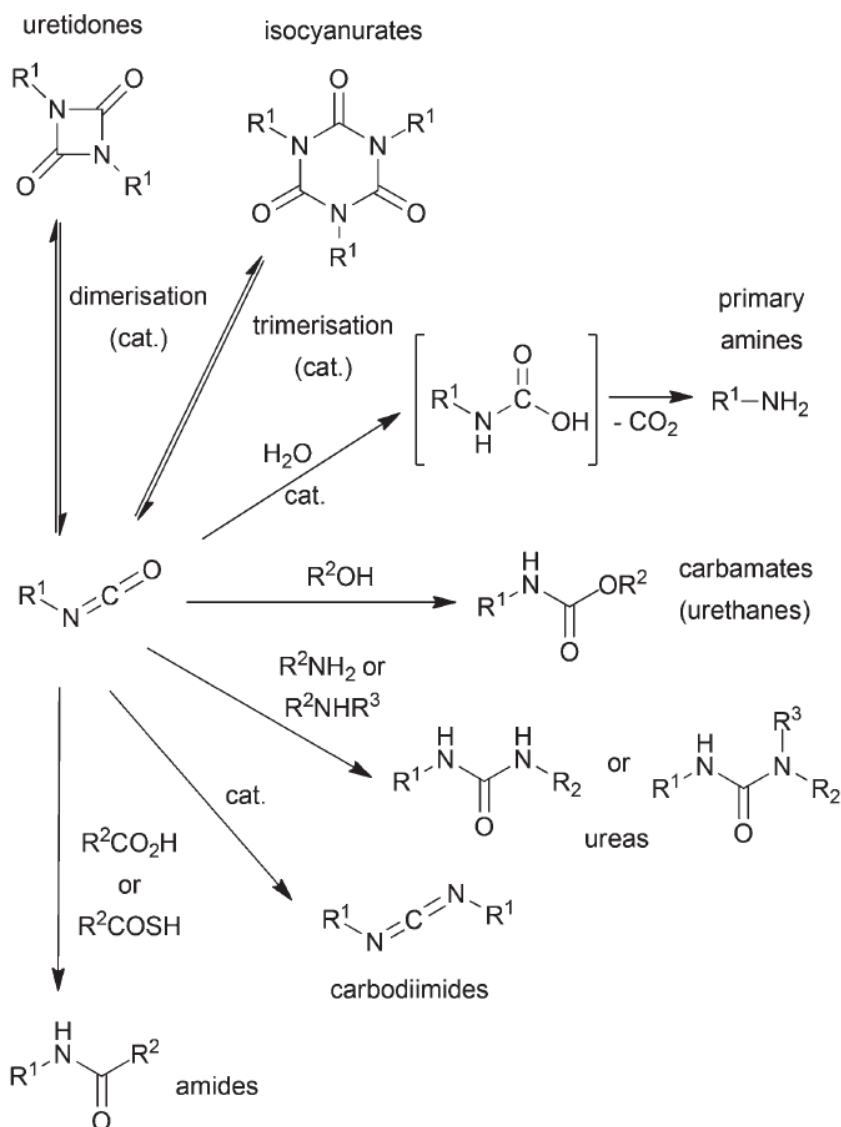


Figure 4. Different chemistry based on isocyanate group. Reproduced from Ref. [13] with permission from the Royal Society of Chemistry.

1.2. Photo-Switching Compounds

Different classifications of photo-responsive systems could be described. Structure, photo-chemical process or finality of the systems are a few of the different ways used to classify them. Zhu et al. [16] classified PRP into several categories based on the photo-sensitive functional groups used for macromolecular preparation: photo-labile protecting (caging) groups [17], reversible dimerization [18, 19], photo-isomerization [20, 21], and weak metal–metal bonds [22]. Therefore, the photo-switchable systems described by Zhu et al. can be stimulated with light at multiple wavelengths, from 200 nm to 750 nm, as indicated in Figure 5, where the wavelength absorption for different PRP are schematically reported.

Blasco et al. [23] recently classified light-induced processes based on different class of photo-induced reaction: thiol-based chemistry [24], cycloaddition reactions (photo [2+2] cycloaddition among others) [25], and photo-dimerization reactions (which will be discussed later).

The photo-chemistry of the photo-dimerizable systems are based on either a $[4\pi+4\pi]$ (anthracene) or $[2\pi+2\pi]$ (cinnamic acid and coumarin) cycloaddition processes. The dimer formation can be switched by another UV irradiation. The general mechanism of a $[2\pi+2\pi]$ -cycloaddition is displayed in Scheme 1, when an alkene is irradiated with UV-light, then an electron promotes from a ground state of the highest occupied molecular orbital (HOMO) to an excited state. This orbital interacts with the lowest unoccupied molecular orbital (LUMO) of the second alkene in a suprafacial contact. This correct symmetry allows the photo-chemical cycloaddition process.

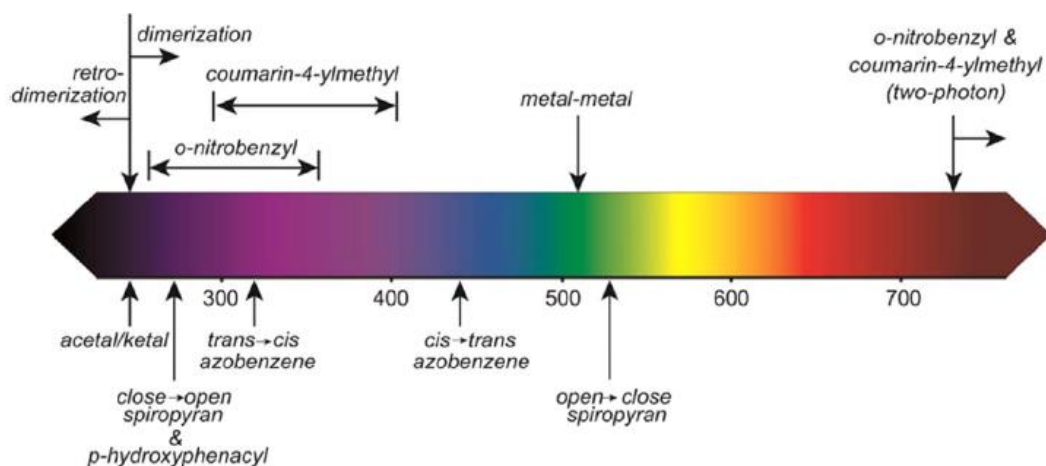
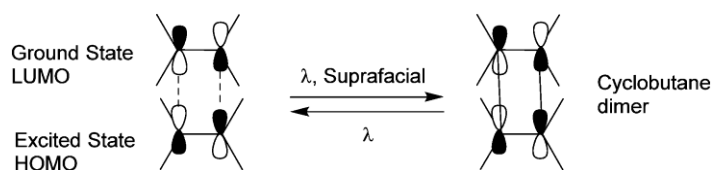


Figure 5. Absorption wavelengths for diverse photo-responsive systems. Reprinted (adapted) with permission from [16]. Copyright (2014) American Chemical Society.



Scheme 1. Suprafacial $[2\pi+2\pi]$ -cycloaddition of two alkenes. Reproduced from Ref. [27] with permission from the Royal Society of Chemistry.

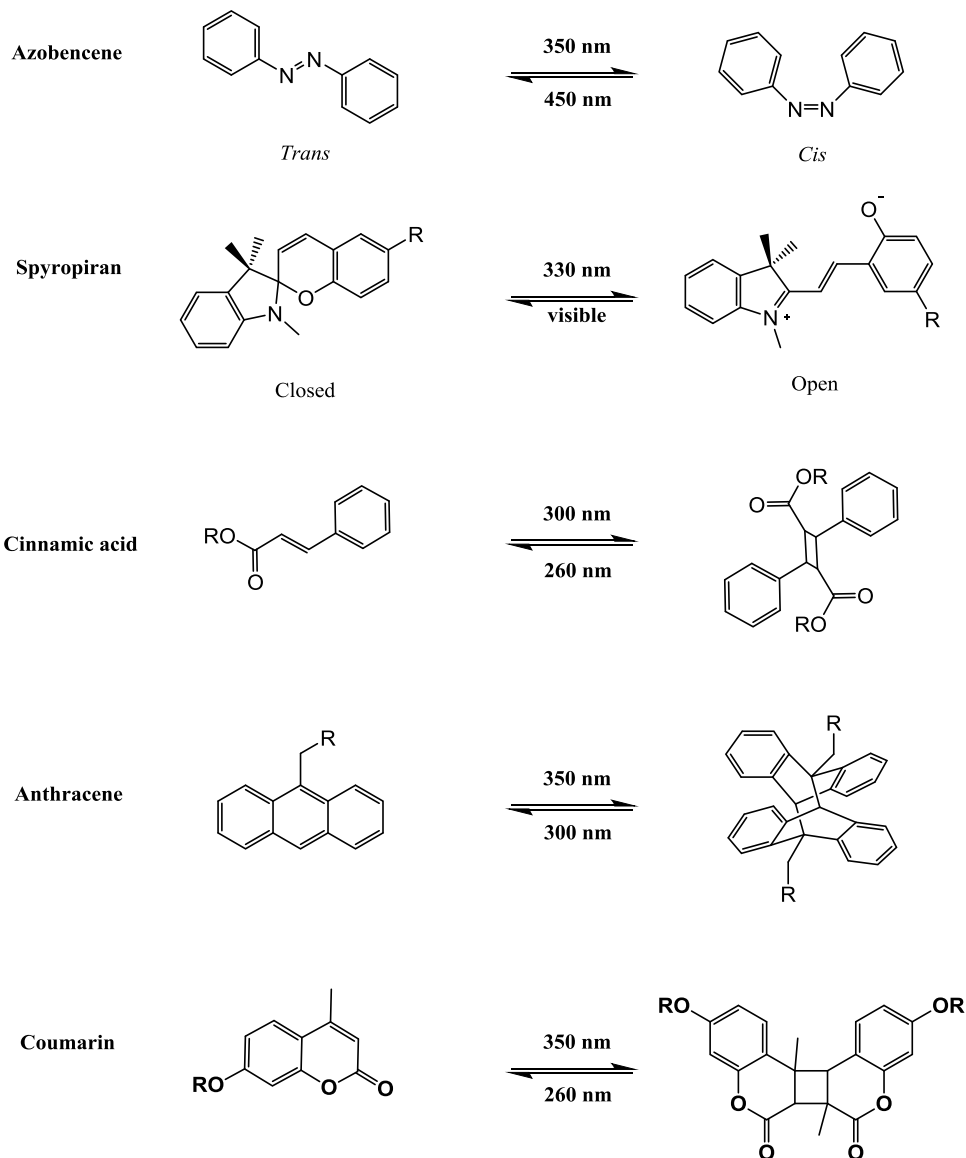


Figure 6. Photo-responsive guests in polymers and their photo-isomers.

There are many groups that can be used as photo-reactive systems in polymers. Examples of photo-isomerization molecules are: azobenzene, dithienylethene, spiropyran,

diarylethene or fulgides. Except azobenzene, these systems are susceptible to undergo changes from an open to a closed form and are also reversible through first order thermal reversion. At this regard, 2-diazo-1-naphthoquinones are a photo-reactive component in photo-resists as well as a good example of photo-induced Wolff rearrangement [26].

Anthracene, cinnamic acid, coumarin, thymine or stilbenes are moieties susceptible to experiment photo-reversible dimerization. The photo-dimerization process can be developed with the formation of one or different cyclobutane isomers, depending on the irradiation conditions. Another option is the formation of different isomers apart from the cyclobutane ring. This is, for instance, the situation of the cinnamic acid or stilbene derivatives, which are subjected to *E-Z* photo-dimerization, or the minor isomer obtained from the irradiation of thymine, 6,4-photo-adduct.

In this chapter, the most representative photo-reactive compounds used in polymer science are also reviewed: azobenzene, spiropyran, cinnamic acid/ester, anthracene and coumarin derivatives (Figure 6).

Azobenzene-Based Systems

Azobenzene derivatives perform an easy *trans-cis* isomerization upon UV irradiation, being the *trans* form the most stable conformation. The reaction is reversible by heat or irradiation with visible light, as shown in Figure 7. Azobenzenes change their geometry from a planar one to non-planar configuration upon irradiation with a drastic decrease in the distance between the *para* carbon atoms from 9.9 Å to 5.5 Å and a corresponding increase in the dipole moment from 0.5 D to 3.1 D. Due to their dissimilar geometries, different properties can be triggered by their photo-response: polarity, electrical properties, membrane dimensions, membrane potential, adsorption, solubility, wettability, swelling, enzyme activity, sol-gel transition of polymer, permeability, ion binding, photo-mechanical cycle, etc. [9, 21, 23].

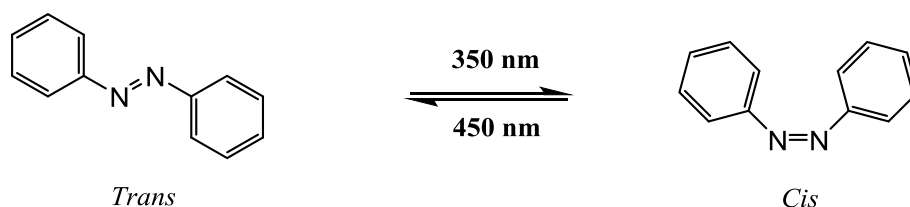


Figure 7. Photo-isomerization reaction of azobenzene.

Spiropyran-Based Systems

Spiropyran, SP, is a photo-responsive system that undergoes a heterocyclic ring cleavage at the C–O spiro bond to form a conjugated chromophore with planar shape, that absorbs intensely in the visible region, this being the merocyanine isomer (Figure 8).

The open-ring form returns to the initial close-ring form either by thermal or photochemical process. Spiropyran derivatives can be entrapped, cross-linked, and introduced as side chain or part of the main chain into the polymer matrices in order to gain a photo-regulation of the membrane potentials [3]. The incorporation of spiropyran systems onto macromolecular supports or inorganic scaffolds allows for the design of robust dynamic materials [28]. Spiropyran was recently used to initiate the ring-opening multibranching polymerization induced by an external light source owing to a reversible photoisomerization of merocyanine [19].

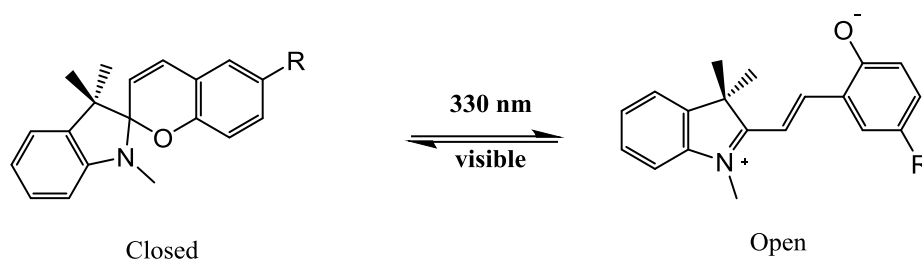


Figure 8. Photo-cleavage reaction of spiropyran.

Cinnamic Acid Systems

Trans-cinnamic acid derivatives are the typical example of $[2\pi + 2\pi]$ photo-dimerization (Figure 9), giving also a model of solid-state reaction [29]. Schmidt et al. have classified the packing of *trans*-cinnamic acid and its derivatives in three different forms: an α -form (where monomers are arranged in a head-to-tail manner), β -form (with the monomers arranged head-to-head), and a γ -form (where the monomers are unfavorably aligned) [30]. Cinnamic acid derivatives have found in nature [31] and exhibit different applications like shape memory [32], anti-tumor activity [33], or antibacterial properties [34].

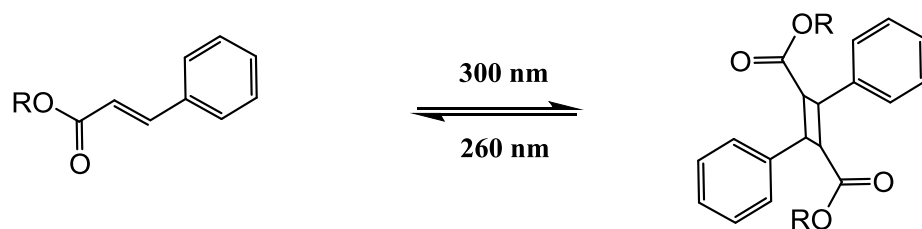


Figure 9. Photo-dimerization reaction of cinnamic acid.

Anthracene Based Systems

Anthracene is a system with three bonded benzene rings. Anthracene derivatives have been extensively investigated specially as organic light-emitting issues. Moreover, anthracenes have been used in optical, electronic and magnetic devices. In medicine, the

anthracene derivatives act as good anti-tumoral drugs and they are carcinogenic to many living beings [35].

Anthracene derivatives have been selected as model systems for crystal-to-crystal photo-dimerizations because of the stack-like motifs which can be found in their crystal structures. This kind of packing leads to short intermolecular face-to-face contacts which facilitate the dimerization driven by light [36].

An interesting application of anthracene-based systems is their photo-dimerization–cycloreversion reactions (Figure 10), which can be used as tools to access highly strained aromatic hydrocarbons. Huang et al. reported the chemical synthesis of oligo-*para*-phenylene-derived nanohoops featuring a rigid dianthracene synthon (see Figure 11). These nanohoops have potential utility as organic optoelectronic materials and building blocks for bottom-up carbon nanotube synthesis [37].

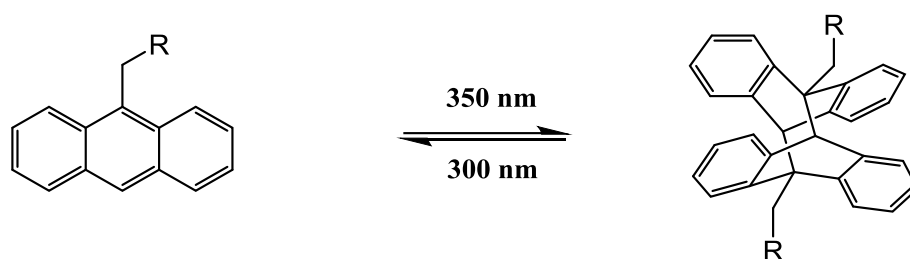


Figure 10. Photo-dimerization reaction of anthracene.

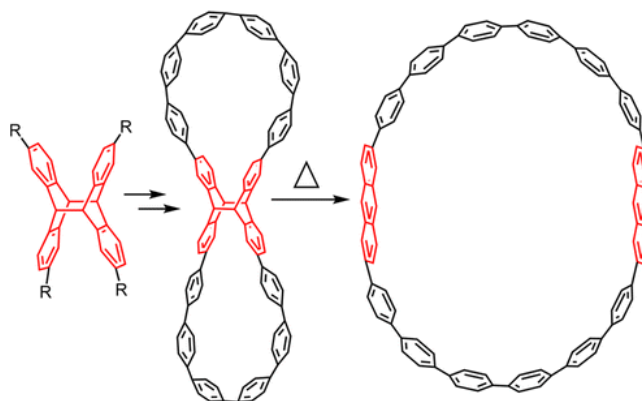


Figure 11. Anthracene-based nanohoops developed by Huang et al. Reprinted (adapted) with permission from [37]. Copyright (2016) American Chemical Society.

Coumarin

Coumarin is a natural constituent of many plants, for example the Tonka bean, whose name come from the French word “coumarou.” Since its discovery in 1820, more than 1000 byproducts have been isolated and over 800 species of plants with naturally presence of coumarin derivatives have been studied. The simplest is the 7-hydroxycoumarin (umbelliferone), which is often considered the precursor of the more

complex coumarins. 4-hydroxycoumarin and 7-hydroxy-4-methyl coumarin are another derivatives also frequently employed. These structures are showed in Figure 12.

The uses for coumarins are as diverse as the structures of the 800 different derivatives of the coumarin family. Coumarins are applied in biochemistry [38-40], medicine [41-44], and polymer science [45-51]. These are also present or used in cosmetic [52, 53], and laser dyes [54, 55]. Very interesting works reported by Trenor et al. [56], Fylaktakidou et al. [57] or Borges et al. [58] have been already published based on coumarin and their properties.

Coumarin derivatives were synthesized by different mechanisms from the 19th century. The first one was the Perkin reaction (1868). Then, in early 1900s, carboxylic acids were used in the Knoevenagel reaction. Moreover, the reaction between resorcinol and ethyl acetoacetate is one of the most used methods to obtain 7-hydroxy-4-methylcoumarin (HMC). This reaction is shown in Figure 13.

In 2003, Nguyen Van et al. developed a ring-closing metathesis by using a Grubb's catalyst [59].

While the most coumarin derivatives are synthesized, there are an important volume of coumarins that have been extracted directly from plants. In 2009, Widelsky et al. isolated five constituents of coumarin from *Angelica Lucida* and evaluated them for antimicrobial activity against Gram positive and Gram negative bacteria as well as fungi [60]. The antimicrobial activity has been ascribed to the inhibition of bacterial nucleic acid synthesis [60]. In this year, Basile at al. extracted several coumarins from the roots of *Ferulago campestris* [61]. They observed that some coumarins (i.e., grandivittin, agasyllin and aegelinol) showed antioxidant activity and it has been ascribed to the fact that coumarins act as radical scavengers. They also found coumarins with antimicrobial performance (aegelinol and agasyllin) showing higher antibacterial activity against Gram-negative than against Gram-positive bacteria.

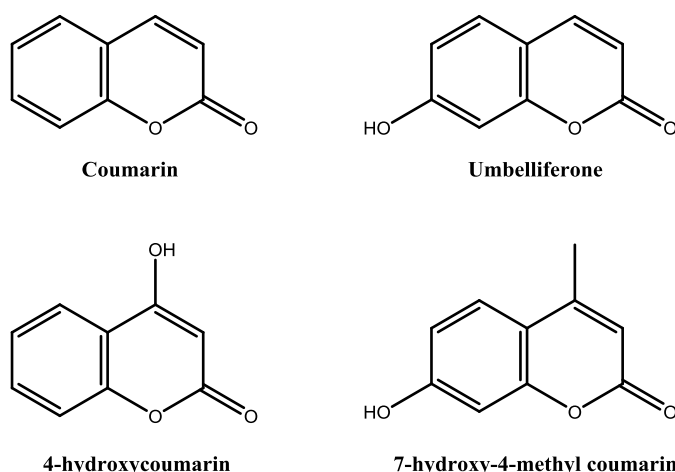


Figure 12. Structures of coumarin and some of their derivatives.

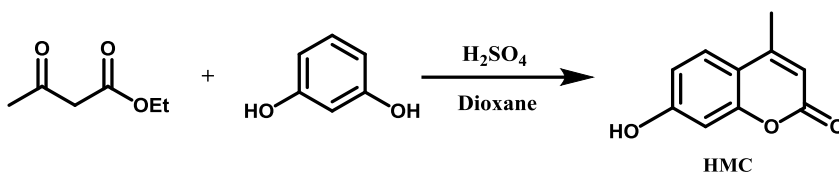


Figure 13. Synthesis of 7-hydroxy-4-methyl coumarin (HMC).

Particularly, on the following part of this chapter we focus the attention on the photo-dimerization of coumarin and on coumarin-based polyurethanes.

2. PHOTO-DIMERIZATION AND PHOTO-CLEAVAGE OF COUMARIN

Coumarin photo-dimerization was discovered in 1902 by Ciamician et al. [62]. In 1966, Krauch et al. [26] confirmed by ¹H-NMR the formation of the four dimers of coumarin at different reaction conditions. Figure 14 shows the structure of these dimers obtained from the UV irradiation of coumarin.

The photo-dimerization process of coumarin is consequence of the [2+2] cycloaddition of the ethylene groups. This is a light-triggered reaction, which is activated at around 300 nm. Photo-cleavage is the reversible process that needs more energy (around 250 nm) to be initiated. Usually, the yield of photo-dimerization/photo-cleavage process decreases with the number of cycles. Figure 15 shows the dimerization process of coumarin and its UV spectrum at various times of irradiation. By decreasing the absorbance band of coumarin monomer at 320 nm, it is possible to quantify the yield of the process [26, 47, 63-66].

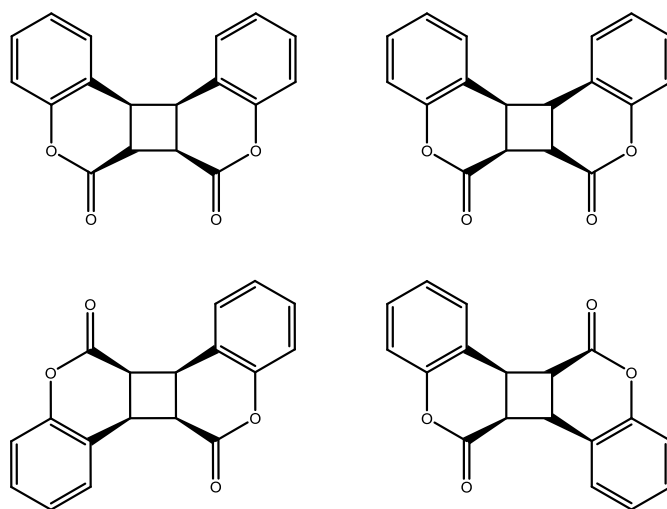


Figure 14. Different structures of coumarin dimers.

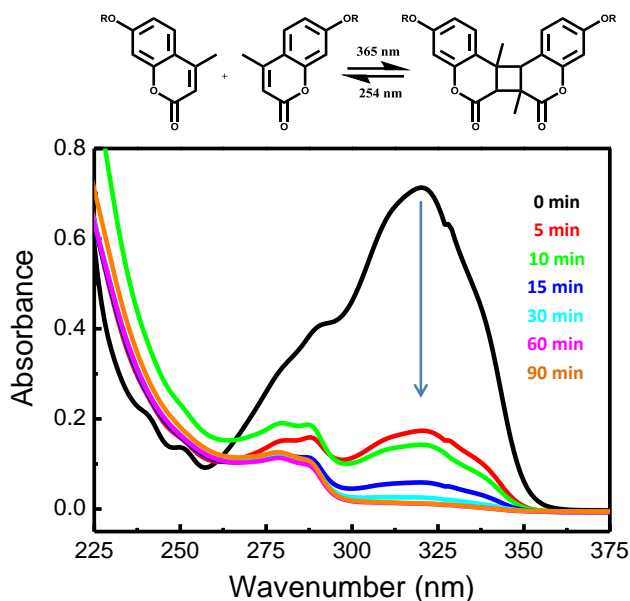


Figure 15. UV-spectra of coumarin at different times of irradiation at 365 nm. The photo-dimerization process decreases the absorbance band of coumarin at 320 nm. Adapted from [67].

3. COUMARINS IN POLYMERS

In recent years, coumarin has been used with polymeric structures in order to form cross-linked systems, supramolecular networks or nanoparticles. In 2016, Long et al. [51] synthesized crosslinked polyurethane micelles based on coumarin with both pH- and UV-response, with the purpose to develop biocompatible drug delivery systems. These micelles were stable in extracellular conditions but can be activated into the cytoplasm by acid conditions, as shown in Figure 16.

Coumarins are also studied by Froimowicz et al. [68] as natural resources to obtain benzoxazine resins for further development of thermosets. However, the main application in polymers is their use as photo-switching system to activate the formation of networks. In 2013, Zhang et al. [69] incorporated coumarin into a tri-star monomer to develop supramolecular structures based on self-assembly with γ -cyclodextrins (γ -CDs), leading to the formation of a non-covalently linked netlike polymer (NNP), which was further converted into its corresponding reticulate polycatenane-like structure (CNP) with a covalent polymer backbone upon UV light irradiation at 365 nm (see Figure 17). These networks can experiment sol-gel transitions under photo-chemical and/or thermal stimuli.

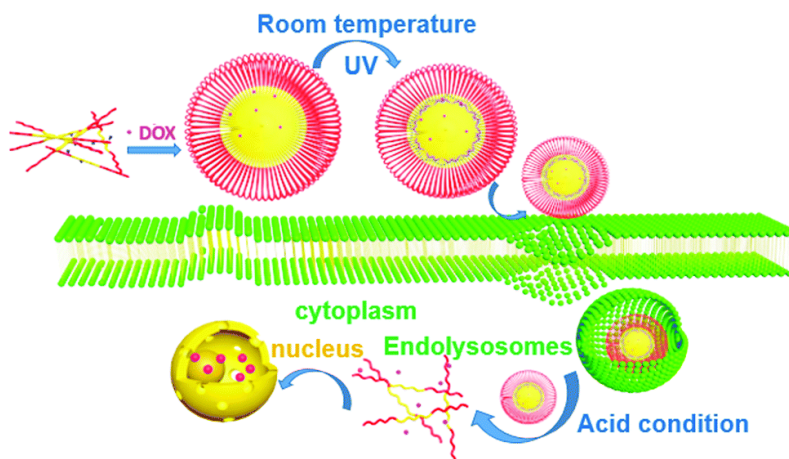


Figure 16. Diagram of polyurethane micelles based on hydrophobic coumarin anticancer drugs and activated by acidic microenvironment inside the tumor tissue. Reproduced from Ref. [51] with permission from the Royal Society of Chemistry.

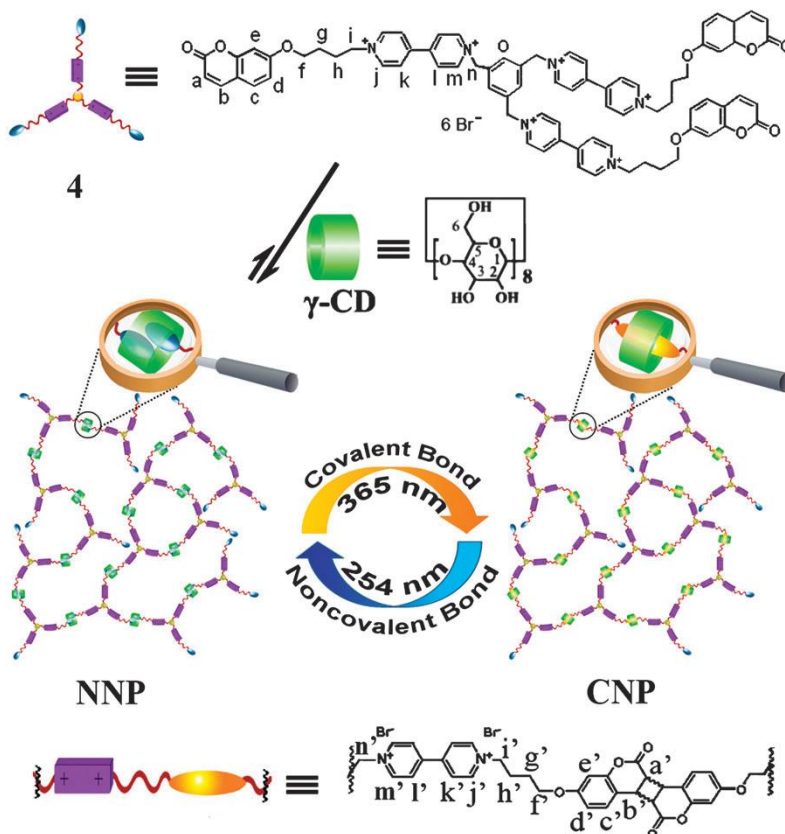


Figure 17. Supramolecular noncovalent linked polymer (NPP) based on coumarin by host-guest contact among tribranched monomers (4) and γ -CDs. Below, the photo-switching between NNP and CNP by UV-light irradiation are shown. Reproduced from Ref. [69] with permission from the Royal Society of Chemistry.

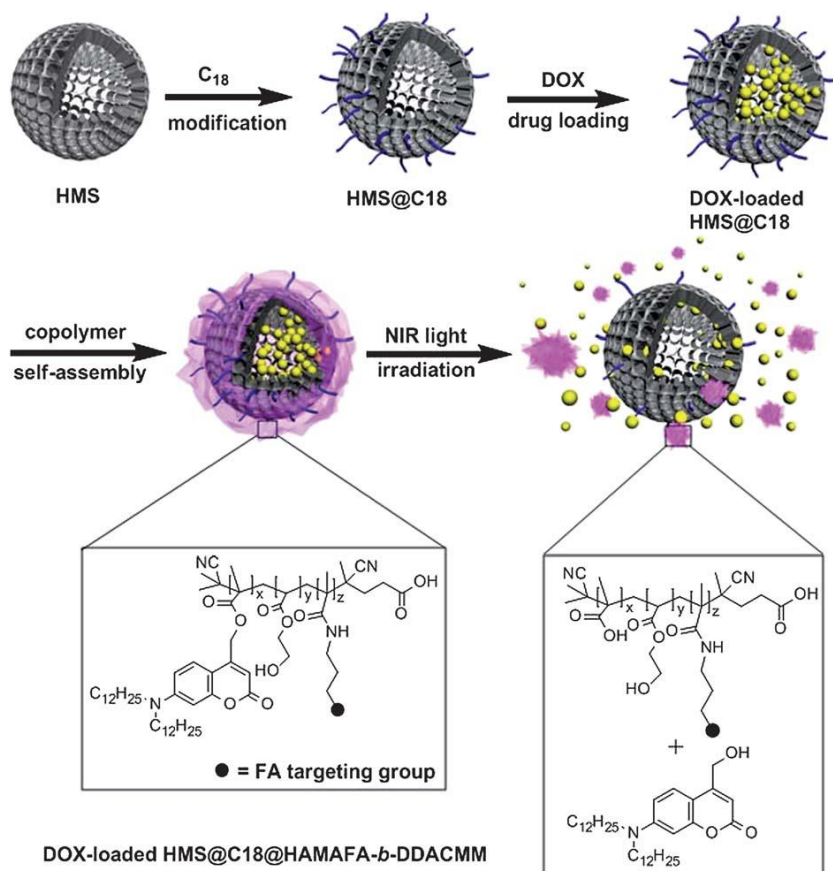


Figure 18. Schematic representation of the development of mesoporous silica/copolymer, for drug delivery and controlled release, by degradation upon NIR light exposure. Reproduced from Ref. [70] with permission from the Royal Society of Chemistry.

Another significant application of coumarin derivatives in polymers involves their photo-responsiveness for optimizing drug delivery systems. In 2013, Ji et al. [70] developed functional and near infrared (NIR) light-triggered nanovehicles for tumor therapy and cell imaging. These nanovehicles were made-up with mesoporous silica modified with a light-responsive block copolymer of [7-(didodecylamino) coumarin-4-yl] methyl methacrylate. Under excitation by NIR light, the pre-loaded drugs could be unconfined from the nanocomposites due to the degradation of the light-responsive copolymers. A diagram of the vehicle loading and its degradation is showed in Figure 18.

4. COUMARIN-BASED POLYURETHANES

An important application of coumarin derivatives is their use as crosslinker group inside the polyurethane chains. PUs are interesting systems to combine with coumarin due to their good mechanical properties. Moreover, the high mobility of the PU chains

stimulates the association between coumarin moieties. Photo-responsive materials need a good UV-light penetration into the polymeric matrix to achieve high photo-dimerization degrees; therefore, the use of translucent or transparent PUs acquires considerable value to enhance their photo-responsive properties. These features provide to the materials an interesting behavior to be applied as self-healing or UV-remendability materials.

In 1997 Chen et al. developed PUs by polyaddition with anti-head-to-head 7-hydroxycoumarin and anti-head-to-tail 7-hydroxy-4-methylcoumarin dimers, which can be self-repaired under UV irradiation [46]. Ling et al. can be considered as one of the biggest developers of coumarin-based PUs during the last years. In 2011 they obtained PU networks based on coumarin dimers that can be self-repaired by UV irradiation [49] (Figure 19). Moreover, in 2012 they worked with mono- and dihydroxyl coumarin derivatives showing a microphase separation in which the rubbery domains are determinant in the photo-remending [50]. In 2014 they obtained PUs based on PEG [71]. By studying these systems with pendant groups of coumarin they showed that the molecular weight of PEG is relevant to obtain high healing efficiency.

Like PEG, PCL is a biodegradable polymer with good physical properties. Seoane et al. developed a photo-reactive PU based on the ring opening polymerization of ϵ -caprolactone by a coumarin diol derivative [72]. The photo-crosslinking process reduced the crystallinity and the melting point of PCL segments. This behavior is an important factor to obtain photo-responsive systems with tailored properties, specifically for their use as coatings. In 2017, our group studied the effect of PCL molecular weight and the concentration of coumarin moieties into photo-responsive PUs [67]. The addition of coumarin increases the thermal stability and the photo-responsiveness with respect to neat polymers. Besides, the photo-dimerization process increases the mechanical properties in the crosslinked PUs, which makes these materials a good option for polymer coatings.

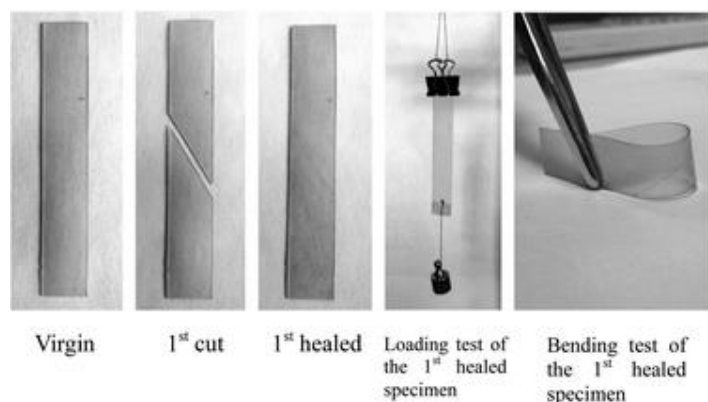


Figure 19. Macro-repairing of fixed samples by UV-light. The fractured surfaces were irradiated at 254 nm and were illuminated at 350 nm for 90 min to heal the crack. Reproduced from Ref. [49] with permission from the Royal Society of Chemistry.

4.1. Nano-Reinforced Polyurethanes

The combination of properties in organic polymers (flexibility, ductility, processability) and a nano scaled inorganic solids (rigidity, thermal stability) can provide to the material a wide range of properties. Different nano-sized fillers are generally used to reinforce PU matrices, such as SiO_2 , Fe_2O_3 , TiO_2 or clay particles. In this sense, polymer/silica composites are the most commonly reported in the literature [73]. Nano-sized silica particles have a large interfacial area and when they are correctly dispersed, these improve the thermal stability of the polymers.

Zhou et al. embedded silica nano-particles with acrylic-based polyurethanes to improve the thermal stability and mechanical properties [74]. Petrovic et al. prepared nanocomposites with higher strength and elongation at break but lower density, modulus, and hardness than the corresponding micron-size silica-filled polyurethanes [75]. Yang et al. dispersed colloidal silica in waterborne polyurethane solutions to obtain hybrids with good thermal stability [76].

In the latest years, nano-silica based polyurethanes have been used in a variety of applications: superhydrophobic coatings [77-79], membranes for gas separation [80, 81] and separators for lithium ion batteries [82]. Recently, our group dispersed fumed silica nanoparticles into polycaprolactone and coumarin-based polyurethanes with an enhancement on thermal stability as well as on photo-responsive properties [83] (see Figure 20).

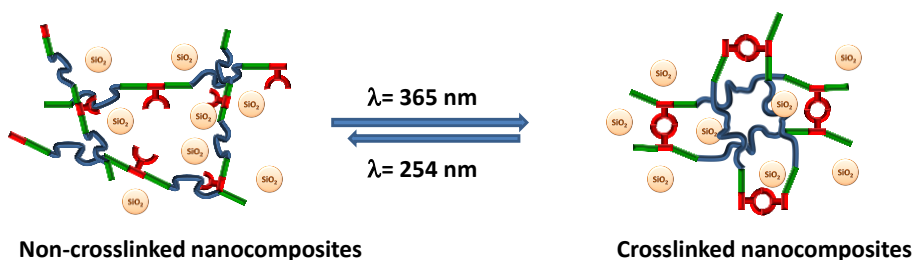


Figure 20. Representation of the UV-crosslinkable PU nanocomposites based on PCL and coumarin with silica nanoparticles. Adapted from [83].

4.2. Photo-Responsive and Self-Healable Materials

Almost all the systems cited previously can be used for the development of self-repaired materials. Cinnamates, disulfide groups or coumarins are reviewed by Fiore et al. as components of optically healable polymers [84]. The main features of self-healing are the macromolecular physical flow and the chemical re-bonding of cleaved moieties. Yang et al. reviewed these parameters as well as the covalent bonding and supramolecular behavior of different photo-responsive systems [85].

5. FINAL REMARKS

Photo-responsive polymers are usually assembled from a non-responsive monomer or polymer and a light-stimulated system. These systems are usually organic compounds (azobenzenes, spiropyrans, cinnamic acid derivatives, anthracene, disulfides and coumarins). Coumarin is a natural compound that experiments reversible photo-dimerization/ photo-cleavage by UV-light influence. The use of coumarin has several applications in biochemistry and medicine, meanwhile in polymer chemistry is employed as photo-crosslinking agent in PUs for coatings, conferring photo-induced self-healing properties to the polymeric matrix. Moreover, when coumarin is used in combination with inorganic nanofillers, the photo-responsive properties of the final nanocomposite are improved. Therefore, self-healing nanocomposites can be developed from coumarin based PUs.

ACKNOWLEDGMENTS

Authors thank MINECO for the MAT2017-88123-P cofinanced with FEDER funds and the Regional Government of Madrid MULTIMAT Challenge: S2013/MIT-2862. L. P. and M. A. acknowledges MINECO for the “Ramon y Cajal” (RYC-2014-15595) and “Juan de la Cierva” (FJCI-2014-20630) contracts.

REFERENCES

- [1] Huang, Y., Dong, R., Zhu, X., Yan, D. Photo-responsive polymeric micelles, *Soft Matter* 10(33) (2014) 6121-6138.
- [2] Zhao, Y. Light-Responsive Block Copolymer Micelles, *Macromolecules* 45(9) (2012) 3647-3657.
- [3] Nicoletta, F. P., Cupelli, D., Formoso, P. De Filpo, G., Colella, V., Gugliuzza, A. Light Responsive Polymer Membranes: A Review, *Membranes* 2(1) (2012) 134.
- [4] Ercole, F., Davis, T., Evans, R. Photo-responsive systems and biomaterials: photochromic polymers, light-triggered self-assembly, surface modification, fluorescence modulation and beyond, *Polymer Chemistry* 1(1) (2010) 37-54.
- [5] Decker, C. Photoinitiated curing of multifunctional monomers, *Acta Polymerica* 45(5) (1994) 333-347.
- [6] Kobatake, S., Takami, S., Muto, H., Ishikawa, T., Irie, M. Rapid and reversible shape changes of molecular crystals on photoirradiation, *Nature* 446(7137) (2007) 778-781.

- [7] Browne, W. R., Feringa, B. L., Light Switching of Molecules on Surfaces, *Annual Review of Physical Chemistry* 60(1) (2009) 407-428.
- [8] Qu, D. H., Wang, Q. C., Zhang, Q. W., Ma, X., Tian, H. Photoresponsive Host-Guest Functional Systems, *Chemical Reviews* 115(15) (2015) 7543-7588.
- [9] Zhao, Y. L., Stoddart, J. F. Azobenzene-Based Light-Responsive Hydrogel System, *Langmuir* 25(15) (2009) 8442-8446.
- [10] Chattopadhyay, D. K., Webster, D. C. Thermal stability and flame retardancy of polyurethanes, *Progress in Polymer Science* 34(10) (2009) 1068-1133.
- [11] Chattopadhyay, D. K., Raju, K. V. S. N. Structural engineering of polyurethane coatings for high performance applications, *Progress in Polymer Science* 32(3) (2007) 352-418.
- [12] Callow, J. A., Callow, M. E. *Trends in the development of environmentally friendly fouling-resistant marine coatings*, 2 (2011) 244.
- [13] Kreye, O., Mutlu, H., Meier, M. A. R. Sustainable routes to polyurethane precursors, *Green Chemistry* 15(6) (2013) 1431-1455.
- [14] Ping, P., Wang, W., Chen, X., Jing, X. Poly(ϵ -caprolactone) Polyurethane and Its Shape-Memory Property, *Biomacromolecules* 6(2) (2005) 587-592.
- [15] Peponi, L., Navarro-Baena, I., Sonseca, A., Gimenez, E., Marcos-Fernandez, A., Kenny, J. M. Synthesis and characterization of PCL-PLLA polyurethane with shape memory behavior, *European Polymer Journal* 49(4) (2013) 893-903.
- [16] Zhu, C., Ninh, C., Bettinger, C. J. Photoreconfigurable Polymers for Biomedical Applications: Chemistry and Macromolecular Engineering, *Biomacromolecules* 15(10) (2014) 3474-3494.
- [17] Pasparakis, G., Manouras, T., Selimis, A., Vamvakaki, M., Argitis, P. Laser-Induced Cell Detachment and Patterning with Photodegradable Polymer Substrates, *Angewandte Chemie International Edition* 50(18) (2011) 4142-4145.
- [18] Wang, D., Jiao, P., Wang, J., Zhang, Q., Feng, L., Yang, Z. Fast photo-switched wettability and color of surfaces coated with polymer brushes containing spiropyran, *Journal of Applied Polymer Science* 125(2) (2012) 870-875.
- [19] Son, S., Shin, E., Kim, B. S. Light-Responsive Micelles of Spiropyran Initiated Hyperbranched Polyglycerol for Smart Drug Delivery, *Biomacromolecules* 15(2) (2014) 628-634.
- [20] Zhu, M. Q., Zhu, L., Han, J. J., Wu, W., Hurst, J. K., Li, A. D. Q. Spiropyran-Based Photochromic Polymer Nanoparticles with Optically Switchable Luminescence, *Journal of the American Chemical Society* 128(13) (2006) 4303-4309.
- [21] Klajn, R. Immobilized azobenzenes for the construction of photoresponsive materials, *Pure and Applied Chemistry*, 2010, p. 2247.
- [22] Tyler, D. R. Photochemically degradable polymers containing metal-metal bonds along their backbones, *Coordination Chemistry Reviews* 246(1) (2003) 291-303.

- [23] Blasco, E., Wegener, M., Barner-Kowollik, C., Photochemically Driven Polymeric Network Formation: Synthesis and Applications, *Advanced Materials* 29(15) (2017) 1604005-n/a.
- [24] Hoyle, C. E., Hensel, R. D., Grubb, M. B. Laser-initiated polymerization of a thiolene system, *Polymer Photochemistry* 4(1) (1984) 69-80.
- [25] Adzima, B. J., Kloxin, C. J., DeForest, C. A., Anseth, K. S., Bowman, C. N. 3D Photofixation Lithography in Diels–Alder Networks, *Macromolecular Rapid Communications* 33(24) (2012) 2092-2096.
- [26] Vleggaar, J. J. M., Huizer, A. H., Kraakman, P. A., Nijssen, W. P. M., Visser, R. J., Varma, C. A. G. O. Photoinduced Wolff-Rearrangement of 2-Diazo-1-naphthoquinones: Evidence for the Participation of a Carbene Intermediate, *Journal of the American Chemical Society* 116(26) (1994) 11754-11763.
- [27] Kaur, G., Johnston, P., Saito, K. Photo-reversible dimerisation reactions and their applications in polymeric systems, *Polymer Chemistry* 5(7) (2014) 2171-2186.
- [28] Klajn, R. Spiropyran-based dynamic materials, *Chemical Society Reviews* 43(1) (2014) 148-184.
- [29] Kaupp, G. Photodimerization of Cinnamic Acid in the Solid State: New Insights on Application of Atomic Force Microscopy, *Angewandte Chemie International Edition in English* 31(5) (1992) 592-595.
- [30] Khan, M., Brunklaus, G., Enkelmann, V., Spiess, H. W. Transient States in [2 + 2] Photodimerization of Cinnamic Acid: Correlation of Solid-State NMR and X-ray Analysis, *Journal of the American Chemical Society* 130(5) (2008) 1741-1748.
- [31] Clifford, M. N. Chlorogenic acids and other cinnamates – nature, occurrence and dietary burden, *Journal of the Science of Food and Agriculture* 79(3) (1999) 362-372.
- [32] Lendlein, A., Jiang, H., Junger, O., Langer, R. Light-induced shape-memory polymers, *Nature* 434(7035) (2005) 879-882.
- [33] Liu, L., Hudgins, W. R., Shack, S., Yin, M. Q., Samid, D. Cinnamic acid: A natural product with potential use in cancer intervention, *International Journal of Cancer* 62(3) (1995) 345-350.
- [34] Burt, S. Essential oils: their antibacterial properties and potential applications in foods—a review, *International Journal of Food Microbiology* 94(3) (2004) 223-253.
- [35] Somashekar, M. N., Chetana, P. R. A Review on Anthracene and Its Derivatives: Applications, *Research & Reviews: Journal of Chemistry* 5(3) (2016) 45-52.
- [36] Salzillo, T., Venuti, E., Della Valle, R. G., Brillante, A. Solid-state photodimerization of 9-methyl-anthracene, *Journal of Raman Spectroscopy* 48(2) (2017) 271-277.
- [37] Huang, Z. A., Chen, C., Yang, X. D., Fan, X. B., Zhou, W., Tung, C. H., Wu, L. Z., Cong, H. Synthesis of Oligoparaphenylene-Derived Nanohoops Employing an

- Anthracene Photodimerization–Cycloreversion Strategy, *Journal of the American Chemical Society* 138(35) (2016) 11144-11147.
- [38] Chen, L., Honsho, Y., Seki, S., Jiang, D. Light-harvesting conjugated microporous polymers: Rapid and highly efficient flow of light energy with a porous polyphenylene framework as antenna, *Journal of the American Chemical Society* 132(19) (2010) 6742-6748.
- [39] Ferguson, L. R. Role of plant polyphenols in genomic stability, *Mutation Research - Fundamental and Molecular Mechanisms of Mutagenesis* 475(1-2) (2001) 89-111.
- [40] Yin Win, K., Feng, S. S. Effects of particle size and surface coating on cellular uptake of polymeric nanoparticles for oral delivery of anticancer drugs, *Biomaterials* 26(15) (2005) 2713-2722.
- [41] Cowan, M. M. Plant products as antimicrobial agents, *Clinical Microbiology Reviews* 12(4) (1999) 564-582.
- [42] Havsteen, B. Flavonoids, a class of natural products of high pharmacological potency, *Biochemical Pharmacology* 32(7) (1983) 1141-1148.
- [43] Lee, A. Y. Y., Levine, M. N., Baker, R. I., Bowden, C., Kakkar, A. K., Prins, M., Rickles, F. R., Julian, J. A., Math, M., Haley, S., Kovacs, M. J., Gent, M. Low-molecular-weight heparin versus a coumarin for the prevention of recurrent venous thromboembolism in patients with cancer, *New England Journal of Medicine* 349(2) (2003) 146-153.
- [44] Vandermeulen, E. P., Van Aken, H., Vermeylen, J. Anticoagulants and spinal-epidural anesthesia, *Anesthesia and Analgesia* 79(6) (1994) 1165-1177.
- [45] Benoit, C., Talitha, S., David, F., Michel, S., Anna, S. J., Rachel, A. V., Patrice, W. Dual thermo- and light-responsive coumarin-based copolymers with programmable cloud points, *Polymer Chemistry* (2017).
- [46] Chen, Y., Chen, K. H. Synthesis and reversible photocleavage of novel polyurethanes containing coumarin dimer components, *Journal of Polymer Science Part A: Polymer Chemistry* 35(4) (1997) 613-624.
- [47] Chen, Y., Wu, J. D., Preparation and photoreaction of copolymers derived from N-(1-phenylethyl)acrylamide and 7-acryloyloxy-4-methyl coumarin, *Journal of Polymer Science Part A: Polymer Chemistry* 32(10) (1994) 1867-1875.
- [48] Chung, J. W., Lee, K., Neikirk, C., Nelson, C. M., Priestley, R. D. Photoresponsive Coumarin-Stabilized Polymeric Nanoparticles as a Detectable Drug Carrier, *Small* 8(11) (2012) 1693-1700.
- [49] Ling, J., Rong, M. Z., Zhang, M. Q. Coumarin imparts repeated photochemical remendability to polyurethane, *Journal of Materials Chemistry* 21(45) (2011) 18373-18380.
- [50] Ling, J., Rong, M. Z., Zhang, M. Q. Photo-stimulated self-healing polyurethane containing dihydroxyl coumarin derivatives, *Polymer* 53(13) (2012) 2691-2698.

- [51] Long, Y. B., Gu, W. X., Pang, C., Ma, J., Gao, H. Construction of coumarin-based cross-linked micelles with pH responsive hydrazone bond and tumor targeting moiety, *Journal of Materials Chemistry B* 4(8) (2016) 1480-1488.
- [52] Yourick, J. J., Bronaugh, R. L. Percutaneous Absorption and Metabolism of Coumarin in Human and Rat Skin, *Journal of Applied Toxicology* 17(3) (1997) 153-158.
- [53] Yamazaki, H., Tanaka, M., Shimada, T. Highly sensitive high-performance liquid chromatographic assay for coumarin 7-hydroxylation and 7-ethoxycoumarin O-deethylation by human liver cytochrome P450 enzymes, *Journal of Chromatography B: Biomedical Sciences and Applications* 721(1) (1999) 13-19.
- [54] Hara, K., Sato, T., Katoh, R., Furube, A., Ohga, Y., Shinpo, A., Suga, S., Sayama, K., Sugihara, H., Arakawa, H. Molecular Design of Coumarin Dyes for Efficient Dye-Sensitized Solar Cells, *The Journal of Physical Chemistry B* 107(2) (2003) 597-606.
- [55] Jones, G., Jackson, W. R., Choi, C. Y., Bergmark, W. R. Solvent effects on emission yield and lifetime for coumarin laser dyes. Requirements for a rotatory decay mechanism, *The Journal of Physical Chemistry* 89(2) (1985) 294-300.
- [56] Trenor, S. R., Shultz, A. R., Love, B. J., Long, T. E. Coumarins in Polymers: From Light Harvesting to Photo-Cross-Linkable Tissue Scaffolds, *Chemical Reviews* 104(6) (2004) 3059-3078.
- [57] Fylaktakidou, K. C., Hadjipavlou-Litina, D. J., Litinas, K. E., Nicolaides, D. N. Natural and synthetic coumarin derivatives with anti-inflammatory/antioxidant activities, *Current Pharmaceutical Design* 10(30) (2004) 3813-3833.
- [58] Borges, F., Roleira, F., Milhazes, N., Santana, L., Uriarte, E. Simple coumarins and analogues in medicinal chemistry: Occurrence, synthesis and biological activity, *Current Medicinal Chemistry* 12(8) (2005) 887-916.
- [59] Nguyen Van, T., Debenedetti, S., De Kimpe, N. Synthesis of coumarins by ring-closing metathesis using Grubbs' catalyst, *Tetrahedron Letters* 44(22) (2003) 4199-4201.
- [60] Widelski, J., Popova, M., Graikou, K., Glowniak, K., Chinou, I. Coumarins from *Angelica Lucida L.* - Antibacterial Activities, *Molecules* 14(8) (2009) 2729.
- [61] Basile, A., Sorbo, S., Spadaro, V., Bruno, M., Maggio, A., Faraone, N., Rosselli, S. Antimicrobial and Antioxidant Activities of Coumarins from the Roots of *Ferulago campestris* (Apiaceae), *Molecules* 14(3) (2009) 939.
- [62] Zhang, X., Wang, H., Liu, C., Zhang, A., Ren, J. Synthesis of Thermoplastic Xylan-Lactide Copolymer with Amidine-Mediated Organocatalyst in Ionic Liquid, *Scientific Reports* 7(1) (2017).
- [63] Chen, Y., Chou, C. F. Reversible photodimerization of coumarin derivatives dispersed in poly(vinyl acetate), *Journal of Polymer Science Part A: Polymer Chemistry* 33(16) (1995) 2705-2714.

- [64] Delzenne, G. A., Laridon, U., Peeters, H. Photopolymerization initiated by O-acyloximes, *European Polymer Journal* 6(7) (1970) 933-943.
- [65] Gnanaguru, K., Ramasubbu, N., Venkatesan, K., Ramamurthy, V. A Study on the Photochemical Dimerization of Coumarins in the Solid State, *Journal of Organic Chemistry* 50(13) (1985) 2337-2346.
- [66] Hammond, G. S., Stout, C. A., Lamola, A. A. Mechanisms of Photochemical Reactions in Solution. XXV. The Photodimerization of Coumarin, *Journal of the American Chemical Society* 86(15) (1964) 3103-3106.
- [67] Salgado, C., Arrieta, M. P., Peponi, L., Fernández-García, M., López, D. Influence of Poly(ϵ -caprolactone) Molecular Weight and Coumarin Amount on Photo-Responsive Polyurethane Properties, *Macromolecular Materials and Engineering* 302(4) (2017).
- [68] Froimowicz, P., Rodriguez Arza, C., Ohashi, S., Ishida, H. Tailor-made and chemically designed synthesis of coumarin-containing benzoxazines and their reactivity study toward their thermosets, *Journal of Polymer Science Part A: Polymer Chemistry* 54(10) (2016) 1428-1435.
- [69] Zhang, Q., Qu, D. H., Ma, X., Tian, H. Sol-gel conversion based on photoswitching between noncovalently and covalently linked netlike supramolecular polymers, *Chemical Communications* 49(84) (2013) 9800-9802.
- [70] Ji, W., Li, N., Chen, D., Qi, X., Sha, W., Jiao, Y., Xu, Q., Lu, J. Coumarin-containing photo-responsive nanocomposites for NIR light-triggered controlled drug release via a two-photon process, *Journal of Materials Chemistry B* 1(43) (2013) 5942-5949.
- [71] Ling, J., Rong, M. Z., Zhang, M. Q. Effect of molecular weight of PEG soft segments on photo-stimulated self-healing performance of coumarin functionalized polyurethanes, *Chinese Journal of Polymer Science* 32(10) (2014) 1286-1297.
- [72] Seoane Rivero, R., Bilbao Solaguren, P., Gondra Zubieta, K., Gonzalez-Jimenez, A., Valentin, J. L., Marcos-Fernandez, A. Synthesis and characterization of a photo-crosslinkable polyurethane based on a coumarin-containing polycaprolactone diol, *European Polymer Journal* 76 (2016) 245-255.
- [73] Zou, H., Wu, S., Shen, J. Polymer/Silica Nanocomposites: Preparation, Characterization, Properties, and Applications, *Chemical Reviews* 108(9) (2008) 3893-3957.
- [74] Zhou, S., Wu, L., Sun, J., Shen, W. The change of the properties of acrylic-based polyurethane via addition of nano-silica, *Progress in Organic Coatings* 45(1) (2002) 33-42.
- [75] Petrović, Z. S., Javni, I., Waddon, A., Bánhegyi, G. Structure and properties of polyurethane-silica nanocomposites, *Journal of Applied Polymer Science* 76(2) (2000) 133-151.

- [76] Yang, C. H., Liu, F. J., Liu, Y. P., Liao, W. T., Hybrids of colloidal silica and waterborne polyurethane, *Journal of Colloid and Interface Science* 302(1) (2006) 123-132.
- [77] Xue, F., Jia, D., Li, Y., Jing, X. Facile preparation of a mechanically robust superhydrophobic acrylic polyurethane coating, *Journal of Materials Chemistry A* 3(26) (2015) 13856-13863.
- [78] Xu, Z., Zhao, Y., Wang, H., Wang, X., Lin, T. A Superamphiphobic Coating with an Ammonia-Triggered Transition to Superhydrophilic and Superoleophobic for Oil–Water Separation, *Angewandte Chemie International Edition* 54(15) (2015) 4527-4530.
- [79] Davis, A., Yeong, Y. H., Steele, A., Bayer, I. S., Loth, E. Superhydrophobic Nanocomposite Surface Topography and Ice Adhesion, *ACS Applied Materials & Interfaces* 6(12) (2014) 9272-9279.
- [80] Khosravi, A., Sadeghi, M., Banadkahi, H. Z., Talakesh, M. M. Polyurethane-Silica Nanocomposite Membranes for Separation of Propane/Methane and Ethane/Methane, *Industrial & Engineering Chemistry Research* 53(5) (2014) 2011-2021.
- [81] Hassanajili, S., Khademi, M., Keshavarz, P. Influence of various types of silica nanoparticles on permeation properties of polyurethane/silica mixed matrix membranes, *Journal of Membrane Science* 453 (2014) 369-383.
- [82] Zhai, Y., Xiao, K., Yu, J., Ding, B. Fabrication of hierarchical structured SiO₂/polyetherimide-polyurethane nanofibrous separators with high performance for lithium ion batteries, *Electrochimica Acta* 154 (2015) 219-226.
- [83] Salgado, C., Arrieta, M. P., Peponi, L., Fernández-García, M., López, D. Silica-nanocomposites of photo-crosslinkable poly(urethane)s based on poly(ϵ -caprolactone) and coumarin, *European Polymer Journal* 93 (2017) 21-32.
- [84] Fiore, G. L., Rowan, S. J., Weder, C. Optically healable polymers, *Chemical Society Reviews* 42(17) (2013) 7278-7288.
- [85] Yang, Y., Ding, X., Urban, M. W. Chemical and physical aspects of self-healing materials, *Progress in Polymer Science* 49–50 (2015) 34-59.

Chapter 8

THERMO-RESPONSIVE POLYMER DISPERSED LIQUID CRYSTALS BASED ON BLOCK COPOLYMERS

*Sheyla Carrasco-Hernandez¹,
Joseba Gomez-Hermoso de Mendoza¹,
Junkal Gutierrez^{1,2} and Agnieszka Tercjak^{1,*}*

¹Group 'Materials + Technologies' (GMT),
Department of Chemical and Environmental Engineering,
Faculty of Engineering, Gipuzkoa, University of the Basque Country (UPV/EHU),
Donostia-San Sebastián, Spain

²Faculty of Engineering Vitoria-Gasteiz,
University of the Basque Country (UPV/EHU), Vitoria-Gasteiz, Spain

ABSTRACT

This Chapter deals with an extensive description related to polymer dispersed liquid crystals based on block copolymers. In addition, a short introduction related to liquid crystals with an emphasis on nematic liquid crystals and polymer dispersed liquid crystals (PDLC) will be given. The introductory part will be followed by a comprehensive discussion related to polymer dispersed liquid crystals and their reversible properties under external stimuli such as thermal gradients or electric and magnetic fields. Finally, different examples of PDLC blends based on block copolymers such as a polymeric matrix will be presented. Furthermore, special attention will be paid to the reversible switching of these smart materials using different characterization techniques such as differential scanning calorimetry (DSC), optical microscopy (OM), photoluminescence spectroscopy (PL), UV-visible spectroscopy (UV-vis), and others.

* Corresponding Author Email: agnieszka.tercjaks@ehu.eus.

Keywords: nematic liquid crystals, block copolymers, polymer dispersed liquid crystals, thermoreversible properties

1. INTRODUCTION

1.1. Liquid Crystals (LCs)

Polymeric materials exist mostly in a solid or liquid state. The mobility of the individual atoms or molecules creates the difference between each state. Solid polymeric materials can switch to a liquid state during the melting transition. Nevertheless, there are materials with intermediate states, named mesophases. These mesophases are the phase transitions between solid and liquid states called the liquid crystal state [1-6]. Consequently, liquid crystals (LCs) are materials in a state, which displays the properties of both conventional liquid and solid crystals at the same time.

In the liquid crystal state, the intermolecular forces, such as dipole-dipole interactions or dispersion forces, are weaker in some directions in comparison to the solid state, however they maintain their associations between molecules in a preferred orientation. The molecules in the liquid crystal state are large and elongated, which allows them to be placed in parallel and can simultaneously move freely with respect to others along their axes. An increase in the temperature (heating process) leads to a molecular movement of LCs that is able to overcome the weaker intermolecular forces, while the stronger ones keep the molecules bound. Consequently, an increase in the temperature provokes a molecular random placement in some directions and a regular one in others as shown in Figure 1. Taking the above into account, LCs are organic materials with different mesophases, which possess properties of both the solid and the liquid state with a long-range orientational order [1-6]. Their capability to self-assemble make them anisotropic materials [7-9], since LCs display different properties depending on the orientation direction.

Generally, LCs can be divided into two classes, thermotropic, and lyotropic LCs. In the case of thermotropic LCs, the molecular orientation depends only on temperature, while in the case of lyotropic LCs, as they are formed from an aqueous solution of amphiphilic molecules such as surfactants, the molecular orientation is directly related to the surfactant concentration [10-15].

In the solid state, thermotropic LC molecules present a regular arrangement, with the same pattern in all directions. Intermolecular forces keep LC molecules in fixed positions. An increase in temperature results in the movement of LC molecules that overcome the intermolecular forces responsible for keeping the order of LC molecules in the solid state, the initiation of random movement, and a change in the state to an isotropic phase or a liquid state [10-15].

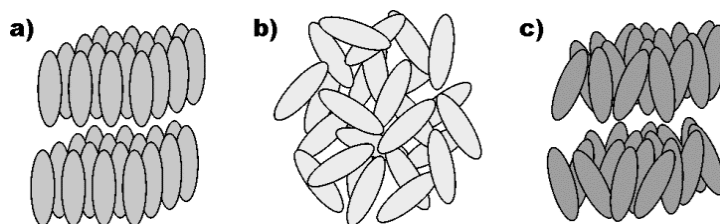


Figure 1. Arrangement of the molecules in a) solid state, b) liquid state, and c) liquid crystal state.

The considered phase transitions in thermotropic LCs are the solid-liquid crystal and the liquid crystal-isotropic liquid transitions. A decrease in the temperature (cooling process) of the isotropic liquid provokes reversible phase transitions, which can be repeated during the heating/cooling cycles [1-5]. The orientation of the molecules in thermotropic LCs is characterized by the director axis pointing in the direction of the average molecular alignment. The director axis describes the long-range order of molecules and depends only on the temperature.

Generally, LC molecules can pass through solid, smectic [16-20], cholesteric [16-18], nematic, and isotropic phase transitions as a function of temperature, which are responsible for the final properties of LCs [19-25] and strongly depend on external conditions such as temperature, chemical composition, external fields, and others [26-30].

In this Chapter we will focus on the nematic LCs.

1.2. Nematic LCs

Nematic liquid crystal (NLC) molecules, with the majority being elongated as rods, do not have a preferred positional order, however they reveal a long-range orientational order. Thus, NLC molecules are located in the same direction however some of them are not completely parallel, thereby, showing a certain deviation. This property is governed by the director axis pointing in the direction of the average molecular alignment, since long axes are approximately parallel [1-10, 31, 32].

The mobility of NLC molecules is similar to that of ordinary isotropic liquids, however, they can be easily aligned by an external field such as magnetic, electric, temperature gradients, and others [33, 34]. Aligned NLCs molecules display the optical properties of uniaxial crystals. Thus, NLCs possess the ability to switch the director axis and as a consequence, the alignment of their rod-like molecules takes place as a response to external stimuli. The NLCs switch from the state of high light dispersion, ON-state, when the director axes are aligned to a transparent state, to OFF-state, when they are not aligned.

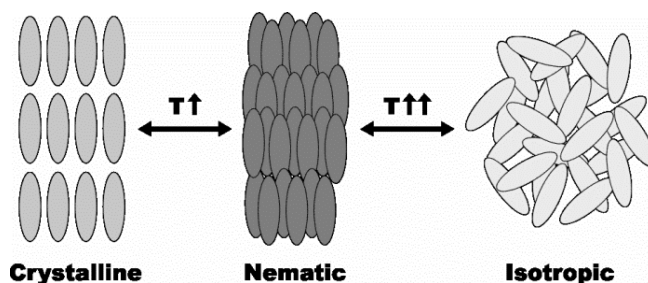


Figure 2. Solid-nematic and nematic-liquid isotropic transitions.

From the thermodynamic point of view, the nematic-isotropic liquid phase transition is a relatively weak first order transition if compared to the solid-nematic transition. Figure 2 shows the solid-nematic and nematic-liquid isotropic transitions of a NLC when a temperature gradient is applied.

The most common approach to describe the nematic phase and nematic-isotropic (N-I) phase transition, is based on the continuous decreasing of the order parameter with an increase in the temperature, dropping drastically to zero at the N-I transition temperature (T_{N-I}). This transition can be described theoretically by using the Landau equation [1-7, 10, 11, 13, 15, 16, 35]. Several theories have been developed to describe the nematic phase and the N-I phase transition. The most widely used approach is the model proposed by de Gennes based on Landau's general description of the phase transition. The Landau-de-Gennes (LDG) theory describes the state of a nematic liquid crystal by a macroscopic order parameter defined in terms of macroscopic quantities [1-7].

The reversible switching process makes NLCs interesting as they can be combined with other materials in order to create innovative applications. LC materials can be used in many different fields as digital thermometers, battery testers and other voltage measuring devices, temperature indicators for medical applications, medical thermography, radiation detection, esthetics, ingredients for cosmetic formulations, non-destructive testing/thermal mapping, aerospace, engineering research, gas/liquid level indicators, and biomedical, among others [7, 16, 18, 41-50].

The alignment capacity of the the rod-like NLC molecules under an external stimulus combined with the processability and properties of the polymeric materials is an interesting pathway to develop polymer dispersed liquid crystal (PDLC) blends, which are used in a wide range of applications in the fields of thermal and electro-optical devices [36-40].

2. POLYMER DISPERSED LIQUID CRYSTAL (PDLC) BLENDS

Polymer blend technology is one of the main areas of research in Polymer and Material Science. Polymer blends combine the properties of their components, leading to

polymeric materials with a wide range of applications [51-55]. Thus, a polymer blend is a physical mixture in which at least two polymers are mixed together to develop novel polymeric materials with synergistic properties.

On the one hand, the main goal of polymer blending is the realization of materials with improved properties for commercial applications, and on the other hand, the preservation of these improved properties to reduce costs and enhance the processability of these materials. All these advantages can be reached through the proper selection of the polymer components and by overcoming limitations such as the difficulty of the dispersion of one polymer into another one due to the high interfacial tension, weak interfacial adhesion, and the instability of the polymer blends.

Depending on both the Gibbs free energy (ΔG_m) of mixing and the second derivative of the Gibbs free energy, polymer blends can be classified as miscible, immiscible, and partially miscible [55-62]. For a miscible polymer blend, $\Delta G_m < 0$ and the second derivative positive, a homogeneous blend is obtained and a unique phase is observed. The miscibility between components depends strongly on the preparation conditions and the polymer blend formulation. The preparation of miscible polymer blends guarantees synergistic properties. For an immiscible or heterogeneous blend, $\Delta G_m > 0$, the second derivative of the free energy function is negative, and in this case several phases corresponding to each component of the polymer blend are detected as a consequence of macrophase separation. When $\Delta G_m \leq 0$ and the second derivative of the free energy function are negative, the polymer blends are partially miscible. In this case, some part of one component of the polymer blend is miscible with the other component forming an interface, which is responsible for good interfacial adhesion.

The miscibility of the polymer blends can be verified by the Fox equation [62-65]. This equation employs the glass transition temperature (T_g) of the polymer blend components to predict the theoretical T_g of a polymer blend. This equation is an easy way to discuss the miscibility of polymer blends. Miscible polymer blends show only one T_g located between the T_g s corresponding to the neat polymer blend components, while immiscible polymer blends possess two T_g s detected at the same temperature range as the T_g of each of the polymer blend components. When investigated polymer blends possess two T_g s located in between the T_g s of each of the polymer blend components and this polymer blend is partially miscible.

Generally, partially miscible polymer blends offer a higher possibility of achieving synergistic properties while incompatible polymer blends are completely immiscible and as a consequence of macrophase separation, have poor mechanical properties [52, 58, 66-70].

The versatility of polymer blends makes them useful in numerous fields of applications such as medical, optical engineering for electronic devices, nanotechnology, and the cosmetic industry, as well as for coatings and adhesives, among others. The

advantages obtained from the mixture of polymeric materials can lead to the development of novel classes of polymer blends by combining polymers with other components.

One of these polymer blends with outstanding synergistic properties, are polymer dispersed liquid crystal (PDLC) blends. The PDLC blends combine properties of thermoplastic polymers and properties of liquid crystals to create novel materials with tailored properties [36-40, 48-50].

As aforementioned, the orientation of the nematic liquid crystal rod-like molecules during the reversible switching process can be changed by applying an external stimulus. This property, jointly with the processability of thermoplastic polymers, make these PDLC blends innovative materials, which can be used in different fields of applications such as optical switches (light shutters), smart windows, and reflective displays, among others [36-40].

The enhancement of the PDLC blend properties in comparison to the properties of the polymer blends is related to the fact that the PDLC blends present, on the one hand, some degree of long-range order and, on the other hand, some degree of mobility. Consequently, properties such as chemical stability, lower flammability, and better processability can be achieved [71-73]. These properties are closely related to the molecular structure of the polymeric chain, which contains rigid liquid crystal phases or mesogens that can be placed in the main chain, in the side chains or in both, thereby allowing the polymer to be oriented in a similar way to neat liquid crystals [60, 74, 75].

The key factor in achieving PDLC blends with tailored properties is the control of the miscibility as a function of the temperature between selected thermoplastic polymers and nematic liquid crystals. The fast cooling rate has led to PDLC blends with smaller nematic domains with a narrow size distribution. On the contrary, the slow cooling rate has led to the coexistence of very large and small nematic domains [76-80]. The PDLC blends consist of NLC droplets with different configurations and orientations homogeneously dispersed in an optically transparent polymer matrix. These very small droplets, only a few microns in size, are responsible for the reversible switching of the PDLC blends by external stimuli [48-50]. The NLC molecules are able to change their orientation by applying an external electric field or a temperature gradient as shown in Figure 3.

The arrangement of the NLC molecules as a function of external stimuli provokes a variation of the intensity of the transmitted light. When an external stimulus is applied, the NLC droplets are oriented and the PDLC blends switch from an opaque to a transparent state. Consequently, the optical properties of the PDLC blends are governed by the nematic liquid crystal phase and are able to maintain their properties in design materials [10, 16-18].

The optical anisotropy of the PDLC blends is closely related to the different values of the NLC and the polymer matrix refractive indices along the optical director axis. This means that they can be optically switched from an opaque state or highly scattering state

(OFF-state), if the director axis is nonaligned to the transparent state (ON-state), and if the director axis is aligned due to the mismatching and matching of the NLC and the polymer refractive index [8, 11, 16, 31, 33, 34, 81-85]. Thus, in the OFF-state, the mismatching between the effective refractive index of the liquid crystal (n_{eff}) and the refractive index of the polymer (n_p) leads to a non-uniform director field inside the liquid crystal droplets, and consequently the PDLC blend films scatter light. In the ON-state, the director field is aligned along the field direction ($n_{\text{eff}} = n_o$) and consequently the PDLC blend films become transparent since the ordinary refractive index n_o of the liquid crystal is equal to n_p .

The switching time between the opaque and transparent states depends on the size, shape, and anchoring energy of the liquid crystal domains. PDLC blends with LC domains a size smaller than the wavelength of visible light do not scatter light efficiently, while LC domains larger than the wavelength of visible light lead to a poor contrast ratio. Consequently, it is desirable to fabricate PDLC blends consisting of LC domains with a uniform characteristic size in the wavelength range of visible light.

Moreover, the switching process is also affected by the contrast ratio between the opaque and transparent states as well as the hysteresis between repeated switching cycles.

In this research field, different optically transparent polymers were used as the matrix in PDLC blends [86-95]. Tercjak et al. [86] have fabricated and studied different PDLC blends based on poly(bisphenol A carbonate) (PC), poly(methylphenylsiloxane) (PMPLSi), poly(styrene-b-ethylene oxide) (PS-b-PEO) block copolymer and a low molecular weight 4'-(hexyloxy)-4-biphenyl-carbonitrile (HOBC). They have also studied the phase diagrams of PC/HOBC, PS-b-PEO/HOBC, and PMPLSi/HOBC blends taking into account the thermal transitions determined by using differential scanning calorimetry (DCS), an optical microscope (OM) and a dynamical mechanical analyzer (DMA). All the PDLC blends investigated by them showed a homogenous isotropic solution of the polymers and the LCs before reversible switching of the PDLC blends from a strong scatter light (OFF-state), thus opaque state, to a transparent state (ON-state).

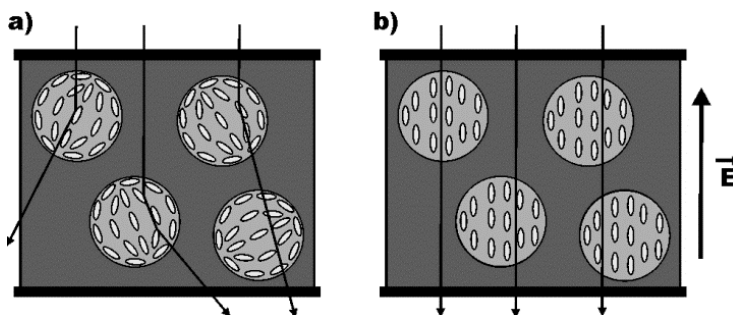


Figure 3. Arrangement of the nematic liquid crystal molecules in a PDLC material, a) light scattered OFF state and b) light transmitted ON state.

Additionally, as it was proved by OM all investigated PDLC blends do not exhibit a liquid-liquid demixing region. Instead of PDLC blends based on PC and PMPLSi, in the case of the PS-*b*-PEO/HOBC blends the strong influence of the addition of PS-*b*-PEO on the temperature in which systems switched from nematic to liquid isotropic state was observed as a consequence of the partial miscibility between PS-block and LC.

Tercjak et al. [86] have also proved that the addition of PC, PS-*b*-PEO or PMPLSi into the PDLC blends hinder crystallization of HOBC if compared with crystallization of neat HOBC. Additionally, the thermo-optical curves of PC/HOBC, PS-*b*-PEO/HOBC and PMPLSi/HOBC in the isotropization region revealed that the nematic-liquid isotropic transition maintained up to 30 wt % HOBC content. Taking in to consideration, both the hindering of crystallization in the PDLC blends and the range in which PDLC blends still show nematic-liquid isotropic transition, specifically designed PDLC blends can be used as smart materials in applications similar to LC applications. Authors have also showed that the addition of PC, PS-*b*-PEO or PMPLSi into the PDLC blends stabilizes them against crystallization as a means of preventing the coalescence of LC droplets.

3. POLYMER DISPERSED LIQUID CRYSTALS (PDLC) BASED ON BLOCK COPOLYMERS

The temperature dependence of the properties of the NLCs in the polymeric matrices makes PDLC blends excellent materials for potential LC applications. The main drawback is the weldline strength between different phases [53, 54, 58, 59]. As explained above, the employment of different methods for predicting the miscibility in blends, is an important area in polymer blend technology [72, 98-100]. A possible way to control and improve the miscibility of the PDLC blend components is the addition of the block copolymers as polymer matrices.

Block copolymers are able to reduce the interfacial tension between components and allow the phase separation to be controlled and consequently, promote higher miscibility between components [101-104]. The ability of the block copolymers to self-assemble and as a consequence to control their morphologies at the nanoscale, offers new possibilities of applications, especially in the field of the miniaturization of opto-electronic and magnetic devices.

Block copolymers are macromolecules consisting of two or more groups of monomers covalently linked in the same polymer chain. The different ways to connect these blocks lead to diverse structures such as diblock AB, triblock ABC or star copolymers. The most interesting property of block copolymers is their ability to self-assemble leading to different structures organized at the nanoscale [105, 106].

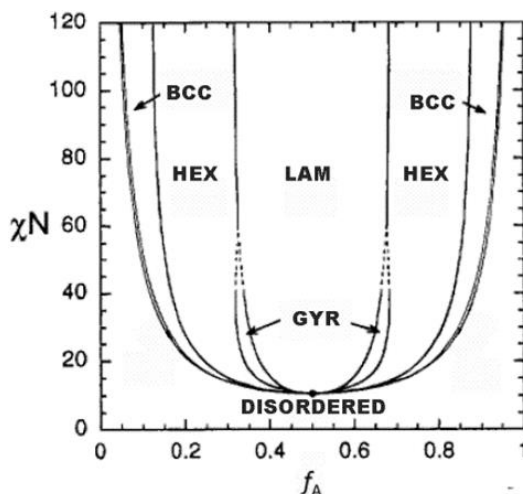


Figure 4. Theoretical phase diagram of an AB diblock copolymer. Reproduced with permission of (Matsen et al.), copyright 1996 ACS Publications.

The different chemical compositions of the blocks and their covalent linkage, lead to well-defined structures with morphologies governed by the Flory-Huggins phase diagram. As can be seen in Figure 4, block copolymers can form different morphologies at the nanoscale such as the body-centered cubic (BCC), hexagonal (HEX), gyroid (GYD) and lamellar (LAM), and disordered structure (DIS) [107-110].

The microphase separation in block copolymers can be controlled by the Flory-Huggins interaction parameter (χ) between monomers, which forms different blocks and the number of polymer repeating units or the degree of polymerization (N). This χ is related to the chemical composition of the blocks and the length of the polymer.

Block copolymers integrated by two monomers display different miscibility with respect to the NLC. Generally, one of the blocks is miscible or partially miscible with the NLC, consequently, NLC can be positioned in one block of the copolymer. Moreover, block copolymers can self-assemble offering nanostructured templates for dispersion of NLC droplets, leading to PDLC materials with electro-optic properties [81-83, 86, 111].

Valenti et al. [111] have fabricated the PDLC blends based on styrene-diene block copolymers as a polymeric matrix and the nematic mixture E7 as a nematic liquid crystal by casting the solvent method in order to study the miscibility between components and the influence of several parameters on the morphology of the PDLC blends. To better understand the role of each block of styrene-diene triblock copolymers, authors also studied PDLC blends with polystyrene and polybutadiene. The results obtained by them revealed a different solubility of the NLC with each block of copolymer, leading to different micro-heterogeneous structures. Valenti et al. [111] have proved that the size, shape, and distribution of NLC droplets changed as a function of the NLC concentration in the PDLC blends. The final morphologies of the PDLC blends investigated by them depended, however, on various parameters especially the affinity between the casting

solvent and the matrix blocks and the critical surface tensions of the NLC and block of copolymer components that were discussed.

Following the work reported by Valenti et al. [111], a PS-*b*-PEO block copolymer was used as a polymer matrix in PDLC blends with HOBC nematic liquid crystals [86, 93]. Authors proved that the addition of even 50 wt % of HOBC liquid crystals into the HOBC/PE-*b*-PEO blend allowed it to obtain a multifunctional nano/mesostructured system as showed in Figure 5.

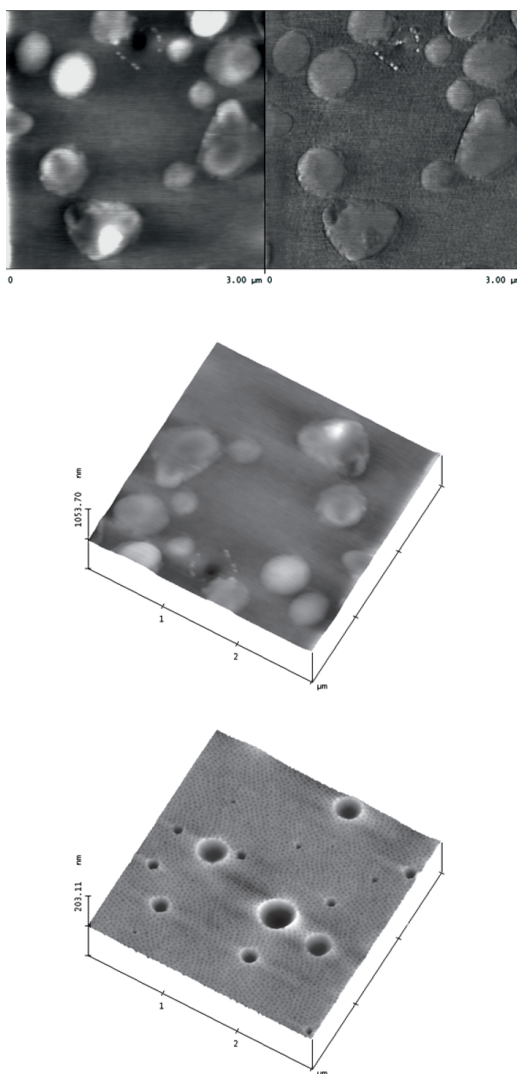


Figure 5. a) AFM height/phase images disordered state b) 3D AFM height image in disordered state c) 3D AFM height image in ordered state of 10 wt % HOBC/PS-*b*-PEO blend. Reproduced with permission of (Tercjak et al.), copyright 2007 Elsevier.

The results obtained evidenced that under the right conditions PDLC blends maintain the properties of a block copolymer since the PS-*b*-PEO block copolymer in these blends self-assembled into well-defined hexagonally closely packed cylinders. The self-

assembly of the PS-*b*-PEO block copolymers in HOBC/PS-*b*-PEO blends contained 5, 10, 30 and 50 wt % HOBC that led to the sub-micron phase segregation of the HOBC liquid crystals. Well-dispersed HOBC liquid crystal droplets with narrow distribution were clearly distinguished in a self-assembled matrix as shown in Figure 5c. The size of the HOBC liquid crystal droplets increased with the increase of the HOBCs in the PDLC blends that were 200-400 nm in diameter for the 50 wt % HOBC/PS-*b*-PEO blends. Thus, the PDLC blends maintained the properties of liquid crystals and consequently the relatively high molecular orientation of the separated mesophase droplets of the HOBC phase refracted plane-polarized light. These blends can switch from a highly light scattering state (OFF-state) to a transparent state (ON-state) when a temperature gradient is applied. Moreover, the self-assembly of the PS-*b*-PEO block copolymer phase hindered the coalescence process of the nematic droplets of the HOBC liquid crystal phase leading to the mesophase separation of the HOBC liquid crystal phase.

In the field of PDLC blends based on block copolymers, Carrasco-Hernandez et al. [112, 113] have used poly(ethylene-*b*-ethylene oxide) (PE-*b*-PEO) block copolymers. They have fabricated PDLC blends employing two different low molecular weight nematic liquid crystals: 4'-(hexyloxy)-4-biphenylcarbonitrile (HOBC) and N-(4-ethoxybenzylidene)-4-butylaniline (EBBA).

The miscibility between each block of the PE-*b*-PEO block copolymer and the HOBC and EBBA nematic liquid crystals and the thermal stability of the PE-*b*-PEO/HOBC and PE-*b*-PEO/EBBA blends were characterized by differential scanning calorimetry (DSC) and thermogravimetric analysis (TGA). The morphology of the fabricated PE-*b*-PEO/HOBC and PE-*b*-PEO/EBBA blends can be visualized using optical microscopy (OM). The miscibility between the PE-*b*-PEO block copolymers and the HOBC and EBBA nematic liquid crystals were directly related to the decrease of the T_m in the HOBC and EBBA liquid crystal phases with an increase of the PE-*b*-PEO block copolymer content as well as the decrease of the degree of crystallization in the liquid crystal phase in the PDLC blends. These results were in good agreement with the theoretical prediction based on the solubility parameters calculated for each block of the PE-*b*-PEO block copolymers and the HOBC and EBBA nematic liquid crystals.

Obtained by the authors, the DSC results confirmed that the PEO block of the PE-*b*-PEO block copolymers showed higher miscibility with the HOBC nematic liquid crystals than with the EBBA nematic liquid crystals as further confirmed by miscibility between the PEO homopolymers and the HOBC and EBBA liquid crystals.

Moreover, the addition of the PE-*b*-PEO block copolymers resulted in an increase in the thermal stability of the PE-*b*-PEO/HOBC and PE-*b*-PEO/EBBA blends which corroborated the partial miscibility between the PDLC blend components. Thermal treatment performed to visualize the liquid crystal character of the PE-*b*-PEO/HOBC and PE-*b*-PEO/EBBA blends indicated that the PDLC blends containing 25 and 50 wt % of

PE-b-PEO block copolymers exhibited a droplet-like morphology with uniform and narrow size distribution of the nematic HOBC or EBBA domains as showed in Figure 6.

As have been reported by Carrasco-Hernandez et al. [112, 113], the introduction of 25 wt % of PE-b-PEO block copolymers into the PE-b-PEO/HOBC blends resulted in coalesced droplets of the HOBC liquid crystal phase clearly observed in Figure 6b, while the addition of 50 wt % of PE-b-PEO block copolymers led to a droplet-like morphology with an average size of the nematic HOBC domains of around $2.5 \pm 0.5 \mu\text{m}$ (Figure 6c). The incorporation of 75 wt % of PE-b-PEO block copolymers (Figure 6d) changed the morphology of the fabricated blends. In this case, only some small bright spherical crystals of PE-b-PEO block copolymers appeared during the black amorphous phase similar to the morphology exhibited by neat PE-b-PEO block copolymers (compare Figure 6d).

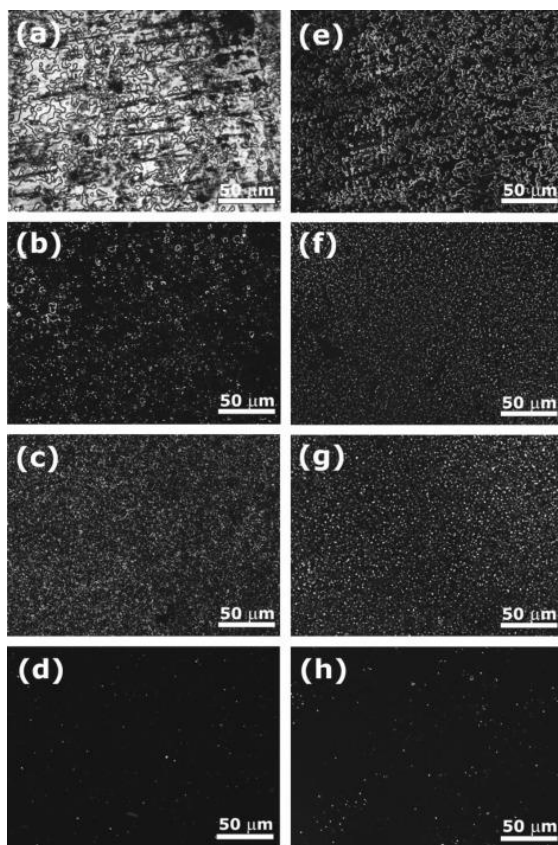


Figure 6. Optical micrographs of (a) HOBC liquid crystals and their PDLC blends with (b) 25 wt %, (c) 50 wt %, (d) 75 wt % PE-b-PEO block copolymer, and (e) EBBA liquid crystals and their PDLC blends with (f) 25 wt %, (g) 50 wt %, (h) 75 wt % PE-b-PEO block copolymers. All OM micrographs were taken between crossed polarizers. Reproduced with permission of (Carrasco-Hernandez et al.), copyright 2016 Elsevier.

The morphology of neat EBBA liquid crystals was similar to the morphology of neat HOBC liquid crystals (Figure 6a and 6e). The PE-b-PEO/EBBA blends containing 25 and 50 wt % of PE-b-PEO block copolymers showed a droplet-like morphology with the uniform size of the nematic EBBA domains. The average size of these mesostable nematic EBBA liquid crystal phases grew with the increase of the PE-b-PEO block copolymer content being $1.5 \pm 0.5 \mu\text{m}$ (Figure 6f) and $3 \pm 0.5 \mu\text{m}$ (Figure 6g) for the PE-b-PEO/EBBA blends modified with 25 and 50 wt % of PE-b-PEO block copolymer content, respectively. The addition of 75 wt % of PE-b-PEO block copolymers into the PE-b-PEO/EBBA blends allowed for envisaging that and for this reason the ratio between component designed materials did not show any liquid crystals droplets (Figure 6h).

The thermo-optical responsive behavior of the PDLC blends based on the PE-b-PEO block copolymers and the HOBC and EBBA nematic liquid crystals were also investigated by Carrasco-Hernandez et al. [113] for the systems with low PE-b-PEO block copolymer content (1, 5, 10 wt %). The presence of nematic-isotropic transitions in these PDLC blends were confirmed by the DSC. The T_{N-I} of the HOBC or EBBA liquid crystal phase in the PE-b-PEO/LC blends were decreased to a few °C with the addition of PE-b-PEO block copolymers if compared with the T_{N-I} of the HOBC or EBBA nematic liquid crystals. Additionally, for all the investigated PDLC blends, the nematic-isotropic transition of the HOBC or EBBA liquid crystal phase occurred almost at the same temperature, regardless of the process, heating or cooling. This behavior indicates that the HOBC or EBBA nematic liquid crystals maintain their ability to switch from an opaque to a transparent state in the PE-b-PEO/LC blends.

The presence of nematic-isotropic transitions in all the investigated PDLC blends, indicate their ability to demonstrate reversible switching during temperature changes. Thus, the liquid crystal phase maintained the nematic-isotropic transitions of the HOBC or EBBA nematic liquid crystals in all the investigated PDLC blends consequently, confirming their ability to switch from an opaque to a transparent state after a temperature gradient. The texture changes as a function of temperature for the investigated HOBC and EBBA nematic liquid crystals and their blends during switching from an opaque to a transparent state were visualized by Carrasco-Hernandez et al. [113] using OM.

The reversible switching process of these PDLC blends were studied by photoluminescence spectroscopy (PL) and UV-visible spectroscopy (UV-vis). The effect of the addition of PE-b-PEO block copolymers to the photoluminescence properties of the HOBC and EBBA liquid crystal phases in the PDLC blends were investigated. Obtained by the authors, the 3D PL spectra of the PE-b-PEO/HOBC and PE-b-PEO/EBBA blends are shown in Figure 7 and 8, respectively.

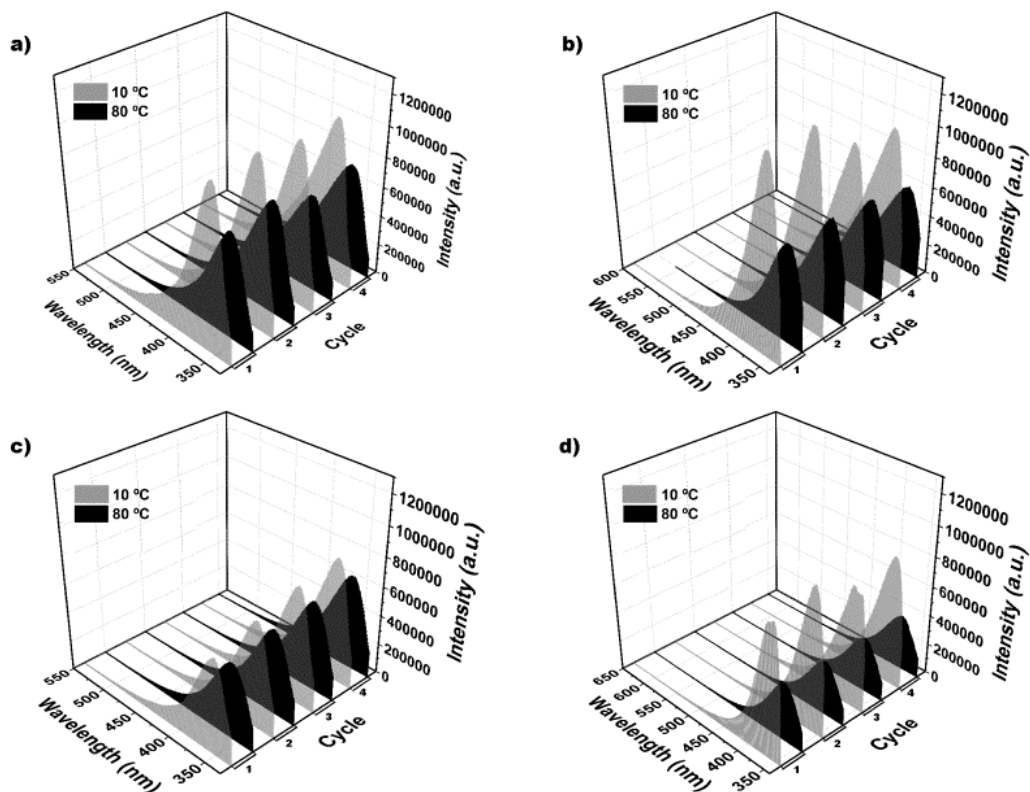


Figure 7. 3D photoluminescence emission spectra at 10 and 80°C of the a) HOBC nematic liquid crystals and PE-b-PEO/HOBC blends with b) 1, c) 5 and d) 10 wt % of PE-b-PEO block copolymer content during four heating/cooling cycles. Reproduced with permission of (Carrasco-Hernandez et al.), copyright 2017 Elsevier.

The reversible photoluminescence changes as a function of the temperature during four heating/cooling cycles, from 10 to 80°C, were monitored in order to deeply study the photoluminescence switching. As mentioned by the authors, the PE-b-PEO block copolymers did not show any emission peaks on the photoluminescence emission spectra taken for excitation wavelengths equal to 333 and 467 nm characteristic for the HOBC and EBBA nematic liquid crystals, respectively.

The PL intensity of the HOBC liquid crystals is much higher than the EBBA liquid crystals. This behavior can be related to the fact that the EBBA liquid crystal phase can act as quencher due to the aniline group in its chemical structure. Consequently, the EBBA liquid crystals maintained thermo-optical reversibility during four heating/cooling cycles while the HOBC liquid crystals lost their reversibility during the repeated heating/cooling cycles. The aniline group present in the EBBA liquid crystal chemical structure acted as a quencher and provoked a lower PL intensity than in the HOBC liquid crystals. However, this was also responsible for the durability of the thermo-optical reversibility when repeated heating/cooling cycles were applied. The addition of the PE-b-PEO block copolymers shifted the maximum emission peak to a higher wavelength and

a lower PL intensity for the PE-b-PEO/HOBC blends and shifted the maximum emission peak to a lower wavelength and a higher PL intensity for the PE-b-PEO/EBBA blends. This behavior was strongly related to the fact that the HOBC nematic liquid crystals are miscible with the PEO blocks while the EBBA nematic liquid crystals are miscible with the PE blocks in the PE-b-PEO block copolymers.

In the case of PE-b-PEO/HOBC blends, the HOBC liquid crystal phase microphase separated from the PEO block domains while in the case of the PE-b-PEO/EBBA blends the EBBA liquid crystal phase microphase separated within the PE block domains. Accordingly, the orientation changes of the HOBC and EBBA nematic liquid crystal phases in the PDLC blends during the switching from an opaque to a transparent state are strongly affected by the partial miscibility of the HOBC liquid crystal phase with the PEO block and EBBA liquid crystal phase with the PEO block of PE-b-PEO block copolymers as shown in Scheme 1.

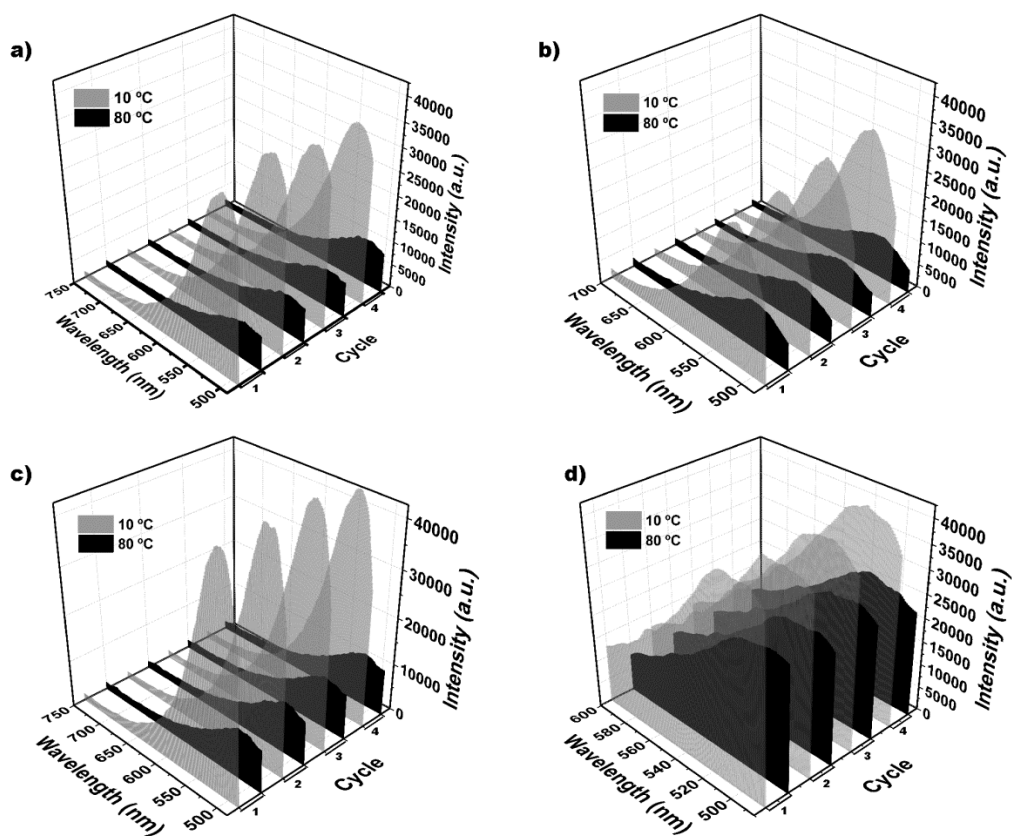
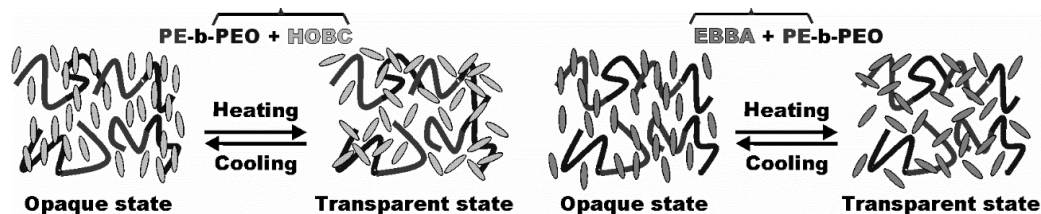


Figure 8. 3D photoluminescence emission spectra at 10 and 80 °C of the a) EBBA nematic liquid crystals and the PE-b-PEO/EBBA blends with b) 1, c) 5 and d) 10 wt % of PE-b-PEO block copolymer content during four heating/cooling cycles. Reproduced with permission of (Carrasco-Hernandez et al.), copyright 2017 Elsevier.



Scheme 1. Schematic illustration of the orientation changes of the HOBC and EBBA liquid crystal phases in the PDLC blends during the switching from an opaque to a transparent state.

The miscibility of the liquid crystals with the different blocks of the PE-b-PEO block copolymers can be responsible for the different photoluminescence behaviors of the PDLC blends based on the HOBC and EBBA nematic liquid crystals.

The transparency and the reversible switching process from opaque to transparent of the PDLC blends based on the HOBC and EBBA nematic liquid crystals as a function of temperature was also studied using UV-vis spectroscopy. The UV-vis transmittance spectra of these PDLC blends were measured at 10 °C (highly scattering state-opaque) and at 80 °C (transparent state). Moreover, the transmittance values were taken at 600 nm during four heating/cooling cycles to quantify the reversibility of this process. The obtained results proved that all the investigated PDLC blends maintained reversible switching from an opaque to a transparent state confirming that they can be employed as thermo-reversible recording materials, thermo-optical devices, and temperature sensors.

Carrasco-Hernandez et al. [114] have used the PE-b-PEO block copolymers as a matrix for the fabrication of the hybrid PE-b-PEO/EBBA electrospun fibers using the co-electrospinning technique. Optimization of the electrospinning processing-window was carried out by varying the concentration of the PE-b-PEO block copolymer solution and playing with three different electrospinning parameters such as voltage, solvent, and the PE-b-PEO block copolymer solution flow rate. The hybrid PE-b-PEO/EBBA electrospun fibers were fabricated modifying the PE-b-PEO block copolymer fibers with low molecular weight EBBA nematic liquid crystals using the coaxial electrospinning technique.

The addition of the EBBA nematic liquid crystals provoked changes in the fiber morphology resulting in a well-ordered lamellar structure. Regarding the hybrid PE-b-PEO/EBBA electrospun fibers developed following the same electrospinning processing window, it was observed that the EBBA nematic liquid crystals improved the hybrid PE-b-PEO/EBBA electrospun fibers formation in width and length due to the higher block copolymer flow rate that provoked changes in the fiber morphology resulting in a well-ordered lamellar structure.

This investigative work proved that the co-electrospinning technique can be successfully employed for the fabrication of hybrid materials based on the PE-b-PEO block copolymers and the EBBA nematic liquid crystals, maintaining the nematic liquid crystal characteristics in the acquired hybrid electrospun fibers.

4. FUTURE TRENDS AND PERSPECTIVE

The PDLC blends based on block copolymers are an interesting class of smart materials, which can find potential application in the fields similar to LC applications. As described in this Chapter, they can switch from an opaque to a transparent state by the application of external stimuli such as thermal gradients, electric or magnetic fields. Moreover, they maintain self-assembly of block copolymers resulting in nanostructured materials, which can act as a template for inorganic nanoparticles. This can be a new trend in this field since inorganic particles can multiply the switching between the opaque and transparent states of these smart materials.

ACKNOWLEDGMENTS

Financial support from Spanish Ministry of Economy, Industry and Competitiveness and European Union in the frame of MAT2015-66149-P project is gratefully acknowledged.

REFERENCES

- [1] Chandrasekhar, S. *Liquid crystals*. Cambridge University Press. Cambridge (UK), 1992.
- [2] de Gennes, P. G., Prost, J. *The physics of liquid crystals*. Oxford University Press. Oxford (UK), 1995.
- [3] Kumar, S. *Liquid crystals*. Experimental study of properties and phase transitions. Cambridge University Press. Cambridge (UK), 2001.
- [4] Singh, S. Phase transitions in liquid crystals. *Phys. Rep.* 2000, 324, 107-269.
- [5] Singh, S. *Liquid crystals: Fundamentals*. World Scientific Publishing Co Pte Ltd. London (UK), 2002.
- [6] Kleman, M., Lavrentovich, O. D. *Soft matter physics: An introduction*. Springer. New York (US), 2003.
- [7] Andrienko, D. *Introduction to liquid crystals*. International Max Planck Research School. Modelling of soft matter. Bad Marienberg (Germany), 2006.
- [8] Collings, P. J. *Liquid Crystals. Nature's delicate phase of matter*. Second Ed., Princeton University Press. Oxford (UK), 2002.
- [9] Khoo, I. C. *Liquid crystals*. Second Ed., John Wiley & Sons. New Jersey (US), 2007.

- [10] Sengupta, A. *Topological microfluidics*. Nematic liquid crystals and nematic colloids in microfluidic environment. Doctoral Thesis. University of Göttingen (Germany), 2013.
- [11] Ramamoorthy, A. *Thermotropic liquid crystals*. Recent advances. Springer. University of Michigan (US), 2007.
- [12] Liu, K., Chen, D., Marcozzi, A., Zheng, L., Su, J., Pesce, D., Zajaczkowski, W., Kolbe, A., Pisula, W., Müllen, K., Clark, N. A., Herrmann, A. Thermotropic liquid crystals from biomacromolecules. *PNAS* 2014, 52, 18596-18600.
- [13] Villanueva-García, M., Gutiérrez-Parra, R. N., Martínez-Richa, A., Roblesa, J. Quantitative structure-property relationships to estimate nematic transition temperatures in thermotropic liquid crystals. *J. Mol. Struct. Theochem* 2005, 727, 63-69.
- [14] Matos, M. R. A., Silva, B. F. B., Marques, E. F. Chain length mismatch and packing effects on the thermotropic phase behavior of salt-free cationic surfactants. *J. Colloid Interf. Sci.* 2013, 405, 134-144.
- [15] Chen, G. Q., Majumdar, A., Wang, D., Zhang, R. Global existence and regularity of solutions for active liquid crystals. *J. Differ. Equations* 2017, 263, 202-239.
- [16] Bata, L. *Advances in liquid crystal research and applications*. First Ed., Akadémiai Kiadó. Budapest (Hungary), 1981.
- [17] Oswald, P., Pieranski, P. *Smectic and columnar liquid crystals*. Taylor & Francis Group, CRS Press. Florida (US), 2006.
- [18] Bahadur, B. *Liquid crystals: Applications and uses*. Vol. 1, World Scientific Publishing Co Pte Ltd. London (UK), 1990.
- [19] Mukherjee, P. K. Smectic-A-smectic-C-smectic-C* Lifshitz point in mixtures of chiral and achiral smectic liquid crystals. *J. Mol. Liq.* 2015, 204, 10-14.
- [20] Guillén-González, F., Tierra, G. Approximation of smectic-A liquid crystals. *Comput. Methods Appl. Mech. Eng.* 2015, 290, 342-361.
- [21] Chakraborty, A., Chakraborty, S., Das, M. K. Critical behavior at the isotropic to nematic, nematic to smectic-A and smectic-A to smectic-C phase transitions in a pyrimidine liquid crystal compound. *Physica B* 2015, 479, 90-95.
- [22] Osiecka, N., Galewski, Z., Juszyńska-Gałązka, E., Massalska-Arodź, M. Studies of reorganization of the molecules during smectic A-smectic C phase transition using infrared spectroscopy and generalized two-dimensional correlation analysis. *J. Mol. Liq.* 2016, 224, 677-683.
- [23] Mirantsev, L. V. Novel possible electro-(magneto-)optic effect in smectic-A liquid crystal cell. *Phys. Lett. A* 2014, 378, 86-89.
- [24] Poursamad, J. B., Hallaji, T. Freedericksz transition in smectic-A liquid crystals doped by ferroelectric nanoparticles. *Physica B* 2017, 504, 112-115.

- [25] Wei, B., Tan, S., Liang, T., Cao S., Wu Y. Synthesis, structural and electrochemical characterization of benzimidazole compounds exhibiting a smectic C liquid crystal phase. *J. Mol. Struct.* 2017, *1133*, 392-397.
- [26] Wang, F., Li, K., Song, P., Wu, X., Chen, H., Cao, H. The effects of thermally induced diffusion of dye on the broadband reflection performance of cholesteric liquid crystals films. *Compos. Part B* 2013, *46*, 145-150.
- [27] Ogiwara, A., Kakiuchida, H. Thermally tunable light filter composed of cholesteric liquid crystals with different temperature dependence. *Sol. Energ. Mat. Sol. C* 2016, *157*, 250-258.
- [28] Therézio, E. M., da Silva, S. F. C., Dalkiranis, G. G., Filho, P. A., Santos, G. C., Ely, F., Bechtold, I. H., Marletta, A. Light polarization states of a cholesteric liquid crystal probed with optical ellipsometry. *Opt. Mater.* 2015, *48*, 7-11.
- [29] Meyer, R. B. Effects of electric and magnetic fields on the structure of cholesteric liquid crystals. *Appl. Phys. Lett.* 1968, *12*, 281-282.
- [30] Lv, K., Liu, D., Li, W., Tian, O., Zhou, X. Reflection characteristics of cholesteric liquid crystal microcapsules with different geometries. *Dyes pigments* 2012, *94*, 452-458.
- [31] Luckhurst, G. R., Sluckin, T. J. *Biaxial nematic liquid crystals*. Theory, simulation and experiment. John Wiley & Sons. University of Southampton (UK), 2015.
- [32] Rego, J. A., Harvey, J. A. A., MacKinnon, A. L., Gatdula, E. Asymmetric synthesis of a highly soluble 'trimeric' analogue of the chiral nematic liquid crystal twist agent Merck S1011. *Liq. Cryst.* 2010, *37*, 37-43.
- [33] Choi, S. S., Morris, S. M., Huck, W. T. S., Coles, H. J. The switching properties of chiral nematic liquid crystals using electrically commanded surfaces. *Soft Matter* 2009, *5*, 354-362.
- [34] Imamura, K., Yoshida, H., Ozaki, M. Reversible switching of liquid crystal micro-particles in a nematic liquid crystal. *Soft Matter* 2016, *12*, 750-755.
- [35] Gramsbergen, E. F., Longa, L., de Jeu, W. H. Landau theory of the nematic-isotropic phase transition. *Phys. Lett.* 1983, *4*, 195-257.
- [36] Yamaguchi, R., Takasu, T. Hybrid aligned nematic liquid crystal smart glass with asymmetrical daylight controls. *J. Soc. Inf. Display* 2015, *23*, 365-370.
- [37] Hoppe, C. E., Galante, M. J., Oyanguren, P. A., Williams, R. J. J. Optical properties of novel thermally switched PDLC films composed of a liquid crystal distributed in a thermoplastic/thermoset polymer blend. *Mater. Sci. Eng C* 2004, *24*, 591-594.
- [38] Parab, S. S., Malik, M. K., Deshmukh, R. R. Dielectric relaxation and electro-optical switching behavior of nematic liquid crystal dispersed in poly(methyl methacrylate). *J. Non-Cryst. Solids* 2012, *358*, 2713-2722.
- [39] Kim, Y., Jung, D., Jeong, S., Kim, K., Choi, W., Seo, Y. Optical properties and optimized conditions for polymer dispersed liquid crystal containing UV curable polymer and nematic liquid crystal. *Curr. Appl. Phys.* 2015, *15*, 292-297.

- [40] Kumar, P., Raina, K. K. Morphological and electro-optical responses of dichroic polymer dispersed liquid crystal films. *Curr. Appl. Phys.* 2007, 7, 636-642.
- [41] Hallcrest, L. C. R. *Handbook of thermochromic liquid crystal technology*. Pickwick Lane. Chicago (US), 2014.
- [42] Meier, G., Sackmann, E., Grabmaier, J. G. *Applications of liquid crystals*. Springer. Berlin (Germany), 1975.
- [43] Brown, G. H. Properties and applications of liquid crystals. *J. Electron. Mater.* 1973, 2, 403-430.
- [44] Li, J. *Refractive indices of liquid crystals and their applications in display and photonic devices*. Thesis doctoral. STARS. University of Central Florida (US), 2005.
- [45] Kwon, K. J., Kim, M. B., Heo, C., Kim, S. G., Back, J. S., Kim, Y. H. Wide color gamut and high dynamic range displays using RGBW LCDs. *Displays* 2015, 40, 9-16.
- [46] Yoshimura, K., Shimamoto, K., Ikeda, M., Ichikawa, K., Naganawa, S. A comparative contrast perception phantom image of brain CT study between high-grade and low-grade liquid crystal displays (LCDs) in electronic medical charts. *Phys. Medica* 2011, 27, 109-116.
- [47] Gago-Calderón, A., Fernández-Ramos, J., Gago-Bohórquez, A. Visual quality evaluation of large LED displays based on subjective sensory perception. *Displays* 2013, 34, 359-370.
- [48] Brennessoltz, M. S., *Stupp EH. Projection displays*. Second Ed., John Wiley & Sons. West Sussex (UK), 2008.
- [49] Drzaic, P. S. *Liquid crystal dispersions*. Vol. 1, World Scientific Publishing Co Pte Ltd. London (UK), 1995.
- [50] Coates D. *Liquid crystal polymers: Synthesis, properties and applications*. Rapra Technology Ltd. Shropshire (UK), 2000.
- [51] Parameswaranpillai, J., Thomas, S., Grohens, Y. *Characterization of polymer blends: Miscibility, morphology, and interfaces*. First Ed., Wiley-VCH. Weinheim (Germany), 2015.
- [52] Bergbreiter, D. E., Martin, C. R. *Control of phase structure in polymer blends, in functional polymers*. Plenum Press. New York (US), 1989.
- [53] Isayeb, A. I. Polymer blend compounding and processing. *Encyclopedia of polymer blends*. Vol. 2, Wiley-VCH. Weinheim (Germany), 2011.
- [54] Ciardelli, F., Penczek, S. *Modification and blending of synthetic and natural macromolecules*. Nato Science Series. Kluwer Academic Publishers. Dordrecht (The Netherlands), 2004.
- [55] Higgins, J. S., Lipson, J. G., White, R. P. A simple approach to polymer mixture miscibility. *Phil. Trans. T. Soc. A* 2010, 368, 1009-1025.

- [56] Koningsveld, R., Stockmayer, W. H., Nies, E. *Polymer phase diagrams: A text book*. Oxford University Press. Oxford (UK), 2001.
- [57] Flory, P. J. *Principles of polymer chemistry*. Cornell University Press. New York (UK), 1953.
- [58] Utracki, L. A., Wilkie, C. A. *Polymer blends handbook*. Second Ed., Springer. Milwaukee (US), 2014.
- [59] Mark, E. J. *Thermodynamics of polymer blends. Physical properties of polymers handbook*. Second Ed., Springer. Ohio (US), 2007.
- [60] Thomas, S., Shanks, R., Sarathchandran, C. *Nanostructured Polymer Blends*. Elsevier. Waltham (US), 2014.
- [61] Robeson, L. M. *Polymer Blends: A comprehensive Review*. Hanser-Garden Inc. Cincinnati (US), 2007.
- [62] Vasile, C., Kulshreshtha, A. K. *Handbook of polymer blends and composites*. Vol. 3B, Rapra Technology Ltd. Shawbury (UK), 2003.
- [63] Brostow, W., Chiu, R., Kalogerias, I. M., Vassilikou-Dova, A. Prediction of glass transition temperatures: Binary blends and copolymers. *Mater. Lett.* 2008, 62, 3152-3155.
- [64] Kuo S. W., Kao H. C., Chang F. C. Thermal behavior and specific interaction in high glass transition temperature PMMA copolymer. *Polymer* 2003;44:6873-6882.
- [65] Zhang G., Zhang J., Wang S., Shen D. Miscibility and phase structure of binary blends of polylactide and poly(methyl methacrylate). *J. Polym. Sci. Pol. Phys.* 2002;41:23-30.
- [66] Yu L, Dean K, Li L. Polymer blends and composites from renewable resources. *Prog. Polym. Sci.* 2006;31:576-602.
- [67] Mano J. F., Koniarova D, Reis RL. Thermal properties of thermoplastic starch/synthetic polymer blends with potential biomedical applicability. *J. Mater. Sci-Mater. M* 2003;14:127-135.
- [68] Mannan H. A., Mukhtar H, Nasir R, Mohshim DF, Mushtaq A. Recent applications of polymer blends in gas separation membranes. *Chem. Eng. Technol.* 2013;36:1838-1846.
- [69] McNeill C. R., Greenham NC. Conjugated-polymer blends for optoelectronics. *Adv. Mater.* 2009;21:3848-3850.
- [70] Narkis M., Srivastava S., Tchoudakov R., Breuer O. Sensors for liquids based on conductive immiscible polymer blends. *Synthetic Met.* 2000;113:29-34.
- [71] Kato T. Self-assembly of phase-segregated liquid crystal structures. *Science* 2002;295:2414-2418.
- [72] Chung T. S. *Thermotropic liquid crystal polymers. Thin-film polymerization, characterization, blends and applications*. Technomic Publishing Co Inc. Pennsylvania (US), 2001.
- [73] Coates D. *Liquid crystal polymers*. Rapra Technology Ltd. Shropshire (UK), 2000.

- [74] Verploegen E, Zhang T, Jung YS, Ross C, Hammond PT. Controlling the morphology of side chain liquid crystalline block copolymer thin films through variations in liquid crystalline content. *Nano Lett.* 2008;10:3434-3440.
- [75] Wei, R., Zhou, L., He, Y., Wang, X., Keller, P. Effect of molecular parameters on thermomechanical behaviour of side-on nematic liquid crystal elastomers. *Polymer* 2013, *54*, 5321-5329.
- [76] Simoni, F. *Nonlinear optical properties of liquid crystals and polymer dispersed liquid crystals*. World Scientific Publishing Co Pte Ltd. London (UK), 1997.
- [77] Drzaic, P. S. *Liquid crystals dispersions*. World Scientific Publishing Co Pte Ltd. London (UK), 1995.
- [78] Coates, D. Polymer dispersed liquid crystals. *J. Mater. Chem.* 1995, *5*, 2063-2072.
- [79] Drzaic, P. S. Polymer dispersed nematic liquid crystal for large area displays and light valves. *J. Appl. Phys.* 1986, *60*, 2142-2148.
- [80] Gill, N., Pojman, J. A., Willis, J., Whitehead, Jr J. B. Polymer-dispersed liquid-crystal materials fabricated with frontal polymerization. *J. Polym. Sci. Pol. Chem.* 2003, *41*, 204-212.
- [81] Tercjak, A., Gutierrez, J., Ocando, C. J., Peponi, L., Mondragon I. Thermoresponsive inorganic/organic hybrids based on conductive TiO₂ nanoparticles embedded in poly(styrene-b-ethylene oxide) block copolymer dispersed liquid crystals. *Acta Mater.* 2009, *57*, 4624-4631.
- [82] Tercjak, A., Serrano, E., Garcia, I., Mondragon, I. Thermoresponsive meso/nanostructured thermosetting materials based on PS-b-PEO block copolymer-dispersed liquid crystal: Curing behavior and morphological variation. *Acta Mater.* 2008, *56*, 5112-5122.
- [83] Tercjak, A., Serrano, E., Mondragon, I. Multifunctional thermally reversible nanostructured thermosetting materials based on block copolymers dispersed liquid crystal. *Macromol. Rapid. Comm.* 2007, *28*, 937-941.
- [84] Ahmad, F., Jamil, M., Lee, J. W., Ri, Y. H., Jeon, Y. J. Characteristics of di- and tri-block copolymers: polymer disperse liquid crystal display. *J. Mod. Optic.* 2014, *61*, 1027-1032.
- [85] Hoppe, C. E., Galante, M. J., Oyanguren, P. A., Williams, R. J. J. Polymer-dispersed liquid crystals based on polystyrene and EBBA: analysis of phase diagrams and morphologies generated. *Macromol. Chem. Phys.* 2003, *204*, 928-935.
- [86] Tercjak, A., Serrano, E., Larrañaga, M., Mondragon, I. Polymer dispersed liquid crystals based on poly(styrene-b-ethylene oxide), poly(bisphenol a carbonate) or poly(methylphenylsiloxane), and 4'-(hexyloxy) 4-biphenyl-carbonitrile: Analysis of phase diagrams and morphologies generated. *J. Appl. Polym. Sci.* 2008, *108*, 1116-1125.

- [87] Sumana, G., Raina, K. K. Synthesis of polysiloxanes and their crosslinking density measurements. *Polym. Mater.* 2002, 19, 281-285.
- [88] Karapinar, R., O'Neill, M., Hird, M. Polymer dispersed ferroelectric liquid crystal films with high electro-optic quality. *J. Phys. D: Appl. Phys.* 2002, 35, 900-905.
- [89] Tercjak, A., Serrano, E., Mondragon, I. Thermally reversible materials based on thermosetting systems modified with polymer dispersed liquid crystals for optoelectronic application. *Polym. Adv. Technol.* 2006, 17, 835-840.
- [90] Craighead, H. G., Cheng, J., Hackwood, S. New display based on electrically induced index matching in an inhomogeneous medium. *Appl. Phys. Lett.* 1982, 40, 22-24.
- [91] Nastał, E., Żurańska, E., Mucha, M. The effect of curing progress on the electrooptical and switching properties of PDLC system. *J. Appl. Polym. Sci.* 1999, 71, 455-463.
- [92] Hoppe, C. E., Galante, M. J., Oyanguren, P. A., Williams, R. J. J. Polymer-dispersed liquid crystals with co-continuous structures generated by polymerization-induced phase separation of EBBA-epoxy solutions. *Macromolecules* 2002, 35, 6324-6331.
- [93] Zucchi, I. A., Resnik, T., Oyanguren, P. A., Galante, M. J., Williams, R. J. J. Comparison of optical properties of thermally reversible light scattering films consisting in dispersions of polystyrene/naphthalene domains or polystyrene/liquid crystal (EBBA) domains in epoxy matrices. *Polymer Bulletin* 2007, 58, 145-151.
- [94] Tercjak, A., Serrano, E., García, I., Ocando, C., Mondragon I. Self-assembled block copolymers as matrix for multifunctional materials modified with low-molecular-weight liquid crystals. *Acta Mater.* 2007, 55, 6436-6443.
- [95] Tercjak, A., Gutierrez J., Ocando O., Mondragon I. Conductive properties of switchable photoluminescence thermosetting systems based on liquid crystals. *Langmuir* 2007, 26, 4296-4302.
- [96] Tercjak, A., Mondragon, I. Relationships between the morphology and thermoresponsive behavior in micro/nanostructured thermosetting matrixes containing a 4'-(hexyloxy)-4-biphenylcarbonitrile liquid crystal. *Langmuir* 2008, 24, 11216-11224.
- [97] Tercjak A., Gutierrez J., Peponi L., Rueda L., Mondragon I. Arrangement of conductive TiO₂ nanoparticles in hybrid inorganic/organic thermosetting materials using liquid crystal. *Macromolecules* 2009, 42, 3386-3390.
- [98] Hempel, P. *Constitutive modeling of amorphous thermoplastic polymers with special emphasis on manufacturing processes*. Karlsruher Institut für Technologie Scientific Publishing. Karlsruhe (Germany), 2016.
- [99] Cogswell, F. N. *Thermoplastic aromatic polymer composites: A study of the structure, processing and properties of carbon fibre reinforced*

- polyetheretherketone and related materials*. Butterworth Heinemann. London (UK), 1992.
- [100] Advani, S. G., Hisiao, K. T. *Manufacturing techniques for polymer matrix composites (PMCs)*. Woodhead Publishing. Philadelphia (US), 2012.
- [101] Eastwood, E., Viswanathan, S., O'Brien, C. P., Kumar, D., Dadmun, M. D. Methods to improve the properties of polymer mixtures: optimizing intermolecular interactions and compatibilization. *Polymer* 2005, *46*, 3957-3970.
- [102] Zhu, S., Liu, Y., Rafailovich, M. H., Sokolov, J., Gersappe, D., Winesett, D. A., Ade, H. Confinement-induced miscibility in polymer blends. *Nature* 1999, *400*, 49-51.
- [103] Bai, Z., Guo, H. Interfacial properties and phase transitions in ternary symmetric homopolymer-copolymer blends: A dissipative particle dynamics study. *Polymer* 2013, *54*, 2146-57.
- [104] Mucha, M. Polymer as an important component of blends and composites with liquid crystals. *Prog. Polym. Sci.* 2003, *28*, 837-73.
- [105] Abetz, V. *Block copolymers I*. Springer. Berlin (Germany), 2005.
- [106] Hadjichristidis, N., Pipas, S., Floudas, G. A. *Block copolymers. Synthetic strategies, physical properties and applications*. John Wiley & Sons. Canada (US), 2003.
- [107] Matsen, M. W., Bates, F. S. Unifying weak and strong segregation block copolymer theories. *Macromolecules* 1996, *29*, 1091-1098.
- [108] Botiz, I., Darling, B. Optoelectronics using block copolymers. *Mater. Today* 2010, *13*, 42-51.
- [109] Hu, H., Goponadhant, M., Osuji, C. O. Directed self-assembly of block copolymers: a tutorial review of strategies for enabling nanotechnology with soft matter. *Soft Matter* 2014, *10*, 3867-3889.
- [110] Mai, Y., Eisenberg, A. Self-assembly of block copolymers. *Chem. Soc. Rev.* 2012, *41*, 5969-5985.
- [111] Valenti, B., Turturro, A., Losio, S., Falqui, L., Costa, G., Cavazza, B, Castellano, M. Styrene-diene block copolymers as embedding matrices for polymer-dispersed liquid crystal films. *Polymer* 2001, *42*, 2427-2438.
- [112] Carrasco-Hernandez, S., Gutierrez, J., Tercjak A. Thermal and optical behavior of poly(ethylene-b-ethylene oxide) block copolymer dispersed liquid crystals blends *Eur. Polym. J.* 2016, *74*, 148-157.
- [113] Carrasco-Hernandez, S., Gutierrez, J., Tercjak A. Optical reversible behavior of poly(ethylene-b-ethylene oxide) block copolymer dispersed liquid crystal blends. *Eur. Polym. J.* 2017, *91*, 187-196.
- [114] Carrasco-Hernandez, S., Gutierrez, J., Peponi L., Tercjak A. Optimization of the electrospinning processing-window to fabricate nanostructured PE-b-PEO and hybrid PE-b-PEO/EBBA fibers. *Polym. Eng. Sci.* 2017, *57*, 1157-1167.

Chapter 9

FRONTAL POLYMERIZATION FOR SMART HYDROGELS

Ivan Navarro Baena^{1,}, Valeria Alzari^{2,*}
and Laura Peponi¹*

¹Instituto de Ciencia y Tecnología de Polímeros, ICTP-CSIC, Madrid, Spain

²Department of Chemistry and Pharmacy,
University of Sassari, Vienna, Sassari, Italy

ABSTRACT

A short review on current work in smart hydrogels field has been presented in this chapter, focusing the attention on the different stimuli to be used for activating hydrogels. Special attention was paid on frontal polymerization as suitable synthetic route for smart hydrogels and their nanocomposites. Therefore, after a brief review on frontal polymerization to design smart hydrogels, a case study has been presented based on the use of the frontal polymerization to obtain smart hydrogels nanocomposites of poly(N-vinylcaprolactam) (PVCL) and its nanocomposites. In particular, hydrogels were reinforced with both silver and hydroxyapatite nanoparticles. Because of the unique properties of these nanoparticles, the nanocomposites presented herein can be considered as very interesting materials for biomedical and antibacterial applications.

Keywords: hydrogels, PVCL, frontal polymerization, nanocomposites, silver nanoparticles, hydroxyapatite

* Corresponding Author Email: ivannavarro.baena@gmail.com; valzari@uniss.it.

ABBREVIATIONS

Hydrogels (HG)
poly(vinyl alcohol) (PVA)
poly(N-vinyl-2-pyrrolidone) (PVP)
poly(ethylene glycol) (PEG)
Poly(2-hydroxyethyl methacrylate) (PHEMA)
poly(ethylene oxide) (PEO)
frontal polymerization (FP)
spontaneous polymerization (SP)
front velocity (V_f)
methyl methacrylate (MMA)
interpenetrating polymer networks (IPN)
dicyclopentadiene (DCPD)
Poly(N-vinylcaprolactam) (PVCL)
poly(N-isopropylacrylamide) (PNIPPA_m)
shape change effect (SCE)
shape memory effect (SME)
critical solution temperature (CST)
upper solution critical temperature (UCST)
low solution critical temperature (LCST)
N-isopropylacrylamide (NIPAA_m)
Poly(acrylic acid) (PAAc)
Poly(acryl amide) (PAA_m)
acrylic acid (AAc)
stearyl acrylate (SA)
methyl acrylate (MA)
Tetraethylene glycol diacrylate (TEGDA)
Aliquat persulfate (APS)
scanning electron microscopy (SEM)

HOW SMART ARE THE HYDROGELS?

Hydrogels (HG) are a special class of polymers able to retain high amounts of water, from 10-20% up to thousands of times their weight. Hydrogels are formed by a network of polymer chains crosslinked via chemical or physical bonds, remaining insoluble in aqueous solutions [1]. In general, the hydrogel polymer chains are formed by hydrophilic monomers, capable to absorb great amounts of water and retain it [2].

A unique classification theory for HG does not exist and, depending on their method of preparation, ionic charge or physical structure, they can be differently classified. In particular, based on their *preparation method*, they may be classified as homopolymers, copolymers, multipolymers or interpenetrating polymeric hydrogels, thus depending on how monomeric unit has been used to form the final cross-linked network [2]. At the same time, hydrogels may be classified as neutral, anionic, cationic or, ampholytic thus taking into account their *ionic charges*. Moreover, based on their *physical structural*, they can be classified as amorphous, semicrystalline or formed by hydrogen-bonded or complexation structures.

Furthermore, as we said before, the polymer chains forming the three-dimensional web of the HG can be *chemically or physically crosslinked*, obtaining two different types of gels: the “physical” and the “chemical” gels. In the first case, the network is formed by molecular entanglements, H-bonding or hydrophobic forces. Moreover, due to these kinds of interactions are reversible and can be disrupted by changes under physical conditions such as temperature, pH, ionic strength, application of stress, or addition of specific solutes, physical gels are also named reversible gels [3, 4]. On the contrary, hydrogels are called “permanent” or “chemical” gels when they are covalently-crosslinked networks [5].

Another classification can derive on the nature of the polymer, natural or synthetic, used to obtain the HG [6]. The most used natural polymers for obtaining HG are chitosan, alginate, fibrin, collagen, gelatin, hyaluronic acid or dextran. In this case, the HG can be classified as biocompatible, biodegradable, and can biologically recognizable moieties to be used for the support of cellular activities. However, the main limitation for using natural polymers is the insufficient mechanical properties that they can provide.

Generally, in order to properly study the hydrogels and their properties, special attention must to be paid to parameters such as the polymer volume fraction in the swollen state, the number average molecular weight between crosslinks and the network mesh size. In particular the first parameter indicates the amount of liquid, which can be imbibed in the HG; the second one indicates the degree of crosslinking and the third one is important to determine the physical properties of the hydrogels including mechanical strength, degradability, and diffusivity of the releasing molecule [7, 8]. In the case of HG for biomedical application its typically mesh size in the swollen state range from 5 to 100 nm [9].

HG can be divided into highly swollen hydrogels, including poly(vinyl alcohol) (PVA), poly(N-vinyl-2-pyrrolidone) (PVP) [10], and poly(ethylene glycol) (PEG) [11], among others, but also in moderately and poorly swollen hydrogels which are based on poly(hydroxyethyl methacrylate) (HEMA) and its derivatives. In 1954, Wichterle and Lim introduced cross-linked PHEMA as biological material [12]. Other hydrogels for biomedical applications include polyacrylamides [13], PVA [14] as well as those based on poly(ethylene oxide) (PEO) [15].

The particular physical properties have made hydrogels very attractive for a large variety of biomedical [16] as well as of pharmaceutical applications [17]. Moreover, other applications include the use of HG as food additives [18], as contact lenses [19], for the reconstruction of artificial organs [20] when they show good mechanical response, and even they have been used as tissue engineering scaffolds, biosensor and in drug delivery systems [21].

The concept of “Shape Memory Hydrogels” was introduced for the first time in 1995 by Osada [22]. These gels are those which their swelling properties change with different external stimuli such as temperature or pH changes among others [22-24]. The interest on the smart hydrogels has been strongly increased in the recent years. As shown in Figure 1, the number of publications on “Smart HG” in the last two decades has notably increased.

Hydrogels can show different smart behavior [25-28], defining as a particular response to certain external stimulus such as temperature, pH, ionic strength, etc. (Figure 2). It is possible to make the difference between shape change effect (SCE) and shape memory effect (SME) in hydrogels [29]. In the first one, the material changes its shape when a stimulus is applied, and by removing the stimulus the shape can be recovered. For instance, swelling/deswelling hydrogels, which change its shape due to the variation of external stimulus, are a class of shape change polymers [29].

On the other hand, shape memory materials can be programmed in a desired temporary shape and the recovery is activated by applying a stimulus. The frontier between both effects is so close allowing their combination in order to design materials with unique properties [30].

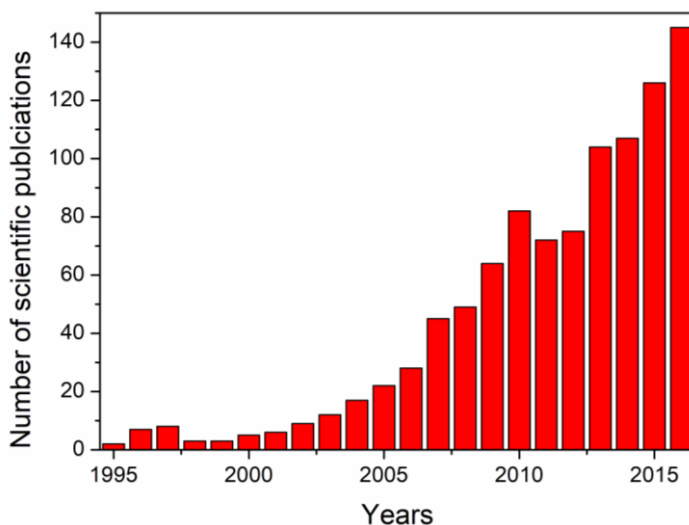


Figure 1. Number of scientific publications in the latest years for the records “Smart hydrogels” (source ISI web of knowledge till 2016).

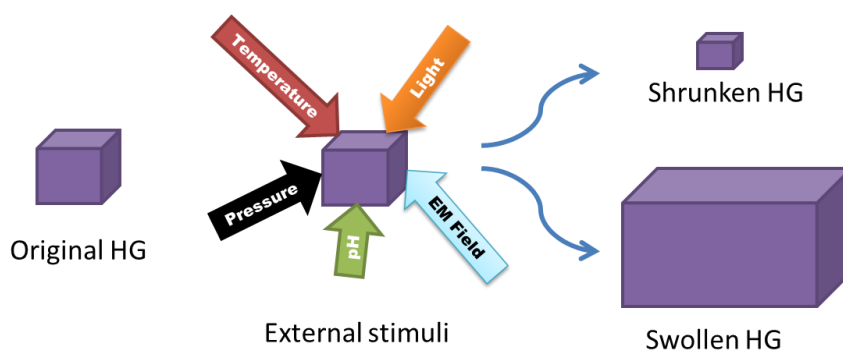


Figure 2. Effects of the external stimuli application on the swelling properties for SCE hydrogels.

Regarding the SCE, the swelling properties are influenced by several factors:

- The degree of crosslinking: the higher is the degree of crosslinking, the lower is the swelling.
- The chemical structure of materials: hydrophilic groups in the molecular chains allow reaching higher swelling level respect to hydrophobic groups.

Temperature is the most widely used stimulus in environmentally responsive polymer systems. The change of temperature is not only relatively easy to control, but also easily applicable both *in vitro* and *in vivo*. For example, temperature-responsive dishes can be utilized as cell sheet manipulation techniques *in vitro* [31-33] and temperature-responsive hydrogels or micelles containing drug can be applied *in vivo* [34-36]. In particular, temperature-sensitive gels have a critical solution temperature (CST). There is a distinction in hydrogels according to their CST: upper solution critical temperature (UCST) and low solution critical temperature (LCST). UCST hydrogels are swollen by the solvent when the temperature is above of USCT and they release the solvent when temperature is below UCST. Whilst LCST hydrogels have an opposite behavior: they are swollen when the temperature is below LCST and they shrink if temperature exceeds LCST.

In particular in this chapter we focus the attention on one of the more innovative technique used to obtain smart hydrogels, that is the frontal polymerization. Moreover, example of different hydrogels obtained by frontal polymerization and also reinforced with different types of nanoparticles has been reported at the end of the chapter.

FRONTAL POLYMERIZATION

In general, chemical reactions can be classified in three main groups depending on the mutual reactivity of their components. Firstly, there are reactions able to happen by

the simple reactant mixing at room temperature or below. Secondly, there are other reactions which happening with a continuous energy providing in heated reactors. Finally, it is possible to find systems that are inert at room temperature but which react fast, and without further energy providing, if ignited (e.g., combustion, explosions). When we work with polymer synthesis the third one it is not so common. A valid alternative solution which is based in this kind of reactions is the photo-polymerization, but this technique is not applicable to all chemical systems and it has several limitations. On the other hand, frontal polymerization (FP) can represent a possible valid alternative technique having practical and economic advantages.

This technique allows the conversion of the monomer into a polymer thanks to the exothermicity of the reaction itself. In this way a reaction front is formed, capable of self-sustaining and propagating within the monomeric mixture.

There are three types of FP:

- 1) Thermal FP, extensively described below.
- 2) Photo Frontal polymerization, where a UV source is used.
- 3) Isothermal Frontal Polymerization, which occurs when the monomer and initiator are dispersed in a preformed polymer, based on the gel effect.

In a thermal FP, a typical glass test tube is filled with the monomeric mixture. A scheme of the typical experimental setup for the frontal polymerization is shown in Figure 3.

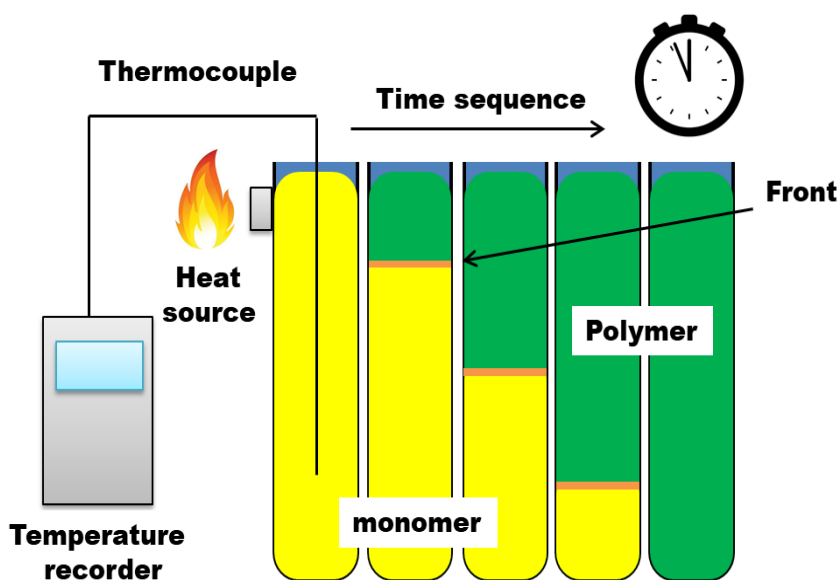


Figure 3. Scheme of the experimental setup for a typical FP.

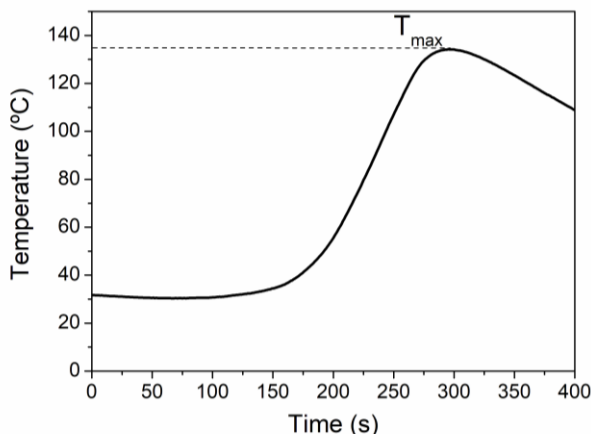


Figure 4. Temperature profile recorded during a typical pure FP experiment.

The reaction is triggered by heating the external wall of the tube to the upper surface of the monomer mixture until the formation of the front becomes evident due to different refractive indexes between the monomer and the polymer. In addition, a thermocouple is immersed in the monomer for measuring the temperature in real time and obtaining the temperature profile.

Two important parameters are taken into account in a thermal FP reaction: T_{\max} (the maximum Temperature of the Front) and V_f (the front velocity): the first is measured through a thermocouple, located at 1 cm from the bottom of the tube; the second is recorded by using a chronometer.

When the FP is the unique mode of polymerization occurring in the reactor at a given time, without spontaneous polymerization (SP), the FP is called *pure*. For this purpose, chemical system has to be almost inert at relatively low temperature and very reactive at the T_{\max} .

A typical temperature profile of a FP experiment is shown in Figure 4. When the initial part of the curve is characterized by slope equal to zero, *pure* FP is occurring. In fact, if no increments of temperature are recorded before the arrival of the front, SP is probably not occurring.

Furthermore, this plot provides other useful information:

- The extent of temperature jump and the value of the maximum reached (T_{\max} , see Figure 4).
- The range interested to heating: it is the monomer zone close to the incoming polymerization front; e.g., its presence can ensure the FP of monomers which are solid at room temperature but that melt immediately before being crossed by the front.

- The “degree of adiabaticity”: the larger the heat loss is, the higher the slope of the curve after T_{\max} is.

T_{\max} is a very important parameter for the final characteristics of the obtained polymer. In fact, it is related to the degrees of conversion and crosslinking, the onset of polymer degradation, bubble formation, etc.

A *pure* FP is often characterized by constant V_f , (Figure 5A). However, such behavior is not always found, because of the bubbles formed during the synthesis which are responsible for a non-constant movement to the front. Furthermore, a linear dependence between front position and time can be found also if SP is simultaneously occurring. So, when other phenomena appear during the FP the time dependence of the front position deviates from linearity, as shown in Figure 5B.

Sometimes, for example if the polymer melts at the T_{\max} , it is responsible for the formation of “fingering”, a phenomenon that is characterized by the dripping of the just formed polymer into the monomeric mixture. This phenomenon can be reduced or prevented by increasing medium viscosity and/or by adding suitable additives within the monomeric mixture [37, 38]. If possible, they should be chosen among those imparting desirable features to the final polymer material [39].

FP presents many advantages, if compared with other traditional polymerization techniques, such as the energy consumption. Thanks to the lack of heat sources, generally requested for carrying out many traditional chemical reactions, FP results a cost-effective technique, reducing the environmental impact and being a “greener” technology. Furthermore, FP is generally, but not exclusively, applicable to solvent-free systems. This technique is relatively simple and fast, monomers can be used as received, without the usual elimination of the dissolved inhibitor, also thanks to the high temperatures typically reached by the fronts. Moreover, by using FP, high conversions of reaction are often found, thus making the final common purification procedures not necessary.

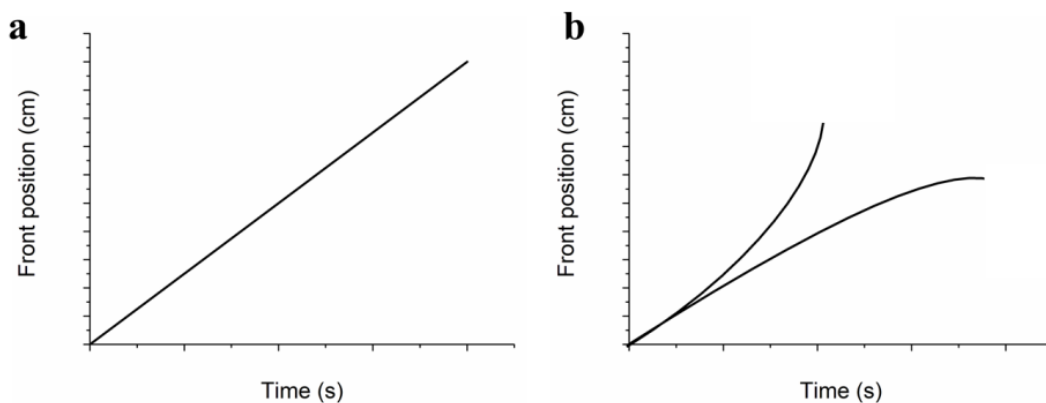


Figure 5. Dependence of front position with the reaction time: A) ideal FP, B) deviation from ideality.

The first studies on FP were performed by Chechilo and Enikolopyan, who applied this technique to methyl methacrylate (MMA) monomer [40, 41]. The reaction was carried out in adiabatic conditions under high pressure (>3000 atm). After this preliminary work, a number of different vinyl monomers were polymerized by FP at ambient pressure [42-44].

The frontal polymerization was effectively used for other systems such as epoxy resins [45, 46] and their interpenetrating polymer networks (IPN) [47]. Morbidelli et al. [48] applied successfully the FP to polymeric blends, discovering that phase separation for poly(methyl methacrylate)/polystyrene blends was reduced by applying FP compared with the blends obtained by mechanical mixing. Analogous results were observed by Pojman et al. [49] in polymer composites. They reported that phase separation was reduced because of the high conversion rate which “freezes” the components in a metastable situation.

Moreover, FP has been successfully applied for the synthesis of copolymers [50]. In fact, the high temperatures reached by the front make both reactivity monomer ratios equal to the unity. As a consequence, all copolymer chains were characterized by the same monomer composition regardless the monomer conversion and avoiding a feed correction during the reaction. Mariani et al. have first polymerized dicyclopentadiene (DCPD) by frontal ring opening metathesis polymerization, extending the applications of FP to other polymeric systems [51]. They also applied FP for the synthesis of DCPD IPNs with acrylates [52], discovering the possibility to take advantage of the heat released by DCPD polymerization to sustain the front of a second monomer (MMA), not able to frontally polymerize alone, thus opening the accessibility of FP to a larger number of polymer systems not considered previously. Washington and Steinbock [53] applied FP for the obtainment of temperature-sensitive hydrogels and Fortenberry and Pojman for the solvent-free synthesis of polyacrylamide [54]. Crivello et al. designed and synthesized glycidyl ethers that undergo frontal polymerization [55] and Chen et al. [56] frontally polymerized PHEMA, and N-methylolacrylamide. Moreover, they studied the development of epoxy resin/polyurethane networks [57] as well as of polyurethane-nanosilica hybrid nanocomposites [58] and PVP [59].

Mariani's group has synthesized several polymers by FP such as polyurethanes [39], different kinds of IPNs [52, 60, 61], unsaturated polyester/styrene resins [62], epoxy resins [63] and poly(diurethanediacylates) [64]. They have also applied FP to the consolidation of porous materials [65] and for the preparation of several hydrogels such as poly(N,N-dimethylacrylamide) [66], stimuli responsive hydrogels based on both poly(N-vinylcaprolactam) (PVCL) and poly(N-isopropylacrylamide) (PNIPPA_m) [67], pH sensitive hydrogels [68] and double responsive (pH and temperature) hydrogels [69]. They have also developed super water absorbent hydrogels of acrylamide and 3-sulfopropyl acrylate [70, 71]. Moreover, Mariani's group has developed some polymer-based nanocomposites reinforced with montmorillonite [72], polyhedral oligomeric

silsesquioxanes [73] and carbon based composites [74], as graphene, to obtain thermosensitives hydrogel nanocomposites based on PNIPPAAm [75] and PVCL [76].

PVCL HYDROGELS OBTAINED BY FRONTAL POLYMERIZATION: A CASE OF STUDY

Poly(N-vinylcaprolactam), PVCL, is formed by a hydrophobic polymer backbone with a cyclic amide attached. The amide group is directly attached to the polymer chain (Figure 6). This is a water soluble polymer which undergoes a thermal induced phase separation when is diluted in water. PVCL is a chemical analogue of PVP, a well-known and widely used pharmaceutical excipient [77, 78]. In particular, PVCL is widely used in hair-care and cosmetic applications [79], and also it has been used in the area of biomedical materials, in stabilization of proteases and in controlled drug delivery and drug release [80-82].

In this chapter, PVCL hydrogels were synthesized by using frontal polymerization.

As it was explained above, the key aspect of this technique is the activation of the polymerization by applying of heat in one point of the sample and its self-propagation until finish the monomer. A front of reaction is formed and propagated, being possible to see with the naked eye the color change from the monomer to polymer. A scheme of the reaction setup was shown in Figure 3.

The polymerization carried out in a test tube of 16 mm diameter where monomer, crosslinker and initiator were mixed. Tetraethylene glycol diacrylate (TEGDA) and Aliquat persulfate (APS) was selected as crosslinker agent and initiator, respectively. The synthesis of the initiator has been done following the previous work of Mariani et al. [83]. The reaction front temperature and the velocity were monitored by measuring the temperature in two different points by using thermocouples.

In order to study the effect of the initiator on the synthesis of PVCL hydrogels, several hydrogels were synthesized using the same amount of crosslinker (1% mol) and varying the amount of initiator.

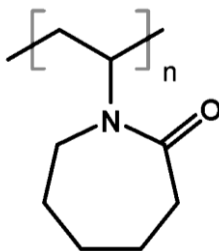


Figure 6. PVCL chemical structure.

Table 1. Hydrogel synthesis parameters

Sample	APS (%mol)	T _{front} (°C)	V _{front} (cm/min)	LCST (°C)
FP01	0.1	105.2	0.4	27
FP02	0.2	122.9	0.5	27,5
FP03	0.3	134.2	0.7	28
FP05	0.5	135.1	0.8	28
CP	0.3	-	-	27

Table 1 summarizes the synthesis parameters, front temperature and velocity, as well as the lower critical solution temperature (LCST) obtained experimentally for samples with different amount of initiator. In order to compare the frontal polymerization obtained gels with those obtained by classical polymerization, a reference PVCL hydrogel was synthesized at 80°C and 12 h reaction. As expected, for the frontal polymerization, the higher is the initiator amount the higher is the front temperature as well as the speed of the front, due to the exothermic character of the reaction.

In particular, PVCL is a LCST hydrogel, thus it shrinks when the higher temperatures and it shows the maximum swelling degree at lower temperatures. This behavior was checked by weighting the hydrogels after being for a certain time at different temperatures. Starting from 22°C the temperature was changed until 44°C, taking data each 2°C. An extra weight at 3°C was done for recording the maximum amount of water of the hydrogels close to water freezing temperature.

Regarding Figure 7, LCST remains unaltered for the different amount of initiator employed. The degree of swelling of the hydrogels is very similar for all the tested temperatures, being different only within the very low temperatures range (near to 0°C). The morphology of the hydrogel cells was observed by scanning electron microscopy (SEM), Figure 8. PVCL hydrogels are formed by nodules of different sizes ranging from 10 micrometers to several hundreds. The nodule shape and sizes of both hydrogels, prepared by frontal and classical polymerization is equivalent, confirming that frontal polymerization is a feasible technique for developing these kinds of hydrogels.

Furthermore, we have prepared nanocomposites using two different fillers: nano-hydroxyapatite particles (nHA) and silver nanoparticles (Ag). Both nanofillers act as reinforcement and can provide new functionalities to the hydrogel matrices. Hydroxyapatite acts as reinforcement and promotes the cell growth. On the other hand, silver nanoparticles have been used for imparting antibacterial properties. The pristine hydrogel synthesized with 0.5% mol of initiator is also displayed as a reference. In Table 2, the synthesis parameters of the composites and the pristine hydrogels are shown.

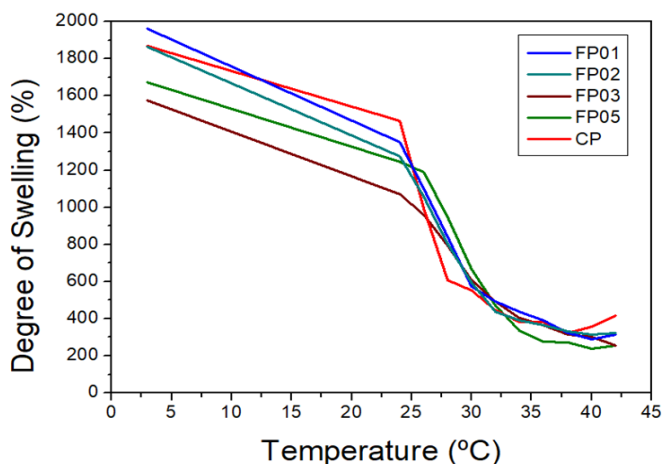


Figure 7. Dependence of the swelling degree with the temperature.

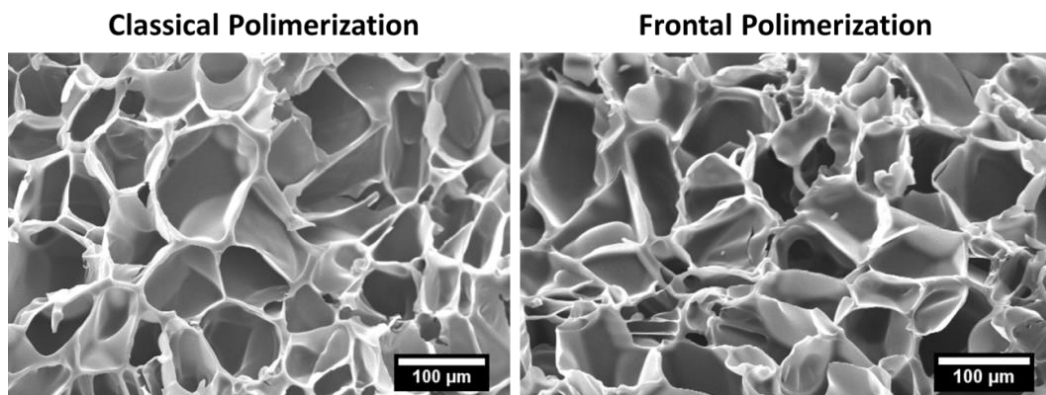


Figure 8. SEM images corresponding to a PVCL hydrogel synthesized by classical polymerization (left) and by frontal polymerization (right).

The synthesis parameters do not change significantly when nHA is added. On the other hand, when silver nanoparticles are used the temperature of the front decreases 16°C. So, silver nanoparticles absorb part of the reaction heat, decreasing the front temperature, while the nHA nanoparticles do not absorb any heat. However, the reaction is complete even in the presence of silver nanoparticles.

Table 2. Synthesis parameters of the nanocomposites

Sample	APS (%mol)	Np (wt %)	T_{front} (°C)	V_{front} (cm/min)	LCST (°C)
FP05	0.5	-	135.1	0.8	28
FP05HA	0.5	1	134	0.9	28
FP05AG	0.5	1	118	0.8	28

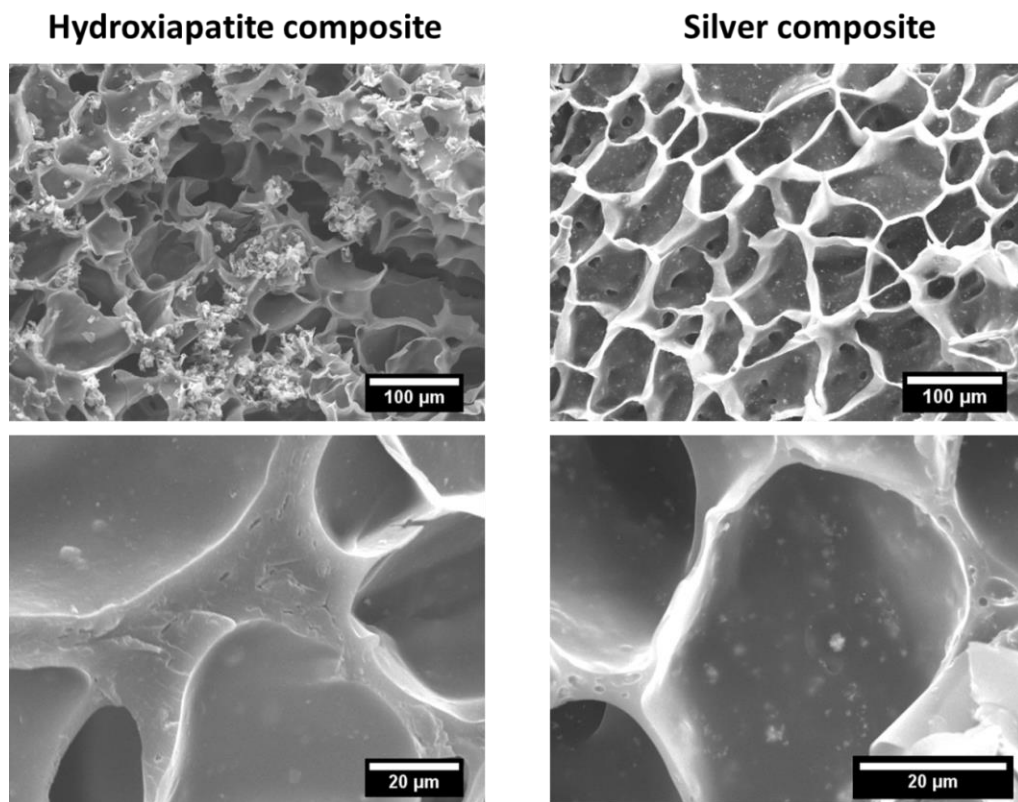


Figure 9. Nanocomposites based on PCL hydrogel matrix reinforced with nano-hydroxyapatite and silver nanoparticles.

SEM characterization was performed in order to study the nanoparticles distribution, Figure 9. In both cases, PVCL hydrogels with cellular structure were developed. In addition, the cells are quite similar to the cells of the pristine hydrogels, showing sizes ranging from 10 micrometers to several hundreds. However, the nanoparticle distribution was better for the silver nanoparticles nanocomposites. Despite the nHa composite shows nanoparticles were embedded within the polymer matrix, there are large aggregates outside, indicating that the integration was not very good. More efforts have to be done in order to remove these aggregates and promote the interaction between PVCL and nHa. On the contrary, silver nanocomposite presents the nanoparticles correctly embedded.

Regarding the swelling behavior of the nanocomposites presented in Figure 10, the LCST behavior is also displayed with the nanoparticles addition and no further changes were detected. It is worth to note that the maximum swelling was for the nanocomposite with the nHa and the lowest for the silver nanoparticles. It seems to be related with the large presence of nHA aggregates which are hydrophilic, and aid to retain more water to the hydrogel.

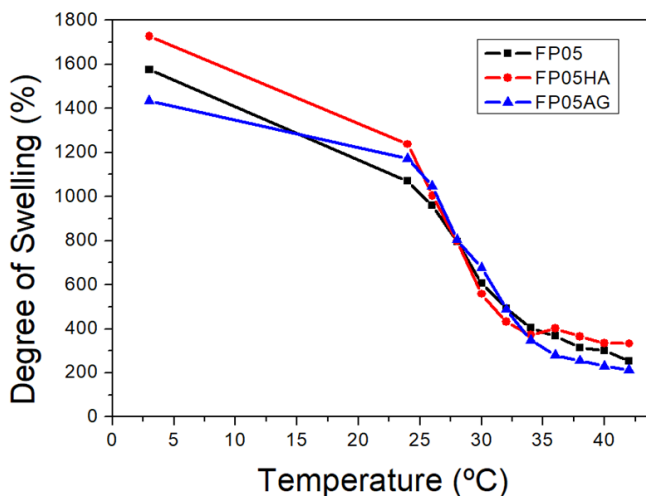


Figure 10. Swelling behavior in the LSCT region for both nanocomposites and the pristine hydrogel prepared by FP.

The correct integration of the silver nanoparticles within the PVCL hydrogels by frontal polymerization motivated the addition of different amounts of nanoparticles in these hydrogel nanocomposites. In particular, five different concentrations were studied.

All the HG nanocomposites were correctly synthesized by FP.

As we mentioned before, silver nanoparticles decreased the maximum temperature reached during the reaction. Moreover, the front rate is also affected by the presence of Ag nanoparticles. In fact, the frontal rate decreases when the amount of nanoparticles increases. Only the nanocomposite with the lowest concentration of nanoparticles presents similar values to the pristine hydrogel.

The morphology of all the nanocomposites was investigated by SEM (Figure 11). All the nanocomposites present the cellular structure of the PVCL hydrogel, and this structure is quite similar to the pristine PVCL hydrogels. In all cases it is possible to detect well dispersed Ag nanoparticles within the polymeric matrix even if high amounts of nanoparticles are added.

In Table 3 the synthesis parameters of the synthesized nanocomposites are presented.

Table 3. HG-Ag nanocomposites: Synthesis parameters

Sample	APS (% mol)	%Ag	T _{max}	V _f (cm/min)
FP05AG01	0.3	0.1	130	0.8
FP05AG03	0.3	0.3	117	0.75
FP05AG1	0.3	1	116	0.73
FP05AG3	0.3	3	115	0.7
FP05AG5	0.3	5	114	0.71
FP05	0.3	0	130	0.8

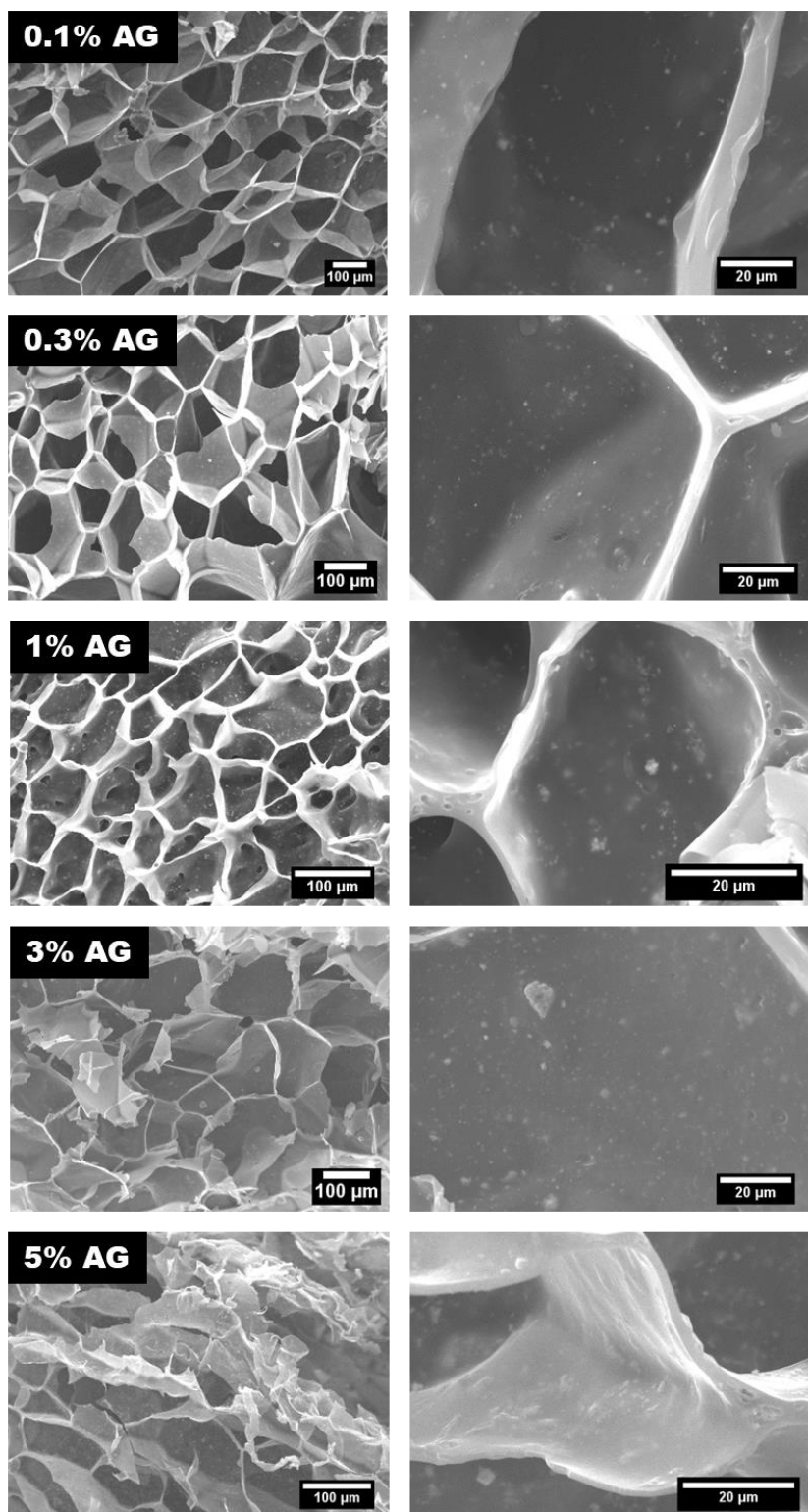


Figure 11. SEM images of the hydrogel nanocomposites with different amounts of silver nanoparticles.

CONCLUSION

In this chapter, we have reviewed the current work in smart hydrogels field. The different stimuli which can be used for activating the hydrogels have been pointed out. In addition, we have presented frontal polymerization as a way for synthesizing and designing smart hydrogels as well as their nanocomposites. In particular, frontal polymerization represents a self-sustaining reaction, and it can be considered an energy-saving way for producing polymer materials, with the additional advantage of short reaction times. Finally, to confirm the potential of FP on the synthesis of smart hydrogels nanocomposites, a study on smart hydrogels based on PVCL and its nanocomposites obtained by adding both Ag and hydroxyapatite nanoparticles has been presented. The characteristic cellular structure of PVCL hydrogels was not modified by using frontal polymerization respect to a classical polymerization, nor because of the presence of the nanoparticles. All the synthesized hydrogels present the thermal-driven smart behavior, with an LCST transition around 28°C. The Ag nanoparticles were well embedded within the polymer walls of the cell even at higher concentration. These preliminary studies demonstrate the potential of the frontal polymerization to prepare hydrogels nanocomposites in very short time and saving energy if compared with the classical methods. Furthermore, the nanocomposites presented here can be considered as very interesting materials for biomedical and antibacterial applications.

ACKNOWLEDGMENTS

Authors thank Spanish Ministry of Economy, Industry and Competitiveness, MINEICO (MAT2017-88123-P) and Regional Government of Madrid (MULTIMAT-CHALLENGE S2013/MIT-2862). LP acknowledges also MINECO for the “Ramon y Cajal” (RYC-2014-15595) contract.

REFERENCES

- [1] Lin, C.-C. and Metters A.T., Hydrogels in controlled release formulations: network design and mathematical modeling. *Advanced drug delivery reviews*, 2006. 58(12): p. 1379-1408.
- [2] Ahn, S.-k., et al., Stimuli-responsive polymer gels. *Soft matter*, 2008. 4(6): p. 1151-1157.
- [3] Campoccia, D., et al., Semisynthetic resorbable materials from hyaluronan esterification. *Biomaterials*, 1998. 19(23): p. 2101-2127.

- [4] Prestwich, G.D., et al., Controlled chemical modification of hyaluronic acid: synthesis, applications, and biodegradation of hydrazide derivatives. *Journal of Controlled Release*, 1998. 53(1): p. 93-103.
- [5] Drumheller, P.D. and Hubbell J.A., Densely crosslinked polymer networks of poly (ethylene glycol) in trimethylolpropane triacrylate for cell-adhesion-resistant surfaces. *Journal of Biomedical Materials Research Part A*, 1995. 29(2): p. 207-215.
- [6] Davis, K.A. and Anseth K.S., Controlled release from crosslinked degradable networks. *Critical Reviews™ in Therapeutic Drug Carrier Systems*, 2002. 19(4-5).
- [7] Mason, M.N., et al., Predicting controlled-release behavior of degradable PLA-b-PEG-b-PLA hydrogels. *Macromolecules*, 2001. 34(13): p. 4630-4635.
- [8] Amsden, B., Solute diffusion within hydrogels. Mechanisms and models. *Macromolecules*, 1998. 31(23): p. 8382-8395.
- [9] Cruise, G.M., D.S. Scharp, and J.A. Hubbell, Characterization of permeability and network structure of interfacially photopolymerized poly (ethylene glycol) diacrylate hydrogels. *Biomaterials*, 1998. 19(14): p. 1287-1294.
- [10] Fang, Y., et al., Facile glycerol-assisted synthesis of N-vinyl pyrrolidinone-based thermosensitive hydrogels via frontal polymerization. *Chemistry of Materials*, 2009. 21(19): p. 4711-4718.
- [11] Turturro, M.V., et al., Kinetic Investigation of Poly (ethylene glycol) Hydrogel Formation via Perfusion-Based Frontal Photopolymerization: Influence of Free-Radical Polymerization Conditions on Frontal Velocity and Swelling Gradients. *Macromolecular Reaction Engineering*, 2013. 7(2): p. 107-115.
- [12] Wichterle, O. and LÍM D., Hydrophilic Gels for Biological Use. *Nature*, 1960. 185: p. 117.
- [13] Tanaka, T., Collapse of gels and the critical endpoint. *Physical Review Letters*, 1978. 40(12): p. 820.
- [14] Alves, M.-H., et al., Poly(Vinyl Alcohol) Physical Hydrogels: New Vista on a Long Serving Biomaterial. *Macromolecular Bioscience*, 2011. 11(10): p. 1293-1313.
- [15] Hoffman, A.S., Hydrogels for biomedical applications. *Advanced Drug Delivery Reviews*, 2012. 64(Supplement): p. 18-23.
- [16] Corkhill, P.H., Hamilton C.J., and Tighe B.J., Synthetic hydrogels VI. Hydrogel composites as wound dressings and implant materials. *Biomaterials*, 1989. 10(1): p. 3-10.
- [17] Kashyap, N., Kumar N., and Kumar M.R., Hydrogels for pharmaceutical and biomedical applications. *Critical Reviews™ in Therapeutic Drug Carrier Systems*, 2005. 22(2).
- [18] Chen, X., et al., Enzymatic and chemoenzymatic approaches to synthesis of sugar-based polymer and hydrogels. *Carbohydrate Polymers*, 1995. 28(1): p. 15-21.

- [19] Ostrovidova, Makeev G., A., and Shamtsian M., Polyfunctional film coatings for medical use. *Materials Science and Engineering: C*, 2003. 23(4): p. 545-550.
- [20] Byrne, M.E., Park K., and Peppas N.A., Molecular imprinting within hydrogels. *Advanced drug delivery reviews*, 2002. 54(1): p. 149-161.
- [21] Razzak, M.T. and Darwis D., Irradiation of polyvinyl alcohol and polyvinyl pyrrolidone blended hydrogel for wound dressing. *Radiation Physics and Chemistry*, 2001. 62(1): p. 107-113.
- [22] Osada, Y. and Matsuda A., Shape memory in hydrogels. *Nature*, 1995. 376(6537): p. 219-219.
- [23] Lundberg, P., et al., pH-triggered self-assembly of biocompatible histamine-functionalized triblock copolymers. *Soft matter*, 2013. 9(1): p. 82-89.
- [24] Han, X.-J., et al., pH-Induced Shape-Memory Polymers. *Macromolecular Rapid Communications*, 2012. 33(12): p. 1055-1060.
- [25] Jeong, B. and Gutowska A., Lessons from nature: stimuli-responsive polymers and their biomedical applications. *Trends in biotechnology*, 2002. 20(7): p. 305-311.
- [26] Kikuchi, A. and Okano T., Intelligent thermoresponsive polymeric stationary phases for aqueous chromatography of biological compounds. *Progress in Polymer Science*, 2002. 27(6): p. 1165-1193.
- [27] Hoffman, A.S., et al., Really smart bioconjugates of smart polymers and receptor proteins. *Journal of Biomedical Materials Research Part A*, 2000. 52(4): p. 577-586.
- [28] Qiu, Y. and Park K., Environment-sensitive hydrogels for drug delivery. *Advanced drug delivery reviews*, 2001. 53(3): p. 321-339.
- [29] Zhao, Q., Qi H.J., and Xie T., Recent progress in shape memory polymer: New behavior, enabling materials, and mechanistic understanding. *Progress in Polymer Science*, 2015. 49-50: p. 79-120.
- [30] Zhang, J.L., et al., Thermo-/chemo-responsive shape memory/change effect in a hydrogel and its composites. *Materials & Design*, 2014. 53: p. 1077-1088.
- [31] Ebara, M., et al., Copolymerization of 2-carboxyisopropylacrylamide with N-isopropylacrylamide accelerates cell detachment from grafted surfaces by reducing temperature. *Biomacromolecules*, 2003. 4(2): p. 344-349.
- [32] Nakajima, K., et al., Intact microglia are cultured and non-invasively harvested without pathological activation using a novel cultured cell recovery method. *Biomaterials*, 2001. 22(11): p. 1213-1223.
- [33] Yamato, M., et al., Release of adsorbed fibronectin from temperature-responsive culture surfaces requires cellular activity. *Biomaterials*, 2000. 21(10): p. 981-986.
- [34] Chilkoti, A., et al., Targeted drug delivery by thermally responsive polymers. *Advanced drug delivery reviews*, 2002. 54(5): p. 613-630.

- [35] Weidner, J., Drug delivery and drug targeting: Drug targeting using thermally responsive polymers and local hyperthermia. *Drug Discovery Today*, 2001. 6(23): p. 1239-1241.
- [36] Jeong, B., et al., % Thermogelling Biodegradable Copolymer Aqueous Solutions for Injectable Protein Delivery and Tissue Engineering. *Biomacromolecules*, 2002. 3(4): p. 865-868.
- [37] Khan, A.M. and Pojman J.A., The use of frontal polymerization in polymer synthesis. *Trends in Polymer Science*, 1996. 8(4): p. 253-257.
- [38] Pojman, J.A., Ilyashenko V.M., and Khan A.M., Free-radical frontal polymerization: self-propagating thermal reaction waves. *Journal of the Chemical Society, Faraday Transactions*, 1996. 92(16): p. 2825-2837.
- [39] Fiori, S., et al., First Synthesis of a Polyurethane by Frontal Polymerization. *Macromolecules*, 2003. 36(8): p. 2674-2679.
- [40] Chechilo, N. and Enikolopyan N., Effect of the concentration and nature of the initiators on the propagation process in polymerization. in *Dokl. Phys. Chem.* 1975.
- [41] Chechilo, N. and Enikolopyan N., Effect of pressure and initial temperature of the reaction mixture during propagation of a polymerization reaction. in *Dokl. Phys. Chem.* 1976.
- [42] Pojman, J.A., Traveling fronts of methacrylic acid polymerization. *Journal of the American Chemical Society*, 1991. 113(16): p. 6284-6286.
- [43] Pojman, J.A., et al., Convective instabilities in traveling fronts of addition polymerization. *The Journal of Physical Chemistry*, 1992. 96(18): p. 7466-7472.
- [44] Pojman, J.A., Nagy I.P., and Salter C., Traveling fronts of addition polymerization with a solid monomer. *Journal of the American Chemical Society*, 1993. 115(23): p. 11044-11045.
- [45] Chekanov, Y., et al., Frontal curing of epoxy resins: comparison of mechanical and thermal properties to batch-cured materials. *Journal of applied polymer science*, 1997. 66(6): p. 1209-1216.
- [46] Kim, C., et al., The continuous curing process for thermoset polymer composites. part 1: Modeling and demonstration. *Journal of Composite Materials*, 1995. 29(9): p. 1222-1253.
- [47] Pojman, J., et al., Binary Frontal Polymerization-A New Method to Produce Simultaneous Interpenetrating Polymer Networks (Sins). *Journal of Polymer Science Part A: Polymer Chemistry*, 1997. 35(2): p. 227-230.
- [48] Tredici, A., et al., Polymer blends by self-propagating frontal polymerization. *Journal of applied polymer science*, 1998. 70(13): p. 2695-2702.
- [49] Nagy, I.P., Sike L., and Pojman J.A., Thermo-chromic composite prepared via a propagating polymerization front. *Journal of the American Chemical Society*, 1995. 117(12): p. 3611-3612.

- [50] Tredici, A., Pecchini R., and Morbidelli M., Self-propagating frontal copolymerization: *J Polym. Chem Sci., Part A*. 1998, 36, p. 1117–1126,.
- [51] Mariani, A., et al., Frontal ring-opening metathesis polymerization of dicyclopentadiene. *Macromolecules*, 2001. 34(19): p. 6539-6541.
- [52] Fiori, S., et al., Interpenetrating polydicyclopentadiene/polyacrylate networks obtained by simultaneous non-interfering frontal polymerization. *e-Polymers*, 2002. 2(1): p. 404-413.
- [53] Washington, R.P. and Steinbock O., Frontal polymerization synthesis of temperature-sensitive hydrogels. *Journal of the American Chemical Society*, 2001. 123(32): p. 7933-7934.
- [54] Fortenberry, D.I. and Pojman J.A., Solvent-free synthesis of polyacrylamide by frontal polymerization. *Journal of Polymer Science Part A: Polymer Chemistry*, 2000. 38(7): p. 1129-1135.
- [55] Crivello, J.V., Design and synthesis of multifunctional glycidyl ethers that undergo frontal polymerization. *Journal of Polymer Science Part A: Polymer Chemistry*, 2006. 44(21): p. 6435-6448.
- [56] Chen, L., et al., First solvent-free synthesis of poly (N-methylolacrylamide) via frontal free-radical polymerization. *Journal of Polymer Science Part A: Polymer Chemistry*, 2007. 45(18): p. 4322-4330.
- [57] Chen, S., et al., Epoxy resin/polyurethane hybrid networks synthesized by frontal polymerization. *Chemistry of materials*, 2006. 18(8): p. 2159-2163.
- [58] Chen, S., et al., Polyurethane–nanosilica hybrid nanocomposites synthesized by frontal polymerization. *Journal of Polymer Science Part A: Polymer Chemistry*, 2005. 43(8): p. 1670-1680.
- [59] Cai, X., S. Chen, and Chen L., Solvent-free free-radical frontal polymerization: A new approach to quickly synthesize poly (N-vinylpyrrolidone). *Journal of Polymer Science Part A: Polymer Chemistry*, 2008. 46(6): p. 2177-2185.
- [60] Illescas, J., et al., Organic–inorganic interpenetrating polymer networks and hybrid polymer materials prepared by frontal polymerization. *Journal of Polymer Science Part A: Polymer Chemistry*, 2013. 51(21): p. 4618-4625.
- [61] Rasso, M., et al., Semi-interpenetrating polymer networks of methyl cellulose and polyacrylamide prepared by frontal polymerization. *Journal of Polymer Science Part A: Polymer Chemistry*, 2017. 55(7): p. 1268-1274.
- [62] Fiori, S., et al., Synthesis and characterization of a polyester/styrene resin obtained by frontal polymerization. *e-Polymers*, 2002. 2(1): p. 769-778.
- [63] Scognamillo, S., et al., Hybrid organic/inorganic epoxy resins prepared by frontal polymerization. *Journal of Polymer Science Part A: Polymer Chemistry*, 2010. 48(21): p. 4721-4725.
- [64] Mariani, A., et al., Frontal polymerization of diurethane diacrylates. *Journal of Polymer Science Part A: Polymer Chemistry*, 2008. 46(10): p. 3344-3352.

- [65] Mariani, A., et al., Frontal polymerization as a convenient technique for the consolidation of tuff. *e-Polymers*, 2009. 9(1): p. 791-802.
- [66] Caria, G., et al., Poly (N, N-dimethylacrylamide) hydrogels obtained by frontal polymerization. *Journal of Polymer Science Part A: Polymer Chemistry*, 2009. 47(5): p. 1422-1428.
- [67] Alzari, V., et al., Stimuli responsive hydrogels prepared by frontal polymerization. *Biomacromolecules*, 2009. 10(9): p. 2672-2677.
- [68] Sanna, R., et al., Polymer hydrogels of 2-hydroxyethyl acrylate and acrylic acid obtained by frontal polymerization. *Journal of Polymer Science Part A: Polymer Chemistry*, 2012. 50(8): p. 1515-1520.
- [69] Nuvoli, L., et al., Double responsive copolymer hydrogels prepared by frontal polymerization. *Journal of Polymer Science Part A: Polymer Chemistry*, 2016. 54(14): p. 2166-2170.
- [70] Scognamillo, S., et al., Thermoresponsive super water absorbent hydrogels prepared by frontal polymerization. *Journal of Polymer Science Part A: Polymer Chemistry*, 2010. 48(11): p. 2486-2490.
- [71] Scognamillo, S., et al., Thermoresponsive super water absorbent hydrogels prepared by frontal polymerization of N-isopropyl acrylamide and 3-sulfopropyl acrylate potassium salt. *Journal of Polymer Science Part A: Polymer Chemistry*, 2011. 49(5): p. 1228-1234.
- [72] Mariani, A., et al., Synthesis and characterization of epoxy resin-montmorillonite nanocomposites obtained by frontal polymerization. *Journal of Polymer Science Part A: Polymer Chemistry*, 2007. 45(11): p. 2204-2211.
- [73] Mariani, A., et al., Polymeric nanocomposites containing polyhedral oligomeric silsesquioxanes prepared via frontal polymerization. *Journal of Polymer Science Part A: Polymer Chemistry*, 2007. 45(19): p. 4514-4521.
- [74] Alzari, V., et al., Stimuli-responsive polymer hydrogels containing partially exfoliated graphite. *Journal of Polymer Science Part A: Polymer Chemistry*, 2010. 48(23): p. 5375-5381.
- [75] Alzari, V., et al., Graphene-containing thermoresponsive nanocomposite hydrogels of poly (N-isopropylacrylamide) prepared by frontal polymerization. *Journal of Materials Chemistry*, 2011. 21(24): p. 8727-8733.
- [76] Sanna, R., et al., Synthesis and characterization of graphene-containing thermoresponsive nanocomposite hydrogels of poly (N-vinylcaprolactam) prepared by frontal polymerization. *Journal of Polymer Science Part A: Polymer Chemistry*, 2012. 50(19): p. 4110-4118.
- [77] Botzolakakis, J., Small L., and Augsburg L., Effect of disintegrants on drug dissolution from capsules filled on a dosator-type automatic capsule-filling machine. *International Journal of Pharmaceutics*, 1982. 12(4): p. 341-349.

- [78] Wan, L.S., Heng P.W., and Ling B., Effect of polyvinylpyrrolidone solutions containing dissolved drug on characteristics of lactose fluidized bed granules. *International Journal of Pharmaceutics*, 1996. 141(1-2): p. 161-170.
- [79] Sanna, R., et al., Poly (N-vinylcaprolactam) nanocomposites containing nanocrystalline cellulose: a green approach to thermoresponsive hydrogels. *Cellulose*, 2013. 20(5): p. 2393-2402.
- [80] Peng, S. and Wu C. *Poly (N-vinylcaprolactam) microgels and its related composites. in Macromolecular Symposia*. 2000. Wiley Online Library.
- [81] Markvicheva, E., et al., Stabilization of proteases by entrapment in a new composite hydrogel. *Applied biochemistry and biotechnology*, 1996. 61(1): p. 75-84.
- [82] Vihola, H., et al., Binding and release of drugs into and from thermosensitive poly (N-vinyl caprolactam) nanoparticles. *European Journal of Pharmaceutical Sciences*, 2002. 16(1): p. 69-74.
- [83] Mariani, A., et al., Phosphonium-based ionic liquids as a new class of radical initiators and their use in gas-free frontal polymerization. *Macromolecules*, 2008. 41(14): p. 5191-5196.

Chapter 10

TUNING POLYMER THERMOSENSITIVITY IN AQUEOUS MEDIA FOR BIOMEDICAL APPLICATIONS

M. Eugenia Pérez-Ojeda^{1,2,}, Enrique Martínez-Campos^{3,†},
Carlos Elvira^{1,‡} and Alberto Gallardo^{1,§}*

¹Institute of Polymer Science and Technology ICTP-CSIC, Madrid, Spain

²Department of Chemistry and Pharmacy,
Friedrich-Alexander-Universität Erlangen-Nürnberg, Erlangen, Germany

³Tissue Engineering Group; Instituto de Estudios Biofuncionales,
Complutense University of Madrid, Madrid, Spain

ABSTRACT

Thermoresponsive polymers have been thoroughly investigated for biomedical uses in many areas; from theragnostics, drug and gene delivery to cell harvesting and tissue engineering. The use of biocompatible smart polymers requires precisely tuning the structure, composition (hydrophobic/hydrophilic balance), polymer length, molecular weight, lateral chains, etc. in order to achieve physical changes in aqueous media at physiological temperature. This chapter intends to describe these issues and how the alteration of the chemical structure of the repetition unit within the backbone, the polymerization degree or end-functionalization, affect the thermal, mechanical and degradation properties of the resulting (co)polymers upon the final application.

Keywords: hydrogels, thermo-responsive, biomedical applications, PNIPAm, polyethers, poly-oxazolines

* Corresponding Author E-mail: eugenia.perez-ojeda@fau.de.

† Email: emartinezcampos79@gmail.com.

‡ Email: celvira@ictp.csic.es.

§ E-mail: gallardo@ictp.csic.es.

ABBREVIATIONS

PLGA	D-L-lactic acid co-glycolic acid
PHB	(R)-3-hydroxybutyrate
EtOx	2-ethyl-2-oxazoline
iPrOx	2-isopropyl-2-oxazoline
AAm	acrylamide
A	acrylate
RGD	arginylglycylaspartic acid
ATRP	atom transfer radical polymerization
CMT	critical micellization temperature
DMAA	dimethylacrylamide
GT	gelation temperature
HPMA	hydroxypropylacrylamide
HEMA	hydroxyethyl methacrylate
LCST	lower critical solution temperature
MA	methacrylate
NtBA	N-tertbutylacrylamide
OEGMA	oligo(ethylene glycol) methacrylate
OEG	oligoethylene glycol
CPropOX	poly (2-cyclopropyl-2-oxazoline)
POXs	poly (2-oxazolines)
PLA	poly L-lactic acid
PP	poly propylene
PCL	poly(ϵ -caprolactone)
PEG	poly(ethylene glycol)
PEA	poly(ethylene adipate)
PEO	poly(ethylene oxide)
PESc	poly(ethylene succinate)
PHA	poly(hexamethylene adipate)
PPF	poly(propylene fumarate)
PPO	poly(propylene oxide)
PCLA	poly(ϵ -caprolactone-co-lactide)
DP	polymerization degree
pNIPAm	poly-N-isopropylacrylamide
PVP	poly-vinylpyrrolidone
USCT	upper critical solution temperature
VPTT	volume phase transition temperature

1. INTRODUCTION TO THERMORESPONSIVE POLYMERS

Certain polymers exhibit thermosensitivity in solution, which is related to an alteration of the balance of polymer-polymer vs. polymer-solvent interactions. Focusing on aqueous media, where this phenomenon may have biomedical significance, there are several polymers showing a lower critical solution temperature, LCST, below which the hydrophilic polymer-water interactions are favored and linear chains are soluble. Above that transition temperature, hydrophobic polymer-polymer interactions are favored and a phase separation or even a precipitation takes place: a phase rich in polymer is formed (Figure 1, A). Clouding occurs as a result of this phase separation, which is why the LCST temperature is often referred to as a cloud point (T_{cp}). A recent review discusses key aspects concerning a correct LCST determination and the most appropriate techniques to do that [1]. An inverse behavior to the LCST phenomenon is also possible. The transition temperature in such case is called Upper Critical Solution Temperature (UCST) (Figure 1, B). However, there are few examples of UCST polymers in water [2].

Natural polymers like polysaccharide derivatives from cellulose, chitosan, gelatin and collagen have often been used as thermoresponsive systems for biomedical applications. However, it is necessary to modify them chemically or to use them in combination with other polymers to be able to control their thermal response and adjust it to that required by the application. Some synthetic polymers such as pNIPAm, polyethers, polyoxazolines, among others, have also been widely applied for the same purpose. This chapter is dedicated to describe how the thermosensitivity of representative synthetic polymers with LCST may be finely tuned by different structural changes. Tuning a LCST in the vicinity of the physiological temperature may be very relevant for some biomedical applications.

Thermoresponsive polymers have been used as carriers for controlled drug release or gene therapy making use of this feature. In addition, many examples have been provided where these smart biomaterials are acting as cell harvesting platforms or other tissue engineering constructs.

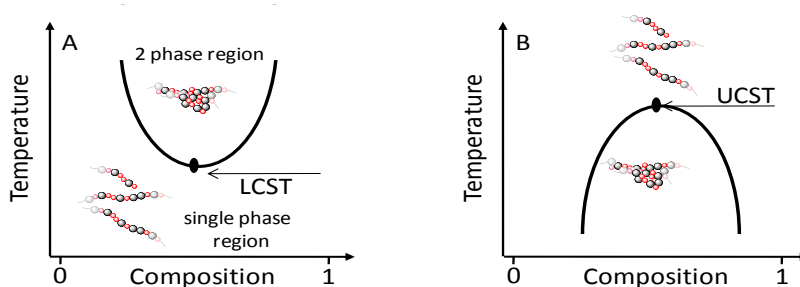


Figure 1. Phase transitions associated with the LCST (A) and UCST (B) behaviors.

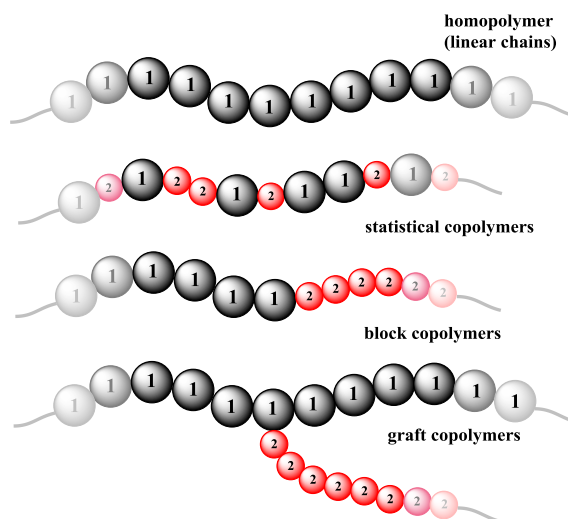


Figure 2. Structural variations in copolymers.

Some of the aspects of polymer thermosensitivity in aqueous media, such as the LCST value, or the extent of the sensitivity, may be modulated by different structural alterations, which can be categorized in different levels. In a prime level, thermosensitivity depends ultimately on the nature of the repetitive unit. In this review some examples of LCST modulation by varying the structural hydrophilic/hydrophobic balance of the repetitive unit and the side chains can be found.

In a second level, polymer chain characteristics may be modulated by copolymerization. If, for example, thermosensitivity is provided by a given unit (i.e., 1), there are several structural possibilities of incorporating additional monomer (i.e., 2 in the case of a binary system), as it is indicated in Figure 2. Statistical copolymers are obtained by the simultaneous polymerization of the two monomeric precursors [3]. Both monomers are incorporated to the growing chains according to the reactivities of the different species (monomers and growing active centers), which finally leads to a unit distribution along the chains that follow a given statistical law. Other structures such as block or graft copolymers cannot be obtained by the simultaneous polymerization of the precursors. Usual procedures for preparing block and graft copolymers are respectively controlled polymerization with sequential addition of the monomers [4] and the use of macromers [5]. In block and graft structures there is no intercalation of other units within the thermosensitive segments. This means that the influence of additional monomers on the LCST value is smaller than in the case of statistical copolymers. Actually these structures have been proposed to modulate other aspects such as the colloidal stability or the gellable nature.

Many thermosensitive systems are based on crosslinked structures, that is, on hydrogels [6]. Hydrogels are polymer networks able to absorb water. Hydrogels are categorized in chemical or physical depending on the type of bonds, covalent and non-

covalent respectively, which compose the crosslinked network. Physical bonds are reversible while chemical crosslinkings are not. In the context of stimuli sensitive materials, this difference is very important since thermosensitivity has been used in physical hydrogels to prepare gellable and injectable materials upon change of temperature. For gellable materials, a gelation temperature, GT, may be defined.

Chemical hydrogels, however, are permanent networks that respond to temperature modifications by change in water uptake and volume. For these chemical networks, the transition temperature is actually called volume phase transition temperature, VPPT, instead of LCST.

2. PNIPAM

2.1. PNIPAm Structure and Biological Applications

Temperature is the most widely used stimulus in environmentally responsive polymer systems. This feature is easy to control and apply in cell cultures or in *in vivo* therapies [7]. In this field, Poly-N-isopropylacrylamide, pNIPAm (Figure 3) and its copolymers with other synthetic or natural structures are the most investigated thermoresponsive systems from the biological point of view [8]. To take advantage of the pNIPAm LCST, near the body temperature, different approaches have been applied to modulate relevant processes [9] especially in drug and gene delivery. In addition, pNIPAm promoted different tailored architectures, such as hydrogels, micelles, films or particles [10] for biological uses.

Cytotoxicity is the first issue to address in order to propose clinical applications in the biomedical field. In this sense, the cytotoxic effect differs between the monomeric and the polymeric form of these systems. Whereas NIPAm monomer is toxic, pNIPAm is widely considered biocompatible, and a research field arises focused on this polymeric family. So far, deep *in vitro* and *in vivo* evaluations with implications in clinical therapies [9] have been accomplished.

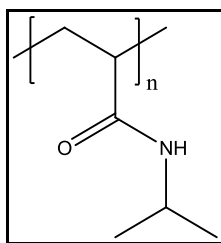


Figure 3. PNIPAm structure.

Thermoresponsive models based on pNIPAm include polymeric micelles, nanoparticles or other carriers to control drug and gene delivery. Since then, a wide range of pNIPAm applications to modulate heating-activated drug release [11] organism-localized delivery [12] or transfection events have been described [13].

Nevertheless, pNIPAm is better known in the field of tissue engineering where it plays a crucial role in the surface design of cell support platforms. Surface chemical composition can also affect cellular processes such as adhesion, proliferation or detachment. In 1990, the Okano group was pioneer in the use of pNIPAm in cell-sheet manipulation techniques, [14] achieving a complete cell sheet detachment from a pNIPAm support just by decreasing the temperature below LCST, [7a] and thus avoiding the use of proteolytic enzymes or physical scrapping. This non-invasive cell harvesting allows conserving the extracellular matrix, cellular and molecular interactions and internal tissue organization [15]. In fact, it has been demonstrated that it also accelerates the subsequent adhesion of the transplant [16]. Cell sheet technology has successfully been applied in soft tissue regeneration. Specialized endothelia and epithelia have been harvested for cornea, skin, oesophagus or blood vessel transplantation [17]. Moreover, cell sheets of myocytes or hepatocytes can help to recover damaged hearts and livers [18]. Other examples on the use of pNIPAm technology are found in harder tissues, such as cartilage or bone [19]. In addition, the possibility of enhancing the cell response through surface activation with biological factors opens huge possibilities in this kind of therapies. Cell adhesion or differentiation can be adjusted to tailor an optimal cell sheet able to fit the organism's requirements [20].

However, the absence of comprehensive studies about each pNIPAm-based support leads to several concerns relative to its harmless use in human organism. It has been shown that features such as the purity of the polymer, the polymerization technique or the specific biological model can affect the biocompatibility results [21]. Although cell cultures provide a well-known experimental model to preliminarily evaluate polymeric applications, specific *in vivo* studies (following ISO or clinical trial requirements) are required to ensure its optimal behavior in patients. Nowadays, certain pNIPAm supports are being tested or already applied in clinical practice [9] serving as an example of biotechnology transfer.

2.2. Thermosensitivity Tuning of pNIPAm

Linear pNIPAm exhibits a LCST around 32°C, very close to the physiological temperature. However, as it has been mentioned before, it may be advantageous to modify some of the aspects of thermosensitivity of the homopolymer pNIPAm. It is well known that the statistical copolymerization with monomeric units that are more hydrophobic or hydrophilic than NIPAm itself shifts the LCST to lower or upper values

respectively. These effects are indicated in Figure 4 where the LCST's variations have been represented as virtual turbidimetry graphs. These variations are composition dependent although if the co-monomer does not participate in the LCST phenomenon, there is a compositional limit from which the thermosensitivity is lost. In this context, it has to be noted that NIPAm is not the only acrylamide exhibiting a LCST [22].

Copolymerization and the tuning of the LCST to higher or lower values may be biologically relevant from different points of view. It may be of interest to design and prepare polymers with a LCST of 37°C or higher values that behave hydrophilic under physiological conditions and exhibit a transition upon heating. In another example, Rochev et al. copolymerized NIPAm with hydrophobic tert-butyl acrylamide to obtain supports for cell culture with enhanced cell adhesive properties [23].

The graph of Figure 5 shows data from literature concerning different NIPAm based copolymers, either with hydrophilic or hydrophobic comonomers.

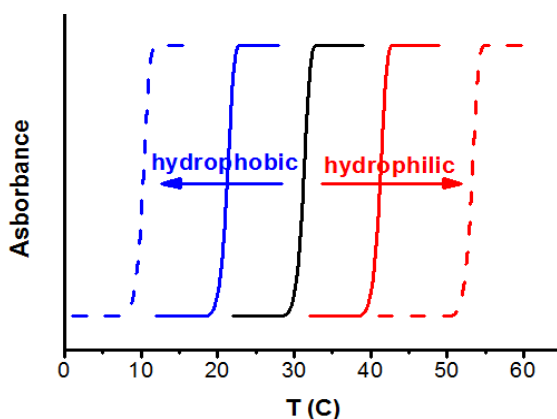


Figure 4. Virtual turbidimetry graphs showing LCST shifts when NIPAm is statistically copolymerized with monomer units more hydrophilic (red) or more hydrophobic (blue) than NIPAm itself.

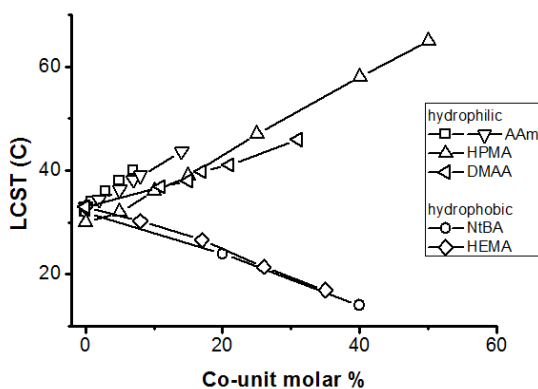


Figure 5. LCST values, taken from literature [24] for several statistical copolymers of NIPAm and other comonomers (acrylamide-AAm, N-tertbutylacrylamide-NtBA, hydropropylacrylamide-HPMA, dimethylacrylamide-DMAA, hydroxyethylmethacrylate-HEMA).

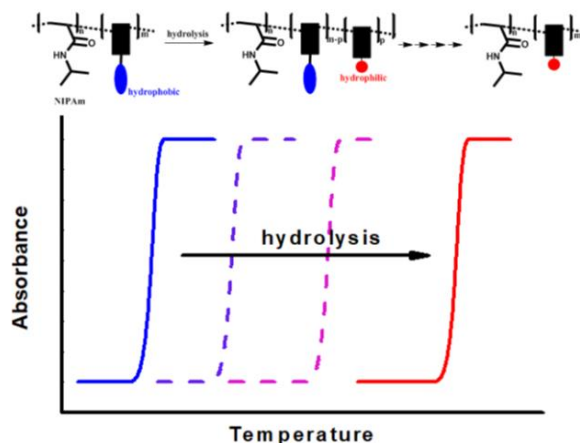


Figure 6. Switchable NIPAm copolymers with degradable side groups.

In 1999 Hennink et al. designed a new concept of LCST tuning, by using a more hydrophobic comonomer than NIPAm but containing a hydrolysable side group that upon incubation in aqueous media lead to a hydrophilic unit and therefore to switchable LCST as it is indicated in Figure 6 [25]. Since this pioneer work, others using the same strategy have been described, which use either hydrolysable [26] or enzyme-sensitive switches [27].

What makes this approach particularly attractive is that, with a proper design, the final hydrophilic polymer may turn to be water soluble and therefore resorbable and eliminable if the molecular weight is appropriate.

NIPAm has been statistically copolymerized with ionizable monomers, both anionizable and cationizable, in order to obtain systems with dual sensitivity, to pH and temperature. In this type of copolymers, thermosensitivity is dependent on the ionization state of the comonomer unit, and therefore is dependent on pH. According to the trend described in Figure 4, the higher the ionization degree of the ionizable units, the higher the LCST of the copolymer. Thermosensitivity may be lost for an ionic content higher than a critical one. This property has been used by Fundueanu et al. to activate thermosensitivity of cationizable systems by electrostatic interaction with an anionic hydrophobic compound [28]. Thermosensitive structures containing cationizable tertiary amines have been prepared to modulate the charge of gene carriers and therefore improve aspects such as cytotoxicity [29].

As mentioned before, block and graft structures have been proposed to modulate aspects such as the colloidal stability. Thus, Voit et al. have reported copolymers of anionizable poly-oxazoline chains grafted on a pNIPAm backbone, which led to nanoentities with thermosensible core and pH-sensitive corona [30]. It has to be mentioned that the nanoentities were stabilized by crosslinking under electron-beam irradiation. Wang et al. anchored pNIPAm chains incorporating PEO grafts to a PP surface in order to obtain thermosensitive self-cleaning surfaces. [31] Beheshti et al.

prepared multiblocks containing PEO and pNIPAm what allowed for modulating the consistency of the entities above LCST (from isolated aggregates to gel-type materials) by changing the length of the blocks [32].

In another outstanding example, Tamate et al. synthesized block copolymers with a PEO-based hydrophilic segment as a dispersion stabilizer and a thermoresponsive segment based on pNIPAm. After crosslinking of the thermoresponsive segment, they obtained polymersomes behaving as self-beating artificial cells [33].

Grafting of pNIPAm onto natural polymers such as polysaccharides may lead to materials with gel-type consistency above LCST; thus it may be used as biocompatible injectable gels, which are very desirable systems in biomedicine. pNIPAm has also been grafted to alginate to offer thermal modulation to the gels obtained upon addition of calcium ions [34].

The previous discussion can be extended to NIPAm-based chemical hydrogels [6] that is, permanent polymer networks. These networks may be constituted by pure pNIPAm chains or by statistical, block or graft copolymers. As it has been mentioned before, the transition temperature is defined in this case as VPTT instead of LCST. Besides, chemical crosslinking has been used to improve the stability of thermosensitive pNIPAm systems. An illustrative example of that is the improvement of the thermogating characteristics of grafted pNIPAm chains, as described by Chen et al. [35].

3. POLYETHERS: POLY(ETHYLENE OXIDE), POLY(PROPYLENE OXIDE) AND POLOXAMERS (PLURONICS®)

3.1. Structures/Composition

3.1.1. PEO, PPO and Their Statistical and Block Combinations

The production of *poly(ethylene oxide) (PEO)* or *polyethylene glycol (PEG)* was first reported in 1859. Both A. V. Laurence and C. A. Wurtz independently isolated products that were identified as polyethylene glycols [36]. PEO is a hydrophilic polymer with the structure shown in Figure 7. Hydrophilic PEO retains a soluble behavior upon heating to 100°C, above this temperature phase separation occurs although further heating may solubilize it again. Thus, the phase diagram of a H₂O/PEO binary mixture is a closed loop which can be modulated by varying the molar mass (higher molecular weight results in lower PEO solubility and therefore the LCST decreases) [37]. Despite their peculiar properties, this polymer family exhibits very high LCST values which are not practical for biological applications. Therefore PEO/water systems are not used by themselves but in combination with other polymers or additives.

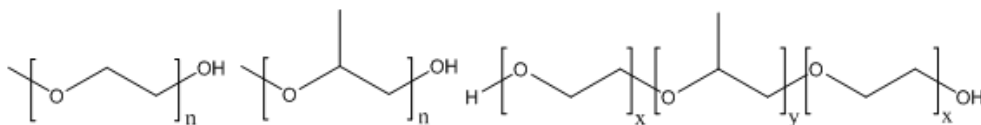


Figure 7. Schematic representation of PEO, PPO and poloxamer structures.

Poly(propylene oxide) PPO introduces a structural modification (see Figure 7) which increases the polyether's hydrophobicity; this translates directly into a decrease in water solubility and therefore the phase transition temperature decreases as well with respect to PEO based materials.

Statistical combination of both monomers results in polymers with intermediate properties with LCST values between both homopolymers which can be tailor-made according to the requirements of an application [38]. The modulation of their thermal behavior/solubility will be explained in more detail in section 3.3.

Commonly, they are bundled in a controlled block structure (see Figure 2). *Poloxamers* are nonionic triblock copolymers composed of a central hydrophobic chain of poly(propylene oxide) flanked by two hydrophilic chains of poly(ethylene oxide) arranged in A-B-A structure: PEO-PPO-PEO (Figure 7) [7a]. The word “poloxamer” was coined by I. Schmolka, who patented for these materials in 1973 [39]. Poloxamers are also known by the trade names Synperonics (Croda), Pluronic (BASF), and Kolliphor (BASF). Due to the generic term “poloxamer,” these copolymers are named with the letter “P” followed by three digits: the first two digits multiplied by 100 give the approximate molecular mass of the PPO core, and the last digit multiplied by 10 gives the percentage of the PEO content. For the Pluronic and Synperonic trade names, coding starts with a letter to define its physical form at room temperature (L = liquid, P = paste, F = flake (solid)) followed by two or three digits. The first digit (two digits in a three-digit number) multiplied by 300 indicates the approximate molecular weight of the hydrophobic PPO; and the last digit multiplied by 10 gives the percentage of the PEO content as for the general nomenclature (e.g., P 127 = poloxamer with a PPO molecular mass of 3,600 g/mol and a 70% PEO content).

With a similar block structure, the *Poloxamine* (Tetronic®) block copolymers (see Figure 8) are a family of 4-arm PPO-PEO block copolymers which also have been used to prepare hydrogel systems for biological purposes [40].

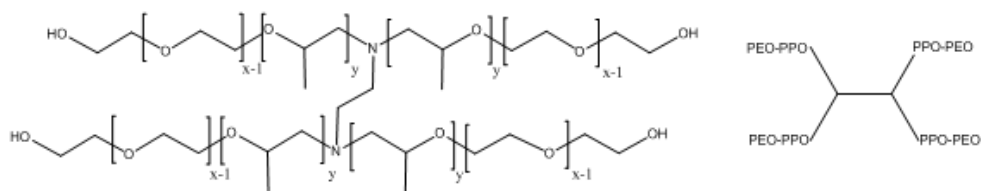


Figure 8. Chemical structure and schematic representation of poloxamines.

Thermal and rheological properties of all these copolymers depend on the PPO block length and the overall molecular weight [41]. PEO and PPO are both water soluble at low temperatures what allows for complete chain miscibility; however, as the temperature increases, the PPO block becomes hydrophobic, dehydrates and the polymer starts forming micelles with a PPO core and a PEO corona (see Figure 9) [42]. Specifically, when the temperature of the poloxamer solution is higher than the critical micellization temperature (CMT), these polymers self-assemble to form stable micelles. Increasing the temperature or the poloxamer concentration to a definite gelation point (GT), these micelles come into contact forming highly ordered networks. This micelle entanglement has been investigated for drug and gene encapsulation and delivery applications. Although they rapidly form hydrogel at a specific temperature, the hydrogels structure is not maintained for a long time under physiological conditions, due to their low molecular weight. Their lack of mechanical strength is nonetheless very interesting for burst drug release as well as for tissue engineering based on injectable and in situ gelling materials [43].

Besides, since the Food and Drug Administration (FDA) approved some poloxamers as inactive materials for pharmaceutical formula and as thickening agents, they have been prolifically applied as drug carriers for diagnosis [44] drug delivery, [45] cell encapsulation [46], gene delivery and cancer therapies [47].

Due to the low mechanical strength of these materials, they have not been largely used for cell harvesting and manipulation. However there are few examples in the literature where temperature-dependent cell detachment has been addressed [48] and applied for instance with adipose-derived stem cells [49] Other examples are focused on enhancing their mechanical properties through chemical crosslinking [6] or modification with peptides what reinforces the stability and improves the cyto-compatibility for cell culturing [46b].

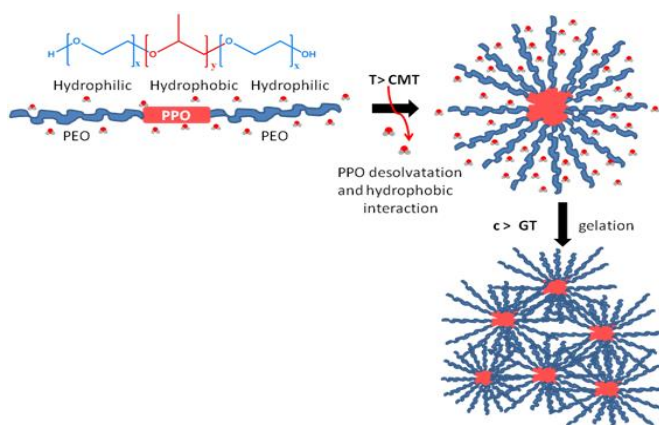


Figure 9. Schematic representation of a Poloxamer's micellization process and the behavior above the critical gelation temperature GT.

Similar triblock copolymers including other central blocks have also been described. The copolymerization of hydrophilic PEO with other monomers makes them better candidates for biological application since the introduction of hydrophobic groups allows for modulating their temperature dependent solubility. Often the PPO block is replaced by biocompatible polyesters such as poly L-lactic acid (PLA), [50] D-L-lactic acid co-glycolic acid (PLGA), [51] poly(hexamethylene adipate (PHA), poly(ethylene adipate) (PEA), poly(ethylene succinate) (PESc) [52] poly(ϵ -caprolactone) (PCL), [53] poly(ϵ -caprolactone-co-lactide)– (PCLA),[54] (R)-3-hydroxybutyrate (PHB) [55] and poly(propylene fumarate) (PPF) [6]. The fact that these polyesters are naturally derived polymers improves the biocompatibility and cell adhesion of the final hydrogel with a view towards their application as smart biofunctional materials [56]. More interestingly for their final application, some of these polyesters are biodegradable [57]. Among them, PLGA is probably one of the most investigated ones since Jeon and co-workers published in 1997 the synthesis of PEO-PGLA-PEO triblock copolymers showing a good biocompatibility, a sol-gel transition at physiological temperature and biodegradability [50a]. Highly controllable biodegradation is possible by simply modulating the ratio of the lactide to the glycolide in the PLGA [58]. Some of PEO-PGLA hydrogels were found to be completely reabsorbed *in vivo* within approximately 1–4 weeks, depending on their composition [59]. However, the degradation products of some polymers, such as PLLA and PLGA, may generate an acidic environment which could cause inflammation at the injection site or protein denaturalization/damage.

3.1.2. Polymers with PEO Side Chains (Grafted Structures)

Surpassing the possibilities of linear PEO and its block-copolymers, oligoethylene glycol (OEG) chains provided with a polymerizable group such as acrylate (A), methacrylate (MA), vinyl, styrene, allyl ether, maleimide, vinyl sulfone, NHS ester groups, etc., allow for better defined architectures by controlled radical polymerization techniques. These methods use the macromer strategy to obtain thermosensitive grafted structures with OEG side chains [60]. Among all the possible OEG-derived polymers, poly(oligoethylene glycol acrylate) (POEGA) and methacrylate (POEGMA) [61] synthesized from conventional (or controlled/living) free-radical polymerization are probably the most used ones [62]. This approach offers excellent control over the polymer composition, functionality, architecture and molecular weight distribution with a wide range of functional monomers to impart the desired functionalities to the polymers.

The OEG-macromer approach is particularly versatile since it allows for grafting hydrophilic OEG chains to polymer backbones of very different nature, and also to introduce multiple variations that will condition the polymer's properties and therefore also its performance and final application. Moreover, the living polymerization allows for defining and controlling the backbone's end group through the functional initiator and studying its influence in the thermoresponsiveness as it will be explained in section 3.3.

Macromer copolymerization empowers combining the advantages of biocompatibility and hydrophilicity that PEO offers with other added-value functional monomers like fluorescent or magnetic label probes, [63] and ionizable monomers (cationic, [64] anionic [65] and zwitterionic [66]). Moreover, the latter allow for the preparation of a dual response system (to temperature and pH) as well as controlling the interaction with the extracellular matrix, etc. Furthermore, incorporation of specific functionalities (e.g., RGD peptide or other biomolecules) synthesized by free-radical polymerization improve upon PEO-based polymer designs [61].

Oligoethylenglycol side chains bearing a polymerizable group allows also for combining within the same macromolecule side chains with different lengths. This will enable to tune the transition temperature as it will be explained in more detail in section 3.3. This can be done statistically or also by synthesizing block copolymers [38]. Obviously, this strategy also permits the pairing to other well-known thermosensitive polymers such as pNIPAm, [31-32, 67] poly(vinyl caprolactone) PVCL [68] or even both of them, [69] among others (either by grafting PEO onto them or by copolymerization with the respective macromonomers obtaining block copolymers).

3.2. Biological Applications of Polyethers

The family of polyethers has an eminent role in a vast variety of biological applications. PEO is generally considered biologically inert and is Generally Regarded as Safe (GRAS) by the FDA. During decades, PEO-based materials have shown a good *in vitro* and *in vivo* biocompatibility even in problematic tissues, such as brain [70] or cornea [71]. Once again, although PEO and other mostly-used copolymers (i.e., with PLA or PCL) have individually demonstrated to be non-cytotoxic, it is necessary to analyze specific materials according to its biological use and patient particularities [72].

Different biomaterial architectures have been proposed for PEO and its copolymers in order to accomplish concrete tasks: coatings for DNA or siRNA administration in gene therapy, [73] nanoparticles [74] to long-term protein systemic delivery or thermosensitive biodegradable hydrogels for controlled drug release. Recently, the attention has been focused on injectable formulations of block copolymers of PEO, PCL and/or other monomers (including PLA or PNIPAm) [51b, 67a] for pulsatile *in situ* release associated to a temperature change [53a, 53b]. This feature may have implications in metabolic disorder treatments (diabetes), [53c, 75] local antitumoral administration, [67f] or controlled release of bioactive agents for tissue regeneration [76]. In the tissue engineering field, a sustained stimulus at mid and long-term stages can improve cell differentiation to relevant phenotypes or matrix secretion, and finally define the regeneration success. Because of that, injectable PEO-based hydrogels are being evaluated in bone regeneration, often in combinations with collagen and hydroxyapatite

[77]. Finally, degradable formulations have also been applied as a filling material in post-surgery treatments, preventing unwanted tissue adhesions or fibrosis [54, 78].

3.3. Thermal Properties and Strategies to Modulate the LCST

As it has been addressed along this chapter for other polymer families, thermosensitivity in aqueous media can be modulated by different structural alterations which differ from the hydrophobic/hydrophilic balance of the backbone to the modification of side chains and end groups. Some of the main parameters that can be adjusted are discussed below.

3.3.1. Influence of Polymer Concentration and Polymerization Degree (DP)

The normal trend observed is: the higher the polymer concentration, the smaller the diffusion rate and phase separation and therefore a higher temperature is needed for the transition. The polymer molar mass (polymerization degree) also affects directly to the transition temperature. For PEO, a higher molecular weight results in lower solubility and therefore the LCST decreases. This is also applicable to other polymers, for example, it has been described that an increase in the PPO molar mass from $M_n = 400$ to 3000 g mol^{-1} results in a LCST shift from 50 to 17°C [38].

3.3.2. Variations of the Side Chain Length

This parameter only concerns the systems containing OEG-grafted chains. Elongation of the lateral OEG chain will increase the hydrophilicity which translated directly into an increase of the LCST. When the side chains are kept constant in length and number, there is obviously a dependence of the LCST with the type of the polymer backbone (vinyl, styrene, acrylate, methacrylate, vinyl ether, etc.). A review from C. Weber et al. [38] presents a detailed comparison between them.

3.3.3. Composition Influence: Hydrophobic/Hydrophilic Balance

This is probably the most important parameter to modulate the thermal response of these kinds of polymers. Increasing mole fraction of the more hydrophobic polymer translates into an average decrease of the copolymer hydrophilicity which results in a decrease of the LCST of the aqueous solution.

Hydrophobic/Hydrophilic balance: Influence in Statistical Copolymers

Statistical copolymerization of an EO with PO permits to obtain copolymers that exhibit a LCST behavior in a temperature range in between the LCST of both homopolymers as it was demonstrated by Bailey and Callard [79]. The authors described a linear decrease of the LCST when increasing the content of PO in the statistical

copolymer. For instance, tuning the PO composition from 50%, 70% and 80% shifted the LCST value from 50 to 40 to 30°C respectively [80].

Hydrophobic/Hydrophilic balance: Influence in Block Copolymers (Ploxamers)

In block copolymers the behavior might differ from that of the statistical ones since the isolated blocks and the interaction among them can influence the overall response. The gelation of poloxamer solutions above certain temperature is attributed to the interaction between the hydrophobic domains (PPO) and the hydrophilic ones (PEO). Their compositions have a strong effect on the structural properties of the micelles: a more hydrophobic Pluronic polymer (longer PPO block) would form easily the micelles with a higher proportion of the dehydrated methyl groups and therefore the LCST and the GT will be lower than the one from a polymer with a shorter PPO block where the hydrophobic interactions are weaker.

The PEO:PPO ratio can be adjusted by modifying the block length or by combination of two different block-copolymers. This balance can be used to modulate the gelation temperature as required. J. M. Zheng et al. [81] and J. Fan et al. [82] described linear equations based on the regression analysis of the effect of the formulation composition on the hydrogel’s gelation temperature by varying the concentrations of two poloxamers with different PEO:PPO ratio and studying the resulting gelation temperatures (Figure 10).

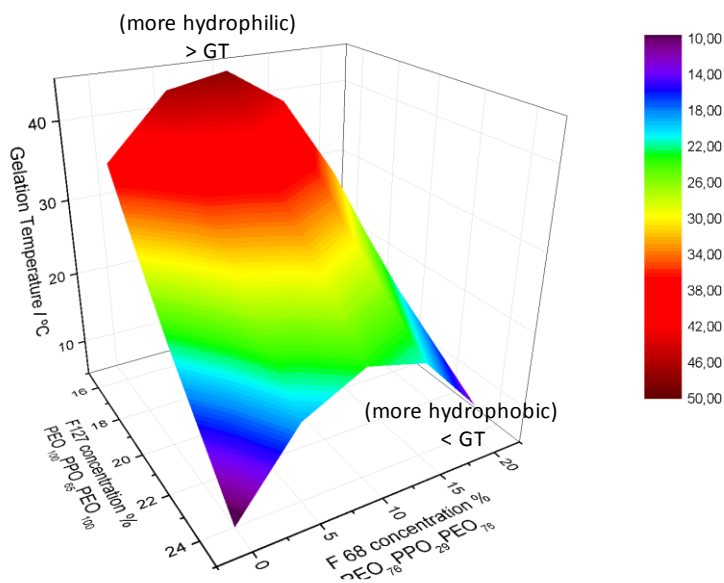


Figure 10. Effect of compositions on the phase transition temperature being F127 and F68 poloxamers with composition 100:65:100 and 76:29:76 respectively (PEO:PPO ratio of F127 and F68 are approximately 3 and 5.2, respectively). Plot from equation from Ref [82].

This hydrophobic/hydrophilic ratio has also been applied to modulate the solubility of other block copolymers where some block were replaced by others structures. For instance, A. Hotta's group has recently studied a PLGA-PEO-PLGA hydrogel varying the molecular weight and the proportion of the hydrophobic PLGA block observing that it is possible to regulate the GT between 25°C and 37°C [51a]. The transition temperature depends on both the total molecular weight and the one of each building block.

Hydrophobic/Hydrophilic balance: Influence in OEG Grafted Structures

The thermal behavior of systems containing OEG grafted chains (section 3.1.2.) strongly depends, as explained above on the side chain length and number of inserted chains, which directly affects the hydrophobic/hydrophilic balance. Therefore the longer the lateral chain, the higher the hydrophilicity and the LCST. Furthermore, this strategy allows for combining different proportions of two thermosensitive parts being both grafted OEG side chains of different lengths (DP) (and thus different thermal responses) onto the same backbone or through the combination of OEG side chains with other thermosensitive units such as NIPAm [31]. Besides, for both cases, statistical and block copolymers are possible. When two thermoresponsive systems are statistically combined an intermediate LCST is usually obtained while a response with two independent transition temperatures can be produced by block copolymers. For these blocky structures, a single intermediate value may be observed as well, although this value is not always the midpoint. The deviation with respect to the midpoint can be attributed to the collapse of the block which possesses the lower LCST which will condition the water diffusion of the second block. For these block copolymer composed of two different OE-macromers higher LCST values than expected for a statistical copolymers would be observed. This difference is more pronounced upon increase of the blocks length. Zhao et al. developed a formula to predict the LCST of block copolymers containing two oligoEO of different DP by considering the LCST from each homopolymer and the DP of each block. (Equation 1) [83].

$$LCST = \frac{DP_1}{DP_1 + DP_2} \times LCST_1 + \frac{DP_2}{DP_1 + DP_2} \times LCST_2$$

Equation 1. LCST of copolymers containing two thermosensitive oligoEO blocks of different DP.

Systems where the LCST from individual blocks are too far away undergo two independent phase transitions.

3.3.4. Variations of the End Group

Despite the fact that the composition of the macromolecule is the most affecting parameter to the polymer's solubility and therefore to its thermal properties, the effects of the endcapping groups of both backbone and side chain are not negligible.

End Group from Lateral Chains

As they are very abundant, they have a remarkable effect on the solubility properties. Besides, being the outer part of the macromolecule, they play an important role in the interaction with the water molecules of the surface. A change from a methyl to an ethyl end group, for example, implies a variation of up to 40-50 °C of the LCST [84].

Backbone's End Group (α , ω)

This effect is only important for low molecular weight polymers. The development of living polymerization techniques has allowed for obtaining well defined end groups and study their influence in micelle formation. Again, the inclusion of hydrophobic groups tends to lower the LCST from the corresponding polymer solution or hydrogel.

3.3.5. Effects of Salt Additives, Surfactants or Co-Solvents

Since the thermoresponsive behavior depends on the interaction between the polymer (hydrophilic/hydrophobic balance within the polymer molecules) and the solvating solvent, it is not surprising that certain additives can influence the position of the LCST. All additives can alter the solvent quality and therefore can alter the polymer-solvent interactions. Therefore, the transition temperature can be shifted to a large extent or it can even disappear [85]. This effect results of paramount importance, since the application of polymers for biological purposes requires the use of buffered media.

The solubility effect of some ions is well known in the protein field since 1888, when F. Hofmeister studied the ability of ions to precipitate proteins out of solution [86]. This knowledge has later been applied to other macromolecules such as polymers [87]. Well hydrated anions (kosmotropes), tend to stabilize macromolecules toward their folded natural state (reducing the LCST). Poorly hydrated anions, (chaotropes), tend to make macromolecules more soluble in water and promote an increase of the LCST (Figure 11). Cations' effect has also been classified in these so called Hofmeister series according to their ability to strengthen the hydrophobic interaction: $\text{NH}_4^+ > \text{K}^+ > \text{Na}^+ > \text{Li}^+ > \text{Mg}^{2+} > \text{Ca}^{2+}$.

A strong kosmotrope salt effect has been observed (stabilization of hydrophobic aggregates in solution) for linear and hyperbranched PEO systems [88]. since salt normally enhances the dehydration process. The LCST values decreased as the salt concentration increased. These studies have also been addressed for some pluronic copolymers for ophthalmic applications since they are necessarily in contact with a saline environment [81].

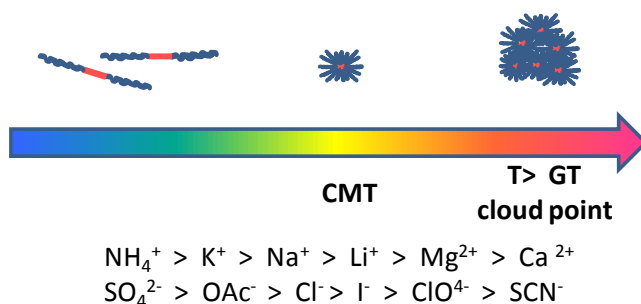


Figure 11. Hofmeister ion effect on Poloxamers.

4. POLY-OXAZOLINES

4.1. POXs Structures and Biological Applications

Poly (2-oxazolines), POXs, are relatively new polymers with -isomeric polypeptide structures that possess applications in the biomedical field in drug and gene delivery, and could have in cell manipulation processes due to their excellent biocompatibility [89]. The first POX was reported in 1960s obtained by ring opening polymerization of 2-oxazoline monomers [90]. Due to the high cost of POXs, industrial applications have not been developed but their living cationic ring-opening polymerization procedures provides an excellent control over their molar mass, polydispersity, monomer composition, chain-end functionality and polymer architecture and therefore over the polymer properties by varying the amidic side chains. An interesting property of POXs is their thermal sensitivity undergoing LCST transitions in aqueous solutions providing them stealth polymer characteristics similar to PEO [91]. Moreover, the structural control of POXs in terms of introduction of functional groups (in the side chain and in chain ends) and the easy preparation of block copolymers, make them excellent candidates for biomedical applications, being considered an alternative to the “gold standard” PEO [92].

The general structure of POXs is depicted in Figure 12. Cationic ring opening polymerization allows for the preparation of POXs with narrow molar mass distributions in which chain transfer has been found to limit their average number molecular weight, M_n , to about 10 KDa [93]. Some attempts to suppress chain transfer by high temperature microwave polymerization, show low polydispersity and higher M_n [94].

POXs are excellent candidates for applications in the biomedical field. First, PEtOx has been approved by the FDA as an indirect food contact agent, similarly to polyvinylpyrrolidone, PVP, or to PEO before its approval for biomedical applications [89]. POXs have been found to be no cytotoxic, even increasing the concentration [95] or the molecular mass of POXs as PMeOx and PEtOx [96].

Most of the studied applications of POXs in this area have been focussed on carriers in controlled drug, gene or protein delivery systems. [89] POXs meet specific requirements needed for the development of next-generation polymer therapeutics such as biocompatibility, high modulation of solubility, variation of size, architecture as well as chemical functionality [97].

As an example, POXs has also been used as effective antitumoral carriers [98] in mice model taking profit of the passive accumulation of polymers in tumor tissue due to enhanced permeability and retention.

Recently, POX-based polymer therapeutics came back into the focus of very intensive research. For example, POX micelles based on di-or triblocks of PMeOx and poly (2-n-butyl-2-oxazoline) have been loaded with drugs such as paclitaxel, amphotericin B and cyclosporine A. These micelles were found to be more stable when containing multiple drugs rather than a single one [99]. Moreover, POXs copolymers based on EtOx with double bond side chains, were post-modified giving rise to thermoresponsive nanoparticles which were applied in radionuclide delivery devices [100].

Poly(L-lysine) dendrimers grafted with polyoxazolines have been described to enhance cytocompatibility and functional group content, [101] allowing for higher active factor loading. This grafting perspective can promote additional applications. On this regard, thermoresponsive polyoxazoline-grafted superparamagnetic iron oxide nanoparticles lead to a tunable cell uptake dependent of temperature, which can present interesting uses *in vitro* and *in vivo* imaging and clinical therapies [102].

4.2. LCST Modulation of POXs

One of the most relevant aspects of POXs is the possibility of properties modulation by variation of the side chain of the monomer. For example, incorporating aromatic side chains or fatty acids results in hydrophobic POXs [103]. Linking long aliphatic side chains to POXs can result in highly crystalline polymers with linear side chains, or amorphous POXs with branched aliphatic side chains [104]. In terms of LCST properties and depending on the nature of the chemical group R the behavior in aqueous solution of POXs (see Figure 12) undergoes from hydrophilic character of PMeOX (R = Me), which is soluble in water from 0 to 100°C, [105] to LCST modulation for POXs with longer aliphatic side chains. Thus, in the case of PEtOX, where R = ethyl, the LCST has been determined to be 61-64°C. [106] In the case of more hydrophobic groups as propyl, named as PnPrOX, the LCST is lower than that of PEtOX, in the range of 25-35°C. [107] A structural isomer of pNIPAm is poly (2-isopropyl-2-oxazoline), PiPrOX, where R = CH(CH₃)₂, it exhibits a LCST of 36°C and its behavior and aggregation are rather unusual as it shows an irreversible crystallization when heated for long time above the

LCST [108]. Finally, the LCST of poly(2-cyclopropyl-2-oxazoline), CPropOX, where $R = \text{CH}(\text{CH}_2)_2$, was determined to be about 30°C which decreases with both increasing polymer molar mass and concentration [109].

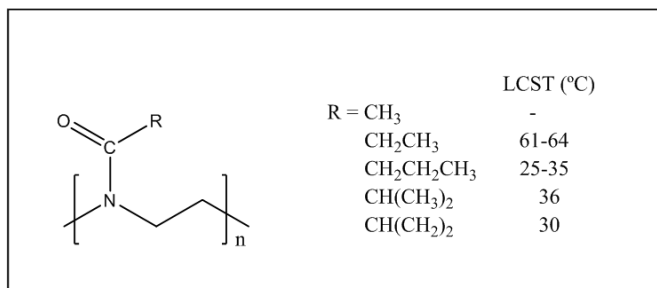


Figure 12. Chemical structure of poly(2-alkyl-2-oxazoline)s and respective LCST depending on the side group.

LCST modulation can also be achieved by copolymerization reactions of different oxazoline monomers. In this sense, Kataoka et al. [108a] have prepared random and gradient oxazoline copolymers with tuned LCST. By copolymerizing 2-n-propyl-2-oxazoline (nPrOx) with either 2-isopropyl-2-oxazoline (iPrOx) or 2-ethyl-2-oxazoline (EtOx) gradient and random copolymers were prepared by cationic polymerization resulting in copolymers with narrow molecular weight distribution. The respective monomer reactivity ratios, obtained by $^1\text{H-NMR}$ analysis, were 3.15 and 0.57 for nPrOx and iPrOx, being considered sufficiently different to form gradient copolymers, P(nPrOx-grad-iPrOx). For nPrOx and EtOx, on the other hand, these values were found to be 1.28 and 1.04 indicating the formation of random copolymers P(nPrOx-ran-EtOx). Both copolymer types followed a simple and practical rule for LCST modulation that depends on the compositional variation between the hydrophobic and hydrophilic oxazoline monomers. P(nPrOx-ran-EtOx) random copolymers showed a clear LCST over a wide temperature range from 24 to 75 °C, increasing with the increase of the EtOx molar fraction, whereas in the case of P(nPrOx-grad-iPrOx) the temperature range is 24-39°C which increasing the LCST increases with increasing iPrOx content.

Similarly, 2-ethyl-2-oxazoline (EtOx) and 2-isopropyl-2-oxazoline (iPrOx) copolymers have been prepared by cationic polymerization giving copolymer with low polydispersity and with modulated LCST [93]. In this case the determined reactivity ratios were found to be 1.78 and 0.79 for EtOx and iPrOx respectively, indicating the formation of gradient copolymers where the trend is a gradual decrease of EtOx and an increase of the iPrOx composition along the backbone to the chain end. In terms of LCST modulation, the prepared copolymers show an LCST increase when increasing the molar content of the hydrophilic co-monomer, i.e., EtOx ranging from 39 to 67°C simply by varying the EtOx/iPrOx molar ratio.

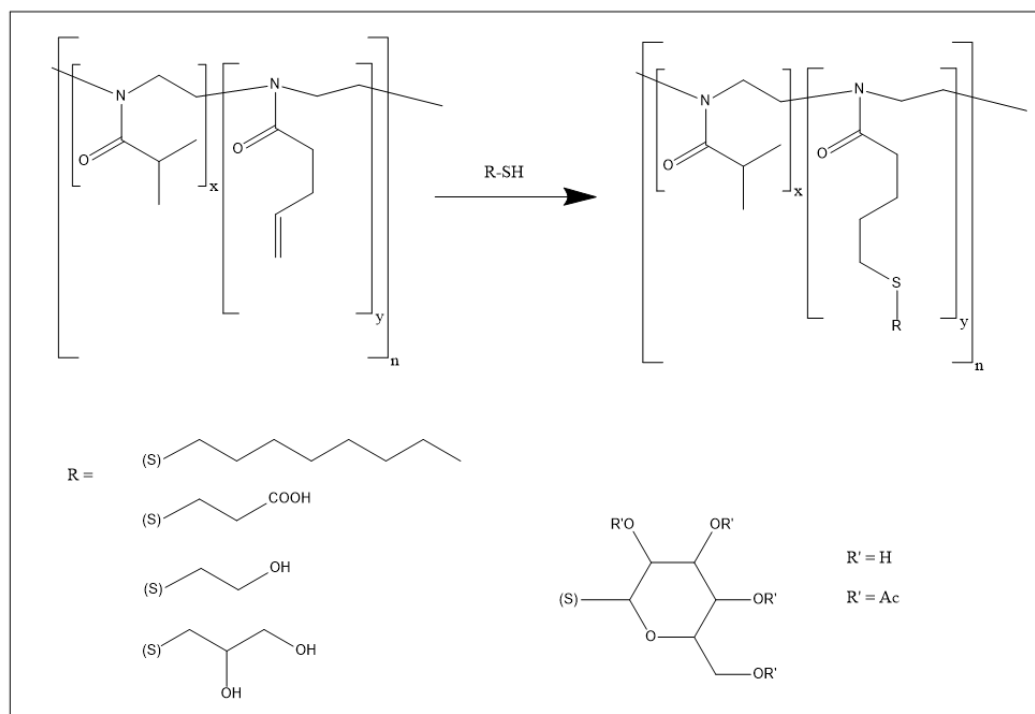


Figure 13. Thermo-responsive poly-oxazolines based copolymers prepared by click modification of poly [2-(iso-propyl/3-butenyl)-2-oxazoline] with ω -functional thiols.

Another family of thermo-responsive poly-oxazolines are based on statistical copolymers of 2-isopropyl-2-oxazoline (iPrOx) and 2-(3-butenyl)-2-oxazoline which can be modified by click addition with ω -functional thiols [110]. Figure 13 shows the preparation of this set of POXs with different hydrophilic groups as carboxylic, hydroxyl, or glucopyranose, or hydrophobic functionalities as aliphatic side chains or acetylated glucopyranose groups.

Turbidimetric studies to obtain the clouds points (LCST) of copolymers with low molar fractions (0.06) of OX monomers with different functionality, showed a LCST range from 30 to 55°C, exhibiting the lowest LCST values those copolymers that incorporate the hydrophobic octane and acetylated glucopyranose groups. The highest are observed for those systems that the hydrophilic propionic acid or glycerol groups. Moreover, the acetylated glucopyranose groups were removed to yield the respective hydroxyl groups. These polymers exhibited a LCST modulated by the copolymer composition ranging from 46 to 85°C.

Other attempts to modulate the LCST of POXs have been based on the effect of polymer end groups and on the preparation of block copolymers [38]. End group functionalized POXs can be achieved by using a functional initiator, and by nucleophilic attack and subsequent modification of the -OH group of the terminal chain end. End groups only affect the LCST of low molecular weight polymers as has been observed in

the case of iPrOx with polymerization degree (DP) of 40, decreasing its LCST in 5°C in comparison with the terminated in –OH from an acrylate group [111]. Moreover, hydrophobic end groups such as octadecyl were found to decrease the LCST 12 and 16°C with one and two end groups respectively, in PiPrOx with DP of 57 [112].

In the case of block copolymers, hydrophilic short PMeOx blocks at the chain end of PiPrOx resulted in an increase of the LCST in 6°C for triblock copolymers as MeOx3-b-iPrOx25-b-MeOx3 [113]. Functionalization of PiPrOx with either one or both chain ends of tri-ethyleneglycol moieties was found to decrease the LCST 5°C. Block copolymers of EtOx with 2-nonyl-2-oxazoline (NonOx), EtOx90-b-NonOx10 showed a LCST of 69°C taking into account that PEtOx with a DP below 100, does not exhibit a LCST in water [114].

5. FINAL REMARKS

Thermoresponsive polymers have been thoroughly investigated for biomedical uses in many areas; from theragnostics, drug and gene delivery to cell harvesting and tissue engineering. The use of biocompatible polymers showing a physical change in aqueous media at physiological temperature requires precisely tuning of the structure, composition (hydrophobic/hydrophilic balance), polymer length, molecular weight, lateral chains, etc. These chemical alterations described along the chapter, can be performed at two levels, by altering the backbone repetition unit from a compositional point of view or by modifying their structure with branches or endcapping groups, but in both cases they directly condition the thermal, mechanical and degradation properties of the polymer adjusting them to that required by the final application.

REFERENCES

- [1] Q. Zhang, C. Weber, U. S. Schubert, R. Hoogenboom, *Materials Horizons* 2017, 4, 109-116.
- [2] M. Boustta, P.-E. Colombo, S. Lenglet, S. Poujol, M. Vert, *Journal of Controlled Release* 2014, 174, 1-6.
- [3] G. Odian, *Principles of polymerization*, John Wiley & Sons, 2004.
- [4] a) A. Goto, T. Fukuda, *Progress in Polymer Science* 2004, 29, 329-385; b) J. Jennings, G. He, S. M. Howdle, P. B. Zetterlund, *Chemical Society Reviews* 2016, 45, 5055-5084.
- [5] D. Uhrig, J. Mays, *Polymer Chemistry* 2011, 2, 69-76.

- [6] L. Klouda, *European Journal of Pharmaceutics and Biopharmaceutics* 2015, 97, 338-349.
- [7] a) A. K. A. S. Brun-Graepi, C. Richard, M. Bessodes, D. Scherman, O. W. Merten, *Progress in Polymer Science* 2010, 35, 1311-1324; b) P. Gilsenan, R. Richardson, E. Morris, *Carbohydrate Polymers* 2000, 41, 339-349.
- [8] a) A. Halperin, M. Kröger, F. M. Winnik, *Angewandte Chemie International Edition* 2015, 54, 15342-15367; b) Y. Guan, Y. Zhang, *Soft Matter* 2011, 7, 6375-6384.
- [9] K. Nagase, M. Yamato, H. Kanazawa, T. Okano, *Biomaterials* 2018, 153, 27-48.
- [10] A. Gandhi, A. Paul, S. O. Sen, K. K. Sen, *Asian Journal of Pharmaceutical sciences* 2015, 10, 99-107.
- [11] I. Ankareddi, C. S. Brazel, *Journal of Applied Polymer Science* 2011, 120, 1597-1606.
- [12] T. Ta, E. Bartolak-Suki, E. J. Park, K. Karrobi, N. J. McDannold, T. M. Porter, *Journal of Controlled Release* 2014, 194, 71-81.
- [13] N. Takeda, E. Nakamura, M. Yokoyama, T. Okano, *Journal of controlled release* 2004, 95, 343-355.
- [14] N. Yamada, T. Okano, H. Sakai, F. Karikusa, Y. Sawasaki, Y. Sakurai, *Macromolecular Rapid Communications* 1990, 11, 571-576.
- [15] B. Chen, F. Xu, N. Fang, K. Neoh, E. Kang, W. N. Chen, V. Chan, *Acta biomaterialia* 2008, 4, 218-229.
- [16] H. E. Canavan, X. Cheng, D. J. Graham, B. D. Ratner, D. G. Castner, *Journal of Biomedical Materials Research Part A* 2005, 75, 1-13.
- [17] a) T. Matsuda, *Journal of Biomaterials Science, Polymer Edition* 2004, 15, 947-955; b) T. Ide, K. Nishida, M. Yamato, T. Sumide, M. Utsumi, T. Nozaki, A. Kikuchi, T. Okano, Y. Tano, *Biomaterials* 2006, 27, 607-614; c) M. Cerqueira, R. P. Pirraco, A. Martins, T. Santos, R. Reis, A. Marques, *Acta biomaterialia* 2014, 10, 3145-3155.
- [18] a) S. Masuda, T. Shimizu, M. Yamato, T. Okano, *Advanced drug delivery reviews* 2008, 60, 277-285; b) Y. Sawa, S. Miyagawa, *BioMed research international* 2013, 2013; c) K. Kim, R. Utoh, K. Ohashi, T. Kikuchi, T. Okano, *Journal of tissue engineering and regenerative medicine* 2015.
- [19] a) M. Sato, M. Yamato, K. Hamahashi, T. Okano, J. Mochida, *The Anatomical Record* 2014, 297, 36-43; b) R. P. Pirraco, H. Obokata, T. Iwata, A. P. Marques, S. Tsuneda, M. Yamato, R. L. Reis, T. Okano, *Tissue Engineering Part A* 2011, 17, 1507-1515.
- [20] H. Shin, S. Jo, A. G. Mikos, *Biomaterials* 2003, 24, 4353-4364.
- [21] M. A. Cooperstein, H. E. Canavan, *Biointerphases* 2013, 8, 19.
- [22] H. Liu, X. Zhu, *Polymer* 1999, 40, 6985-6990.

- [23] Y. Rochev, T. Golubeva, A. Gorelov, L. Allen, W. Gallagher, I. Selezneva, B. Gavrilyuk, K. Dawson, in *Trends in Colloid and Interface Science XV*, Springer, 2001, pp. 153-156.
- [24] a) Z. Shen, K. Terao, Y. Maki, T. Dobashi, G. Ma, T. Yamamoto, *Colloid and Polymer Science* 2006, 284, 1001-1007; b) B. Luan, B. W. Muir, J. Zhu, X. Hao, *RSC Advances* 2016, 6, 89925-89933; c) V. P. Gilcreest, W. M. Carroll, Y. A. Rochev, I. Blute, K. A. Dawson, A. V. Gorelov, *Langmuir* 2004, 20, 10138-10145.
- [25] D. Neradovic, W. L. Hinrichs, J. J. Kettenes-van den Bosch, W. E. Hennink, *Macromolecular Rapid Communications* 1999, 20, 577-581.
- [26] a) Z. Cui, B. H. Lee, C. Pauken, B. L. Vernon, *Journal of Biomedical Materials Research Part A* 2011, 98, 159-166; b) J. Guan, Y. Hong, Z. Ma, W. R. Wagner, *Biomacromolecules* 2008, 9, 1283-1292.
- [27] D. J. Overstreet, H. D. Dhruv, B. L. Vernon, *Biomacromolecules* 2010, 11, 1154-1159.
- [28] G. Fundeanu, M. Constantin, I. Asmarandei, V. Harabagiu, P. Ascenzi, B. C. Simionescu, *Journal of Biomedical Materials Research Part A* 2013, 101, 1661-1669.
- [29] Z. Shen, B. Shi, H. Zhang, J. Bi, S. Dai, *Soft Matter* 2012, 8, 1385-1394.
- [30] S. Zschoche, J. C. Rueda, M. Binner, H. Komber, A. Janke, K. F. Arndt, S. Lehmann, B. Voit, *Macromolecular Chemistry and Physics* 2012, 213, 215-226.
- [31] Y. Ye, J. Huang, X. Wang, *ACS applied materials & interfaces* 2015, 7, 22128-22136.
- [32] N. Beheshti, K. Zhu, A. L. Kjøniksen, K. D. Knudsen, B. Nyström, *Soft Matter* 2011, 7, 1168-1175.
- [33] R. Tamate, T. Ueki, R. Yoshida, *Advanced Materials* 2015, 27, 837-842.
- [34] M. S. Lencina, A. E. Ciolino, N. A. Andreucetti, M. A. Villar, *European Polymer Journal* 2015, 68, 641-649.
- [35] Y. C. Chen, R. Xie, M. Yang, P. F. Li, X. L. Zhu, L. Y. Chu, *Chemical engineering & technology* 2009, 32, 622-631.
- [36] J. Bailey, Frederick E.; Koleske, Joseph V., *Alkylene oxides and their polymers.*, Vol. 35, Marcel Dekker, New York, 1990.
- [37] S. Saeki, N. Kuwahara, M. Nakata, M. Kaneko, *Polymer* 1976, 17, 685-689.
- [38] C. Weber, R. Hoogenboom, U. S. Schubert, *Progress in Polymer Science* 2012, 37, 686-714.
- [39] I. Schmolka, US 3740421, 1973.
- [40] Y. B. Lee, Y. M. Shin, E. M. Kim, J. Y. Lee, J. Lim, S. K. Kwon, H. Shin, *Journal of Materials Chemistry B* 2016, 4, 6012-6022.
- [41] P. Alexandridis, T. Alan Hatton, *Colloids and Surfaces A: Physicochemical and Engineering Aspects* 1995, 96, 1-46.

- [42] C. Alvarez-Lorenzo, J. Gonzalez-Lopez, M. Fernandez-Tarrio, I. Sandez-Macho, A. Concheiro, *European journal of pharmaceuticals and biopharmaceutics* 2007, 66, 244-252.
- [43] a) E. Cho, J. S. Lee, K. Webb, *Acta biomaterialia* 2012, 8, 2223-2232; b) L. Yu, J. Ding, *Chemical Society Reviews* 2008, 37, 1473-1481; c) J. Cortiella, J. E. Nichols, K. Kojima, L. J. Bonassar, P. Dargon, A. K. Roy, M. P. Vacant, J. A. Niles, C. A. Vacanti, *Tissue engineering* 2006, 12, 1213-1225; d) L. S. Yap, M. C. Yang, *Colloids and Surfaces B: Biointerfaces* 2016, 146, 204-211; e) H. Yu, Y. Liu, H. Yang, K. Peng, X. Zhang, *Macromolecular rapid communications* 2016, 37, 1723-1728; f) T. Li, M. Zhang, J. Wang, T. Wang, Y. Yao, X. Zhang, C. Zhang, N. Zhang, *The AAPS journal* 2016, 18, 146-155.
- [44] L. Liu, K.-T. Yong, I. Roy, W.-C. Law, L. Ye, J. Liu, J. Liu, R. Kumar, X. Zhang, P. N. Prasad, *Theranostics* 2012, 2, 705.
- [45] X. Xiong, K. Tam, L. Gan, *Journal of nanoscience and nanotechnology* 2006, 6, 2638-2650.
- [46] a) H. Lee, T. G. Park, *Journal of Biomedical Materials Research Part A* 2009, 88, 797-806; b) S. Peng, J. Y. Lin, M. H. Cheng, C. W. Wu, I. M. Chu, *Materials Science and Engineering: C* 2016, 69, 421-428.
- [47] a) M. Gao, H. Xu, C. Zhang, K. Liu, X. Bao, Q. Chu, Y. He, Y. Tian, *Drug development and industrial pharmacy* 2014, 40, 1557-1564; b) Y. Xie, Q. Long, Q. Wu, S. Shi, M. Dai, Y. Liu, L. Liu, C. Gong, Z. Qian, Y. Wei, *Rsc Advances* 2012, 2, 7759-7771.
- [48] A. Higuchi, T. Yamamoto, K. Sugiyama, S. Hayashi, T. M. Tak, T. Nakagawa, *Biomacromolecules* 2005, 6, 691-696.
- [49] H. H. Jung, K. Park, D. K. Han, *Journal of Controlled Release* 2010, 147, 84-91.
- [50] a) B. Jeong, Y. H. Bae, D. S. Lee, S. W. Kim, *Nature* 1997, 388, 860-862; b) H. J. Chung, Y. Lee, T. G. Park, *Journal of Controlled Release* 2008, 127, 22-30; c) D. G. Abebe, T. Fujiwara, *Biomacromolecules* 2012, 13, 1828-1836; d) T. Vermonden, N. E. Fedorovich, D. van Geemen, J. Alblas, C. F. van Nostrum, W. J. Dhert, W. E. Hennink, *Biomacromolecules* 2008, 9, 919-926; e) L. M. Loiola, B. A. Más, E. A. Duek, M. I. Felisberti, *European Polymer Journal* 2015, 68, 618-629.
- [51] a) M. Miyazaki, T. Maeda, K. Hirashima, N. Kurokawa, K. Nagahama, A. Hotta, *Polymer* 2017, 115, 246-254; b) A. Alexander, J. Khan, S. Saraf, S. Saraf, *Journal of controlled release* 2013, 172, 715-729; c) P. Y. Lee, E. Cobain, J. Huard, L. Huang, *Molecular therapy* 2007, 15, 1189-1194.
- [52] a) M. Song, D. Lee, J. Ahn, D. Kim, S. Kim, *Journal of Polymer Science Part A: Polymer Chemistry* 2004, 42, 772-784; b) Y. S. Jung, W. Park, H. Park, D. K. Lee, K. Na, *Carbohydrate polymers* 2017, 156, 403-408.

- [53] a) M. Boffito, P. Sirianni, A. M. Di Rienzo, V. Chiono, *Journal of Biomedical Materials Research Part A* 2015, 103, 1276-1290; b) C. Gong, S. Shi, P. Dong, B. Kan, M. Gou, X. Wang, X. Li, F. Luo, X. Zhao, Y. Wei, *International journal of pharmaceutics* 2009, 365, 89-99; c) S. Payyappilly, S. Dhara, S. Chattopadhyay, *Journal of Biomedical Materials Research Part A* 2014, 102, 1500-1509; d) M. J. Hwang, J. M. Suh, Y. H. Bae, S. W. Kim, B. Jeong, *Biomacromolecules* 2005, 6, 885-890.
- [54] Z. Zhang, J. Ni, L. Chen, L. Yu, J. Xu, J. Ding, *Journal of Biomedical Materials Research Part B: Applied Biomaterials* 2012, 100, 1599-1609.
- [55] a) Q. Zhao, G. Cheng, H. Li, X. Ma, L. Zhang, *Polymer* 2005, 46, 10561-10567; b) K. Chaturvedi, K. Ganguly, A. R. Kulkarni, M. N. Nadagouda, J. Stowbridge, W. E. Rudzinski, T. M. Aminabhavi, *RSC Advances* 2013, 3, 7064-7070.
- [56] Y. J. Kim, Y. T. Matsunaga, *Journal of Materials Chemistry B* 2017.
- [57] a) M. Mochizuki, M. Hiramami, *Polymers for advanced technologies* 1997, 8, 203-209; b) H. Tan, K. G. Marra, *Materials* 2010, 3, 1746-1767.
- [58] a) M. Qiao, D. Chen, X. Ma, Y. Liu, *International Journal of Pharmaceutics* 2005, 294, 103-112; b) L. Yu, Z. Zhang, J. Ding, *Biomacromolecules* 2011, 12, 1290-1297.
- [59] M. K. Nguyen, D. S. Lee, *Macromolecular bioscience* 2010, 10, 563-579.
- [60] S.-i. Yamamoto, J. Pietrasik, K. Matyjaszewski, *Macromolecules* 2007, 40, 9348-9353.
- [61] E. Bakaic, N. M. Smeets, T. Hoare, *RSC Advances* 2015, 5, 35469-35486.
- [62] G. Vancoillie, D. Frank, R. Hoogenboom, *Progress in Polymer Science* 2014, 39, 1074-1095.
- [63] a) C. Pietsch, A. Vollrath, R. Hoogenboom, U. S. Schubert, *Sensors* 2010, 10, 7979-7990; b) R. París, I. Quijada-Garrido, O. García, M. Liras, *Macromolecules* 2011, 44, 80-86.
- [64] S.-i. Yamamoto, J. Pietrasik, K. Matyjaszewski, *Macromolecules* 2008, 41, 7013-7020.
- [65] J. A. Jones, N. Novo, K. Flagler, C. D. Pagnucco, S. Carew, C. Cheong, X. Z. Kong, N. A. Burke, H. D. Stöver, *Journal of Polymer Science Part A: Polymer Chemistry* 2005, 43, 6095-6104.
- [66] D. Dong, J. Li, M. Cui, J. Wang, Y. Zhou, L. Luo, Y. Wei, L. Ye, H. Sun, F. Yao, *ACS applied materials & interfaces* 2016, 8, 4442-4455.
- [67] a) A. Alexander, J. Khan, S. Saraf, S. Saraf, *European Journal of Pharmaceutics and Biopharmaceutics* 2014, 88, 575-585; b) Z. Li, Z. Fan, Y. Xu, W. Lo, X. Wang, H. Niu, X. Li, X. Xie, M. Khan, J. Guan, *ACS applied materials & interfaces* 2016, 8, 10752-10760; c) D. Liu, T. Wang, X. Liu, Z. Tong, *Biomedical Materials* 2012, 7, 055008; d) T. Trongsatitkul, B. M. Budhlall, *Polymer Chemistry* 2013, 4, 1502-1516; e) N. A. B. Vieira, J. R. Neto, M. J. Tiera, *Colloids and*

- Surfaces A: Physicochemical and Engineering Aspects* 2005, 262, 251-259; f) H. S. Abandansari, E. Aghaghafari, M. R. Nabid, H. Niknejad, *Polymer* 2013, 54, 1329-1340.
- [68] K. Van Durme, S. Verbrugghe, F. E. Du Prez, B. Van Mele, *Macromolecules* 2004, 37, 1054-1061.
- [69] a) K. A. Bovaldinova, M. M. Feldstein, N. E. Sherstneva, A. P. Moscalets, A. R. Khokhlov, *Polymer* 2017, 125, 10-20; bZ. Ye, Y. Li, Z. An, P. Wu, *Langmuir* 2016, 32, 6691-6700.
- [70] K. Bjugstad, K. Lampe, D. Kern, M. Mahoney, *Journal of Biomedical Materials Research Part A* 2010, 95, 79-91.
- [71] B. Ozcelik, K. D. Brown, A. Blencowe, K. Ladewig, G. W. Stevens, J. P. Y. Scheerlinck, K. Abberton, M. Daniell, G. G. Qiao, *Advanced healthcare materials* 2014, 3, 1496-1507.
- [72] E. Wenande, L. Garvey, *Clinical & Experimental Allergy* 2016, 46, 907-922.
- [73] J. Kim, P. H. Kim, S. W. Kim, C. O. Yun, *Biomaterials* 2012, 33, 1838-1850.
- [74] J. S. Suk, Q. Xu, N. Kim, J. Hanes, L. M. Ensign, *Advanced drug delivery reviews* 2016, 99, 28-51.
- [75] W. S. Shim, J. H. Kim, H. Park, K. Kim, I. C. Kwon, D. S. Lee, *Biomaterials* 2006, 27, 5178-5185.
- [76] X. J. Loh, P. Peh, S. Liao, C. Sng, J. Li, *Journal of Controlled Release* 2010, 143, 175-182.
- [77] a) P. Ni, Q. Ding, M. Fan, J. Liao, Z. Qian, J. Luo, X. Li, F. Luo, Z. Yang, Y. Wei, *Biomaterials* 2014, 35, 236-248; b) S. Fu, P. Ni, B. Wang, B. Chu, L. Zheng, F. Luo, J. Luo, Z. Qian, *Biomaterials* 2012, 33, 4801-4809.
- [78] a) B. Yang, C. Gong, Z. Qian, X. Zhao, Z. Li, X. Qi, S. Zhou, Q. Zhong, F. Luo, Y. Wei, *BMC biotechnology* 2010, 10, 65; b) B. Yang, C. Gong, X. Zhao, S. Zhou, Z. Li, X. Qi, Q. Zhong, F. Luo, Z. Qian, *International journal of nanomedicine* 2012, 7, 547; cQ. Wu, N. Wang, T. He, J. Shang, L. Li, L. Song, X. Yang, X. Li, N. Luo, W. Zhang, *Scientific reports* 2015, 5.
- [79] F. Bailey, R. Callard, *Journal of applied polymer science* 1959, 1, 56-62.
- [80] J. Persson, A. Kaul, F. Tjerneld, *Journal of Chromatography B: Biomedical Sciences and Applications* 2000, 743, 115-126.
- [81] G. Wei, H. Xu, P. T. Ding, S. M. Li, J. M. Zheng, *Journal of Controlled Release* 2002, 83, 65-74.
- [82] D. Liu, T. Jiang, W. Cai, J. Chen, H. Zhang, S. Hietala, H. A. Santos, G. Yin, J. Fan, *Advanced healthcare materials* 2016, 5, 1513-1521.
- [83] B. Zhao, D. Li, F. Hua, D. R. Green, *Macromolecules* 2005, 38, 9509-9517.
- [84] S. Aoshima, H. Oda, E. Kobayashi, *Journal of Polymer Science Part A: Polymer Chemistry* 1992, 30, 2407-2413.

- [85] N. K. Pandit, J. Kisaka, *International journal of pharmaceutics* 1996, 145, 129-136.
- [86] F. Hofmeister, *Archiv für experimentelle Pathologie und Pharmakologie* 1888, 24, 247-260.
- [87] B. A. Deyerle, Y. Zhang, *Langmuir* 2011, 27, 9203-9210.
- [88] M. Luzon, C. Boyer, C. Peinado, T. Corrales, M. Whittaker, L. Tao, T. P. Davis, *Journal of Polymer Science Part A: Polymer Chemistry* 2010, 48, 2783-2792.
- [89] O. Sedlacek, B. D. Monnery, S. K. Filippov, R. Hoogenboom, M. Hruby, *Macromolecular rapid communications* 2012, 33, 1648-1662.
- [90] a) W. Seeliger, W. Thier, *Angewandte Chemie International Edition* 1966, 5, 612-617; b) T. Bassiri, A. Levy, M. Litt, *Journal of Polymer Science Part C: Polymer Letters* 1967, 5, 871-879.
- [91] R. Konradi, B. Pidhatika, A. Mühlebach, M. Textor, *Langmuir* 2008, 24, 613-616.
- [92] M. Barz, R. Luxenhofer, R. Zentel, M. J. Vicent, *Polymer Chemistry* 2011, 2, 1900-1918.
- [93] J. S. Park, K. Kataoka, *Macromolecules* 2006, 39, 6622-6630.
- [94] C. R. Becer, R. M. Paulus, S. Höppener, R. Hoogenboom, C. A. Fustin, J. F. Gohy, U. S. Schubert, *Macromolecules* 2008, 41, 5210-5215.
- [95] R. Luxenhofer, G. Sahay, A. Schulz, D. Alakhova, T. K. Bronich, R. Jordan, A. V. Kabanov, *Journal of Controlled Release* 2011, 153, 73-82.
- [96] J. Kronek, Z. Kroneková, J. Lustoň, E. Paulovičová, L. Paulovičová, B. Mendrek, *Journal of Materials Science: Materials in Medicine* 2011, 22, 1725-1734.
- [97] R. Luxenhofer, Y. Han, A. Schulz, J. Tong, Z. He, A. V. Kabanov, R. Jordan, *Macromolecular rapid communications* 2012, 33, 1613-1631.
- [98] P. Chytil, T. Etrych, Č. Koňák, M. Šírová, T. Mrkvan, J. Bouček, B. Řihová, K. Ulbrich, *Journal of Controlled Release* 2008, 127, 121-130.
- [99] Y. Han, Z. He, A. Schulz, T. K. Bronich, R. Jordan, R. Luxenhofer, A. V. Kabanov, *Molecular pharmaceutics* 2012, 9, 2302-2313.
- [100] M. Hruby, S. K. Filippov, J. Panek, M. Novakova, H. Mackova, J. Kucka, K. Ulbrich, *Journal of Controlled Release* 2010, 148, e60-e62.
- [101] R. England, J. Hare, P. Kemmitt, K. Treacher, M. Waring, S. Barry, C. Alexander, M. Ashford, *Polymer Chemistry* 2016, 7, 4609-4617.
- [102] S. Kurzhals, N. Gal, R. Zirbs, E. Reimhult, *Nanoscale* 2017, 9, 2793-2805.
- [103] R. Hoogenboom, *European journal of lipid science and technology* 2011, 113, 59-71.
- [104] K. Kempe, A. Vollrath, H. W. Schaefer, T. G. Poehlmann, C. Biskup, R. Hoogenboom, S. Hornig, U. S. Schubert, *Macromolecular rapid communications* 2010, 31, 1869-1873.
- [105] S. Salzinger, S. Huber, S. Jaksch, P. Busch, R. Jordan, C. M. Papadakis, *Colloid and Polymer Science* 2012, 290, 385-400.

- [106] D. Christova, R. Velichkova, W. Loos, E. J. Goethals, F. Du Prez, *Polymer* 2003, 44, 2255-2261.
- [107] T. B. Bonn , K. L dtke, R. Jordan, P.  t p nek, C. M. Papadakis, *Colloid and Polymer Science* 2004, 282, 833-843.
- [108] a) J. S. Park, K. Kataoka, *Macromolecules* 2007, 40, 3599-3609; b) T. M. Allen, P. R. Cullis, *Science* 2004, 303, 1818-1822.
- [109] M. M. Bloksma, C. Weber, I. Y. Perevyazko, A. Kuse, A. Baumg rtel, A. Vollrath, R. Hoogenboom, U. S. Schubert, *Macromolecules* 2011, 44, 4057-4064.
- [110] C. Diehl, H. Schlaad, *Macromolecular bioscience* 2009, 9, 157-161.
- [111] J. S. Park, Y. Akiyama, Y. Yamasaki, K. Kataoka, *Langmuir* 2007, 23, 138-146.
- [112] R. Obeid, F. Tanaka, F. o. M. Winnik, *Macromolecules* 2009, 42, 5818-5828.
- [113] S. Huber, N. Hutter, R. Jordan, *Colloid and Polymer Science* 2008, 286, 1653-1661.
- [114] H. M. Lambermont-Thijs, R. Hoogenboom, C. A. Fustin, C. Bomal-D'Haese, J. F. Gohy, U. S. Schubert, *Journal of Polymer Science Part A: Polymer Chemistry* 2009, 47, 515-522.

Chapter 11

SMART ANTIMICROBIAL SURFACES

*Alexandra Muñoz-Bonilla** and *Marta Fernández-García†*

Instituto de Ciencia y Tecnología de Polímeros (ICTP-CSIC),
Madrid, Spain

ABSTRACT

Bacterial colonization and biofilm formation on material surfaces is a serious problem in medical devices and, in general, in human healthcare. In recent years, polymeric coatings with inherent antibacterial properties have acquired relevance as a practical alternative to combat biofilm formation. Basically, there are two main types of antimicrobial surfaces, bactericidal and antifouling surfaces, in which each type presents its inherent drawbacks. Thus, many efforts have been made to develop surfaces with both characters, bactericidal and bacteria-resistant properties. Of particular interest results smart antimicrobial surfaces that can reversible switch in response to external stimuli between bactericidal and antifouling character to release dead bacteria attached onto the surfaces. In this chapter, we highlight the recent developments performed on smart surfaces with switchable capacity between biocidal activity and self-cleaning properties in response to stimulus such as pH, temperature, aqueous environment, ionic strength, light and electrical field.

Keywords: biofilm, antimicrobial, responsive surfaces, bactericidal activity, bacteria release

* Corresponding Author Email: sbonilla@ictp.csic.es.

† Corresponding Author Email: marta fg@ictp.csic.es.

INTRODUCTION

Bacterial adhesion on surfaces, which often leads to the subsequent formation of biofilm, is a serious problem in many fields such as medical [1], food industry [2] or even in cosmetics [3]. Microbial surface contamination involves the transmission of infections by contact, which is particularly critical in hospitals. These 'hospital-acquired' infections are a growing problem and a major challenge to beat. Indeed, the majority of the nosocomial infections are related to biofilm formation, which normally exhibits resistance toward conventional antibiotics and is associated with persistent infections. For instance, bacterial infections associated with implanted devices such as catheters and prosthetics cause the most serious postsurgical complications, approximately between 4% and 6% of implants become infected during the early implantation periods. These postsurgical infections often need implant removal and re-implantation because the efficacy of the antibiotics administered systematically is rather low.

Therefore, the development of strategies to prevent or eliminate bacterial contamination and biofilm formation on material surfaces has attracted much attention over the past few decades. Mainly, two general approaches have been explored to avoid the formation of biofilm based on polymer coatings. On one hand, antifouling coatings including poly(ethylene glycol)-based materials, glycopolymers and zwitterionic polymers, which prevent the adhesion of biomolecules such proteins and bacteria [4-6]. Such surfaces can effectively reduce the initial bacterial attachment but only during a short period due to detachment and degradation process. After the adhesion of bacteria onto the surface, these bacteria secrete extracellular matrices and rapidly proliferate leading to the formation of the biofilm. In the second main approach, biocidal agents are incorporated into the materials including antibiotics, nanoparticles (NPs), cationic polymers and antimicrobial peptides [7-11]. The biocidal agent can be either covalently attached or physically incorporated to be released. The antimicrobial agent leaching surfaces can be very efficient even against adherent bacteria but the release of the biocidal is difficult to control, and usually lack for long-term uses; whereas the surfaces with the biocidal compounds covalently tethered to the surface normally require complex synthetic steps and, in some cases, the activity of the agent attached to the surface is reduced [12]. In any case, in bactericidal surfaces, the surface would remain contaminated by the dead bacteria, which diminish the biocidal activity of the surface and also provide a favorable environment for further bacteria attachment and biofilm formation.

Therefore, an ideal antibacterial surface should overcome all these limitations, preventing the initial bacterial adhesion, killing bacteria in case of attachment and finally shedding the dead bacteria to clean the surface and achieve a long-term activity [13, 14]. In recent years, several novel surfaces have been developed with switchable capacity between biocidal activity and self-cleaning properties to release the dead bacteria [15].

These smart antimicrobial surfaces constitute a very promising approach that is attracting a great attention to combat bacterial biofilms. Such surfaces are able to reversibly vary their physicochemical properties in response to external stimuli by changes in their chemistry, molecular conformation and structure; thus, the ability to attach, kill, and release bacteria can be controlled by simply modifying the external conditions. These stimuli can be physical, chemical, or biological, typically include temperature, pH, enzymes, light and ionic strength.

This chapter is focused on the recent development and relevant strategies employed for generation of such smart antimicrobial surfaces and the specific stimuli used to trigger antimicrobial action.

pH-RESPONSIVE SURFACES

The pH is a relevant stimulus for antibacterial coatings. Although, in general the ideal environment for bacterial growth is around neutral pH, variation in the pH is generally implied in many bacterial colonization and biofilm formation. Typically, when biofilm formation occurs the local environment becomes more acidic as a result of the bacterial metabolism [16]. This is critical, for instance, in dental caries. *Streptococcus mutans*, a major oral pathogen, produces acids from the fermentation of food and dramatically decreases the pH; consequently a demineralization of the tooth surface can take place provoking the formation of caries [17].

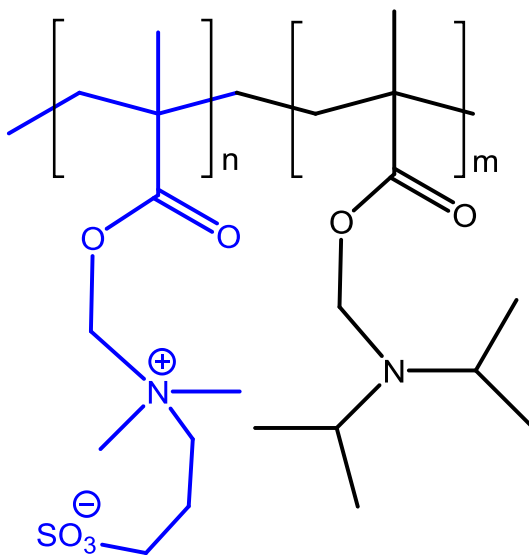
Smart and self-defensive antibacterial coatings based on pH-responsive polymers have been explored taking advantage of this pH variation at the immediate environment. Indeed, it can be said that the bacteria themselves act as external stimulus as their metabolism implies the local pH drop. The decrease of the pH produces changes in the pH-responsive polymers used in such as films that can provoke variations in the surface wettability or even the release of antibiotics. Thus, these smart surfaces may be carefully designed to be able of killing the bacteria in one state and releasing the dead bacteria in the other state.

There are many approaches reported in literature based on controlled-release antibacterial surfaces triggered by acidification of the local environment. However, most of them are studies limited to killing action rather than shedding of dead bacteria [18, 19]. Similarly, other studies are focused on coatings with pH-triggered hydrophobicity, as higher hydrophobicity implies more resistant to colonization [20]. However, antibacterial coatings following a kill and release strategy that also avoid the accumulation of dead bacteria require a most sophisticated design.

For example, polymer films of zwitterionic block copolymer micelles have been developed with the dual function, anti-adhesive and antibacterial agent releasing in response to changes in the pH [21]. The block copolymers, poly[3-dimethyl

(methacryloyloxyethyl) ammonium propane sulfonate-*b*-2-(diisopropylamino)ethyl methacrylate] (β PDMA-*b*-PDPA) (see Scheme 1) self-assembly into micelles in an aqueous environment above pH 6.5 and can be loaded with the antimicrobial agent triclosan. The zwitterionic shell of β PDMA provides anti-adhesive properties to the film, while in acidic conditions the triclosan is released due to the disintegration of the micelles, showing a remarkable antibacterial effect against *Staphylococcus aureus*.

Recently, an antibacterial surface with switchable capability of killing and releasing bacteria has been developed by Chen and co-workers [22]. In this work, nanowire arrays on silicon wafers were first modified with poly(methacrylic acid) (PMAA) by surface-initiated atom transfer radical polymerization (SI-ATRP). PMAA is a pH-responsive polymer with carboxyl groups on its repeat units. In acidic aqueous solution the polymer collapses, whereas at basic conditions the polymer presents high density of negative charges and swells. The PMAA coating was employed as reservoir for the controllable loading and release of a natural antimicrobial lysozyme and also for the bacteria release. At acidic pH the grafted PMAA chains collapse, enabling the loading of lysozyme (see Figure 1). Then, under typical neutral pH, some of the PMAA extend and the loaded lysozyme is released, killing the bacteria attached onto the surface. Subsequently, at basic pH the chains are totally extended and negatively charged to repel the dead bacteria, thus cleaning the surface and allowing the reloading of the antibacterial agent. In addition, the reusability of the surfaces was tested by repeated cycles of loading and releasing of lysozyme, maintaining their killing efficiency above 90%.



Scheme 1. Structure of β PDMA-*b*-PDPA copolymer.

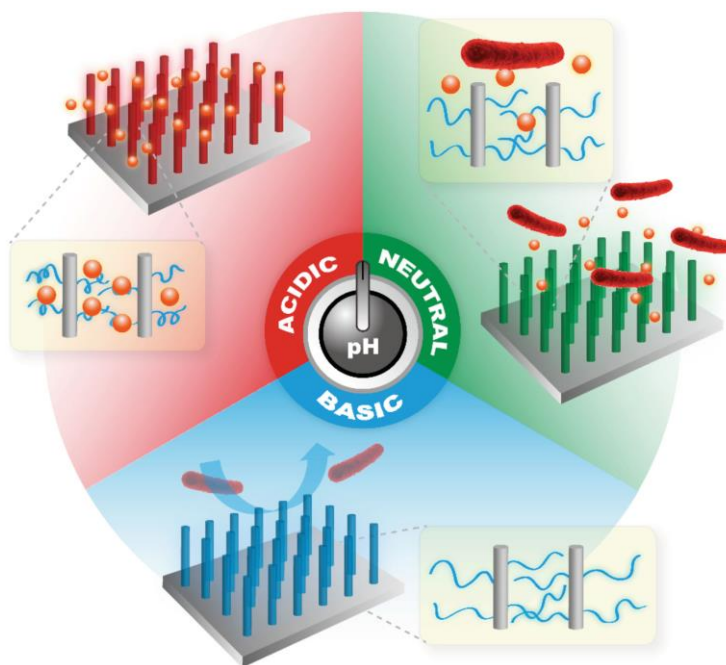


Figure 1. Schematic representation of a smart antibacterial surface with pH-responsive capability of killing and releasing dead bacteria. Reproduced with permission from reference [22]. Copyright 2016 Wiley.

These smart antibacterial films acting by pH-triggered delivery of the antimicrobial agent need to be repeatedly loaded for the renewal of the activity. As an alternative, non-leaching smart surfaces have been also proposed following different strategies. For example, surfaces with hierarchical polymer brush architecture were prepared consisting of an outer layer of pH-responsive PMAA and an inner layer of the antimicrobial peptides [23]. By this way, the PMAA layer resists the initial attachment of bacteria under physiological conditions; and when acidification occurs due to the bacterial colonization, the PMAA chains collapse, and the antimicrobial peptides result exposed for killing the invasive bacteria. Finally, the dead bacteria can be released from the surface when the environmental pH increases and the PMAA chains recover their hydrophobicity. Remarkably, these hierarchical surfaces demonstrated to maintain the antibacterial activity and the low bacterial adhesion after two cycles.

In another non-leaching approach, switchable antimicrobial and antifouling hydrogels were designed to respond by changing the environmental pH [24, 25]. Hydrogels are interesting materials that have been used in many biomedical applications, such as wound dressing, tissue engineering scaffolds and drug delivery systems. In particular, zwitterionic hydrogel based on carboxybetaine was prepared, in which the hydroxyl groups can reversible switch between the zwitterionic form and cationic form (Figure 2).

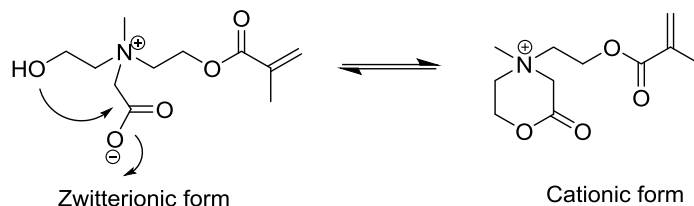


Figure 2. Chemical structures of the monomers based on carboxybetaine with hydroxyl groups able to switch between zwitterionic and cationic lactone forms [24].

Concretely, under acidic environment the hydrogels are in cationic lactone form with antimicrobial ability, able to kill the entrapped bacteria. Then, under neutral or basic conditions the hydrogel converts into zwitterionic form with antifouling properties, thus the dead bacteria can be released from the surface. The hydrogels exhibit significant activity in the cationic form, killing over 99.99996% of *Escherichia coli* K12 attached on the surface while enable the release of ~99.5% of dead bacteria.

Next, this group used a different approach, the combination of monomers with different charge, i.e., positively charged quaternary amine [2-(acryloyloxy)ethyl] trimethyl ammonium chloride (TMA), and negatively-charged carboxylic acid 2-carboxyethyl acrylate (CAA) [26]. At neutral and basic pHs, the copolymer is uncharged giving non-fouling property. When the carboxylic acid group becomes protonated at low pH, the copolymer is positively charged. The adhesion was tested against *Staphylococcus epidermidis* bacteria under flow conditions during 3 h of contact. The number of bacterial cells that adhered to the copolymer brush coated surface showed a 6-fold difference between acidic and neutral pH test conditions, while no significant differences were observed in comparison to the positive bare gold and negative poly(sulfobetaine methacrylate) (PSBMA) controls. PSBMA was selected since it is completely deprotonated within a wide range of pH values.

TEMPERATURE-RESPONSIVE SURFACES

Bacteria infections often lead to an increase of the temperature; thereby this temperature variation is a very useful stimulus to promote the killing action in the antibacterial surfaces. Most of the temperature-responsive antimicrobial surfaces are based on poly(*N*-isopropylacrylamide) (PNIPAAm), which is one of the most widely used thermo-responsive polymers with a lower critical solution temperature (LCST) of approximately 32°C, near the body temperature. In fact, the LCST of PNIPAAm can be adjusted by changing the molecular weight or modifying the hydrophobic/hydrophilic balance, for instance, by copolymerization [27]. These PNIPAAm-based surfaces are able to reversible switch between hydrophobic at higher temperature favoring the adhesion

and the bacteria killing; and hydrophilic a lower temperatures, which facilitates the release of dead bacteria. López's group has developed a series of smart antibacterial surfaces based on PNIPAAm, which display switchable killing and bacteria releasing actions by changing temperature [28-32].

Nanopatterned surfaces consisting of parallel lines of PNIPAAm brushes and antimicrobial quaternary ammonium compounds (QAS) attached between these lines were fabricated by interferometric lithography combined with surface-initiated polymerization (Figure 3a) [28]. Above the LCST of PNIPAAm, the chains collapse permitting the attachment of bacteria, i.e., *E. coli* K12 and simultaneously exposing the QAS for killing function; while at lower temperature, below the LCST, the PNIPAAm chains become hydrophilic and expand; fact that provokes the release of dead bacteria. Figure 3b shows the attachment and detachment of *E. coli* bacteria on these smart surfaces. Similar strategy was followed in another publication but using a sustainable environmentally benign biocide such as the antimicrobial enzyme, lysozyme, instead of QAS [30].

The López's group has also developed multifunctional films with both antimicrobial activity and fouling-release ability employing resonant infrared, matrix-assisted pulsed laser evaporation (RIR-MAPLE) [31, 32], which is a very promising technique based on the deposition of organic thin films by infrared laser ablation of a host emulsion matrix. This technique enables a sequential co-deposition mode, which also allowing the preparation of blend films with a precise control of the concentration component.

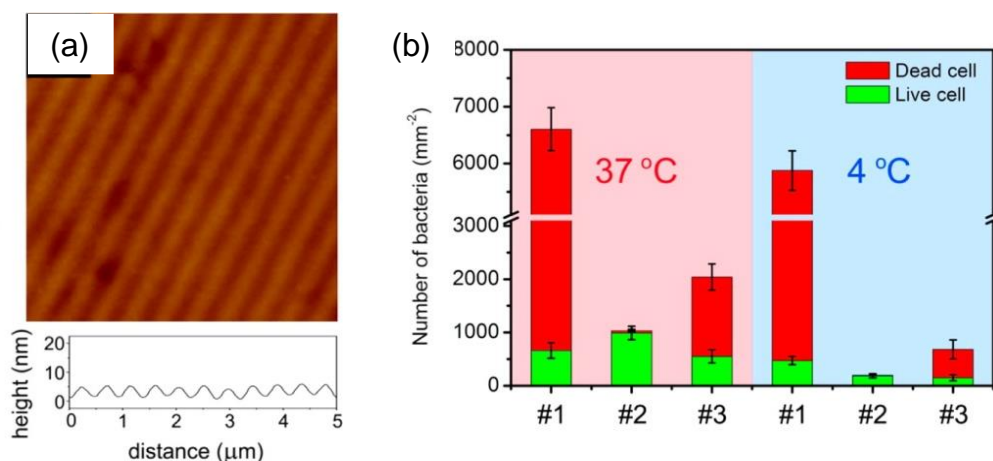


Figure 3. a) AFM image of the nanopatterned surface b) Number of attached *E. coli* bacteria (live and dead) on smart surface (#3) in comparison with films composed only by QAS (#1) and nanopatterned films of PNIPAAm (#2), at different incubation temperatures. Adapted with permission from reference [28]. Copyright 2013 ACS.

Likewise, at 37°C the film promotes bacterial attachment and is able to kill the majority of bacteria, whereas when the temperature decreases the hydration of the PNIPAAm leads to the bacterial detachment. The killing efficiency of PNIPAAm/QAS films [31] was higher than the corresponding nanopatterned films previously described due to the higher surface roughness obtained by RIR-MAPLE. Blends of PNIPAAm with oligo(*p*-phenylene-ethynylene) (OPE) prepared by RIR-MAPLE also exhibited significant results [32]. OPE shows very effective biocidal activity under ultraviolet-A light; however, the accumulation of dead bacteria on the films limits its effectiveness. The preparation of these smart surfaces by RIR-MAPLE overcomes this drawback.

In spite of the significant performance of those smart surfaces, their fabrication requires complex strategies or not very accessible equipment. Other approaches have been explored for the production of smart antibacterial films based on thermo-responsive polymers, for instance by using a one-step photopolymerization method [33]. In this work, silver nanoparticles with biocidal activity were combined with PNIPAAm for the formation of antimicrobial nanocomposite films on glass surfaces previously modified with 3-methacryloxypropyltrimethoxysilane (MPS). The films were synthesized by photopolymerization using the photoinitiator 2,2-dimethoxy-2-phenyl acetophenone (DMPA), which produces free radicals under UV light, initiates the polymerization of NIPAAm and facilitates the synthesis of Ag NPs from silver nitrate (Figure 4).

Similarly, these surfaces were able to respond to changes of the environmental temperature. At 37°C, films assist the attachment of *E. coli* bacteria and their killing by Ag NPs actions, whereas at temperature below the LCST of PNIPAAm the chains swell releasing the dead bacteria. However, the antimicrobial activity at 37°C was not as high as typically found for Ag NPs, may be due their low accessibility of the nanoparticles embedded in the polymer matrix.

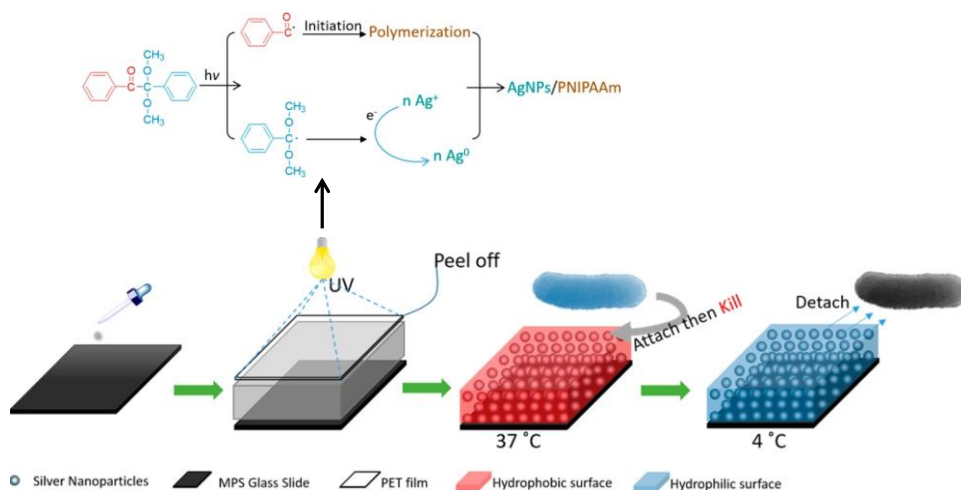


Figure 4. Preparation of smart polymer surfaces by photopolymerization. Adapted with permission from reference [33]. Copyright 2016 ACS.

In another strategy, the brushes of thermoresponsive and bactericidal polymers were attached onto the substrates by host-guest self-assembly approach of β -cyclodextrin (β -CD) and adamantane (Ad) [34]. Adamantane terminated PNIPAAm and the bactericidal poly[2-(methacryloyloxy)ethyl]-trimethylammonium chloride (PMT) were synthesized by ATRP and were assembled onto silicon wafer grafted with β -CD. These surfaces showed switchable antifouling property and bactericidal activity in response to temperature variation. In addition, they demonstrated high stability even upon immersion into a disassembling agent solution, and durability during repeated cycles.

Instead of blending thermoresponsive polymers with antimicrobial agents, another alternative is the preparation of copolymers containing both functions in the same structure. For instance, NIPAAm was copolymerized with the bactericidal quaternary ammonium salts (2-(dimethylamino)-ethyl methacrylate (DMAEMA+)) [35]. Concretely, the copolymer brushes of P(NIPAAm-co-DMAEMA+) were synthesized by surface-initiated reversible addition-fragmentation chain transfer (SI-RAFT) polymerization from polydimethylsiloxane and glass substrates. These coatings switch between two states: hydrophobic and killing at high temperatures and hydrophilic and antifouling at lower temperatures. The surfaces showed bactericidal efficiency against Gram-negative *E. coli* and Gram-positive *S. aureus*, and the reversibly changes between bactericidal and antifouling were examined through four incubation-release cycles against *S. aureus* bacteria. The proportion of dead bacteria in the first deposition was 15.5% and 16.4% of living *S. aureus*. After washing the surface with cold water the percentage decreased to 1.4% and 1.1% for dead and living bacteria, respectively. Similar results were found for the rest of the cycles, which demonstrated that the incorporation of bactericidal quaternary ammonium salts does not impede the antifouling properties of the copolymer brushes. The same research group has prepared antimicrobial coatings based on terpolymer brushed following the same strategy [36]. The terpolymer was a combination of temperature-responsive *N*-vinylcaprolactam (VCL), bactericidal DMAEMA+ and hydrophilic 2-methacryloyloxyethyl phosphorylcholine (MPC) P(VCL-co-DMAEMA+-co-MPC). The use of thermo-responsive VCL improved the biocompatibility in comparison with PNIPAAm-based polymers because VCL does not contain amide derivatives, while the incorporation of the MPC component in the terpolymer coating significantly augmented the antifouling and release properties of the surfaces.

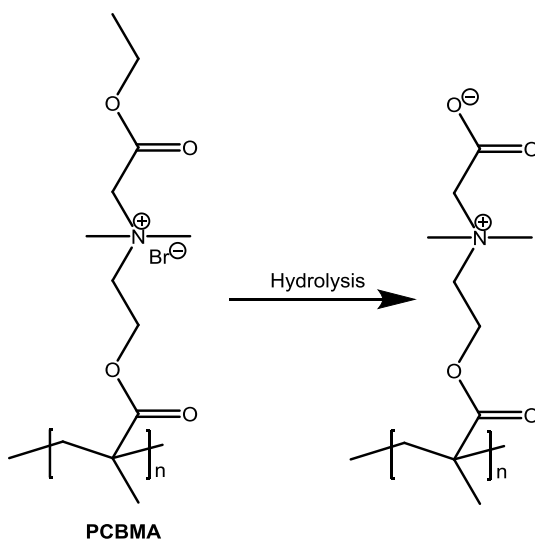
DRY-WET-RESPONSIVE SURFACES

Medical devices can be contaminated in dry state by airborne bacteria before their use in patients, which normally involves an aqueous environment; thus, the antimicrobial materials should be effective also in dry conditions. Smart polymer surfaces have been developed to response to aqueous medium, typically involving hydrolysis reactions.

These surfaces are able to kill bacteria in dry condition (*in vitro*) whereas in aqueous medium (*in vivo*) exert antifouling properties to avoid further attachment of bacteria.

As previously commented, Jiang's group has developed polymer derivatives of zwitterionic carboxybetaine, which can switch between the antimicrobial lactone form and the antifouling zwitterionic form while the intramolecular hydrogen bonds will enhance the mechanical property of the zwitterionic hydrogel [24]. In a posterior approach to obtain polymer surfaces that change from bactericidal to antifouling, this group used poly(*N,N*-dimethyl-*N*-(ethoxycarbonylmethyl)-*N*-[2'-(methacryloyloxy) ethyl]-ammonium bromide) (PCBMA), which was grafted by SI-ATRP onto a gold surface [37]. This cationic antimicrobial polymer was able to kill more than 99.9% of *E. coli* K12 bacteria in 1 h, and can be hydrolyzed to form the antifouling zwitterionic polymer able to release 98% of the dead bacterial cells (see Scheme 2). However, this system was not able to provide reversibility, which is a great disadvantage. To overcome this fact, they developed a smart polymer capable of repeatedly switches between antimicrobial and antifouling forms [38].

This new system is based on previously described system, which is able to switch between zwitterionic and cationic lactone forms. When the surface is coated with the morpholinone-based polymer, PCB-ring, is able to kill over 99.9% of *E. coli* K12 attached on it under dry conditions. While in neutral or basic aqueous environments, PCB-ring is hydrolyzed to zwitterionic carboxybetaine-based polymer, PCB-OH, and immediately the surface releases dead bacteria and at the same time resists bacteria adhesion in the aqueous media. PCB-OH can be back to PCB-ring under weak acid conditions, thereby regenerating the killing function (see Figure 5).



Scheme 2. Chemical structures of antimicrobial cationic PCBMA and its resulting zwitterionic polymer after hydrolysis.

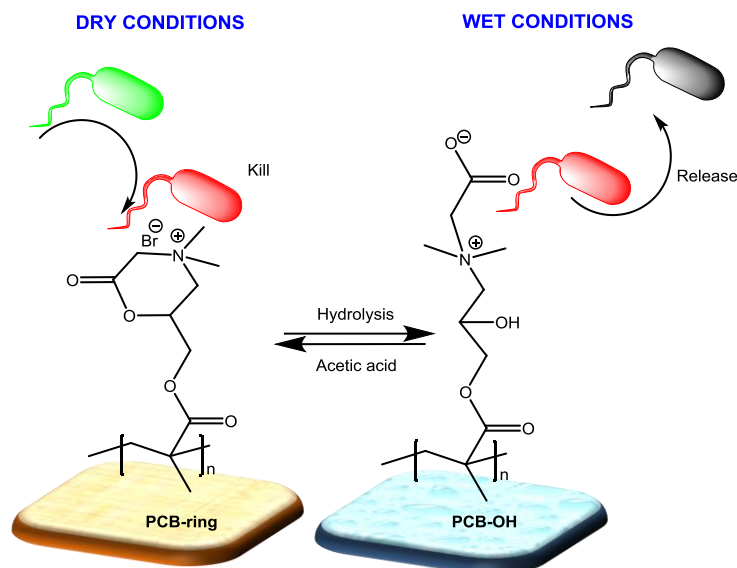


Figure 5. Smart surface based on antimicrobial cationic *N,N*-dimethyl-2-morpholinone-based polymer (PCB-ring) and the zwitterionic carboxybetaine-based polymer (PCB-OH).

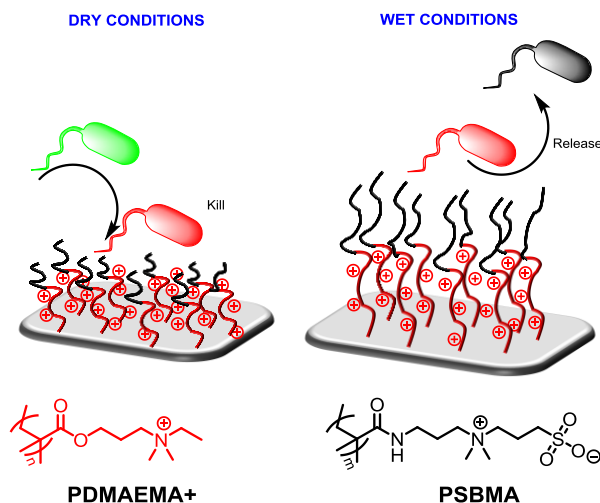


Figure 6. Smart surface based on antimicrobial and antifouling block copolymer.

Very recently, Yang et al. [39] have proposed a surface-initiated photoiniferter-mediated polymerization (SI-PIMP) strategy to construct a hierarchical antibacterial surface consisting of a zwitterionic outer layer and a polycationic bactericidal background layer (see Figure 6). This zwitterionic outer layer does not affect the antibacterial efficiency of antimicrobial layer in dry conditions, but allows the release of dead bacteria in aqueous environment as well as protects from the attachment of planktonic bacteria. More importantly, this layer physically impedes the contact of the

mammalian cells with the cationic groups, thus moderating the toxicity of polycationic surfaces in wet conditions. The silane-terminated iniferted was anchored to a silicon substrate from which a block copolymer was obtained. In a first step, DMAEMA monomer was polymerized and then extended with 3-((3-methacrylamidopropyl)dimethylammonio)propane-1-sulfonate (SBMA) monomer and finally, quaternized with 1-bromoethane. The killing efficiencies of the resulting surface in dry conditions against *S. aureus* and *E. coli* bacteria were ~80.5% and ~77.2%, respectively. This means that there are remaining colonies that can be irreversible attached to the surface, replicate, and form biofilm. However, this surface under wet conditions was capable of easily release the bacteria due to the presence of PSBMA segments in the copolymer.

IONIC-STRENGTH-RESPONSIVE SURFACES

Polyelectrolytes attached to surfaces can response to variation in the ionic strength. In electrolyte solutions with high ionic strength conditions, the charges of the pendant groups in the polymer chains are separated, and the decrease of electrostatic repulsions leads to collapsed conformations, whereas in low ionic strength conditions the brushes remain extended [40]. In addition, the type of counterions and the interactions between polyelectrolytes and counterions offer possibility to modulate the wettability of surfaces and then, the antifouling properties. Huang et al. [41] have developed a special strategy to release bacteria from bactericidal surfaces *via* clicking kosmotropic counterions into cationic polyelectrolyte brushes for reversible switching of surface functions between killing and release of bacteria. They grafted *via* SI-ATRP bactericidal poly((trimethylamino)ethyl methacrylate chloride) (PTMAEMA) brushes to gold thermal-deposited onto glass slide surface. Afterwards, the surfaces were tested against Gram-positive *S. epidermidis* and Gram-negative *E. coli*, and *Stenotrophomonas maltophilia* bacteria. Subsequently, the samples were placed in NaCl, MgSO₄, sodium citrate and sodium hexametaphosphate (PP) solutions to release dead bacteria. Among all, the kosmotropic PP⁶⁻ anion effectively repels adsorbed bacteria to a release rate of more than 93% (see Figure 7), due to conformational changes, strong hydration and electrostatic repulsion. However, the rate gradually decreases after five killing/release cycles.

In a recent work, brushes of poly(1-(2-methacryloyloxyhexyl)-3-methylimidazolium bromide) PIL(Br) were grafted to commercial polydimethylsiloxane (PDMS) surface *via* visible light-induced polymerization at room temperature [42]. Lithium bis(trifluoromethanesulfonyl) amide (Tf₂N) was used as counteranion exchanger, that provokes a change in the wettability of the surface from hydrophilic to hydrophobic. Before the anion exchange, the PIL(Br) chains are in an extended conformation showing bactericidal activity, while the PIL(Tf₂N) brushes adopt a collapsed conformation leading

to the release of dead bacteria. In this scenario, the switchability between killing and release bacteria was maintained over three cycles.

Chen et al. [43] have prepared brushes of poly(3-(1-(4-vinylbenzyl)-1H-imidazol-3-ium-3-yl) propane-1-sulfonate) (PVBIPS) *via* SI-ATRP onto gold surface, which can be switched reversibly and repeatedly between protein capture/release of Gram-negative *Pseudomona aeruginosa* and *S. epidermidis* bacteria. They controlled the surface wettability but not the killing effect. In a posterior improvement, they combined antimicrobial triclosan covalently attached to PVBIPS brushes through the reaction between phenolic hydroxyl groups and sulfonic groups [44]. The live/dead assay for PVBIPS and PVBIPS-g-triclosan showed that these surfaces exhibit excellent bacteria release capability (see Figure 8) ~99% for each bacteria. However, PDVBIPS surface did not show bactericidal activity, opposite to the surface with PVBIPS-g-triclosan, which was able to kill ~97% and ~95% of attached *E. coli* and *S. aureus*, respectively. Both properties were preserved after three cycles.

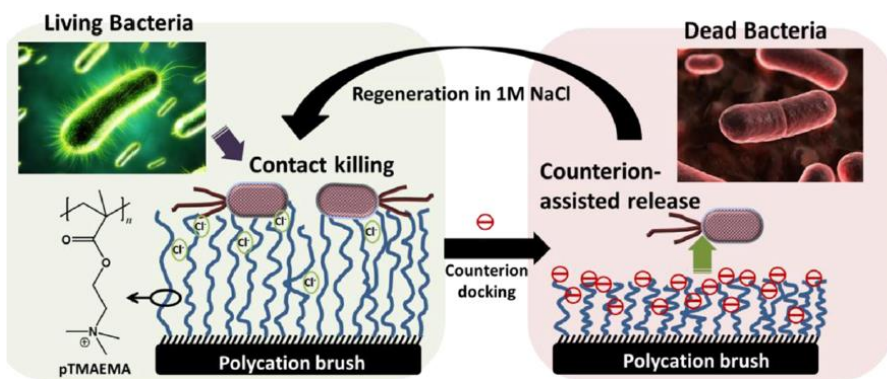


Figure 7. Schematic illustration of contact killing and counterion-assisted release of bacteria on antimicrobial surfaces. Adapted with permission from reference [41]. Copyright 2015 ACS.

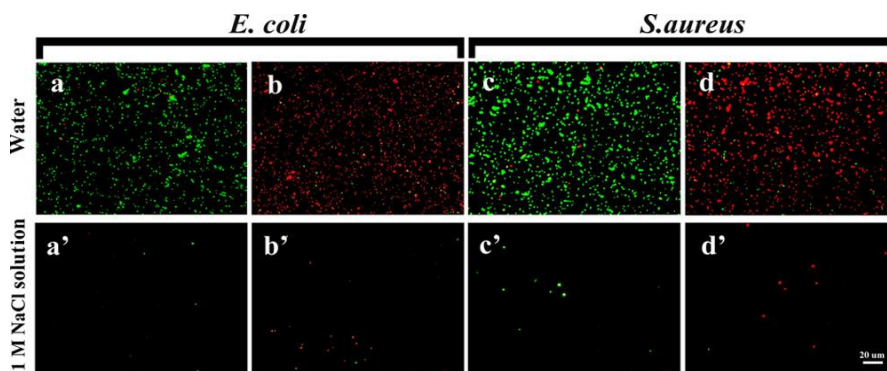


Figure 8. Representative fluorescence microscopy images of bacteria attachment on (a, a', c, c') PVBIPS and (b, b', d, d') PVBIPS-g-triclosan before and after the treatment of 1 M NaCl solution (green staining represents live bacteria, and red staining represents dead bacteria). Adapted with permission from reference [44]. Copyright 2015 ACS.

PHOTO-RESPONSIVE SURFACES

Smart surfaces based on external stimuli such as temperature, pH or ionic strength; do not often reach the equilibrium in a rapid manner. In addition, it is difficult to focus the stimuli and the spatial control of applying. Photo-responsive surfaces can overtake these aspects. The light can be focused even on a submicron-sized area and the reaction of photo-activation typically proceeds rapidly. Besides, light is noninvasive and can be suitable for biological systems.

For the preparation of photo-responsive smart surfaces with reversible switching properties, the photoreaction used has to be also reversible. In this sense, photoswitchable molecules such as azo-compounds and spiroopyran in which their properties changes reversibly are preferred for this applications [45, 46]. Recently, antimicrobial surfaces with the capability of reversible switching between bactericidal and antifouling character were developed involving photoswitchable molecules [47, 48]. In these publications, the switchability also implies host-guest interactions based on supramolecular chemistry.[34, 49] In a first publication, Chen and coworkers [47] prepared systems able to photo-reversible capture and release bacteria. These systems were based on surfaces containing azobenzene groups as guest and β -cyclodextrin-mannose conjugates (CD-M) as host. The azo groups in *trans* configuration immobilize the CD-M molecules by forming host-guest inclusion complexes. These surfaces showed capacity to specifically catch 1-fimbriated bacteria due to the mannose units located at the CDs, which exhibit an enhanced performance due to the glycocluster effect.[50] Then, the azo groups photoisomerize under irradiation with UV light to *cis* form, which results in the dissociation of the complex and the release of the captured bacteria.

This group has extended this approach to fabricate surfaces with photoswitchable bactericidal activity and bacteria-releasing ability [48]. In a similar way, they developed systems composed of surfaces bearing azobenzene groups as guest and, in this case, the β -cyclodextrin was conjugated with seven quaternary ammonium salt groups (CD-QAS) leading a biocidal derivative. Similarly, the azo groups in *trans* form were able to immobilize the biocidal CD-QAS molecules by forming host-guest inclusion complexes (see Figure 9).

These surfaces exhibited significant bactericidal activity with killing efficiencies higher than 90% against *E. coli* bacteria. Subsequently, upon irradiation with UV light (365 nm), the azobenzene groups was transformed to *cis* form, which resulted in the dissociation of the inclusion complex and thereby, the release of dead bacteria attached onto the surfaces. The surface can be regenerated for its reuse, by irradiation with visible light (450 nm) and addition of new CD-QAS compounds.

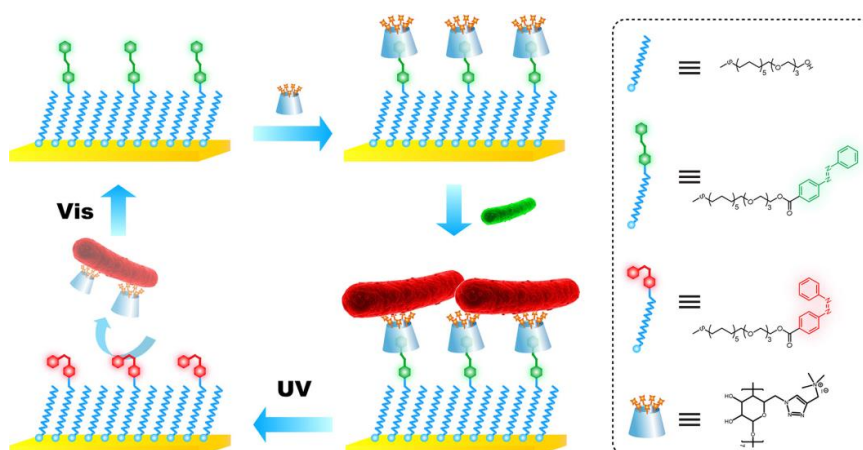


Figure 9. Scheme of the antibacterial surfaces with photoswitchable bactericidal activity and bacteria-releasing ability. Reproduced with permission from reference [48]. Copyright 2017 ACS.

ELECTRO-RESPONSIVE SURFACES

The application of electrical field is also a convenient stimulus for the fabrication of antimicrobial smart surfaces. Similarly to light irradiation, the response to a changing electric field takes place quickly in comparison with chemically induced changes. In particular, smart surfaces based on conjugated conductive polymers could be promising candidates, for instance, in bioelectronics applications, in which the surface requires to be clean with the purpose of reducing infections and maintaining the performance of the device, i.e., the conductivity and activity. Cao et al. [51] have designed a surface based on a conductive zwitterionic poly(sulfobetaine-3,4-ethylenedioxythiophene) (PSBEDOT) (see Figure 10), which also exhibits switchable antimicrobial-antifouling properties.

The polymeric films were obtained by electropolymerization in aqueous solution onto different substrates, indium tin oxide coated polyethylene terephthalate (ITO-PET) substrate and gold coated surface plasmon resonance (SPR) sensor chips. The antifouling properties of the prepared surfaces were first evaluated by testing the adsorption of proteins, bovine aorta endothelial cells and mouse NIH 3T3 fibroblast cells. The conductive coating demonstrated to resist non-specific protein and cell attachment. Then, switchable capability between antifouling and antimicrobial was studied under different potentials against *E. coli* K12 as model bacteria. In the oxidized state (0.6 V), PSBEDOT becomes positively charged, showing antibacterial action able to kill over 89% of attached cells. Whereas in the reduced state (0 V) PSBEDOT is in its zwitterionic form, the surface resists the attachment of high concentration of bacteria, and can release more than 96.7% of the dead bacteria in 1 h. Therefore, this study demonstrated the potential of electro-responsive conductive surfaces with antimicrobial properties for diverse bioelectronic applications.

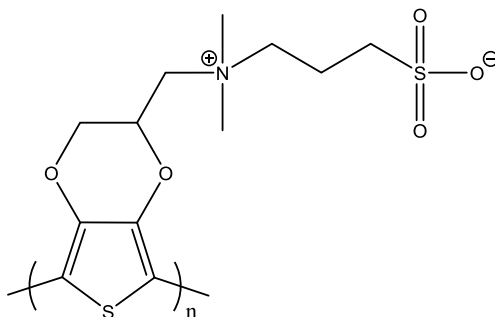


Figure 10. Chemical structure of zwitterionic poly(sulfobetaine-3,4-ethylenedioxythiophene) (PSBEDOT) used in electro-responsive surfaces [51].

CONCLUSION

Over the past few years, several smart antimicrobial surfaces have been developed with switchable capacity of killing and releasing bacteria in response to external stimuli. These surfaces combine the biocidal activity and the bacteria-release capability that confers self-cleaning properties to achieve a long-term activity. Those facts suppose a great advance compared with conventional antibacterial surfaces. Although considerable progress has been done, and significant results have been obtained, many challenges are still remained. Many efforts need to be put in the influence of the micro- and nano-topography, which could help to improve the performance of the surfaces. Besides, the real biological environment is complex and synthetic surfaces need other specific properties, such as hemocompatibility for blood-contacting devices or enhanced osteoblast adhesion for orthopedic implants. In fact, *in vivo* investigations are required also to study the toxicological effect and biocompatibility of these surfaces.

ACKNOWLEDGMENTS

Authors want to acknowledge the financial supported (Project MAT2016-78437-R) by the MINECO, the Agencia Estatal de Investigación (AEI, Spain) and Fondo Europeo de Desarrollo Regional (FEDER, EU).

REFERENCES

- [1] Francolini I, Donelli G. Prevention and control of biofilm-based medical-device-related infections. *FEMS Immunology & Medical Microbiology* 2010;59:227-38.

- [2] Srey S, Jahid IK, Ha S-D. Biofilm formation in food industries: A food safety concern. *Food Control* 2013;31:572-85.
- [3] Giacomel CB, Dartora G, Diefethaeler HS, Haas SE. Investigation on the use of expired make-up and microbiological contamination of mascaras. *International Journal of Cosmetic Science* 2013;35:375-80.
- [4] Mi L, Jiang S. Integrated Antimicrobial and Nonfouling Zwitterionic Polymers. *Angewandte Chemie International Edition* 2014;53:1746-54.
- [5] Yang WJ, Neoh K-G, Kang E-T, Teo SL-M, Rittschof D. Polymer brush coatings for combating marine biofouling. *Progress in Polymer Science* 2014;39:1017-42.
- [6] Campoccia D, Montanaro L, Arciola CR. A review of the biomaterials technologies for infection-resistant surfaces. *Biomaterials* 2013;34:8533-54.
- [7] Alvarez-Paino M, Juan-Rodríguez R, Cuervo-Rodríguez R, Tejero R, López D, López-Fabal F, et al. Antimicrobial films obtained from latex particles functionalized with quaternized block copolymers. *Colloids and Surfaces B: Biointerfaces* 2016;140:94-103.
- [8] Alvarez-Paino M, Bonilla P, Cuervo-Rodríguez R, López-Fabal F, Gómez-Garcés JL, Muñoz-Bonilla A, et al. Antimicrobial surfaces obtained from blends of block copolymers synthesized by simultaneous ATRP and click chemistry reactions. *European Polymer Journal* 2017;93:53-62.
- [9] Costa F, Carvalho IF, Montelaro RC, Gomes P, Martins MCL. Covalent immobilization of antimicrobial peptides (AMPs) onto biomaterial surfaces. *Acta Biomaterialia* 2011;7:1431-40.
- [10] Jo YK, Seo JH, Choi B-H, Kim BJ, Shin HH, Hwang BH, et al. Surface-Independent Antibacterial Coating Using Silver Nanoparticle-Generating Engineered Mussel Glue. *ACS Applied Materials & Interfaces* 2014;6:20242-53.
- [11] Wo Y, Xu L-C, Li Z, Matzger AJ, Meyerhoff ME, Siedlecki CA. Antimicrobial nitric oxide releasing surfaces based on S-nitroso-N-acetylpenicillamine impregnated polymers combined with submicron-textured surface topography. *Biomater Sci* 2017;5:1265-78.
- [12] Li Y, Wei S, Wu J, Jasensky J, Xi C, Li H, et al. Effects of Peptide Immobilization Sites on the Structure and Activity of Surface-Tethered Antimicrobial Peptides. *The Journal of Physical Chemistry C* 2015;119:7146-55.
- [13] Yu Q, Wu Z, Chen H. Dual-function antibacterial surfaces for biomedical applications. *Acta Biomaterialia* 2015;16:1-13.
- [14] Salwiczek M, Qu Y, Gardiner J, Strugnell RA, Lithgow T, McLean KM, et al. Emerging rules for effective antimicrobial coatings. *Trends in Biotechnology* 2014;32:82-90.
- [15] Cavallaro A, Taheri S, Vasilev K. Responsive and “smart” antibacterial surfaces: Common approaches and new developments (Review). *Biointerphases* 2014;9:029005.

- [16] Lee H-S, Dastgheyb SS, Hickok NJ, Eckmann DM, Composto RJ. Targeted Release of Tobramycin from a pH-Responsive Grafted Bilayer Challenged with *S. aureus*. *Biomacromolecules* 2015;16:650-9.
- [17] Li L, He J, Eckert R, Yarbrough D, Lux R, Anderson M, et al. Design and Characterization of an Acid-Activated Antimicrobial Peptide. *Chemical Biology & Drug Design* 2010;75:127-32.
- [18] Zhuk I, Jariwala F, Attygalle AB, Wu Y, Libera MR, Sukhishvili SA. Self-Defensive Layer-by-Layer Films with Bacteria-Triggered Antibiotic Release. *ACS nano* 2014;8:7733-45.
- [19] Wang B, Liu H, Wang Z, Shi S, Nan K, Xu Q, et al. A self-defensive antibacterial coating acting through the bacteria-triggered release of a hydrophobic antibiotic from layer-by-layer films. *Journal of Materials Chemistry B* 2017;5:1498-506.
- [20] Lu Y, Wu Y, Liang J, Libera MR, Sukhishvili SA. Self-defensive antibacterial layer-by-layer hydrogel coatings with pH-triggered hydrophobicity. *Biomaterials* 2015;45:64-71.
- [21] Onat B, Bütün V, Banerjee S, Erel-Goktepe I. Bacterial anti-adhesive and pH-induced antibacterial agent releasing ultra-thin films of zwitterionic copolymer micelles. *Acta Biomaterialia* 2016;40:293-309.
- [22] Wei T, Yu Q, Zhan W, Chen H. A Smart Antibacterial Surface for the On-Demand Killing and Releasing of Bacteria. *Advanced Healthcare Materials* 2016;5:449-56.
- [23] Yan S, Shi H, Song L, Wang X, Liu L, Luan S, et al. Nonleaching Bacteria-Responsive Antibacterial Surface Based on a Unique Hierarchical Architecture. *ACS Applied Materials & Interfaces* 2016;8:24471-81.
- [24] Cao B, Tang Q, Li L, Humble J, Wu H, Liu L, et al. Switchable Antimicrobial and Antifouling Hydrogels with Enhanced Mechanical Properties. *Advanced Healthcare Materials* 2013;2:1096-102.
- [25] Cao Z, Brault N, Xue H, Keefe A, Jiang S. Manipulating Sticky and Non-Sticky Properties in a Single Material. *Angewandte Chemie International Edition* 2011;50:6102-4.
- [26] Mi L, Bernards MT, Cheng G, Yu Q, Jiang S. pH responsive properties of non-fouling mixed-charge polymer brushes based on quaternary amine and carboxylic acid monomers. *Biomaterials* 2010;31:2919-25.
- [27] Schild HG. Poly(N-isopropylacrylamide): experiment, theory and application. *Progress in Polymer Science* 1992;17:163-249.
- [28] Yu Q, Cho J, Shivapooja P, Ista LK, López GP. Nanopatterned Smart Polymer Surfaces for Controlled Attachment, Killing, and Release of Bacteria. *ACS Applied Materials & Interfaces* 2013;5:9295-304.
- [29] Yu Q, Shivapooja P, Johnson LM, Tizazu G, Leggett GJ, López GP. Nanopatterned polymer brushes as switchable bioactive interfaces. *Nanoscale* 2013;5:3632.

- [30] Yu Q, Ista LK, López GP. Nanopatterned antimicrobial enzymatic surfaces combining biocidal and fouling release properties. *Nanoscale* 2014;6:4750-7.
- [31] Yu Q, Ge W, Atewologun A, López GP, Stiff-Roberts AD. RIR-MAPLE deposition of multifunctional films combining biocidal and fouling release properties. *J Mater Chem B* 2014;2:4371-8.
- [32] Yu Q, Ge W, Atewologun A, Stiff-Roberts AD, López GP. Antimicrobial and bacteria-releasing multifunctional surfaces: Oligo (p-phenylene-ethynylene)/poly (N-isopropylacrylamide) films deposited by RIR-MAPLE. *Colloids and Surfaces B: Biointerfaces* 2015;126:328-34.
- [33] Yang H, Li G, Stansbury JW, Zhu X, Wang X, Nie J. Smart Antibacterial Surface Made by Photopolymerization. *ACS Applied Materials & Interfaces* 2016;8:28047-54.
- [34] Shi Z-Q, Cai Y-T, Deng J, Zhao W-F, Zhao C-S. Host-Guest Self-Assembly Toward Reversible Thermoresponsive Switching for Bacteria Killing and Detachment. *ACS Applied Materials & Interfaces* 2016;8:23523-32.
- [35] Wang B, Xu Q, Ye Z, Liu H, Lin Q, Nan K, et al. Copolymer Brushes with Temperature-Triggered, Reversibly Switchable Bactericidal and Antifouling Properties for Biomaterial Surfaces. *ACS Applied Materials & Interfaces* 2016;8:27207-17.
- [36] Wang B, Ye Z, Xu Q, Liu H, Lin Q, Chen H, et al. Construction of a temperature-responsive terpolymer coating with recyclable bactericidal and self-cleaning antimicrobial properties. *Biomater Sci* 2016;4:1731-41.
- [37] Cheng G, Xue H, Zhang Z, Chen S, Jiang S. A Switchable Biocompatible Polymer Surface with Self-Sterilizing and Nonfouling Capabilities. *Angewandte Chemie International Edition* 2008;47:8831-4.
- [38] Cao Z, Mi L, Mendiola J, Ella-Menye J-R, Zhang L, Xue H, et al. Reversibly Switching the Function of a Surface between Attacking and Defending against Bacteria. *Angewandte Chemie International Edition* 2012;51:2602-5.
- [39] Yan S, Luan S, Shi H, Xu X, Zhang J, Yuan S, et al. Hierarchical Polymer Brushes with Dominant Antibacterial Mechanisms Switching from Bactericidal to Bacteria Repellent. *Biomacromolecules* 2016;17:1696-704.
- [40] Moya S, Azzaroni O, Farhan T, Osborne VL, Huck WTS. Locking and Unlocking of Polyelectrolyte Brushes: Toward the Fabrication of Chemically Controlled Nanoactuators. *Angewandte Chemie International Edition* 2005;44:4578-81.
- [41] Huang C-J, Chen Y-S, Chang Y. Counterion-Activated Nanoactuator: Reversibly Switchable Killing/Releasing Bacteria on Polycation Brushes. *ACS Applied Materials & Interfaces* 2015;7:2415-23.
- [42] Dong Y-S, Xiong X-H, Lu X-W, Wu Z-Q, Chen H. Antibacterial surfaces based on poly(cationic liquid) brushes: switchability between killing and releasing via anion counterion switching. *J Mater Chem B* 2016;4:6111-6.

- [43] Chen H, Yang J, Xiao S, Hu R, Bhaway SM, Vogt BD, et al. Salt-responsive polyzwitterionic materials for surface regeneration between switchable fouling and antifouling properties. *Acta Biomaterialia* 2016;40:62-9.
- [44] Wu B, Zhang L, Huang L, Xiao S, Yang Y, Zhong M, et al. Salt-Induced Regenerative Surface for Bacteria Killing and Release. *Langmuir* 2017;33:7160-8.
- [45] He D, Arisaka Y, Masuda K, Yamamoto M, Takeda N. A photoresponsive soft interface reversibly controls wettability and cell adhesion by conformational changes in a spiropyran-conjugated amphiphilic block copolymer. *Acta Biomaterialia* 2017;51:101-11.
- [46] Russev M-M, Hecht S. Photoswitches: From Molecules to Materials. *Advanced Materials* 2010;22:3348-60.
- [47] Zhan W, Wei T, Cao L, Hu C, Qu Y, Yu Q, et al. Supramolecular Platform with Switchable Multivalent Affinity: Photo-Reversible Capture and Release of Bacteria. *ACS Applied Materials & Interfaces* 2017;9:3505-13.
- [48] Wei T, Zhan W, Yu Q, Chen H. Smart Biointerface with Photoswitched Functions between Bactericidal Activity and Bacteria-Releasing Ability. *ACS Applied Materials & Interfaces* 2017;9:25767-74.
- [49] Wei T, Zhan W, Cao L, Hu C, Qu Y, Yu Q, et al. Multifunctional and Regenerable Antibacterial Surfaces Fabricated by a Universal Strategy. *ACS Applied Materials & Interfaces* 2016;8:30048-57.
- [50] Lundquist JJ, Toone EJ. The Cluster Glycoside Effect. *Chemical Reviews* 2002;102:555-78.
- [51] Cao B, Lee C-J, Zeng Z, Cheng F, Xu F, Cong H, et al. Electroactive poly(sulfobetaine-3,4-ethylenedioxythiophene) (PSBEDOT) with controllable antifouling and antimicrobial properties. *Chemical Science* 2016;7:1976-81.

Chapter 12

POLYMERS FOR SMART PACKAGING SOLUTIONS

Marco Monti and Marta Zaccone*

Proplast, Rivalta Scrivia, AL, Italy

ABSTRACT

In the last years, smart (or intelligent) packaging has been one of the most promising technologies in the food packaging industry. In fact, the possibility of making people aware of the safety and the quality of the food they are going to eat, has a huge potential impact in terms of both health of the consumer and reduction of food waste. In this field, many technical opportunities have been developed, based on a physical or a chemical reaction that results in a visible change of color which communicates to the consumer the change in the food quality. Being some of the most used materials in food packaging, polymers have often a main role also in the smart solutions, also thanks to their versatility and the possibility to be modified and tailored to obtain the expected features. This chapter represents a brief overview of the smart packaging solutions related to the polymer world.

Keywords: smart packaging, nanotechnology, nanoparticles, food, beverage

INTRODUCTION

In the last decades, the goal of preserving the quality of food as long as possible has been one of the main issue of the food industry. This topic, apart from the obvious daily advantage of avoiding food and money waste of each family, has had a more relevant effect in decreasing the general waste of food due to its degradation. In fact, as reported

* Corresponding Author Email: marco.monti@proplast.it.

by the study of Food and Agriculture Organization (FAO) of the United Nations presented in 2011 [1], approximately one-third of the edible parts of food produced for human consumption, is lost or wasted throughout the supply chain, from initial agricultural production to the final household consumption. This data are even more impressive paying attention to the fact that, in industrialized countries, more than 40% of the food loss occurs at retail and consumer levels (Figure 1), and this is mainly due to the fact that people throw away food because it is spoiled or beyond its expiry date.

The technical approach for extending the shelf life of food has been traditionally working on the development of increasingly higher gas barrier films and materials. Indeed, this solution hinders the gases which are detrimental for the food preservation to get in contact with the food itself. In the last decade, the development of packaging solutions, which can actively interact with both the food itself and the atmosphere around it, has brought for instance to oxygen or ethylene scavenging materials or antimicrobial solutions. This has led to very interesting solutions that can make the shelf life of the packed food longer. This is the so-called *active* packaging.

In the last years, a new opportunity for food packaging has become of great interest, starting from the simple consideration that the packaging is by definition physically in between the food and the consumer. Taking advantage of this position, it can directly interact both with the food and the consumer, collecting information from the food itself and making it available to the person who wants to consume it. Information that the packaging can collect and that may be of interest for the consumer can be for instance about the freshness and the quality of a perishable product or the temperature of beverage that is supposed to be served hot, rather than the thermal history of one food whose cold chain is important. In other words, the packaging *communicates* to the consumer information regarding what he or she is going to eat or drink. In this case, we can refer to as *smart* (or *intelligent*) packaging [2].

An example of smart packaging is reported in Figure 2, where an indicator changes its colour as the level of maturity of the packed fruit increases [3].

Although the smart packaging technologies have strong advantages, it is worth noting that they are still in a development phase and not fully commercially available. The reason can be found on the one hand in a lack of industrially accessible technologies that is still present, despite the overwhelming outcomes reported in the scientific literature. On the other hand, food packaging products suffer the fact that the consumers never think in buying *them*, because they are just buying their content (i.e., the food or the beverage): therefore, in the food packaging industry the cost is an issue more than in the other industrial sectors. As a consequence, the smart packaging solutions represent an additional cost that often the food industries are not ready to accept.

In this chapter, we report a brief review of scientific and technical solutions that have been developed in the field of the polymer-based smart packaging technologies.

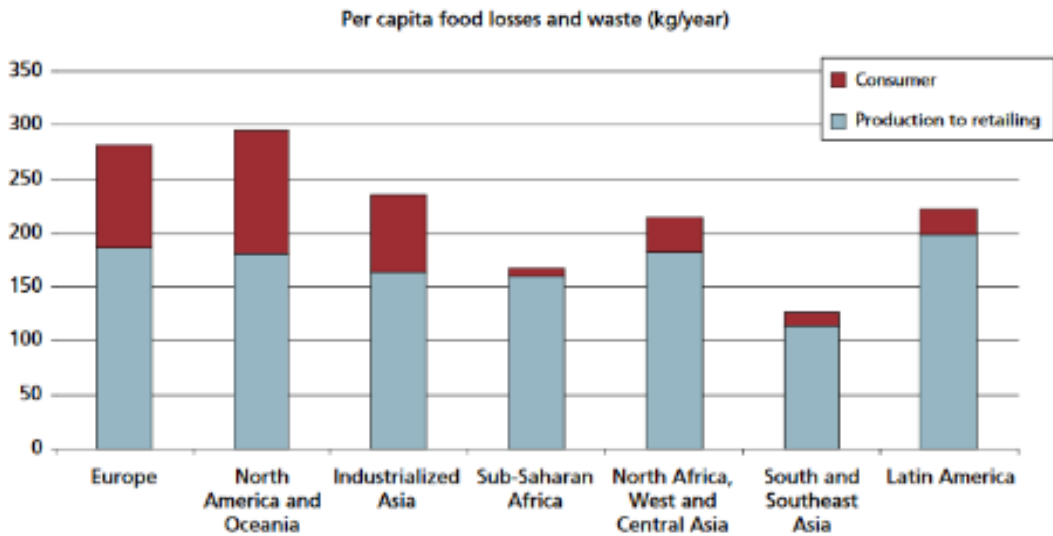


Figure 1. Per capita waste and food losses, at consumption and pre-consumption stages, in different regions [1].



Figure 2. Example of smart packaging [3].

TIME-TEMPERATURE INDICATORS (TTI)

The first attempts in developing smart packaging solutions date back to 90s [4], and have been about the so-called *time-temperature indicators* (TTI). They have the aim of supplying information about the thermal history of the packed food, in order to give precise information regarding the real preservation state. In fact, the expiry date reported on the packaging of the food refers to an estimation calculated considering a correct conservation. If, for some reason, this cannot be guaranteed, the food can deteriorate earlier than predicted, with the danger of being eaten by the consumer with a detrimental effect on his or her health. Moreover, several food products need to follow a strict cold chain logistics from the production to the delivery to the consumer's kitchen, for

preserving the high quality and being healthy. In these cases, a TTI can be helpful. In general, for safety reasons, the consumers need to be aware whether the food they are going to eat has been heated above or cooled below a temperature that is critical for the food itself, with the potential survival of microorganisms and protein denaturation [5, 6]. As an example, it is well known how detrimental could be for the food undergoing frequent freezing and defrosting cycles.

From the technical point of view, these systems can be manufactured following two different approaches. A first method consists in utilizing the migration across a porous material of a colorant/pigment, whose kinetics is biased by the temperature and connected to the time from the packing phase. A second technique uses as indicator a chemical reaction, which produces a change in colour and is led by either chemical substances produced by the food, or by the oxygen, in case it is not supposed to be there. In general, the working mechanism of a TTI is based on mechanical, chemical, enzymatic or microbiological irreversible changes, which result in a visible response in the form of a mechanical deformation, colour development or colour movement [2].

In the literature, several studies report the development of systems that can act as a TTI [5]. Lee et al. [7] reported the results of a study about the development of an oxygen indicator based on a colorimetric UV-activation, using titania nanoparticles. These nanoparticles photosensitize the reduction of methylene blue by triethanolamine in a polymer encapsulation medium, using UVA light. When the indicator is UV irradiated, it whitens and remains in this colourless state in the dark, until it is exposed to oxygen. After this exposure, its original colour is re-established. The authors underline that the indicator is reusable and the rate of recovery of colour is proportional to the level of oxygen, and that it is printable as an ink on many surfaces, including glass and plastic.

Mills and Hazafy [8] published a study in which they used nanocrystalline SnO₂ as a photosensitizer in an oxygen indicator. An electron donor, glycerol, a redox dye, methylene blue, and an encapsulating polymer, hydroxyethyl cellulose (HEC), constitute this indicator. Upon an UV-B light exposure, the indicator is activated (photobleached) as the methylene blue is photoreduced by the SnO₂ nanoparticles. When no oxygen is present, the film stays whitened. Then it recovers its original colour, when exposed to oxygen. Unlike TiO₂-based solutions, their indicator is not activated by UVA light from white fluorescent lamps, but by UVB light. They explain that the half-life of the original colour recovery of the activated film, t_{50} , is straight proportional to the level of oxygen, present in the environment. This is a clear advantage of using this indicator in packaging with a modified atmosphere as a possible quality assurance indicator.

Aniceto Pereira et al. [9] developed a TTI based on a PVA/Chitosan polymer mixture, doped with anthocyanins extracted from *Brassica oleracea var. capitata*, which is able to detect changes in the pH of packaged food products when subjected to improper storage temperature. They tested the efficiency of the TTI on pasteurized milk, with evident changes in the coloration of the film (Figure 3).

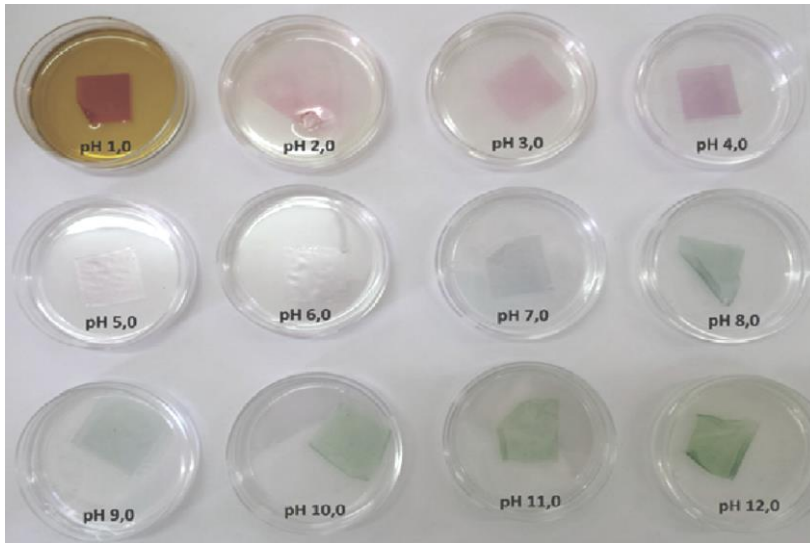


Figure 3. TTI color response at different pH conditions for a modified PVA film [9].

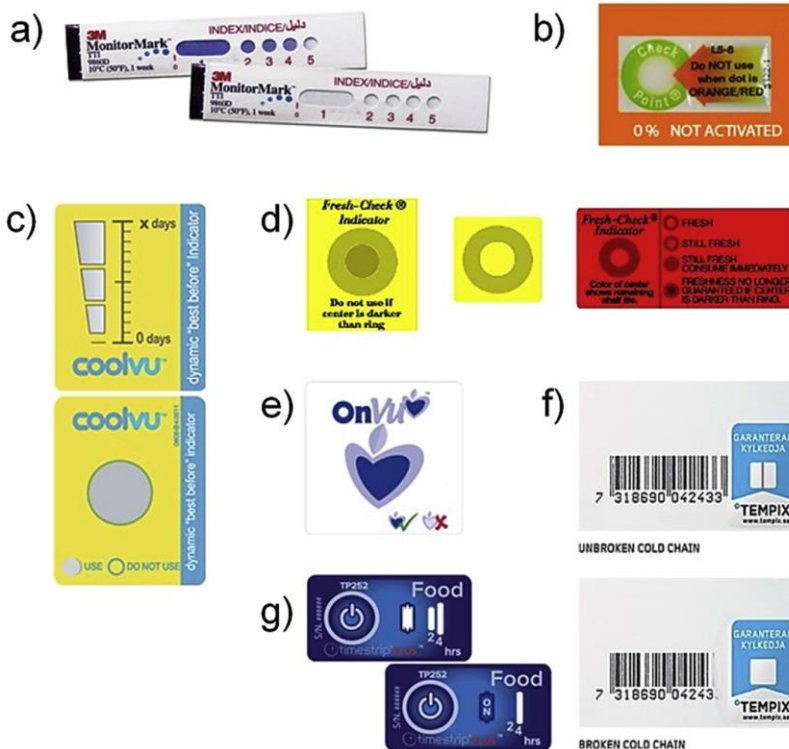


Figure 4. Examples of time-temperature indicators. a) Monitor Mark™ by 3M (USA); b) Fresh-Check® by Lifelines Technologies Inc. (USA); c) CoolVu™ by Freshpoint (Switzerland); d) Checkpoint® by Vitsab International AB (Sweden); e) OnVu™ by Freshpoint (Switzerland); f) Tempix® by Tempix AB (Sweden); g) Timestrip® by Timestrip Plc (UK) [5].

Nonetheless, even though the developed TTI shows very interesting properties and efficiency in terms of change of colour, the authors note that its stiffness is different from the one of the commercial polymers applied in food packaging, and this could hinder its direct application in the industrial world.

The milk is one of the food/beverage products that could benefit from TTI. In fact, for this product, the management of the cold chain logistics needs special care and its monitoring by TTIs can be potentially of paramount importance for food safety and quality.

As another example of how TTIs can be used for milk quality monitoring, Lu et al. [10] studied a new time-temperature indicator based on an enzymatic reaction, diffusion and demobilization technology. They tested it in order to monitor the milk shelf life, obtaining good stability and reliability at dynamic storage conditions.

Nopwinyuwong et al. [11] synthesized Polydiacetylene (PDA)/silica nanocomposites by self-assembly method, starting from polymerizable amphiphilic diacetylene monomers. The response in terms of change of colour of both PDA/SiO₂/surfactant and surfactant-free PDA/SiO₂ aqueous solutions was considerably affected by both time and temperature and this led their system to be used as a new polymer-based TTI.

FRESHNESS INDICATORS

A very useful communication of the smart packaging to the consumer is related to the freshness of food. A specific class of indicators are dedicated to this kind of communication to the consumer. Freshness indicators are smart devices, which allow the monitoring of food quality throughout storage and transportation. This type of indicators provides direct information on the freshness of the products and is based on the reaction of its materials, with the chemical compounds produced during the deterioration of the food. The development of these indicators over the last two decades was pushed by the increasing consumer demand for healthy and fresh food [12].

As in the case of TTIs, the chemical reaction produces a change in colour, detectable by the consumer. This is particularly useful for the end-users. In fact, on the one hand the food can deteriorate earlier than the expiry date, with the danger for the health of the consumer. On the other hand, the food can be still good after the expiry date and the indicator can help the consumer preventing from throwing the food away if not necessary.

As already mentioned, the TTI indicators described in the previous section, are about detecting oxygen. Differently, the freshness indicators are asked to detect microbial growth or chemical changes occurring to the food, which can be several and depend upon the nature of the packed food. The reaction between the microbial growth metabolites and

the indicators integrated within the package provides visual information regarding the quality of the product [13, 14].

For this reason, the advance of this family of indicators is considerably more complicated. A great variety of freshness indicators, which react in the presence of quality indicating metabolites, can be found in the scientific literature [15].

It is important to underline that the formation of these metabolites depends on several factors, such as the nature of the packed food, spoilage flora and the type of packaging. For this reason, the suitable quality indicating metabolites as target molecules for these indicators are several.

Numerous authors presented studies on freshness indicators mechanisms, based on a change of colour of the indicator, due to the occurrence of microbial metabolites produced during spoilage [16-18]. Nonetheless, this type of indicators, which are based on broad-spectrum colour changes, have some disadvantages. In fact, a deficiency of specificity in colour changes could lead to an indication of contamination in food products, even if a significant quality deterioration does not occur. The possibilities of false positives are likely to discourage producers from using indicators unless precise indication of spoilage can be guaranteed. Other described techniques are based on optical or electronic measurements [19-21].

Several freshness indicators, in particular designed for seafood products, are based on the total amount of emitted volatile basic nitrogen (i.e., TVB-N), specifically volatile amines, which are formed when the food spoils. They can be identified by different methods, such as conductometric and pH variations. On the other hand, hydrogen sulphide indicators can be employed to evaluate the quality of meat products. This chemical compound, which is released by meat during ripening, is correlated with the colour of myoglobin, which is considered a positive qualitative attribute for meat products. Smolander et al. [22] developed a freshness indicator specifically built for modified atmosphere packed poultry meat. Other possible indicators for meat products decomposition are represented by biogenic amines such as histamine, putrescine, tyramine and cadaverine, which were studied in literature [23, 24].

Moreover, Khalil et al. [25] have designed a device for the revealing of ammonia or volatile amines, based on the change of colour of pH-dyes on PTFE-carrier solid phase indicator film.

Detection systems, patented by Miller et al. [26] and studied by Loughran and Diamond [27], are based on the idea of an indicator provided on a substrate and reacting to volatile amines with a colour change, hence indicating freshness of packaged food. In 1999, COX Technologies launched FreshTag®, based on the aforementioned studies. This device is a colorimetric indicator label, which reacts to volatile amines produced during storage of fish and seafood products.

It's Fresh! Inc (<http://www.itsfresh.com/>) produces a commercial food freshness indicator, which is suitable for different meat-containing food products, such as poultry,

beef and pork and seafood. The consumer can place the indicator directly inside a storage bag or container, and then placed in the refrigerator for 8 hours. If the colour of the indicator changes from pink to yellow, the quality of the product can be considered as deteriorated.

Other examples are represented by both SensorQ™ by FQSI Inc., which indicates spoilage in fresh meat and poultry products [28] and RipeSense™, a ripeness indicator which allows consumers to choose fruit that best appeals to their tastes [29], by detecting aroma components or gases (e.g., ethylene), released by the fruit and involved in the ripening process.

Another application, developed for both commercial and military industries, is Toxin Guard™ by Toxin Alert, Inc. (Ontario, Canada), which is a polyethylene-based packaging film that can detect the presence of specific pathogenic bacteria (*Salmonella*, *Campylobacter*, *Escherichia coli* O157 and *Listeria*) with the aid of immobilized antibodies. As the analyte (toxin, microorganism) touches the material, it will be bound first to a specific, labelled antibody and then to a capturing antibody, printed as a certain pattern [30].

The method can also be used to the recognition of pesticide residues or proteins resulting from genetic modifications. Lawrence Berkeley National Laboratory has developed specific materials for indicators in order to detect *Escherichia coli* O157 enterotoxin [31]. This sensor, incorporated in the material of the packaging, is formed by a cross-polymerised polydiacetylene and it has a deep blue colour. The molecules, which specifically bind the toxin, are confined in this polydiacetylene matrix and as the toxin is bound to the film, the colour of the film varies from blue to red.

Several sensors are based on resistive metallic oxides (MOS), which interact with the microbial metabolite molecules varying their electrical conductivity. Similar to these devices, electrically conductive nanocomposite sensors were developed. They can detect pathogenic bacteria, such as *Salmonella* spp., *Bacillus cereus* and *Vibrio parahaemolyticus*, realised by spoiling food [32]. Finally, biochips based on DNA molecules are developing. This technique will be able to detect bacteria in meat, fish and fruit food products.

THERMOCROMIC INDICATORS

Thermocromic sensors and devices represent another kind of smart packaging solution, which can make the consumer aware of the food temperature by a change in the colour of the part in which they are embedded or printed. These sensors are typically used in food products, which need to be served hot (e.g., drink or ready-to-eat food). They can be developed either by using a thermocromic additive to be mixed with the polymer (always available as a masterbatch) or by a thermocromic ink.

Thermochromic masterbatches are commercially available and they can be diluted in the suitable polymeric matrix, in order to obtain a thermochromic formulation to be used in the production of the packaging. As an example, the British company TMCHallcrest produces a series of thermochromic masterbatches, with the brand name Chromazone™. These materials are based on a reversible thermochromic mechanism and the temperature at which the colour variation occurs can be modulated, making these products suitable for a number of food packaging applications, where different service temperature are required. Based on the formulation of the thermochromic additive, different colours can be obtained, as reported in the Figure 6 below [33].



Figure 5. Thermochromic colors in baby spoons [33].

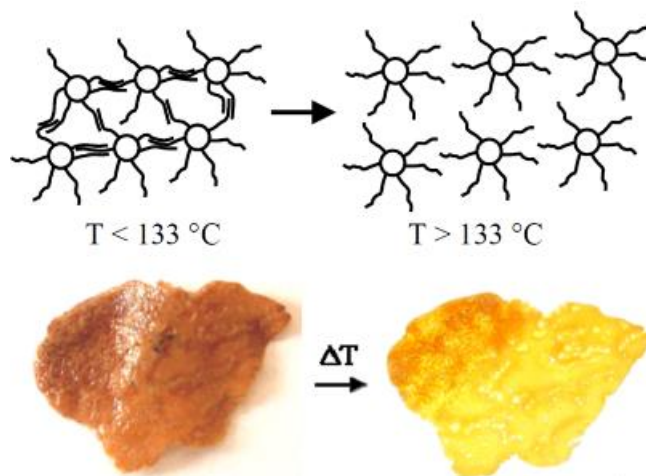


Figure 6. Thermochromic nanoparticles, scheme and picture [34].

From the scientific literature point of view, several studies have been published in the last years [34-36]. As an example, Carotenuto et al. [34] developed silver thiolate

nanoparticles, which allow the final material to have a chromic toning above a certain temperature. This phenomenon can be explained by a partial crystallization of the thiol chains (see Figure 6). Even though the produced thermochromic effect has been clearly demonstrated, the change in colour occurs at 133°C (not be easily tuned without chemically modifying it), which is a temperature barely suitable for the food. This outcome, together with the fact that such nanoparticles are not suitable to the food contact according to the current legislation, makes the application of this technical solution quite difficult in the food industry.

The authors of this chapter have worked in the last years in the development of thermochromic packaging for baby-food (unpublished results) to support an Italian company that had the goal of making the parents aware about when the food is at the right temperature for their children. Polyethylene (PE) was used as polymer matrix, as it is the one already used for that application. The use of the Chromazone™ masterbatch allowed creating a tailored formulation, suitable for the polyolefin matrix used in the project. A modulated quantity of additive was added and an evident thermochromic effect was detected, as observed in Figure 7. A thermochromic colour variation was seen when the sample was immersed in the warm water. In this case, the correct masterbatch and the corresponding variation of colour was selected based on a precise temperature, directly required for this food application, at which the colour change is expected (about 40°C). The study has also involved the manufacturing of thermochromic additives by following the aforementioned chemical approach [34], obtaining the same interesting results (as reported in Figure 8), and further confirming the effectiveness of that method.



Figure 7. Injection molded samples with thermochromic masterbatch.



Figure 8. Extruded wire of thermochromic nanocomposites.

Thermochromic inks constitute a different technical solution for thermochromic smart packaging. They are based on thermosensitive inks, directly printed on the packaging, like shrinkable sleeves of beverage cans. The colour of the ink changes when the temperature is within a specific pre-determined range, which is considered the best condition for food consumption. The modification of the colour can also deliver a short message to the consumer, such as for instance “ready to serve,” simply by using the ink for writing or drawing the message itself. However, one of the main drawback of this kind of temperature indicators is represented by the difficulty in distinctly observing the colour change.

Inks colour change could be either irreversible or reversible. Irreversible and invisible thermochromic ink, as long as it is exposed to high temperature, develops into an intense colour when exposed to a certain temperature. This colour change will remain stable and permanent even if a new change of the temperature occurs [37]. Reversible thermochromic inks change their colour if heated or frozen: therefore, they return to their original state if the temperature comes back to its original value. As an example, Ctiinks [38] produces thermochromic inks for products (e.g., beverage, see Figure 9) where there is an expectation of hot or cold from the consumer. These types of thermochromic inks are often used as temperature-activated inks on the packaging labels to induce a colour change.

Finally, touch-activated thermochromic inks show an image or a different colour from the original one, printed below once scrubbed or touched. These particular liquid crystal inks - when rubbed or touched - modify their colour within the visible spectrum. High-temperature thermochromic inks vary colour just below the pain threshold, alerting consumers about a safety hazard [40].



Figure 9. Examples of cold-activated inks on packaging labels [39].

REFERENCES

- [1] Gustavsson, J., Cederberg, C., Sonesson, U., van Otterdijk, R., Meybeck A., (2011). *Global food losses and food waste – Extent, causes and prevention*, FAO, Rome.
- [2] Kerry, J., Butler, P., editors, (2008). *Smart Packaging Technology for fast moving consumers goods*, John Wiley and Sons Ltd., Chichester, UK.
- [3] R. L., (2004). *Ripeness indicator proves fruitful*, Packaging World.
- [4] Taoukis, P. S., Labuza, T. P., (1989). Applicability of time–temperature indicators as shelf life monitors of food products, *Journal of Food Science*, 54: 783–789.
- [5] Ghaani, M., Cozzolino, C. A., Castelli, G., Farris, S., (2016). An overview of the intelligent packaging technologies in the food sector, *Trends in Food Science & Technology*, 51: 1-11.
- [6] Pault, H., (1995). Brain boxes or simply packed? *Food Processing*, 64: 23-26.
- [7] Lee, S. K., Sheridan, M., Mills, A., (2005), Novel UV-Activated Colorimetric Oxygen Indicator, *Chemistry of Materials*, 17: 2744–2751.
- [8] Mills, A., Hazafy, D., (2009). Nanocrystalline SnO₂-based, UVB-activated, colourimetric oxygen indicator, *Sensors and Actuators B*, 136: 344–349.
- [9] Pereira, V. A. Jr, Queiroz de Arruda, I. N., Stefani, R., (2015). Active chitosan/PVA films with anthocyanins from Brassica oleraceae (Red Cabbage) as Time–Temperature Indicators for application in intelligent food packaging, *Food Hydrocolloids*, 43: 180-188.
- [10] Lu, L., Zheng, W., Lv, Z., Tang, Y., (2013). Development and application of time-temperature indicators used on food during the cold chain logistics. *Packaging Technology and Science*, 26: 80-90.

- [11] Nopwinyuwong, A., Kitaoka, T., Boonsupthip, W., Pechyen, C., Suppakul, P., (2014). Effect of cationic surfactants on characteristics and colorimetric behavior of polydiacetylene/silica nanocomposite as time–temperature indicator, *Applied Surface Science*, 314: 426-432.
- [12] Siro, I., (2012). Active and intelligent packaging of food., In Bhat, R., Alias, A. K., Paliyath, G., (Eds.), *Progress in food preservation*, 23-48.
- [13] Kerry, J. P., O’Grady, M. N., Hogan, S. A., (2006). Past, current and potential utilisation of active and intelligent packaging systems for meat and muscle-based products: A review, *Meat Science* 74:113–130.
- [14] Kuswandi, B., Maryska, C., Jayusra, A. A., Heng, L. Y., (2013). Real time onpackage freshness indicator for guavas packaging. *Food Measure*, 7: 29–39.
- [15] Smolander, M., (2004). Freshness indicators for packaging, *Food Science and Technology*, 18 (IV): 26–7.
- [16] Williams, J. R., Myers, K. E., Owens, M. M., Bonne, A. A., (2006). Food quality indicator, *United States Patent Application Publication* US 2006/0057022 A1.
- [17] Smolander, M., Hurme, E., Koivisto, M., Kivinen, S., (2004). Indicator, PCT, *International Patent Application* WO 2004/102185 A1.
- [18] Smolander, M., Hurme, E., Latva-Kala, K., Luoma, T., Alakomi, H.-L., Ahvenainen, R., (2002). Myoglobin-based indicators for the evaluation of freshness of unmarinated broiler cuts, *Innovative Food Science and Emerging Technologies* 3: 277–285.
- [19] Pacquit, A., Frisby, J., Diamond, D., Lau, K. T., Farrel, A., Quilty, B., Diamond, D., (2007). Development of smart packaging for the monitoring of fish spoilage, *Food Chemistry*, 102: 466– 470.
- [20] Pacquit, A., Lau, K. T., McLaughlin, H., Frisby, J., Quilty, B., Diamond, D., (2006). Development of a volatile amine sensor for the monitoring of fish spoilage, *Talanta*, 69: 515–520.
- [21] Byrne, L., Lau, K. T., Diamond, D., (2002). Monitoring of headspace total volatile basic nitrogen from selected fish species using reflectance spectroscopic measurements of pH sensitive films, *Analyst*, 127: 1338–1341.
- [22] Smolander, M., Hurme, E., Latva-Kala, K., Luoma, T., Alakomi, H.-L., Ahvenainen, R. (2002). Myoglobin-based indicators for the evaluation of freshness of unmarinated broiler cuts, *Innovative Food Science and Emerging Technologies*, 3: 277–285.
- [23] Kaniou, I., Samouris, G., Mouratidou, T., Eleftheriadou, A., Zantopoulos, N., (2001). Determination of biogenic amines in fresh unpacked and vacuum-packed beef during storage at 4°C, *Food Chemistry*, 74: 515–519.
- [24] Rokka, M., Eerola, S., Smolander, M., Alakomi, H.-L., Ahvenainen, R., (2004). Monitoring of the quality of modified atmosphere packaged broiler chicken cuts

- stored in different temperature conditions. B. Biogenic amines as quality-indicating metabolites, *Food Control*, 15: 601–607.
- [25] Khalil, G. E., Putnam, D. L., Hubbard, T. W., (2003). Ammonia detection and measurement device, *United States Patent Application Publication US 2003/0003589 A1*.
- [26] Miller, D. W., Wilkes, J. G., Conte, E. D., (1999). Food quality indicator device, *PCT International Patent Application WO 99/04256*.
- [27] Loughran, M., Diamond, D., (2000). Monitoring of volatile bases in fish sample headspace using an acidochromic dye, *Food Chemistry*, 69: 97–103.
- [28] O’Grady, M. N., Kerry, J. P., (2008). Smart packaging technologies and their application in conventional meat packaging systems, *Meat Biotechnology*, 425-451.
- [29] Poças, M. F. F., Delgado, T. F., Oliveira, F. A. R., (2008). Smart Packaging Technologies for Fruits and Vegetables, *Smart Packaging Technologies for Fast Moving Consumer Goods* 151-166.
- [30] Bodenhamer, W. T., (2000). *Method and apparatus for selective biological material detection*, US Patent 6051388.
- [31] Quan, C., Stevens, R., (1998). Protein coupled colorimetric analyte detectors, *PCT International Patent Application WO 98/36263*.
- [32] Arshak, K., Adley, C., Moore, E., Cunniffe, C., Campion, M., Harris, J., (2007). Characterisation of polymer nanocomposite sensors for quantification of bacterial cultures, *Sensors Actuators B* 126: 226–31.
- [33] <http://www.newcolorchem.com/default.php?action=protext&id=84>.
- [34] Carotenuto, G., Nicolais, F., (2009). Reversible Thermochromic Nanocomposites Based on Thiolate-Capped Silver Nanoparticles Embedded in Amorphous Polystyrene, *Materials* 2: 1323-1340.
- [35] Carotenuto, G., Palomba, M., De Nicola, S., (2012). A new high-soluble precursor for in situ silver nanoparticle generation in polymers, *e-Polymers*, 85.
- [36] Carotenuto, G., (2001). Dependence of the order–disorder transition temperature of 1-octadecanethiol/silver system on the substrate size, *Journal of Materials Science Letters* 20: 663– 665.
- [37] Tollan, C. M., Marcilla, R., Pomposo, J. A., Rodriguez, J., Aizpurua, J., Molina, J., Mecerreyes, D., (2009). Irreversible Thermochromic Behavior in Gold and Silver Nanorod/Polymeric Ionic Liquid Nanocomposite Films, *Applied Materials and Interfaces* 1(II): 348-352.
- [38] <http://www.packagingid.com/thermochromicink/>.
- [39] <https://www.plastech.biz/news/Ball-further-enhances-thermochromic-ink-technology-4499>.
- [40] Roya, A. Q., Elham, M., (2016). Intelligent food packaging: Concepts and innovations, *Journal of ChemTech Research* 9 (VI): 669-676.

Chapter 13

**SMART COATINGS:
DEVELOPMENT OF ANTIOXIDANT
EDIBLE FILMS BASED ON SODIUM CASEINATE
AND HYDROXYTYROSOL**

Marina Patricia Arrieta^{1,*} and Mercedes Ana Peltzer^{2,3,†}

¹Institute of Polymer Science and Technology (ICTP-CSIC), Madrid, Spain

²Department of Science and Technology, University of Quilmes,
Buenos Aires, Argentina

³National Scientific and Technical Research Council (CONICET),
Buenos Aires, Argentina

ABSTRACT

The increasing production of biobased and biodegradable polymers provides to the food industry the opportunity to offer alternative solutions with lower environmental impact. Among the available biopolymers, caseinates show excellent edible film formability, the ability to form thin and flexible layers, interesting for edible coating systems. Hydroxytyrosol (HT) is a natural antioxidant occurring in olives and mostly recovered from residues of olive oil production. However, many authors suggested that it is also available in olive oil. The HT is an ortho-diphenol with a marked antioxidant activity related to the electron donating ability of hydroxyl groups in the ortho position and subsequent formation of stable intramolecular hydrogen bonds with the phenoxylic radical. This chapter begins with generalities regarding the interest of smart materials in the food packaging field, focusing the attention on antioxidant active packaging systems as well as the interest on the use of edible active coatings for these applications. Then, it

* Corresponding Author Email: marrieta@ictp.csic.es.

† Corresponding Author Email: mercedes.peltzer@unq.edu.ar.

is reported the development of active edible films based on sodium caseinate and HT. The most important results regarding a full characterization of the obtained active films in terms of visual, structural, thermal, mechanical and barrier properties; together with the evaluation of the antioxidant properties of the developed films are described throughout this chapter and it was possible to conclude that this system is a good alternative to avoid or retard foodstuff oxidation and though increase food shelf life.

Keywords: edible films, biopolymers, sodium caseinate, antioxidant, hydroxytyrosol

1. INTRODUCTION

Continuous changes in life style have led to significant changes in consumers' habits, demanding for higher quality and longer shelf life food products. The more and more consumers requirements joined with the appearance of new regulations in the food supply chain (i.e., food processing, transport, distribution and storage) have led to a demand of more advanced packaging systems. In consequence, advanced polymeric systems with innovative functions are gaining considerable interest in the food packaging field. In this context, smart polymers have gained particular attention in the food industry, which continuously demands innovative food packaging formulations not only for extending the food shelf life, but also for guarantying food safety, quality and traceability [1]. Smart polymers are polymeric systems that exhibit special functions in response to external conditions, thus, such polymers are also called stimuli-responsive polymers [2]. In the food packaging field, there are mainly two packaging approach technologies which allows monitoring the condition of packaged food or contributes to preserve and extend their shelf life: intelligent packaging and active packaging [3, 4]. Intelligent packaging monitor the condition of packaged food or the environment surrounding the food with the main purpose to indicate when food products are spoiled or some specific conditions changed [5]. Meanwhile, active packaging takes advantages from the positive interactions between the packaging material with active components deliberately incorporated and the packed food products. In this way, these systems slow down the food deterioration process and further extend its shelf-life by gradually releasing the active compound from the packaging to the food, either to the head space or into the surface of the packed food, where mainly food deterioration/contamination take place (Figure 1).

Active packaging can be classified as absorbers or emitters systems. Among the absorbers, those that are mostly described in literature are moisture, oxygen, ethylene and carbon dioxide scavengers [6-8]. Oxygen is responsible for oxidation of food constituents and proliferation of aerobic bacteria and molds; indeed, it is responsible for quality and nutritional losses due to the change in colour, flavor or oxidation of sensitive vitamins. One strategy, to minimize this situation is by using oxygen scavengers systems, which are able to reduce oxygen inside the package to less than 0.01%. The oxygen scavenging

technologies that exist are based on iron power oxidation, ascorbic acid oxidation, enzymatic oxidation, among others [9]. The removal of ethylene and/or inhibition of the effect of ethylene in stored environments are fundamental to maintain postharvest quality of climacteric products. The ethylene trapping technologies related to active systems are those that use potassium permanganate (KMnO_4)-based mechanisms and new palladiums based materials [10]. One promising technology for adsorption of certain gases, such as ethylene, is by the use of metal-organic-framework (MOF) based mesh-adjustable molecular sieves (MAMS) [11, 12]. The excess of water inside the packaged of high water activity products promotes bacterial and molds growth, resulting in a reduction of shelf life and loss of food quality. An effective way of controlling water accumulation in a package that is not permeable to water vapor is by using a moisture absorber. The most common one is a super absorbent polymer located between two layers of a microporous polymer [13]. Regarding the emitters, it is possible to find the CO_2 emitters, preservatives releasers (antimicrobials and antioxidants), ethanol emitters, among others. CO_2 emitters are very useful for their antimicrobial effect to extend food shelf life. One example of these systems is the so-called $\text{CO}_2^{\text{®}}$ Fresh Pads, mainly used for meat, poultry and fish products. These systems are based on pads, which are able to absorb drip losses from the muscle and react with citric acid and sodium bicarbonate present in the pad, to generate CO_2 [13]. However, the most common active emitters packaging are the antimicrobial and antioxidant packaging. In fact, active packaging formulations have become the most important challenge for the modern food industry to extend the shelf life of food [14]. In this context, biologically active compounds have gained interest in food industry, especially in view of recent outbreaks of contamination associated with food products [15]. Oxidation is one of the major problems affecting food quality [4, 14]. This is why antioxidants, and particularly phenols, are largely used as additives to reduce lipid oxidation and protect food nutrients against oxidation [16], and thus extending the food product shelf life as they limit the oxygen transfer and the reactivity of free radicals [14]. Therefore, the use of antioxidant active packaging systems results interesting because they allow preventing the food oxidation process by reducing, or even avoiding, the direct incorporation of antioxidants to the foodstuff.

On the other hand, there is a growing tendency in the food industry to replace the petrochemical based polymer frequently used in this field for more sustainable alternatives. Therefore, the use of biobased polymers has gained considerable attention during the two last decades. Biobased polymers are those polymers obtained from natural resources. Different classifications of the biobased polymers have been proposed depending on the evolution of the synthesis process as it is shown in Figure 2.

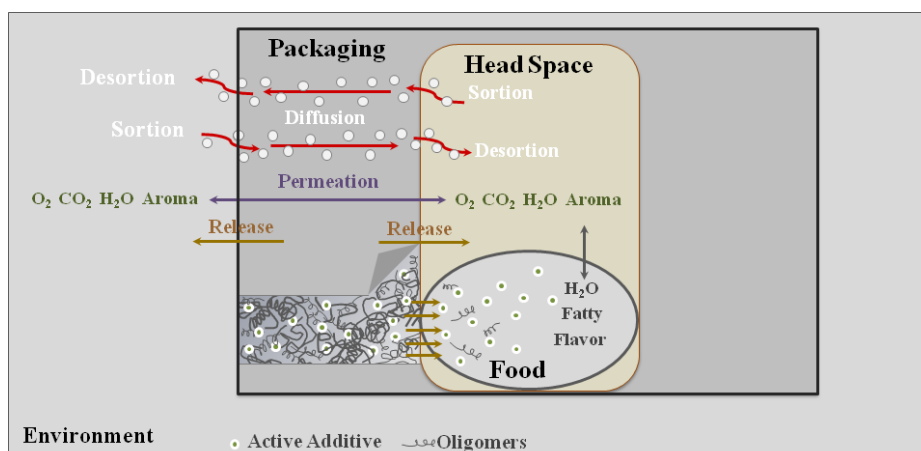


Figure 1. Schematic representation of transfer process involved in food related materials.

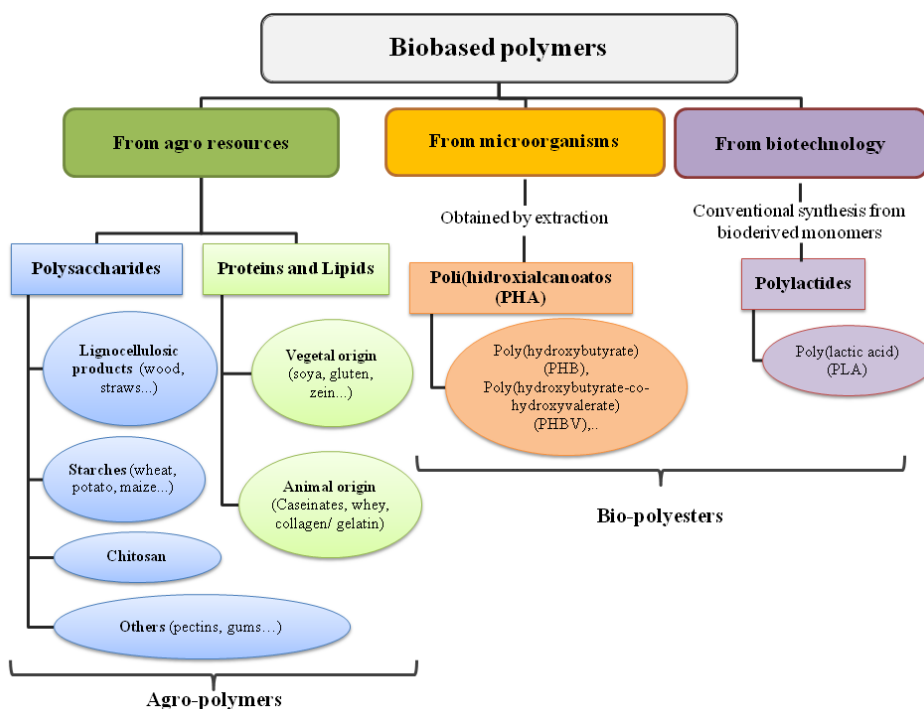


Figure 2. Classification of biobased polymers (Adapted from Averous 2004) [17].

Bio-polyesters, particularly poly(lactic acid) (PLA), are currently introduced in the market mainly because they can be processed by usual thermoplastic processing technologies already available in the plastic processing industry, such as extrusion, injection molding, sheet extrusion, blow molding, thermoforming and film forming [18]. However, the main drawback for the development of antioxidant packaging formulations is that their transformation temperatures are generally too high for active compounds, which generally cannot be heated at the high temperatures used for their transformation

[19, 20]. Thus, agro-polymers (proteins, polysaccharides and lipids) have gained interest as carrier for antioxidant compounds. Additionally, agro-polymers can be processed as biopackaging materials, some of them being edible materials interesting for food coating applications [14]. The main advantage of edible materials over synthetic food packaging polymers is that they can be consumed with the food, reducing the current problem of plastic food packaging waste generation [21]. Packaging materials are removed from the food, while edible coatings are part of the foodstuff [22]. Thus, edible coatings are interesting sustainable alternatives for traditional food packaging, which currently generates a high amount of plastic wastes. Moreover, the continuously demand of consumers for higher quality, convenience and food safety as well as longer shelf life food products have led to an increasing interest into edible coatings in the food industry [23]. Among all the multipurpose applications of edible films in the food industry, such as coating to enhance the nutritional value of food products or as carriers of other additives, the use of edible films has important functions for food protection: restriction of moisture loss, control of gas permeability, preservation of structural integrity of the foodstuff, etc. [23, 24].

Within biopolymers, proteins have attracted considerable industrial and researcher attention during the last years, although edible films can be also prepared using polysaccharides and lipids [16]. Among proteins, milk proteins such as casein, caseinates (i.e.,: sodium (NaC) and calcium caseinates CaC)) or whey proteins have been considered as suitable raw materials for making edible coatings, as they have numerous functional properties that make them excellent materials for edible coating-forming agents [16, 25]. Milk proteins show similar or lower mechanical strengths than films from wheat and soy proteins, and cellulose based films [26]. In fact, edible coatings based on milk proteins have a soft transparent aspect and good oxygen barrier performance at low relative humidity [16]. Caseins represent 75-80% of all milk proteins and it is organized on a micellar structure which consists of α , β and κ -casein [27]. In the form of caseinates it has been shown that they can act as water soluble emulsifiers able to create stable emulsions, which are further easy to apply as coatings on foodstuff [28]. In fact, caseinates have random coil nature and are able to form extensive intermolecular hydrogen and electrostatic bonds that can easily form films from aqueous solutions [29]. Moreover, due to the high number of polar groups within its structure, caseinates also show strong adhesion to various substrates, making them an excellent barrier to non-polar substance; including oxygen, carbon dioxide and aromas [30, 31]. However, due to the inherent brittleness of caseinates, plasticizers should be added to improve their ductile performance and to get the flexibility required for food coatings purposes [31].

Among other caseinate plasticizers (i.e., acetylated monoglyceride [28], poly(ethylene glycol) [32], sorbitol [29], etc.), glycerol has been proposed as the most effective caseinates plasticizer since it contributes to the reduction in material brittleness by the limitation of protein cross-linking and reduction of intra and intermolecular

hydrogen bonds [33], while increasing intermolecular spacing and thus reducing mechanical strength of the edible films [29]. From an environmental point of view, another interesting point is that glycerol is a by-product of biodiesel production; and thus its use as plasticizer is a positive way to increase its added value from a low-grade by-product to a useful plasticizer [31, 34]. In this sense, Siew et al., studied NaC systems plasticized with glycerol and PEG. They observed that plasticizers reduced the viscosity of the film forming solution, since plasticizer disrupt the protein-protein and protein-solvent interactions through hydrogen bonding of the plasticizer molecules with the caseinate chain and water molecules leading to smaller protein aggregates. Glycerol has a larger effect on the mechanical properties of the film. Moreover, PEG based formulations showed higher water vapor permeation (WVP) properties. Fabra et al., studied NaC based films plasticized with glycerol and sorbitol, and the results showed that glycerol was more effective as plasticizer than sorbitol for caseinate matrices due to the fact that films with 90 wt% of sorbitol presented similar tensile properties to NaC with 40-50 wt% of glycerol [29].

As commented before, oxidation is one of the main causes of food deterioration; therefore it is important to find a solution to prevent it. Antioxidant active packaging, which was the first type of active packaging available, prevents oxidation by either absorbing components that contribute to oxidation such as oxygen or radicals, or by releasing antioxidants inside the packaging, in particular to the surface where the oxidation process is mainly produced, as previously described. Food grade antioxidants should be employed to the formulation of these systems, since once they are released to the food product they become a food ingredient [35]. Natural antioxidants, from plants and herbs origin, are those mostly used for these purposes. Plants that belong to the *Lamiaceae* family include aromatic herbs such as basil, mint, rosemary, sage, savory, marjoram, oregano, hyssop, thyme and lavender, among others. Most of them have been used to extract active phenolic components with bioactive capacity such as antioxidants, antimicrobial, among other interesting properties [36]. Oregano (*Origanum vulgare L.*) and thyme (*Thymus vulgaris L.*) have been studied widely for their antioxidant activity, due to the high content of phenolic compounds: carvacrol and thymol [37-41] and their incorporation in polymeric matrices to develop active systems were highly described [31, 42, 43]. For instance, caseinate based matrices (NaC and CaC) has been incorporated with carvacrol and the films showed antibacterial properties [42] as well as improved flexibility [31]. The antioxidant activity of aqueous tea infusions was related to their chemical composition and compared with the antioxidant activity of natural (ascorbic acid and α -tocopherol) and synthetic antioxidants (butylated hydroxytoluene (BHT) and butylated hydroxyanisole (BHA)) [44]. NaC plasticized with glycerol has been used for the development of antioxidant coatings by adding α -tocopherol with improved water vapor permeability [45]. Green tea aqueous extracts were incorporated in gelatin matrices in order to provide gelatin edible films with antioxidant capacity [46].

Table olives, very consumed in Mediterranean diet, contain biologically active phenolic compounds. Oleuropein is the most predominant phenolic compound in the fresh fruit and due to its bitterness it should be removed to make olive fruit palatable. This action is carried out by salt curing or acid hydrolysis, and the products of this hydrolysis are hydroxytyrosol (HT) and tyrosol (T) [47]. It is also well known that aqueous residues of the production of olive oil contain valuable products. Hamza & Sayadi 2016, reported that olive mill wastewater contains high concentration of aromatic compounds, and represents a potential source of valuable molecules, in particular ortho-diphenols. These molecules are known for their antioxidant properties and their main interest from the food industry is to be used as alternatives to synthetic antioxidants [48]. Indeed, after the extraction of oil from the olive, many phenolic compounds remain in the by-product alperujo, extracts of which contain a similar phenolic profile to that of the original fruit [49]. It was described that olive mill waste is rich in a diverse range of biophenols and typically contains about 98% of the phenols present in olive fruit, either in the wastewater (approx. 53%) or in the pomace (approx. 45%). This disposal is considered as a significant environmental issue and its reutilization could be an advantageous practice. More than 50 biphenols and related product were identified in olive mill waste, such as phenyl alcohols, phenolic acids, secoiridoids, and flavonoids, most of them with high bio-antioxidant activity [50]. Many of the benefits of olives are associated to the hydroxytyrosol presence, one of the most extensively studied phenolics compounds in olives [51-56]. It is an o-diphenol with a marked antioxidant activity related to the electron donating ability of hydroxyl groups in the ortho position and subsequent formation of stable intramolecular hydrogen bonds with the phenoxylic radical [49]. HT is characterized by a strong antioxidant activity, similar to 2,6-di-tert-butyl-p-hydroxytoluene (BHT) and 3-tert-butyl-6-hydroxyanisole (BHA), two synthetic antioxidant used for formulations [48]. In addition, it was demonstrated that its antioxidant power was similar to other natural antioxidants such as thymol, 6-gingerol and zingerone, and contributes to the stability of virgin olive oil [57, 58].

The incorporation of HT in polymeric matrices was also studied, as an antioxidant for the polymer matrix, with a good performance in polypropylene materials acting as antioxidant [59], and it might be considered as a promising alternative to be used in active packaging formulations. Beltran et al., incorporated HT in poly(ϵ -caprolactone) (PCL) and studied the effect of the antioxidant on thermal, physical and mechanical properties of the polymer, in addition to the study of the release of the compound to methanol at different times [60]. The incorporation of the antioxidant was effective, however, since HT is a polar compound its incorporation to hydrophilic matrices is expected to be more efficient.

In this work, the addition of HT in edible polymeric matrices based on sodium caseinate to develop biodegradable antioxidant active coating systems, will be studied.

Throughout this chapter the full characterization of these innovative systems will be described to assess the possibility to use them for food coating applications.

2. MATERIALS AND METHODS

2.1. Materials

Sodium (NaC) was kindly supplied in powder form by Ferrer Alimentación S.A (Barcelona, Spain). Anhydrous glycerol (99.5%) was purchased from Sigma Aldrich (Móstoles, Madrid, Spain). Hydroxytyrosol (purity 97%) was kindly provided by Fine & Performance Chemicals Ltd.

2.1.1. Edible Films Preparation

Edible films were prepared by solvent casting method. The casting solution was prepared following the method previously developed [31], with slight modifications. In brief, the film forming solutions were prepared in distilled water with 5 wt% of NaC and the amount of glycerol required to obtain NaC:glycerol 1:0.35 ratio (in weight). The film forming solutions were then heated at 65°C for 10 minutes under continuous stirring (1100 rpm) and further cooled at room temperature. Then, the amount of hydroxytyrosol (HT) required to obtain NaC:HT 1:0.05 and 1:0.10 ratios was added, with homogenization for 3 min at room temperature (1100 rpm). To eliminate air bubbles, the film forming solutions were ultrasonicated using an ultrasound cycle process of degasification for 2 min followed by a rest during 30 s at room temperature 5 consecutive times in an Elma S30 (Elmasonic). The film forming solutions were then kept 3 h at 4°C to perform the removal of any air bubbles [61]. Edible films were prepared by pouring the degasified film-forming solutions into polyethylene Petri dishes (85 or 150 mm diameter) and they were allowed to dry for approximately 48 h at room temperature.

The average thickness of films was measured with a digital micrometer Permascope MP Q (Fischer) ± 0.001 mm at ten random positions over the film surface.

2.2. Methods

2.2.1. Visual Appearance and UV-visible Measurements

The visual appearance of films was checked by taken photographs. The absorption spectra in the 200-700 nm region of plasticized NaC based edible films were investigated by means of a Perkin Elmer (Lambda 35, USA) UV-VIS spectrophotometer.

2.2.2. Colourimetric Properties

Edible film colour properties were measured in the CIELAB colour space by using a KONICA CM-3600d COLORFLEX-DIFF2, HunterLab, Hunter Associates Laboratory, Inc, (Reston, Virginia, USA). The instrument was previously calibrated with a white standard tile. Colour coordinates, L (lightness), a* (red-green) and b* (yellow-blue) as well as the yellowness index (YI) were measured at random positions over the edible film surface. Average values of at least five measurements were calculated. Total color difference (ΔE) was calculated with respect to the control NaC edible film (NaC-G) as:

$$\Delta E = \sqrt{\Delta a^{*2} + \Delta b^{*2} + \Delta L^2} \quad (\text{Equation 1})$$

2.2.3. Scanning Electron Microscopy (SEM)

SEM micrographs of the surfaces as well as of the cryo-fractured cross-sections of plastizyced NaC based edible films were obtained with a PHILIPS XL30 Scanning Electron Microscope (SEM). In order to increase samples' electrical conductivity they were previously coated with a palladium/gold layer in vacuum conditions to be further observed by SEM.

2.2.4. Fourier Transform Infrared Spectroscopy

Attenuated total reflectance - Fourier transform infrared spectroscopy (ATR-FTIR) measurements of NaC based edible films were conducted by a Spectrum One FTIR spectrometer (Perkin Elmer instruments). Spectra were obtained in the 4000-650 cm^{-1} region at room temperature in transmission mode with a resolution of 4 cm^{-1} .

2.2.5. Mechanical Properties

The mechanical properties of edible films were evaluated by tensile test measurements. They were conducted at room temperature by using a universal testing machine (3344 Instron Instrument, Fareham Hants, UK) equipped with a 100 N load cell, at a crosshead speed of 25 $\text{mm}\cdot\text{min}^{-1}$ and initial length of 50 mm. Rectangular strips (10 x 100 mm^2) samples were used and at least five specimens were tested for each edible film formulation. Young modulus and elongation at break were calculated from the resulting stress-strain curves.

2.2.6. Dynamic Light Scattering

The particle size and particle size distribution of the sodium caseinate dispersion were determined with a dynamic light scattering (DLS) analyzer (Zetasizer Nano series ZS, Malvern Instrument Ltd., U.K.) equipped with a He-Ne laser beam at 658 nm and with a detection angle of 173°. Samples were dissolved in distilled water (1 mg/mL) and the experiments were performed at 20°C. The particle size value of NaC reported was the average of at least five consecutive runs.

2.2.7. Thermogravimetric Analysis

Thermogravimetric (TGA) measurements of plasticized NaC based edible films were performed in a TA-TGA Q500 thermal analyzer under dynamic mode weighing around 5-10 mg. Measurements were run from 30 to 700°C at 10°C min⁻¹ under nitrogen and oxidative atmosphere. The initial degradation temperatures (T_{ini}) were taken at 10% of mass loss and temperatures at the maximum degradation rate (T_{max}) were obtained from the first derivative of the TGA curves (DTG).

2.2.8 Antioxidant Activity of Film Forming Solution

The antioxidant activity was determined by means of 2,2-diphenyl-1-picrylhydrazyl (DPPH) method [51]. DPPH method is widely used mainly because it is simple, inexpensive and robust techniques [53]. It is an indicator radical that can be inhibited either by direct reduction via single electron transfer (SET) or by radical quenching via hydrogen atom transfer (HAT) [52, 62] due to the presence of a radical or an antioxidant [63]. It can be easily followed by the reduction of the characteristic DPPH wavelength absorption spectrum at 517 nm. The antioxidant activity of the film forming solutions was performed in triplicate and calculated as percentage of inhibition (I%) values expressed as gallic acid (GA) concentration using the Equation 2:

$$I (\%) = \frac{A_{control} - A_{sample}}{A_{control}} \times 100\% \quad (\text{Equation 2})$$

2.2.9. Oxygen Transmission Rate

The oxygen transmission rate (OTR) was measured to study the oxygen permeability of edible films by using a Systech Instruments 8500 oxygen permeation analyzer (Metrotec S.A, Spain) at room temperature and 2.5 atm. Edible film samples (14 cm diameter circle) were compressed between the upper and lower diffusion chamber at 25 ± 2°C. Pure oxygen (99.9% purity) was introduced into the upper half of the sample chamber while nitrogen (99.9% purity) was injected into the lower half.

2.2.10. Surface Wettability

Surface wettability of films was studied through static water contact angle measurements with a standard goniometer (EasyDrop-FM140, KRÜSS GmbH, Hamburg, Germany) equipped with a camera. Drop Shape Analysis SW21; DSA1 software was used to test the water contact angle (WCA) at room temperature. The contact angle was determined by randomly putting 5 drops of distilled water (≈ 5 μL) with a syringe onto the film surfaces and measured after 30 seconds [64]. Meanwhile, to determine the water contact angle evolution, photos were taken every 5 seconds.

3. RESULTS

3.1. Visual Appearance and UV-Vis Measurements

Plasticized NaC based edible films, with thickness of about $100 \pm 10 \mu\text{m}$, resulted transparent films, allowing seeing through them (Figure 3-a). After the addition of HT, the plasticized NaC edible films, with thickness ranging between 140 and 150 μm , kept their transparency but adquired a greenish tonality (Figure 3-b and c). These findings were corroborated by absorption measurements in the visible and UV region of the spectra (Figure 3-d) as well as by colourimetric measurements in the CIELab space (Table 1).

The control plastiziced NaC edible film (NaC-G) showed high transmission in the visible region of the spectra (400-700 nm) and the transparency value determined at 600 nm reached 86 %. Meanwhile, the presence of HT reduced the light transmission of the visible region of the spectra, decreasing the transparency to 75% for NaC-G-HT5 and to 68% for NaC-G-HT10 at 600 nm. Regardeless, UV region of the control plastiziced NaC edible film (NaC-G) showed again highest transmission in the UV-A spectra region (between 350 nm and 475 nm) with respect of HT added edible films (NaC-G-HT5 and NaC-G-HT10). Meanwhile, the most part of the UV-B region (between 280 nm and 315 nm, which causes the most photochemical degradation of plastics) [65] as well as UV-C region (100-280 nm, generally created from artificial light sources) [65] are not transmitted. In the case of HT added edible films it was observed that HT produced further UV bloking effect in the UV-A spectra region.

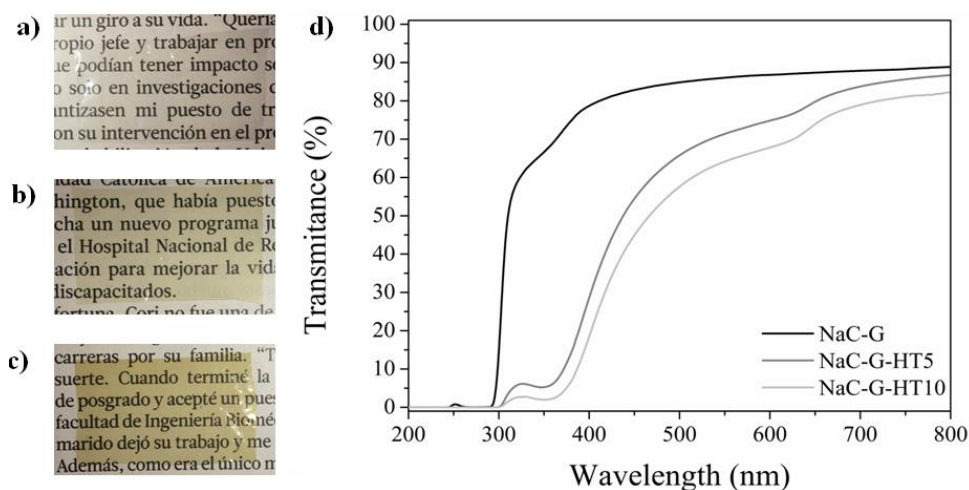


Figure 3. Visual appearance of edible films: a) NaC-G, b) NaC-G-HT5, c) NaC-G-HT10 and d) UV-Vis spectra of edible films.

Table 1. Color parameters from CIELab space and YI of edible films

Edible film	<i>L</i>	<i>a</i> *	<i>b</i> *	ΔE	<i>YI</i>
NaC-G	93.4 ± 0.6 ^a	-1.33 ± 0.06 ^a	3.3 ± 1.3 ^a	-	5.3 ± 2.4 ^a
NaC-G-HT5	85.7 ± 0.6 ^b	-2.99 ± 0.05 ^b	15.8 ± 0.9 ^b	14.8 ± 0.4 ^a	27.9 ± 1.7 ^b
NaC-G-HT10	83.1 ± 0.7 ^c	-2.99 ± 0.04 ^b	19.1 ± 0.8 ^c	18.9 ± 0.5 ^b	34.3 ± 1.5 ^c

^{a-c} Different superscripts within the same column indicate significant differences between formulations ($p < 0.05$).

Table 1 summarizes the color parameters obtained for NaC-G, NaC-G-HT5 and NaC-G-HT5 based edible films. NaC-G showed the highest *L* value typical from high brightness materials and *L* was significantly reduced by HT presence. The addition of HT also produced a green and yellow tonality as revealed by the deviation towards negative values of the *a** coordinate (indicative of a deviation towards green) and the deviation towards positive values for *b** coordinate (indicative of a deviation towards yellow). Therefore, the yellow index (*YI*), generally used to describe the change in color of a sample from clear toward yellow, was also determined. As expected, *YI* values showed the maximum value for the NaC-G-HT10 edible film, followed by NaC-G-HT5 and finally for the plasticized NaC system. The total color differences produced by the addition of HT were significantly different to the control NaC-G edible film and the ΔE value increased with higher amounts of HT. In fact the total color differences were significantly higher than 2.0, which is used as the threshold of perceptible color difference for the human eye [66].

The results from optical and colourimetric analysis showed that although the addition of HT produced a green-yellow tonality all edible formulations allowed seeing through the films, even those formulations with the highest amount of HT (10 wt%). It should be mentioned that transparency is one of the most important requirements for consumers acceptance in consideration of the potential use of these films in food coating applications [22]. Moreover, HT added NaC-G edible films can also offer a light barrier between 250 nm and 600 nm, which result interesting to protect some food products from the light [15].

3.2. Particle Size of Sodium Caseinate Film Forming Solution

The HT effect on the sodium caseinate particle size as well as on their distribution was studied by dynamic light scattering (DLS) measurements. The particle size and their distribution in the film forming solution seems to be interesting due to its impact on the properties of the edible films such as mechanical properties and barrier performance [67].

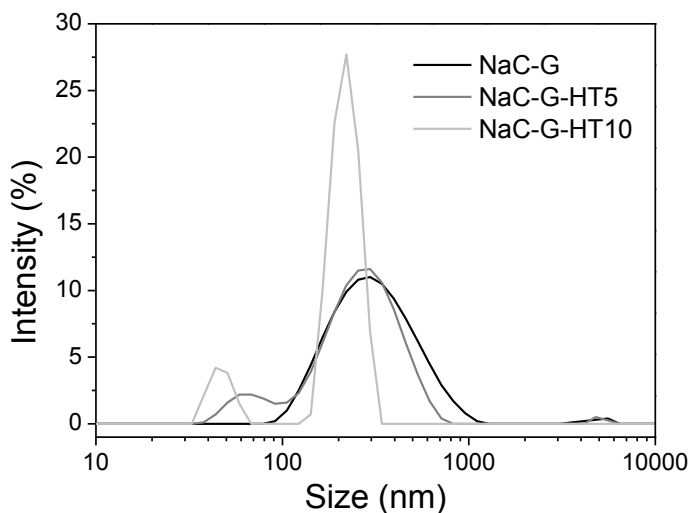


Figure 4. Particle size distributions of NaC-G, NaC-G-HT10 and NaC-G-HT5.

As seen in Figure 4, NaC-G system showed a bimodal size distribution, in accordance with the literature [68, 69]. NaC-G shows the main peak (from 80 nm to 1200 nm) centered at around 295 nm and a second small peak at about 5500 nm, suggesting the presence of aggregates. It is known that caseinates particles in water form aggregates since the use of water as solvent affects the hydration and volume of NaC and, thus, their particle size [69]. Meanwhile, further aggregates are due to the caseinates ability to form extensive intermolecular hydrogen bonds. With the addition of HT smaller particles size were obtained, as it reveals the peak centered at around 295 nm in NaC-G-HT5 and that at around 50 nm in NaC-G-HT10. While the mean peak remains centered at 295 nm in NaC-G-HT5, it is centered at 220 in NaC-G-HT10. This suggests a lower degree of aggregation of the NaC particles in the dispersion, and this effect became more remarkable as the HT amount increased. In fact, NaC-G-HT10 showed more homogeneous particle size distribution since the main peak became narrow (from 122 nm to 342 nm). This behaviour could be related with the fact that HT interacts with the NaC protein interrupting the protein-protein interaction and thus leading to less casein aggregates.

3.3. Structural Characterization

3.3.1. Scanning Electron Microscopy

In Figure 5 are shown the SEM micrographs of the surface and cross-fractured sections of edible films. As it is expected for plasticized sodium caseinate edible films [22, 31, 70], all formulations showed mostly homogeneous and smooth surfaces with no apparent phase separation (Figure 5 a, c and e).

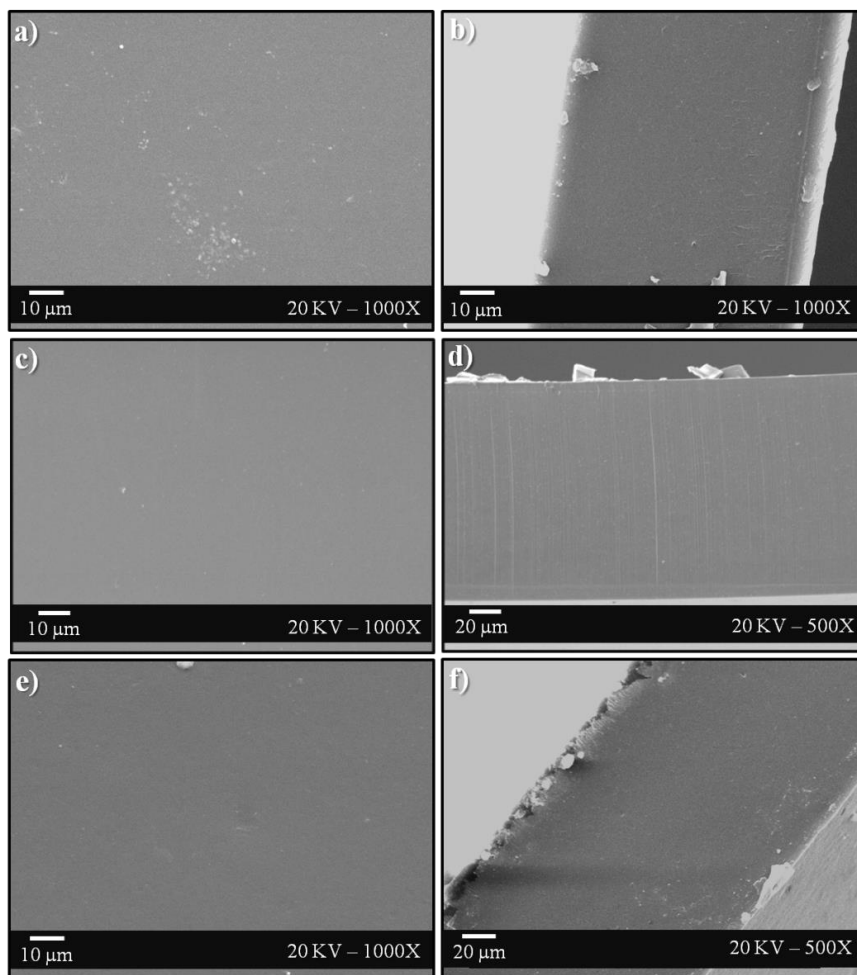


Figure 5. SEM micrographs of edible films surfaces (left side) and cryo-fracture cross sections (right side): NaC-G (a and b), NaC-G-5HT (c and d) and NaC-G-10HT (e and f).

One of the foremost drawbacks observed in edible films prepared by solvent casting process is the presence of small holes, due to the bubbles bursting through the surface when solvent vaporization occurred [71]. The processing conditions used here, that is ultrasound degasification process followed by the cooling of the film forming solution, allowed yielding films without physical defects (i.e.,: cracks or bubbles) (Figure 5 b, d and f). No interfaces were observed in those formulations containing HT, NaC-G-5HT (Figure 5 c and d) and NaC-G-10HT (Figure 5 e and f), indicating a good compatibility between the essential oil and the plasticized sodium caseinate polymeric matrix.

3.3.2. Fourier Transform Infrared Spectroscopy

Figure 6 shows FTIR spectra of plasticized sodium caseinate films with HT 5 and 10 wt% and the control sample without HT (NaC-G). There was an increase in the broad band between 3650 and 3200 cm^{-1} corresponding to the stretching of $-\text{OH}$ bond, when the

HT was added to the samples. The small shoulder at 3080 cm^{-1} is linked to NH bond of proteins [72]. Then, the region between 2925 cm^{-1} and 2965 cm^{-1} , corresponds to the C-H bonding, in particular CH_2 and CH_3 , respectively. Amide I and amide II bands are located at 1630 cm^{-1} and 1540 cm^{-1} , respectively. When HT was added to the formulations, the band at 1630 cm^{-1} was shifted to lower wavenumbers, due to the tendency of the NH group to form hydrogen bonding with other molecules, in this case water, glycerol and HT [33, 73]. This effect demonstrated that there is a good incorporation of the antioxidant in the protein matrix. Indeed, the presence of HT is evidenced in the region between 1300 cm^{-1} and 923 cm^{-1} . In particular there was an increase in the intensity of the bands at 1241 cm^{-1} corresponding to the deformation in-plane of phenolic compounds.

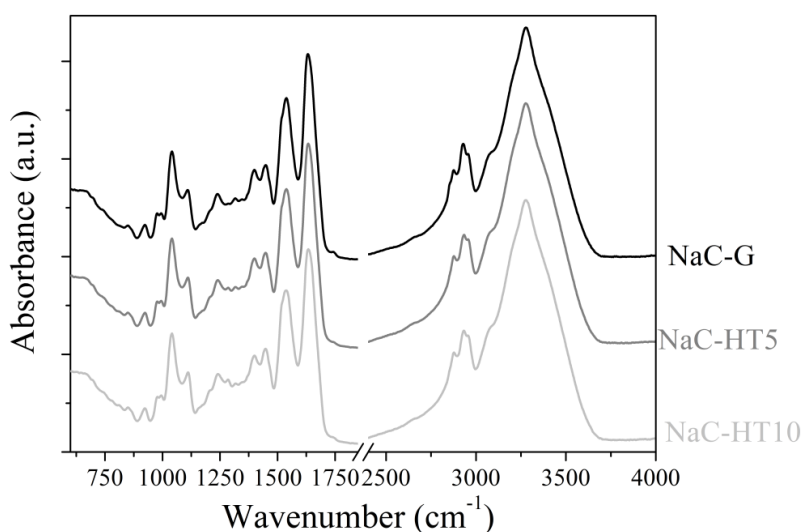


Figure 6. FTIR spectra of plasticized sodium caseinate films without HT and with 5 wt% and 10 wt% of HT.

3.4. Mechanical Properties

The mechanical performance of edible films intended to be used as food coatings is very relevant. In fact, the material should have enough ductility for films manufacturing and at the same time the enough stiffness to protect foodstuff from the environment. It has been observed that plasticizer is required for NaC film forming because the inherent brittleness of NaC matrix results in fragile films that crack before testing the tensile properties [31]. This is why in the present work glycerol was added as plasticizer. The stiffness of plasticized NaC based materials was evaluated from the Young modulus (Figure 7-a), while the elongation at break was used to evaluate the stretching ability of the edible films (Figure 7-b).

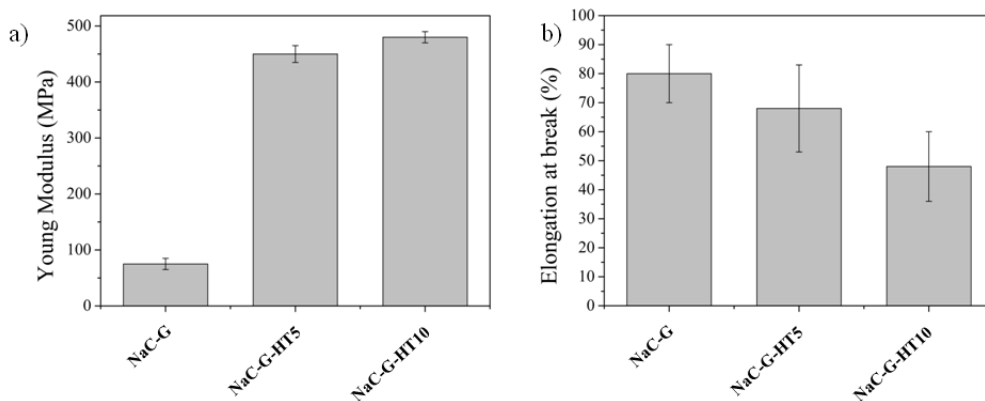


Figure 7. Mechanical properties of edible films a) Young modulus and b) elongation at break.

The Young modulus increased with the addition of HT. This behavior may be attributed to the fact that HT positively interacts with NaC protein chains during the film formation, limiting the polymer chain mobility and lead to a more rigid material. In addition, since HT is a highly polar compound; it may compete with protein chains for water molecules, increasing protein-protein interaction and producing a stiffer structure. This is linked to the lower values of elongation at break obtained for the active samples, comparing with the control NaC-G edible film, but they still showed enough ability to stretch out. The elongation at break of the control NaC-G film was around 80%, underlining the ductile behavior of the plasticized caseinate system as previously observed in the literature [29, 31].

3.5. Thermogravimetric Analysis

3.5.1. Degradation under Inert Atmosphere of Nitrogen

TGA thermograms, under inert atmosphere, of the prepared plasticized (35% wt) and non-plasticized biobased films, and those added with 5 and 10 wt% of HT are shown in Figure 8. Degradation of the samples could be separated in three steps. The first one, from 30-100°C (not shown in the thermogram), corresponds to water evaporation and at the end of this first step, starts HT degradation. The second step, between 200 and 300°C, with approximately a weight loss of 35%, corresponds to the degradation of plasticizer. Non-plasticized film did not present this degradation step and its main degradation starts at 300°C, at the beginning of the third degradation step for plasticized samples. Though, a third step corresponds to the full degradation of the protein and this happened between 300 and 700°C. From derivate curve (DTG) showed in Figure 8-b, peak temperature corresponding to the maximum degradation rate temperature (T_{max}) of each degradation step was easily determined.

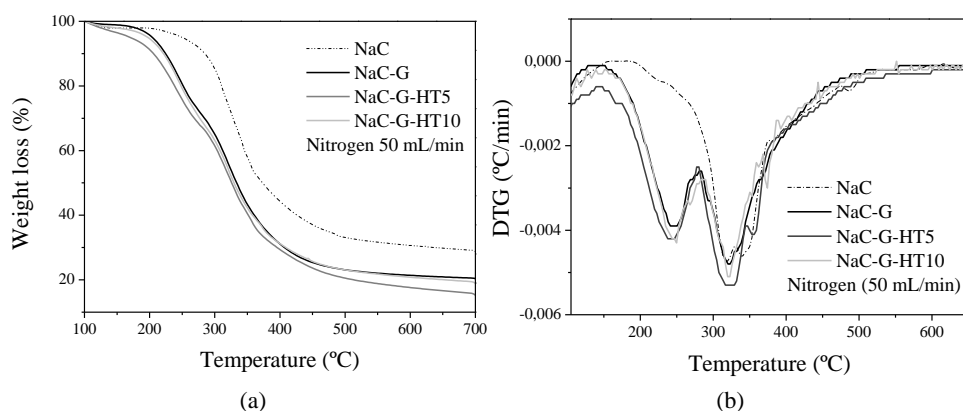


Figure 8. Thermograms of NaC films in nitrogen (50 mL/min). a) Weight loss (%) vs temperature; b) Degradation rate vs Temperature (DTG).

Table 2. Parameters from TGA assay

Sample	Main degradation temperatures under N ₂			% Residue at 700 °C
	T _{ini} (°C)	T _{max1} (°C)	T _{max2} (°C)	
NaC	238	-	317	28
NaC-G	210	248	323	19
NaC-G-HT5%	166	244	323	14
NaC-G-HT10%	190	250	323	19

Results showed that the addition of HT in caseinate films did not affect negatively thermal properties of the samples.

In Table 2, parameters calculated from thermograms are shown. No significant differences were observed between samples regarding T_{max} values. On the other hand, T_{ini} was decreased with the addition of HT, maybe due to the early decomposition of HT under these conditions. However, it was possible to see that higher concentrations of HT increased again the initial degradation temperature, this mean that higher concentration of the antioxidant is needed to maintain thermal stability of the caseinate films.

3.5.2 Degradation under Oxidant Atmosphere of Oxygen

Indeed, degradation under oxidant atmosphere presented several steps, but the profile seems to be different to the previous one under inert atmosphere. Differences between samples are more evident when the analysis was performed in oxygen. From Figure 9 is possible to see that degradation of NaC-G-HT10 film happened later than the other two studied samples. In fact, this could be attributed to an antioxidant effect on the matrix itself. Table 3 shows parameters of TGA curves. Again, 10% of HT was necessary to find an appreciable increase in thermal properties, since an appreciable increase in T_{ini} was observed for these samples. Thus, the presence of HT at the highest value of 10 wt% acts as a thermo-oxidative stabilizer for the NaC matrix.

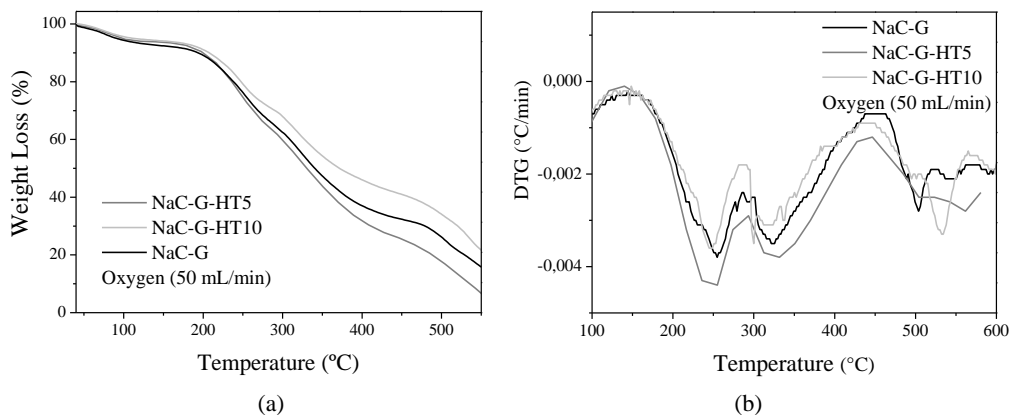


Figure 9. Thermograms of NaC films in oxygen (50 mL/min). a) Weight loss (%) vs temperature; b) Degradation rate vs Temperature (DTG).

Table 3. Parameters from TGA assay

Sample	Main degradation temperatures under O ₂		
	T _{ini} (°C)	T _{max2} (°C)	T _{max3} (°C)
NaC-G	192	255	324
NaC-G-HT5%	198	248	324
NaC-G-HT10%	207	247	323

3.6. Antioxidant Activity

The main objective of antioxidant added coating films is to reduce food lipid oxidation process on food surface during storage [16]. Thus, the antioxidant activity of the film forming solution was demonstrated by measuring the radical scavenging ability, since scavenging of radicals is one of the main antioxidant mechanisms [74]. HT antioxidant reduces the DPPH radicals by acting as a donor of a hydrogen atom [62]. As the HT proportion increased from 0 to 10 wt%, the DPPH scavenging activity expressed as gallic acid (GA) concentration increased from 0 to 49.5 ppm. It is known that the solubility characteristics of the antioxidant can determine its effectiveness. HT shows high solubility in water ($\approx 50 \text{ g L}^{-1}$) and, consequently, HT based materials usually show high antioxidant activity in aqueous solutions (i.e., aqueous food simulants [15]).

3.7. Surface Wettability

Surface wettability is a relevant property for coating materials intended to be used in contact with food, since it will directly influence many other functional properties of the

polymeric material such as the permeability towards water vapor, selective adsorption, adhesion, printing, controlled release of molecules, the beginning of biodegradation process, etc. [75]. Thus, water contact angle measurements are frequently measured to evaluate the hydrophilic/hydrophobic character of polymeric materials. NaC is a highly hydrophilic polymer and the WCA resulted in $54.4^\circ \pm 1.1^\circ$ NaC-G, while it increased with HT addition to $66.0^\circ \pm 0.8^\circ$ for NaC-G-HT5 and $70.3^\circ \pm 1.6^\circ$ for NaC-G-HT10. Edible film formulations became slightly more hydrophobic due to the presence of HT, suggesting that the HT interacts with the protein matrix and water molecules interrupting the water-protein interaction and enhancing protein-protein bonding. As a consequence of the high hydrophilic nature of NaC-G matrix after 5 seconds the WCA significantly decreased in these films (from $54.4^\circ \pm 1.0^\circ$ to $52.4^\circ \pm 0.9^\circ$), while it was maintained for HT added films after around 30 s (Figure 10). However, a swelling phenomenon took then place, interrupting the HT-protein interactions showing significant changes in the WCA values. Subsequently, a fast water absorption mechanism solubilized the NaC-G edible film. Water drops took 60 s to solubilize the NaC-G-HT materials, while around 80 s were needed to solubilize NaC-G samples due to the higher amount of polymeric matrix (NaC-G) in this formulation (65 wt%). These results suggest that the presence of HT produced an induction period in the polymeric matrix water absorption process, due to the limited polymer chain mobility in NaC-G-HT based materials.

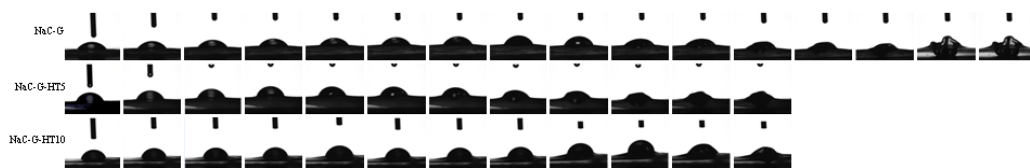


Figure 10. Water contact angle evolution of plasticized NaC edible films (photos were taken every 5 seconds).

3.8. Oxygen Barrier

Coating barrier performance was evaluated by means of oxygen transmission rate (OTR.e). NaC-based films showed excellent oxygen barrier properties, even when caseinate matrix is plasticized with glycerol (NaC-G edible film $1.5 \pm 0.1 \text{ cm}^3 \text{ mm m}^{-2} \text{ day}^{-1}$) [42]. The addition of 5 wt% of HT increased the oxygen permeation of NaC-G to $2.0 \pm 0.1 \text{ cm}^3 \text{ mm m}^{-2} \text{ day}^{-1}$ in NaC-G-HT5. This behavior could be related with the lower NaC particle size of HT added emulsions, discussed in DLS results. No significant changes were observed with higher addition of amounts of HT (NaC-G-HT10 = $2.2 \pm 0.4 \text{ cm}^3 \text{ mm m}^{-2} \text{ day}^{-1}$) [76]. Nevertheless, it should be highlighted that NaC-G-HT films still showed excellent oxygen barrier properties, with similar OTR.e values of poly(ethylene

terphthalate) (PET) films ($3 \text{ cm}^3 \text{ mm m}^{-2} \text{ day}^{-1}$) [77]. Therefore, NaC-G-HT based formulations resulted to be an attractive alternative for food coating applications were barrier to oxygen is critical to avoid or reduce oxidative processes.

CONCLUSION

Antioxidant edible coatings result in smart materials that can provide a long-term food protection through an increase on stability of the packed food by the addition of antioxidant active agents, in comparison with the direct addition of the antioxidant into the foodstuff. Additionally, edible coatings will not result in any environmental drawbacks. Prepared active films showed good mechanical and thermal properties to be used as food coating/packaging. Slight increase in thermoxidative stability of the samples was observed for the additivated films with HT. Visual aspect of the material was good, with a change in the colour of the films but the transparency was not altered. As the HT proportion increased from 0 to 10 wt%, the DPPH scavenging activity expressed as gallic acid (GA) concentration increased considerably. The addition of hydroxytyrosol at two levels in plasticized sodium caseinate films to develop antioxidant active films resulted in a good alternative to avoid or retard foodstuff oxidation and though increase food shelf life.

ACKNOWLEDGMENTS

Authors gratefully thank Prof. Alfonso Jiménez (University of Alicante, Spain) for his collaboration and useful discussions. Prof. Juan López Martínez (Polytechnic University of Valencia, Spain) and Dr. Marta Fernández García (ICTP-CSIC, Spain) are acknowledged for their assistance with characterization techniques. M. P. Arrieta thanks the Spanish Ministry of Economy and Competitiveness (MINECO) for Juan de la Cierva contract (FJCI-2014-20630). M. A. Peltzer thanks to the National Scientific and Technical Research Council (CONICET) for being a member of the institution. Authors want to thank Ferrer Alimentación S. A., for providing the sodium caseinate.

REFERENCES

- [1] Vanderroost M, Ragaert P, Devlieghere F, De Meulenaer B. Intelligent food packaging: The next generation. *Trends in Food Science & Technology*. 2014;39(1):47-62.

- [2] Peponi L, Arrieta MP, Mujica-Garcia A, López D. Smart Polymers. *Modification of Polymer Properties* 2016. p. 131-154.
- [3] López-Gómez A, Cerdán-Cartagena F, Suardíaz-Muro J, Boluda-Aguilar M, Hernández-Hernández ME, López-Serrano MA, et al., Radiofrequency Identification and Surface Acoustic Wave Technologies for Developing the Food Intelligent Packaging Concept. *Food Engineering Reviews*. 2015;7(1):11-32.
- [4] Arrieta MP, Sessini V, Peponi L. Biodegradable poly(ester-urethane) incorporated with catechin with shape memory and antioxidant activity for food packaging. *European Polymer Journal*. 2017;94:111-124.
- [5] Biji K, Ravishankar C, Mohan C, Gopal TS. Smart packaging systems for food applications: a review. *Journal of Food Science and Technology*. 2015:1-11.
- [6] Muhamad II, Salleh E, Khairudin N, Salehudin MH, Karim NA. Active and smart packaging film for food postharvest treatment. *Postharvest Biology and Technology of Horticultural Crops: Principles and Practices for Quality Maintenance*. 2015:217.
- [7] Brody AL, Strupinsky E, Kline LR. *Active packaging for food applications*: CRC press; 2001.
- [8] Day BPF. Active packaging of food. In: Kerry J, Butler P, editors. *Smart packaging technologies for fast moving consumer goods*: John Wiley & Sons; 2008. p. 1-17.
- [9] Realini CE, Marcos B. Active and intelligent packaging systems for a modern society. *Meat Science*. 2014;98(3):404-419.
- [10] Terry LA, Ilkenhans T, Poulston S, Rowsell L, Smith AW. Development of new palladium-promoted ethylene scavenger. *Postharvest Biology and Technology*. 2007;45(2):214-220.
- [11] Rouquerol J, Rouquerol F, Llewellyn P, Maurin G, Sing KS. *Adsorption by powders and porous solids: principles, methodology and applications*: Academic press; 2013.
- [12] Kuppler RJ, Timmons DJ, Fang Q-R, Li J-R, Makal TA, Young MD, et al., Potential applications of metal-organic frameworks. *Coordination Chemistry Reviews*. 2009;253(23):3042-3066.
- [13] Kerry JP, O'Grady MN, Hogan SA. Past, current and potential utilisation of active and intelligent packaging systems for meat and muscle-based products: A review. *Meat Science*. 2006;74(1):113-130.
- [14] Benbettaïeb N, Tanner C, Cayot P, Karbowski T, Debeaufort F. Impact of functional properties and release kinetics on antioxidant activity of biopolymer active films and coatings. *Food chemistry*. 2018;242(Supplement C):369-377.
- [15] Fortunati E, Luzi F, Dugo L, Fanali C, Tripodo G, Santi L, et al., Effect of hydroxytyrosol methyl carbonate on the thermal, migration and antioxidant properties of PVA-based films for active food packaging. *Polymer International*. 2016;65(8):872-882.

- [16] Helal A, Desobry S, Banon S, Shamsia SM. Antioxidant activity and bioaccessibility of phenols-enriched edible casein/caseinate coatings during in vitro digestion. *Journal of Dairy Research*. 2015;82(1):56-63.
- [17] Avérous L. Biodegradable Multiphase Systems Based on Plasticized Starch: A Review. *Journal of Macromolecular Science, Part C*. 2004;44(3):231-274.
- [18] Arrieta MP, Fortunati E, Dominici F, Rayón E, López J, Kenny JM. Multifunctional PLA–PHB/cellulose nanocrystal films: Processing, structural and thermal properties. *Carbohydrate Polymers*. 2014;107(Supplement C):16-24.
- [19] Colak BY, Peynichou P, Galland S, Oulahal N, Prochazka F, Degraeve P. Antimicrobial Activity of Nisin and Natamycin Incorporated Sodium Caseinate Extrusion-Blown Films: A Comparative Study with Heat-Pressed/Solution Cast Films. *Journal of Food Science*. 2016;81(5):E1141-E1150.
- [20] Arrieta MP, López J, Ferrándiz S, Peltzer MA. Characterization of PLA-limonene blends for food packaging applications. *Polymer Testing*. 2013;32(4):760-768.
- [21] Bustos C RO, Alberti R FV, Matiacevich SB. Edible antimicrobial films based on microencapsulated lemongrass oil. *Journal of Food Science and Technology*. 2016;53(1):832-839.
- [22] Fabra MJ, Talens P, Chiralt A. Microstructure and optical properties of sodium caseinate films containing oleic acid-beeswax mixtures. *Food Hydrocolloids*. 2009;23(3):676-683.
- [23] Arvanitoyannis I, Psomiadou E, Nakayama A. Edible films made from sodium caseinate, starches, sugars or glycerol. *Part 1. Carbohydrate Polymers*. 1996;31(4):179-192.
- [24] Introzzi L, Fuentes-Alventosa JM, Cozzolino CA, Trabattoni S, Tavazzi S, Bianchi CL, et al., “Wetting Enhancer” Pullulan Coating for Antifog Packaging Applications. *ACS Applied Materials & Interfaces*. 2012;4(7):3692-3700.
- [25] Arrieta MP, Peltzer MA, Garrigos MC, Jiménez A. Antibacterial biofilms based on calcium caseinate incorporated with carvacrol. *Microbes in Applied Research: Current Advances and Challenges*, Malaga, Spain, 14 - 16 September 20112012. p. 469-473.
- [26] Banerjee R, Chen H, Wu J. Milk protein-based edible film mechanical strength changes due to ultrasound process. *Journal of Food Science*. 1996;61(4):824-828.
- [27] Belyamani I, Prochazka F, Assezat G. Production and characterization of sodium caseinate edible films made by blown-film extrusion. *Journal of Food Engineering*. 2014;121:39-47.
- [28] Avena- Bustillos RJ, Krochta JM. Water Vapor Permeability of Caseinate- Based Edible Films as Affected by pH, Calcium Crosslinking and Lipid Content. *Journal of Food Science*. 1993;58(4):904-907.

- [29] Fabra MJ, Talens P, Chiralt A. Tensile properties and water vapor permeability of sodium caseinate films containing oleic acid–beeswax mixtures. *Journal of Food Engineering*. 2008;85(3):393-400.
- [30] Pérez Córdoba LJ, Sobral PJA. Physical and antioxidant properties of films based on gelatin, gelatin-chitosan or gelatin-sodium caseinate blends loaded with nanoemulsified active compounds. *Journal of Food Engineering*. 2017;213:47-53.
- [31] Arrieta MP, Peltzer MA, Garrigós MDC, Jiménez A. Structure and mechanical properties of sodium and calcium caseinate edible active films with carvacrol. *Journal of Food Engineering*. 2013;114(4):486-494.
- [32] Siew DCW, Heilmann C, Eastal AJ, Cooney RP. Solution and film properties of sodium caseinate/glycerol and sodium caseinate/polyethylene glycol edible coating systems. *Journal of Agricultural and Food Chemistry*. 1999;47(8):3432-3440.
- [33] Pereda M, Aranguren MI, Marcovich NE. Characterization of chitosan/caseinate films. *Journal of Applied Polymer Science*. 2008;107(2):1080-1090.
- [34] Ye Z, Xiu S, Shahbazi A, Zhu S. Co-liquefaction of swine manure and crude glycerol to bio-oil: Model compound studies and reaction pathways. *Bioresource Technology*. 2012;104(Supplement C):783-787.
- [35] EU Commission. *EU Guidance to the Commission Regulation (EC) No 450/2009 of 29 May 2009 on active and intelligent materials and articles intended to come into contact with food*. 2009.
- [36] Gómez-Estaca J, Giménez B, Montero P, Gómez-Guillén MC. Incorporation of antioxidant borage extract into edible films based on sole skin gelatin or a commercial fish gelatin. *Journal of Food Engineering*. 2009;92(1):78-85.
- [37] Vichi S, Zitterl-Eglseer K, Jugl M, Franz C. Determination of the presence of antioxidants deriving from sage and oregano extracts added to animal fat by means of assessment of the radical scavenging capacity by photochemiluminescence analysis. *Nahrung - Food*. 2001;45(2):101-104.
- [38] Zandi P, Ahmadi L. Antioxidant Effect of Plant Extracts of Labiatae Family. *Journal of Food Science and Technology*. 2000;37(4):436-439.
- [39] Takácsová M, Příbela A, Faktorová M. Study of the antioxidative effects of thyme, sage, juniper and oregano. *Food/Nahrung*. 1995;39(3):241-243.
- [40] Ramos M, Jiménez A, Peltzer M, Garrigós MC. Development of novel nano-biocomposite antioxidant films based on poly (lactic acid) and thymol for active packaging. *Food chemistry*. 2014;162:149-155.
- [41] Peltzer M, Wagner J, Jimenez A. Migration study of carvacrol as a natural antioxidant in high-density polyethylene for active packaging. *Food Additives and Contaminants - Part A Chemistry, Analysis, Control, Exposure and Risk Assessment*. 2009;26(6):938-946.

- [42] Arrieta MP, Peltzer MA, López J, Garrigós MDC, Valente AJM, Jiménez A. Functional properties of sodium and calcium caseinate antimicrobial active films containing carvacrol. *Journal of Food Engineering*. 2014;121(1):94-101.
- [43] Quesada J, Sendra E, Navarro C, Sayas-Barberá E. Antimicrobial Active Packaging including Chitosan Films with *Thymus vulgaris* L. *Essential Oil for Ready-to-Eat Meat. Foods*. 2016;5(3):57.
- [44] Kulišić T, Dragović-Uzelac V, Miloš M. Antioxidant Activity of Aqueous Tea Infusions Prepared from Oregano, Thyme and Wild Thyme. *Food Technology & Biotechnology*. 2006;44(4).
- [45] Fabra MJ, Hambleton A, Talens P, Debeaufort F, Chiralt A. Effect of ferulic acid and α -tocopherol antioxidants on properties of sodium caseinate edible films. *Food Hydrocolloids*. 2011;25(6):1441-1447.
- [46] Gimenez B, Moreno S, López-Caballero M, Montero P, Gómez-Guillén M. Antioxidant properties of green tea extract incorporated to fish gelatin films after simulated gastrointestinal enzymatic digestion. *LWT-Food Science and Technology*. 2013;53(2):445-451.
- [47] Charoenprasert S, Mitchell A. Factors influencing phenolic compounds in table olives (*Olea europaea*). *Journal of Agricultural and Food Chemistry*. 2012;60(29):7081-7095.
- [48] Hamza M, Sayadi S. The Possibility of Recovering of Hydroxytyrosol from Olive Milling Wastewater by Enzymatic Bioconversion. In: Boskou D, Clodoveo ML, editors. *Products from Olive Tree*. Rijeka: InTech; 2016. p. Ch. 14.
- [49] Rodríguez- Gutiérrez G, Duthie GG, Wood S, Morrice P, Nicol F, Reid M, et al., Alperujo extract, hydroxytyrosol, and 3, 4- dihydroxyphenylglycol are bioavailable and have antioxidant properties in vitamin E- deficient rats—a proteomics and network analysis approach. *Molecular nutrition & food research*. 2012;56(7):1131-1147.
- [50] He J, Alister-Briggs M, de Lyster T, Jones GP. Stability and antioxidant potential of purified olive mill wastewater extracts. *Food chemistry*. 2012;131(4):1312-1321.
- [51] Okada Y, Okada M. Scavenging Effect of Water Soluble Proteins in Broad Beans on Free Radicals and Active Oxygen Species. *Journal of Agricultural and Food Chemistry*. 1998;46(2):401-406.
- [52] Gómez-Estaca J, López-de-Dicastillo C, Hernández-Muñoz P, Catalá R, Gavara R. Advances in antioxidant active food packaging. *Trends in Food Science & Technology*. 2014;35(1):42-51.
- [53] López de Dicastillo C, Navarro R, Guarda A, Galotto MJ. Development of Biocomposites with Antioxidant Activity Based on Red Onion Extract and Acetate Cellulose. *Antioxidants*. 2015;4(3):533-547.

- [54] Fernández-Bolaños JG, López Ó, Fernández-Bolaños J, Rodríguez-Gutiérrez G. Hydroxytyrosol and derivatives: Isolation, synthesis, and biological properties. *Current Organic Chemistry*. 2008;12(6):442-463.
- [55] Schaffer S, Podstawa M, Visioli F, Bogani P, Müller WE, Eckert GP. Hydroxytyrosol-rich olive mill wastewater extract protects brain cells in vitro and ex vivo. *Journal of Agricultural and Food Chemistry*. 2007;55(13):5043-5049.
- [56] Obied HK, Allen MS, Bedgood DR, Prenzler PD, Robards K, Stockmann R. Bioactivity and analysis of biophenols recovered from olive mill waste. *Journal of Agricultural and Food Chemistry*. 2005;53(4):823-837.
- [57] Aeschbach R, Löliger J, Scott B, Murcia A, Butler J, Halliwell B, et al., Antioxidant actions of thymol, carvacrol, 6-gingerol, zingerone and hydroxytyrosol. *Food and Chemical Toxicology*. 1994;32(1):31-36.
- [58] Attya M, Benabdelkamel H, Perri E, Russo A, Sindona G. Effects of conventional heating on the stability of major olive oil phenolic compounds by tandem mass spectrometry and isotope dilution assay. *Molecules*. 2010;15(12):8734-8746.
- [59] Peltzer M, Jiménez A. Determination of oxidation parameters by DSC for polypropylene stabilized with hydroxytyrosol (3,4-dihydroxy-phenylethanol). *Journal of Thermal Analysis and Calorimetry*. 2009;96(1):243-248.
- [60] Beltrán A, Valente AJM, Jiménez A, Garrigós MC. Characterization of poly(ϵ -caprolactone)-based nanocomposites containing hydroxytyrosol for active food packaging. *Journal of Agricultural and Food Chemistry*. 2014;62(10):2244-2252.
- [61] Matsakidou A, Biliaderis CG, Kiosseoglou V. Preparation and characterization of composite sodium caseinate edible films incorporating naturally emulsified oil bodies. *Food Hydrocolloids*. 2013;30(1):232-240.
- [62] Galano A. Free Radicals Induced Oxidative Stress at a Molecular Level: The Current Status, Challenges and Perspectives of Computational Chemistry Based Protocols. *Journal of the Mexican Chemical Society*. 2015;59:231-262.
- [63] Prior RL, Wu X, Schaich K. Standardized methods for the determination of antioxidant capacity and phenolics in foods and dietary supplements. *Journal of Agricultural and Food Chemistry*. 2005;53(10):4290-4302.
- [64] Fombuena V, Balart J, Boronat T, Sánchez-Nácher L, Garcia-Sanoguera D. Improving mechanical performance of thermoplastic adhesion joints by atmospheric plasma. *Materials and Design*. 2013;47:49-56.
- [65] Auras R, Harte B, Selke S. An overview of polylactides as packaging materials. *Macromolecular bioscience*. 2004;4(9):835-864.
- [66] Paravina RD, Ontiveros JC, Powers JM. Curing- Dependent Changes in Color and Translucency Parameter of Composite Bleach Shades. *Journal of Esthetic and Restorative Dentistry*. 2002;14(3):158-166.

- [67] Fabra MJ, Jiménez A, Atarés L, Talens P, Chiralt A. Effect of Fatty Acids and Beeswax Addition on Properties of Sodium Caseinate Dispersions and Films. *Biomacromolecules*. 2009;10(6):1500-1507.
- [68] Xuexin W, Golding M. Effects of urea addition on the structural and material properties of sodium caseinate solutions and emulsions. *Food Hydrocolloids*. 2014;42(Part 1):162-170.
- [69] Sosa-Herrera MG, Martínez-Padilla LP, Delgado-Reyes VA, Torres-Robledo A. Effect of agave fructans on bulk and surface properties of sodium caseinate in aqueous media. *Food Hydrocolloids*. 2016;60(Supplement C):199-205.
- [70] Pereda M, Aranguren MI, Marcovich NE. Caseinate films modified with tung oil. *Food Hydrocolloids*. 2010;24(8):800-808.
- [71] Chalier P, Ben Arfa A, Preziosi-Belloy L, Gontard N. Carvacrol losses from soy protein coated papers as a function of drying conditions. *Journal of Applied Polymer Science*. 2007;106(1):611-620.
- [72] Kong J, Yu S. Fourier transform infrared spectroscopic analysis of protein secondary structures. *Acta biochimica et biophysica Sinica*. 2007;39(8):549-559.
- [73] Gao C, Stading M, Wellner N, Parker ML, Noel TR, Mills EC, et al., Plasticization of a protein-based film by glycerol: a spectroscopic, mechanical, and thermal study. *Journal of Agricultural and Food Chemistry*. 2006;54(13):4611-4616.
- [74] Fortunati E, Luzi F, Fanali C, Dugo L, Giovanna Belluomo M, Torre L, et al., Hydroxytyrosol as active ingredient in poly(vinyl alcohol) films for food packaging applications. *Journal of Renewable Materials*. 2017;5(2):81-95.
- [75] Arrieta MP, Fortunati E, Burgos N, Peltzer MA, López J, Peponi L. Nanocellulose-Based Polymeric Blends for Food Packaging Applications. *Multifunctional Polymeric Nanocomposites Based on Cellulosic Reinforcements*. 2016. p. 205-252.
- [76] Ramos M, Arrieta MP, Beltran A, Garrigós MC. Characterization of PLA, PCL and sodium caseinate active bio-films for food packaging applications. *Food Packaging: Procedures, Management and Trends*. 2012. p. 63-78.
- [77] Burgos N, Martino VP, Jiménez A. Characterization and ageing study of poly (lactic acid) films plasticized with oligomeric lactic acid. *Polymer degradation and stability*. 2013;98(2):651-658.

Chapter 14

IS YOUR POLYMER SMART ENOUGH? BETTER MAKE A HYBRID!

***Daniela Anahí Sánchez-Téllez^{1,2,*}, Lucía Téllez-Jurado, PhD¹
and Luís María Rodríguez-Lorenzo, PhD^{2,3}***

¹Department of Engineering in Metallurgy and Materials,
Instituto Politécnico Nacional-ESIQIE,
Mexico City, Mexico

²Networking Biomedical Research Centre in Bioengineering,
Biomaterials and Nanomedicine, CIBER-BBN, Spain

³Institute of Polymer Science and Technology-
Spanish Research Council (CSIC), Madrid, Spain

ABSTRACT

The main advantages of inorganic–organic hybrids are the combination of frequent dissimilar properties of organic and inorganic components in one material and the opportunity to develop an almost unlimited set of new materials with a large spectrum of known and yet unknown properties, because of the many possible combinations. Usually, in composite materials, polymer networks serve as organic matrices and inorganic components (Si, Ti, Sn, Al-based compounds, etc.) serve as fillers dispersed into the polymer network. These composites can be considered within Class I hybrids. In this class, weak bonds between components can be found such as Van der Waals forces or hydrogen bonds. Moreover there is Class II hybrids where components are linked by strong chemical bonds such as ionic or ionic-covalent bonds. Two types of reactions can be used to synthesize Class II hybrids: the simultaneous polymerization and the sequential polymerization of organic and inorganic monomers. Different structures can be obtained by altering the polymerization procedure: inorganic phase nanodomains

* Corresponding Author Email: danielatellez06@gmail.com.

dispersed into the organic matrix; networks with bicontinuous phase structure; networks with ordered inorganic phase; and organic-inorganic block copolymer networks with inorganic junction domains. The chemistry of inorganic-organic network hybrids is mainly developed using hybrid molecular precursors such as organically modified metal-alkoxides or oligomers of general formula $R'_n\text{Si}(\text{OR})_{4-n}$ or $(\text{OR})_{4-n}\text{Si-R}''\text{-Si}(\text{OR})_{4-n}$ with $n = 1,2,3$, respectively. Several stimuli responsive hybrids have been manufactured for different applications: drug delivery systems based on mesoporous silica supports (MSS) have been described responding to physical, chemical or biochemical stimuli; antibacterial hybrids based on photocatalyst reactions; smart biosensing systems based on thin metallic and inorganic nanofilms with natural peptides, glutathione or aminothiols are also being described responding to complex opto-electronic interactions; graphene-based bilayer and multilayer actuators made from graphene and conducting polymers are described responding to chemical variations; and self-healing graphene-polymer hybrids are described responding to near-infrared region (NIR) irradiation. These materials are among the highlighted examples of hybrid smart materials.

Keywords: hybrids, *sol-gel*, silica supports, drug delivery, antibacterial, graphene

INTRODUCTION

Smart polymers are stimuli-responsive polymers which can be sensitive to a number of factors such as pH, temperature, humidity, wavelength or intensity of light and electric or magnetic fields. These polymers can respond in several ways: altering color or transparency; becoming conductive or permeable to water; changing and recovering their shape. Smart polymers are used in specialized applications such as biodegradable packaging [1] and tissue or biomedical engineering [2] as extensively described in this book.

Thermo-responsive polymers, such as polyurethanes [3], can be an example. They undergo modification of their elasticity, due to alterations in the bulk amorphous (soft segment) or crystal (hard segment) mobility. The switching temperature (T_s) depends on the physical or chemical crosslinking, the degree of crosslinking and the ratio of soft and hard segments. Moreover, the shape-memory effects are strongly dependent on the molecular architecture of the polymers such as the structure and the orientation of polymer chains. Therefore, this kind of smart materials requires: 1) blocks (soft and hard segments) which act as switching segments and 2) crosslinked points (networks) which determine the permanent shape of the material. Thermoresponsive materials have gained importance in the last few years in the biomedical field. They can act as drug delivery systems in the human body as long as the trigger temperatures are set in the range of 35–37°C. Thermo-responsive polymers undergo a reversible alterable phase (or volume) transition in response to a change in temperature, which can act as a trigger, externally and/or remotely applied. This property allows the manipulation of the material *via* ‘on-demand’ remote control as well as ‘on-off’ switchable control by temperature [3].

Adding to this kind of materials the possibility to get special features (such as nano-/micro-sized fibrous structures with a high surface area and high porosity) gives them the opportunity to be used simultaneously as cell scaffolds for tissue engineering. However, smart fibers, made from thermo-responsive polymers, present high water solubility, causing their structure to collapse while the material dissolves, limiting their application as scaffolds. Thus, the design of more stable new formulations has risen. The aim should be to enhance their biodegradability, biocompatibility, stability and mechanical/chemical properties *via* either chemical modification or functionalization.

Other examples of responsive polymers are based on hydrogels. Hydrogels are three-dimensional hydrophilic polymer networks made up of water-soluble polymers, crosslinked by either covalent or physical methods [4, 5]. Hydrogels are viable materials for multiple applications due to their ability to retain large portions of water, to swell to distend and to exhibit large changes in dimensions (volume changes of several- to 10-fold are common) [6, 7]. The hydrophilic characteristics of hydrogels are caused by the presence of special hydrophilic molecules (-OH, -CONH, -CONH₂, and -SO₃H) found in the polymeric components, giving them different absorption potentials [6] and the ability to respond to a range of different stimuli including: temperature, pH, salt, specific (bio)chemical signals, and electric fields [7]; depending on their molecular composition, undergoing large volume changes in response. Smart hydrogels may have the ability to undergo not only volume change but also shape change. Homogeneous hydrogels undergo inhomogeneous volume change (inducing shape change) when exposed to inhomogeneous stimuli. In order to make a hydrogel that undergo shape change in response to a uniform stimulus, it is necessary to introduce an embedded inhomogeneity into the hydrogel. This inhomogeneity should be incorporated during the synthesis and the manufacture of the hydrogel. The options are: using bilayers, aligned reinforcements or spatially variable crosslinking [8]. Consequently, the great value of these inhomogeneous hydrogels is the combination of the potential and limitations of each precursor; for example, the incorporation of stiffer components, like silica-based domains which restrain swelling in hydrogels in certain positions or directions, or the use of natural polysaccharides-based polymers, hybridized with inorganic materials (hydroxyapatite, SiO₂, or demineralized bone matrix) which limit the number and type of hydrophilic molecules, determining their degradation kinetics and enhancing biological and mechanical properties.

When using tunable properties and functionalization of smart polymers to form hybrids, the new materials may acquire better properties, since the self-alterable dynamic properties and the high sensitivity to small changes in the environment; an adequate degradation kinetics and mechanical properties, given by inorganic components, can entirely produce a new range of properties [3].

WHY IS IT IMPORTANT TO INTRODUCE INORGANICS?

Continuing with examples in the biomedical field, even though there is a great progress in designing materials which can replace natural tissues, scientists are far from matching nature's ability to engineer biomacromolecules, tissues and organs in terms of structure, versatility, adaptability and synthetic process. Biopolymers such as proteins, peptides, nucleic acids and polysaccharides have been used as vital structural components to design materials which can replace, restore or regenerate any tissue in the body. In order to improve and expand the properties and applications of these macromolecules, synthetic and/or inorganic components can be attached to modify the starting organic materials. The attached components can change the materials properties in response to environmental variations, affecting the overall properties of the biomaterial and forming smart hybrid biomaterials [9].

Introducing an inorganic phase into a polymer leads to heterogeneous composite material. However, according to the size of heterogeneities, they can be defined as microcomposites, nanocomposites and molecular composites. The organic-inorganic polymers are classified as hybrids or nanocomposites since the organic and inorganic components blended in a single system on molecular or nano scale level. Under optimum conditions, hybrid materials show synergy of properties of both organic and inorganic components.

Usually, in hybrid materials, polymer networks serve as organic matrices and inorganic components (Si, Ti, Sn or Al-based compounds), working as fillers dispersed into the polymer and forming organic-inorganic networks with different structures and morphologies. These characteristics, along with a well dispersion of the inorganic phase into the organic matrix, are important to determine the properties of the heterogeneous systems. Excellent mechanical, thermal and scratch resistant properties can be tailored by a fine morphology and microphase separated nanosized (1-100 nm) inorganic domains.

The design of materials with some specific properties, such as better degradation kinetics, requires the incorporation of inorganic components into polymeric matrices. The integration of nanotubes with different chemical composition into hybrid scaffolds may provide them bioactive and mechanical properties. This is the case of three-dimensional porous collagen sponges, incorporated with single-walled carbon nanotubes [10]. The incorporation of the single-walled carbon nanotubes improved cell proliferation and sGAG production in the *in vivo* microenvironment, since the nanotubes could be internalized by cells, benefiting the controlled and localized delivery of biological factors.

TYPES AND CHEMISTRY OF HYBRIDS (CLASS I AND II HYBRIDS)

Hybrid materials are divided into two classes: Class I and Class II [11]. In Class I, weak bonds can be found between components (Van der Waals forces or hydrogen bonds) whereas in Class II, strong chemical bonds are present between components (ionic or ionic-covalent bonds) as represented in Figure 1.

Thus, no clear borderline can be drawn between the terms “nanocomposite” and “hybrid”. Commonly, the term “nanocomposite” defines discrete structural units used in the nanometer range and the term “hybrid material” defines inorganic units formed *in situ* from molecular precursors.

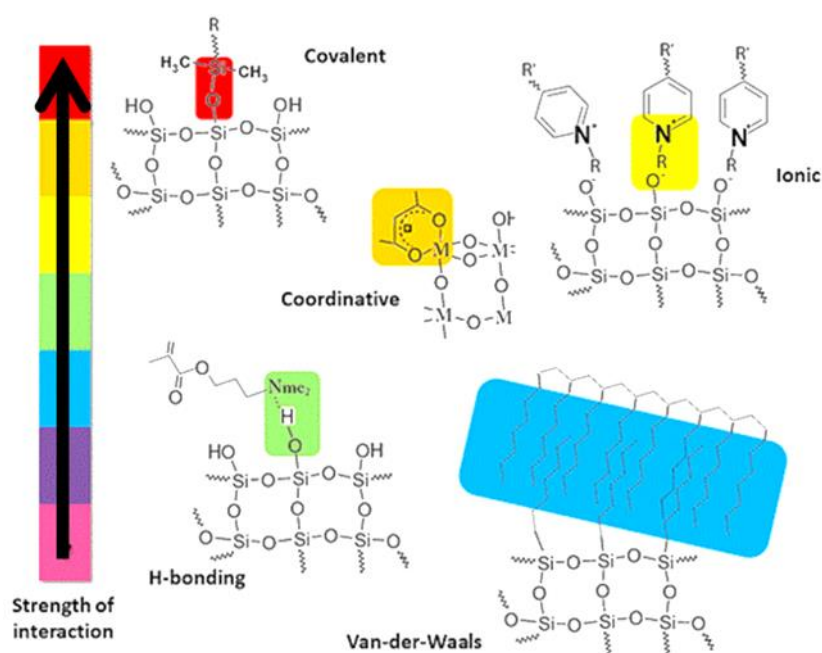


Figure 1. Interactions found in hybrid materials and their relative strength. Blends of inorganic and organic components are generally considered to be Class I hybrids because no strong chemical interactions are formed between the inorganic and the organic building blocks [12, 13]. When two different networks, one inorganic and the other organic, interpenetrate each other without strong chemical interactions, Class I hybrids are also formed (these are called interpenetrating networks or IPNs). Class II hybrids are formed when discrete inorganic building blocks are covalently bonded with organic polymers or when inorganic and organic polymers are covalently connected with each other [14, 15].

Structural properties can also be used to distinguish various hybrid materials. There are networks defined by inorganic nanobuilding blocks, which can present three basic types of networks: a) networks with inorganic blocks covalently attached as pendant units; b) networks with inorganic blocks as crosslink units; and c) networks with physically admixed inorganic blocks without a covalent bond as displayed in Figure 2.

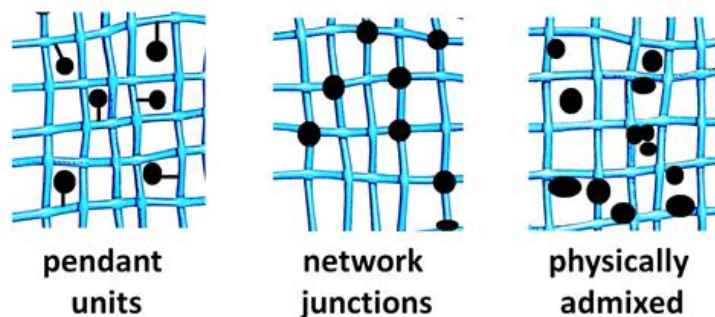


Figure 2. Organic-inorganic networks with inorganic blocks as pendant unit, as network junctions and physically admixed inorganic blocks.

Class II hybrids are the main subject of this chapter because of the variety of properties that can be designed and the possibility of introducing further stimuli-responsive functionalities coming from the polymers. In Class II hybrids, organic groups (R') can be introduced into an inorganic network as either network modifiers or network formers. The organic group (R') can be any organo-functional group. If R' is a nonhydrolyzable organic group (Si- CH_3 , Si-phenyl) it is introduced as a network modifier [16]. If R' can react with itself (R' contains a vinyl, methacryl, epoxy or amino group) or with additional polymerizable monomers, it is introduced as a network former [17, 18].

Two types of reactions can be used to synthesize Class II hybrids; the simultaneous polymerization and the sequential polymerization of the organic and the inorganic monomers (*via* hydrolytic – polycondensation) as summarized in Figure 3.

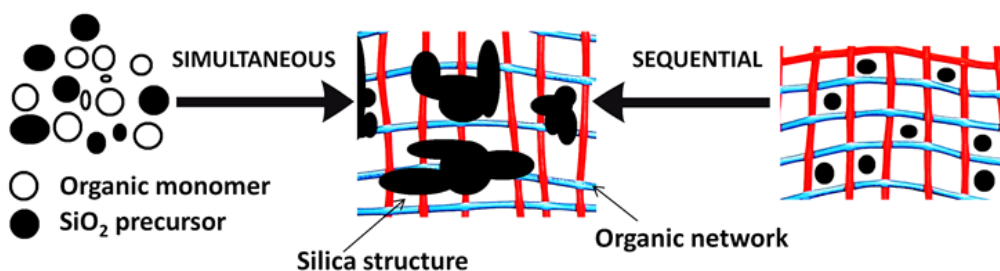


Figure 3. Synthesis procedure of an organic-silica network, generating an *in situ* silica phase.

In these reactions, the hybrid network structure and the morphology can be controlled by: 1) the reaction conditions, mainly by modifying the catalyses of the *sol-gel* process (acid, basic or neutral pH catalysis); 2) selecting different molecular architectures from the organic-inorganic precursors; 3) altering the polymerization procedure; 4) grafting the organic-inorganic interphase. Therefore, Class II hybrids can present several morphologies when processed: 1) networks with inorganic phase nanodomains dispersed

into the organic matrix; 2) networks with bicontinuous phase structure; 3) networks with ordered inorganic phase; 4) organic-inorganic block copolymer networks with inorganic junction domains [19, 20]. The chemistry of inorganic-organic network hybrids is mainly developed using hybrid molecular precursors such as organically modified metal-alkoxides or oligomers of general formula $R'_n\text{Si}(\text{OR})_{4-n}$ or $(\text{OR})_{4-n}\text{Si}-R''-\text{Si}(\text{OR})_{4-n}$ with $n = 1, 2, 3$, respectively, and silicon containing material. The organic groups introduce new properties to the inorganic network, as flexibility, hydrophobicity, hydrophilicity, refractive index modification, etc. [21, 22]; and the inorganic network introduces specific optical, electronic or magnetic properties in organic polymer matrices [23, 24]. These possibilities clearly reveal the power of hybrid materials to generate complex systems in a kind of LEGO© approach.

SOL-GEL METHOD, A VIA TO SYNTHESIZE HYBRIDS

Hybrid synthesis reactions should have the character of classical covalent bond formation in solution. One of the most prominent processes, which fulfill this demand is *sol-gel* process. This process allows controlling the mixing of two or more dissimilar phases to form hybrids under mild reaction conditions. Using *sol-gel* process as a polymerization technique overcomes the difficulty of dispersion of inorganic fillers since the inorganic precursors are initially dispersed on a molecular level in an organic matrix.

Sol-gel process consists in inorganic polymerization of molecular precursors (metal alkoxides $\text{M}(\text{OR})_n$, $\text{M} = \text{Si, Ti, Zr, Al}$, etc, and $\text{OR} = \text{OC}_n\text{H}_{2n+1}$) within organic solvents at a low temperature to form inorganic frameworks of metal oxo-polymers. The inorganic polymerization proceeds in two stages: the hydrolysis and the condensation of the metal alkoxides. The hydrolysis occurs when adding water or a water/alcohol solution to the metal alkoxide in order to introduce hydroxyl groups, forming a *sol* made of highly reactive MOH ($\text{M} = \text{metal}$) species. Hydrolysis is followed by the condensation of MOH species through alcoxolation, oxolation and ololation mechanisms in competition among them to form the *gel* [25]. The oxo metallic network progressively grows from the solution, leading to the formation of oligomers, oxopolymers, colloids and a solid phase. These reactions are described as SN_2 nucleophilic substitutions. The chemical reactivity of metal alkoxides towards hydrolysis and condensation depends on the electronegativity of the metal ion and the ability to increase its coordination number [26]. Finally, the *gels* are aged and dried at room temperature and by thermal treatments. Figure 4 shows an example of hydrolysis-condensation reactions.

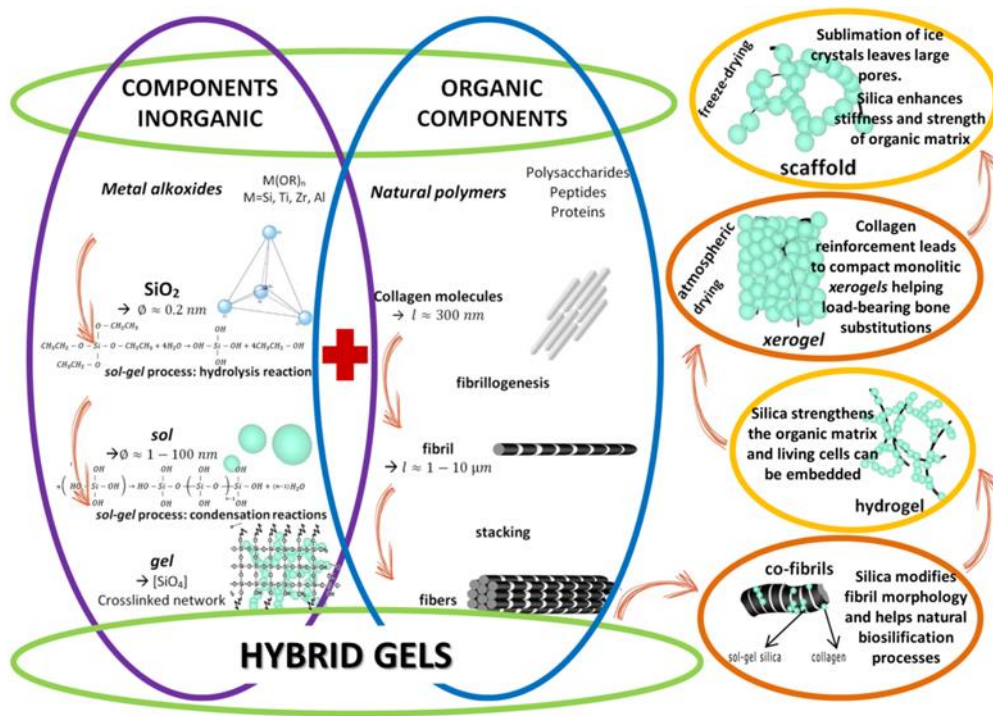


Figure 4. Hydrolysis – condensation reactions of organic-inorganic hybrids. From soft mineralized gels to hard compact *xerogels* [4].

A *sol* is a dispersion of colloidal particles with sizes between 1 to 1000 nm kept by electrostatic and Van der Waals forces within a medium different from the particles state (solid-liquid, solid-gas, and liquid-gas). A *gel* is an interconnected rigid structure with polymeric chains and micro pores. In order to obtain a low density *aerogel*, the liquid is removed by transforming it into gas, applying hypercritical conditions to the interconnected solid structure of the *gel*, avoiding the structure to contract. On the other hand, when the liquid is removed *via* atmospheric pressure through evaporation (drying), the *gel* structure shrinks/contracts and a *xerogel* is formed. Although a dried *gel* is stabilized when the adsorbed physical water is eliminated between 100 – 180°C, there is still a high concentration of hydroxyl groups on the pores surface. Finally, the *gel* can be densified, by reducing the size and number of pores through thermal treatments. A variety of organic-inorganic networks can be formed when using this technology to synthesize hybrid materials [28-30]. SiO₂ glass-type materials have been obtained mainly from alkoxy silanes and the hydrolysis of the tetraethoxysilane (TEOS) which is the most common monomer to form silica network *in situ* within an organic matrix [31, 32].

What it is important in these materials is that the inorganic phase domains, formed by the *sol-gel* process in the organic-inorganic networks, are polydisperse in size and heterogeneous in chemical composition. Better nanostructured organic-inorganic polymers are prepared using well defined inorganic nanobuilding blocks with

predetermined molecular architecture. A large variety of organofunctional nanobuilding blocks are studied, being the polyhedral oligomeric silsesquioxanes (POSS) [33] and the tetrahedral SiO₂ structures [34] the ones with more attention. These three-dimensional inorganic structures give local reinforcement and immobilization to a polymer chain, showing an improvement of properties, such as increased T_g, modulus, degradability, decomposition temperature [35], reduced flammability [36, 37] and increased gas permeability [38, 39]. However, the properties, the structure and the morphology of the inorganic-polymer hybrids are determined by the strength of two types of competing interactions: 1) between inorganic and polymer components (inorganic-chain interaction) [40] and 2) between inorganic units (inorganic-inorganic interaction). When the inorganic-inorganic interactions are stronger, the inorganic phase tends to separate and form aggregates [41]. Therefore, the main objective is to determine the phase structure evolution along with the size of the heterogeneity domains and the geometrical description of the structure, by using fractal geometry during the random processes of polymerization or aggregation [42, 43]. This is why finding an adequate amount of inorganic and organic precursors is of great importance when processing hybrid materials. In order to form an organic-inorganic nanostructured network, the inorganic units have to aggregate within the organic matrix. As to control the hybrid network structure and morphology, there is the need to control the inorganic units aggregation, which will be influenced by: a) the inorganic block topology in the network, either as a pendant unit or as a network crosslinker; b) an organic substituent into the inorganic block which can affect miscibility with an organic matrix; c) the covalent bonding to the organic matrix; d) the polymerization procedure of the network synthesis.

SMART HYBRIDS

As stated in a former section, the main advantages of inorganic–organic hybrids are: the combination of frequent dissimilar properties of organic and inorganic components in one material; the opportunity to develop an almost unlimited set of new materials with a large spectrum of known and yet unknown properties, because of the many possible combinations. Several stimuli responsive hybrids and their applications are summarized in this section as examples of these characteristics. Few significant examples are described below to give a general overview.

Stimuli responsive drug delivery systems have generated special interest to the scientific community in recent years [44, 45]. Numerous controlled-release systems based on mesoporous silica supports (MSS) have been described using physical [46], chemical [47] or biochemical [48] stimuli. One of the first reported examples was developed by Lin et al. [49]. MSSs were capped with gluconic acid-modified insulin (G-Ins) and loaded with cyclic adenosine monophosphate (cAMP). The nanomaterial demonstrated to

be glucose-sensitive because it releases both G-Ins and cAMP. Moreover, Shi et al. [50] reported an insulin loaded nanocarrier coated with GOx enzyme-multilayers which were cross-linked with glutaraldehyde. This nanocarrier acted as gatekeepers to control the release of insulin in response to glucose. Another example was recently developed by Asefa et al. [51] who described the preparation of MSNs for insulin release by tethering insulin molecules onto boronic acid functionalized MSSs and then coated the material with a shell of pH sensitive polymer polyacrylic acid. The material exhibited both pH- and glucose- dependent release of insulin. In another promising approach, mesoporous hybrid gated materials were synthesized by grafting nanometric silica with 1-propyl-1-H-benzimidazole groups, loaded with fluorescent isothiocyanate-labeled insulin (FITC-Ins) and capped during the formation of inclusion complexes between β -cyclodextrin-modified enzyme glucose oxidase (CD-GOx) and the benzimidazole groups, grafted on the mesoporous support. The designed nanodevice for controlled insulin release is based on the recognition of glucose with the glucose oxidase enzyme and hydrolyzed into gluconic acid ($pK_a = 3.6$). The generation of gluconic acid induces a local drop in pH which would cause the protonation of the benzimidazol groups ($pK_a = 5.55$) and the unthreading of the inclusion complexes between benzimidazol and CD-GOx; the final result is the delivery of entrapped insulin with the formation of a solid [52]. This approach presents some advantages versus other reported glucose-triggered insulin release, such as the storage of insulin into the pores which prevents its degradation.

Sol-gel method has also been applied to prepare *flame retarded polymer based devices* [53]. The need of developing halogen-free flame materials is mandatory to preserve human security and environmental protection. The combination of a nanofiller with silicon, phosphorus and nitrogen-containing flame retardants has been verified to present anti-flammability properties and several researches are focused on this composition [54]. As an example, Chiang et al. [55] studied the influence of diethylphosphatoethyltriethoxysilane/TEOS on the thermal properties of epoxy nanocomposites. They reported the formation of a char and enhancement of thermal stability at high temperature in phosphorylated silica based nanocomposites. In a different approach [56] and to improve the flame retardant properties of PA6 polymers, *in situ* generation of phosphorylated silica, *via* an extrusion process, was investigated. The *in situ* synthesis of the silico-phosphorated phase from the SiP or SiP/TEOS hydrolysis–condensation reactions leads to a different combustion behavior, compared with neat PA6. PA6 behavior is characteristic of a non-charring material whereas those materials based on SiP inorganic precursors behave as “charring” compounds, which form a fire protective residue. This flame behavior confirmed the synergistic effect between Si and P and the potential to provide very specific properties to polymer nanocomposites, using the association of *sol-gel* chemistry and polymer processing.

Antibacterial hybrids can also be synthesized. Nanometer-size TiO_2 particles in the anatase crystalline form are known to possess photocatalyst properties when illuminated by UV light with wavelength <385 nm [57]. The general scheme of the photocatalytic damage of microorganism cells by TiO_2 photocatalytic properties involves: 1) photoexcited TiO_2 catalyst produces electron-hole pairs which migrate to the TiO_2 surface; 2) photogenerated holes in TiO_2 can react with adsorbed H_2O or OH^- groups in the catalyst/water interface to produce the highly reactive hydroxyl radicals, therefore electrons can react with oxygen vacancies to form superoxide ions; 3) various highly active oxygen species generated can oxidize organic compounds/cells adsorbed on the TiO_2 surface, causing microorganisms death. In order to improve the efficiency and prepare applicable antibacterial materials, it is necessary to generate electron-hole pairs by extending the excitation wavelength to the visible light region and to achieve a reduced recombination rate on the newly created electron-hole carriers. This is usually made by tailoring the particle size and the pore-size distributions, generating structural defects to induce space-charge separation *via* metal dopants [58]. Because of the majority of photoexcited charge carriers [electrons (e^-) and holes (h^+)] may undergo a rapid recombination; single component semiconductor nanoparticles exhibit relatively poor photocatalytic efficiency. On the other hand, semiconductor-metal nanocomposites exhibit increased efficiency of photocatalytic activity because of a reduction in the e^- - h^+ recombination rate due to better charge separation between electrons [59].

The incorporation of titanium dioxide into polymeric matrices transfers the biocidal properties to the corresponding polymer-based compounds [60]. Nanostructured smart systems, based on metallic and inorganic loaded liposomes, cyclodextrins or dendrimers, are also being prepared and tested as drug delivery systems and on self-cleaning textiles [60]. Hybrid materials, based on TiO_2 and poly(ϵ -caprolactone) (PCL), have been fabricated and used in biomedical applications. Interpenetrating networks are formed by hydrogen bonds between $\text{Ti}\backslash\text{OH}$ groups in the *sol-gel* intermediate species and carbonyl groups in the polymer repeating units. The bioactivity of the synthesized systems was proven by the formation of a hydroxyapatite layer on the surface of samples, soaked into a fluid simulating human blood plasma (SBF). MTT cytotoxicity tests and Trypan Blue dye exclusion tests showed that all the hybrids had a non-cytotoxic effect on NIH-3T3 mouse embryonic fibroblasts; however activation of the bactericidal effect tests are not performed yet [61].

TiO_2 based nano-structured materials have been also applied for anti-bacterial modification of textile and polymeric materials. Meilert et al. have used polycarboxylic acids as spacers to attach TiO_2 nano-particles to fabrics [62]. Plasma pretreatment has been used for the generation of active groups on the surface to combine them with TiO_2 nanoparticles [63]. Wang et al. have used argon plasma grafting nano-particles on wool surface [64]. Won et al. have produced nanoparticles in the polymeric matrix by reducing metallic salts under the irradiation with UV light [60].

Nanostructured *smart biosensing systems*, based on gold (Au)- and silver (Ag)- thin nanofilms with natural peptides, glutathione, or simplest stable aminothiol, are also being developed [65]. These materials are highly promising in biomedicine and environmental monitoring. They are sensitive to pH and optical signal enhancement during bioassays; these characteristics are attributed to the complex opto-electronic interactions of incoming photonic signals in the nanomaterial interface [66].

Graphene-based smart materials are one type of smart hybrids with several potential applications. Graphene materials include: 1) mechanically exfoliated perfect graphene; 2) chemical vapor deposited high-quality graphene; 3) chemically modified graphene, for example, graphene oxide (GO); 4) reduced graphene oxide (rGO) and their macroscopic assemblies or composites. What make them attractive for high-performance stimuli-responsive or ‘smart’ materials are their high specific surface area and their excellent mechanical, electrical, optical and thermal properties. These properties combine well with the good elasticity, light weight and high transparency provided by polymers [67].

Graphene-based biosensors, with the configuration of a field-effect transistor, usually show a high signal-to-noise ratio. This is mainly due to the high carrier mobility and low electronic noise of graphene. The binding of biomolecules on the surface of graphene channels can sensitively change the carrier density of graphene and/or screen its surface impurities. The long-range electrostatic interaction between graphene and the substrate electrode can also be modulated [68]. On the basis of these factors, the conductance of graphene can be sensitively changed *via* interaction with biomolecules. For example, the conductance of a p-type GO was increased by attaching a negatively charged single-stranded DNA (ssDNA) to its surface *via* the formation of GO–DNA hybrids. This conductance was further increased by hybridizing ssDNA with its complementary DNA; moreover it could be completely restored by removing the complementary DNA [69].

GO is also a promising carrier for pH-controlled drug delivery systems because of its 2D structure, adjustable functional groups and good biocompatibility. For example, the cancer drug doxorubicin was loaded on the surfaces of GO sheets via hydrogen bonding and π – π stacking interactions [70]. The microenvironment of focus (for example, tumor) is more acidic than normal tissues, leading to the protonation of hydrophobic drugs and thus the weakening of their interactions with GO. Therefore, the drug can be selectively released from GO sheets into the target focus. However, GO sheets are prone to aggregate in physiological buffers because of the existence of ions which screen their surface charges. Therefore, they have to be modified with polymers or functional groups to increase their solubility in this medium for drug delivery. For example, polyethylene glycol-functionalized GO showed good dispersability in various biological media. A poly(vinyl alcohol)–GO hybrid hydrogel, simply fabricated by mechanical blending, exhibited a reversible pH-induced *gel–sol* transition, enabling it to a selective release of vitamin B12 in a neutral phosphate buffer solution [71]. In another study, Pluronic

copolymer (F127)-stabilized rGO was loaded with doxorubicin, showing a high-loading efficiency of 289% (w/w) for controlled delivery in acid medium [72]. The change mechanism is based on the surface charges of GO sheets and the electrostatic repulsion forces between them. They can be modulated by pH value of dispersion. For example, adding acid to a GO dispersion induces the protonation of the negatively charged carboxyl groups of the GO sheets, weakening their electrostatic repulsion force and enhancing their hydrogen-bonding attraction force. In a strong acid medium, GO sheets tend to aggregate into irregular particles or to form a self-assembled hydrogel because of their insufficient mutual repulsion force. Increasing the pH value of a GO solution induces the opposite effects. Accordingly, switching the pH of a GO dispersion between high and low values can induce reversible *sol-gel* transition or dispersion and aggregation of the GO sheets. In another research, rGO sheets, covalently conjugated with polyethylenimine and polyethylene glycol, showed a high capacity of loading doxorubicin [73]. The loaded doxorubicin can be efficiently released by glutathione and NIR irradiation to kill cancer cells.

In a different application, *graphene-based* bilayer and multilayer *actuators* are made of graphene and other functional materials as actuation or supporting layers. Conducting polymers are frequently applied as one of the actuation layers. The volume of a conducting polymer film changes dramatically (>2%) upon electrochemical doping and dedoping. For example, upon electrochemical oxidation or reduction, a PPy film was shown to expand or contract, particularly in its cross-section direction [74]. The graphene film underwent volume contraction or swelling by hole or electron injection. The different volume-changing behavior of the two materials provides an opportunity for designing a rational PPy–graphene bilayer or multilayer actuator with excellent performance.

Thermoresponsive polymer–graphene compounds have also been used to construct thermally responsive systems for versatile applications. Poly(*N*-isopropylacrylamide) (PNIPAM) is the most widely used polymer for this purpose, because of its biocompatibility, water-solubility and low critical solution temperature (LCST), 32°C. For example, a GO–PNIPAM hybrid was used to develop thermoresponsive fluorescent switches or sensors [75]. In this material, PNIPAM was covalently modified with fluorescent moieties. At temperatures below the LCST, the PNIPAM chains swelled and the composite exhibited strong photoluminescence. In contrast, at temperatures above the LCST, the PNIPAM chains contracted and the distances between the fluorescent moieties and the surfaces of the GO sheets were shortened, leading to the quenching of photoluminescence. After cooling the solution, the photoluminescence signal can be totally recovered. Following this mechanism, a reversible on–off photoluminescence switching can be made with temperature variation.

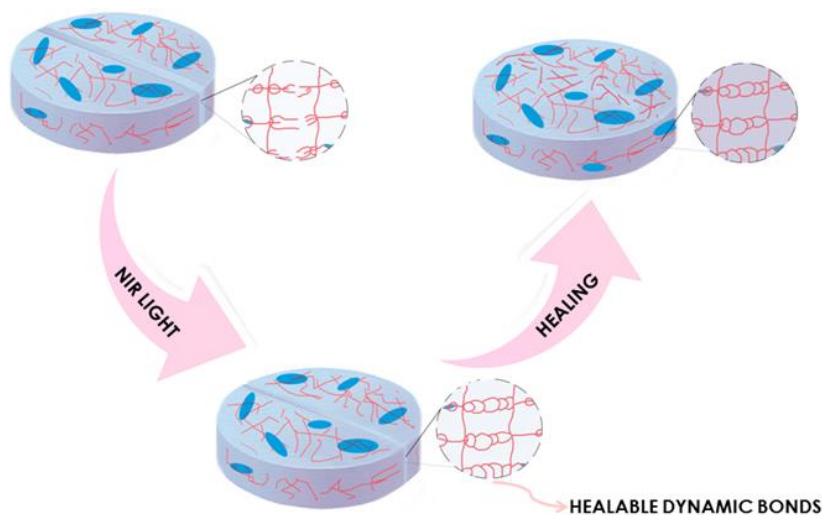


Figure 5. A GO–polymer hydrogel for light-responsive (NIR: near-infrared region) self-healing [67].

Self-healing materials are capable of spontaneous self-repairing on the sites of damage. Conventional self-healing materials are mainly based on polymeric hydrogels or films, because they can heal themselves *via* interchain dynamic bonding (for example, hydrogen bonding, dynamic covalent bonding, ionic bonding and supramolecular interactions) [76]. However, most of these polymers, PNIPAM, poly(vinyl alcohol) or thermoplastic polyurethane, are mechanically too weak to achieve repeated healing, which limits their practical applications. Developing self-healing materials with high mechanical strength and high healing efficiency remains challenging. Furthermore, carbon based materials have good compatibility with many polymers because of their large conjugated structures and large number of oxygenated functional groups, giving them excellent mechanical strength. In graphene–polymer hybrids exposed to NIR irradiation, the graphene component converts light energy to heat, inducing the diffusion and entanglement of polymer chains at the broken interface, in order to heal the fracture as shown in Figure 5 [77]. The graphene content balances the mechanical strength and healing efficiency of the material. These self-healing hydrogels have potential applications in surgical dressing, artificial tissues and biomedical devices.

In summary, the combination of inorganic and organic components used to synthesized hybrids may yield a new set of properties and applications in polymer based materials. In this chapter, the functionalities of inorganic components given to polymers were briefly introduced. The differences in chemical bonding between class I and class II hybrids, described. *Sol-gel* method used to synthesize class II hybrids, explained. And some of the most promising responsive hybrids, depending on the nature of the stimuli they respond to, were highlighted.

REFERENCES

- [1] Marturano V, Cerruti P, Giamberini M, Tylkowski B, Ambrogio V. Light-responsive polymer micro-and nano-capsules. *Polymers*. 2017;9:8.
- [2] Baudis S, Behl M, Lendlein A. Smart polymers for biomedical applications. *Macromolecular Chemistry and Physics*. 2014;215:2399-402.
- [3] Kim YJ, Matsunaga YT. Thermo-responsive polymers and their application as smart biomaterials. *Journal of Materials Chemistry B*. 2017;5:4307-4321.
- [4] Sánchez-Téllez DA, Téllez-Jurado L, Rodríguez-Lorenzo LM. Hydrogels for cartilage regeneration, from polysaccharides to hybrids. *Polymers*. 2017;In Press.
- [5] Rodriguez-Lorenzo LM, Saldana L, Benito-Garzon L, Garcia-Carrodegua R, de Aza S, Vilaboa N, et al. Feasibility of ceramic-polymer composite cryogels as scaffolds for bone tissue engineering. *Journal of Tissue Engineering and Regenerative Medicine*. 2012;6:421-433.
- [6] Gyles DA, Castro LD, Carréra Silva Jr JO, Ribeiro-Costa RM. A review of the designs and prominent biomedical advances of natural and synthetic hydrogel formulations. *European Polymer Journal*. 2017;88:373-392.
- [7] Jeon SJ, Hauser AW, Hayward RC. Shape-Morphing Materials from Stimuli-Responsive Hydrogel Hybrids. *Accounts of Chemical Research*. 2017;50:161-169.
- [8] Baker AB, Wass DF, Trask R. Thermally induced reversible and reprogrammable actuation of tough hydrogels utilising ionoprinting and iron coordination chemistry. *Sensors and Actuators B*. 2018;254:519-525.
- [9] Cobo I, Li M, Sumerlin BS, Perrier S. Smart hybrid materials by conjugation of responsive polymers to biomacromolecules. *Nature Materials*. 2015;14:143-159.
- [10] Jeon JE, Vaquette C, Theodoropoulos C, Klein TJ, Hutmacher DW. Multiphasic construct studied in an ectopic osteochondral defect model. *Journal of the Royal Society Interface*. 2014;11:20140184.
- [11] KICKELBICK G. *Introduction to Hybrid Materials*. Hybrid Materials: Wiley-VCH Verlag GmbH & Co. KGaA; 2007. p. 1-48.
- [12] Vargas Becerril N, Téllez Jurado L, Rodriguez-Lorenzo LM. Adsorption of fibronectin on hydroxyapatite functionalized with alendronate. *Journal of the Australian Ceramic Society*. 2013;49:60-67.
- [13] Vargas-Becerril N, Patiño-Carachure C, Rodriguez-Lorenzo LM, Téllez-Jurado L. Synthesis of hybrid compounds apatite-alendronate by reactive milling and effects on the structure and morphology of the apatite phase. *Ceramics International*. 2013;39:3921-3929.
- [14] Téllez L, Rubio J, Rubio F, Morales E, Oteo JL. Synthesis of inorganic-organic hybrid materials from TEOS, TBT and PDMS. *Journal of Materials Science*. 2003;38:1773-1780.

- [15] Téllez L, Rubio J, Rubio F, Morales E, Oteo JL. FT-IR study of the hydrolysis and polymerization of tetraethyl orthosilicate and polydimethyl siloxane in the presence of tetrabutyl orthotitanate. *Spectroscopy Letters*. 2004;37:11-31.
- [16] Eduok U, Faye O, Szpunar J. Recent developments and applications of protective silicone coatings: A review of PDMS functional materials. *Progress in Organic Coatings*. 2017;111:124-163.
- [17] Fernando D, Attik N, Cresswell M, Mokbel I, Pradelle-Plasse N, Jackson P, Grosogeat B, Colon P. Influence of network modifiers in an acetate based sol-gel bioactive glass system. *Microporous and Mesoporous Materials*. 2018;257:99-109.
- [18] Sánchez-Téllez DA, Téllez-Jurado L, Chávez-Alcalá JF. Bioactivity and degradability of hybrids nano-composites materials with great application as bone tissue substitutes. *Journal of Alloys and Compounds*. 2015;615:670-675.
- [19] Tamayo A, Téllez L, Rubio J, Rubio F, Oteo JL. Effect of reaction conditions on surface properties of TEOS-TBOT-PDMS hybrid materials. *Journal of Sol-Gel Science and Technology*. 2010;55:94-104.
- [20] Téllez L, Balmori H, Valenzuela MA, Rubio J, Rubio F, Oteo JL. Pore structure and texture of organic/inorganic hybrid materials. *Ceramic Engineering and Science Proceedings*. 2006;27:387-397.
- [21] Jiménez-Gallegos R, Téllez-Jurado L, Rodríguez-Lorenzo LM, San Román J. Modulation of the hydrophilic character and influence on the biocompatibility of polyurethane-siloxane based hybrids. *Boletín de la Sociedad Española de Cerámica y Vidrio*. 2011;50:1-8.
- [22] Ralbag N, Ruiz-Cabello FJM, Rodríguez Valverde MA, Gutkin V, Sfez R, Avnir D. Continuous thermal control of hydrophilicity/hydrophobicity changes of hybrid films and of their directionally: kinetics and substrate effects. *Journal of Colloids and Interface Science*. 2017;505:692-702.
- [23] Mun SY, Lim HM, Lee S-H. Thermal and electrical properties of epoxy composite with expanded graphite-ceramic core-shell hybrids. *Materials Research Bulletin*. 2018;97:19-23.
- [24] Jittiarporn P, Sikong L, Kooptarnond K, Taweepreda W, Stoenescu S, Badilescu S, Truong VV. Truong. Electrochromic properties of MoO₃-WO₃ thin films prepared by a sol-gel method, in the presence of a triblock copolymer template. *Surface & Coatings Technology*. 2017;327:66-74.
- [25] Brinker J, Scherer GW. *Sol-gel science: the physics and chemistry of sol-gel processing*. Academic press; 2013.
- [26] Peña-Alonso R, Téllez J, Rubio J, Rubio F. Surface chemical and physical properties of TEOS-TBOT-PDMS hybrid materials. *Journal of Sol-Gel Science and Technology*. 2006;38:133-145.

- [27] Sánchez-Téllez DA, Téllez-Jurado L, Rodríguez-Lorenzo LM. Optimization of the CaO and P₂O₅ contents on PDMS-SiO₂-CaO-P₂O₅ hybrids intended for bone regeneration. *Journal of Materials Science*. 2015;50:5993-6006.
- [28] Téllez L, Tamayo A, Mazo MA, Rubio F, Rubio J. Preparation and characterisation of mixed silicon oxycarbide materials. *Boletín de la Sociedad Española de Cerámica y Vidrio*. 2010;49:105-112.
- [29] Téllez L, Rubio J, Valenzuela MA, Rubio F, Oteo JL. Effect of Ti concentration on the structure and texture of SiTiOC glasses. *Materials Characterization*. 2009;60:506-512.
- [30] Tamayo A, Téllez J, Peña-Alonso R, Rubio F, Rubio J. Surface changes during pyrolytic conversion of hybrid materials to oxycarbide glasses. *Journal of Materials Science*. 2009;44:5743-5753.
- [31] Peña-Alonso R, Téllez J, Tamayo A, Rubio F, Rubio J, Oteo JL. Silicon-titanium oxycarbide glasses as bimodal porous inorganic membranes. *Journal of the European Ceramic Society*. 2007;27:969-973.
- [32] Téllez L, Rubio F, Peña-Alonso R, Rubio J. FT-IR spectroscopy study of the reaction of obtention of hybrid materials. *Boletín de la Sociedad Española de Cerámica y Vidrio*. 2004;43:883-890.
- [33] Dire S, Bottone D, Callone E, Maniglio D, Bénois I, Ribot F. Hydrophobic coatings by thiol-ene click functionalization of silsesquioxanes with tunable architecture. *Materials*. 2017;10:913.
- [34] Zajickova Z. Advances in the development and applications of organic-silica hybrid monoliths. *Journal of Separation Science*. 2017;40:25-48.
- [35] Gao W, Qian X, Wang S. Preparation of hybrid silicon materials microcapsulated ammonium polyphosphate and its application in thermoplastic polyurethane. *Journal of Applied Polymer Science*. 2018;135:45742.
- [36] Cheng XW, Liang CX, Guan JP, Yang XH, Tang RC. Flame retardant and hydrophobic properties of novel sol-gel derived phytic acid/silica hybrid organic-inorganic coatings for silk fabric. *Applied Surface Science*. 2018;427:69-80.
- [37] Ren Y, Zhang Y, Gu Y, Zeng Q. Flame retardant polyacrylonitrile fabrics prepared by organic-inorganic hybrid silica coating via sol-gel technique. *Progress in Organic Coatings*. 2017;112:225-233.
- [38] Jiménez-Gallegos R, Téllez-Jurado L, Rodríguez-Lorenzo LM, San Román J. Synthesis and characterization of siloxane-polyurethane hybrid materials. *Key Engineering Materials*. 2009;396-398:481-484.
- [39] González-García DM, Téllez-Jurado L, Jiménez-Gallegos R, Rodríguez-Lorenzo LM. Novel non-cytotoxic, bioactive and biodegradable hybrid materials based on polyurethanes/TiO₂ for biomedical applications. *Materials Science and Engineering C*. 2017;75:375-384.

- [40] Martínez-Valencia AB, Carbaja-De la Torre G, Torres-Sanchez R, Tellez-Jurado L, Esperanza-Ponce HE. Production of polyurethane/nano-hydroxyapatite hybrid materials and microstructural characterization. *International Journal of Physical Sciences*. 2011;6:2731-2743.
- [41] Téllez L, Tamayo A, Mazo MA, Rubio F, Rubio J. Influence of TiO₂ on the pore structure and texture of SiO₂-PDMS hybrid materials. *Materials Research Society Symposium Proceedings*. 2005;847:183-188.
- [42] Sánchez-Téllez Rodríguez-Lorenzo LM, Mazo MA, Rubio J, Tamayo A. Surface effects on the degradation mechanism of bioactive PDMS-SiO₂-CaO-P2O5 hybrid materials intended for bone regeneration. *Ceramics International*. 2017;43:476-483.
- [43] Tamayo A, Téllez L, Rodríguez-Reyes M, Mazo MA, Rubio F, Rubio J. Surface properties of bioactive TEOS-PDMS-TiO₂-CaO ormosils. *Journal of Materials Science*. 2014;49:4656-4669.
- [44] Beltran-Osuna AA, Perilla JE. Colloidal and spherical mesoporous silica particles: synthesis and new technologies for delivery applications. *Journal of Sol-Gel Science and Technology*. 2016;77:480-496.
- [45] Sancenon F, Pascual L, Oroval M, Aznar E, Martínez-Manez R. Gated Silica Mesoporous Materials in Sensing Applications. *Chemistryopen*. 2015;4:418-437.
- [46] Liu J, Detrembleur C, De Pauw-Gillet MC, Mornet S, Jerome C, Duguet E. Gold nanorods coated with mesoporous silica shell as drug delivery system for remote near infrared light-activated release and potential phototherapy. *Small*. 2015;11:2323-2332.
- [47] Zhang XX, Li FF, Guo SY, Chen X, Wang XL, Li J, et al. Biofunctionalized polymer-lipid supported mesoporous silica nanoparticles for release of chemotherapeutics in multidrug resistant cancer cells. *Biomaterials*. 2014;35:3650-3665.
- [48] Bhat R, Ribes A, Mas N, Aznar E, Sancenon F, Marcos MD, et al. Thrombin-responsive gated silica mesoporous nanoparticles as coagulation regulators. *Langmuir*. 2016;32:1195-1200.
- [49] Zhao YN, Trewyn BG, Slowing, II, Lin VSY. Mesoporous silica nanoparticle-based double drug delivery system for glucose-responsive controlled release of insulin and cyclic AMP. *Journal of the American Chemical Society*. 2009;131:8398-8400.
- [50] Zhao WR, Zhang HT, He QJ, Li YS, Gu JL, Li L, et al. A glucose-responsive controlled release of insulin system based on enzyme multilayers-coated mesoporous silica particles. *Chemical Communications*. 2011;47:9459-9461.
- [51] Jain RN, Huang X, Das S, Silva R, Ivanova V, Minko T, Asefa T. Functionalized mesoporous silica nanoparticles for glucose- and pH-stimulated release of insulin. *Journal of Inorganic and General Chemistry*. 2014;640:616-623.

- [52] Oroval M, Diez P, Aznar E, Coll C, Marcos MD, Sancenon F, et al. Self-regulated glucose-sensitive neoglycoenzyme-capped mesoporous silica nanoparticles for insulin delivery. *Chemistry-a European Journal*. 2017;23:1353-1360.
- [53] Bounor-Legare V, Cassagnau P. In situ synthesis of organic-inorganic hybrids or nanocomposites from sol-gel chemistry in molten polymers. *Progress in Polymer Science*. 2014;39:1473-1497.
- [54] Ramani A, Hagen M, Hereid J, Zhang JP, Delichatsios M. Interaction of a phosphorus-based FR, a nanoclay and PA6. Part 2 interaction of the complete PA6 polymer nanocomposites. *Fire and Materials*. 2010;34:77-93.
- [55] Chiu YC, Ma CCM, Liu FY, Chiang CL, Riang L, Yang JC. Effect of P/Si polymeric silsesquioxane and the monomer compound on thermal properties of epoxy nanocomposite. *European Polymer Journal*. 2008;44:1003-1011.
- [56] Du L, Qu B, Zhang M. Thermal properties and combustion characterization of nylon 6/MgAl-LDH nanocomposites via organic modification and melt intercalation. *Polymer Degradation and Stability*. 2007;92:497-502.
- [57] Fu GF, Vary PS, Lin CT. Anatase TiO₂ nanocomposites for antimicrobial coatings. *Journal of Physical Chemistry B*. 2005;109:8889-8898.
- [58] Yu JC, Zhang LZ, Zheng Z, Zhao JC. Synthesis and characterization of phosphated mesoporous titanium dioxide with high photocatalytic activity. *Chemistry of Materials*. 2003;15:2280-2286.
- [59] Lu ZX, Zhou L, Zhang ZL, Shi WL, Xie ZX, Xie HY, et al. Cell damage induced by photocatalysis of TiO₂ thin films. *Langmuir*. 2003;19:8765-8768.
- [60] Dastjerdi R, Montazer M. A review on the application of inorganic nano-structured materials in the modification of textiles: Focus on anti-microbial properties. *Colloids and Surfaces B-Biointerfaces*. 2010;79:5-18.
- [61] Catauro M, Bollino F, Papale F, Marciano S, Pacifico S. TiO₂/PCL hybrid materials synthesized via sol-gel technique for biomedical applications. *Materials Science & Engineering C-Materials for Biological Applications*. 2015;47:135-141.
- [62] Meilert KT, Laub D, Kiwi J. Photocatalytic self-cleaning of modified cotton textiles by TiO₂ clusters attached by chemical spacers. *Journal of Molecular Catalysis a-Chemical*. 2005;237:101-108.
- [63] Bozzi A, Yuranova T, Kiwi J. Self-cleaning of wool-polyamide and polyester textiles by TiO₂-rutile modification under daylight irradiation at ambient temperature. *Journal of Photochemistry and Photobiology a-Chemistry*. 2005;172:27-34.
- [64] Wang SH, Hou WS, Wei LQ, Jia HS, Liu XG, Xu BS. Antibacterial activity of nano-SiO₂ antibacterial agent grafted on wool surface. *Surface & Coatings Technology*. 2007;202:460-465.

- [65] Yu M, Zhou C, Liu J, Hankins JD, Zheng J. Luminescent gold nanoparticles with pH-dependent membrane adsorption. *Journal of the American Chemical Society*. 2011;133:11014-11017.
- [66] Ranjan R, Esimbekova EN, Kirillova MA, Kratasyuk VA. Metal-enhanced luminescence: Current trend and future perspectives- A review. *Analytica Chimica Acta*. 2017;971:1-13.
- [67] Yu X, Cheng H, Zhang M, Zhao Y, Qu L, Shi G. Graphene-based smart materials. *Nature Reviews Materials*. 2017;2:17046.
- [68] Liu Y, Dong X, Chen P. Biological and chemical sensors based on graphene materials. *Chemical Society Reviews*. 2012;41:2283-2307.
- [69] Mohanty N, Berry V. Graphene-based single-bacterium resolution biodevice and DNA transistor: Interfacing graphene derivatives with nanoscale and microscale biocomponents. *Nano Letters*. 2008;8:4469-4476.
- [70] Liu J, Cui L, Losic D. Graphene and graphene oxide as new nanocarriers for drug delivery applications. *Acta Biomaterialia*. 2013;9:9243-9257.
- [71] Bai H, Li C, Wang X, Shi G. A pH-sensitive graphene oxide composite hydrogel. *Chemical Communications*. 2010;46:2376-2378.
- [72] Hu H, Yu J, Li Y, Zhao J, Dong H. Engineering of a novel pluronic F127/graphene nanohybrid for pH responsive drug delivery. *Journal of Biomedical Materials Research - Part A*. 2012;100 A:141-148.
- [73] Kim H, Lee D, Kim J, Kim TI, Kim WJ. Photothermally triggered cytosolic drug delivery via endosome disruption using a functionalized reduced graphene oxide. *ACS Nano*. 2013;7:6735-6746.
- [74] Liu J, Wang Z, Xie X, Cheng H, Zhao Y, Qu L. A rationally-designed synergetic polypyrrole/graphene bilayer actuator. *Journal of Materials Chemistry*. 2012;22:4015-4020.
- [75] Lee J, Yang H, Park CH, Cho HH, Yun H, Kim BJ. Colorimetric Thermometer from graphene oxide platform integrated with red, green, and blue emitting, responsive block copolymers. *Chemistry of Materials*. 2016;28:3446-3453.
- [76] Zhang E, Wang T, Zhao L, Sun W, Liu X, Tong Z. Fast self-healing of graphene oxide-hectorite clay-poly(N,N -dimethylacrylamide) hybrid hydrogels realized by near-infrared irradiation. *ACS Applied Materials and Interfaces*. 2014;6:22855-22861.
- [77] Huang L, Yi N, Wu Y, Zhang Y, Zhang Q, Huang Y, et al. Multichannel and repeatable self-healing of mechanical enhanced graphene-thermoplastic polyurethane composites. *Advanced Materials*. 2013;25:2224-2228.

Chapter 15

POLYMERS FOR ADDITIVE MANUFACTURING

***Thibault Ghigonetto,¹ Carmen M. González-Henríquez²,
Mauricio A. Sarabia-Vallejos³ and Juan Rodríguez-Hernández^{1,*}***

¹Instituto de Ciencia y Tecnología de Polímeros (ICTP),
Consejo Superior de Investigaciones Científicas (CSIC),
Chemistry and Properties of Polymeric Materials Department, Madrid, Spain

²Universidad Tecnológica Metropolitana, Facultad de Ciencias Naturales,
Matemáticas y del Medio Ambiente,
Departamento de Química, Santiago, Chile

³Pontificia Universidad Católica de Chile, Escuela de Ingeniería,
Departamento de Ingeniería Estructural y Geotecnia, Santiago, Chile

ABSTRACT

Additive manufacturing (AM), also generally known as 3D printing permits the fabrication of fully customized objects with a high level of geometrical complexity implying rapid fabrication time as well as low cost. Among the materials used for additive manufacturing include metals and ceramics in addition to polymers. Nevertheless, the synthetic versatility as well as the wide range of material properties that can be achieved using polymers have established this type of materials amongst the most widely employed. Herein, we describe the basic principles applied when considering printing mechanisms, as well as the advantages and disadvantages of the most relevant AM technologies. Moreover, the characteristics of the polymers employed for each technology are described including discussion of some illustrative examples of their principal applications.

* Corresponding Author Email: Email:jrodriguez@ictp.csic.es.

Keywords: additive manufacturing, stereolithography, fused deposition modeling, laser sintering, thermoplastics, photopolymerization

INTRODUCTION

1) Introduction to Additive Manufacturing

The ISO/ASTM standard terminology defines additive manufacturing (AM) as the “process of joining materials to make parts from 3D model data, usually layer upon layer, as opposed to subtractive manufacturing and formative manufacturing methodologies” [1]. “Subtractive manufacturing” refers to traditional manufacturing methodologies such as casting, forming, molding, and machining, usually constituting complex processes that require tooling, machinery, computers, and robots.

During the last 30 years of evolution in AM, other appellations have been also employed for AM processes including: rapid prototyping, rapid manufacturing, rapid tooling, freeformed fabrication, additive fabrication, additive techniques, layer manufacturing or solid freeformed fabrication. As mentioned by Campbell and Ivanova [2], AM is today widely considered as a disruptive technology that offers a new paradigm for engineering design and manufacturing that could have significant economic, geopolitical, environmental, intellectual property, and security implications.

How Does AM Work?

As described in Figure 1, AM starts with a three-dimensional (3D) model using computer aided design (CAD) modelling software (Step 1) [1]. The file obtained is converted into a stl file format (Step 2) and transferred to the AM machine (Step 3) which is digitized and sliced into model layers. The machine is then set up to adjust the printing conditions (Step 4) including energy source (temperature, laser intensity, etc.) or z-resolution (provided by the layer thickness). Other parameters depend on the AM technique selected, such as the exposure time in the case of stereolithography, or the nozzle material flow in the case of FDM. With the experimental conditions selected, the AM system prints the layers in a build, adding each new layer on top of the prior layer (Step 5). The final steps, involve the removal of the printed parts (Step 6), then post-processing to remove the supporting material (Step 7) and finally the application (Step 8).

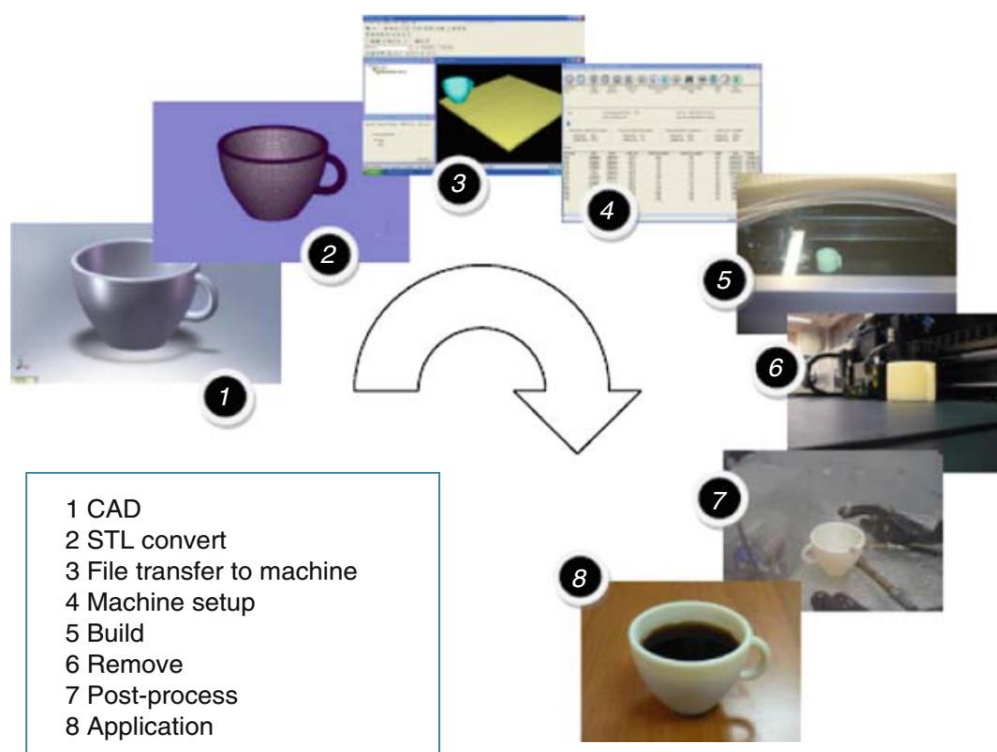


Figure 1. Steps involved in the fabrication of a cup by AM. Reproduced with permission from ref. [1].

Advantages of Additive Manufacturing in Comparison to Other Technologies

Additive manufacturing offers important advantages over other currently employed technologies [3]. AM permits the fabrication of fully customized geometrically complex products in an economic manner for a limited production. Some reports established that AM is cost effective in comparison, for instance, with plastic injection molding for targeted production runs ranging from 50 to 5,000 units. Other authors estimate that AM is competitive with plastic injection molding for the targeted fabrications below 1,000 items [4]. The basis of the low production cost is related to the nonrequirement of molds or costly tools, the nonrequirement of milling or sanding processes and the full automatization of the process.

Another crucial advantage is related to the design of the AM printed parts. Designs can easily be created and modified according to any specific change and can be shared so that manufacturing can be easily carried out in many different places simultaneously. In fact, AM allows for the quick fabrication of prototypes with different versions for lab testing without the need of costly retooling. Moreover, replacement parts can be produced by third-party providers utilizing the original designs provided by the manufacturer. As a result, an inventory is not required that can impose additional costs if finished goods remain unsold.

Finally, it is worth mentioning that AM offers important improvements in terms of environmental implications. AM makes a more efficient use of the materials and permits an environmentally friendly design. Typically, lower amounts of energy are consumed in comparison to subtractive processes. AM does not require additive chemicals and facilitates in most of the cases the reuse of the material.

Applications of AM Parts

AM fabricated parts have found application in many different fields (Figure 2). The importance of AM has been steadily growing during the last 20 years and today AM parts meet the requirements of many different industrial areas including textiles, aerospace, automotive, furniture, electronics, jewelry, sports, tool and mold making, toys/collectibles industry, and more recently they have been implemented in biomedical applications including implants/prosthetics, dental, and surgical devices/aids [3, 5].



Figure 2. Utilization of additive manufacturing across various industries. Reproduced with permission from ref. [2].

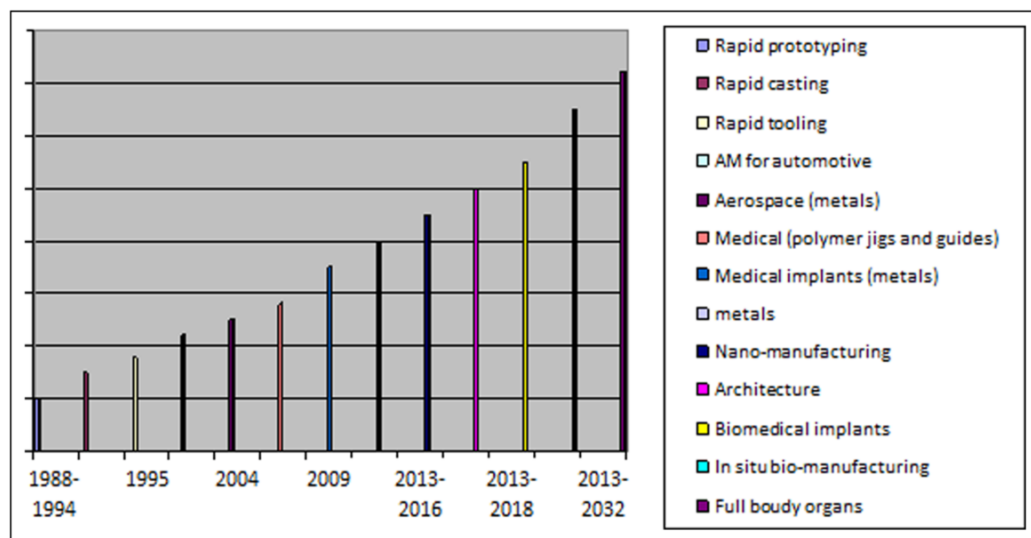


Figure 3. AM timeline for different applications. Reproduced with permission from ref. [6].

One should also note that the range of applications has evolved during the last decades. The AM application timeline suggested by Mawale et al. [6] is shown in Figure 3. As shown in the Figure, a clear evolution from rapid prototyping to series production can be observed. Currently studied applications include aerospace, medical devices, implants or manufacturing. The future of AM should, according Mawale et al., work on the efficiency of AM processes to decrease the final price. In terms of applications, the present state of the art still requires further investigation within certain areas including the development of biomedical devices, *in-situ* bio-manufacturing or the fabrication of full body organs.

2) Brief Summary of the AM Technologies

ASTM International has classified AM technologies into seven categories: (a) material extrusion, (b) powder bed fusion, (c) vat photopolymerization, (d) material jetting, (e) binder jetting, (f) sheet lamination, and (g) directed energy deposition [7, 8]. Whilst today a variety of materials are used within AM, which range from thermoplastics or photopolymers to ceramics or metallic powders, we will center our attention on those techniques which employ polymeric materials. Among these techniques, material extrusion, powder bed fusion and vat photopolymerization have employed polymeric materials extensively. For this reason, this chapter will focus on the polymers employed in these three methodologies.

(a) Material Extrusion

Without any doubt the most extended AM technology is material extrusion, a method in which material is selectively dispensed through a nozzle [9]. In general, any polymer or polymer-based material can be employed to produce flow through a moving orifice when heating and pressure are applied. Maintaining both the pressure applied and the nozzle speed constant, the material deposited will have a constant cross-sectional diameter. As shown in Figure 4, the material or materials (if a supporting material is required) is deposited on a support as required by the design. Once a layer is completed, the machine will move the nozzle upwards, or move the part downwards (typically 100-300 μm), so that a new layer can be created on top of the previous one. The steps of a common extrusion-based system include [10]:

- Loading of material.
- Liquification of the material.
- Application of pressure to move the material through the nozzle.
- Extrusion.
- Plotting according to a predefined path and in a controlled manner.
- Bonding of the material to itself or secondary build materials to form a coherent solid structure.
- Inclusion of support structures to enable complex geometrical features.

There are two primary approaches taken towards using an extrusion process. The first technology was initially developed by Stratasys, company founded by Scott and Lisa Crump in the late 1980s. In this case, the material was molten inside a heated nozzle channel permitting the material to flow out through the nozzle and undertake bonding with adjacent material before solidifying (Figure 4). This approach, known as Fused Deposition Modelling (FDM) is, due to the cheap components employed, the most extended AM technology and currently largely employed to fabricate low-cost 3D printers.

The second approach uses non-viscous flowable slurries as material for the extrusion and is usually carried out without heating. This alternative has been employed, for instance, to extrude food items [11]. Equally, this approach is convenient for the AM of biomaterials loaded with living organisms including cells. In this case, the limited temperature conditions in which cells can be employed, do not allow the use of the previous FDM methodology. Commercially available biomedical cell printers use this approach, which in addition feature large-diameter nozzles to minimize shear loading on the cells as they are deposited – thus they can enhance cell viability [12].

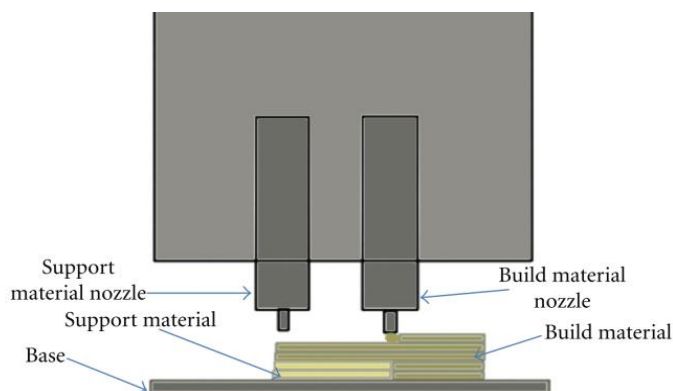


Figure 4. Fused deposition modeling. Reproduced with permission from ref. [13].

FDM presents several advantages including the non-requirement of a chemical post-processing or resins to cure, the low price of both the machine and materials resulting in a more cost effective process [14, 15]. There are, however, disadvantages in the use of this technology such as the low resolution both in x-y and z axis limited by the nozzle dimensions, the low fabrication speed (even when working in the sparse mode, which limits the amount of plastic to be deposited) and moreover the anisotropy of the fabricated parts [16].

(b) Powder Bed Fusion

Powder bed fusion, later called Selective Laser Sintering (SLS) was first commercialized by Deckard and Beaman through the DTM Corporation [9]. As is schematically shown in Figure 5, in SLS a thin layer of powder is sintered or fused by the application of a laser beam. The fabrication process occurs as follows: the chamber, filled with nitrogen in order to avoid eventual oxidation and/or degradation, is heated just below the melting point of the material. This pre-heating of the powder (which should be uniform over the entire surface) is crucial for two different reasons. Firstly, this temperature will limit the amount of laser energy required to consolidate the material and therefore limit the eventual material degradation. Secondly, large thermal cycles of heating and cooling cause proportional expansion and contraction, thus are prone to produce undesirable warping of the printed part.

Once the chamber temperature is controlled, a thin powder layer is applied and leveled using a counter-rotating roller. Then, the laser applied fuses the powder at a specific location for each layer as specified by the design, forming the slice cross-section. The construction bed is then lowered a certain amount depending on the layer thickness desired; the laser is then applied again. This process is repeated upon completion of each layer.

For the cross-section formation, as described by Shirazi et al. [17] there are three main mechanisms proposed:

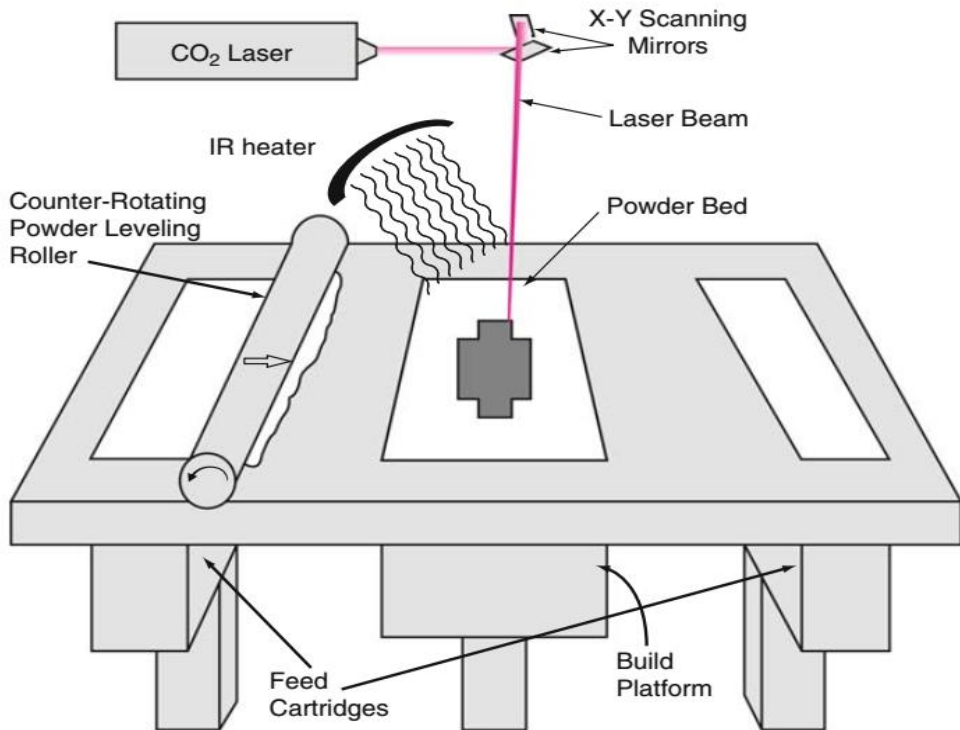


Figure 5. Schematic setup of the Selective Laser Sintering process. Reproduced with permission from ref. [17].

- a) Solid-state sintering is a thermal process that induces the binding upon heating between $T_m/2$ and T_m .
- b) Liquid phase assisted sintering is employed to favor the sintering of the materials and involves the addition of an additive to the powder that melts before the matrix phase. This method has been, for instance, used in the fabrication of 3D ceramic materials.
- c) Full melting (more adapted for metallic and ceramic materials rather than polymers) allows the fabrication of highly dense materials upon complete melting the powders by the laser beam.

In addition to the material properties, process factors such as part bed temperature, laser energy density or layer thickness are important parameters to consider during the fabrication of 3D printed parts via SLS [18, 19].

The main advantages of SLS technology are:

- a) Firstly, SLS accommodates the use of a wide range of materials including recycling of unused powder.

- b) Secondly, SLS does not require the use of support structures which are required for many other additive processes such as FDM, mainly because the part is supported by the surrounding unfused powder.
- c) Finally, SLS produces parts that are tougher and more stable than those obtained by for instance SLA.

Among the most important limitations of this technology has to be the limited accuracy which is restricted by the size of the material particles, usually circa 50-80 μm in general. Moreover, the process requires a constant temperature held close to the material melting point, which is also uniformly distributed throughout the entire chamber. Finally, as mentioned previously, oxidation needs to be prevented by using an inert gas atmosphere in many cases.

(c) Vat Photopolymerization Processes

This AM technique involves the use of liquid photopolymers that are spatially cured by light-activated polymerization [9]. Chuck Hull, in the mid-1980s, was the pioneer in using UV curable materials that when exposed to a scanning laser, produced solid polymer patterns. More interestingly, he found that by curing one layer over a previous layer, a solid 3D part could be fabricated [20]. He founded the company 3D systems and the first commercial AM machine produced was the SLA-1, introduced in 1987.

This technique is known as stereolithography (SLA) and is depicted in Figure 6, there are two different main SLA techniques distinguished by their patterning process [21]:

- Scanning-based SLA (SSLA) or direct writing. In SSLA a laser beam with small diameter (~ 0.1 mm) scans large areas by small rotations of a mirror.
- Projection-based SLA (PSLA) that is also called maskless or dynamic mask method. PSLA uses a dynamic mask for generating 2D patterns with micrometer-scale resolution.

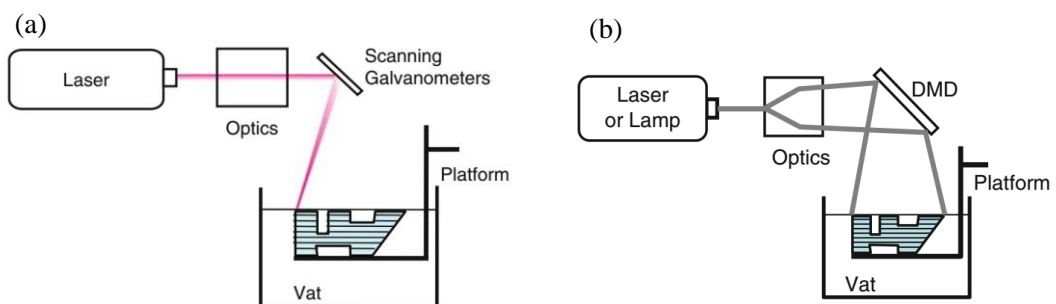


Figure 6. Schematic diagrams of the approaches to photopolymerization processes: (a) SSLA and (b) PSLA Reproduced with permission from ref. [10].

As mentioned previously, the SLA principle relies on a photopolymerization process that enables the conversion of a liquid monomer/oligomer mixture to a solidified polymer typically using ultraviolet light. UV light activates a photoinitiator and the polymerization reaction starts in those areas directly exposed [22]. A platform is required (as shown in Figure 6) to anchor the AM part and support the overhanging structures. Then, the UV laser is precisely applied to certain regions of the liquid surface where the resin solidifies. When the layer is finished the platform moves downwards, a new layer of liquid resin wets the AM part and the process is repeated again [23]. When the process is finished, the excess resin is drained (often for reuse) and the AM part is washed typically using ethanol [14, 15]. The speed required to fabricate the part prevents complete in situ conversion of the photopolymerization reaction and usually a post-curing step is carried out thereafter.

One of the major advantages of this approach is the high resolution of the fabricated parts. The depth of cure, which ultimately determines the z axis resolution, is controlled by the photoinitiator, the irradiant exposure conditions (wavelength, power and exposure time/velocity) and the eventual incorporation of dyes, pigments or other added UV absorbers, since these processes typically involve UV sources in the form of UV lasers or UV LEDs. The photo-induced layer thickness typically varies between 50–200 μm . The step size is selected based on a balance between decreased build times and enhanced resolution. A newer version of this process has been developed with a higher resolution and is called microstereolithography. This new process features an attainable layer thickness of less than 10 μm [24]. Among the drawbacks, most notably the mechanical stability of the printed objects is lower in comparison, for instance, with those obtained by SLS. Furthermore, there are issues still remaining concerning the biocompatibility of the materials employed [25].

Other AM techniques are also on the market that similarly uses polymers for the fabrication of 3D printed parts. These include, binder jetting or polyjet; information about these methodologies can be found elsewhere [1, 13, 26, 27].

POLYMERS EMPLOYED IN FUSED DEPOSITION MODELLING

As mentioned above, fused deposition modeling (FDM) is an additive manufacturing process in which a thin solid plastic filament passes through a nozzle/print head in order to melt and extrude it. The most widespread materials employed for FDM are hence thermoplastic polymers such as poly(lactic acid) (PLA) and acrylonitrile butadiene styrene (ABS) materials, which can be used in most of the commercially available FDM machines. Nevertheless, other polymers have equally been employed in FDM fabrication such as polycarbonate (PC) (including its blends of PC-ABS, and the medical grade PC,

i.e., PC-ISO), polyphenylsulfone (PPSF), polycaprolactone (PCL), polyamide (Nylon) or high density polyethylene [10].

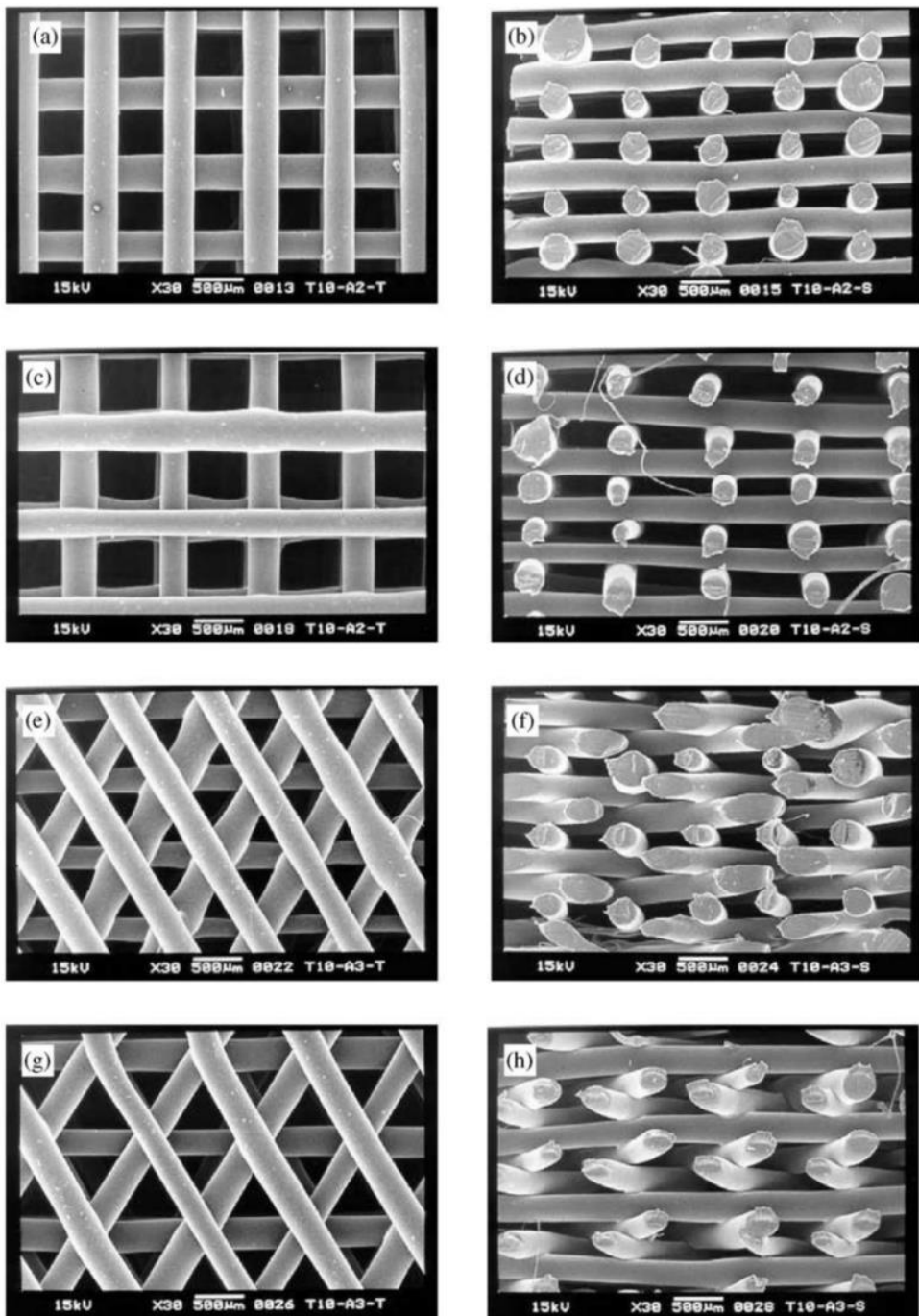


Figure 7. Scaffolds prepared by Zein et al. using poly(ϵ -caprolactone) (PCL) in a FDM 3D printer.

FDM is more apt for amorphous polymers rather than highly crystalline polymers that are more suitable for SLS processes – as will be depicted. The reason for this relies in the fact that FDM is a much better extruder of viscous materials. Amorphous polymers do not have a clear melting point and the material becomes softer by increasing the temperature. As a result, it is easy to modulate the pressure conditions required to extrude the material by finely tuning the temperature of the nozzle. In contrast to amorphous polymers, high crystalline polymers present a clear material change upon heating due to the fusion of the crystals that are physically observed by an abrupt transition in a precise temperature region from a solid state to a liquid state. In this case, a homogeneous extrusion will be hardly controlled. While this is the general rule, it is also true that crystalline materials such as PCL are currently being employed in FDM. For instance, Zein et al. [28] employed the FDM for producing poly(ϵ -caprolactone) (PCL) scaffolds with different geometrically consistent honeycomb-like patterns and fully interconnected porous channels (Figure 7).

In some cases, the design of a 3D part requires incorporating a support material that can be easily removed when the part is finished.. In FDM two polymers have been typically employed for this purpose. On the one hand, poly(vinyl alcohol) (PVA) with an approximate printing temperature of 170-190°C has been used due to its water-solubility. On the other hand, high impact polystyrene (HIPS) is an excellent support material for ABS parts as it is very similar to ABS in its properties. HIPS can be dissolved in Limonene whereas acetone can be employed for ABS.

In addition to the pure polymers described above other polymer-based materials have been employed that can be classified in three different groups:

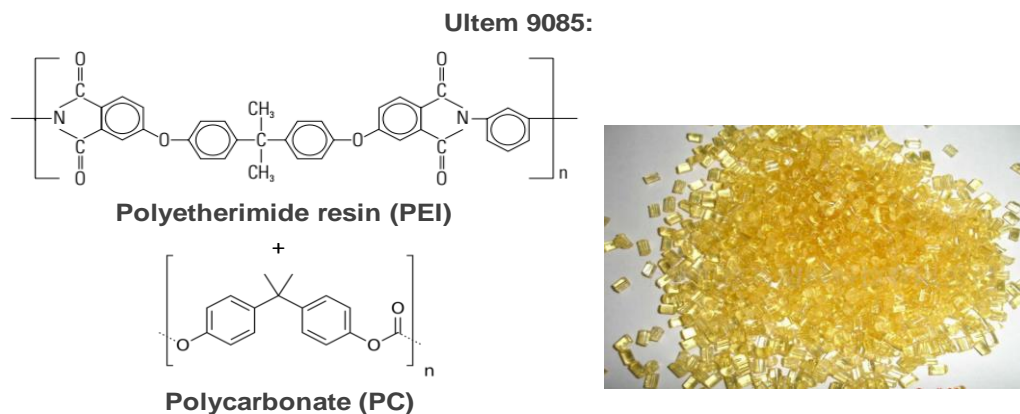


Figure 8. Chemical structure of Ultem 9085 composed of a blend of polyetherimide resin (PEI) and polycarbonate (PC).

(a) Polymer Blends

Blending allows for the easy preparation of a wide variety of materials that combine the properties of two or more different polymers. An illustrative example of the excellent properties of a polymer blend employed for FDM is the commercially available Ultem 9085 [29]. Ultem 9085 is a blend of a polyetherimide resin (PEI) and polycarbonate (PC) as illustrated in Figure 8. This material has unique characteristics that make OSU 55/55 suitable for aerospace and confined space applications. In particular, Ultem exhibits an improved ductility and flow, is transparent, possesses high strength and stiffness and good chemical resistance.

(b) Microscale Composites

Microscale composites have been prepared using microparticles and ceramic powders, fibers or piezoelectric materials [30]. For instance, copper microparticles (of $\sim 10\ \mu\text{m}$ in diameter) were incorporated into ABS by Nikzad et al. [31]. They found that these composites presented an improved storage modulus and thermal conductivity as well as a reduced coefficient of thermal expansion. Other microparticles employed include iron used to increase the thermal conductivity [32], Al and Al_2O_3 that reduce the frictional coefficient [33] or ceramic particles to prepare materials with improved dielectric permittivity [30].

(c) Nanocomposites

Similar to the microscale composites, in the fabrication of nanocomposites several authors have also employed nano-dimensional particles. For example, Perez et al. [34] that with the addition of 5 wt% nanotitanium dioxide (TiO_2), a 13.2% increase in the tensile strength of printed composite parts was shown in comparison to unfilled polymer parts. However, all printed composite parts showed reduced elongation and more brittle feature in these cases.

Moreover, carbon nanotubes and even graphene has also been incorporated into thermoplastic filaments and employed for FDM printing. Rymansaib et al. [35] prepared carbon nanofibres (CNFs) and graphite flake microparticles that were added to polystyrene with the aim of making new conductive blends suitable for 3D-printing. The polystyrene/CNF/graphite (80/10/10 wt%) composite provides good conductivity and provides a stable electrochemical interface with a well-defined active geometric surface area. The printed electrodes formed a stable interface to the polystyrene shell, which gave good signal to background voltammetric responses, and were reusable after polishing.

POLYMERS FOR STEREOLITHOGRAPHY (SLA)

SLA is a liquid-based process that consists of curing or solidification of a photosensitive polymer when an ultraviolet laser illuminates the resin. The photosensitive resins are composed of three main components:

- a) A photoinitiator, which absorbs the light and generates the active species.
- b) A reactive multifunctional monomer or oligomer, or mixture of both that gives rise to a crosslinking polymerization. The backbone of the oligomer can be varied widely and is designed to confer specific mechanical and physical properties to the polymerized material.
- c) A reactive diluent, the role of which is to adjust the viscosity of the mixture to an acceptable level for application to a substrate; it also participates in the polymerization reaction.

Eventually, flexibilizers and stabilizers may also be incorporated in the photosensitive mixture. Most materials used are conventional epoxy, acrylate resins, or thermoplastic elastomers. The original monomers were combinations of multifunctional acrylates which formed cross-linked resins [36].

(a) Photopolymerization Processes

Depending on the type of photopolymerization chemistry involved, two different types of resins [37] are commercially available nowadays:

(i) Free-Radical Photopolymerization

In this type of resins, the UV irradiation on the photoinitiator produces a homolytic cleavage of a single/double bond and formation of two radicals. This initiation step is followed by the propagation or eventual transference, i.e., the incorporation of monomeric units; albeit the transfer of the radical to another growing chain. Finally, termination occurs by any of the three possible mechanisms; a) Combination: Two chain ends simply couple together to form one long chain. One can determine if this mode of termination is occurring by monitoring the molecular weight of the propagating species: Combination will result in doubling of molecular weight. b) Radical disproportionation: A hydrogen atom from one chain end is abstracted to another, producing a polymer with a terminal unsaturated group and a polymer with a terminal saturated group. c) Combination of an active chain end with an initiator radical.

Two different types of initiators are employed for free-radical photopolymerizable resins. On the one hand, type I photoinitiators are unimolecular free-radical generators;

that is to say, upon the absorption of UV-light a specific bond within the initiators structure undergoes homolytic cleavage to produce free radicals. Typical type I photoinitiators are hydroxyacetophenone (HAP) or phosphineoxide (TPO). On the other hand, type II photoinitiators require a co-initiator, usually an alcohol or amine, functional groups that can readily have hydrogens abstracted, in addition to the photoinitiator. The absorption of UV light by a Type-II photoinitiator causes an excited electron state in the photoinitiator that will abstract a hydrogen atom from the co-initiator, and in the process, splitting a bonding pair of electrons.

Not only the type of initiator but the concentration as well as the molar absorption coefficient are crucial on the absorption and therefore on the resolution achieved.

Even if it is outside of the scope of this chapter, it is worth mentioning that other important parameters need to be considered since they are directly related to the kinetics. Such additional parameters include: the presence of oxygen, the temperature and the UV light intensity.

(ii) Cationic Photopolymerization

Similarly to radical photopolymerization, in the case of cationic photopolymerization, a photoinitiator is in charge of the conversion of UV light into initiating species. However, in this case, the initiator molecule is converted into a strong acid species (either a Lewis or Brönsted acid) that initiates polymerization by UV light absorption. Most cationic photoinitiators are comprised of a cationic and anionic pair with a distinct role in the polymerization. The cationic portion of the photoinitiator molecule is responsible for the absorption of UV radiation while the anionic portion of the molecule becomes the strong acid after UV absorption [38]. Provided the initiation step occurs, the cationic polymerization mechanism proceeds similar to other chain-growth polymerizations through propagation, termination and chain transfer steps.

(b) Materials Employed for SLA

The ideal monomers used in SLA (typically comonomers and reactive oligomers) should have a relatively low to modest overall viscosity and be able to rapidly form crosslinked polymers. Acrylates for free radical photopolymerization and epoxy monomers for cationic photopolymerization are most commonly encountered as photo-based printing materials. However, photopolymerizable epoxies offer better mechanical properties. In contrast to acrylate resins, they have exceptionally low volume shrinkage and good dimensional stability.

(i) Polymers Employed

SLA is a precise, fast and cheap technology to fabricate intricate geometries when required, among other examples, to produce implantable scaffolds for tissue engineering applications. However, biomaterials that are biocompatible and biodegradable in the human body are required for this purpose. As described by Choi et al. [39] biodegradable scaffolding implies that the scaffold is “gradually degraded chemically *in vivo* leaving the desired shape of the regenerated tissue without causing cytotoxicity”. Moreover, biocompatibility indicates that “the surface of the scaffold remains chemically compatible such that cells attach to and grow on the scaffold without inducing any undesired reactions (or immune responses) with neighboring tissues”. In this context, several biodegradable and biocompatible materials have been synthesized and adapted for their use in SLA.

Cooke et al. [40] reported a poly(propylene fumarate) (PPF) scaffold, accomplishing the requirements of biodegradability and biocompatibility, when fabricated in a conventional SL system [39]. Other examples of using PPF for the fabrication of scaffolds were reported by Lee et al. [41]. They used poly(propylene fumarate) (PPF) as the biomaterial, diethyl fumarate (DEF) as the solvent and bisacrylphosphine oxide (BAPO) as the photoinitiator. After optimizing the experimental conditions, including the resin composition (by satisfying both the viscosity limitation and the mechanical requirement), laser parameters such as critical exposure (E_c) and penetration depth (D_p), the authors succeeded in the fabrication of scaffolds with a high accuracy in the xy -plane while minimizing the overcuring of the resin in z -axis.

Also poly(ϵ -caprolactone) (PCL) is an excellent candidate material for biocompatible/biodegradable support. PCL is degraded by hydrolysis of its ester linkages in physiological conditions (such as in the human body) and has therefore received great attention for its use as an implantable biomaterial. In particular it is especially interesting for the preparation of long term implantable devices, owing to its degradation rate which is even slower than that of polylactide. Elomaa and coworkers [42] investigated a photocrosslinkable PCL-based resin which was developed and applied using stereolithography. No additional solvents were required during the structure preparation process. Three-armed PCL oligomers of varying molecular weights were synthesized and then functionalized with methacrylic anhydride; they were then photocrosslinked, resulting in high gel content networks. As illustrated in Figure 9, the scaffolds precisely matched the computer-aided designs, with no observable material shrinkage. The average porosity was $70.5 \pm 0.8\%$, and the average pore size was $465 \mu\text{m}$. The pore network was highly interconnected.

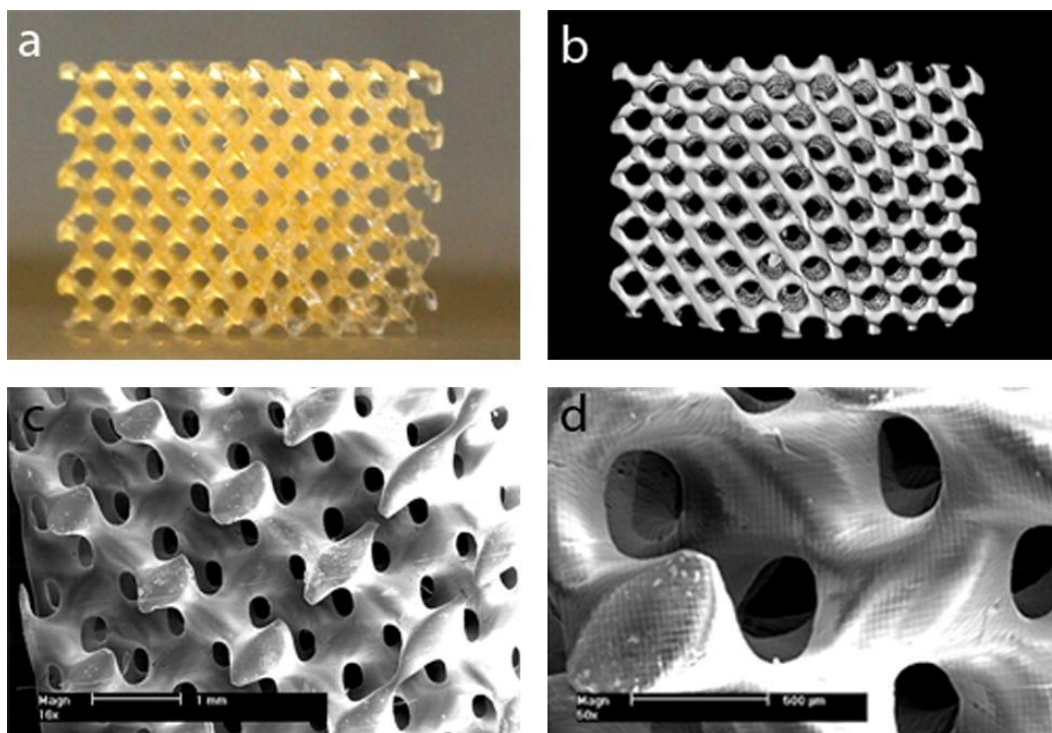


Figure 9. Photograph (a), μ CT visualization (b) and SEM images (c and d) of a scaffold built by stereolithography using 1500-m macromer. Reproduced with permission from ref. [42].

Elasticity and flexibility are also interesting properties of some polymeric materials. Processing of these polymers by stereolithography would produce flexible and elastic three-dimensional structures that, in comparison with hydrogels may significantly improve the mechanical resistance of the 3D printed part. With this objective, Schüller-Ravoo et al. [43] fabricated flexible and elastic poly(trimethylene carbonate) (PTMC) structures using a three-armed methacrylated PTMC macromer (obtained by reaction of trimethylene carbonate, glycerol, and methacrylic anhydride). Upon seeding of bovine chondrocytes into the scaffolds, the cells adhered and spread on the PTMC surface. After culturing for 6 weeks, cells with a round morphology were present, indicative of the differentiated chondrocyte phenotype. In cartilage tissue engineering, chondrocytes adopt a round shape indicating the presence of differentiated cells producing cartilage specific proteoglycans and collagen fibrils of high collagen type II over type I ratio.

The high resolution obtained using SLA permitted the fabrication of a myriad of microfluidic devices with high versatilities in terms of design. In addition acrylate based resins provide high clarity although not complete transparency. Au et al. [44] described the fabrication of fluidic valves and pumps that can be stereolithographically printed in optically-clear, biocompatible plastic and integrated within microfluidic devices at low cost. User-friendly fluid automation devices can be printed and used by non-specialized personnel as replacement for costly robotic pipettors or tedious manual pipetting.

Engineers can manipulate the designs as digital modules into new devices of expanded functionality. Moreover, SL benefits from the possibility of a modular design. Au et al. designed a valve in an electronic file that could be digitally connected to other functional modules to easily build more complex devices. As shown in Figure 10, the fabricated fluidic switch operates by connecting two valves V1 and V2 to a common outlet. Different dye outputs are produced by opening the appropriate valves (images c-e).

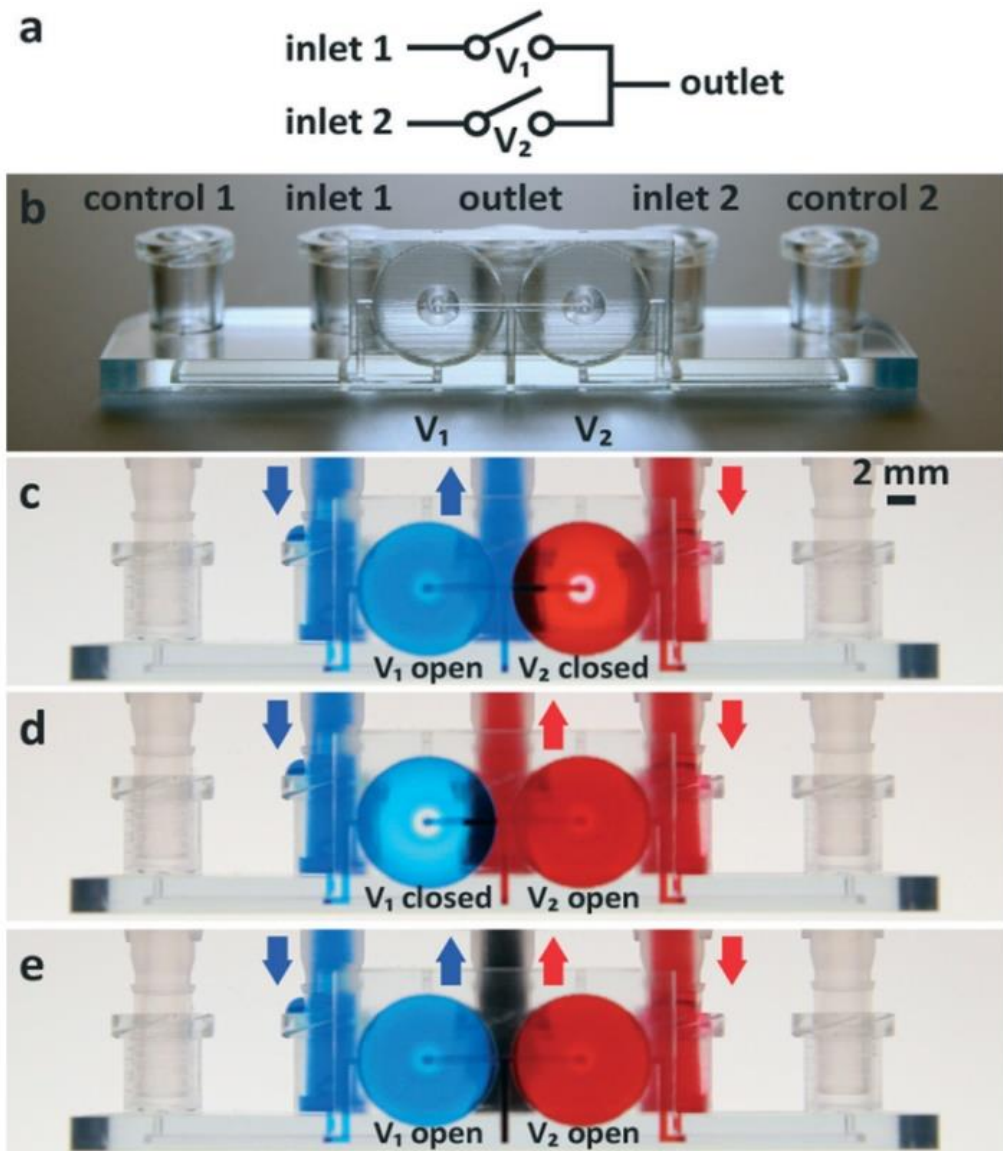


Figure 10. 3D-printed switch. Circuit diagram photograph of the two-valve switch. (c–e) Photographs of a dye-filled switch in three different actuation states. Reproduced with permission from ref. [44].

(ii) Ceramic and Metal Composites

It is difficult to obtain good mechanical properties (a high level of hardness and a high mechanical resistance to fluid pressure) as well as thermal and electrical conductivity when photopolymers are used. As a result, the fabrication of composites by dispersing a particular additive (typically ceramic or metallic particles) in the photosensitive resin has been extensively employed to improve the final material properties. For instance, a printable diamond polymer composite was developed by Kalsoom et al. [45] for the fabrication of low cost thermally conducting devices. They fabricated the composite by simply suspending the HPHT diamond microparticles within the commercial acrylate based resin at concentrations as high as 30% (w/v), avoiding any additional chemical reactions or further modifications. A heating system was set at 100°C and used to evaluate the heat transfer performance of the printed sinks. The difference in temperatures and heat distribution of the heat sink printed from the basic resin and the composite material, each heated for 10 min, was determined using a thermal imaging camera. As depicted in Figure 11, the IR images for the AP and APD-30 composite heat sinks showed that the temperature of the composite heat sink was almost 5–8°C higher for all three regions (i.e., top, middle and bottom) compared to the basic AP heat sink, thus demonstrating that the composite material improved the heat distribution away from the heated surface.

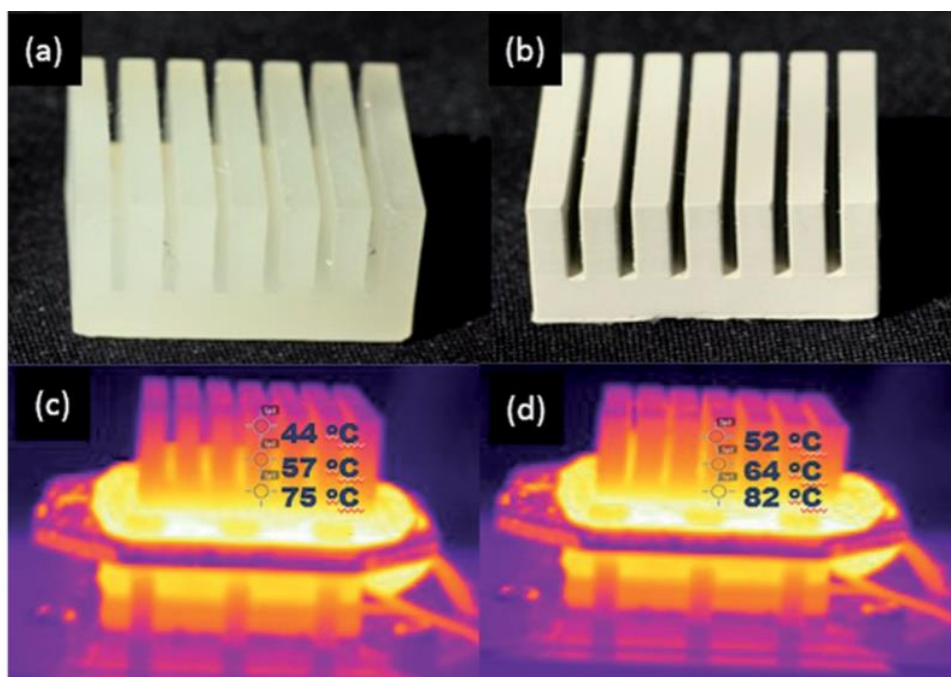


Figure 11. (a) 3D printed heat sink using commercial acrylate resin, (b) 3D printed heat sink using 30% (w/v) composite material, (c) IR images of polymer heat sink heated for 10 min at 100°C and (d) IR image of composite heat sink heated for 10 min at 100°C.

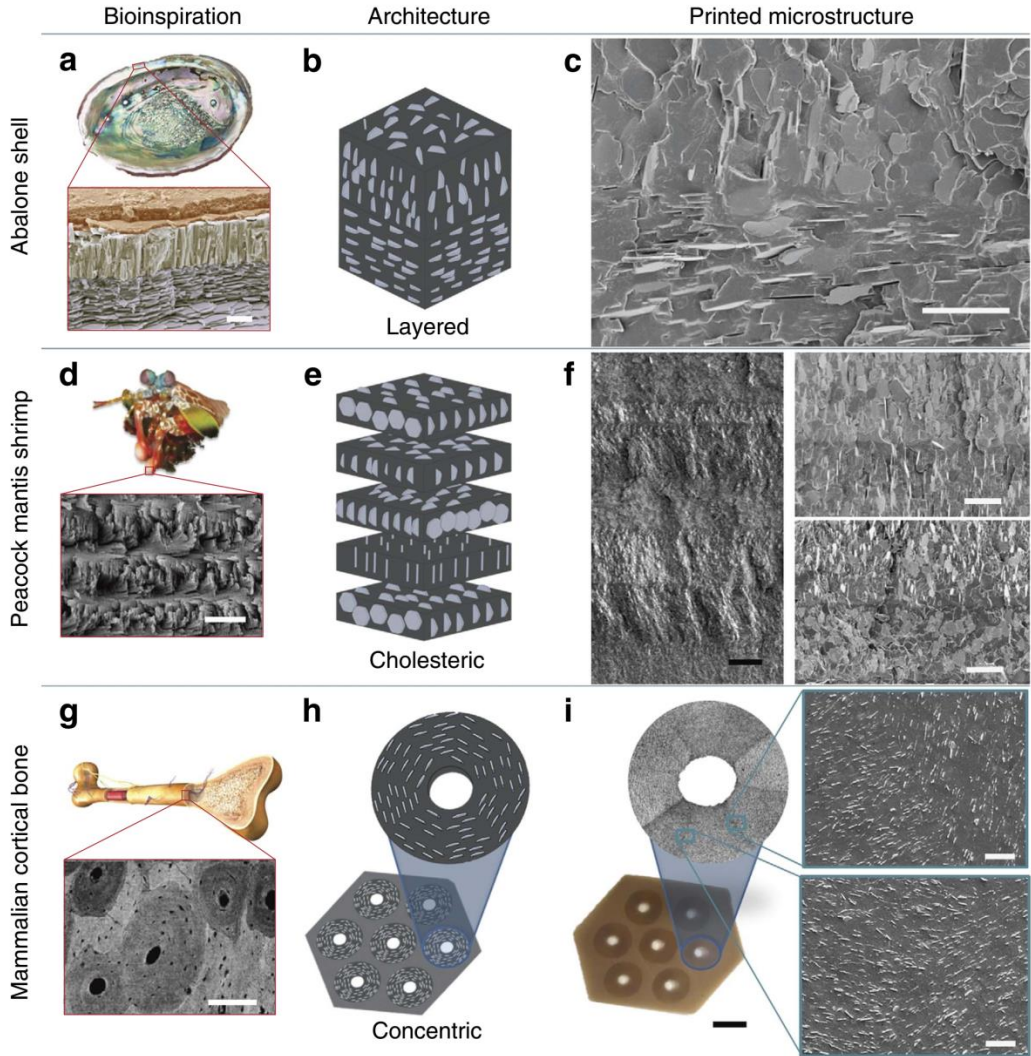


Figure 12. Bioinspired composites with microstructured architectures can be recreated with 3D magnetic printing. (a) The Haliotidae sp. Abalone shell exhibits a layered structure of calcite prisms topping in-plane aragonite platelets (nacre). This architecture is (b) simplified and (c) 3D magnetic printed. (d) The dactyl club of the peacock mantis shrimp exhibits a cholesteric architecture of mineralized chitin fibres. This architecture is (e) simplified and (f) 3D magnetic printed. (g) The mammalian cortical bone exhibits concentric plywood structures of lamellae-reinforced osteons. This architecture is (h) simplified and (i) 3D magnetic printed. All printed microstructures are acrylateurethane co-polymers reinforced by 15 volume percent alumina platelets. Scale bar, 5 μm in a; 25 μm in c; 15 μm in d; 50 μm (black) and 20 μm (white) in f; 200 μm in g; and 5 μm (black) and 25 μm (white) in i. Reproduced with permission from ref. [46].

In addition to the incorporation of a particular ceramics or metallics, a current challenge to the adaption of additive manufacturing technology of reinforced composites also involves the ability to provide orientation of the reinforcing co-composites. In particular, the orientation of fibres during the printing process. An illustrative example of

the efforts in this direction was reported by Martin et al. [46]. By using a 3D Magnetic-Printing Process they created an SLA-based 3D printing framework capable of printing dense ceramic/polymer composites in which the direction of the ceramic-reinforcing particles could be finely tuned within each individual voxel of printed material. As shown in Figure 12, they were able to recreate choice reinforcement architectures exhibited by biologically discontinuous fibre composite systems including the osteon structures within the mammalian cortical bone, the layered nacreous shell of abalones and the cholesteric reinforced dactyl club of the peacock mantis shrimp.

SELECTIVE LASER SINTERING: POLYMERS POWDERS AND COMPOSITES

One of the major advantages of SLS is related to the great variety of materials “*a priori*” that could be employed. These include polymers, metals and their combinations, combinations of metals and ceramics and combinations of metals and polymers [24, 47, 48].

Examples of polymers that could be used are; acrylic styrene, polycaprolactone or polyamide (nylon), all of which result in 3D printed parts that show similar mechanical properties to parts prepared by injection [47, 49]. It is also possible to use composites or reinforced polymers, for instance polyamide with reinforced by fiberglass or with metals like copper.

(a) Polymer Choice: Semi-Crystalline and Amorphous

Two types of thermoplastics have been typically employed in SLS, i.e., semi-crystalline and amorphous [50]. From a morphological point of view the main difference between the two types of polymers is related to their molecular arrangement. Whereas, an amorphous material has the chain molecules arranged in a random manner, a semi-crystalline material present chains with an ordered structure. This difference confers to each type of material and thier different thermal properties which determine, in turn, the fabrication parameters in SLS. In both cases, upon heating, a glass transition temperature (T_g) can be observed [51, 52]. A majority of semicrystalline polymers have a glass transition temperature (T_g) below or close to room temperature (-100 to 50°C) while the amorphous polymers typically employed have a T_g of $\sim 100^\circ\text{C}$. Moreover, semycrystalline polymers present a melting temperature (T_m) above 100°C (between 100 and 400°C) at which a considerable volume change occurs and the material rapidly changes from rigid

to a liquid form. This transition does not appear in amorphous polymers that present a progressively rubbery morphology with no obvious transitions [53-55].

In addition to the semicrystalline or amorphous nature of the material, both T_g and T_m are also related to the molecular weight of the polymer employed. Therefore, an optimization of the SLS experimental conditions is required for each thermoplastic material. Other processing considerations include the particle size, the powder flow, thickness of the deposited powder layer, the power of the laser or the relative humidity just to mention a few of them [56].

For instance, the power and scanning speed of the laser applied in an SLS system is directly related to the mechanical properties of the 3D printed parts. When, semi-crystalline polymers are employed, the laser heats the material above the T_m . In this situation, the material remains hard until an appropriate quantity of heat is absorbed, at which point it is rapidly changed into a viscous liquid. To the opposite, amorphous polymer powders are consolidated upon heating above the T_g . In comparison to semi-crystalline polymers, amorphous materials are much more viscous and therefore require more intense heating to establish the appropriate particle interconexion [57]. Associated to heating and cooling processes, shrinkage is a serious issue in SLS. In particular, the use of semicrystalline polymers produces strong material contraction upon with freezing. In order to minimize this drawback, the chamber where the 3D part will be constructed is preheated allowing the powders to be in a furnace below their melting temperature during long periods of time (up to a duration of hours) [53].

In addition to the laser intensity, decreasing the laser scanning speed leads to the production of denser parts as a result of the longer interaction time between the powder and the laser beam [58]. A higher laser scan speed results in less energy transferred to the materials [59].

Semi-crystalline polymers are primarily used with an intrinsic selection criteria ideally including:

- a broad process temperature window between polymer melting upon heating and recrystallization upon cooling.
- a narrow melt transition.
- a high melting enthalpy to minimize unwanted sintering associated with thermal conductivity.

(b) Polymer and Polymer Blends Employed in SLS

Nylons in their different variants are without any doubt the most extensively employed polymer employed for SLS. An illustrative example of the use of Nylon for SLS was reported by Das et al. [60] that prepared scaffolds from Nylon-6. They carried

out biocompatibility tests that showed that Nylon-6 scaffolds fabricated by SLS can support cell viability. To investigate the biocompatibility of scaffolds, cells were either in direct contact with the Nylon-6 disks (CoCulture group) or subjected to conditioned media (Conditioned Media group).

Polycaprolactone (PCL) is a semi-crystalline material with high thermal stability and a degradation period of approximately two years [61] and has been extensively employed for SLS. Due to the good biocompatibility, bioresorbability, and processability of PCL, this polymer has found application in tissue engineering [62] and cartilage repair [63-65] purposes amongst others.

Eshraghi et al. [66] studied the mechanical and microstructural properties of polycaprolactone scaffolds with one-dimensional, two-dimensional, and three-dimensional orthogonally oriented porous architectures produced by selective laser sintering (Figure 13).

Amorphous synthetic polymers such as polycarbonate or polystyrene have been also employed for SLS. These polymers tend to yield weaker, more porous structures than the semi-crystalline polymer powders, although relatively brittle polystyrene parts can be strengthened and toughened by substitution with poly(styrene-co-acrylonitrile) or ABS [56].

Finally, cellulose and its derivatives used as coating materials for drugs, drug-releasing scaffolds and in other biomedical applications are also projected for incorporation into orthopedic implants, and thus have been also employed for SLS. Salmoria et al. [19] reported the rapid fabrication of starch-cellulose and cellulose acetate scaffolds by selective laser sintering and the evaluation of the laser power, laser scan speed and the polymer particle size influence on the scaffold properties. The fine adjustment of process parameters was fundamental in order to warranty the processability of biodegradable cellulose based polymers by SLS. As depicted in Figure 14, the specimens with lower particle size presented a higher degree of sintering, higher mechanical strength and a significant level of closed pores, as indicated by the density measurements and fractography analyses.

Blending, as a tool to obtain polymeric materials with variable properties, has also been employed to fabricate 3D printed parts by SLS. However, the examples reported are rather scarce. An illustrative example of this strategy was reported by Salmoria et al. [67], therein they prepared blends of polyamide (PA2200) and high-density polyethylene (HDPE) particles with average sizes of 60 and 100 μm . PA2200 showed higher absorption of laser energy than HDPE during the sintering of blend specimens, with subsequent thermal energy transfer to the melting of the HDPE phase. The authors reported the formation of heterogeneous microstructures of PA2200/HDPE blended specimens with co-continuous and dispersed phases depending on the quantity of HDPE.

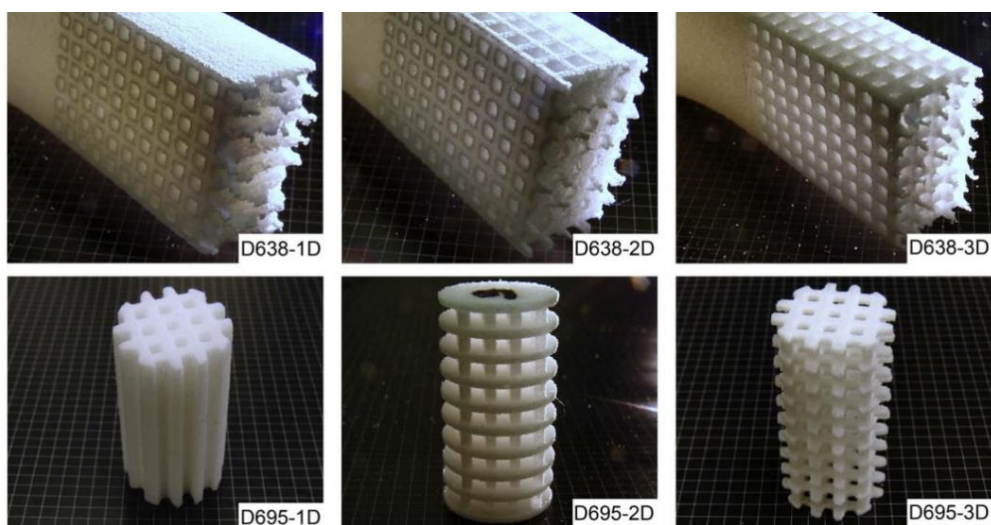
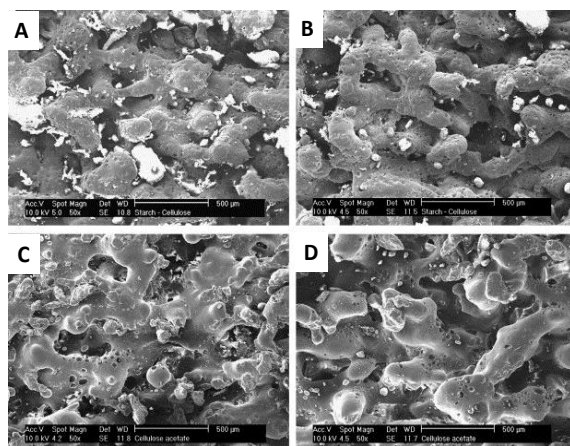


Figure 13. Scaffolds with one-dimensional, two-dimensional, and three-dimensional orthogonally oriented porous architectures produced by selective laser sintering. Reproduced with permission from ref. [66].



Specimen	Particle size	$\rho_{\text{volumetric}}$ (g cm^{-3})	
A	Starch-cellulose	106–125 μm	0.522
B	Starch-cellulose	150–212 μm	0.475
C	Cellulose acetate	106–125 μm	0.460
D	Cellulose acetate	150–212 μm	0.367

Figure 14. The micrographs of the sintered specimen surfaces of *starch-cellulose* (A) particles of 106–125 μm (B) of 150–212 μm and *Cellulose acetate* (C) particles of 106–125 μm (D) 150–212 μm . Reproduced with permission from ref. [19].

(c) Composites Prepared Using Micro/Nano Fillers

A large number of investigations have been made to improve the mechanical and physical properties of polymeric laser sintered parts by reinforcing them with different charges. For instance, the incorporation of ceramics (which are rather brittle) into polymers improved the mechanical properties and enabled the shaping of hard ceramics [68–70]. In general, polymeric materials employed for SLS have been charged with:

(i) *Micron-Sized Inorganic Fillers such as Glass Beads, Silicon Carbide, Hydroxyapatite and Aluminium Powder*

Chung and Suman [71] prepared composites of Nylon-11 filled with different volume fractions of glass beads (0–30%). The results showed that the tensile and compressive modulus increased whilst the strain at break and strain at yield decreased as a function of glass bead volume fraction.

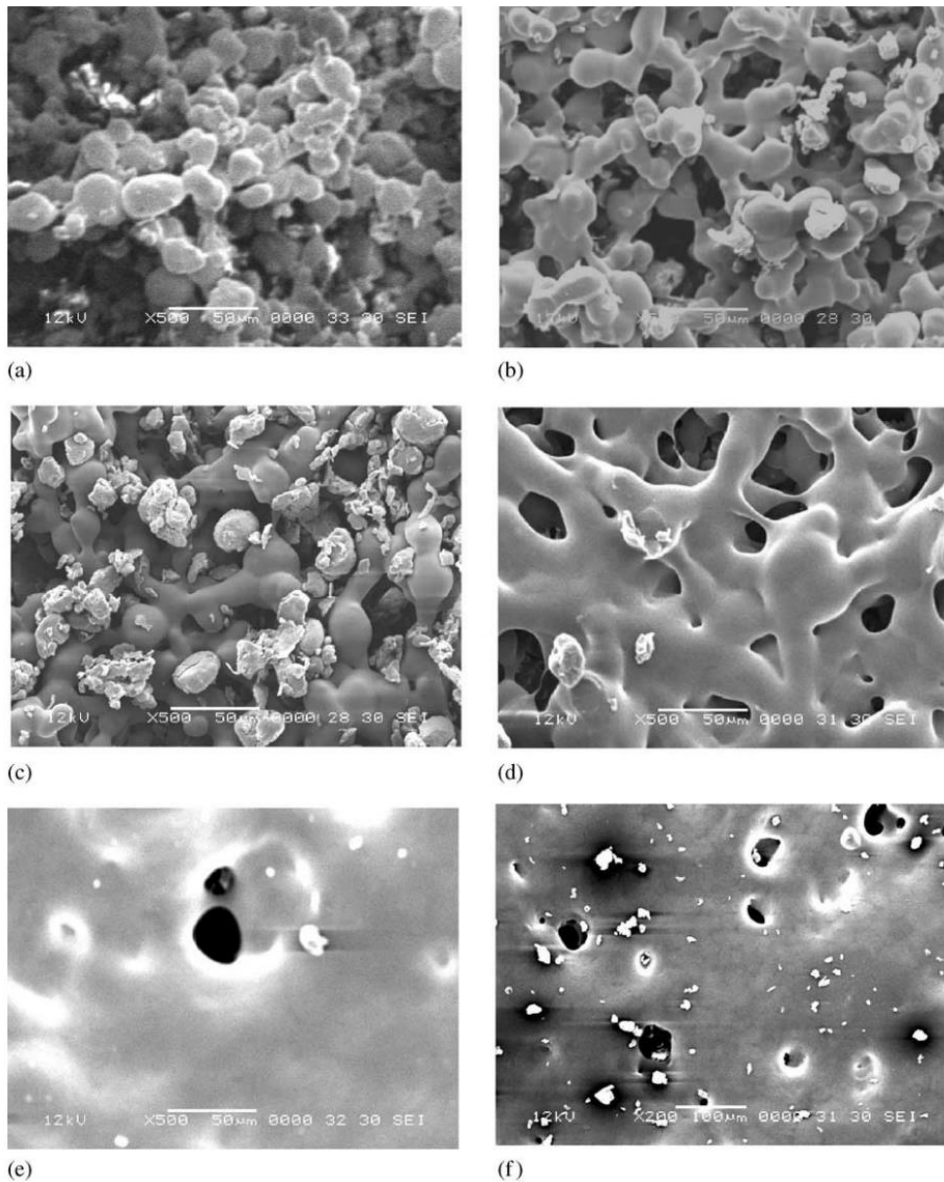
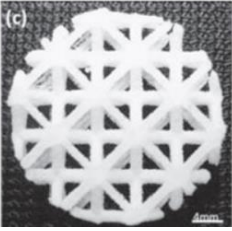
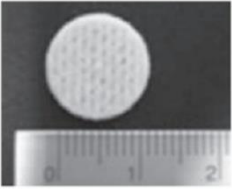
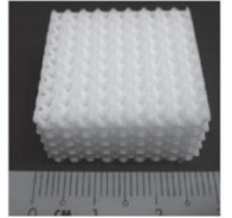
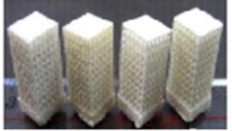
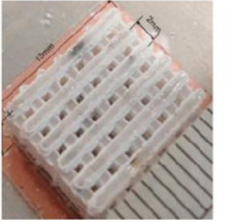
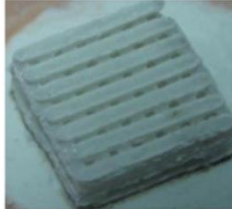


Figure 15. Micrograph of sintered pure PEEK specimens produced at a part bed temperature of 140C and laser power settings of (a) 9 W, (b) 12 W, (c) 16 W, (d) 20 W, (e) 24W, and (f) 28W. Reproduced with permission from ref. [72].

Table 1. Summary of mechanical and biological properties of laser sintered tissues and scaffolds. Adapted from ref. [17]

Material	Physical properties	Biological properties	Image of the final part	Ref.
PCL	Porosity: 85% Micropores: 40–100 μm	A high density of cells was observed on the scaffold after 6 days		[65]
PCL	Porosity: 83% Micropores: 300–400 μm	The porcine adipose-derived stem cells (pASC) proliferated well and differentiated into osteoblasts successfully in the scaffold		[74]
PCL	Porosity: 40–84%	A confluent monolayer of cells with an elongated morphology could be observed on the wells fed with the scaffold extract		[75]
CP/PHBV CHA/PLLA	Porosity of the PHBV polymer scaffolds: $64.6 \pm 2.0\%$ CP/PHBV scaffolds: $62.6 \pm 1.2\%$ PLLA polymer scaffolds: $69.5 \pm 1.3\%$ CHA/PLLA scaffolds: $66.8 \pm 2.5\%$	All scaffolds were facilitated proliferation of and ALP expression by SaOS-2 cells. Viability assays of SaOS-2 cells after 3 days of culture on sintered scaffolds		[76]
HA/ β -TCP	Porosity: 61% Interconnected macroporous structure of the scaffold with a rectangular pore size range of 0.8–1.2 μm	MG63 cells exhibited elongated and flattened morphology on the TCP/HAP scaffolds, and the cells were connected with cellular micro-extensions		[77]
Forsterite based scaffolds with 20% nano-58S bioactive glass	Interconnected porous scaffold with pore size 0.5 to 0.8 μm	Cells attached and spread well on the forsterite/nano-58S		[78]

To create the scaffolds, Tan et al. [72] employed rapid prototyping (RP) techniques to overcome the limitations encountered with conventional manual-based fabrication processes. For that purpose, the authors prepared scaffolds based on polyetheretherketone (PEEK) and hydroxyapatite (HA) powders physically blended and processed on a commercial SLS system. PEEK has a glass transition at approximately 143°C and melts at approximately 343°C. Since PEEK has a much lower melting point than HA, it is possible to induce sintering of PEEK at temperatures near T_g , and moreover to bind and partially expose the HA particles within the sintered PEEK matrix. However, the laser power and the bed temperature play a crucial role on the sintering process (Figure 15). On the one hand, the sintering of PEEK is more successful at higher part bed temperatures for each of the different laser power settings tested; as evidenced from the quantity and prominence of neck formation between particles. On the other hand, when the laser power was increased to 12 W and higher at a part bed temperature setting of 140°C was used, the sintering results obtained appeared more promising; as can be observed from Figure 15c–f.

In addition, Xia et al. [73] selected hydroxyapatite (HA) as reinforcement and fabricated a set of PCL based scaffolds by SLS. Scanning electronic microscopy (SEM) showed that the nano-HA/PCL scaffolds exhibited predesigned, well-ordered macropores and interconnected micropores and featured a 130% improvement on the compressive strength. Human bone marrow stromal cells were seeded onto the nano-HA/PCL or PCL scaffolds and cultured for 28 days in vitro. As indicated by the level of cell attachment and proliferation, the nano-HA/PCL showed excellent biocompatibility, comparable to that of PCL scaffolds.

A brief summary of examples of scaffolds prepared by SLS reported in the literature are included in Table 1.

(ii) Nano-Sized Fillers such as Clay, Carbon Nanofibres, Nanosilica, and Nano- Al_2O_3 Particles

The impact resistance of sintered tissues and scaffolds can also be improved using nanocomposites. For instance, Zheng et al. [79] prepared nano- Al_2O_3 particles coated with polystyrene (PS) by emulsion polymerization and used them as fillers to reinforce PS based composites prepared by selective laser sintering (SLS). The influence of the treated and untreated nanoparticles on the sintering behavior and mechanical properties of the laser sintered specimens were investigated. They found that there were many uneven holes in the untreated composites. In contrast, for the treated composites, due to the nanoparticle surfaces treated by emulsion polymerization, the absorbance of the laser light was improved and the nanoparticles dispersed in the polymer matrix with good uniformity. As a result, a full dense structure was obtained and the properties were enhanced. In particular, the impact strength increased by 50% and the tensile strength increased by up to 300% in comparison to the unfilled PS respectively.

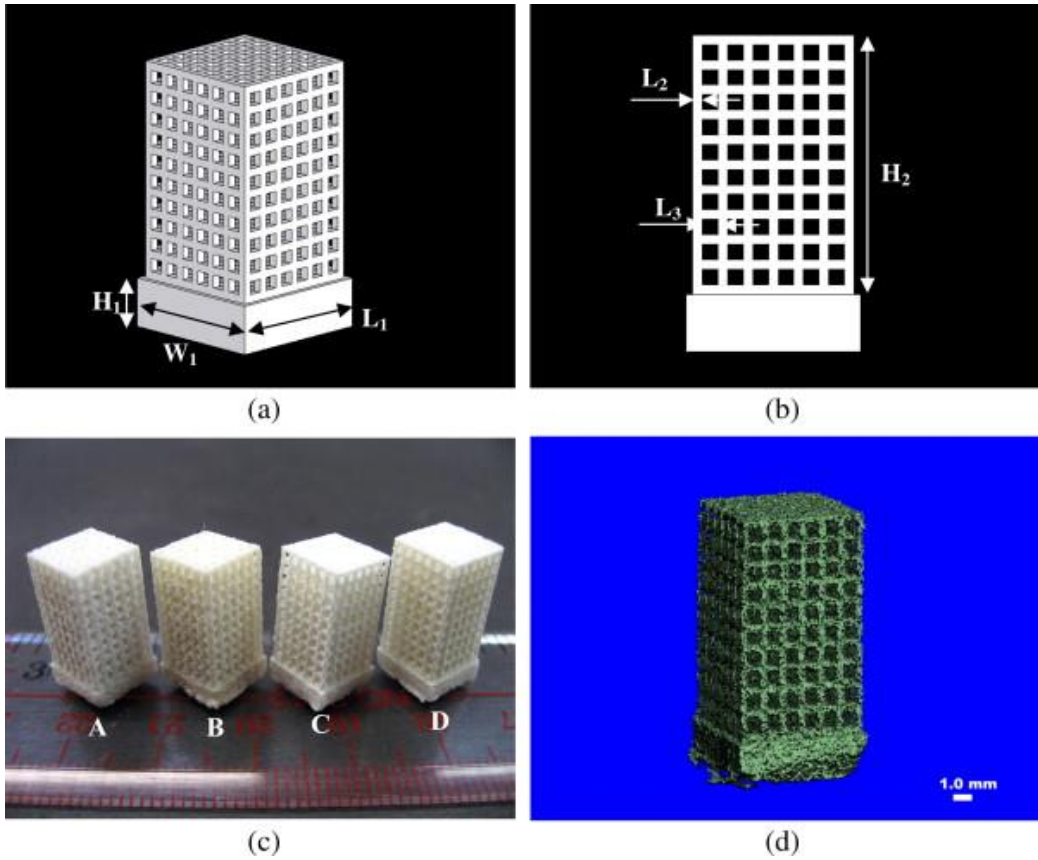


Figure 16. (a)-(b) Schematic diagrams of the scaffold model in diametric and side; (c) scaffolds produced by SLS: (A) PHBV; (B) Ca-P/PHBV; (C) PLLA; (D) CHAp/PLLA. (d) MicroCT image of a Ca-P/PHBV scaffold. Reproduced with permission from ref. [76].

Nanocomposites have been, similarly to microcomposites, employed for the fabrication of scaffolds. For example, Bin et al. [76] prepared three-dimensional nanocomposite microspheres based on calcium phosphate (Ca-P)/poly(hydroxybutyrate-co-hydroxyvalerate) (PHBV) and carbonated hydroxyapatite (CHAp)/poly(l-lactic acid) (PLLA) employed, in turn, to fabricate scaffolds (Figure 16). The sintered scaffolds had controlled material microstructure, totally interconnected porous structure and high porosity. According to the authors, *in vitro* biological evaluation showed that SaOS-2 cells had high cell viability and normal morphology and phenotype after 3 to 7 days culture on all scaffolds. The incorporation of Ca-P nanoparticles significantly improved cell proliferation and alkaline phosphatase activity for Ca-P/PHBV scaffolds, whereas CHAp/PLLA nanocomposite scaffolds exhibited a similar level of cell response compared with PLLA polymer scaffolds.

CONCLUSION

The development of a wide variety of additive manufacturing (AM) technologies currently offer versatile platforms for tailor-made fabrication of fully-customized products in a decentralized and cost-effective fashion. Besides its initial use, which was limited to being a tool for rapid prototyping and small-scale production of customized items, additive manufacturing has become an interesting methodology to fabricate components with unusual shapes for a wide variety of applications ranging from architecture to biomedicine.

This review has provided a general and introductory overview of the most extensively employed methodologies used to fabricate AM parts using polymers as base materials in three different forms, i.e., filaments, liquid resins or powders. A description of the particular concerns to be considered in each case has been discussed. Equally, recent examples of novel polymeric materials developed for AM as well as their applications have been thoroughly described.

Future, novel developments in terms of equipments and materials will offer new opportunities for the use of AM printed materials to be applied as functional technical parts, medical parts or micro-fabrication; a challenge still remaining for which many research groups are actively involved in with the intent to turn AM into production technology.

ACKNOWLEDGMENTS

The authors acknowledge financial support given by FONDECYT Grant N° 1170209. M.A. Sarabia acknowledges the financial support given by CONICYT through the doctoral program Scholarship Grant. J. Rodriguez-Hernandez acknowledges financial support from the Spanish National Science Foundation (CSIC) and the Ministerio de Economía y Competitividad (MINECO) (Project MAT2016-78437-R). Finally, this study was funded by VRAC Grant Number L216-04 of Universidad Tecnológica Metropolitana.

REFERENCES

- [1] I. Gibson, D. Rosen, B. Stucker, *Additive manufacturing technologies: 3D printing, rapid prototyping, and direct digital manufacturing*, Springer 2014.

- [2] T.A. Campbell, O.S. Ivanova, Additive manufacturing as a disruptive technology: implications of three-dimensional printing, *Technology & Innovation* 15(1) (2013) 67-79.
- [3] B. Berman, 3-D printing: The new industrial revolution, *Business horizons* 55(2) (2012) 155-162.
- [4] B. Sedacca, Hand built by lasers [additive layer manufacturing], *Engineering & Technology* 6(1) (2011) 58-60.
- [5] J. Gausemeier, N. Echterhoff, M. Wall, *Thinking ahead the Future of Additive Manufacturing—, Analysis of Promising Industries*, Heinz Nixdorf Institute, University of Paderborn Product Engineering, Paderborn 14 (2011).
- [6] M.B. Mawale, A.M. Kuthe, S.W. Dahake, Additive layered manufacturing: State-of-the-art applications in product innovation, *Concurrent Engineering* 24(1) (2016) 94-102.
- [7] S.K.Y. Miura, S. Kobayashi, M. Iwamoto, Y. Imanishi, J. Umemura, *Chem. Phys. Lett.* 315 (1999) 1.
- [8] D.L. Bourell, Perspectives on additive manufacturing, *Annual Review of Materials Research* 46 (2016) 1-18.
- [9] A.J.S.R.H. Wieringa, *Macromolecules* (29) (1996) 2032.
- [10] I. Gibson, D. Rosen, B. Stucker, *Additive Manufacturing Technologies Rapid Prototyping to Direct Digital Manufacturing*. 2010, Springer.
- [11] C.W.F.Y.C. Chang, *Polym. Prepr.* (38) (1997) 945.
- [12] N. Jones, *Science in three dimensions: the print revolution*, 2012.
- [13] K.V. Wong, A. Hernandez, A review of additive manufacturing, *ISRN Mechanical Engineering* 2012 (2012).
- [14] C.K. Chua, K.F. Leong, C.S. Lim, *Rapid prototyping: principles and applications*, World Scientific, 2010.
- [15] K. Cooper, *Rapid prototyping technology: selection and application*, CRC press, 2001.
- [16] S. Morvan, R. Hochsmann, M. Sakamoto, ProMetal RCT (TM) process for fabrication of complex sand molds and sand cores, *Rapid Prototyping* 11(2) (2005) 1-7.
- [17] S.F.S. Shirazi, S. Gharekhani, M. Mehrali, H. Yarmand, H.S.C. Metselaar, N.A. Kadri, N.A.A. Osman, A review on powder-based additive manufacturing for tissue engineering: selective laser sintering and inkjet 3D printing, *Science and technology of advanced materials* 16(3) (2015) 033502.
- [18] K.C. Kolan, M.C. Leu, G.E. Hilmas, M. Velez, Effect of material, process parameters, and simulated body fluids on mechanical properties of 13-93 bioactive glass porous constructs made by selective laser sintering, *Journal of the mechanical behavior of biomedical materials* 13 (2012) 14-24.

- [19] G.V. Salmoria, P. Klauss, R.A. Paggi, L.A. Kanis, A. Lago, Structure and mechanical properties of cellulose based scaffolds fabricated by selective laser sintering, *Polymer Testing* 28(6) (2009) 648-652.
- [20] H. Lipson, The shape of things to come: frontiers in additive manufacturing, *Frontiers of Engineering* (2011) 33-44.
- [21] M.M. Emami, F. Barazandeh, F. Yaghmaie, Scanning-projection based stereolithography: Method and structure, *Sensors and Actuators A: Physical* 218 (2014) 116-124.
- [22] D. Pham, C. Ji, Design for stereolithography, *Proceedings of the Institution of Mechanical Engineers, Part C: Journal of Mechanical Engineering Science* 214(5) (2000) 635-640.
- [23] P.F. Jacobs, *Rapid prototyping & manufacturing: fundamentals of stereolithography*, Society of Manufacturing Engineers 1992.
- [24] J.W. Halloran, V. Tomeckova, S. Gentry, S. Das, P. Cilino, D. Yuan, R. Guo, A. Rudraraju, P. Shao, T. Wu, Photopolymerization of powder suspensions for shaping ceramics, *Journal of the European Ceramic Society* 31(14) (2011) 2613-2619.
- [25] N.P. Macdonald, F. Zhu, C. Hall, J. Reboud, P. Crosier, E. Patton, D. Wlodkowic, J. Cooper, Assessment of biocompatibility of 3D printed photopolymers using zebrafish embryo toxicity assays, *Lab on a Chip* 16(2) (2016) 291-297.
- [26] I. Gibson, D.W. Rosen, B. Stucker, *Additive manufacturing technologies*, Springer. 2010.
- [27] X. Xu, S. Meteyer, N. Perry, Y.F. Zhao, Energy consumption model of Binder-jetting additive manufacturing processes, *International Journal of Production Research* 53(23) (2015) 7005-7015.
- [28] K. Leong, C. Cheah, C. Chua, Solid freeform fabrication of three-dimensional scaffolds for engineering replacement tissues and organs, *Biomaterials* 24(13) (2003) 2363-2378.
- [29] R.H. Wieringa, A.J. Schouten, *Macromolecules* 29 (1996) 3032-3034.
- [30] D. Isakov, Q. Lei, F. Castles, C. Stevens, C. Grovenor, P. Grant, 3D printed anisotropic dielectric composite with meta-material features, *Materials & Design* 93 (2016) 423-430.
- [31] M. Nikzad, S. Masood, I. Sbarski, Thermo-mechanical properties of a highly filled polymeric composites for fused deposition modeling, *Materials & Design* 32(6) (2011) 3448-3456.
- [32] S. Masood, W. Song, Thermal characteristics of a new metal/polymer material for FDM rapid prototyping process, *Assembly Automation* 25(4) (2005) 309-315.
- [33] K. Boparai, R. Singh, H. Singh, Comparison of tribological behaviour for Nylon6-Al-Al₂O₃ and ABS parts fabricated by fused deposition modelling: This paper

- reports a low cost composite material that is more wear-resistant than conventional ABS, *Virtual and Physical Prototyping* 10(2) (2015) 59-66.
- [34] A.R.T. Perez, D.A. Roberson, R.B. Wicker, Fracture surface analysis of 3D-printed tensile specimens of novel ABS-based materials, *Journal of Failure Analysis and Prevention* 14(3) (2014) 343-353.
- [35] Z. Rymanasib, P. Iravani, E. Emslie, M. Medvidović-Kosanović, M. Sak-Bosnar, R. Verdejo, F. Marken, All-Polystyrene 3D-Printed Electrochemical Device with Embedded Carbon Nanofiber-Graphite-Polystyrene Composite Conductor, *Electroanalysis* 28(7) (2016) 1517-1523.
- [36] P.J. Bártolo, *Stereolithography: materials, processes and applications*, Springer Science & Business Media 2011.
- [37] E. Andrzejewska, Photopolymerization kinetics of multifunctional monomers, *Progress in polymer science* 26(4) (2001) 605-665.
- [38] <https://polymerinnovationblog.com/uv-curing-part-five-cationic-photopolymerization/>.
- [39] J.-W. Choi, R. Wicker, S.-H. Lee, K.-H. Choi, C.-S. Ha, I. Chung, Fabrication of 3D biocompatible/biodegradable micro-scaffolds using dynamic mask projection microstereolithography, *Journal of Materials Processing Technology* 209(15) (2009) 5494-5503.
- [40] M.N. Cooke, J.P. Fisher, D. Dean, C. Rimnac, A.G. Mikos, Use of stereolithography to manufacture critical-sized 3D biodegradable scaffolds for bone ingrowth, *Journal of Biomedical Materials Research Part B: Applied Biomaterials* 64(2) (2003) 65-69.
- [41] K.-W. Lee, S. Wang, B.C. Fox, E.L. Ritman, M.J. Yaszemski, L. Lu, Poly (propylene fumarate) bone tissue engineering scaffold fabrication using stereolithography: effects of resin formulations and laser parameters, *Biomacromolecules* 8(4) (2007) 1077-1084.
- [42] L. Elomaa, S. Teixeira, R. Hakala, H. Korhonen, D.W. Grijpma, J.V. Seppälä, Preparation of poly (ϵ -caprolactone)-based tissue engineering scaffolds by stereolithography, *Acta biomaterialia* 7(11) (2011) 3850-3856.
- [43] S. Schüller-Ravoo, S.M. Teixeira, J. Feijen, D.W. Grijpma, A.A. Poot, Flexible and Elastic Scaffolds for Cartilage Tissue Engineering Prepared by Stereolithography Using Poly(trimethylene carbonate)-Based Resins, *Macromolecular Bioscience* 13(12) (2013) 1711-1719.
- [44] A.K. Au, N. Bhattacharjee, L.F. Horowitz, T.C. Chang, A. Folch, 3D-printed microfluidic automation, *Lab on a Chip* 15(8) (2015) 1934-1941.
- [45] U. Kalsoom, A. Peristyy, P. Nesterenko, B. Paull, A 3D printable diamond polymer composite: a novel material for fabrication of low cost thermally conducting devices, *RSC Advances* 6(44) (2016) 38140-38147.

- [46] J.J. Martin, B.E. Fiore, R.M. Erb, Designing bioinspired composite reinforcement architectures via 3D magnetic printing, *Nature communications* 6 (2015).
- [47] H.-H. Tang, M.-L. Chiu, H.-C. Yen, Slurry-based selective laser sintering of polymer-coated ceramic powders to fabricate high strength alumina parts, *Journal of the European Ceramic Society* 31(8) (2011) 1383-1388.
- [48] G.V. Salmoria, R.A. Paggi, A. Lago, V.E. Beal, Microstructural and mechanical characterization of PA12/MWCNTs nanocomposite manufactured by selective laser sintering, *Polymer Testing* 30(6) (2011) 611-615.
- [49] M. Krzmar, S. Dolinsek, *Selective laser sintering of composite materials technologies*, na2010.
- [50] U. Ajoku, N. Hopkinson, M. Caine, Experimental measurement and finite element modelling of the compressive properties of laser sintered Nylon-12, *Materials Science and Engineering: A* 428(1) (2006) 211-216.
- [51] J. Bicerano, J.T. Seitz, Molecular origins of toughness in polymers, *Polymer Toughening* (1996) 1-59.
- [52] G. Wisanrakkit, J. Gillham, The glass transition temperature (T_g) as an index of chemical conversion for a high-T_g amine/epoxy system: chemical and diffusion-controlled reaction kinetics, *Journal of Applied Polymer Science* 41(11-12) (1990) 2885-2929.
- [53] J.-P. Kruth, G. Levy, F. Klocke, T. Childs, Consolidation phenomena in laser and powder-bed based layered manufacturing, *CIRP Annals-Manufacturing Technology* 56(2) (2007) 730-759.
- [54] M. Schmidt, D. Pohle, T. Rechtenwald, Selective laser sintering of PEEK, *CIRP Annals-Manufacturing Technology* 56(1) (2007) 205-208.
- [55] H. Ho, W. Cheung, I. Gibson, Effects of graphite powder on the laser sintering behaviour of polycarbonate, *Rapid Prototyping Journal* 8(4) (2002) 233-242.
- [56] R. Goodridge, C. Tuck, R. Hague, Laser sintering of polyamides and other polymers, *Progress in Materials Science* 57(2) (2012) 229-267.
- [57] J.J. Beaman, J.W. Barlow, D.L. Bourell, R.H. Crawford, H.L. Marcus, K.P. McAlea, *Solid freeform fabrication: a new direction in manufacturing*, Kluwer Academic Publishers, Norwell, MA 2061 (1997) 25-49.
- [58] F.L. Amorim, A. Lohrengel, V. Neubert, C.F. Higa, T. Czelusniak, Selective laser sintering of Mo-CuNi composite to be used as EDM electrode, *Rapid Prototyping Journal* 20(1) (2014) 59-68.
- [59] D. Gu, Y. Shen, Influence of Cu-liquid content on densification and microstructure of direct laser sintered submicron W-Cu/micron Cu powder mixture, *Materials Science and Engineering: A* 489(1) (2008) 169-177.
- [60] S. Das, S.J. Hollister, C. Flanagan, A. Adewunmi, K. Bark, C. Chen, K. Ramaswamy, D. Rose, E. Widjaja, Freeform fabrication of Nylon-6 tissue engineering scaffolds, *Rapid Prototyping Journal* 9(1) (2003) 43-49.

- [61] P.A. Gunatillake, R. Adhikari, Biodegradable synthetic polymers for tissue engineering, *Eur Cell Mater* 5(1) (2003) 1-16.
- [62] J.M. Williams, A. Adewunmi, R.M. Schek, C.L. Flanagan, P.H. Krebsbach, S.E. Feinberg, S.J. Hollister, S. Das, Bone tissue engineering using polycaprolactone scaffolds fabricated via selective laser sintering, *Biomaterials* 26(23) (2005) 4817-4827.
- [63] M.I. Sabir, X. Xu, L. Li, A review on biodegradable polymeric materials for bone tissue engineering applications, *Journal of materials science* 44(21) (2009) 5713-5724.
- [64] V.J. Mkhabela, S.S. Ray, Poly (ϵ -caprolactone) nanocomposite scaffolds for tissue engineering: a brief overview, *Journal of nanoscience and nanotechnology* 14(1) (2014) 535-545.
- [65] W. Yeong, N. Sudarmadji, H. Yu, C. Chua, K. Leong, S. Venkatraman, Y. Boey, L. Tan, Porous polycaprolactone scaffold for cardiac tissue engineering fabricated by selective laser sintering, *Acta biomaterialia* 6(6) (2010) 2028-2034.
- [66] S. Eshraghi, S. Das, Mechanical and microstructural properties of polycaprolactone scaffolds with one-dimensional, two-dimensional, and three-dimensional orthogonally oriented porous architectures produced by selective laser sintering, *Acta biomaterialia* 6(7) (2010) 2467-2476.
- [67] G. Salmoria, J. Leite, C. Ahrens, A. Lago, A. Pires, Rapid manufacturing of PA/HDPE blend specimens by selective laser sintering: microstructural characterization, *Polymer Testing* 26(3) (2007) 361-368.
- [68] C. Shuai, P. Feng, B. Yang, Y. Cao, A. Min, S. Peng, Effect of nano-zirconia on the mechanical and biological properties of calcium silicate scaffolds, *International Journal of Applied Ceramic Technology* 12(6) (2015) 1148-1156.
- [69] F. Wiria, K. Leong, C. Chua, Y. Liu, Poly- ϵ -caprolactone/hydroxyapatite for tissue engineering scaffold fabrication via selective laser sintering, *Acta biomaterialia* 3(1) (2007) 1-12.
- [70] L. Shor, S. Güçeri, X. Wen, M. Gandhi, W. Sun, Fabrication of three-dimensional polycaprolactone/hydroxyapatite tissue scaffolds and osteoblast-scaffold interactions in vitro, *Biomaterials* 28(35) (2007) 5291-5297.
- [71] H. Chung, S. Das, Processing and properties of glass bead particulate-filled functionally graded Nylon-11 composites produced by selective laser sintering, *Materials Science and Engineering: A* 437(2) (2006) 226-234.
- [72] K.H. Tan, C.K. Chua, K.F. Leong, C.M. Cheah, P. Cheang, M.S. Abu Bakar, S.W. Cha, Scaffold development using selective laser sintering of polyetheretherketone-hydroxyapatite biocomposite blends, *Biomaterials* 24(18) (2003) 3115-3123.
- [73] Y. Xia, P. Zhou, X. Cheng, Y. Xie, C. Liang, C. Li, S. Xu, Selective laser sintering fabrication of nano-hydroxyapatite/poly- ϵ -caprolactone scaffolds for bone tissue engineering applications, *International journal of nanomedicine* 8 (2013) 4197.

- [74] H.-T. Liao, K.-H. Chang, Y. Jiang, J.-P. Chen, M.-Y. Lee, Fabrication of tissue engineered PCL scaffold by selective laser-sintered machine for osteogenesis of adipose-derived stem cells: the research has proven that a bone tissue-engineered scaffold can be made using the selective laser sintering method, *Virtual and Physical Prototyping* 6(1) (2011) 57-60.
- [75] N. Sudarmadji, J. Tan, K. Leong, C. Chua, Y. Loh, Investigation of the mechanical properties and porosity relationships in selective laser-sintered polyhedral for functionally graded scaffolds, *Acta biomaterialia* 7(2) (2011) 530-537.
- [76] B. Duan, M. Wang, W.Y. Zhou, W.L. Cheung, Z.Y. Li, W.W. Lu, Three-dimensional nanocomposite scaffolds fabricated via selective laser sintering for bone tissue engineering, *Acta biomaterialia* 6(12) (2010) 4495-4505.
- [77] C. Shuai, P. Li, J. Liu, S. Peng, Optimization of TCP/HAP ratio for better properties of calcium phosphate scaffold via selective laser sintering, *Materials Characterization* 77 (2013) 23-31.
- [78] J. Deng, P. Li, C. Gao, P. Feng, C. Shuai, S. Peng, Bioactivity improvement of forsterite-based scaffolds with nano-58S bioactive glass, *Materials and Manufacturing Processes* 29(7) (2014) 877-884.
- [79] H. Zheng, J. Zhang, S. Lu, G. Wang, Z. Xu, Effect of core-shell composite particles on the sintering behavior and properties of nano-Al₂O₃/polystyrene composite prepared by SLS, *Materials Letters* 60(9) (2006) 1219-1223.

Chapter 16

**FROM 3D TO 4D-PRINTING:
ON THE ROAD TO SMART 3D-PRINTED
POLYMER DEVICES**

Jérémy Odent^{1,}, Antoniya Toncheva^{1,2*},
Philippe Dubois^{1,‡} and Jean-Marie Raquez^{1,‡}*

¹Laboratory of Polymeric and Composite Materials,
Center of Innovation and Research in Materials and Polymers,
University of Mons, Mons, Belgium

²Laboratory of Bioactive Polymers, Institute of Polymers,
Bulgarian Academy of Sciences, Sofia, Bulgaria

ABSTRACT

The scientific and technological progress reached a point that allows for exciting 3D printing technologies. Applied to the additive manufacturing industry, said technologies offer the possibility to create polymer devices with controlled architectures such as personalized prototypes, hydrogels, biomedical and flexible electronic devices, as well as sensors and actuators with controlled properties and a specific set of desired functionalities. Alongside this advancement, a new class of polymers defined as “smart polymer materials”, are described, with a main utility built around the capacity to exhibit adaptive properties that fulfill previously impossible functions post application of environmental changes. Direct 3D printing of such stimuli-responsive materials allowed the development of a brand new 4D printing technology with an outlined time dimension. This chapter will cover a comparative review of the two most frequently explored AM technologies - fused deposition modeling and stereolithography with a specific focus on

* These authors contribute equally to this work

‡Corresponding Author Email: philippe.dubois.raquez@umons.ac.be;
jean-marie.raquez@umons.ac.be.

the practical use in “smart materials” 3D printing. Potential applications for the printed parts and some critical remarks are also mentioned.

Keywords: smart polymers, additive manufacturing, fused deposition modeling, stereolithography, 3D-printing, 4D-printing

INTRODUCTION

1. From Additive Manufacturing to Smart Materials

Slowly yet steadily, additive manufacturing (AM) technologies have become a major player in the fabrication of polymer devices. Private companies, government and public sector have openly declared an interest into applying this method in smart devices fabrication while pursuing direct practical. AM also known as 3D printing, has been herein recognized as a milestone technology for future advances in manufacturing [1-4]. Based on a layer by layer fabrication, with resolution in the range in micro- and nanometers per layer, the computer-assisted printing significantly speeds up the development of custom 3D objects without actually inflating the costs. AM technologies using polymeric materials include selective laser sintering [5], fused deposition modeling (FDM) [6] and stereolithography (SLA) [7] techniques. While FDM is the most promising candidate for fabricating parts out of multi-materials, SLA offers the highest versatility with respect to the freedom in material development, scalability and speed of fabrication.

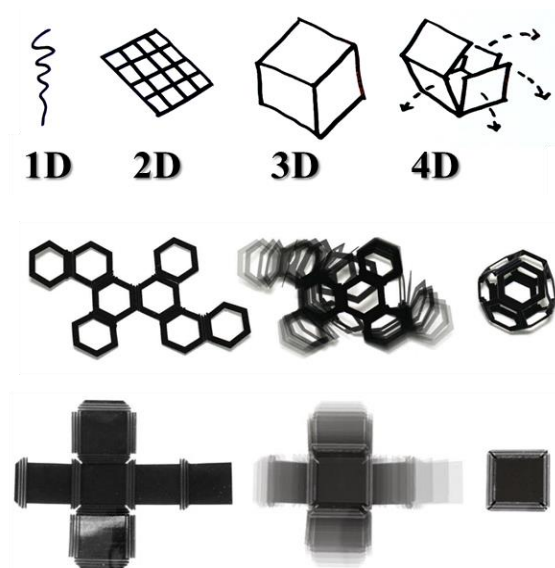


Figure 1. Schematic illustration of the 4D printing concept whereas the 3D-printed structure can change shape over time given external stimulus [8, 9].

Despite the irrefutable progress made around 3D printing and its unquestionable potential benefits, the technique still suffers from rigid and static properties of the printed parts and a difficulty with the actuation or transformation to a desirable shape. However, the emergence of a new class of polymers defined as “smart materials” has somewhat changed the accepted way to conceptualize and design polymer devices. Generally, the term “smart material” is used to describe a material capable of responding to an external stimulus by changing its shape, volume and physical properties, such as Young’s modulus, stiffness, and resistance [10]. By attaching this additional attribute of “smartness”, new functional systems are linked to various polymeric devices - sensors, actuators and soft-robotics. Combining these stimuli-responsive materials and AM techniques resulted in 3D objects that carry unique responses to a variety of external or environmental stimuli such as changes in temperature, humidity, pH, solvent vapor, *etc.* [11, 12]. This progress gave birth to the 4D printing technology with a fourth dimension defined as the material’s transformation over time (Figure 1) [8, 9]. The key element here is the time, where the actuation, the sensor properties and the programmability are directly embedded into the material structure and occur in desired time frames. The resulting new properties mainly rely on an appropriate combination of “smart materials” in the right three-dimensional geometry. Subsequently, shape-changing, self-actuating, self-healing or any other multi-functionality can be obtained as an expected response triggered by changes in the environment. This approach has immediate potential implications in e.g., robotics, biomedical devices, building construction, aerospace, electronics and sensors. As an example, the U.S. Army has already virtually adapted the technology to produce woodland camouflage fabrics, able to mimic natural or even artificial backgrounds by bending the light reflected from the clothing [13].

In this chapter, the focus would be on some of the most recent advancements in AM techniques, with an accent on 3D printing for the design of “smart polymer” materials. A special mention would go to the 4D printing methodology. The discussion would be built around FDM and SLA, the two most well-established techniques in the field. More information about other currently existing AM processing methods is available in Chapter 10 “Polymers for Additive Manufacturing” of this book and readers are kindly invited to refer its content. At the end of the chapter, some practical daily life applications are described and envisioned, and future perspectives and critical remarks are also outlined.

2. 3D Printing

2.1. Fused Deposition Modeling

FDM as part of the AM industry is a fast-growing prototyping technology, offering an opportunity to create functional parts with complex geometrical shape within an

acceptable time frames. The core of the process is melting a uniform mono-filament to a semi-liquid state, followed by a layer-by-layer extrusion onto an adapted platform. The adhesion between the layers is guaranteed by a simple contact between the deposited filaments solidifying in the final object [14]. FDM usable materials are limited to most commonly used commercially available thermoplastic polymers (polylactide - PLA, acrylonitrile-butadiene-styrene, polyethylene terephthalate, Nylon®, thermoplastic polyurethane and polycarbonate). Main beneficial factors for those are a low melting temperature, biocompatibility, resorbability and large scale industrial production. For the correct application of FDM, the melt viscosity of the material is of great importance. It should be high enough to ensure structural support, while simultaneously being low enough to enable the layer-to-layer deposition [15]. Some advantages of FDM-based printers are the low cost, high speed and simplicity of the process. However, one common difficulty is that the polymer or the composite material should be prepared in filament shape with a specific diameter (generally 1.75 mm) and capable of undergoing the extrusion process. In cases where nanofillers are loaded in the polymer matrix, their homogeneous dispersion ends up being of particular importance for the final properties of the printed part.

Currently, some advances in the development of composite 3D methodology also allow for the use of pre-blended materials and polymer nanocomposites. Various nanofillers such as carbon fiber [16], carbon black [17], short fibers (including chopped carbon fibers) [18], polymer fibrils [19], carbon nanotubes [10], and glass fibers [20] were mixed into thermoplastic filaments for direct use. The result was a notable reinforcement of the materials in term of mechanical properties. Using 3D printers with two or more printer nozzles enables the production of smart polymer systems for everyday materials. It should be noted that the process parameters (such as working temperature, layer thickness, printing orientation, raster width and angle and air gap) and their direct impact on the final device morphology and properties are not in the scope of this chapter. Detailed information can be found in the study published by Sood et al. [21].

Even though AM through material extrusion is a convenient method for the manufacturing thermoplastic components, a key obstacle facing the 3D-printed plastic parts is the weak welding between adjacent filaments. Often when using FDM, the adhesion between the adjacent filaments in the final 3D-printed device is a result of simple surface contact to contact of the molten material. There are several important difficulties that need to be dealt with: *(i)* fast surface cooling of the previously deposited filament decreases the possibility to interact with the subsequent deposited molten filament, *(ii)* the formation of crystalline phase in the previously deposited filaments during their cooling (decreased mobile amorphous phase of the macromolecules and low probability to interact with the subsequent filament) and *(iii)* an irregular volume contraction alongside the deposited filaments resulting in “wave”-shaped profile instead of straight one. All these effects could lead to delamination of the filament layers and the

subsequent mechanical failure of the final product and limited engineering application. These anisotropic mechanical properties often measure different volume strength when stress is applied: greater along the filament length deposition and weaker in any other direction (Figure 2). In addition to that, some limitations related to the mechanical construction of the equipment are present such as: printing direction (x and y) deviation and vibrations during the printing process. By combining the knowledge acquired in various scientific fields and the expertise of the technological progress linked to the FDM machine construction. In this context, several scientific studies were published with the goal of increasing the interface between the individual filaments. Some scientific projects are focused on the post-treatment of the filament (heating or coating) or on the formation of covalent bonds between the filaments, e.g., thermoreversible reactions.

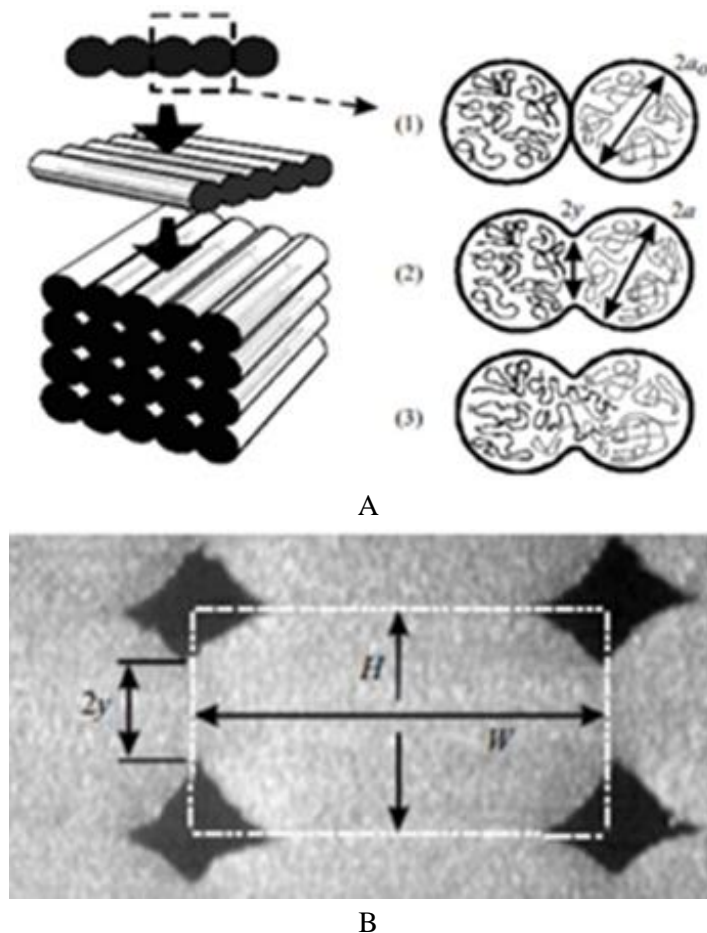
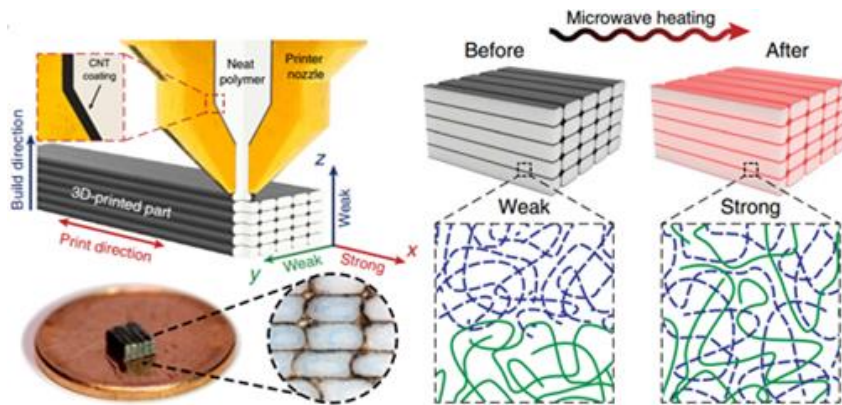


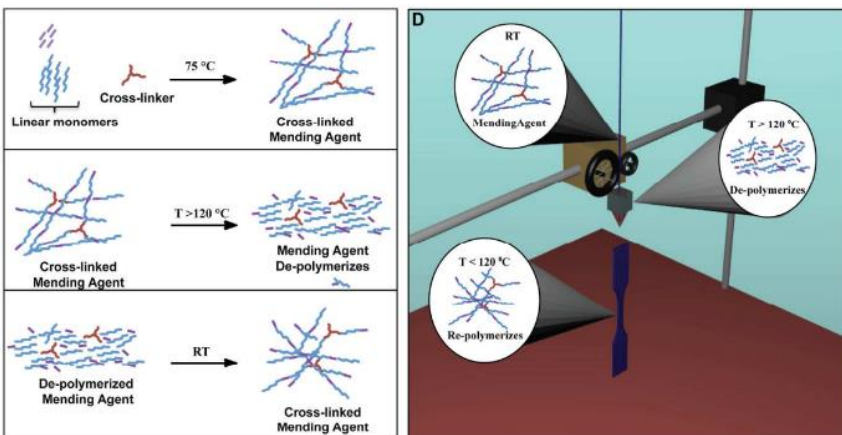
Figure 2. Different degree of contacts between two adjacent filaments: 1-surface contacting, 2-neck growth, 3-molecular diffusion at interface and randomization (A) and SEM microphotograph of the cross-sectional area of the filaments (B) [23].

In the literature, several approaches were proposed to improve the strength of FDM fabricated parts. The focus is on the bead width, the air gap, the working temperature and the faster orientation while goal is to increase the surface contacting the filaments interface, its' the neck growth and molecular diffusion (Figure 2).

Another promising setup is to perform microwave irradiation assisted FDM. This idea has been investigated by Sweeney et al. The experiment used PLA filaments coated with multiwalled carbon nanotubes (0.5 - 20 wt%) for their local heating properties and percolation network [22]. Specifically, localized nanofillers only at the surface of the filaments allowed the production of 3D-printed parts with properties approaching those made from conventional manufacturing such as injection-molding. The presence of microwave-responsive heating elements on the fibers surface, allowed the local selective heat and relaxation of the polymer macromolecules thus increasing their interfaces entanglement (Figure 3A). As a result, enhanced adhesion between the filaments and improved weld fracture strength by 275% were obtained. The authors successfully demonstrated a technique for designing new 3D-printed materials with enhanced mechanical properties resulting in nanomaterial networks.



A



B

Figure 3. (Continued).

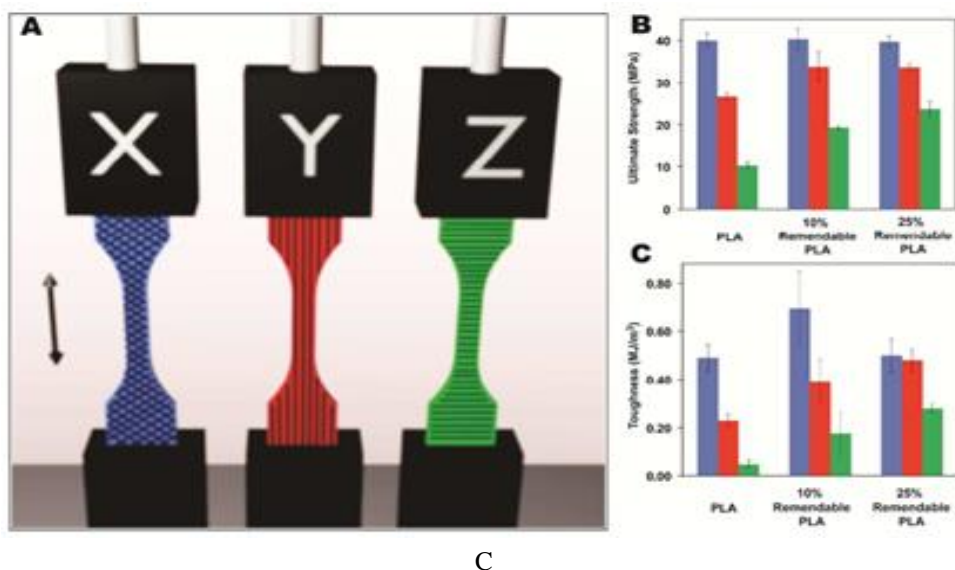


Figure 3. Different approaches for filament adhesion enhancement: chain interpenetration (A) or covalent bonding (B and C) [22, 24, 25].

Another possibility to improve the materials mechanical-properties is to explore the fibers interface chemistry. Monomers, oligomers and small molecules playing the role of crosslinker are a valid path in this scenario. Their functionalization with moieties capable of undergoing thermally reversible dynamic Diels-Alder has shown some promising results [24, 26]. To address the covalent chemical adhesion at a molecular level, PLA functionalized with maleimide moieties and a furan-containing mending agent as crosslinker have been used (Figure 3B). The advantage of this approach is that the thermo-reversible network in the extruded filament thermally *de*-polymerizes during the heat cycle of the print process and *re*-polymerizes during the cooling step. When different dogbone type patterns (X, Y, Z) were tested, depending on the direction of the deposited filaments (Figure 3C), it was established that both strength and toughness end up being improved (130% and 460%, respectively along the *z*-axis). Recycling of the polymer matrix was also possible without its additional chemical modifications. Such self-healing mechanisms have also been described by Yang et al. where new covalent bonds occurred within the polymer structure by using multi-furan monomer and bismaleimide [25]. In this case, isotropic 3D thermoset parts in terms of mechanical properties and with more than 95% interlayer adhesion were designed. In advantage to the multi-axial toughness, a smooth surface of the finished product was obtained. Improvement of the printed parts' mechanical properties can be reached when an inert gas atmosphere is used during the print process. Acrylonitrile-butadiene-styrene and polyamide materials demonstrated high mechanical load (increase in elongation at break and tensile strength up to 30%) due to the absence of the macromolecular chain oxidation processes and related-polymer degradation when exposed at high printing temperature [27]. Another possibility to

overcome the anisotropic mechanical effect (improved interfilamentous junctions) is to introduce crosslinks among the polymer chains by exposing 3D-printed copolymer blends to ionizing radiation. Shaffer et al. demonstrated that gamma rays irradiation of polymer/radiation sensitizers (i.e., trimethylolpropane triacrylate and triallysocyanurate) blends during the printing process, induce crosslinking of the parts resulting in enhanced thermomechanical properties of the final PLA-based material [28]. All these approaches ensure good adhesion between the individual filaments, which is of importance for the successful producing of 3D-printed parts with sufficient mechanical properties and reproducible functionalities in the case of shape memory systems such as actuators.

Of particular interest are the custom-design polymer devices with predefined structure and unique functionality such as self-healing and-deployable structure, actuators, origami structures, biosensor, fixation and fitting parts and others. These polymers are also suitable for smart robotic mechanisms and soft actuation. For their fabrication, a new class of polymers can be used - shape memory polymers (SMPs) capable to memorize their original shape, to acquire a metastable temporary one upon deformation and to revert back to the permanent shape when exposed to an appropriate stimulus. The polymer material's ability to achieve shape recovery from the fixed temporary shape to the initial one is defined as shape-memory effect (SME). This property can be quantified using the shape fixity ratio (R_f) or the ability of the material to fix the temporary shape and the shape recovery ratio (R_r), which represents the extent to get back to the original shape. Usually, the major actuation is directly related to the thermal transitions glass temperature (T_g) or melting temperature (T_m) of the polymeric matrix. In addition, full shape recovery may be caused by other stimuli such as magnetic field, light and electrical current where functional nanofillers (magnetic, plasmonic nanoparticles, carbon nanotubes) are incorporated in the nanocomposite material [29]. In the present chapter, we will define smart 3D materials as materials produced by a 3D technique and capable of recovering their initial shape when exposed to diverse stimuli, while 4D materials would be those capable to change their shape over time once they are 3D-printed and this without external force.

The emergence of SMPs opens the door to the production of new type of filaments from non-commercially available polymers with good processability. Extruded mono-filaments from ternary blends between styrene-*b*-(ethylene-*co*-butylene)-*b*-styrene, polyethylene wax and low-density polyethylene were produced by Chen et al. [30]. The 3D smart materials had the advantage to memorize at least three temporary shapes at specific temperatures via dual, triple and quadruple heating process (Figure 4A). This gradual shape recovery was explained with the presence of multiple individual melting peaks characteristic for polymer matrix composition (heterogeneous microstructures),

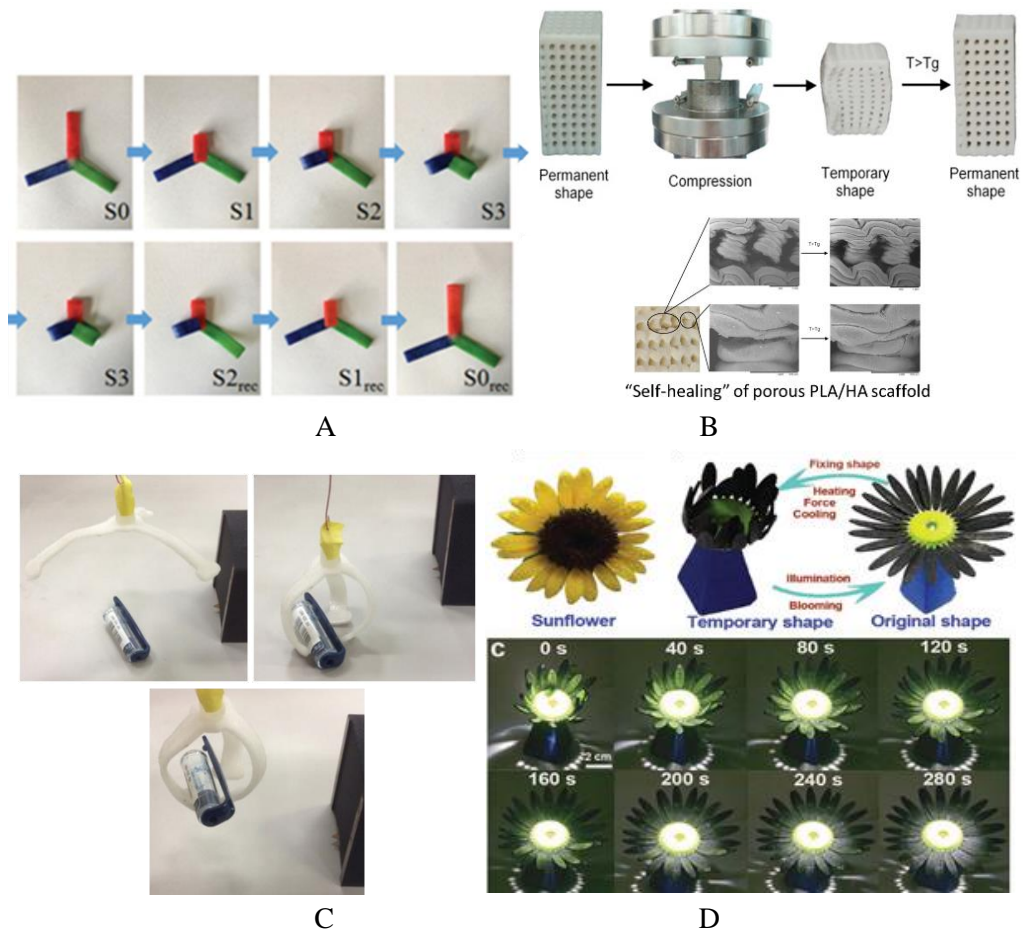


Figure 4. Digital images of 3D-printed SMPs by FDM with quadruple shape memory effect through bending test (A) [30], with self-healing properties (B) [31] or for catching and transport of objects (C) [33]; Photo-responsive materials with light-triggered shape recovery (D) [34].

offering broad thermally switching transitions. As a consequence, it was demonstrated that 3D-printed objects for rapid prototyping with tunable SME can be easily prepared with specific topological structures, particularly in comparison to other conventionally used thermoplastic-shaping techniques (such as casting or molding). Another nanofiller used for SMP filaments production was hydroxyapatite (HA, 15 wt%) [31]. In this case the porous scaffolds (with an average pore size and porosity of 700 μm and 30 vol%) were reinforced by the dispersed HA particles acting as nucleation agents on PLA phase. The incorporation of the ceramic particles inhibited the growth of cracks during compression-heating-compression cycles revealing the self-healing properties of the material (Figure 4B). The authors then established the advantage of FDM as a disruptive technique for the production of personalized porous scaffolds and implants as self-fitting small bone defect replacements with R_r of 98% and absence of delamination.

Thermally-triggered parts can be done from filaments made of an ionomeric thermoplastic SMP-zinc-neutralized poly(ethylene-co-methacrylic acid) [32]. In this case, the shape-memory effect is obtained via two networks: nanodomains with long relaxation times of supramolecular crosslinks formed by ionic bonds (permanent network) and ethylene crystals (temporary network). Printed parts with more complex geometry can be used for catching and transporting objects as presented in Figure 4C [33]. In this study, the filaments were produced from polyurethanes with various T_g (i.e., from 145°C to 195°C).

FDM also finds an application in the fabrication of light triggered devices, where the chemical stability and properties of the photo-sensible compounds are preserved during the printing process by avoiding their UV illumination, as in the case of SLA. Photo-responsive shape memory (nano)composites from polyurethane as smart polymer with advisable T_m and carbon black for its excellent photo-thermal conversion efficiency were described [34]. Remote light control (light source or sunshine) of the printed parts was demonstrated using complex geometric shapes such as a cubic frame and a sun flower-shaped structure (Figure 4D). In both cases the original shape recovered fast (within few minutes with good R_r) due to the effective conversion of light into heat. This approach confirms the potential application of 3D-printed materials as biomimetic solar tracking sensors or smart solar cell systems in FDM.

2.2. Stereolithography

Based on a spatially controlled layer by layer solidification of a liquid resin by photopolymerization, SLA allows a high quality surface resolution, dimensional accuracy, a variety of material options that includes transparent materials and a growing library of compatible materials enabling the fabrication of large-scale 3D objects [7]. The advantages of SLA compared to all other AM techniques regarding accuracy and resolution as micron-sized structures with sub-micron resolution have been established using this setup [35]. Most SLA formulations are based on chain-growth polymerization from concentrated solutions of low molecular weight species that typically form dense, brittle networks [36]. Among the limited commercial availability of liquid resins suitable for SLA, acrylics for their propensity to light-initiated free radical polymerization and epoxies for their propensity to cationic photopolymerization are commonly used in SLA formulations, together with their high solubility in many common solvents. Thiolene photo-curable resins was also tentatively implemented in the SLA area [37]. Multi-functional monomers are then typically used to introduce more crosslinking sites and tune the mechanical properties of the resulting cured resins. While the number of available photo-curable resins is now rapidly expanding, a customizable manufacturing setup is currently being developed, as a way to cover the printability of other range of materials, and possibly combining performances of different materials in the resulting 3D objects. For example, Tumbleston et al. [16] recently used acrylate photo-chemistry in a newly developed continuous liquid interface production (Carbon 3D Inc.). In this study, a

modified version of SLA that can print up to 10 cm scale objects in minutes (instead of hours) by creating an oxygen depletion zone in liquid resins, was presented. Another modified version of SLA includes digital mask projection SLA [38], digital light processing [39], micro-SLA [40] and two-photon polymerization [41] to polymerize

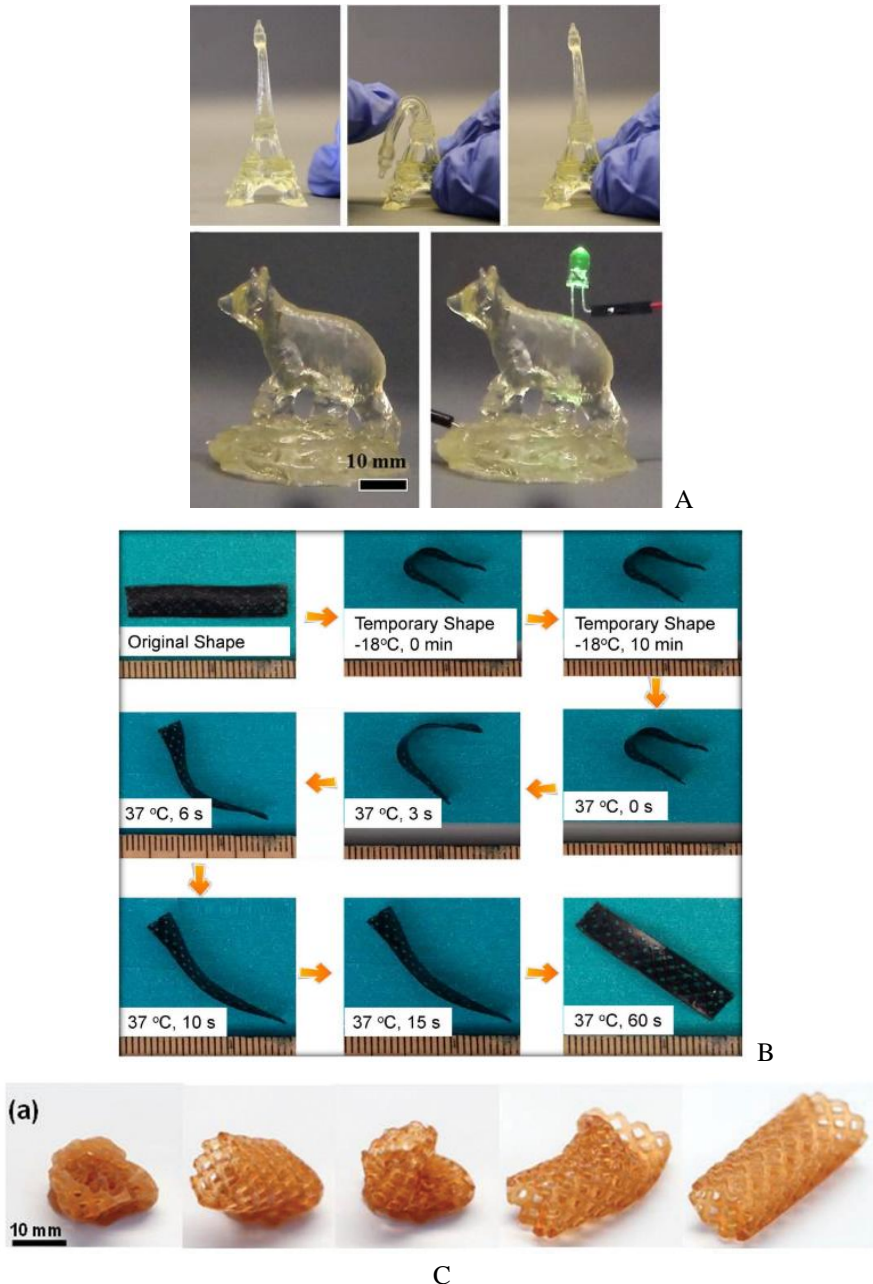


Figure 5. Digital images of SLA printed materials with shape-memory properties for highly elastic and conductive hydrogels (A) [42], tissue engineering scaffolds (B) [43] and vascular stents fabrication (C) [44].

objects starting from a liquid resin. Scientists are constantly looking for a better solution in order to 3D print parts that are not only structurally sound, but get functionalized with active materials to impart “smartness” into the resulting objects.

As part of said “smart materials”, SMPs are a subject of successful SLA printing with various applications. New approach for highly elastic, transparent hydrogels obtained by SLA was proposed by Odent et al. [42] The composite materials presented dynamic and reversible network of ionic interactions resulting in single platform of tunable stiffness, toughness, extensibility, and resiliency. In addition, the presence of silica nanoparticles resulted in the reinforcement of the mechanical performances of the printed material. The electroconductivity of the material conveys a potential application in soft robotics and compliant conductors field (Figure 5A). Composite hydrogels with magnetic responsiveness were designed by Hassen et al. [45]. Poly(ethylene glycol) dimethacrylate was used for its shape-memory properties and the magnetic remote control was provided by adding physically embedded carbonyl iron particles. An interesting approach for biocompatible 3D scaffolds as tissue engineering for human bone marrow mesenchymal stem cells proliferation were proposed by Miao et al. [43]. In this case renewable soybean oil epoxidized acrylate was used as a liquid resin conferring the shape-memory properties of the porous scaffolds. Their shape-recovery is mainly thermally-triggered with T_g of 20°C, offering the possibility to easily generate the glass/rubber phases (permanent/temporary shape) at a temperature close to the human body one (Figure 5B). Cytotoxicity analysis performed on the printed materials had significantly higher cell adhesion and proliferation than traditional polyethylene glycol diacrylate, and had no statistical difference from the widely used polyesters [PLA and poly(ϵ -caprolactone)]. 3D minimally invasive medical devices such as vascular or tracheal stents with complex geometry and shape-memory effect were shaped from methacrylated macromonomers (Figure 5C) [44] or methacrylated polycaprolactone precursor, respectively [46].

3. 4D Printing

4D-printing adds the fourth dimension of time, whereas the 3D-printed structure can change shape, functionality or properties over time once triggered by an external stimulus [11, 12]. Therefore, “smart materials” can be seen as those which provide a means of achieving stimuli-responsiveness into the resulting 3D object that would have otherwise been lacking. The latter is evident once the fabrication of self-assembling origami, where a 2D structure automatically folds into a complicated 3D component is considered [47, 48]. The development of active materials with desirable properties that are also compatible with printers is then crucial for steady advancements in 4D printing. Usually, a 4D-printed structure is created by combining several active materials in the appropriate distribution into a single, one-time printed structure [49]. At the core of this technology

lies a control over two key capabilities: the *material design* and the *structure design* relates to the transformation of the as-printed object due to the properties of the material and design geometric mechanisms respectively. These will be discussed in additional details in the following sections.

3.1. Structural Design

Designing the orientation and location of “smart materials” into 3D-printed objects can facilitate their structural changes in response to external stimuli. However, the change under these conditions does not always lead to increase their dimensionality - an anisotropy, i.e., inhomogeneity with different magnitudes towards any directions is therefore required to generate a transformation such as bending and twisting. Self-transforming materials could then be achieved either by applying gradients of field to homogeneous materials or by applying non-gradient stimuli to inhomogeneous materials [50]. While self-transforming objects using homogeneous materials is technically complicated, a force gradient must be formed and kept for a long period of time, inhomogeneous materials easily switching configurations thanks to the difference in strength of these constituting components. Herein, it is easily understandable that 3D printing technology is one of the most powerful tools to create complex 3D shapes with varied material distributions through spatial arrangement. Such a structuring approach can be categorized as *uniform distribution*, *gradient distribution* and *special patterns* (Figure 6).

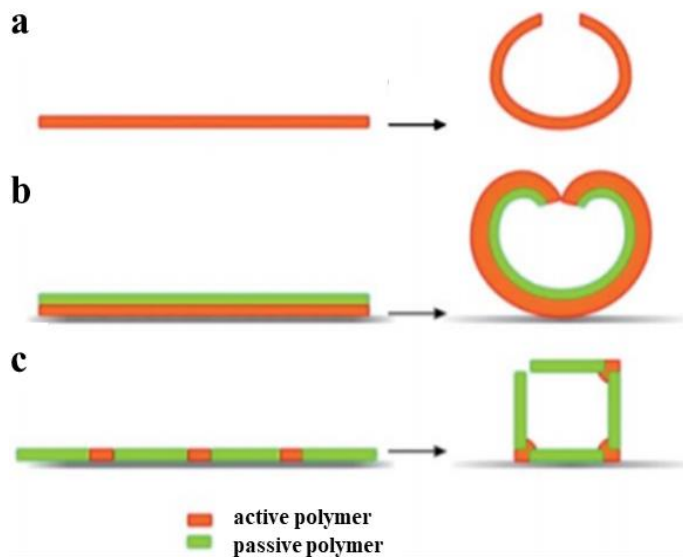


Figure 6. Approaches for structure design of self-transforming materials using uniform distribution (A), gradient distribution (B) and special patterns (C) [50].

3.1.1. Uniform Distribution

This approach is based on homogeneous active materials having directional anisotropy of properties [50]. Among them, shape-shifting materials are probably the most well-known 4D systems of this category having the ability to switch its geometric configuration from one to another in a fully controllable manner when exposed to an appropriate stimulus [51]. In this respect, *shape-changing* (or so-called actuation) should be distinguished from his *shape-memory* counterpart - the former spontaneously change its shape in response to an external stimulus and return to the original shape once the stimulus is turned off. On contrary, the shape-memory effect requires a programming step through deformation of the permanent shape and its fixation in a temporary one, which is retained, until an appropriate stimulus is applied (e.g., moisture, pH change and light) [52, 53]. The use of polymers with multi-responsiveness into a uniformly distributed printed structure therefore allowed the creation of original designs for self-transforming and multi-triggering materials. In this context, details about 4D-printed materials with respect to specific stimuli would be discussed hereafter - the authors kindly return the reader to the appropriate '*Material Design*' section.

3.1.2. Gradient Distribution

The gradient distribution of a single material means that the density of the structure is different at various locations. As a result, the material does not uniformly expand or shrink but folds and unfolds. Bilayers are probably the first structures with gradient distribution - one of the layers is passive, so its properties remain unchanged while the second layer is active and its volume or shape is changed when a stimulus is applied [50]. The proof of concept is demonstrated on the example of star-like patterned polycaprolactone/poly(*N*-isopropylacrylamide) bilayers, capable of controlled capture and release of cells upon heating (Figure 7A) [54]. Fabricating photolithographically patterned bilayer in all the three dimensions is therefore a straightforward way to design and fabricate actuators for repeated sensing in response to continuous environmental change. Several self-folding structures were accordingly created by employing the bilayer design [55-60]. The latter include thermo-responsive SMP/elastomer bilayer laminate in which the shape-change is actuated by the thermal mismatch strain between the two layers upon heating [61]. Likewise, the successful combination of FDM and SLA approaches for the manufacture of complex multi-material magnetic scaffolds in the form of coaxial and bilayer structures suitable for the regeneration of complex tissues were considered [62]. Lastly, Ge et al. investigated the designing variables that are crucial for creating laminate architecture by directly imprinting fibers of SMPs into an elastomeric matrix [48]. 3D-printed flat layered composite structures consisting of multiple active SMP fibers with different T_g in a rubbery matrix to control the transformation of the structure were further developed by Wu et al. (Figure 7B) [63]. Utilizing heat-shrinkable PLA strips, which are printed by FDM on a fixed sheet, Zhang et al. had fabricated smart

3D lightweight structures, whose initial bilayer microstructure can be switched between flat and 3D configuration under appropriate thermal stimuli [64, 65]. Inspired by Nature, Gladman et al. printed composite hydrogel bilayer architectures with programmable anisotropy controlled by the alignment of cellulose fibrils in a soft acrylamide matrix that morph into given target shapes on immersion in water [66].

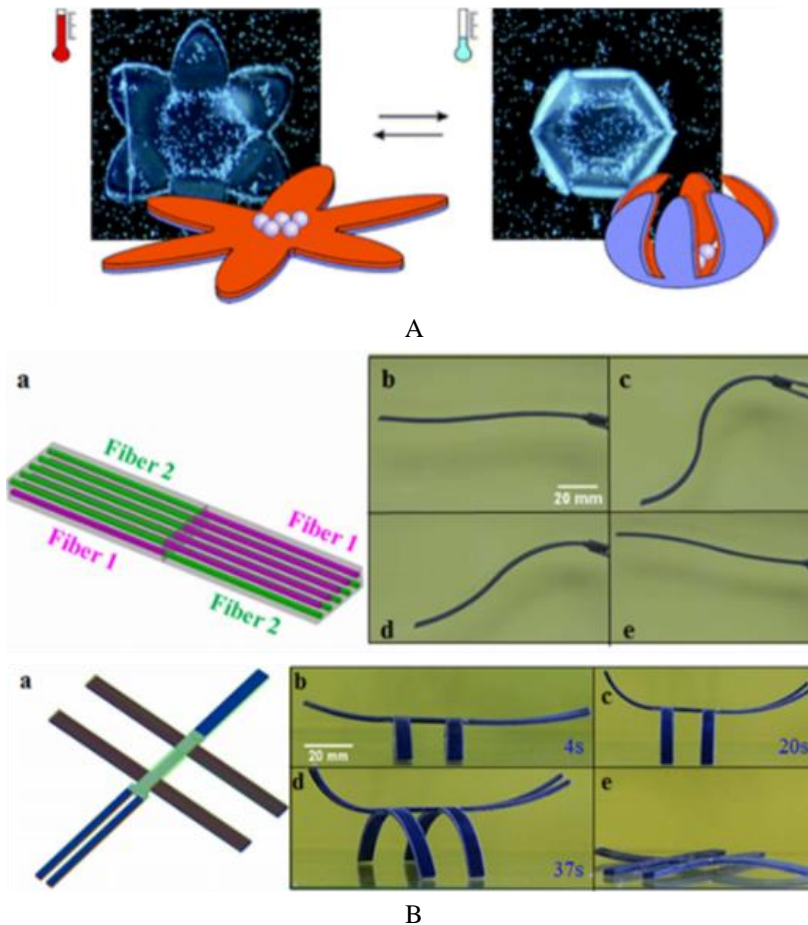


Figure 7. Thermo-responsive star-shaped self-folding capsules in the form of photocrosslinked bilayer (A) [54], and two-layer laminate designed leading to an active “wave” shape when heated or mimicking an insect when immersed in hot water (B) [63].

While the approach is very simple and could be one-step fabricated using a single material, the formed bilayer structures are, hinge-free, i.e., exclusively leading to rounded shapes during the folding. Such limitations pushed researchers to improve the ways to 3D print structural elements in an attempt to convey reliable and large curvature actuation, which is partially covered by gradient-structures or subsequently by special patterns. Usually, gradient materials consist of a layered structure wherein there is a varying layer composition along one axis. One example of such a structurally sound design is shown by

Tibbits et al. using thin surface disk with a gradient distribution of rigid material from the center point to a circumference with full expanding material to fold into otherwise unattainable designed structures depending on the duration of immersion in water (Figure 8) [67]. A method for producing gradient structures with extrusion-type 3D printing was later introduced by Giannatsis et al. following three main steps: (i) defining the geometry and material distribution of each layer in the form of a grayscale image, (ii) generating a set of points distributed according to the gray tone of the image and (iii) constructing a continuous path through the points for guiding material deposition by the 3D printer [68]. Unlike bilayer materials, gradient materials have a continuous change of composition and microstructure along one direction, which helps with avoiding problematic sharp interfaces between discrete layers, a common cause of failure in many engineered parts [69]. Photolithography is a common technique to crosslink and thus permanently preserve a gradient structure. SLA should then outmatch other AM techniques with respect to the fabrication of gradient-structured materials, whereas the time of exposure and the crosslinking density would govern the direction of the gradient.

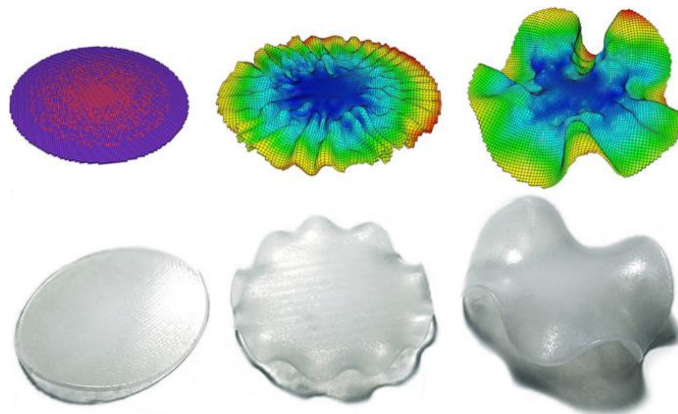


Figure 8. Gradient-structured material and the results of its immersion in water over time [67].

3.1.3. Special Patterns

The approach is based on the use of patterned components of the passive polymer with insertion of an active one. The object's transformation thereby depends on the collective action of those building blocks. For instance, Tibbits et al. combined rigid plastic and active expandable polymer materials in various spatial arrangements in their experiments - the rigid material gives the structure and angle limits for folding while the active material swells after encountering water, forcing the rigid material to bend in its final-state 3D configuration (Figure 9A) [8, 9, 67, 70]. Embedding certain targeted smart hinges inside the structure thereby enable reliable self-transforming behavior. Ge et al. designed self-evolving structures that can be programmed to sense the environment and actively self-deform when exposed to water [47] or even thermomechanically programmed to get complex 3D configurations [48]. Using different combinations of

flexible hinges and rigid segments of metal and polymer thin films, Bassik et al. successfully constructed complex and highly-defined 3D patterned structures [71]. Fabricating such designs is however technically complicated as it might require mask alignment during several steps of photolithography but it also allows fabrication of the broadest range of self-folding structures [72]. Even so, origami-inspired self-folding structures have been recently designed and reviewed by Peraza-Hernandez et al. [73]. Among them, Santangelo et al. focused on understanding the mechanics in which an origami structure can be designed to fold [74]. Kwok et al. presented a design optimization framework for using AM to fabricate flat origami structures that can be self-folded into a target 3D shape [75]. Felton, Tolley et al. conjointly developed a novel method of self-folding hinges and models to rapidly fabricate origami using shape-memory composites and predict the final geometry of the folding state and the overall folding torque (Figure 9B) [76, 77]. A model was also successfully used to predict the bending characteristics, e.g., bending curvature and bending angle, of a series of 3D-printed hydrogel-based inks capable of reversible shape deformation in response to hydration and temperature [78].

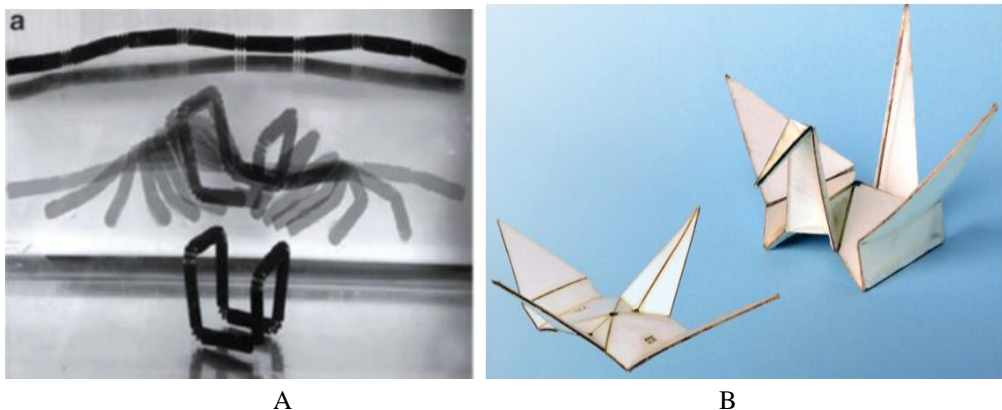


Figure 9. 4D-printed special patterns made of rigid plastic and active expandable polymer materials which expands when exposed to water (A) [9], and origami-inspired self-folding structure using current as a stimulus (through the related heating Joule effect) (B) [76].

While such structural designs have not been yet fully exploited through solid freeform fabrication technology due to the difficulty of implementing multiple materials in a single geometry, SLA has probably been the primary technology focus on creating multi-material structures [79]. Although this technique would not typically be considered a strong candidate for using multiple materials, as it would require the management of possible contamination between multiple viscous resins, it still offers the highest resolution and accuracy with a variety of materials options and easy access to the building chamber. Strategies for building multi-material structures were then conceived to have finally been the focus of recent researches [80-83]. During these developments,

others 3D printing techniques such as direct inks writing or even hybrid manufacturing systems were exploited to build multi-material parts [84, 85]. They are myriad issues, ranging from the processing of different materials to the combined performance of the materials in the final object, that are still challenging with the building of multiple materials in AM but it probably offers novel ways to fabricate, assemble, and morph structures in the right spatial arrangement.

3.2. Material Design

Designing novel active materials having configuration-changing abilities given environmental conditions has been widely used in 4D printing. Shape-morphing is probably one of its main descendant, allowing for a global deformation, which can stretch, fold and bend given environmental/external changes. Stimuli-wise, 4D printing can be categorized as induced by temperature, humidity, pH, light or magnetism [86].

3.2.1. Temperature

An advantageous activation method for 4D printing is the use of heat to trigger the “smart material” for shape-change purposes. So far, the most extensively investigated group of thermo-responsive materials are SMPs, which can revert its shape from a temporary to a permanent one by absorbing thermal energy. In this respect, Choong et al. used a thermally responsive network based on a dual-component phase switching mechanism to build parts of complex geometries having shape-memory behavior using SLA technology (Figure 10A) [87]. In additional research, SMPs fibers were precisely printed into an elastomeric matrix by Ge et al. in order to create an active composite capable of origami folding patterns [47, 48]. Other examples by Ge et al. included the use of a family of photo-curable methacrylate based copolymer networks to demonstrate a new 4D-printing approach that can create high resolution multi-material SMP architectures (Figure 10B) [88]. Liu et al. used 3D-printed thermally responsive SMPs to create actively deployable tensegrities that respond to environmental stimuli in a sequential fashion [89]. Mao et al. also created sequential self-folding structures by 3D-printing hinges with different digital SMPs into components [90]. The latter rapidly self-folds to specified shapes in controlled changing sequences when subjected to a uniform temperature. Multi-shape active composites consisting of families of SMP fibers with different T_g were printed by Wu et al. to control the transformation of the structure [91]. As a result, after being programmed into a temporary shape by a simple thermal-mechanical training program, the printed composite is able to change into multiple geometries and then recover the flat permanent state when stimulated by temperature. Conventional thermo-responsive SMPs can also result in heat-shrinkage. In this respect, Zhang et al. exploited uniform internal strain stored in printed material to fabricate heat-shrinkable polymer, which possesses controllable thermo-structural response and spontaneous pattern transformation under heating [64, 65]. Adaptive structures capable of

self-expanding and self-shrinking by means of four-dimensional printing technology were further developed by Bodaghi et al. [92]. Bakarich et al. here described relatively fast and reversible skeletal muscle-like linear actuation in 3D-printed hydrogels that are both mechanically robust and thermally actuated for their incorporation into a smart valve [93]. To that purpose, they used a thermally responsive covalent crosslinked network of poly(*N*-isopropylacrylamide) to function as both - the toughening agent and the provider of actuation through reversible volume transitions.

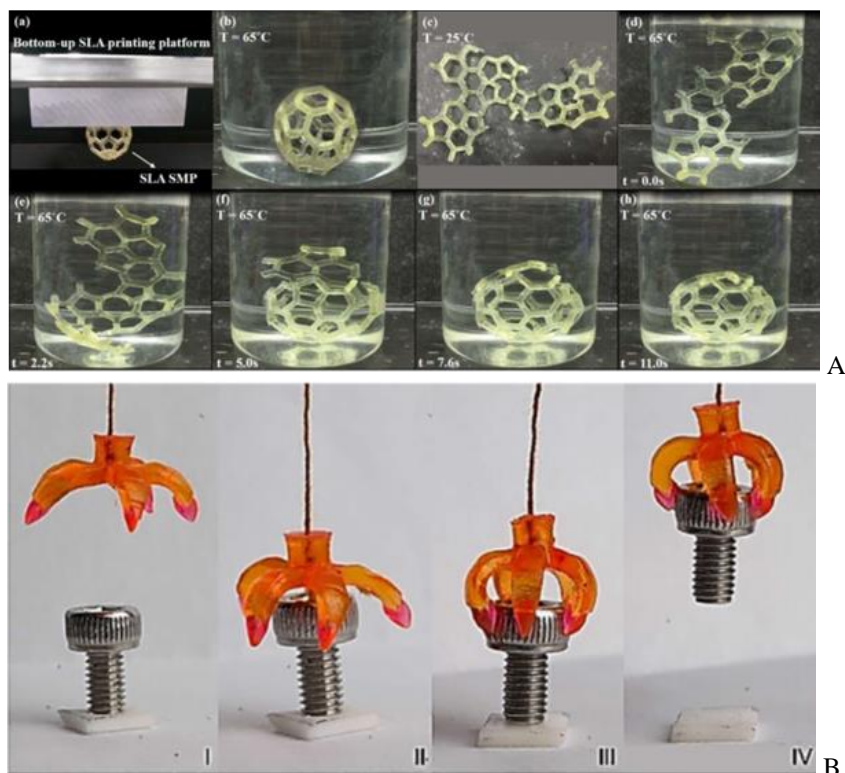
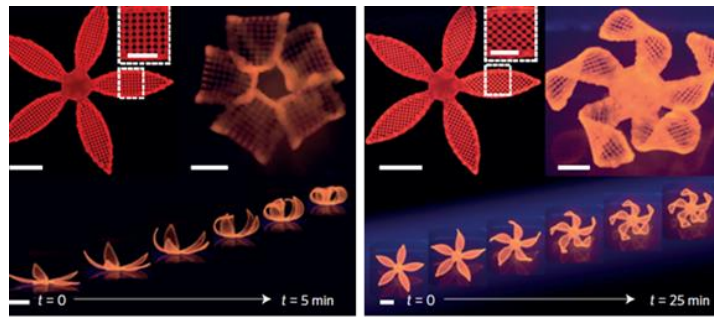


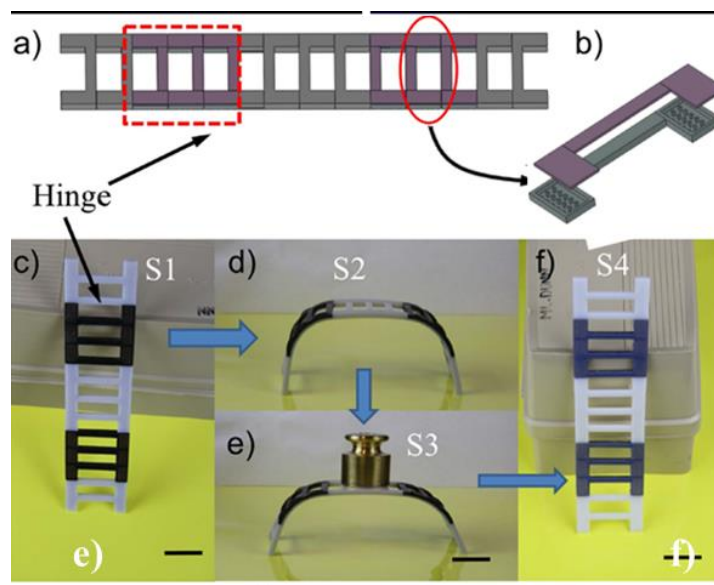
Figure 10. Folding/unfolding cycle for 4D-printed thermally-responsive buckminsterfullerene SMP (A) [87] and SMP gripper that reversibly grabs and releases the objects (B) [88].

3.2.2. Humidity

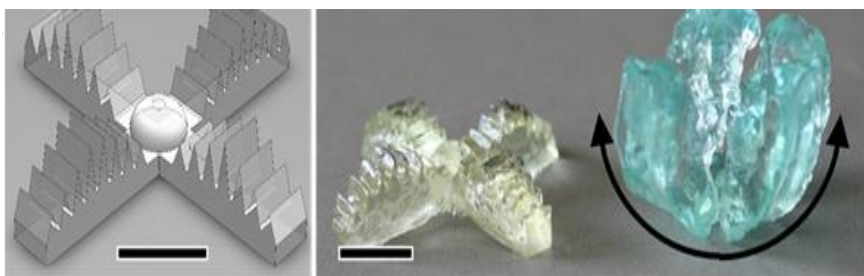
Hydrogels that swell when solvent molecules diffuse into polymer network is probably the second mainly used system to realize 4D-printing. Tibbitts et al. described 3D-printed “smart materials” that expand to induce the transformation when exposed to moisture [8, 9, 67, 70]. His group even controlled the bending angle and direction of the expanding materials by placing rigid components in select areas that prevent the hygroscopic material from expanding in unintended directions. For instance, Tibbitts et al. addressed the challenge of designing active printed materials for complex self-evolving deformations by utilizing hydrophilic materials that expand when submerged in water to



A



B



C

Figure 11. Complex flower morphologies generated by printing bilayers architectures that morph into given target shapes on immersion in water (A) [66], example of active ladder capable of two-way actuation upon the swelling of hydrogel hinges and the heating of SMP hinges (B) [95] and ionic hydrogel composite-based multi-armed gripper, as designed, and printed to rapidly swell from initially flat and open to curved and enclosed when immersed in water (C) [97].

induce various programmed shape changes [70]. Inspired by biomimetics, Gladman et al. created a 4D printing system composed of stiff cellulose fibrils embedded in a soft acrylamide hydrogel ink to programmably fabricate plant-inspired architectures that change shape on immersion in water (Figure 11A) [66]. Huang et al. recently reported ultrafast digital printing of multi-dimensional responsive polymers including hydrogels and SMPs having variable degree of monomer conversion and cross-linking density [94]. In essence, the subsequent immersion in water induced differential swelling in the pixelated polymer networks, turning the 2D polymer films into a 3D object. Active materials capable of two-way actuation were further demonstrated by Mao et al. upon the combination of SMPs and hydrogels in 3D-printed architectures [95]. This approach used the swelling of a hydrogel for the shape change and the temperature-dependent modulus of a SMP to drive the shape-change in a prescribe way (Figure 11B). Duigou et al. used the hygroscopicity of natural wood fibres for the production of original self-bending devices that actuate in a moisture gradient [96]. By controlling the orientation of particles in materials during printing using an external magnetic force, Kokkinis et al. managed to align fused silica particles into the materials to fabricate shape-changing objects [84]. Finally, Odent et al. demonstrated novel 3D-printed ionic composite hydrogels that allowed for fast diffusive swelling for practical implantation of large osmotically driven actuators [97].

3.2.3. Other Stimuli-Responsiveness

While the most common activation method for 4D-printing utilizes temperature and water to trigger shape change, other stimuli such as pH, light and magnetism, although still poorly exploited, have been recently considered in 4D-printing and present new opportunities for designing smart devices. For instance, Nadgorny et al. 3D-printed poly(2-vinylpyridine) objects that exhibited dynamic and reversible pH-dependent swelling. The printed hydrogels also acted as flow-regulating valves, controlling the flow rate depending on the pH [98]. The key to their formulation is the pyridine chemistry combined to a post-printing functionalization approach, which provide a fine-tuning of the degree of swelling by a precise choice of quaternizing reagents and their stoichiometry. Focusing on materials that could be reconfigured multiple times into different shapes with the use of different stimuli, Kuksenok et al. designed a composite that integrates functionalized photo-responsive fibers with thermo-responsive gels [99]. In particular, the single composite can display multiple functionalities as the application of light and heat produces distinctly different responses in these gel-fiber composites. In a new investigation, the sequential folding behavior of polystyrene sheets using the degree of transparency of line pattern was studied by Liu et al. as well as Lee et al. for their use in the design and manufacture of self-folding origami structures [100, 101]. This approach to self-folding then employed localized absorption of light on an otherwise compositionally homogeneous substrate into a hinging response (Figure 12A). Finally,

and in order to ensure optimal part design for potential magnetic applications, Bollig et al. investigated the effects of common 3D-printed structural features on the magnetic properties of the final printed object constructed from a magnetic iron-thermoplastic composite [102]. Magnetic iron oxide III nanoparticles were further employed by Ji et al. to develop digital light processing 3D printing resin, which enabled the free-assembly manufacturing of soft actuators with complex architectures [103]. As proof of concept, a flexible gripper allowing for remote control of gripping and transferring cargo in the presence of magnetic field was demonstrated.

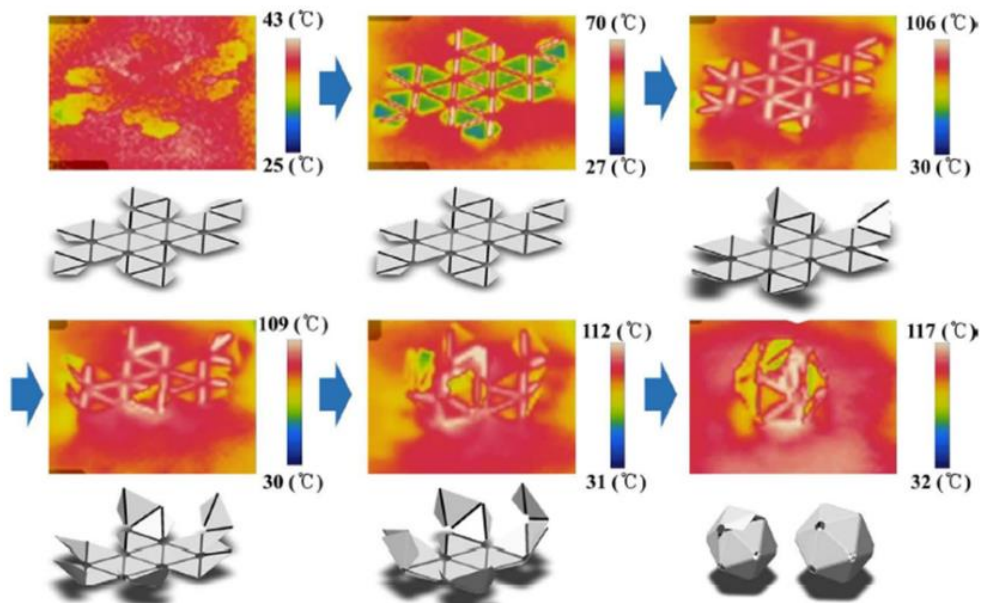


Figure 12. Icosahedral shape deformation of polystyrene sheets using sequential folding behavior (A) [101].

PERSPECTIVES AND CONCLUSION

Over the last years, 3D printing technology has been leading a revolution in the materials science research and manufacturing in term of object design with complex geometry and composition, as well as the fabrication of smart polymer systems with astonishing properties and rapid prototyping. Based on the technological progress, it is now possible to combine different methods such as FDM or SLA with the goal of achieving unique material properties and functionalities. Despite the great advantages of the here listed approaches and the promising application of the produced devices, major challenges in the 3D prototyping are still remaining:

FDM Challenges

- 1) Except for the commercially available polymer filaments based on PLA, ABS, PET and others, the production of new polymer (or composite) filaments is challenging due to the relatively low quantity of the synthesized polymers and the homogeneous dispersion of the nanofillers. In addition to this, new demands on the reactive extrusion processing were defined such as: facilities for filaments fabrication with precise diameter (1.75 mm), their collecting during the cooling step and eventual surface coating.
- 2) FDM faces some problems regarding the large-scale fabrication of mechanically robust 3D-printed parts along with some difficulties related to the slow speed and single material printing. New trend in this aspect is the manufacturing of 3D printers with multiple nozzles while filaments with different composition are used.
- 3) As discussed in this chapter, the problem with the anisotropic mechanical properties of the printed parts needs quick solutions. A potential solution is a post treatment of the surface (plasma, coating, solvent vapor exposure). The materials' surface morphology (roughness and distance between the deposited filaments) affecting directly the device properties can be additionally controlled by the use of printing nozzles with different diameter: the smaller is the diameter, the greater should be the resolution of process. Another set of challenges with an effect on the multi-axial mechanical loads of FDM printed parts are the presence of residual stress (warping and delamination of the printed components when an appropriate post processing steps are not taken) and dimensional errors (the parts are no longer meeting the dimensional specifications).

SLA Challenges

- 1) Despite the possibility to produce polymer devices by SLA from a great range of photo-sensible polymers, initiators and cross-linking agents, one main limitation of this technique is related to the poor mechanical properties of the final parts. Therefore, the major obstacle here would concern the reinforcement of the materials *via* incorporation of nanofillers or additional generation of supramolecular structures. This imposes the development of new types of liquid resins and photo-sensitive low molecular weight polymers suitable for SLA with desired functionalities to fit specific applications.
- 2) Even if the resolution of the SLA technique is superior to the one of the FDM (100 nm compared to 0.1 mm, respectively), the main way to prepare the monomers is in solution. This restricts the fabrication to soft materials, limiting

the exploration of new horizons for thermoplastic polymers (mostly soluble in organic solvents). A possible solution could be found in more complex solvent mixtures, but the risk of the printer damaging (solvent vapors) and the question of work security are unsolved.

- 3) Today as part of the AM techniques, 4D-printing has several unique advantages over 3D-printing that may lead to widespread implementation. Depending on the potential application dual-, triple- or multi-responsive materials can be designed. The main difficulty in this field is the speed and degree of responsiveness of the “smart materials”. Some of them can sense stimulus but only provide minimal actuation or only respond after a very long time.

ACKNOWLEDGMENTS

This research has been funded by the European Commission and Région Wallonne FEDER program in the frame of ‘Pôle d’Excellence Materia Nova’ and OPTI2MAT program of excellence, by the Interuniversity Attraction Poles program initiated by the Belgian Federal Science Policy Office (PAI 6/27 and P7/05) and by FNRS-FRFC. Financial support from the BEWARE (BELgium WALLonia REsearch, project convention no. 410161) Fellowships Academia programme co-funded by the COFUND programme of the European Union (FP7-Marie Curie Actions) is gratefully acknowledged. J.-M. Raquez is ‘chercheur qualifié’ by the F.R.S.-FNRS.

REFERENCES

- [1] Wong, K. V., and Hernandez, A. (2012). A Review of Additive Manufacturing. *ISRN Mechanical Engineering*, 2012: 10.
- [2] Gibson, L., Rosen, D., and Stucker, B. (2015). *Additive manufacturing technologies: 3D Printing, Rapid Prototyping, and Direct Digital Manufacturing* In: Springer.
- [3] Yan, X., and Gu, P. (1996). A review of rapid prototyping technologies and systems. *Computer-Aided Design*, 28 (4): 307-318.
- [4] Chua, C. K., and Leong, K. F. (2015). *3D Printing and Additive Manufacturing: Principles and Applications* In: World Scientific.
- [5] Yap, C. Y., Chua, C. K., Dong, Z. L., Liu, Z. H., Zhang, D. Q., Loh, L. E., and Sing, S. L. (2015). Review of selective laser melting: Materials and applications. *Applied Physics Reviews*, 2 (4): 041101.

- [6] Mohan, N., Senthil, P., Vinodh, S., and Jayanth, N. (2017). A review on composite materials and process parameters optimisation for the fused deposition modelling process. *Virtual and Physical Prototyping*, 12 (1): 47-59.
- [7] Bártolo, P. J. (2011). *Stereolithography: Materials, Processes and Applications* In: Springer.
- [8] Tibbits, S. (2014). 4D Printing: Multi-Material Shape Change. *Architectural Design*, 84 (1): 116-121.
- [9] Campbell, T. A., Tibbits, S., and Garrett, B. (2014). The programmable world. *Sci Am*, 311 (5): 60-65.
- [10] Shofner, M. L., Lozano, K., Rodríguez-Macías, F. J., and Barrera, E. V. (2003). Nanofiber-reinforced polymers prepared by fused deposition modeling. *Journal of Applied Polymer Science*, 89 (11): 3081-3090.
- [11] Momeni, F., M.Mehdi Hassani, N. S., Liu, X., and Ni, J. (2017). A review of 4D printing. *Materials & Design*, 122 (Supplement C): 42-79.
- [12] Li, X., Shang, J., and Wang, Z. (2017). Intelligent materials: a review of applications in 4D printing. *Assembly Automation*, 37 (2): 170-185.
- [13] Rubežienė, V., Padleckienė, I., Baltušnikaitė, J., and Varnaitė, R. (2008). Evaluation of Camouflage Effectiveness of Printed Fabrics in Visible and Near Infrared Radiation Spectral Ranges. *Journal of Materials Science*, 14: 361-365.
- [14] Wang, X., Jiang, M., Zhou, Z., Gou, J., and Hui, D. (2017). 3D printing of polymer matrix composites: A review and prospective. *Composites Part B: Engineering*, 110 (Supplement C): 442-458.
- [15] Hussam, K. M., Rui, G., Célio, F., João, N., Sousa, C. O., and Lima, F. L. (2017). On the use of high viscosity polymers in the fused filament fabrication process. *Rapid Prototyping Journal*, 23 (4): 727-735.
- [16] Matsuzaki, R., Ueda, M., Namiki, M., Jeong, T.-K., Asahara, H., Horiguchi, K., Nakamura, T., Todoroki, A., and Hirano, Y. (2016). Three-dimensional printing of continuous-fiber composites by in-nozzle impregnation. *Scientific reports*, 6: 23058.
- [17] Leigh, S. J., Bradley, R. J., Pursell, C. P., Billson, D. R., and Hutchins, D. A. (2012). A Simple, Low-Cost Conductive Composite Material for 3D Printing of Electronic Sensors. *PLOS ONE*, 7 (11): e49365.
- [18] Tekinalp, H. L., Kunc, V., Velez-Garcia, G. M., Duty, C. E., Love, L. J., Naskar, A. K., Blue, C. A., and Ozcan, S. (2014). Highly oriented carbon fiber-polymer composites via additive manufacturing. *Composites Science and Technology*, 105 (Supplement C): 144-150.
- [19] Auad, M. L., Richardson, T., Orts, W. J., Medeiros, E. S., Mattoso, L. H. C., Mosiewicki, M. A., Marcovich, N. E., and Aranguren, M. I. (2011). Polyaniline-modified cellulose nanofibrils as reinforcement of a smart polyurethane. *Polymer International*, 60 (5): 743-750.

- [20] Zhong, W., Li, F., Zhang, Z., Song, L., and Li, Z. (2001). Short fiber reinforced composites for fused deposition modeling. *Materials Science and Engineering: A*, 301 (2): 125-130.
- [21] Sood, A. K., Ohdar, R. K., and Mahapatra, S. S. (2010). Parametric appraisal of mechanical property of fused deposition modelling processed parts. *Materials & Design*, 31 (1): 287-295.
- [22] Sweeney, C. B., Lackey, B. A., Pospisil, M. J., Achee, T. C., Hicks, V. K., Moran, A. G., Teipel, B. R., Saed, M. A., and Green, M. J. (2017). Welding of 3D-printed carbon nanotube–polymer composites by locally induced microwave heating. *Science Advances*, 3 (6).
- [23] Parandoush, P., and Lin, D. (2017). A review on additive manufacturing of polymer-fiber composites. *Composite Structures*, 182 (Supplement C): 36-53.
- [24] Davidson, J. R., Appuhamillage, G. A., Thompson, C. M., Voit, W., and Smaldone, R. A. (2016). Design Paradigm Utilizing Reversible Diels–Alder Reactions to Enhance the Mechanical Properties of 3D Printed Materials. *ACS Applied Materials & Interfaces*, 8 (26): 16961-16966.
- [25] Yang, K., Grant, J. C., Lamey, P., Joshi-Imre, A., Lund, B. R., Smaldone, R. A., and Voit, W. (2017). Diels–Alder Reversible Thermoset 3D Printing: Isotropic Thermoset Polymers via Fused Filament Fabrication. *Advanced Functional Materials*, 27 (24): n/a-n/a.
- [26] Appuhamillage, G. A., Reagan, J. C., Khorsandi, S., Davidson, J. R., Voit, W., and Smaldone, R. A. (2017). 3D printed remendable polylactic acid blends with uniform mechanical strength enabled by a dynamic Diels-Alder reaction. *Polymer Chemistry*, 8 (13): 2087-2092.
- [27] Lederle, F., Meyer, F., Brunotte, G.-P., Kaldun, C., and Hübner, E. G. (2016). Improved mechanical properties of 3D-printed parts by fused deposition modeling processed under the exclusion of oxygen. *Progress in Additive Manufacturing*, 1 (1): 3-7.
- [28] Shaffer, S., Yang, K., Vargas, J., Di Prima, M. A., and Voit, W. (2014). On reducing anisotropy in 3D printed polymers via ionizing radiation. *Polymer*, 55 (23): 5969-5979.
- [29] Pilate, F., Toncheva, A., Dubois, P., and Raquez, J.-M. (2016). Shape-memory polymers for multiple applications in the materials world. *European Polymer Journal*, 80: 268-294.
- [30] Chen, S., Zhang, Q., and Feng, J. (2017). 3D printing of tunable shape memory polymer blends. *Journal of Materials Chemistry C*, 5 (33): 8361-8365.
- [31] Senatov, F. S., Niaza, K. V., Zadorozhnyy, M. Y., Maksimkin, A. V., Kaloshkin, S. D., and Estrin, Y. Z. (2016). Mechanical properties and shape memory effect of 3D-printed PLA-based porous scaffolds. *Journal of the Mechanical Behavior of Biomedical Materials*, 57 (Supplement C): 139-148.

- [32] Zhao, Z., Peng, F., Cavicchi, K. A., Cakmak, M., Weiss, R. A., and Vogt, B. D. (2017). Three-Dimensional Printed Shape Memory Objects Based on an Olefin Ionomer of Zinc-Neutralized Poly(ethylene-co-methacrylic acid). *ACS Applied Materials & Interfaces*, 9 (32): 27239-27249.
- [33] Yang, Y., Chen, Y., Wei, Y., and Li, Y. (2016). 3D printing of shape memory polymer for functional part fabrication. *The International Journal of Advanced Manufacturing Technology*, 84 (9): 2079-2095.
- [34] Yang, H., Leow, W. R., Wang, T., Wang, J., Yu, J., He, K., Qi, D., Wan, C., and Chen, X. (2017). 3D Printed Photoresponsive Devices Based on Shape Memory Composites. *Advanced Materials*, 29 (33): n/a-n/a.
- [35] Maruo, S., and Ikuta, K. (2002). Submicron stereolithography for the production of freely movable mechanisms by using single-photon polymerization. *Sensors and Actuators A: Physical*, 100 (1): 70-76.
- [36] Melchels, F. P. W., Feijen, J., and Grijpma, D. W. (2010). A review on stereolithography and its applications in biomedical engineering. *Biomaterials*, 31 (24): 6121-6130.
- [37] Zhou, J., Zhang, Q., Zhang, H., Tan, J., Chen, S., Liu, Q., Ma, M., and Xin, T. (2016). Evaluation of thiol-ene photo-curable resins using in rapid prototyping. *Rapid Prototyping Journal*, 22 (3): 465-473.
- [38] Pan, Y., Zhou, C., and Chen, Y. (2012). *Rapid Manufacturing in Minutes: The Development of a Mask Projection Stereolithography Process for High-Speed Fabrication*. (54990): 405-414.
- [39] Tyge, E., Pallisgaard, J. J., Lillethorup, M., Hjaltalin, N. G., Thompson, M. K., and Clemmensen, L. H. (2015). Characterizing Digital Light Processing (DLP) 3D Printed Primitives In *Image Analysis: 19th Scandinavian Conference, SCIA 2015, Copenhagen, Denmark, June 15-17, 2015. Proceedings*, Cham: Springer International Publishing: 302-313.
- [40] Beluze, L., Bertsch, A., and Renaud, P. (1999). Microstereolithography: a new process to build complex 3D objects. *Proc. Soc. Photo-Opt. Instrum. Eng.*, 1: 808-817.
- [41] Park, S. H., Yang, D. Y., and Lee, K. S. (2009). Two-photon stereolithography for realizing ultraprecise three-dimensional nano/microdevices. *Laser & Photonics Reviews*, 3 (1-2): 1-11.
- [42] Odent, J., Wallin, T. J., Pan, W., Kruemplestaedter, K., Shepherd, R. F., and Giannelis, E. P. (2017). Highly Elastic, Transparent, and Conductive 3D-Printed Ionic Composite Hydrogels. *Advanced Functional Materials*, 27 (33): n/a-n/a.
- [43] Miao, S., Zhu, W., Castro, N. J., Nowicki, M., Zhou, X., Cui, H., Fisher, J. P., and Zhang, L. G. (2016). 4D printing smart biomedical scaffolds with novel soybean oil epoxidized acrylate. *Scientific reports*, 6: 27226.

- [44] Zarek, M., Layani, M., Cooperstein, I., Sachyani, E., Cohn, D., and Magdassi, S. (2016). 3D Printing of Shape Memory Polymers for Flexible Electronic Devices. *Advanced Materials*, 28 (22): 4449-4454.
- [45] Hassan, R. U., Jo, S., and Seok, J. (2018). Fabrication of a functionally graded and magnetically responsive shape memory polymer using a 3D printing technique and its characterization. *Journal of Applied Polymer Science*, 135 (11): n/a-n/a.
- [46] Zarek, M., Mansour, N., Shapira, S., and Cohn, D. (2017). 4D Printing of Shape Memory-Based Personalized Endoluminal Medical Devices. *Macromolecular Rapid Communications*, 38 (2): n/a-n/a.
- [47] Qi, G., Conner, K. D., Qi, H. J., and Martin, L. D. (2014). Active origami by 4D printing. *Smart Materials and Structures*, 23 (9): 094007.
- [48] Ge, Q., Qi, H. J., and Dunn, M. L. (2013). Active materials by four-dimension printing. *Applied Physics Letters*, 103 (13): 131901.
- [49] Raviv, D., Zhao, W., McKnelly, C., Papadopoulou, A., Kadambi, A., Shi, B., Hirsch, S., Dikovskiy, D., Zyracki, M., Olguin, C., Raskar, R., and Tibbits, S. (2014). *Active Printed Materials for Complex Self-Evolving Deformations*. 4: 7422.
- [50] Ionov, L. (2011). Soft microorigami: self-folding polymer films. *Soft Matter*, 7 (15): 6786-6791.
- [51] Behl, M., and Lendlein, A. (2007). Shape-memory polymers. *Materials Today*, 10 (4): 20-28.
- [52] Zhou, J., and Sheiko, S. S. (2016). Reversible shape-shifting in polymeric materials. *Journal of Polymer Science Part B: Polymer Physics*, 54 (14): 1365-1380.
- [53] Sun, L., Huang, W. M., Ding, Z., Zhao, Y., Wang, C. C., Purnawali, H., and Tang, C. (2012). Stimulus-responsive shape memory materials: A review. *Materials & Design*, 33 (Supplement C): 577-640.
- [54] Stoychev, G., Puretskiy, N., and Ionov, L. (2011). Self-folding all-polymer thermoresponsive microcapsules. *Soft Matter*, 7 (7): 3277-3279.
- [55] Bassik, N., Abebe, B. T., Laflin, K. E., and Gracias, D. H. (2010). Photolithographically patterned smart hydrogel based bilayer actuators. *Polymer*, 51 (26): 6093-6098.
- [56] Azam, A., Laflin, K. E., Jamal, M., Fernandes, R., and Gracias, D. H. (2011). Self-folding micropatterned polymeric containers. *Biomedical Microdevices*, 13 (1): 51-58.
- [57] Simpson, B., Nunnery, G., Tannenbaum, R., and Kalaitzidou, K. (2010). Capture/release ability of thermo-responsive polymer particles. *Journal of Materials Chemistry*, 20 (17): 3496-3501.
- [58] Randhawa, J. S., Leong, T. G., Bassik, N., Benson, B. R., Jochmans, M. T., and Gracias, D. H. (2008). Pick-and-Place Using Chemically Actuated Microgrippers. *Journal of the American Chemical Society*, 130 (51): 17238-17239.

- [59] Tang, Z., Gao, Z., Jia, S., Wang, F., and Wang, Y. (2017). Graphene-Based Polymer Bilayers with Superior Light-Driven Properties for Remote Construction of 3D Structures. *Advanced Science*, 4 (5): n/a-n/a.
- [60] Toncheva, A., Willocq, B., Khelifa, F., Douheret, O., Lambert, P., Dubois, P., and Raquez, J.-M. (2017). Bilayer solvent and vapor-triggered actuators made of cross-linked polymer architectures via Diels-Alder pathways. *Journal of Materials Chemistry B*, 5 (28): 5556-5563.
- [61] Chao, Y., Zhen, D., Wang, T. J., Martin, L. D., and Qi, H. J. (2017). Shape forming by thermal expansion mismatch and shape memory locking in polymer/elastomer laminates. *Smart Materials and Structures*, 26 (10): 105027.
- [62] De Santis, R., D'Amora, U., Russo, T., Ronca, A., Gloria, A., and Ambrosio, L. (2015). 3D fibre deposition and stereolithography techniques for the design of multifunctional nanocomposite magnetic scaffolds. *Journal of Materials Science: Materials in Medicine*, 26 (10): 250.
- [63] Wu, J., Yuan, C., Ding, Z., Isakov, M., Mao, Y., Wang, T., Dunn, M. L., and Qi, H. J. (2016). *Multi-shape active composites by 3D printing of digital shape memory polymers*. 6: 24224.
- [64] Zhang, Q., Zhang, K., and Hu, G. (2016). *Smart three-dimensional lightweight structure triggered from a thin composite sheet via 3D printing technique*. 6: 22431.
- [65] Zhang, Q., Yan, D., Zhang, K., and Hu, G. (2015). *Pattern Transformation of Heat-Shrinkable Polymer by Three-Dimensional (3D) Printing Technique*. 5: 8936.
- [66] Sydney Gladman, A., Matsumoto, E. A., Nuzzo, R. G., Mahadevan, L., and Lewis, J. A. (2016). Biomimetic 4D printing. *Nat Mater*, 15 (4): 413-418.
- [67] Skylar, T., Carrie, M., Carlos, O., Daniel, D., and Shai, H. (2014). 4D Printing and Universal Transformation. *Proceedings of the 34th Annual Conference of the ACADIA 2014: Design Agency* 539-548.
- [68] Giannatsis, J., Vassilakos, A., Canellidis, V., and Dedoussis, V. (2016). Fabrication of graded structures by extrusion 3D Printing. *Proceeding of the 2015 IEEE International Conference on Industrial Engineering and Engineering Management*.
- [69] Claussen, K. U., Scheibel, T., Schmidt, H.-W., and Giesa, R. (2012). Polymer Gradient Materials: Can Nature Teach Us New Tricks? *Macromolecular Materials and Engineering*, 297 (10): 938-957.
- [70] Raviv, D., Zhao, W., McKnelly, C., Papadopoulou, A., Kadambi, A., Shi, B., Hirsch, S., Dikovskiy, D., Zyracki, M., Olguin, C., Raskar, R., and Tibbits, S. (2014). Active Printed Materials for Complex Self-Evolving Deformations. *Scientific Reports*, 4: 7422.
- [71] Bassik, N., Stern, G. M., Jamal, M., and Gracias, D. H. (2008). Patterning Thin Film Mechanical Properties to Drive Assembly of Complex 3D Structures. *Advanced Materials*, 20 (24): 4760-4764.

- [72] Ionov, L. (2012). Biomimetic 3D self-assembling biomicroconstructs by spontaneous deformation of thin polymer films. *Journal of Materials Chemistry*, 22 (37): 19366-19375.
- [73] Edwin, A. P.-H., Darren, J. H., Richard, J. M., Jr., and Dimitris, C. L. (2014). Origami-inspired active structures: a synthesis and review. *Smart Materials and Structures*, 23 (9): 094001.
- [74] Santangelo, C. D. (2017). Extreme Mechanics: Self-Folding Origami. *Annual Review of Condensed Matter Physics*, 8 (1): 165-183.
- [75] Kwok, T.-H., Wang, C. C. L., Deng, D., Zhang, Y., and Chen, Y. (2015). Four-Dimensional Printing for Freeform Surfaces: Design Optimization of Origami and Kirigami Structures. *Journal of Mechanical Design*, 137 (11): 111413-111413-111410.
- [76] Felton, S. M., Tolley, M. T., Shin, B., Onal, C. D., Demaine, E. D., Rus, D., and Wood, R. J. (2013). Self-folding with shape memory composites. *Soft Matter*, 9 (32): 7688-7694.
- [77] Michael, T. T., Samuel, M. F., Shuhei, M., Daniel, A., Daniela, R., and Robert, J. W. (2014). Self-folding origami: shape memory composites activated by uniform heating. *Smart Materials and Structures*, 23 (9): 094006.
- [78] Naficy, S., Gately, R., Gorkin, R., Xin, H., and Spinks, G. M. (2017). 4D Printing of Reversible Shape Morphing Hydrogel Structures. *Macromolecular Materials and Engineering*, 302 (1): 1600212-n/a.
- [79] Wicker, R. B., and MacDonald, E. W. (2012). Multi-material, multi-technology stereolithography. *Virtual and Physical Prototyping*, 7 (3): 181-194.
- [80] Choi, J.-W., Kim, H.-C., and Wicker, R. (2011). Multi-material stereolithography. *Journal of Materials Processing Technology*, 211 (3): 318-328.
- [81] Hochan, K., Jae- Won, C., and Ryan, W. (2010). Scheduling and process planning for multiple material stereolithography. *Rapid Prototyping Journal*, 16 (4): 232-240.
- [82] Arcaute, K., Mann, B., and Wicker, R. (2010). Stereolithography of spatially controlled multi-material bioactive poly(ethylene glycol) scaffolds. *Acta Biomaterialia*, 6 (3): 1047-1054.
- [83] Ge, Q., Sakhaei, A. H., Lee, H., Dunn, C. K., Fang, N. X., and Dunn, M. L. (2016). Multimaterial 4D Printing with Tailorable Shape Memory Polymers. 6: 31110.
- [84] Kokkinis, D., Schaffner, M., and Studart, A. R. (2015). Multimaterial magnetically assisted 3D printing of composite materials. *Nature Communications*, 6: 8643.
- [85] Amit, J. L., Eric, M., and B., W. R. (2012). Integrating stereolithography and direct print technologies for 3D structural electronics fabrication. *Rapid Prototyping Journal*, 18 (2): 129-143.

- [86] Leist, S. K., and Zhou, J. (2016). Current status of 4D printing technology and the potential of light-reactive smart materials as 4D printable materials. *Virtual and Physical Prototyping*, 11 (4): 249-262.
- [87] Choong, Y. Y. C., Maleksaeedi, S., Eng, H., Wei, J., and Su, P.-C. (2017). 4D printing of high performance shape memory polymer using stereolithography. *Materials & Design*, 126 (Supplement C): 219-225.
- [88] Ge, Q., Sakhaei, A. H., Lee, H., Dunn, C. K., Fang, N. X., and Dunn, M. L. (2016). Multimaterial 4D Printing with Tailorable Shape Memory Polymers. *Scientific Reports*, 6: 31110.
- [89] Liu, K., Wu, J., Paulino, G. H., and Qi, H. J. (2017). Programmable Deployment of Tensegrity Structures by Stimulus-Responsive Polymers. *Scientific Reports*, 7 (1): 3511.
- [90] Mao, Y., Yu, K., Isakov, M. S., Wu, J., Dunn, M. L., and Jerry Qi, H. (2015). Sequential Self-Folding Structures by 3D Printed Digital Shape Memory Polymers. *Scientific Reports*, 5: 13616.
- [91] Wu, J., Yuan, C., Ding, Z., Isakov, M., Mao, Y., Wang, T., Dunn, M. L., and Qi, H. J. (2016). Multi-shape active composites by 3D printing of digital shape memory polymers. *Scientific Reports*, 6: 24224.
- [92] Bodaghi, M., Damanpack, A. R., and Liao, W. H. (2016). Self-expanding/shrinking structures by 4D printing. *Smart Materials and Structures*, 25 (10): 105034.
- [93] Bakarich, S. E., Gorkin, R., Panhuis, M. i. h., and Spinks, G. M. (2015). 4D Printing with Mechanically Robust, Thermally Actuating Hydrogels. *Macromolecular Rapid Communications*, 36 (12): 1211-1217.
- [94] Huang, L., Jiang, R., Wu, J., Song, J., Bai, H., Li, B., Zhao, Q., and Xie, T. (2017). Ultrafast Digital Printing toward 4D Shape Changing Materials. *Advanced Materials*, 29 (7): 1605390-n/a.
- [95] Mao, Y., Ding, Z., Yuan, C., Ai, S., Isakov, M., Wu, J., Wang, T., Dunn, M. L., and Qi, H. J. (2016). 3D Printed Reversible Shape Changing Components with Stimuli Responsive Materials. *Scientific Reports*, 6: 24761.
- [96] Le Duigou, A., Castro, M., Bevan, R., and Martin, N. (2016). 3D printing of wood fibre biocomposites: From mechanical to actuation functionality. *Materials & Design*, 96 (Supplement C): 106-114.
- [97] Odent, J., Wallin, T. J., Pan, W., Kruemplestaedter, K., Shepherd, R. F., and Giannelis, E. P. (2017). Highly Elastic, Transparent, and Conductive 3D-Printed Ionic Composite Hydrogels. *Advanced Functional Materials*: 1701807-n/a.
- [98] Nadgorny, M., Xiao, Z., Chen, C., and Connal, L. A. (2016). Three-Dimensional Printing of pH-Responsive and Functional Polymers on an Affordable Desktop Printer. *ACS Applied Materials & Interfaces*, 8 (42): 28946-28954.

- [99] Kuksenok, O., and Balazs, A. C. (2016). Stimuli-responsive behavior of composites integrating thermo-responsive gels with photo-responsive fibers. *Materials Horizons*, 3 (1): 53-62.
- [100] Liu, Y., Boyles, J. K., Genzer, J., and Dickey, M. D. (2012). Self-folding of polymer sheets using local light absorption. *Soft Matter*, 8 (6): 1764-1769.
- [101] Lee, Y., Lee, H., Hwang, T., Lee, J.-G., and Cho, M. (2015). Sequential Folding using Light-activated Polystyrene Sheet. *Scientific Reports*, 5: 16544.
- [102] Bollig, L. M., Patton, M. V., Mowry, G. S., and Nelson-Cheeseman, B. B. (2017). Effects of 3-D Printed Structural Characteristics on Magnetic Properties. *IEEE Transactions on Magnetics*, 53 (11): 1-6.
- [103] Ji, Z., Yan, C., Yu, B., Wang, X., and Zhou, F. (2017). Multimaterials 3D Printing for Free Assembly Manufacturing of Magnetic Driving Soft Actuator. *Advanced Materials Interfaces*, 4 (22): 1700629-n/a.

EDITOR CONTACT INFORMATION

Laura Peponi, PhD

Researcher

Instituto de Ciencia y Tecnología de Polímeros ICTP-CSIC
[Institute of Polymer Science and Technology, ICTP-CSIC]

Madrid, Spain

Email: lpeponi@ictp.csic.es

Jean-Marie Raquez, PhD

Laboratory of Polymeric and Composite Materials

University of Mons, Mons, Belgium

Email: JeanMarie.RAQUEZ@umons.ac.be

INDEX

#

2-ethyl-2-oxazoline (EtOx), 246, 263, 264, 266
2-isopropyl-2-oxazoline (iPrOx), 246, 263, 264, 265, 266
3D-printing, ix, xvi, 60, 367, 392, 408, 414
4D-printing, xvi, 392, 402, 408, 409, 411, 414

A

acrylic acid (AAc), 224
active packaging, xiii, 296, 309, 310, 311, 314, 315, 331, 332
additive manufacturing, vi, ix, xiv, xvi, 81, 356, 357, 358, 364, 374, 383, 384, 385, 391, 392, 393, 414, 415, 416
aerospace field, 18, 20
aliquat persulfate (APS), 224, 232, 233, 234, 236
antibacterial, xii, xiv, 72, 89, 183, 185, 194, 196, 223, 233, 238, 275, 276, 277, 278, 279, 280, 282, 285, 289, 290, 291, 292, 293, 294, 314, 330, 336, 345, 353
antibacterial surface, 276, 277, 278, 279, 280, 285, 289, 290, 291, 292, 293, 294
antifouling surfaces, xii, 275
antimicrobial, xii, 185, 195, 196, 275, 276, 277, 278, 279, 280, 281, 282, 283, 284, 285, 287, 288, 289, 291, 292, 293, 294, 296, 311, 314, 330, 332, 353
antioxidant, vi, xiii, 55, 185, 196, 309, 310, 311, 312, 314, 315, 318, 323, 325, 326, 328, 329, 330, 331, 332, 333
arginylglycylaspartic acid (RGD), 246, 257
associative and chain-transfer reactions, 99

atom transfer radical polymerization (ATRP), 246, 278, 283, 284, 286, 287, 291

B

bacteria release, 275, 278, 287
bacterial colonization and biofilm, 277
bactericidal activity, 275, 283, 286, 287, 288, 289, 294
bending test, 17, 399
beverage, 295, 296, 300, 305
biobased polymers, 311, 312
biodegradable polymers, xiii, 32, 309
biofilm, xii, 275, 276, 277, 286, 290, 291
biofilm formation, xii, 275, 276, 277
bio-inspired materials, 2
biomedical applications, vi, 7, 10, 18, 19, 20, 24, 30, 39, 57, 72, 75, 80, 83, 193, 225, 239, 240, 245, 247, 262, 279, 291, 345, 349, 351, 353, 358, 377
biomedical materials, xv, 30, 84, 93, 232, 239, 240, 267, 268, 269, 270, 271, 354, 384, 386, 416
biomedicine, 19, 253, 346, 383
biopolymers, xiii, 309, 310, 313, 338
block copolymers, vi, xi, 9, 25, 93, 113, 199, 200, 206, 207, 209, 210, 211, 212, 213, 214, 215, 220, 221, 222, 253, 254, 257, 259, 260, 262, 265, 266, 277, 291, 354

C

cell-sheet manipulation, 250
chains movement, 156
chain-transfer reactions, 100, 104

- characterization of SME, 15
 chemo-responsive, 12, 21, 28, 85, 91, 240
 coordination bonds, 108, 110
 copolymer, xi, xiv, 8, 13, 25, 27, 29, 40, 47, 51, 57,
 113, 141, 146, 149, 150, 151, 160, 167, 171, 176,
 177, 178, 179, 189, 192, 196, 205, 207, 208, 209,
 210, 211, 212, 213, 214, 219, 220, 222, 231, 241,
 243, 252, 258, 259, 260, 264, 265, 277, 278, 280,
 283, 285, 286, 292, 293, 294, 336, 340, 347, 350,
 398, 408
 copolymerization, 240, 242, 248, 250, 251, 256, 257,
 258, 264, 280
 copolymers of ethylene-vinyl acetate (EVA), x, 10,
 35, 39, 47, 48, 49, 50, 51, 52, 53, 54, 55, 57, 58
 coumarin, vi, xi, 14, 28, 114, 175, 178, 180, 182,
 184, 185, 186, 187, 188, 189, 190, 191, 192, 195,
 196, 197, 198
 covalent bonding, v, 123, 124, 126, 140, 191, 343,
 348, 397
 covalent bonds, xi, xiii, xvi, 8, 11, 98, 99, 100, 123,
 124, 125, 126, 140, 141, 335, 339, 395, 397
 critical micellization temperature (CMT), 246, 255
 critical solution temperature, 224, 227, 246, 347
 critical solution temperature (CST), 224, 227, 233,
 246, 247, 280, 347
 crosslinking, 8, 10, 14, 26, 38, 112, 125, 128, 130,
 135, 136, 140, 141, 147, 175, 177, 190, 192, 221,
 227, 230, 252, 253, 255, 330, 336, 337, 368, 398,
 400, 406
 crosslinks, 10, 41, 81, 90, 117, 126, 127, 128, 129,
 130, 131, 132, 133, 136, 138, 225, 398, 400
 cyclic thermo-mechanical compression tests, 18
 cyclic thermo-mechanical tensile tests, 16, 18
- D**
- damage, ix, x, xi, xvi, 39, 95, 96, 97, 98, 106, 109,
 111, 112, 123, 125, 128, 133, 134, 138, 139, 141,
 149, 150, 151, 152, 154, 155, 156, 158, 159, 160,
 161, 162, 163, 164, 165, 166, 167, 168, 169, 170,
 171, 172, 256, 345, 348, 353
 degree of crosslinking, 225, 227, 336
 dicyclopentadiene (DCPD), 224, 231, 242
 dielectric type, 14
 Diels-Alder, ix, xi, xvi, 11, 65, 100, 102, 112, 114,
 123, 124, 125, 127, 128, 140, 397, 416, 419
 Diels-Alder chemistry, xi, xvi, 123, 128, 140
 dimerization, 116, 175, 180, 182, 183, 184, 186, 187,
 190, 192, 197
 dimethylacrylamide (DMAA), 231, 243, 246, 251,
 354
 dispersed liquid crystals (PDLC), xi, 199, 202, 204,
 205, 206, 207, 208, 209, 210, 211, 213, 214, 215,
 217, 220, 221, 222
 dissociative, 99, 100, 101, 102, 103, 104, 106
 dissociative reactions, 99, 100, 101, 104, 106
 disulfide bonds, 105, 117, 130, 131, 136, 137, 138,
 145, 148
 disulfide exchange, xi, xvi, 118, 123, 126, 130, 131,
 137, 138, 140
 disulfide exchange reaction, xi, xvi, 123, 126, 130,
 131, 137, 138, 140
 D-L-lactic acid co-glycolic acid (PLGA), 19, 246,
 256, 260
 drug delivery, x, xi, xiv, 14, 15, 19, 30, 59, 82, 175,
 177, 187, 189, 193, 226, 232, 238, 239, 240, 255,
 267, 271, 279, 336, 343, 345, 346, 352, 354
 dry-wet-responsive surfaces, 283
 dual sensitivity, 252
 dynamic bonds, 100, 101, 111, 118, 124, 141
 dynamic chemistry, 95
 dynamic covalent reactions, 98, 99, 106
- E**
- edible coatings, 313, 328
 edible films, vi, xiii, 56, 309, 310, 313, 314, 316,
 317, 318, 319, 320, 321, 322, 323, 324, 327, 330,
 331, 332, 333
 elastomer, 10, 24, 26, 27, 29, 30, 57, 65, 79, 92, 115,
 117, 123, 127, 128, 130, 133, 136, 137, 142, 143,
 144, 145, 146, 148, 404, 419
 electro-activated SMPs, 14
 electro-responsive surfaces, 289, 290
 ethylene copolymers, x, 9, 35, 39, 54
- F**
- fixing domain, 6
 food, xii, xiii, 33, 55, 82, 194, 226, 255, 262, 276,
 277, 291, 295, 296, 297, 298, 300, 301, 302, 303,
 304, 305, 306, 307, 308, 309, 310, 311, 312, 313,
 314, 315, 316, 320, 323, 326, 328, 329, 330, 331,
 332, 333, 334, 360
 front velocity (V_f), 154, 224, 229, 230, 236

frontal polymerization (FP), xii, 220, 223, 224, 227, 228, 229, 230, 231, 232, 233, 234, 236, 238, 239, 241, 242, 243, 244
 furan, 65, 125, 128, 130, 139, 143, 147, 397
 fused deposition modeling, xiv, 81, 356, 364, 385, 391, 392, 393, 415, 416

G

gelation temperature (GT), 246, 249, 255, 259, 260
 glass/rubber transition, 9
 graphene, xiv, 14, 24, 28, 67, 71, 73, 77, 88, 89, 90, 91, 138, 139, 140, 144, 145, 232, 243, 336, 346, 347, 348, 354, 367, 419

H

hardness test, 156, 161
 host-guest interactions, 110, 288
 humidity, ix, x, 1, 8, 12, 13, 35, 36, 68, 313, 336, 376, 393, 408
 humidity/water-activated SME, 12
 hybrids, xiii, 3, 55, 61, 136, 141, 191, 220, 335, 336, 337, 338, 339, 340, 341, 342, 343, 345, 346, 348, 349, 350, 351, 353
 hydrogels (HG), vi, ix, xi, xii, xiv, xv, xvi, 6, 21, 23, 81, 84, 91, 93, 98, 101, 118, 120, 121, 175, 176, 178, 223, 224, 225, 226, 227, 231, 232, 233, 235, 236, 238, 239, 240, 242, 243, 244, 245, 248, 249, 253, 255, 256, 257, 279, 280, 292, 337, 348, 349, 354, 371, 391, 401, 402, 409, 411, 417, 421
 hydrogen bonding, 8, 13, 68, 75, 79, 85, 106, 109, 118, 120, 124, 126, 158, 161, 167, 169, 170, 172, 314, 323, 346, 348
 hydrolysable side group, 252
 hydrophilic cellulose nanocrystals, 13
 hydrophilic component, 13
 hydrophobic/hydrophilic balance, xii, xvii, 245, 258, 260, 266
 hydroxyapatite, xii, 25, 55, 223, 233, 235, 238, 257, 337, 345, 349, 352, 379, 381, 382, 388, 399
 hydroxyethyl methacrylate (HEMA), 225, 246, 251
 hydroxypropylacrylamide (HPMA), 246, 251
 hydroxytyrosol, vi, xiii, 309, 310, 315, 316, 328, 329, 332, 333, 334

I

indentation, xi, 149, 151, 154, 155, 156, 157, 159, 160, 162, 163, 164, 170
 intelligent packaging, 306, 307, 310, 329
 interpenetrating polymer networks (IPN), 8, 63, 65, 224, 231, 241, 242
 intrinsic healing, 95, 97, 135, 139
 intrinsically healable materials, 110
 ionic type, 14
 ionomer healing, 149
 ionomeric resin, 35, 39, 40
 ionomers, xi, 11, 24, 25, 26, 40, 41, 58, 124, 127, 142, 146, 147, 149, 150, 151, 152, 153, 154, 155, 157, 158, 160, 161, 164, 168, 169, 170, 171, 172, 173

L

laser sintering, 356, 377, 378, 381, 384, 385, 387, 388, 389, 392
 light-responsive, 13, 72, 110, 176, 177, 189, 192, 193, 195, 348
 light-responsive SMPs, 13
 light-triggered, 28, 88, 175, 186, 189, 192, 197, 399
 liquid crystals, xi, xvi, 6, 199, 200, 204, 208, 209, 210, 211, 212, 214, 215, 216, 217, 218, 220, 221, 222
 low energy-transfer damages, vi, 149, 150, 171
 lower critical solution temperature (LCST), 224, 227, 233, 234, 235, 238, 246, 247, 248, 249, 250, 251, 252, 253, 254, 258, 259, 260, 261, 262, 263, 264, 265, 266, 280, 281, 282, 347

M

maleimide, 65, 115, 125, 128, 130, 139, 140, 143, 256, 397
 melting/crystallization transition, 9
 methacrylate (MA), 10, 92, 128, 131, 133, 224, 246, 256, 258, 278, 280, 283, 286, 329, 330, 331, 332, 334, 350, 351, 352, 354, 387, 408
 methyl methacrylate (MMA), 189, 217, 219, 224, 231
 moisture-sensitive, 13, 27

N

nanocomposites, v, x, xi, xii, xvi, 13, 20, 23, 24, 25, 27, 28, 29, 31, 35, 38, 39, 41, 42, 47, 48, 49, 50, 51, 52, 55, 56, 57, 58, 59, 61, 62, 67, 68, 69, 71, 75, 77, 79, 80, 83, 84, 87, 88, 90, 91, 92, 112, 138, 140, 144, 148, 175, 189, 191, 192, 197, 198, 223, 231, 233, 234, 235, 236, 237, 238, 242, 243, 244, 300, 305, 308, 333, 334, 338, 344, 345, 353, 367, 381, 382, 394

nanofillers, x, 6, 14, 38, 39, 47, 59, 60, 62, 67, 68, 69, 70, 71, 72, 73, 74, 75, 76, 77, 78, 79, 80, 81, 82, 138, 139, 192, 233, 344, 394, 396, 398, 399, 413

nano-hydroxyapatite particles, 233

nanoparticles, x, xii, 14, 28, 35, 38, 54, 71, 88, 90, 97, 187, 193, 195, 215, 216, 220, 221, 223, 227, 233, 234, 235, 236, 238, 244, 250, 257, 263, 276, 282, 295, 298, 303, 304, 345, 352, 354, 381, 382, 398, 412

nanotechnology, 83, 84, 90, 177, 203, 222, 269, 295, 388

natural bentonite, x, 35, 39, 47, 54

natural rubber, 38, 57, 113, 127, 128, 133, 135, 144, 145, 146, 147, 148

nematic liquid crystals, xi, 199, 200, 204, 208, 209, 211, 212, 213, 214, 217

network, xiii, 8, 9, 11, 14, 15, 21, 39, 41, 45, 47, 53, 55, 56, 63, 65, 66, 68, 70, 72, 75, 79, 85, 86, 89, 90, 91, 97, 98, 101, 104, 111, 125, 126, 127, 130, 131, 134, 135, 138, 141, 142, 144, 147, 148, 163, 224, 225, 238, 239, 249, 332, 335, 340, 341, 342, 343, 350, 370, 396, 397, 400, 402, 408, 409

N-isopropylacrylamide (NIPAAm), 224, 240, 243, 249, 280, 282, 283, 292, 293, 347

non-covalent interactions, 106, 124

N-tertbutylacrylamide (NtBA), 246, 251

Nucrel®, x, 35, 39, 40, 41, 42, 43, 44, 45, 46, 54, 150, 151, 153, 160, 161, 163, 166, 167, 170, 171, 172

O

oligo(ethylene glycol) methacrylate (OEGMA), 246

oligoethylene glycol (OEG), 246, 256, 258, 260

order-disorder transition, 5, 150, 156, 158, 164, 169, 172

P

pea starch, 47, 57

penetration, 58, 150, 152, 153, 173, 190, 370

permanent networks and switching phases, 9

permanent phase, 36

permanent shape, xv, 5, 6, 7, 8, 14, 16, 17, 37, 38, 41, 47, 63, 72, 336, 398, 404

photo-crosslinking reaction, 14

photopolymerization, 282, 356, 359, 363, 364, 368, 369, 386, 400

photo-responsive, xi, 14, 175, 176, 177, 180, 182, 189, 190, 191, 192, 197, 288, 411, 422

photo-responsive polymers, xi, 14, 175, 176

photo-thermal effect, 14, 71

pH-responsive polymeric systems, 15

pH-Responsive Surfaces, 277

physical, xi, xii, xiii, xiv, xvii, 8, 11, 16, 20, 36, 38, 41, 45, 63, 65, 71, 72, 77, 92, 96, 97, 99, 100, 111, 123, 150, 175, 179, 190, 191, 198, 203, 222, 224, 225, 226, 245, 248, 250, 254, 266, 277, 295, 315, 322, 336, 337, 342, 343, 350, 368, 378, 393

plasticizing effect of water, 12

PNIPAm, 245, 249, 257

poloxamers, 253, 254, 255, 259, 262

poly (2-cyclopropyl-2-oxazoline) (CPropOX), 246, 264

poly (2-oxazolines) (POXs), 246, 262, 263, 265

poly L-lactic acid (PLA), 10, 19, 23, 32, 55, 69, 87, 93, 178, 179, 239, 246, 256, 257, 312, 330, 334, 364, 394, 396, 397, 399, 402, 404, 413, 416

poly propylene (PP), 246, 252, 286

poly(2-hydroxyethyl methacrylate) (PHEMA), 224, 225, 231

poly(acryl amide) (PAAm), 224

poly(acrylic acid) (PAAc), 224

poly(ethylene adipate) (PEA), 246, 256

poly(ethylene glycol) (PEG), 71, 75, 76, 77, 79, 80, 85, 91, 178, 179, 190, 197, 224, 225, 239, 246, 253, 276, 313, 420

poly(ethylene glycol) (PEG), 71, 75, 76, 77, 79, 80, 85, 91, 178, 179, 190, 197, 224, 225, 239, 246, 253, 276, 313, 420

poly(ethylene oxide) (PEO), 19, 71, 72, 129, 205, 206, 208, 209, 210, 211, 212, 213, 214, 220, 222, 224, 225, 246, 252, 253, 254, 255, 256, 257, 258, 259, 260, 261, 262

poly(ethylene succinate) (PESc), 246, 256

poly(ethylene-co-methacrylic acid) copolymer, 39
 poly(hexamethylene adipate) (PHA), 246, 256
 poly(N-isopropylacrylamide) (PNIPAm), 224, 231, 280, 404, 409
 poly(N-vinyl-2-pyrrolidone) (PVP), 224, 225, 231, 232, 246, 262
 poly(N-vinylcaprolactam) (PVCL), xii, 223, 224, 231, 232, 233, 234, 235, 236, 238, 257
 poly(propylene fumarate) (PPF), 246, 256, 370
 poly(propylene oxide) (PPO), 246, 253, 254, 255, 256, 258, 259
 poly(vinyl alcohol) (PVA), 71, 72, 75, 83, 224, 225, 239, 298, 299, 306, 329, 334, 346, 348, 366
 poly(ϵ -caprolactone-co-lactide) (PCLA), 246, 256
 poly(ϵ -caprolactone) (PCL), 9, 10, 11, 19, 23, 25, 55, 58, 65, 66, 67, 71, 75, 76, 78, 79, 80, 81, 178, 179, 190, 191, 193, 235, 246, 256, 257, 315, 334, 345, 353, 365, 366, 370, 377, 380, 381, 389
 polyethers, 9, 245, 247, 253, 257
 polymer dispersed liquid crystals, vi, xi, 199, 200, 206, 220, 221
 polymerization degree (DP), xii, 245, 246, 258, 260, 266
 poly-N-isopropylacrylamide, 246
 poly-N-isopropylacrylamide (pNIPAm), 246, 247, 249, 250, 252, 253, 257, 263
 poly-oxazolines, 245, 262, 265
 polyurethanes, xi, 9, 10, 12, 13, 19, 25, 26, 27, 58, 61, 68, 79, 84, 87, 88, 91, 92, 93, 104, 106, 113, 114, 115, 117, 118, 119, 120, 127, 136, 138, 141, 142, 143, 144, 145, 148, 175, 176, 177, 178, 186, 187, 188, 189, 191, 193, 195, 197, 198, 231, 241, 242, 336, 348, 350, 351, 352, 354, 394, 400, 415
 programming, 6, 7, 11, 12, 16, 36, 37, 47, 63, 73, 82, 89, 404
 puncture tests, 149, 151, 153, 155, 163, 166, 167, 168

R

(R)-3-hydroxybutyrate (PHB), 32, 246, 256, 330
 responsive surfaces, 275, 286, 288
 reversibility, 12, 97, 98, 124, 125, 126, 128, 129, 130, 140, 212, 214, 284
 recovery, 3, 5, 6, 7, 8, 9, 10, 11, 12, 13, 14, 16, 17, 18, 28, 31, 36, 37, 39, 42, 43, 45, 55, 57, 63, 64, 65, 69, 71, 72, 73, 75, 77, 78, 79, 80, 87, 88, 89, 105, 113, 125, 131, 132, 133, 134, 135, 137, 150,

153, 154, 155, 156, 157, 159, 160, 161, 162, 163, 164, 165, 166, 167, 168, 169, 170, 172, 226, 240, 298, 398, 399, 402
 reversible hydrogen bonding, 150, 160, 171
 reversible photochemical reaction, 14
 reversible properties, xi, 199
 rubber, 3, 41, 113, 126, 127, 128, 129, 130, 132, 133, 134, 136, 137, 138, 139, 140, 141, 143, 145, 146, 147, 148, 173, 402

S

scanning electron microscopy (SEM), 125, 151, 163, 224, 233, 234, 235, 236, 237, 317, 321, 322, 371, 381, 395
 scratch, xi, 69, 137, 142, 149, 150, 152, 164, 165, 166, 169, 172, 173, 338
 scratch tests, 149
 self-cleaning properties, xii, 77, 275, 276, 290
 self-healing, v, ix, xi, xiv, xv, xvi, 18, 20, 21, 23, 24, 39, 58, 71, 78, 82, 91, 96, 98, 106, 109, 110, 111, 112, 113, 114, 115, 117, 118, 119, 120, 121, 123, 124, 125, 126, 127, 128, 129, 130, 131, 132, 133, 136, 137, 138, 139, 140, 141, 143, 144, 145, 146, 147, 148, 149, 150, 151, 168, 173, 175, 190, 191, 192, 195, 197, 198, 336, 348, 354, 393, 397, 398, 399
 self-healing materials, ix, xv, xvi, 18, 20, 71, 98, 111, 112, 114, 117, 120, 124, 198, 348
 self-repairing, 96, 119, 348
 shape change effect (SCE), 224, 226, 227
 shape memory, ix, x, xi, xv, xvi, 1, 2, 3, 4, 6, 7, 8, 9, 10, 11, 12, 13, 14, 18, 19, 20, 21, 22, 23, 24, 25, 26, 27, 28, 30, 31, 35, 36, 37, 38, 39, 40, 41, 47, 48, 49, 50, 51, 54, 55, 56, 57, 58, 80, 83, 84, 85, 86, 87, 88, 89, 90, 91, 92, 93, 111, 137, 138, 142, 146, 147, 148, 150, 163, 175, 179, 183, 193, 224, 226, 240, 329, 398, 399, 400, 416, 417, 418, 419, 420, 421
 shape memory alloys (SMAs), 3, 4, 5, 21, 22, 61
 shape memory ceramics (SMCs), 4, 5, 6, 18, 21, 61
 shape memory effect (SME), 2, 3, 4, 6, 7, 10, 12, 13, 15, 16, 18, 20, 21, 22, 23, 26, 29, 30, 39, 41, 55, 57, 61, 62, 63, 64, 65, 66, 67, 69, 71, 73, 75, 79, 80, 81, 82, 85, 87, 88, 90, 91, 93, 137, 138, 148, 163, 224, 226, 398, 399, 416
 shape memory hydrogels, 23, 226
 shape memory nanocomposites, 18, 38, 88, 89, 90

- shape memory polymeric nanocomposites, 6
- shape memory polymers, ix, xv, xvi, 1, 7, 9, 10, 11, 18, 19, 20, 23, 25, 26, 28, 30, 31, 36, 39, 54, 55, 56, 58, 84, 85, 93, 113, 398, 418, 419, 420, 421
- shape memory polymers (SMPs), ix, x, xv, xvi, 1, 5, 6, 7, 8, 9, 10, 11, 12, 14, 15, 16, 18, 19, 20, 23, 25, 26, 28, 30, 31, 36, 38, 39, 54, 55, 56, 58, 59, 61, 62, 63, 64, 67, 70, 72, 74, 75, 78, 80, 81, 82, 84, 85, 93, 113, 398, 399, 402, 404, 408, 411, 418, 419, 420, 421
- shape-memory composite, 60, 407
- shape-memory materials (SMMs), 2, 3, 4, 6, 61
- shape-memory polymer, ix, xv, xvi, 12, 24, 28, 30, 31, 60, 61, 83, 84, 85, 86, 87, 88, 89, 90, 91, 92, 113, 194, 240
- silica, x, xiv, 35, 39, 41, 43, 47, 54, 55, 112, 113, 189, 191, 197, 198, 300, 307, 336, 337, 340, 342, 343, 344, 351, 352, 353, 402, 411
- silica nanoparticles, x, 35, 39, 41, 44, 54, 112, 191, 198, 352, 353, 402
- silica supports, xiv, 336, 343
- silver nanoparticles, 146, 223, 233, 234, 235, 236, 237, 282, 308
- simple bending test, 15, 16, 17
- smart antimicrobial surfaces, vi, xii, 275, 277, 290
- smart materials, ix, xii, xiii, xiv, xvi, xvii, 20, 23, 29, 31, 36, 54, 60, 61, 83, 84, 87, 88, 89, 90, 92, 113, 114, 144, 146, 147, 199, 206, 215, 309, 328, 336, 346, 354, 392, 393, 398, 402, 403, 409, 414, 418, 419, 420, 421
- smart packaging, vi, xiii, 295, 296, 297, 300, 302, 305, 306, 307, 308, 329
- smart polymers, xii, xv, 21, 57, 240, 245, 310, 329, 337, 392
- SMP-based medical devices, 19
- sodium caseinate, vi, xiii, 33, 309, 310, 315, 317, 320, 321, 322, 323, 328, 330, 331, 332, 333, 334
- sol-gel, 114, 127, 131, 141, 177, 178, 182, 187, 256, 336, 340, 341, 342, 350, 351, 352, 353
- spontaneous polymerization (SP), 182, 224, 229, 230
- stable, 7
- starch nanocrystals (SNCs), x, 35, 38, 39, 51, 53, 54, 57
- stearyl acrylate (SA), 224, 292, 329
- stereolithography, xiv, 81, 356, 363, 368, 370, 371, 385, 386, 391, 392, 400, 415, 417, 419, 420, 421
- stimuli-responsive, 95
- stimuli-responsive, v, xiv, xvii, 1, 2, 20, 24, 35, 62, 111, 137, 240, 310, 336, 340, 346, 349, 391, 393, 402, 411
- stimulus, ix, x, xii, xv, 1, 2, 6, 8, 13, 22, 27, 29, 35, 36, 54, 59, 61, 63, 78, 81, 83, 84, 91, 96, 98, 100, 101, 124, 136, 137, 202, 204, 226, 227, 249, 257, 275, 277, 280, 289, 337, 392, 393, 398, 402, 404, 407, 414, 418, 421
- strain fixity ratio (R_f), 16, 18, 40, 43, 44, 46, 47, 48, 50, 53, 63, 75, 398
- strain recovery ratio (R_r), 16, 18, 40, 43, 44, 46, 48, 50, 53, 54, 63, 68, 75, 77, 79, 398, 399, 400
- stretch-induced crystallization, 47, 51
- sulfur vulcanization, 130
- supramolecular chemistry, 106, 177, 288
- supramolecular interaction, 8, 11, 78, 98, 106, 109, 110, 124, 348
- supramolecular Interactions, 106
- Surlyn®, x, xi, 35, 39, 40, 41, 42, 44, 45, 46, 54, 149, 150, 151, 152, 153, 157, 158, 159, 160, 161, 162, 163, 164, 165, 166, 167, 168, 169, 170, 171, 172
- swelling properties, 226, 227
- switching domain, 6, 7, 9, 10, 12, 38, 63, 64, 65
- switching phase, 11, 36, 47

T

- temperature-responsive hydrogels, 227
- temperature-responsive surfaces, 280
- temporary shape, xv, 4, 5, 6, 7, 9, 11, 14, 15, 16, 18, 36, 37, 38, 40, 44, 45, 47, 48, 54, 63, 64, 72, 226, 398, 402, 408
- tetraethylene glycol diacrylate (TEGDA), 224, 232
- thermally activated process, 149
- thermally-activated, v, x, 4, 9, 14, 19, 35, 39, 47, 48, 50, 51, 53
- thermally-activated shape memory, v, 35, 39, 47, 48, 50, 51, 53
- thermally-activated SMPs, 9, 19
- thermo-mechanical cycle experiments, 16, 36, 39
- thermoplastic starch, x, 32, 35, 38, 39, 47, 54, 55, 219
- thermoplastics, xv, 6, 10, 106, 116, 356, 375
- thermo-responsive, vi, 9, 12, 19, 39, 48, 53, 79, 199, 245, 265, 280, 282, 283, 337, 404, 408, 411, 418, 422
- thermoreponsive polymers, xvi, 247, 283

thermo-reversible bonds, 11
thermoreversible properties, 200
three-point flexural test, 15, 16, 17
tuning of the LCST, 251

U

ultrasound, 15, 28, 30, 316, 322, 330
upper solution critical temperature (UCST), 224,
227, 246, 247

V

vitrimers, 103, 104, 113, 116, 127
volume phase transition temperature (VPPT), 246,
249, 253

W

water-responsive, 12, 55, 62

Π

π - π Stacking, 109